re-BUS

You have downloaded a document from
RE-BUŚ
repository of the University of Silesia in Katowice

Title: Zastosowanie różnych technik analitycznych do badania reakcji oscylacyjnych wybranych aminokwasów białkowych

Author: Agnieszka Godziek

Citation style: Godziek Agnieszka. (2017). Zastosowanie różnych technik analitycznych do badania reakcji oscylacyjnych wybranych aminokwasów białkowych. Praca doktorska. Katowice : Uniwersytet Śląski

© Korzystanie z tego materiału jest możliwe zgodnie z właściwymi przepisami o dozwolonym użytku lub o innych wyjątkach przewidzianych w przepisach prawa, a korzystanie w szerszym zakresie wymaga uzyskania zgody uprawnionego.

UNIWERSYTET ŚLĄSKI W KATOWICACH
Biblioteka Uniwersytetu Śląskiego
Ministerstwo Nauki i Szkolnictwa Wyższego

Rozprawa doktorska

Zastosowanie różnych technik analitycznych do badania reakcji oscylacyjnych wybranych aminokwasów białkowych

Agnieszka Godziek

Promotor pracy:
Dr hab. Mieczysław Sajewicz
Zakład Chemii Ogólnej i Chromatografii
Instytut Chemii
Uniwersytet Śląski w Katowicach

Uniwersytet Śląski
Wydział Matematyki, Fizyki i Chemii
Instytut Chemii

Katowice 2017

Składam serdeczne podziękowania

Panu Doktorowi Mieczysławowi Sajewiczowi za cenne wskazówki, kierownictwo nad pracą, a także za wszelką udzieloną pomoc podczas realizacji pracy.

Pani Profesor Teresie Kowalskiej za opiekę naukową poświęcony czas oraz nieocenioną pomoc i cenne wskazówki w trakcie wykonywania badań i redagowania niniejszej pracy.

Pragnę również serdecznie podziękować moim Rodzicom za wiarę w moje możliwości i wsparcie na każdym etapie edukacji oraz Piotrowi za cierpliwość i wsparcie duchowe.

Za wsparcie finansowe w postaci stypendium otrzymanego przeze mnie w ramach programu „DoktoRIS – Program stypendialny na rzecz innowacyjnego Śląska" współfinansowanego przez Unię Europejską w ramach Europejskiego Funduszu Społecznego.

KAPITAŁ LUDZKI
NARODOWA STRATEGIA SPÓJNOŚCI

UNIA EUROPEJSKA
EUROPEJSKI
FUNDUSZ SPOŁECZNY

SPIS TREŚCI

I. WSTĘP

Aminokwasy białkowe jako podstawowe jednostki budulcowe wszystkich żywych organizmów nie zostały dotychczas wystarczająco dobrze przebadane pod kątem ich samoorganizacji w roztworach abiotycznych. Proces ten jest charakterystyczny dla wszystkich przebadanych aminokwasów białkowych. W wyniku samoorganizacji aminokwasów powstają proste struktury peptydowe, które również mogą samoorganizować się do bardziej skomplikowanych struktur, jakimi są nano- oraz mikrostruktury peptydowe.

Pojęcie nanorurek, czy nanosfer peptydowych znane jest od początku lat 90-tych ubiegłego stulecia [1-3] jednak dopiero obecny stan wiedzy oraz zaawansowana aparatura badawcza pozwalają na lepsze poznanie tych niezwykłych struktur. Badania nad nanorurkami, nanosferami, czy nanowłóknami peptydowymi prowadzone są wprawdzie w różnych ośrodkach badawczych (np. [4-6]), jednak w żadnym z nich samoorganizacja peptydów nie jest prowadzona począwszy od prostych aminokwasów białkowych. Jak do tej pory, żaden ośrodek badawczy nie zainteresował się podstawowymi badaniami nad mechanizmem samorzutnego powstawania nanostruktur peptydowych z czystych optycznie aminokwasów białkowych w układach abiotycznych.

Istnieją duże szanse na zastosowanie odpowiednich nanomateriałów peptydowych w wielu dziedzinach, np. w medycynie [7], jako nośniki leków, w biotechnologii [8-9], inżynierii tkankowej [5], czy kosmetyce, jako dodatki wzmacniające działanie antyoksydacyjne, czy przeciwstarzeniowe. Dotychczasowa nauka o aminokwasach, peptydach i białkach całkowicie pomija fakt samorzutnej peptyzacji tych związków w układach abiotycznych, dlatego więc badanie tych zjawisk znacznie rozszerzy stan obecnej wiedzy o tych prostych składnikach budulcowych każdego żywego organizmu.

II. CZĘŚĆ LITERATUROWA

1. AMINOWKASY

Aminokwasy wchodzą w skład wszystkich białek, polipeptydów i peptydów, przez co są podstawowymi jednostkami budulcowymi wszystkich żywych organizmów. Związki te pełnią również inne funkcje biologiczne będąc substratami w utlenianiu komórkowym, biorą udział w syntezie związków ważnych biologicznie, m.in. zasad azotowych, są ponadto neuroprzekaźnikami, neurohormonami, a także zwykłymi hormonami [10]. Cechą wspólną tej grupy związków jest ich budowa. Wszystkie aminokwasy w swojej strukturze zawierają co najmniej jedną grupę aminową ($–NH_2$) oraz co najmniej jedną grupę karboksylową (–COOH).

1.1. BUDOWA *α*-AMINOKWASÓW

Pierwszym odkrytym aminokwasem była asparagina, wyizolowana przez dwóch francuskich chemików Robiqueta i Vauquelina w 1804 roku z soku asparagusa [11]. Następnie w 1810 roku Wollaston wyizolował cystynę z kamieni moczowych [12]. Kolejno w 1819 roku Proust podczas badań nad serem wyizolował leucynę, a rok później Braconnot otrzymał glicynę z hydrolizatu żelatyny [13]. Od pierwszych odkryć w literaturze opisano już ponad 700 różnych aminokwasów [14], z czego znaczną większość stanowią aminokwasy w postaci wolnej lub w połączeniach niebiałkowych [15]. Znanych jest również 20 aminokwasów wchodzących w skład białek, tzw. aminokwasy białkowe. Większość z nich (wyjątkiem jest prolina i hydroksyprolina) posiada grupę aminową w pozycji *α* oraz łańcuch boczny przyłączony do tego samego atomu węgla [16].

α-Aminokwasy zbudowane są z centralnie usytuowanego atomu węgla, do którego przyłączone są grupa aminowa, grupa karboksylowa, atom wodoru oraz wyróżniająca dany aminokwas reszta *R*, zwana często łańcuchem bocznym. Rys. 1 przedstawia ogólny schemat budowy aminokwasów zarówno w postaci wolnej od ładunku elektrycznego, jak i w postaci obojnaczego jonu [17].

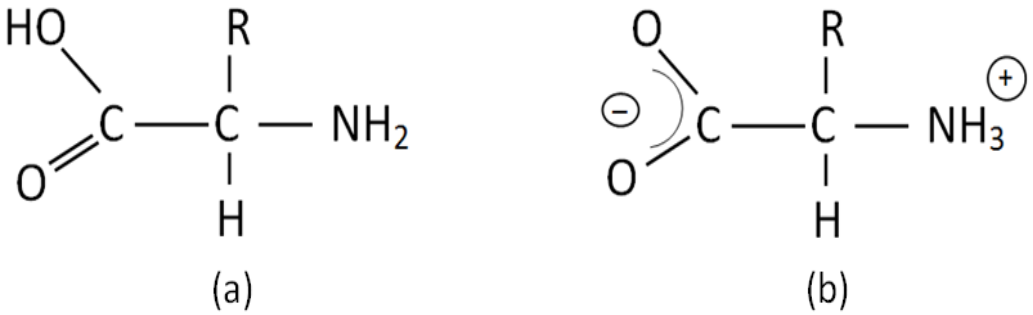

Rys. 1. Ogólny schemat budowy aminokwasów w postaci (a) wolnej od ładunku elektrycznego oraz (b) w postaci jonu obojnaczego

Aminokwasy w zależności od natury łańcucha bocznego wykazują różne właściwości fizykochemiczne. Jedne mają charakter kwasowy, inne zasadowy, jedne reszty aminokwasowe są aromatyczne, inne polarne. Jeszcze inne łańcuchy boczne tworzą wiązania wodorowe czy kowalencyjne, a inne stabilizują cząsteczkę. Łańcuch boczny *α*-aminokwasów może zawierać łańcuch alifatyczny, pierścień aromatyczny, dodatkową grupę aminową bądź karboksylową, grupę wodorotlenową, czy siarkę [18]. Rys. 2 przedstawia budowę dwudziestu podstawowych *L*-*α*-aminokwasów budujących białka.

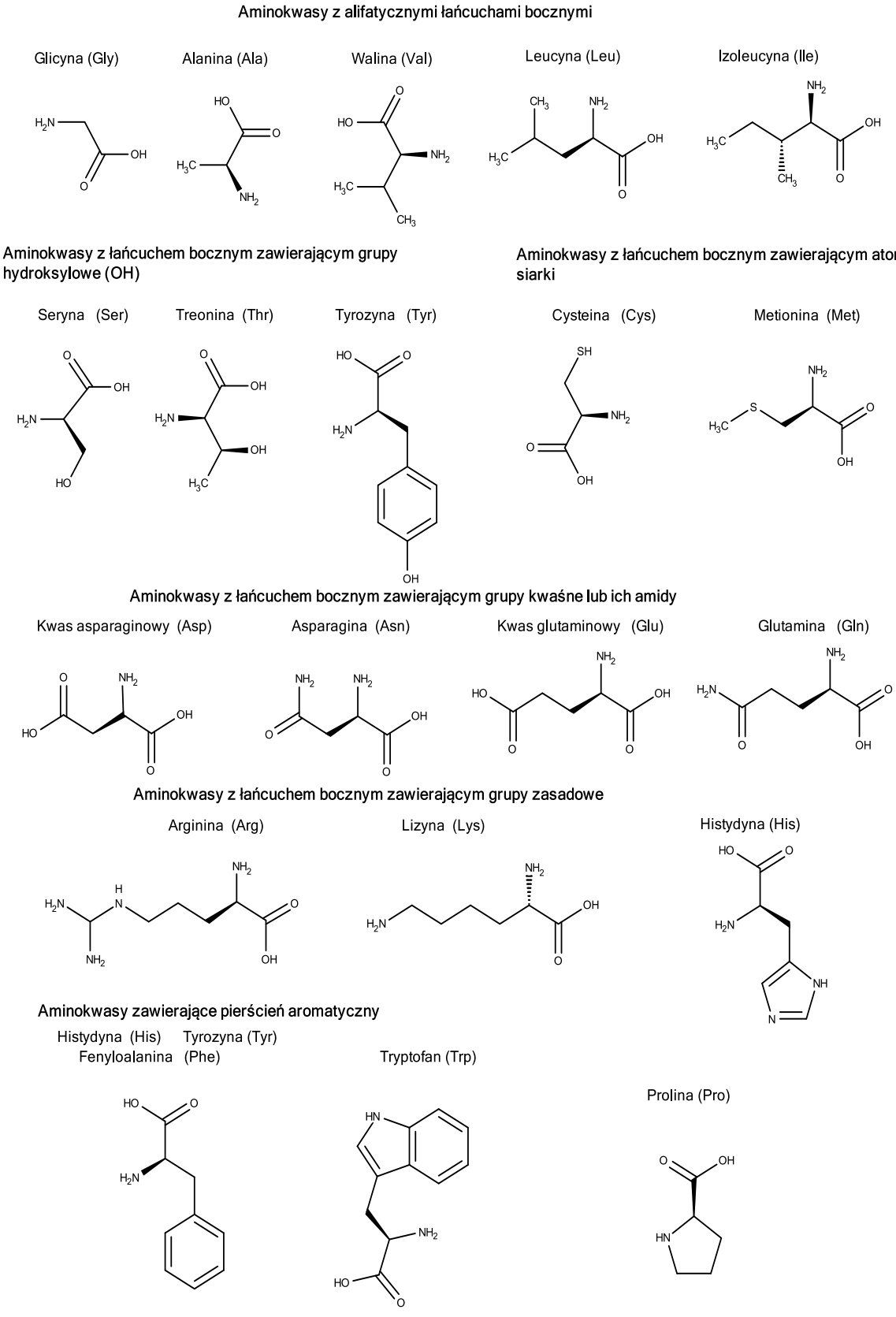

Rys. 2. Wzory przestrzenne *L*-α-aminokwasów występujących w białkach

1.2. WŁAŚCIWOŚCI OPTYCZNE AMINOKWASÓW

Jedną z cech charakterystycznych wszystkich aminokwasów białkowych jest fakt, iż posiadają w swojej strukturze asymetryczny atom węgla *α*, przez co wykazują aktywność optyczną. Wyjątkiem jest glicyna, która nie posiada centrum chiralności i nie skręca płaszczyzny światła spolaryzowanego. Enancjomery wykazują niemalże identyczne właściwości fizyczne, wyjątkiem jest ich zachowanie wobec światła spolaryzowanego. Jeden enancjomer skręca płaszczyznę światła spolaryzowanego w prawo, a drugi w lewo. Mają one taką samą temperaturę topnienia czy wrzenia, taką samą gęstość oraz wszystkie pozostałe dające się oznaczyć stałe fizyczne również są takie same. Enancjomery posiadają także praktycznie takie same właściwości chemiczne, jednak tutaj wyjątek stanowi ich zachowanie wobec związków optycznie czynnych [19-20]. Ze względu na te właściwości rozdział enancjomerów jest niezwykle trudny, choć bardzo istotny. Na Rys. 3 przedstawiono ogólny wzór aminokwasów szeregu *L* (z greckiego *levo* – lewy) oraz *D* (z greckiego *dextro*- prawy) będących sowimi lustrzanymi odbiciami.

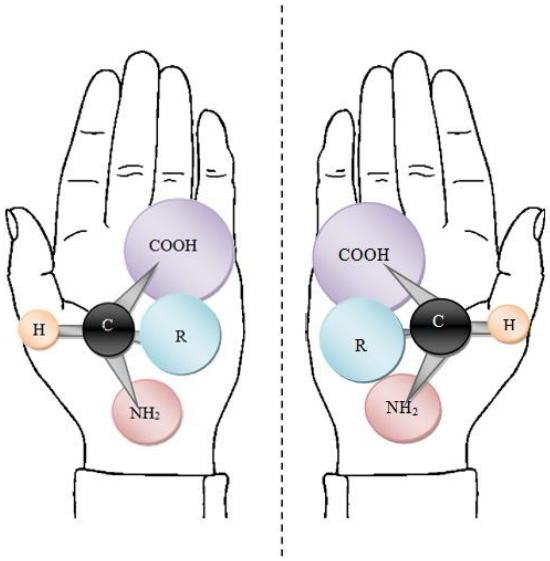

Rys. 3. Izomery *L*- oraz *D*- aminokwasów

Wśród aminokwasów można spotkać również związki, które posiadają dwa centra chiralności. Postać o konfiguracji *L* przy węglu *α* oznaczana jest jako forma *L*. Postać, której konfiguracja przy obu atomach chiralnych jest przeciwna oznaczana jest jako forma *D*. Diastereoizomery oznaczane są jako *L*-allo oraz *D*-allo. Wśród

aminokwasów białkowych treonina, izoleucyna oraz hydroksyprolina posiadają dwa chiralne atomy węgla. Na Rys. 4 zostały przedstawione cztery wzory przestrzenne hydroksyproliny [21].

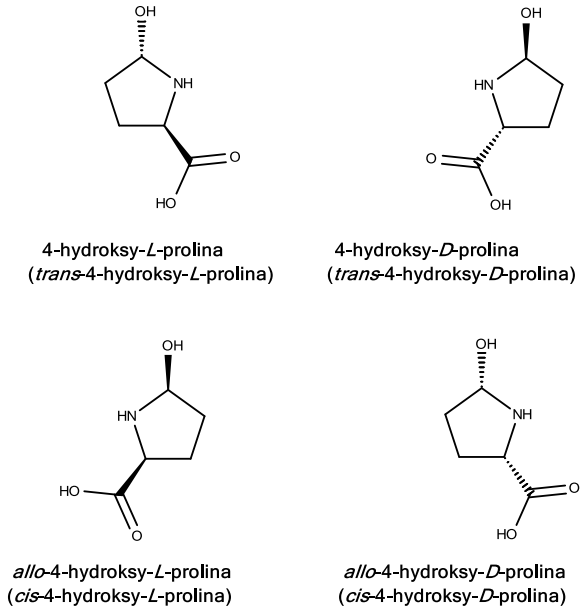

Rys. 4. Wzory przestrzenne *L*-hydroksyproliny, *D*-hydroksyproliny, *L-allo*-hydroksyproliny oraz *D-allo*-hydroksyproliny

Aminokwasy otrzymywane na drodze syntezy chemicznej zawierają taką samą ilość izomeru *D*, co izomeru *L*, jednak aminokwasy występujące w organizmach żywych należą niemalże wyłącznie do szeregu *L* [22]. Izomery szeregu *D* aminokwasów są powszechnie spotykane w świecie organizmów żywych. Już w 1920 roku stwierdzono obecność oktopiny zbudowanej z *L*-argininy oraz *D*-alaniny w tkance mięśniowej ośmiornicy oraz przegrzebków, a także nieco później obecność peptydu poli-*D*-glutaminowego w błonie komórkowej bakterii wąglika (*Bacillus anthracis*) [23]. Ówcześnie takie przykłady występowania *D*-aminokwasów uważano za wyjątki potwierdzające regułę homochiralności w świecie organizmów żywych, jednak pod koniec XX w. stwierdzono obecność aminokwasów szeregu *D* również u zwierząt, w tym także u ludzi. Przykładowo potwierdzono obecność *D*-kwasu asparaginowego w ludzkich zębach [24], *α*-krystaliny w soczewce pacjentów cierpiących na zaćmę [25], czy obecność *β*-amyloidu w mózgu pacjentów cierpiących na chorobę Alzheimera

[26]. Ponadto powiązano występowanie wielu aminokwasów szeregu *D* z występowaniem różnych chorób. Odkładanie się *D*-aminokwasów takich, jak *D*-alanina, *D*-arginina, *D*-asparagina oraz *D*-seryna wpływa na rozwój choroby Alzheimera, obecność *D*-seryny zauważono również w mózgu osób chorych na schizofrenię oraz chorobę Parkinsona [27-28]. Obecność reszt aminokwasowych o konfiguracji *D* w łańcuchu peptydowym może wynikać z różnych mechanizmów, jak na przykład konwersja wolnej grupy *L*-aminokwasowej do jej odpowiednika *D* przed włączeniem aminokwasu do łańcucha peptydowego lub w wyniku enzymatycznej modyfikacji posttranslacyjnej łańcucha peptydowego [23].

1.3. ROZPUSZCZALNOŚĆ AMINOKWASÓW

Aminokwasy zarówno w fazie stałej, jak i w silnie polarnych rozpuszczalnikach występują w formie jonu obojnaczego. Słaba rozpuszczalność w rozpuszczalnikach niepolarnych jest związana z ich jonową siecią krystaliczną. Dowodem na występowanie jonowej dipolarnej struktury aminokwasów jest brak pasm charakterystycznych grupy aminowej czy karboksylowej w widmach adsorpcyjnych, NMR, IR, czy w widmach Ramana.

Aminokwasy poza kilkoma wyjątkami są dobrze rozpuszczalne w wodzie, amoniaku, a także w innych polarnych rozpuszczalnikach, natomiast w etanolu, metanolu, czy acetonitrylu są słabo rozpuszczalne. Nie rozpuszczają się w rozpuszczalnikach niepolarnych takich, jak heksan, benzen czy eter.

Rozpuszczalność aminokwasów zależy również od ich struktury. Lepszą rozpuszczalność wykazują związki z hydrofilowym łańcuchem bocznym. Szczególnie słabo rozpuszczalne w wodzie są aminokwasy aromatyczne (fenyloalanina, tyrozyna, tryptofan) [21].

1.4. REAKCJA PEPTYZACJI

Emil Fischer znany niemiecki chemik, w 1902 roku zauważył, że białka zawierają stosunkowo niewiele wolnych grup karboksylowych i aminowych. Na podstawie tej obserwacji zasugerował, że reakcja łączenia się dwóch aminokwasów to kondensacja z udziałem tych właśnie grup pochodzących od dwóch aminokwasów biorących udział w reakcji. W wyniku takiej reakcji powstaje wiązanie peptydowe (zwane też wiązaniem amidowym) [29]. Schemat reakcji peptyzacji został przedstawiony na Rys. 5.

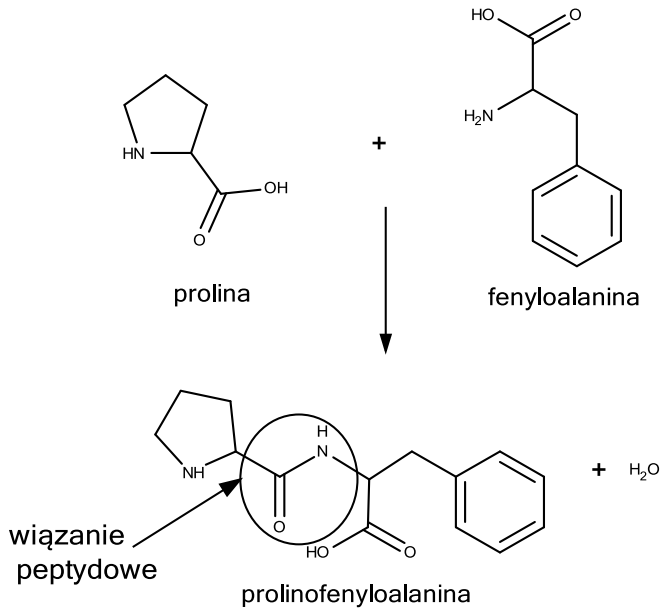

Rys. 5. Reakcja peptyzacji fenyloalaniny i proliny z zaznaczonym wiązaniem peptydowym

Peptydy mogą składać się z kilku, kilkunastu, lub większej liczby aminokwasów. Można zatem wyróżnić di-, tri-, tetra- i polipeptydy. Oligopeptydami nazywamy peptydy zbudowane z co najwyżej 10 aminokwasów, polipeptydami zaś takie, które zawierają mniej, niż 100 jednostek aminokwasowych. Peptydy zawierające więcej, niż 100 reszt aminokwasowych nazywane są białkami [30]. Można wyróżnić cztery formy występowania białek:

- Struktura pierwszorzędowa białka – jest to najprostsza forma występowania białek, które są liniowymi polimerami utworzonymi z aminokwasów połączonych wiązaniami peptydowymi. W niektórych przypadkach dwa łańcuchy polipeptydowe mogą być połączone wiązaniami poprzecznymi, najczęściej są to mostki disiarkowe [17]. Schematyczny łańcuch polipeptydowy został przedstawiony na Rys. 6.

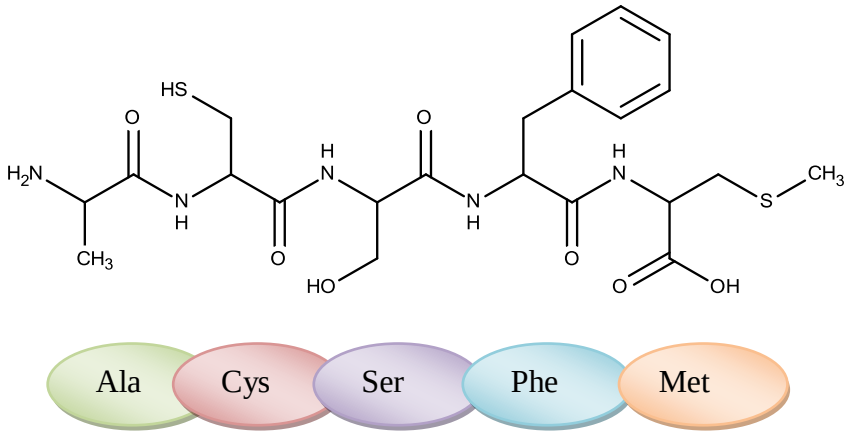

Rys. 6. Łańcuch polipeptydowy złożony z następujących aminokwasów: alanina-cysteina-seryna-fenyloalanina-metionina

- Struktura drugorzędowa białka – jest to struktura posiadająca uporządkowane ułożenie łańcuchów polipeptydowych białek wskutek tworzenia się regularnych wewnątrzcząsteczkowych wiązań wodorowych pomiędzy atomem tlenu jednej grupy amidowej (–C=O), a atomem wodoru innej grupy amidowej (–N–H) w łańcuchu polipeptydowym. Wyróżnia się trzy formy uporządkowania:
  - α-helisa – jest strukturą cylindryczną posiadającą niepolarny rdzeń otoczony przez polarne grupy boczne ułożone heliakalnie po zewnętrznej stronie. Struktura α-helisy jest stabilizowana przez wiązania wodorowe utworzone pomiędzy grupą –C=O aminokwasu a grupą –N–H aminokwasu oddalonego o cztery reszty aminokwasowe. W rezultacie za wyjątkiem aminokwasów na początku i na końcu helisy wszystkie reszty aminokwasowe biorą udział w tworzeniu wiązań wodorowych. Każda reszta aminokwasowa przesunięta jest w stosunku do sąsiedniej o 0,15 nm i obrócona o kąt 100^{o}, co sprawia, że na każdy obrót helisy przypada 3,6 reszt aminokwasowych, a skok helisy wynosi 0,54 nm. Helisa może być zarówno prawo- jak i lewoskrętna, jednak

w helisach prawoskrętnych występuje mniej zawad sterycznych pomiędzy łańcuchami bocznymi a szkieletem, przez co są energetycznie uprzywilejowane [17], [31]. Struktura α-helisy z zaznaczonymi wiązaniami wodorowymi pomiędzy grupami amidowymi odpowiednich aminokwasów została przedstawiona na Rys. 7.

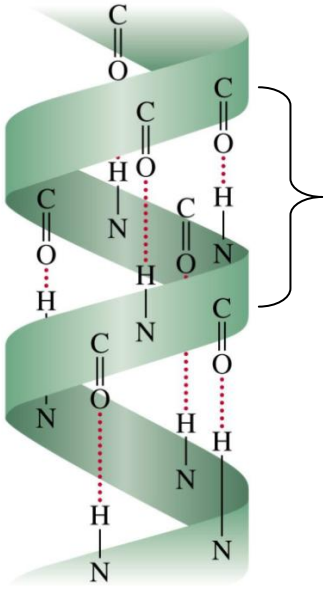

Rys. 7. Struktura α-helisy z zaznaczonymi wiązaniami wodorowymi pomiędzy grupami amidowymi odpowiednich aminokwasów [32]

- β-harmonijka – składa się przynajmniej z dwóch łańcuchów polipeptydowych, zwanych nićmi β. Struktura β-harmonijki składa się, z co najmniej dwóch nici β połączonych wiązaniami wodorowymi. Odległość pomiędzy sąsiadującymi aminokwasami na osi długiej wynosi 0,35 nm, a reszty aminokwasowe sąsiadujących aminokwasów zwrócone są w przeciwnych kierunkach. Strukturę nici β z zaznaczonymi resztami aminokwasowymi przedstawiono na Rys. 8.

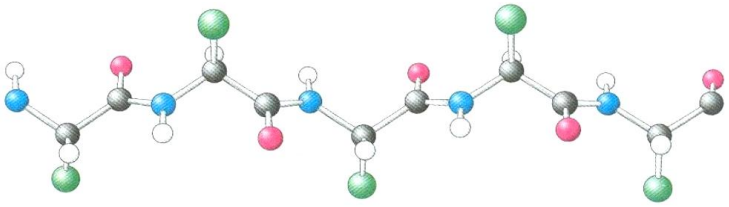

Rys. 8. Struktura β-nici z zaznaczonymi resztami aminokwasowymi (kolor zielony) raz na górze, a raz na dole łańcucha polipeptydowego [17]

Sąsiadujące łańcuchy w *β*-harmonijce mogą był ułożone w przeciwnych kierunkach (antyrównoległa *β*-harmonijka) albo w tym samym kierunku (równoległa *β*-harmonijka). W przypadku ułożenia antyrównoległego, wiązania wodorowe tworzą się między grupami –N–H oraz –C=O każdego aminokwasu z jednej nici *β* z aminokwasem sąsiedniego łańcucha. W przypadku ułożenia równoległego *β*-harmonijki sytuacja jest nieco bardziej skomplikowana. Grupa –N–H każdego aminokwasu połączona jest wiązaniem wodorowym z grupą –C=O aminokwasu sąsiedniej nici, natomiast grupa –C=O łączy się wiązaniem wodorowym z grupą –N–H aminokwasu przesuniętego wzdłuż łańcucha o 2 reszty aminokwasowe. Struktury *β*-harmonijki mogą być tworzone przez wiele nici (zwykle 4–5, ale czasem nawet 10 i więcej), które mogą być ułożone równolegle, antyrównolegle lub mieszanie. Na Rys. 9 przedstawiono strukturę *β*-harmonijki [17], [31].

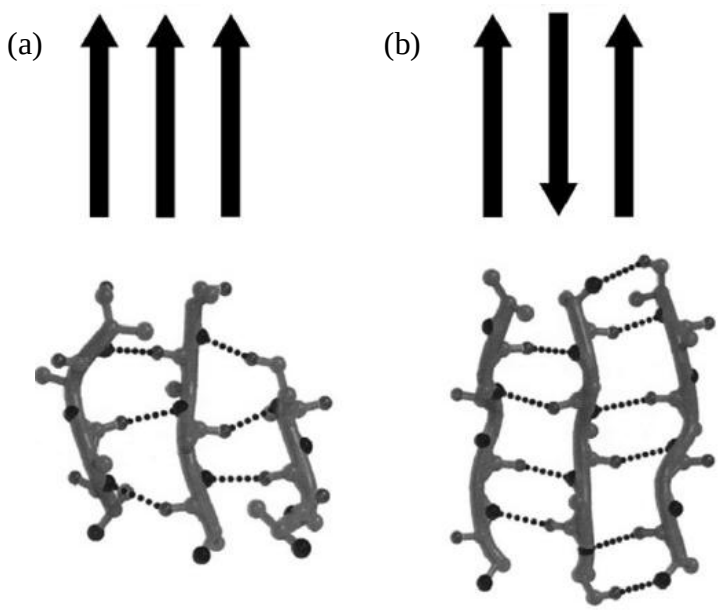

Rys. 9. Schematyczny model struktury *β*-harmonijki (a) struktura równoległa; (b) struktura antyrównoległa [33]

- zwrot *β* oraz pętla *Ω* – zdecydowana większość białek to cząsteczki ściśle upakowane o globularnych kształtach. Jest to możliwe do uzyskania dzięki zmianom kierunku łańcucha polipeptydowego, które dokonują się poprzez występowanie zwrotów *β* oraz pętli *Ω*. Najbardziej popularnym elementem występującym w strukturach białek jest zwrot *β* (Rys. 10(a)), zbudowany

z czterech reszt aminokwasowych w łańcuchu polipeptydowym połączonych wiązaniem wodorowym pomiędzy grupą –C=O pierwszej reszty aminokwasowej (1.) z grupą –N–H czwartej reszty aminokwasowej (4.) stabilizując strukturę zwrotu (Rys. 10 (b)). Pętle *Ω* są natomiast odpowiedzialne za odwrócenie kierunku łańcucha i nie posiadają regularnej, określonej struktury (Rys. 10(c)). Zarówno zwroty *β* jak i pętle *Ω* występują na powierzchni białek, dlatego też biorą udział w oddziaływaniach pomiędzy białkami, a innymi cząsteczkami [34].

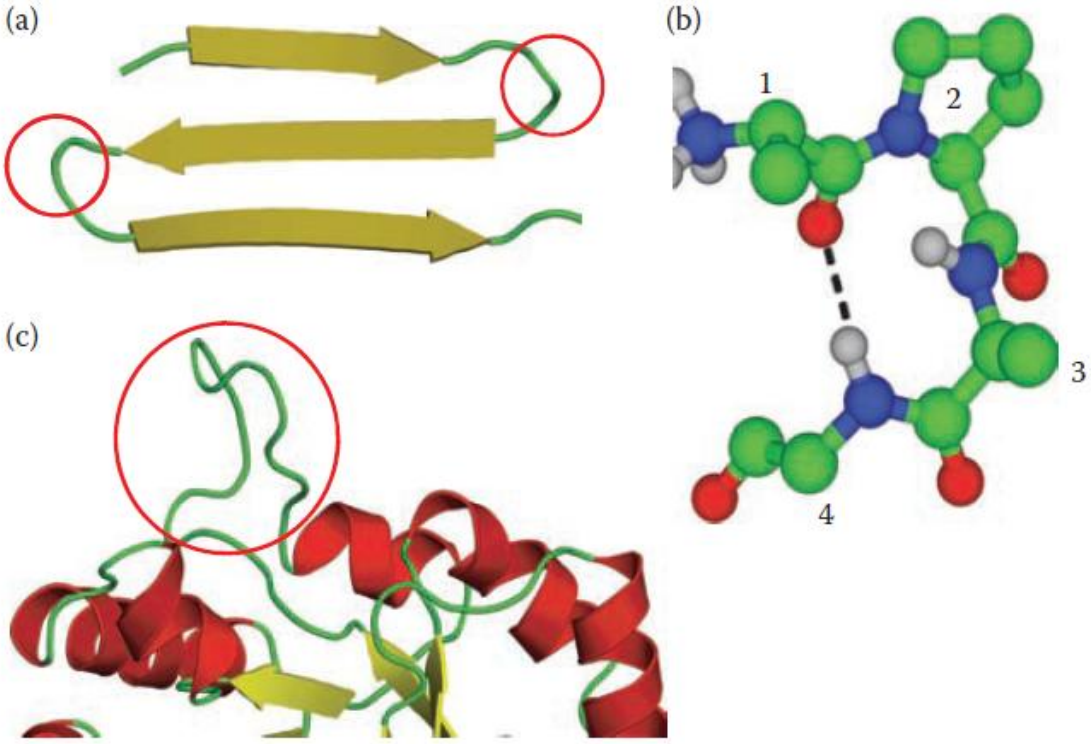

Rys. 10. Zwrot *β* oraz pętla *Ω*. (a) Zwrot *β* w strukturze *β*-harmonijki (zaznaczone w czerwonych okręgach); (b) struktura *β*-zwrotu. W łańcuchu polipeptydowym grupę –C=O 1. reszty aminokwasowej łączy wiązanie wodorowe z grupą –N–H 4. reszty aminokwasowej, stabilizując strukturę *β*-zwrotu; (c) Struktura pętli *Ω* zaznaczona czerwonym okręgiem [34]

- Struktura trzeciorzędowa białka – określa poziom organizacji białka. Strukturę trzeciorzędową białka tworzą przestrzennie rozmieszczone elementy struktury drugorzędowej. Struktura ta jest stabilizowana przez różne wiązania chemiczne oraz oddziaływania międzycząsteczkowe, jak np. mostki disiarkowe nadające

trwałość strukturze, oddziaływania jonowe, oddziaływania van der Waalsa, czy oddziaływania hydrofobowe. Można wyróżnić dwa typy struktury trzeciorzędowej: globularne (Rys. 11(a)) (kuliste białka rozpuszczalne w wodzie) oraz włókniste (Rys. 11(b)) (białka nierozpuszczalne w wodzie) [34].

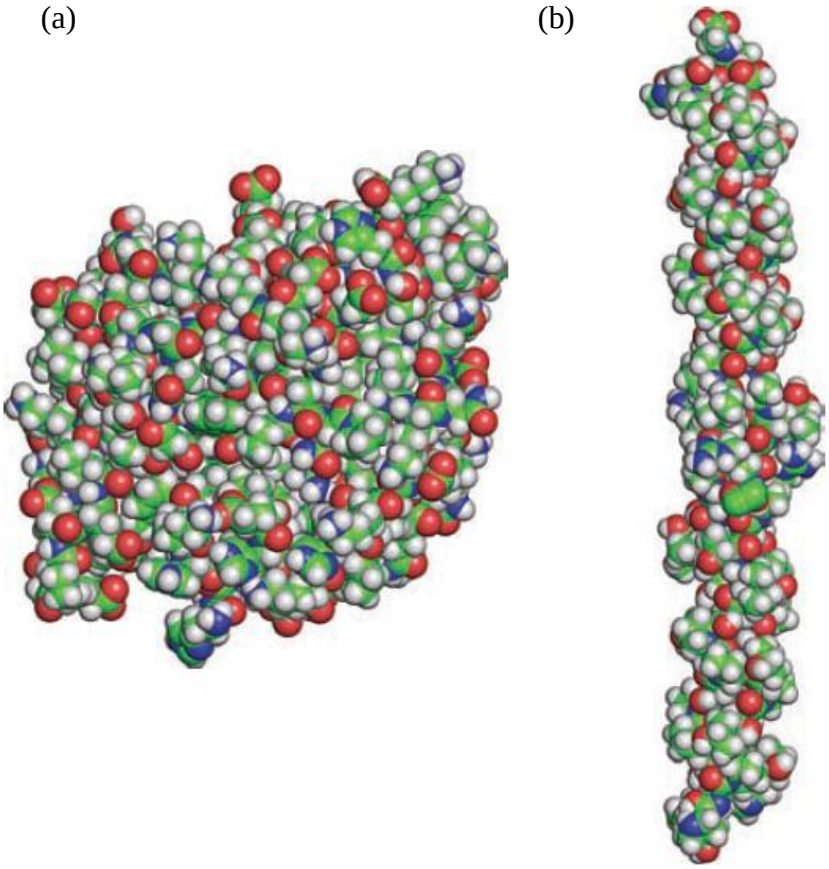

Rys. 11. Struktura trzeciorzędowa białka (a) globularne białko reprezentowane przez enzym anhydrozy węglowej; (b) włókniste białko reprezentowane przez kolagen [34]

- Struktura czwartorzędowa białka – odnosi się do wzajemnego ułożenia łańcuchów polipeptydowych (zwanych w tym przypadku podjednostkami) i natury oddziaływań między nimi. Najprostszą strukturą czwartorzędową jest dimer składający się z dwóch podjednostek (Rys. 12(a)); białka mogą wykazywać strukturę bardzo złożoną – zbudowaną z dziesiątek podjednostek. Podjednostki połączone są ze sobą wiązaniami niekowalencyjnymi. Na Rys. 12 przedstawiono przykładowe ułożenia podjednostek w czwartorzędowej strukturze białka [31], [34].

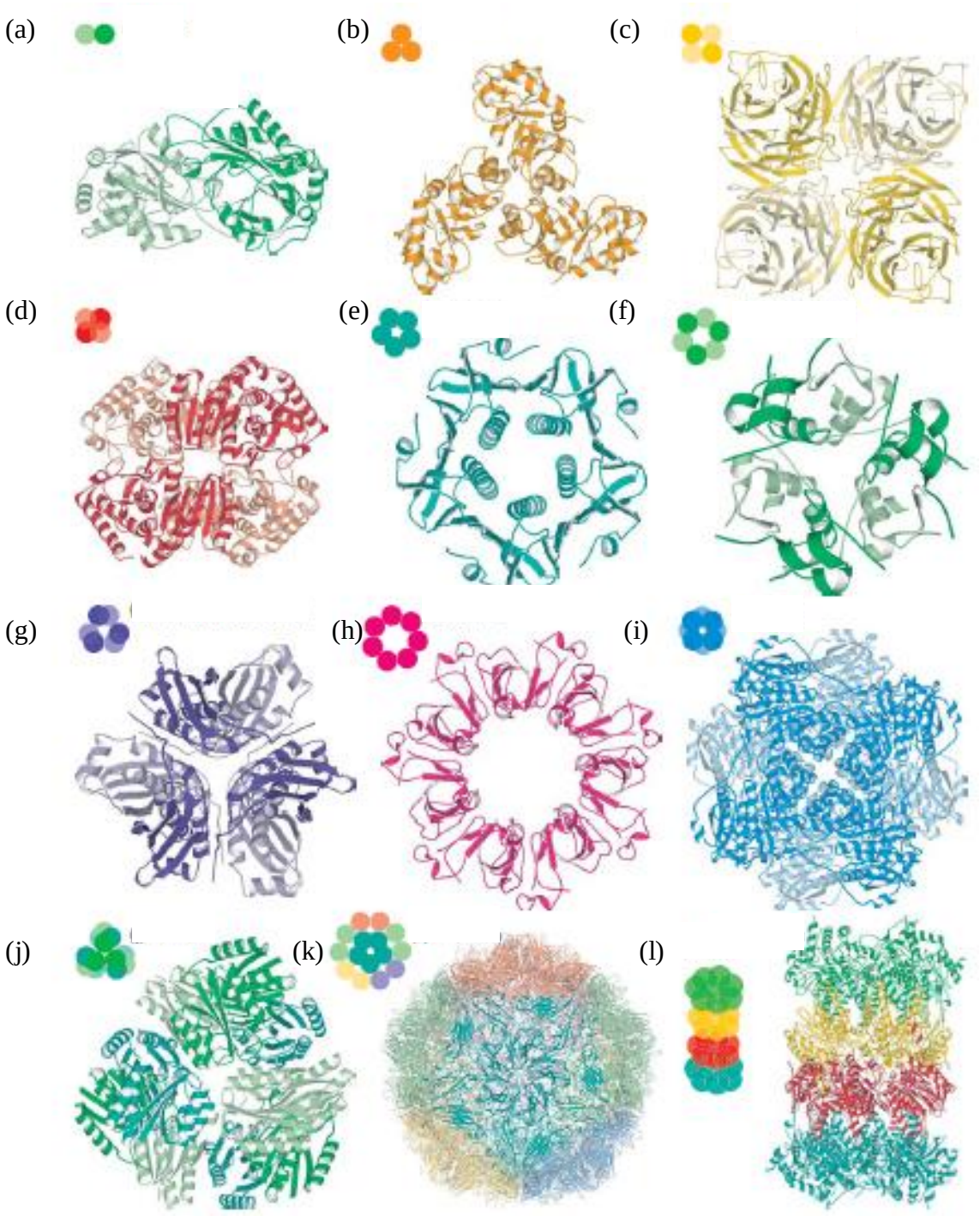

Rys. 12. Przykładowe ułożenia podjednostek w czwartorzędowej strukturze białka (a) dimer; (b) trimer; (c) płaski tetramer; (d) tetramer; (e) pentamer; (f) płaski heksamer; (g) heksamer; (h) heptametr; (i) oktamer; (j) dodekamer; (k) icosahedron; (l) pseudo heptamer [35]

2. WŁAŚCIWOŚCI FIZYKOCHEMICZNE BADANYCH AMINOKWASÓW BIAŁKOWYCH

W niniejszej rozprawie zostaną omówione właściwości fizykochemiczne wybranych aminokwasów białkowych takich, jak cysteina, fenyloalanina, histydyna, hydroksyprolina, metionina, prolina, seryna oraz treonina. Aminokwasy te zostały wytypowane do badań spośród 20 aminokwasów białkowych ze względu na zróżnicowanie w budowie chemicznej łańcucha bocznego. Wybrano dwa aminokwasy z łańcuchem bocznym zawierającym dodatkowe grupy hydroksylowe, dwa aminokwasy zawierające siarkę oraz aminokwasy zawierające pierścień aromatyczny, a także prolinę będącą iminokwasem, oraz jej pochodną hydroksyprolinę, zawierającą dodatkową grupę hydroksylową. Wybrane aminokwasy pełnią ważne funkcje życiowe w żywych organizmach, co również zostało wzięte pod uwagę podczas planowania eksperymentu.

2.1. CYSTEINA

L-Cysteina (kwas (2*R*)-2-amino-3-sulfanylopropanowy), o wzorze strukturalnym przedstawionym na Rys. 13, została odkryta w 1884 roku przez Baumanna, jako produkt redukcji cystyny, która została odkryta w 1810 roku przez Wollastona [12] jako składnik kamieni moczowych. Struktury cystyny i cysteiny zostały określone na drodze syntezy chemicznej w latach 1903-1904 [36].

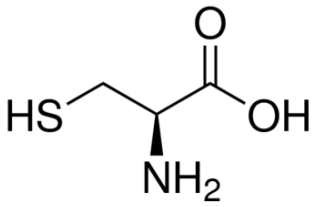

Rys. 13. Budowa przestrzenna *L*-cysteiny

Cysteina w swojej strukturze zawiera grupę tiolową (–SH), dzięki której może tworzyć mostki disiarkowe, będące jednym z czynników wpływających na trzeciorzędową strukturę białka. Cysteina występuje szczególnie obficie w wełnie i włosach, występuje niemalże we wszystkich białkach z wyjątkiem kolagenu i żelatyny. Cysteinę trudno otrzymać z hydrolizatów białek ze względu na fakt, iż szybko ulega utlenieniu do cystyny (dwie cząsteczki cysteiny połączone mostkiem disiarkowym). Ponadto aminokwas ten odgrywa kluczową rolę w organizmie żywym podczas odtruwania organizmu z metali ciężkich, chroni organizm przed szkodliwym

działaniem alkoholu i papierosów, a także jest niezbędny do syntezy białek osocza, kreatyny, uczestniczy również w syntezie glukagonu i insuliny. Ponadto cysteina posiada silne właściwości przeciwutleniające [37]. Podstawowe właściwości fizykochemiczne cysteiny zostały przedstawione w Tab.1.

Tab. 1. Właściwości fizykochemiczne *L*-cysteiny [21]**,** [36]**,** [38-39]

Wzór sumaryczny	$C_3H_7NO_2S$
Masa molowa	121,16 $g \cdot mol^{-1}$
Wygląd	Biały proszek
Rozpuszczalność w H_2O	17,4 $g \cdot 100cm^{-3}$; 25°C
Gęstość	1,49 $g \cdot cm^{-3}$ w 20 °C
Punkt izoelektryczny	5,07
Skręcalność właściwa w H_2O $[\alpha]_D$	-16,51
Toksyczność	LD_{50}>1,890 g/kg (szczur wędrowny, podawane doustnie)

W 1908 roku Sir Archibald Edward Garrod opisał zaburzenia metaboliczne wywoływane przez cystynę, włączając tę chorobę do opisanych przez siebie wrodzonych błędów metabolizmu [40]. Cystynuria jest rzadkim, ale ważnym powodem występowania kamieni nerkowych. Jest to choroba genetyczna, polegająca na reabsorpcji cystyny oraz innych aminokwasów, takich, jak arginina, lizyna i ornityna w kanalikach nerkowych. Ze względu na niską rozpuszczalność cystyny w moczu ryzyko występowania kamieni przez całe życie jest duże [41]. Ogólnoświatowy poziom występowania cystynurii szacuje się na 1 : 7 000, jednak zróżnicowanie w zależności od regionu jest wielkie. Cystynuria najczęściej występuje wśród libijskich Żydów (1 : 2 500), najrzadziej natomiast w Szwecji [42-43].

Drugą chorobą związaną z zaburzonym metabolizmem cysteiny jest cystynoza (choroba genetyczna powodująca odkładanie się cystyny w organizmie). Spowodowana jest ona utratą funkcji genu CTNS, kodującego cystynozynę – białko transportujące. Brak genu powoduje odkładanie się cystyny w organizmie, która niszczy komórki i tworzy kryształki, które gromadząc się w narządach i tkankach powodują ich uszkodzenia. Choroba najczęściej atakuje nerki, oczy, mięśnie, wątrobę, tarczycę, trzustkę, a czasem nawet mózg. Jest to rzadka choroba występująca z częstotliwością od 1 : 100 000 do 1 : 200 000 noworodków na świecie [44].

2.2. FENYLOALANINA

L-Fenyloalanina (kwas *α*-amino-*β*-fenylopropionowy), o wzorze strukturalnym przedstawionym na Rys. 14, została po raz pierwszy wyizolowana w 1879 roku przez Schulza oraz Barbieri'ego z łubinu żółtego. Już trzy lata później Erlenmeyer oraz Lipp uzyskali po raz pierwszy fenyloalaninę na drodze syntezy chemicznej z fenyloacetaldehydu, wodoru, cyjanku i amoniaku. Po dokonaniu pierwszej syntezy chemicznej Schulze oraz Barbieri w 1883 ustalili strukturę chemiczną fenyloalaniny, która jest aromatycznym aminokwasem występującym w przyrodzie [36].

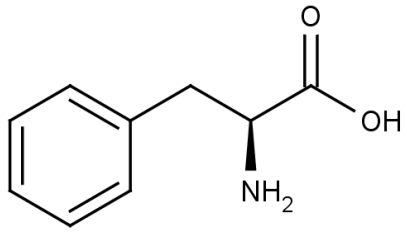

Rys. 14. Budowa przestrzenna *L*-fenyloalaniny

Fenyloalanina jest istotnym aminokwasem białkowym. Organizm sam nie jest w stanie wyprodukować tego związku, dlatego też musi zostać on dostarczony do organizmu z pożywieniem. Fenyloalanina jest niezbędna do prawidłowego funkcjonowania ośrodkowego układu nerwowego, jest w stanie przeniknąć barierę krew-mózg, dlatego jest użyteczna w leczeniu zaburzeń mózgowych. Ponadto organizm przekształca fenyloalaninę w neuroprzekaźniki takie, jak adrenalinę, dopaminę oraz noradrenalinę [45]. Tab. 2 przedstawia właściwości fizykochemiczne fenyloalaniny.

Tab. 2. Właściwości fizykochemiczne *L*-fenyloalaniny [21]**,** [36]**,** [46-47]

Wzór sumaryczny	$C_9H_{11}NO_2$
Masa molowa	165,19 $g \cdot mol^{-1}$
Wygląd	Biały krystaliczny proszek
Rozpuszczalność w H_2O	2,96 $g \cdot 100cm^{-3}$; 25°C
Gęstość	0,46 $g \cdot cm^{-3}$ w 20 °C
Punkt izoelektryczny	5,76
Skręcalność właściwa w H_2O $[\alpha]_D$	-34,51
Toksyczność	LD_{50}>5,287 g/kg (szczur, podawane dootrzewnowo)

W 1934 roku norweski lekarz Følling opisał zaburzenia metaboliczne wywoływane przez ten aminokwas i nazywał je fenyloketonurią [48], która jest najczęściej występującym zaburzeniem katabolizmu aminokwasów. Do 1960 roku większość dzieci rodzących się z tą wadą genetyczną miało poważnie uszkodzony mózg. Jednak wprowadzenie diety ubogiej w fenyloalaninę w leczeniu fenyloketonurii przez Bickela [49] oraz opracowanie testu diagnostycznego (test Guthriego) w 1960 roku przez Guthriego [50], pozwalającego na masowe badania noworodków sprawiły, iż wczesna diagnoza choroby oraz wprowadzenie odpowiedniej diety pozwalają uniknąć poważnego upośledzenia mózgu u chorych na tę chorobę genetyczną. Fenyloketonuria występuje z częstotliwością od 1 : 4 000 do 1 : 200 000, w zależności od regionu na świecie. W Europie średnia wartość to jedno chore dziecko na 10 000 urodzeń [51]. Najczęściej choroba występuje w Turcji i Irlandii Północnej (1 : 4 000), ze względu wysoki stopień pokrewieństwa w populacji [52-53], najrzadziej zaś w Finlandii (1 : 100 000) [54]. W USA choroba występuje raz na 15 000 urodzeń, w Ameryce Łacińskiej zaś od 1 : 50 000 do 1 : 25 000; współczynnik ten jest z reguły wyższy w południowej części Ameryki Łacińskiej [55]. Stopień rozpowszechnienia fenyloketonurii jest najbardziej zróżnicowany w Azji i wynosi od 1 : 15 000 do 1 : 100 500 w różnych regionach Chin [56-57], 1 : 200 000 w Tajlandii [58] oraz 1 : 70 000 w Japonii [59].

W wyniku tej wrodzonej choroby genetycznej organizm nie posiada enzymu przekształcającego fenyloalaninę w tyrozynę, przez co poziom fenyloalaniny we krwi jest coraz wyższy, a ilość tyrozyny jest niewystarczająca dla prawidłowego funkcjonowania organizmu. Fenyloketonuria powoduje nieodwracalne uszkodzenie ośrodkowego układu nerwowego, powodując upośledzenie umysłowe i zaburzenia neurologiczne. Szybka diagnoza i leczenie restrykcyjną dietą ubogą w fenyloalaninę wprowadzone już w pierwszych dniach życia noworodka pozwala uzyskać prawidłowy rozwój dziecka, również umysłowy [60-61].

2.3. HISTYDYNA

L-Histydyna (kwas *α*-amino-*β*-(imidazolo-γ-ilo)propanowy), o wzorze strukturalnym przedstawionym na Rys. 15, została po raz pierwszy wyizolowana z kwaśnego hydrolizatu białka przez niemieckiego biochemika Kossela w 1896 roku. Struktura histydyny, która posiada pierścień imidazolowy, została objaśniona przez Pauly'ego w 1904 roku i potwierdzona poprzez syntezę chemiczną z diaminoacetonu przez Pymana w 1911 roku [36].

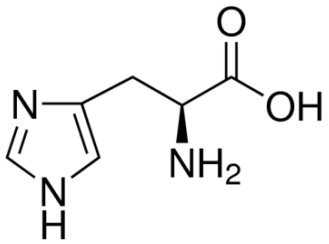

Rys. 15. Budowa przestrzenna *L*-histydyny

L-Histydyna jest kluczowym aminokwasem, który licznie występuje w hemoglobinie, jest niezbędny do produkcji zarówno białych, jak i czerwonych krwinek. Jest aminokwasem o szczególnie silnych właściwościach antyoksydacyjnych przez swoje wysokie powinowactwo do tlenu singletowego (szybkość reakcji histydyny z tlenem singletowym wynosi 10^8 mol·s^{-1}). Ponadto histydyna pomaga w usuwaniu metali ciężkich (miedź, nikiel, cynk, czy żelazo) z organizmu [62]. Histydyna stanowi także składnik budulcowy mioglobiny odpowiedzialnej za gromadzenie tlenu w tkance mięśniowej [63], uczestniczy w syntezie kwasów nukleinowych, a także jest prekursorem histaminy. Podstawowe właściwości fizykochemiczne histydyny zostały przedstawione w Tab. 3.

Tab. 3. Właściwości fizykochemiczne *L*-histydyny [21]**,** [36]**,** [64-65]

Wzór sumaryczny	$C_6H_9N_3O_2$
Masa molowa	155,15 g·mol^{-1}
Wygląd	Biały proszek krystaliczny
Rozpuszczalność w H_2O	4,19 g·100cm^{-3}; 25^{o}C
Gęstość	0,47 g·cm^{-3} w 20 ^{o}C
Punkt izoelektryczny	7,69
Skręcalność właściwa w H_2O $[\alpha]_D$	-38,53
Toksyczność	LD_{50} >15 g/kg (szczur, podawane doustnie)

W 1961 roku Ghadimi opisał zaburzenie przemiany materii przejawiające się podwyższonym poziomem histydyny we krwi oraz moczu chorego, nazywając tę chorobę histydynemią. Choroba ta łączy się z upośledzeniem umysłowym, a także z zaburzeniem mowy i słuchu [66], [36]. Przyczyną histydynemii jest niewystarczająca aktywność amoniakoliazy histydynowej w wątrobie, co zaburza przekształcanie histydyny w urokanian [15]. Ta wrodzona wada genetyczna występuje z częstotliwością od 1 : 8600 w Quebec (Kanada) do 1 : 180 000 w Nowym Jorku (USA) [67].

2.4. HYDROKSYPROLINA

4-Hydroksy-*L*-prolina (kwas (2*S*,4*R*)-4-hydroksypirolidyno-2-karboksylowy), o wzorze strukturalnym przedstawionym na Rys. 16, jest jednym z aminokwasów budujących białka. Została odkryta przez niemieckiego chemika Fischera w 1902 roku w hydrolizacie żelatyny. Racemiczna mieszanina hydroksyproliny została po raz pierwszy otrzymana na drodze syntezy chemicznej przez Leuchsa w 1905 roku z epichlorohydryny i soli sodowej estru malonowego.

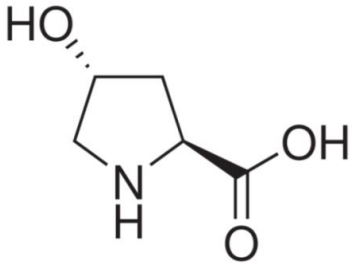

Rys. 16. Budowa przestrzenna *trans*-4-hydroxy-*L*-proliny

Hydroksyprolina jest bardzo istotna dla organizmów żywych ze względu na fakt, iż wchodzi ona w skład helisy kolagenu, która zawiera powtarzające się sekwencje aminokwasów Gly-*X*-*Y*, w której hydroksyprolina występuje na pozycji *Y* [68]. Kolagen jest podstawowym budulcem tkanki łącznej i ścięgien. Ponadto kolagen odpowiedzialny jest za elastyczność skóry, a jego zanik rozpoczyna procesy starzenia [69]. Hydroksyprolina jest również niezbędna w wielu procesach fizjologicznych, jest substratem podczas syntezy glicyny oraz glukozy [70]. Podstawowe właściwości fizykochemiczne hydroksyproliny zostały zebrane w Tab. 4.

Tab. 4. Właściwości fizykochemiczne 4-hydroksy-*L*-proliny [21], [36], [71]	
Wzór sumaryczny	$C_5H_9NO_3$
Masa molowa	131,13 $g \cdot mol^{-1}$
Wygląd	Bezbarwne kryształki
Rozpuszczalność w H_2O	36,1 $g \cdot 100\ cm^{-3}$; 25°C
Gęstość	Brak danych
Punkt izoelektryczny	5,83
Skręcalność właściwa w H_2O $[\alpha]_D$	-75,96
Toksyczność	Brak dostępnych danych

Znana jest również choroba metaboliczna związana z niedoborem oksydazy hydroksyproliny, która utlenia hydroksyprolinę do *L*-*α*-pirolino-3-hydroksy-5-karboksylanu – hiperhydroksyprolinemia. Początkowo została wykryta u dziecka z upośledzeniem umysłowym, jednak kolejni pacjenci byli zarówno fizycznie, jak i psychicznie zdrowi. Hiperhydroksyprolinemia charakteryzuje się znacznym podwyższeniem stężenia hydroksyproliny w osoczu oraz w moczu chorych, nie stwierdzono jednak nieprawidłowości w metabolizmie kolagenu, ani wpływu na katabolizm proliny, ponieważ zaatakowany enzym bierze udział jedynie w katabolizmie hydroksyproliny. Hiperhydroksyprolinemia jest niezwykle rzadką chorobą, która wydaje się być nieszkodliwa dla zdrowia [72], [36].

2.5. METIONINA

L-Metionina (kwas 2-amino-4-(metylotio)butanowy), o wzorze strukturalnym przedstawionym na Rys. 17, została odkryta w 1922 roku przez Muellera, jako substancja obecna w kwaśnym hydrolizacie kazeiny podczas badań nad czynnikiem wzrostu hemolitycznych paciorkowców [73]. Rok później strukturę metioniny, jako aminokwasu zawierającego siarkę, zaproponował Mueller, po opracowaniu sposobu otrzymywania dużych ilości tego aminokwasu z kazeiny [74]. W międzyczasie Muellerowi udało się również opracować sposoby otrzymywania metioniny z innych źródeł, w tym z albuminy, białek jaj, edestyny i wełny. Struktura chemiczna została ustalona na drodze syntezy chemicznej z *β*-metylotiolpropylo aldehydu przez Bargera i Coynea w 1928 roku [75].

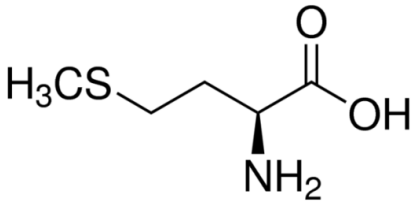

Rys. 17. Budowa przestrzenna *L*-metioniny

Metionina obok cysteiny jest jednym z dwóch aminokwasów białkowych, zawierających w swojej strukturze siarkę. Obficie występuje w kazeinie i białku jaj. W żywym organizmie metionina pełni ważne funkcje: wpływa na przemianę lipidową, jest niezbędna w syntezie choliny, kreatyny i adrenaliny, uczestniczy ponadto w procesie transmetylacji [76]. Metionina jest regulatorem układu mięśniowego i nerwowego, jest silnym antyoksydantem, działa detoksykacyjnie, reguluje pracę tarczycy, jest także potrzebna do biosyntezy cysteiny, karnityny oraz lecytyny [16]. Podstawowe właściwości fizykochemiczne metioniny zostały zebrane w Tab. 5.

Tab. 5. Właściwości fizykochemiczne *L*-metioniny [21]**,** [77-78]

Wzór sumaryczny	$C_5H_{11}NO_2S$
Masa molowa	149,21g·mol^{-1}
Wygląd	Białe ciało stałe
Rozpuszczalność w H_2O	5,06 g·100cm^{-3}; 25^{o}C
Gęstość	1,34 g·cm^{-3}
Punkt izoelektryczny	5,74
Skręcalność właściwa w H_2O $[\alpha]_D$	-9,99
Toksyczność	LD_{50}>36 g/kg (szczur, podawane doustnie)

Zaburzenia metabolizmu metioniny wywołują następujące choroby: homocystynurię, cystationurię oraz hipermetioninemię. Pierwsza z nich jest związana z zaburzeniem metabolizmu metioniny, spowodowanym niedoborem oraz niską aktywnością *β*-syntazy cystationinowej. Enzym ten katalizuje reakcję przekształcenia homocysteiny do cysteiny przy udziale pirydoksyny (witamina B_6), wskutek czego w osoczu gromadzi się *L*-homocysteina przy jednoczesnym niedoborze *L*-cysteiny, a także pojawia się wysoki poziom metioniny w moczu. Gromadząca się homocysteina oraz inne metabolity metioniny powodują uszkodzenia włókien kolagenu i elastyny. Pacjenci z homocystynurią cierpią na drgawki, opóźnienie umysłowe, choroby układu

krążenia, zaczerwienienie skóry, dyslokacje soczewki oraz stłuszczenie wątroby, jednak odpowiednio wczesne rozpoznanie choroby oraz rozpoczęcie leczenia pozwala uniknąć upośledzenia umysłowego [79]. Homocystynuria jest dość rzadką chorobą, występuje średnio jednokrotnie na 335 000 urodzeń na całym świecie; najczęściej choroba ta występuje w Katarze (1 : 3 000) [80], najrzadziej zaś w Japonii (1 : 900 000) [81].

Cystationuria spowodowana jest niedoborem enzymu *γ*-cystationazy i nie wykazuje charakterystycznych cech patologicznych. Charakteryzuje się zwiększonym poziomem cystationiny osoczowej w moczu. Cystationuria uważana jest za łagodną nieprawidłowość biochemiczną, występującą jednokrotnie na 14 000 urodzeń [82].

Hipermetioninemia natomiast to choroba wynikająca z nadmiaru metioniny we krwi, spowodowana nieprawidłowym metabolizmem tego aminokwasu (niedobór adenozylotransferazy metioniny). Choroba ta często nie daje żadnych objawów, jednak chorzy mogą wykazywać problemy z przyswajaniem wiedzy, umiejętnościami motorycznymi, ociężałością umysłową, ospałością, a także mogą mieć problemy z wątrobą [72]. Występowanie tej choroby szacuje się średnio na 1 : 100 000 zdrowych urodzeń [83].

2.6. PROLINA

L-Prolina (kwas pirolidyno-2-karboksylowy), jako jeden z nielicznych aminokwasów, została najpierw zsyntetyzowana na drodze chemicznej z malonianu *α,δ*-dibromopropylu w 1900 roku przez Willstättera [84], a dopiero rok później została odkryta jako składnik białka w przyrodzie przez Fischera [85]. Prolina o wzorze strukturalnym przedstawionym na Rys. 18 jest jednym z aminokwasów białkowych, które organizm może sam wytworzyć z argininy oraz kwasu glutaminowego.

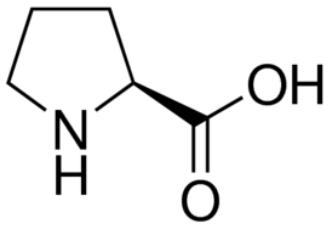

Rys. 18. Budowa przestrzenna *L*-proliny

Prolina spełnia wiele ważnych funkcji w organizmie człowieka, m.in. jest potrzebna do syntezy białek (w okresie wzrostu, podczas choroby, czy w trakcie gojenia się ran), stanowi podstawowy element kolagenu, niezbędnego do prawidłowej pracy stawów i ścięgien, a także odpowiedzialnego za elastyczność skóry. Bierze ponadto udział w reakcjach przeciwutleniających, a jej niedobór może prowadzić do obniżenia wydajności organizmu, niedoboru kolagenu, czy zaburzyć prawidłową budowę ścian tętnic [15], [22]. Podstawowe właściwości fizykochemiczne proliny zostały zebrane w Tab. 6.

Tab. 6. Właściwości fizykochemiczne *L*-proliny [21]**,** [86-87]

Wzór sumaryczny	$C_5H_9NO_2$
Masa molowa	115,13 $g \cdot mol^{-1}$
Wygląd	Biały proszek krystaliczny
Rozpuszczalność w H_2O	162,3 $g \cdot 100cm^{-3}$; 25°C
Gęstość	1,35 $g \cdot cm^{-3}$
Punkt izoelektryczny	6,3
Skręcalność właściwa w H_2O $[\alpha]_D$	-86,16
Toksyczność	LD_{50} > 5,110 g/kg (szczur, podawane doustnie)

Podczas metabolizmu prolina jest utleniana przez dehydrogenazę prolinową do 2-*Δ*'-pirolino-5-karboksylanu, który następnie przekształca się do semialdehydu glutaminowego, który z kolei jest utleniany przez dehydrogenazę zależną od NAD^+ lub $NADP^+$ do glukogennego glutaminianu [16]. Zaburzenia w metabolizmie zarówno na pierwszym, jak i na drugim etapie wywołują choroby genetyczne zwane hiperprolinemią typu I oraz II. Hiperprolinemia typu I jest spowodowana niedoborem dehydrogenazy prolinowej i przejawia się wzrostem stężenia proliny w osoczu oraz wydalaniam proliny, hydroksyproliny i glicyny z moczem. Hiperprolinrmia typu II spowodowana jest przez brak dehydrogenazy. Pacjęci z hiperprolidemią mają drgawki, opóźnienie umysłowe oraz choroby nerek [72]. Znaleziono również związek pomiędzy hiperprolidemią a schizofenią u ludzi [88].

2.7. SERYNA

L-Seryna (kwas α-amino-β-hydroksypropionowy), o wzorze strukturalnym przedstawionym na Rys. 19, została po raz pierwszy wydzielona z hydrolizatu białek jedwabiu przez Cramera w 1865 roku. Określił on również skład pierwiastkowy seryny, a ponadto stwierdził, iż jest ona podobna do alaniny [89]. Następnie w 1902 roku Fischer i Leuchs określili strukturę seryny na drodze syntezy chemicznej z aldehydu glikolowego i cyjanohydryny [90].

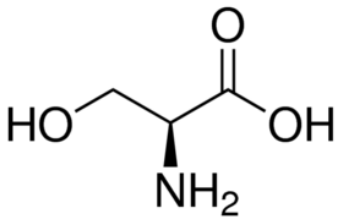

Rys. 19. Budowa przestrzenna *L*-seryny

Seryna w organizmie człowieka wpływa na rozwój układu nerwowego (zwłaszcza mózgu). Niedobory seryny występują u ludzi cierpiących na niektóre choroby psychiczne. Jest ważna dla metabolizmu tłuszczy i kwasów tłuszczowych, uczestniczy w metabolizmie komórkowym, w produkcji immunoglobulin i przeciwciał, a także wraz z glicyną uczestniczy w syntezie substancji purynowych i pirymidynowych. Stanowi także składnik osłonki mielinowej nerwów i łagodzi ból [72], [91]. Właściwości fizykochemiczne seryny zostały przedstawione w Tab.7.

Tab. 7. Właściwości fizykochemiczne *L*-seryny [36]**,** [92-93]

Wzór sumaryczny	$C_3H_7NO_3$
Masa molowa	105,09 $g \cdot mol^{-1}$
Wygląd	Biały proszek
Rozpuszczalność w H_2O	41,3 $g \cdot 100cm^{-3}$; 25°C
Gęstość	1,6 $g \cdot cm^{-3}$ w 22 °C
Punkt izoelektryczny	5,68
Skręcalność właściwa w H_2O $[\alpha]_D$	-7,5
Toksyczność	LD_{50} > 14,000 g/kg (szczur, podawane doustnie)

Seryna jest aminokwasem endogennym, organizm jest w stanie sam go zsyntezować z 3-fosfoglicerynianu. Reakcja przebiega w trzech etapach. W pierwszym z nich następuje utlenienie 3-fosfoglicerynianu do 3-fosfohydroksypirogronianu (w obecności dehydrogenazy fosfoglicerynianowej), następnie ulega on transmitancji do 3-fosfoseryny, która ulega hydrolizie dając serynę, która również może zostać otrzymana w odwrotnej reakcji powstawania glicyny, katalizowanej przez hydroksymetylotransferazę serynową [22].

Niedobór dehydrogenazy fosfoglicerynianowej jest ciężką, choć potencjalnie uleczalną chorobą metabolizmu u ludzi. Chorzy mają niskie stężenie seryny oraz glicyny w osoczu i płynie mózgowo-rdzeniowym. Objawami choroby jest spowolnienie psychoruchowe, małogłowie, nadciśnienie, opóźnienie wzrostu, a także epilepsja. W złagodzeniu choroby pomaga odpowiednia dieta bogata w serynę, która wystarcza do uzyskania odpowiedniego rozwoju psychicznego i fizycznego [36].

2.8. TREONINA

L-Treonina (kwas *α*-amino-*β*-hydroksymasłowy), o wzorze strukturalnym przedstawionym na Rys. 20, została odkryta, jako ostatni aminokwas białkowy przez Schryvera i Bustona w 1925 roku z białek owsa [36]. Dziesięć lat później Rose wraz ze współpracownikami wyizolowali treoninę z hydrolizatu kazeiny, ustalili także jej strukturę na drodze syntezy chemicznej [94].

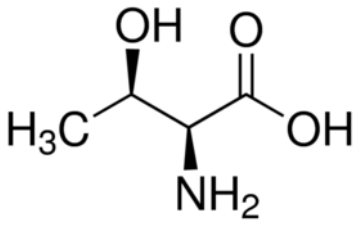

Rys. 20. Budowa przestrzenna *L*-treoniny

L-Treonina jest niezbędnym aminokwasem dla prawidłowego funkcjonowania zarówno układu nerwowego, jak i wspomaga działanie układu odpornościowego i pokarmowego. Ponadto reguluje pracę wątroby i serca. Uczestniczy w produkcji przeciwciał, kolagenu i elastyny, jest także niezbędna dla prawidłowej budowy szkliwa zębów, pracy tarczycy, czy metabolizmu tłuszczów w wątrobie [95]. Podstawowe właściwości fizykochemiczne *L*-treoniny zostały zebrane w Tab. 8.

Tab. 8. Właściwości fizykochemiczne *L*-treoniny [21]**,** [36]**,** [96-97]	
Wzór sumaryczny	$C_4H_9NO_3$
Masa molowa	119,12 $g \cdot mol^{-1}$
Wygląd	bezbarwne ciało stałe
Rozpuszczalność w H_2O	9,54 $g \cdot 100cm^{-3}$; 25°C
Gęstość	1,45 $g \cdot cm^{-3}$
Punkt izoelektryczny	5,64
Skręcalność właściwa w H_2O $[\alpha]_D$	-28,46
Toksyczność	LD_{50} > 3,098 g/kg (szczur, śródotrzewnowo)

Treonina razem z izoleucyną, waliną i metioniną wpływają na dwie choroby metaboliczne: kwasicę propionową (wywołaną przez defekt enzymu karboksylazy propionylo-koenzymu *A*) oraz kwasicę metylomalonową (spowodowaną przez niedobór enzymu mutazy metylomalonylo-koenzymu *A*). Po spożyciu białka zawierającego wymienione aminokwasy u chorych występuje ciężka kwasica oraz objawy zatrucia. Objawy obu kwasic pojawiają się już kilka dni po urodzeniu dziecka, są to wymioty oraz brak apetytu, a także chorzy nie przybierają na wadze. W okresach zaostrzeń choroby pojawia się wiotkość mięśni, a także senność przechodząca w śpiączkę, która może powodować zgon. Leczenie obu tych zaburzeń metabolizmu ogranicza się do zwalczania objawów kwasicy i nawadniania, a także do stosowania diety ubogiej w treoninę, izoleucynę, walinę oraz metioninę [36], [98-99].

3. REAKCJE OSCYLACYJNE

Reakcje oscylacyjne są niezwykłymi procesami chemicznymi, które na pierwszy rzut oka wydają się chaotyczne, jednak cechują się uporządkowaniem. Procesy te początkowo nie były akceptowane przez środowisko naukowe przez pozorną sprzeczność z II zasadą termodynamiki i wciąż niektórzy chemicy patrzą na nie z niedowierzaniem. Jednak reakcje oscylacyjne są wszechobecne w życiu codziennym. Począwszy od kamieni półszlachetnych takich, jak np. malachit, agat czy lazuryt, powstałych w wyniku zajścia reakcji oscylacyjnych (pierścienie Lieseganga) [100], poprzez procesy zachodzące w żywych organizmach takie, jak skurcze mięśnia sercowego, okresowe zmiany potencjałów na błonie komórek nerwowych, czy powstawanie kamieni nerkowych, które również kierowane są przez procesy oscylacyjne [101], a kończąc na charakterystycznym ubarwieniu w świecie zwierząt, które jest wynikiem zachodzących reakcji oscylacyjnych. Jako przykłady mogą posłużyć rozmieszczenie plamek żyrafy, prążków zebry czy tygrysa [102], a także ubarwienie ryb tropikalnych [103-104].

3.1. WSTĘP DO REAKCJI OSCYLACYJNYCH

Reakcje oscylacyjne są reakcjami wprowadzającymi swoisty chaos w świat ogólnie pojmowanej chemii. Już podczas pierwszego spotkania z chemią można dowiedzieć się, że w miarę przebiegu reakcji maleje stężenie substratów przy jednoczesnym wzroście stężenia produktów, a proces reakcji można opisać przy pomocy funkcji monotonicznej.

Reakcji oscylacyjnych nie da się opisać funkcją monotoniczną. Stężenia zarówno substratów, jak i produktów zmieniają się w sposób niemonotoniczny. Podczas przebiegu reakcji obserwuje się spadek, a następnie wzrost stężenia zarówno substratów, produktów jak i produktów przejściowych reakcji, które z reguły towarzyszą takim procesom [101]. Rys. 21 przedstawia zachowanie składników klasycznej reakcji chemicznej (Rys. 21(a)) oraz periodyczne zmiany stężeń produktów przejściowych *X* oraz *Y* podczas przebiegu reakcji oscylacyjnej (Rys. 21(b)).

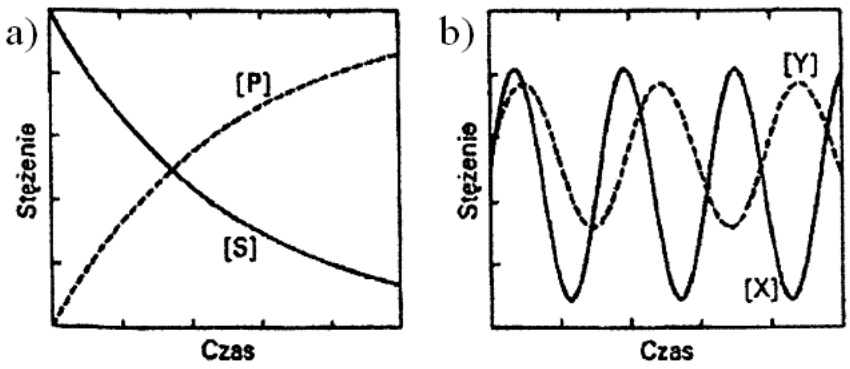

Rys. 21. Porównanie czasowych zmian (a) stężenia substratów [*S*] oraz produktów [*P*] w klasycznej reakcji chemicznej oraz (b) produktów przejściowych [*X*],[*Y*] w reakcji oscylacyjnej [101]

Aby reakcja wykazywała charakter oscylacyjny muszą zostać spełnione następujące warunki: układ musi wykazywać silne niezrównoważenie pod względem kinetycznym, niezbędna jest obecność równań wykazujących silną nieliniowość (np. równanie kinetyczne co najmniej drugiego lub wyższych rzędów), a także obecność sprzężeń zwrotnych dodatnich i ujemnych o naprzemiennym działaniu (np. autokataliza oraz autoinhibicja) [101].

3.2. MODELE TEORETYCZNE

Kwestia modelowania przebiegu reakcji oscylacyjnych jest skomplikowana, modele bywają bardzo złożone, a procesy, które opisują często nie są do końca poznane. Trudność, jaką stanowi stworzenie modelu, który będzie dokładnie opisywał przebieg reakcji oscylacyjnej doskonale pokazuje najbardziej znana reakcja Biełousowa-Żabotyńskiego, która została po raz pierwszy opisana w latach 50’ ubiegłego wieku [105-106]. Powstało wiele modeli teoretycznych opisujących tę reakcję, jednak najbardziej znanym jest model stworzony przez Fielda, Korosa oraz Noyesa w 1972 roku i nazwany od nazwisk autorów modelem FKN [107]. Mimo, iż istnieją inne modele opisujące przebieg tej reakcji, to żaden z nich nie wyjaśnia do końca jej niezwykle skomplikowanego przebiegu. Mimo tych trudności warto odnaleźć pewne ważne etapy stanowiące źródło zachowania oscylacyjnego, aby w przyszłości z większą łatwością doszukiwać się procesów oscylacyjnych w świecie procesów rzeczywistych. Modelowanie rozpoczyna się od napisania układu równań różniczkowych opisujących zmiany stężeń reagentów występujących w określonej

reakcji. Powstałe równania mogą być zwyczajne (jedyną zmienną niezależną jest czas) lub cząstkowe (do zmiennej niezależnej, jaką jest czas dochodzą zmienne przestrzenne). Przebieg stężeń reagentów w funkcji zmiennych niezależnych powinien przynajmniej w pewnym zakresie wykazywać charakter oscylacyjny, np. jedna z szybkości reakcji powinna mieć charakter nieliniowy [101].

3.2.1. MECHANIZM REAKCJI OSCYLACYJNYCH AMINOKWASÓW

Wyniki wcześniejszych badań prowadzonych na Uniwersytecie Śląskim w Katowicach wykazały, iż zarówno pojedyncze niskocząsteczkowe związki chiralne należące do grup aminokwasów [108-110] hydroksykwasów [111-114] czy leków z grupy profenów [115-118], jak i ich mieszaniny ulegają samorzutnym reakcjom oscylacyjnym. Mechanizm inwersji chiralnej w środowisku wodnym z zaznaczonymi formami niechiralnymi na przykładzie cysteiny (z *L*-Cys do *D*-Cys) przedstawia się następująco:

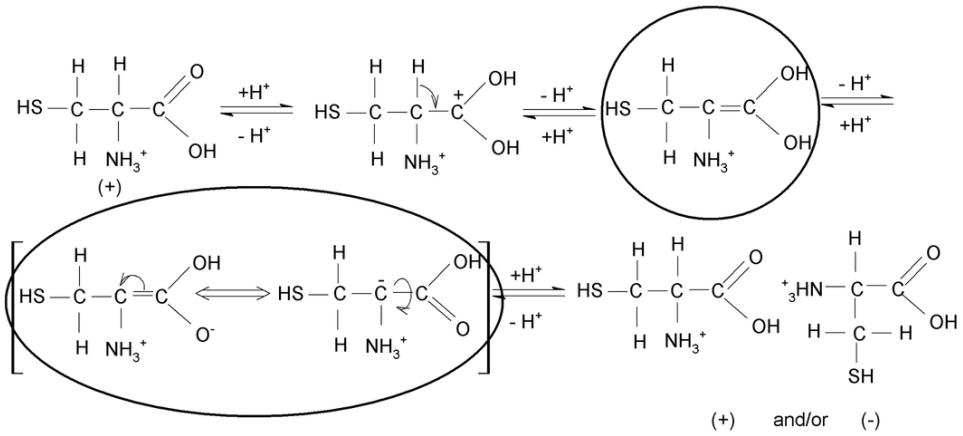

Schemat 1. Mechanizm inwersji chiralnej w środowisku wodnym z zaznaczonymi formami niechiralnymi na przykładzie cysteiny

Mechanizm samorzutnej peptyzacji α-aminokwasów w środowisku wodnym przedstawia się następująco:

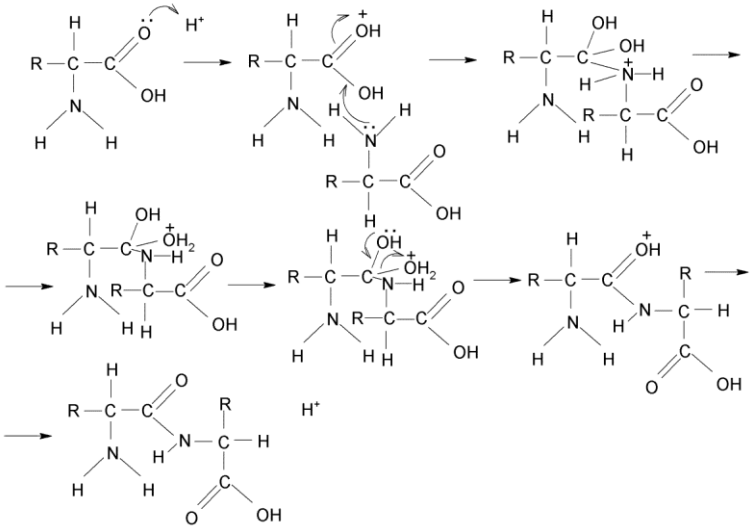

Schemat 2. Mechanizm samorzutnej peptyzacji α-aminokwasów w środowisku wodnym

Mechanizm peptyzacji w przypadku par aminokwasów białkowych jest analogiczny do powyższego i przedstawia się następująco (na przykładzie pary aminokwasów cysteiny oraz proliny):

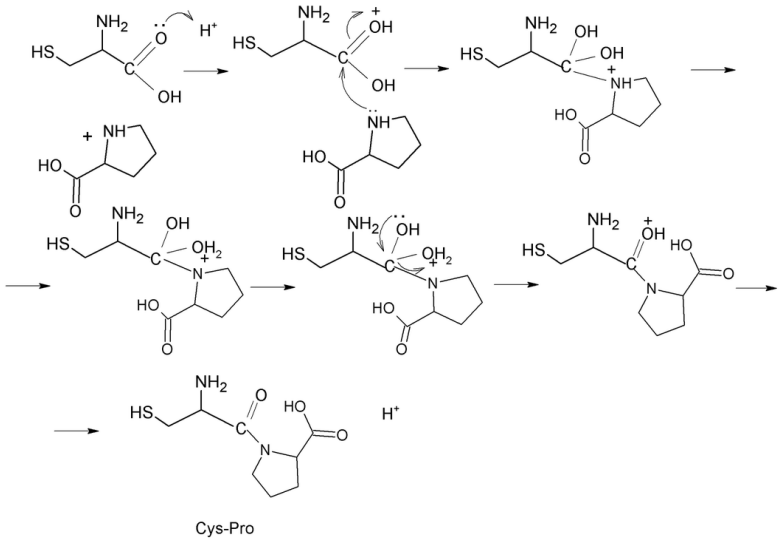

Schemat 3. Mechanizm peptyzacji zachodzący w układzie dwuskładnikowym na przykładzie pary aminokwasów cysteiny oraz proliny

Ponadto na podstawie wcześniejszych badań wykazano, że oscylacyjna inwersja chiralna przebiega równolegle z oscylacyjną peptyzacją. Ogólny schemat obu tych równolegle przebiegających procesów (na przykładzie cysteiny) przedstawia się następująco:

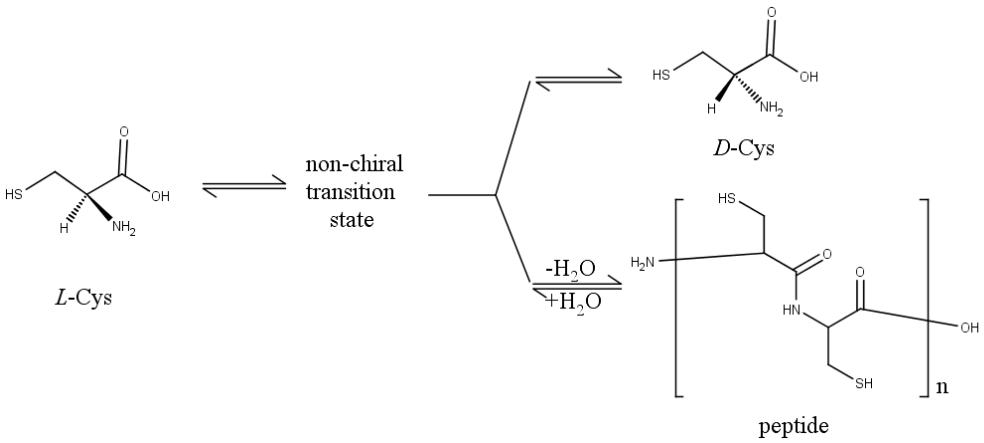

Schemat 4. Schemat równoległego procesu inwersji chiralnej i peptyzacji w układzie jednoskładnikowym na przykładzie cysteiny

W przypadku badań prowadzonych dla mieszanin aminokwasów do układu wprowadzano dwa aminokwasy, dlatego też poza homopeptydami zarówno jednego jak i drugiego aminokwasu mogą tworzyć się produkty mieszane. Ogólny schemat obu tych równolegle przebiegających procesów (na przykładzie pary aminokwasów cysteiny oraz proliny) przedstawia się następująco:

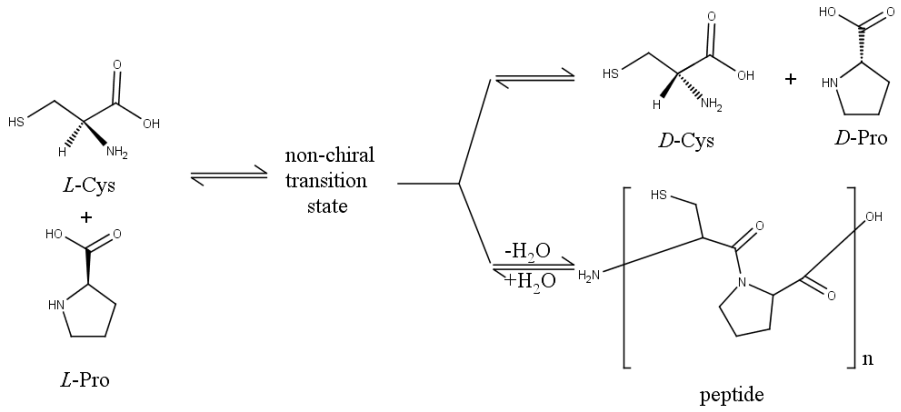

Schemat 5. Schemat równoległego procesu inwersji chiralnej i peptyzacji w układzie dwuskładnikowym na przykładzie pary aminokwasów cysteiny i proliny

3.2.2. MODEL PRZEBIEGU REAKCJI OSCYLACYJNEJ PEPTYZACJI AMINOKWASÓW W UKŁADZIE DWUSKŁADNIKOWYM

Model ten uwzględnia trzy indywidua: prekursor *P* (np. aminokwas), krótki oligomer *E* wywodzący się z prekursora (np. peptyd), agregat (prawdopodobnie micela *M*), który powstaje z kilku molekuł *E*. W modelu tym założono, że micela może kształtować się w dwojaki sposób – niekatalizowany (micele tworzą się z oligomerów) oraz katalizowany (micele służą, jako szablony do powstawania większych micel).

Reakcje elementarne przebiegają w następujący sposób:

Oscylator 1:

$n_{11}P_1 \rightarrow E_1$	$v = k_{01}P_1$	*(oligomeryzacja)*
$n_{21}E_1 \rightarrow M_1$	$v = k_{u1}E_1$	*(niekatalizowana agregacja)*
$2M_1 + n_{21}E_1 \rightarrow 3M_1$	$v = k_{a1}M_1^2E_1$	*(katalizowana agregacja)*
$M_1 \rightarrow$ produkty	$v = k_{b1}M_1$	*(rozkład)*

Oscylator 2:

$n_{12}P_2 \rightarrow E_2$	$v = k_{02}P$	*(oligomeryzacja)*
$n_{22}E_2 \rightarrow M_2$	$v = k_{u2}E_2$	*(niekatalizowana agregacja)*
$2M_2 + n_{22}E_2 \rightarrow 3M_2$	$v = k_{a2}M_2^2E_2$	*(katalizowana agregacja)*
$M_2 \rightarrow$ produkty	$v = k_{b2}M_2$	*(rozkład)*

Rys. 22 przedstawia niemonotoniczne zmiany stężeń obu oscylatorów w funkcji czasu. Każdy z wykresów jest charakterystyczny dla jednego z czterech możliwych scenariuszy przebiegu procesu kondensacji.

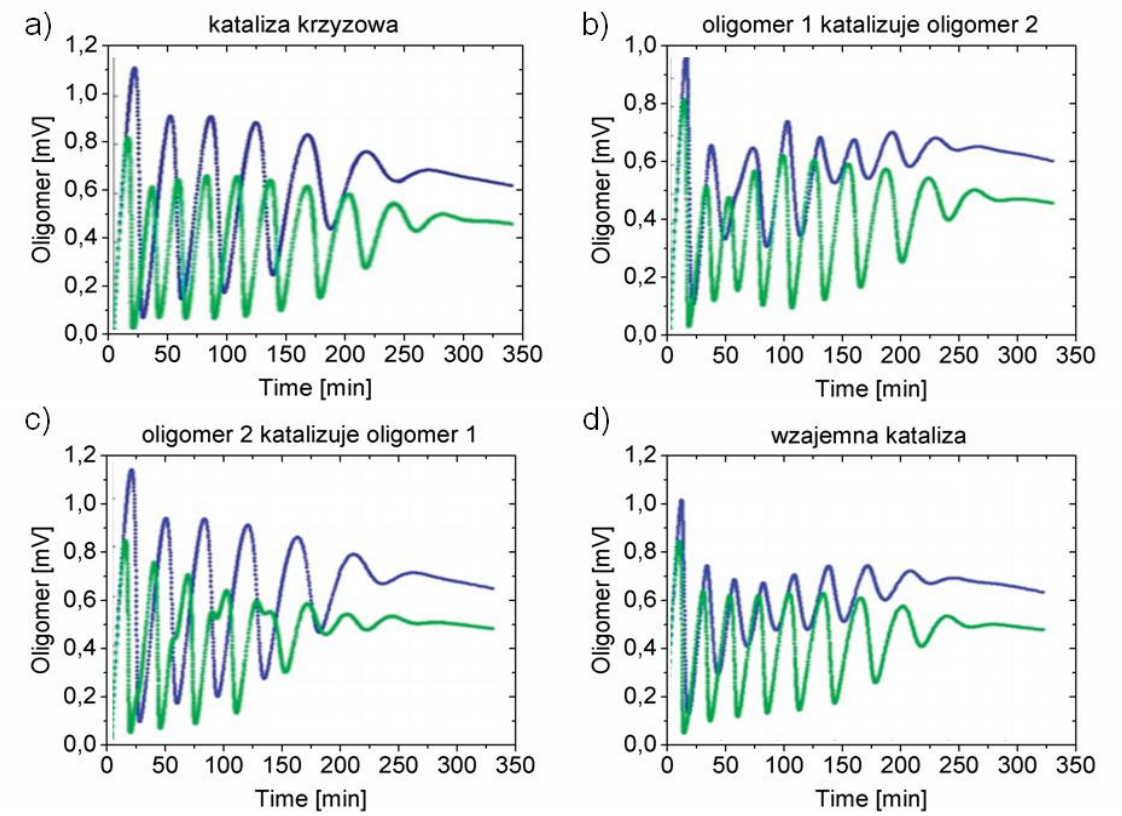

Rys. 22. Zależność sygnału analitycznego oscylatorów (kolor niebieski – oscylacje oligomeru pierwszego; kolor zielony – oscylacje oligomeru drugiego) w funkcji czasu. a) kataliza krzyżowa; b) oligomer 1 katalizuje oligomer; c) oligomer 2 katalizuje oligomer 1; d) wzajemna kataliza [119]

Wykresy przedstawione na Rys. 22 pokazują cztery możliwe zachowania dwóch oscylatorów. Rys. 22(a) przedstawia sytuację, w której oba oscylatory oscylują niezależnie (drugi oligomer jest szybszy (28s) od oligomeru pierwszego (38s)), jednak maksima ich stężeń są silnie skorelowane. Kolejne dwa scenariusze przedstawione na Rys. 22(b)-(c) pokazują sytuację, w której pierwszy oligomer katalizuje oligomer drugi i odwrotnie. Oscylatory te nie oscylują synchronicznie, choć można zaobserwować pewną zależność pomiędzy nimi. W przypadku drugim w początkowej fazie oscylatory drgają synchronicznie, by w końcowym etapie procesu wypaść z synchronizacji. Ostatni wykres dotyczy wzajemnej katalizy (Rys. 22(d)) i zgodnie z nim każdy z oligomerów katalizuje zarówno siebie, jak i drugi oscylator, przy czym okres oscylacji jest tutaj taki, jak dla szybszego oligomeru, podczas gdy oligomer wolniejszy dopasowuje się do zachowania swojego szybszego partnera [119].

4. SAMOORGANIZACJA PEPTYDÓW

Samoorganizację (*ang. self-assembly*) można zdefiniować, jako samorzutne łączenie się pojedynczych elementów w uporządkowaną strukturę, bez ingerencji człowieka. Typowe nanostruktury powstałe w wyniku samoorganizacji zawierają wiązania wodorowe, jonowe, hydrofobowe oraz van dar Waalsa, które nadają im trwałość [120]. Struktury otrzymane w wyniku samoorganizacji mogą przypominać kształt nanorur [121], nanowłókien [122], nanodysków, nanowstążek czy nanosfer [123]. Zjawisko samoorganizacji występuje naturalnie w przyrodzie, np. podczas tworzenia się podwójnej helisy DNA, czy podczas tworzenia się błon komórkowych.

Pojęcie nanorurek czy nanosfer peptydowych znane jest już od początku lat 90' ubiegłego stulecia [1-3], jednak popularność zdobyły dopiero z początkiem XXI w. Wśród struktur samoorganizujących się w nano- oraz mikrostruktury peptydowe są najbardziej popularnymi ze względu na fakt, iż peptydy można w łatwy sposób zsyntezować przy zastosowaniu metod w fazie stałej, co pozwala na specyficzne modyfikacje w sekwencji aminokwasów na poziomie molekularnym. Funkcjonalizacja peptydów jest łatwa do przeprowadzenia, a struktury supramolekularne mogą zostać zaprojektowane na pomocą inżynierii molekularnej [124]. Ponadto peptydy są w pełni biokompatybilne z ludzkim ciałem, co wpływa na szerokie spektrum potencjalnych zastosowań.

4.1. SPOSOBY OTRZYMYWANIA NANOSTRUKTUR PEPTYDOWYCH

Pierwsze doniesienia literaturowe na temat nanostruktur peptydowych pojawiły się w 1993 roku, kiedy to Ghadiri wraz z współautorami opublikowali prace, w których zaprezentowali cykliczne nanorurki peptydowe oraz ich potencjalne zastosowanie. Nanorurki te zbudowane są z cyklicznych peptydów złożonych z *D*- oraz *L*-aminokwasów, które są zdolne do samoorganizacji, w wyniku której układają się jedne na drugich tworząc nanorurki o pożądanej średnicy. Peptydy można również funkcjonalizować np. pierścieniami aromatycznymi zdolnymi do przenoszenia ładunku, co umożliwia zastosowanie takich struktur w elektronice molekularnej [1-2]. Schemat samoorganizacji peptydów został przedstawiony na Rys. 23.

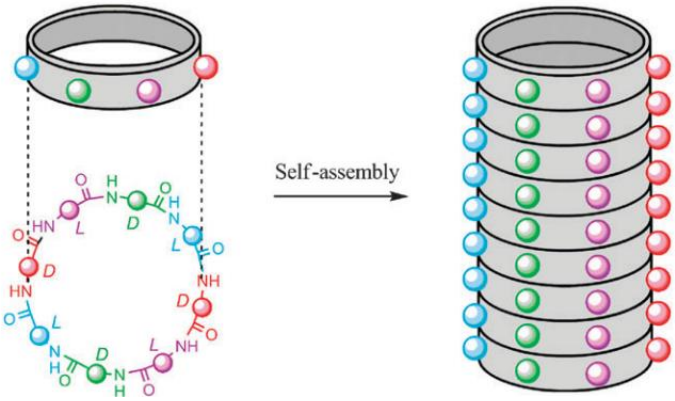

Rys. 23. Schemat samoorganizacji nanorurek peptydowych z cyklicznych peptydów zawierających *D*- oraz *L*-aminokwasy, po raz pierwszy opracowany przez Ghadiria wraz z współautorami [125]

Kolejnym podejściem do projektowania nanostruktur peptydowych jest zasada uzupełniających się ładunków, polegająca na projektowaniu peptydów w taki sposób, aby samoorganizowały się pod względem oddziaływań elektrostatycznych pomiędzy dodatnio i ujemnie naładowanymi resztami aminokwasowymi w peptydach. Po raz pierwszy taką metodę samoorganizacji peptydów zaproponował Zhang wraz ze współautorami w 1993 roku [126]. Metoda ta polega na projektowaniu łańcuchów peptydowych, zawierających mniej więcej po 50% peptydów naładowanych dodatnio (lizyna oraz arginina) oraz ujemnie (kwas glutaminowy oraz kwas asparaginowy) [127]. Peptydy te w roztworach wodnych szybko ulegają samoorganizacji tworząc nanowłókna, które w wyniku dalszych procesów mogą tworzyć hydrożele. Żele te z powodzeniem są stosowane w inżynierii tkankowej, czy podczas regeneracji uszkodzonych tkanek. Schemat samoorganizacji peptydów oparty na zasadzie uzupełniających się ładunków został przedstawiony na Rys. 24.

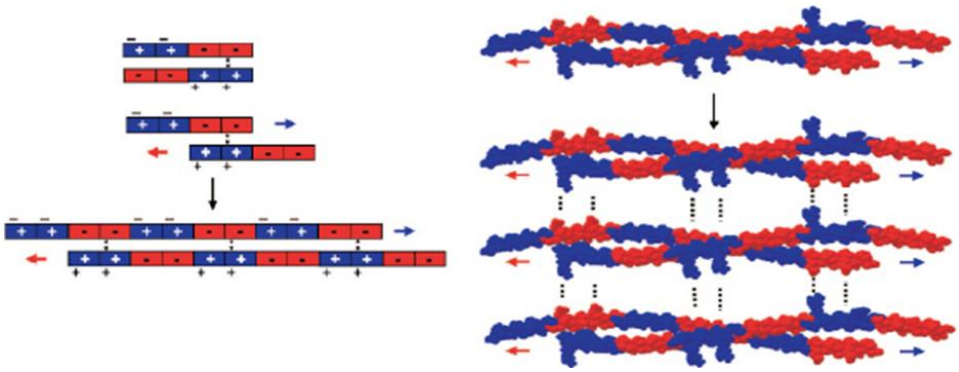

Rys. 24. Schemat samoorganizacji peptydów oparty na zasadzie uzupełniających się ładunków. Konstrukcja bloków peptydowych o odmiennych ładunkach pozwala na efektywną samoorganizację monomerów peptydowych do dobrze uporządkowanych nanowłókien, a nawet do hydrożeli peptydowych [128].

Inne podejście do projektowania nanostruktur peptydowych wzoruje się na zachowaniu środków powierzchniowo czynnych. Bazując na budowie typowego surfaktantu (hydrofilowa głowa i hydrofobowy ogon) projektuje się peptydy, które mają naśladować ich budowę. Typowy peptyd naśladujący surfaktant składa się z dwóch części: część hydrofobowa składa się z kilku aminokwasów hydrofobowych, takich jak glicyna, alanina, walina, leucyna i izoleucyna o różnych stopniach hydrofobowości. Modyfikując skład aminokwasów w łańcuchu można kontrolować całkowitą hydrofobowość peptydu. Część druga to hydrofilowa głowa złożona z jednego lub dwóch aminokwasów hydrofilowych, takich, jak arginina, lizyna, czy histydyna (dodatnio naładowana głowa) lub kwas asparaginowy czy kwas glutaminowy (ujemnie naładowana głowa). Odpowiednio dobierając peptydy wchodzące w cześć hydrofilową peptydu można projektować dodatnio lub ujemnie naładowane peptydy na wzór surfaktantów [129].

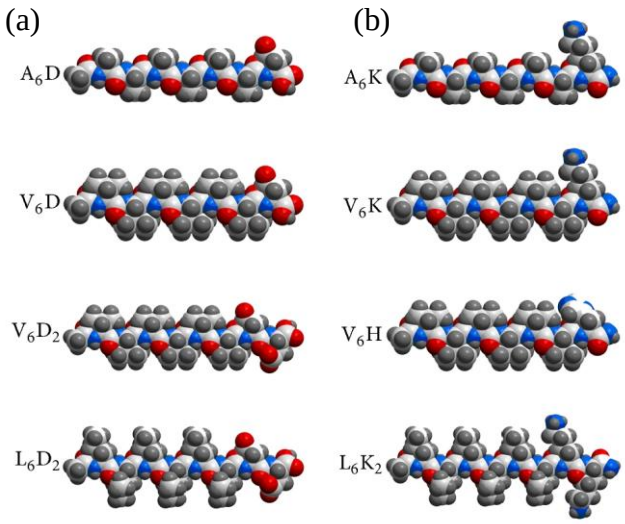

Rys. 25. Modele cząsteczkowe kilku typowych cząsteczek peptydów na wzór surfaktantów; (a) ujemnie i (b) dodatnio naładowane peptydy; A – alanina, D – kwas asparaginowy, V – walina, L – leucyna, K – lizyna, H – histydyna; szary – atom wodoru, czerwony – atom tlenu, niebieski – atom azotu [129]

Zasada samoorganizacji jest analogiczna do tej, jaką obserwujemy w zachowaniu się środków powierzchniowo czynnych. Peptydy mogą układać się ogon do ogona tworząc dwuwarstwowe rurki (Rys. 26(a)), mogą także tworzyć micele układając się ogonami do środka, a głowami na zewnątrz (Rys. 26(b)). Ostatnią możliwością jest tworzenie warstw peptydowych na powierzchni (Rys. 26(c)).

W zależności od zaprojektowanego peptydu można otrzymać różne kształty nanostruktur w procesie samoorganizacji, co pokazuje wielkie spektrum możliwości podczas projektowania takich materiałów w zależności od potencjalnego zastosowania.

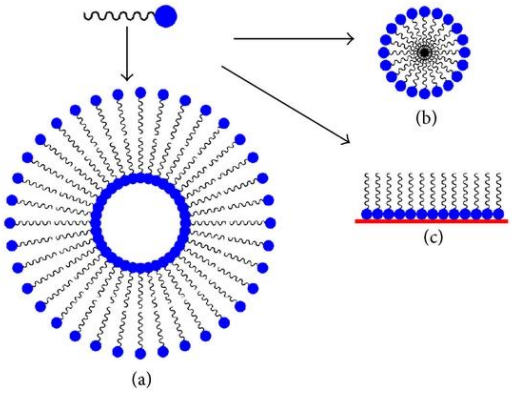

Rys. 26. Schematyczne modele nanocząstek otrzymanych w wyniku samoorganizacji peptydów projektowanych na podobieństwo surfaktantów (a) dwuwarstwowa rura, (b) micela, (c) pojedyncza warstwa na powierzchni [129]

Następne podejście do projektowania nanostruktur peptydowych jest wzorowane na naturalnym procesie samoorganizującego się białka w uporządkowane nanostruktury *β*-amyloidu. Występowanie włókien amyloidowych jest związane z wieloma chorobami, w tym m. in. z chorobą Alzheimera [130-131], chorobą Parkinsona [132], [133], czy cukrzycą typu II [134]. Niezależnie od badań nad wpływem chorobotwórczym włókien amyloidowych, prowadzone są badania nad syntetycznymi peptydami zdolnymi do samoorganizacji we włókna amyloidowe. Zazwyczaj włókna amyloidowe tworzone są przez polipeptydy zbudowane z 30-40 reszt aminokwasowych, ale mogą być tworzone także przez większe białka. Podczas badań wykazano, że również krótsze peptydy (tetra- czy heksapeptydy) posiadają zdolność do samoorganizacji w typowe włókna amyloidowe. Stwierdzono ponadto, że heksapeptyd Asn-Phe-Gly-Ala-Ile-Leu (asparagina-fenyloalanina-glicyna-alanina-izoleucyna-leucyna) tworzy włókna amyloidowe in vitro, natomiast pentapeptyd pozbawiony asparaginy tworzy włókniste struktury, lecz o innej budowie [135]. Na podstawie dalszych badań [136] stwierdzono, że zamiana fenyloalaniny na alaninę w strukturze peptydu powoduje utratę zdolności do tworzenia włókien amyloidowych [137-138], co sugeruje, że obecność aromatycznych aminokwasów w krótkich peptydach wpływa na zdolność samoorganizacji peptydów do włókien amyloidowych. Prowadząc dalsze badania odkrywano kolejne, coraz mniejsze peptydy amyloidogenne,

takie, jak pentapeptyd Asn-Phe-Leu-Val-His (asparagina-fenyloalanina-leucyna-walina-histydyna), będący fragmentem HIAPP (*ang. Human Islet Amyloid Polypeptide*), oraz Asn-Phe-Gly-Ser-Val-Gln (asparagina-fenyloalanina-glicyna-seryna-walina-glutamina) będący fragmentem peptydu aortowego [139]. Również skrócony tetrapeptyd Asp-Phe-Asn-Lys (asparagina-fenyloalanina-kwas asparaginowy-lizyna) tworzy włókna amyloidowe, jednak ich struktura jest mniej uporządkowana. Poszukiwanie najmniejszego peptydu posiadającego zdolność do samoorganizacji doprowadziło do wniosku, iż dipeptyd fenyloalaniny tworzy nanorurki, co otworzyło nową klasę peptydów ulegających samoorganizacji, tzw. nanostruktury aromatyczne [140].

Ostatnia z omawianych klas nanostruktur opiera się na wykorzystywaniu krótkich peptydów aromatycznych do tworzenia uporządkowanych nanostruktur. Difenyloalanina (FF) jest najszerzej przebadanym dipeptydem z tej klasy związków. Utworzone nanorurki FF są bardzo sztywne, trwałe termicznie oraz stabilne w rozpuszczalnikach organicznych [141]. Tworzą się samorzutnie przez rozpuszczenie liofilizowanej formy peptydów w 1,1,1,3,3,3-heksafluoro-2-propanolu oraz rozcieńczenie tak przygotowanych roztworów w wodzie redestylowanej do żądanego stężenia [142]. Inną metodą otrzymywania nanostruktur peptydowych jest rozpuszczenie liofilizowanego peptydu w ultraczystej wodzie podgrzanej do 65^{o}C, termostatowanie roztworu przez 30 minut w zadanej temperaturze, a następnie stopniowe ochładzanie roztworu do temperatury pokojowej [143]. Wzór strukturalny oraz typowe zdjęcie mikroskopowe nanorurki fenyloalaniny zostały przedstawione na Rys. 27.

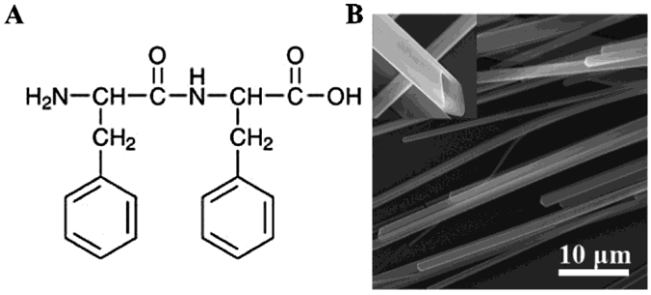

Rys. 27. (a) Wzór strukturalny dipeptydu fenyloalaniny, (b) mikrografia przedstawiająca nanorurki fenyloalaniny wykonana skaningowym mikroskopem elektronowym [144]

Liczne badania prowadzone nad samoorganizacją dipeptydu fenyloalaniny wykazały, że peptyd FF może również samoorganizować się do innych nanostruktur. W zależności od warunków doświadczalnych mogą się tworzyć nanopęcherze, nanodruty [145], nanowłókna [146-147], naszyjniki [148-149], mikropręty [150-151], czy hydrożele [152-153].

Kolejnym krótkim dipeptydem aromatycznym ulegającym samoorganizacji do nanostruktur peptydowych jest difenyloglicyna, która różni się od fenyloalaniny jedynie brakiem jednej grupy $–CH_2$ w łańcuchu węglowym, a w wyniku samoorganizacji tworzy nanosfery peptydowe. Podobnie drobne zmiany wprowadzane do peptydu FF, jak na przykład dołączenie cysteiny do łańcucha peptydowego, powoduje zmianę otrzymanej struktury na nanosferę [154]. Schematyczny model przedstawiający proces samoorganizacji peptydów difenyloalaniny do nanorurek oraz difenyloglicyny do nanosfer peptydowych przedstawiono na Rys. 28.

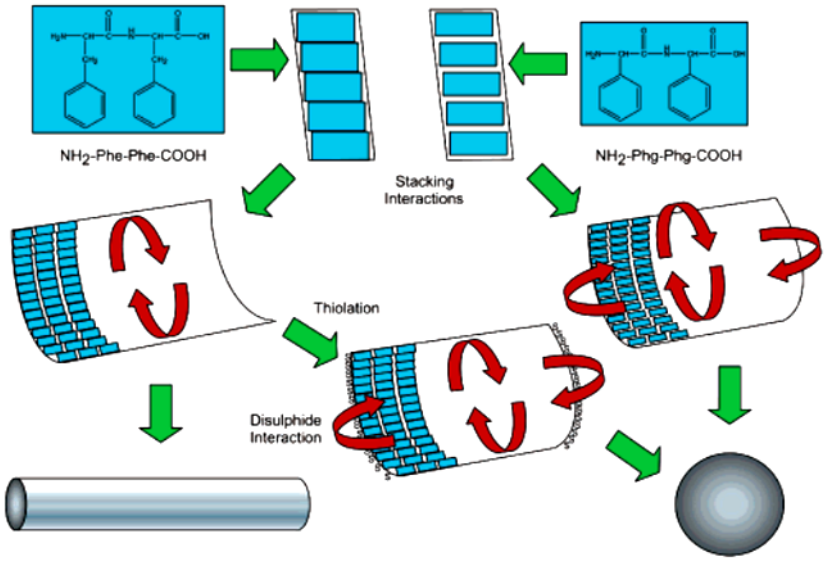

Rys. 28. Schematyczny model przedstawiający proces samoorganizacji peptydów difenyloalaniny do nanorurek oraz difenyloglicyny do nanosfer peptydowych. Interakcje pomiędzy ugrupowaniami aromatycznymi peptydów sugerują układanie się peptydów w pofałdowane arkusze stabilizowane wiązaniami wodorowymi, a następnie ich zwijanie wzdłuż jednej z osi tworząc rurkę. Tworzenie struktur sferycznych może wynikać z zamknięcia arkusza wzdłuż dwóch osi, podobnie wprowadzenie grupy tiolowej pochodzącej od cysteiny powoduje zamykanie arkusza również na drugiej osi [154]

4.2. PRZYKŁADOWE ZASTOSOWANIA NANOSTRUKTUR PEPTYDOWYCH

Możliwości zastosowań nanomateriałów peptydowych są bardzo rozległe i obejmują m. in. inżynierię tkankową, biosensory, nośniki leków, leki przeciwbakteryjne czy przeciwwirusowe. Przewagą nanomateiałów peptydowych jest ich biokomplatybilność, możliwość wzbogacenia peptydu o dowolny motyw molekularny, a także możliwość dobierania aminokwasów w taki sposób, aby otrzymać materiał o odpowiednich właściwościach.

Biomedyczne zastosowania nanostruktur peptydowych są bardzo rozległe i obejmują między innymi tworzenie trójwymiarowych rusztowań z samoorganizujących się peptydów, które pobudzają komórki kostne do wzrostu. Takie hydrożele mają szerokie zastosowanie np. w stomatologii podczas leczenia ubytków kostnych, spowodowanych przez choroby uzębienia [155]. Peptydowe hydrożele znajdują również zastosowanie jako matryce zewnętrzne przyspieszające wzrost komórek skóry [156]. Ponadto wykazano, że peptydowe opatrunki zmniejszają obrzęk rany, przyspieszają proces tworzenia i zanikania strupa, a także przyspieszają proces gojenia się rany po oparzeniach II stopnia u szczurów [157]. Prowadzone są również badania nad zastosowaniem samoorganizujących się peptydów jako nośników leków [158], jako rusztowań wspomagających wzrost aksonów w uszkodzonym rdzeniu kręgowym [159], czy jako macierze pobudzające naprawę tkanki chrzęstnej [160]. Samoorganizujące struktury peptydowe znajdują również zastosowanie jako biosensory do wykrywania m. in. glukozy [161], związków fenolowych [162], neurotoksyn [163], NADH, etanolu [164], kaspazy 3 [165], do wykrywania pałeczek dżumy [166], czy bakterii E. Coli [167]. Nanostruktury peptydowe wykazują również właściwości przeciwbakteryjne [168] oraz przeciwwirusowe [169-170], a także wykazują właściwości przeciwstarzeniowe, przez co z powodzeniem mogą być stosowane jako dodatki do kosmetyków, intensyfikujące produkcję kolagenu [171].

III. CEL PRACY

Celem badawczym niniejszej rozprawy było:

- Badanie technikami chromatograficznymi (HPLC-ELSD, TLC) wybranych pojedynczych aminokwasów białkowych oraz ich mieszanin pod kątem ich zdolności do ulegania oscylacyjnej inwersji chiralnej i/lub samorzutnej peptyzacji w środowisku abiotycznym;
- Identyfikacja powstałych produktów reakcji peptyzacji aminokwasów z wykorzystaniem układów HPLC-MS, LC-MS, MS oraz TLC-MS;
- Sprawdzenie, czy w przypadku par aminokwasów produktami reakcji peptyzacji są jedynie homo-, czy również heteropeptydy (HPLC-MS, LC-MS, MS);
- Sprawdzenie, czy powstałe proste peptydy mogą organizować się w struktury nano- oraz mikropeptydowe (SEM);
- Znalezienie zależności między budową cząsteczkową wyjściowych aminokwasów, a kształtem otrzymanych nanostruktur (SEM);
- Śledzenie zmian zmętnienia oraz skręcalności właściwej przechowywanych roztworów aminokwasów w celu lepszego zrozumienia zachodzących procesów (turbidymetria i polarymetria).

IV. GLOSARIUSZ

- His – histydyna
- HPLC – (*ang. High Performance Liquid Chromatography)* wysokosprawna chromatografia cieczowa
- HPLC-ELSD – (*ang. High Performance Liquid Chromatography with Light Scattering detector*) wysokosprawna chromatografia cieczowa z detektorem rozproszenia światła
- Hyp – hydroksyprolina
- LC-MS – (*ang. Liquid Chromatography/Mass Spectrometry*) chromatografia cieczowa z detektorem spektrometrii mas
- Met – metionina
- Phe – fenyloalanina
- Pro – prolina
- SEM – (*ang. Scanning Electron Microscope*) skaningowy mikroskop elektronowy
- Ser – seryna
- Thr – treonina
- TLC – (*ang. Thin Layer Chromatography*) chromatografia cienkowarstwowa
- TLS-MS – (*ang. Thin Layer Chromatography - Mass Spectrometry*) sprzężenie chromatografii cienkowarstwowej ze spektrometrią mas

V. CZĘŚĆ EKSPERYMENTALNA

1. ODCZYNNIKI I MATERIAŁY

Podczas prowadzenia badań korzystano z odczynników chemicznych i materiałów przedstawionych w Tab. 9-12.

Tab. 9. Ogólna charakterystyka aminokwasów stosowanych podczas badań

Aminokwas (1)	**Wzór chemiczny** (2)	**Czystość** (3)	**Producent** (4)
L-Cysteina	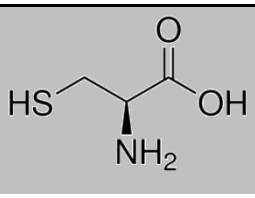	≥ 98%	Reanal, Budapeszt, Węgry
L-Fenyloalanina	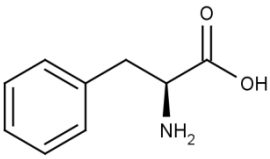	≥ 98%	Merck KGaA, Darmstadt, Niemcy
L-Histydyna	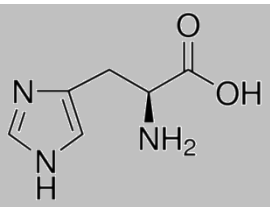	≥ 98%	Reanal, Budapeszt, Węgry
L-Hydroksyprolina	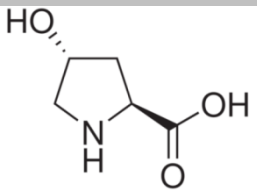	≥ 98%	Sigma-Aldrich, St. Louis, MO, USA
L-Metionina	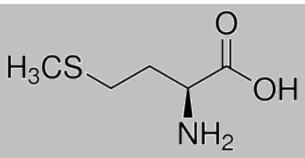	≥ 98%	Reanal, Budapeszt, Węgry
L-Prolina	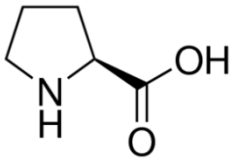	≥ 98%	Merck KGaA, Darmstadt, Niemcy

(1)	(2)	(3)	(4)
L-Seryna	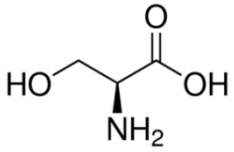	≥ 98%	Reanal, Budapeszt, Węgry
D-Seryna	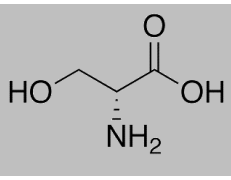	≥ 98%	Sigma-Aldrich, St. Louis, MO, USA
DL-Seryna	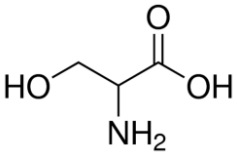	≥ 98%	Sigma-Aldrich, St. Louis, MO, USA
L-Treonina	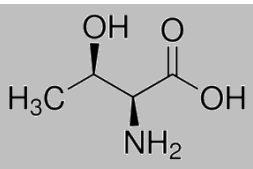	≥ 98%	Reanal, Budapeszt, Węgry

Tab. 10. Ogólna charakterystyka cieczy stosowanych, jako rozpuszczalniki badanych substancji i/lub jako fazy ruchome w badaniach chromatograficznych

Rozpuszczalnik	Wzór chemiczny	Czystość	Producent
Acetonitryl	CH_3CN	≥ 99,9%	Sigma-Aldrich, St. Louis, MO, USA
Metanol	CH_3OH	≥ 99,9%	Sigma-Aldrich, St. Louis, MO, USA
2-Butanol	$CH_3CH_2CH(OH)CH_3$	≥ 99%	Sigma-Aldrich, St. Louis, MO, USA
1- Propanol	C_3H_7OH	≥ 99,9%	Sigma-Aldrich, St. Louis, MO, USA
2-Propanol	$(CH_3)_2CHOH$	≥ 99,9%	Roth, Karlsruhe, Niemcy
Kwas octowy	CH_3COOH	CZDA	POCH, Gliwice, Polska
Woda amoniakalna	NH3 · H_2O	CZDA	POCH, Gliwice, Polska
Pirydyna	C_5H_5N	CZDA	Sigma-Aldrich, St. Louis, MO, USA
Woda	H_2O	redestylowana, dejonizowana	Laboratorium Uniwersytetu Śląskiego, Katowice, Polska

Tab. 11. Ogólna charakterystyka ciał stałych stosowanych do sporządzenia roztworów użytych podczas badań

Związek chemiczny	Wzór chemiczny	Czystość	Producent
Czterowodny octan manganu(II)	$(CH_3CO_2)_2Mn \cdot 4H_2O$	≥ 99%	Sigma-Aldrich, St. Louis, MO, USA
Azotan(V) cynku(II)	$Zn(NO_3)_2$	CZDA	POCH, Gliwice, Polska
Ninhydryna	$C_9H_6O_4$	CZDA	POCH, Gliwice, Polska
Siedmiowodny siarczan(VI) miedzi(II)	$CuSO_4 \cdot 7H_2O$	CZDA	POCH, Gliwice, Polska
Winian sodowo-potasowy	$KNaC_4H_4O_6$	≥ 99%	POCH, Gliwice, Polska
Wodorotlenek sodu	NaOH	CZDA	POCH, Gliwice, Polska

Tab. 12. Ogólna charakterystyka materiałów stosowanych, jako fazy stacjonarne w chromatografii cieczowej

Faza stacjonarna	Rodzaj chromatografii	Wymiary kolumny i średnica ziarna	Producent
Mikrokrystaliczna celuloza (komercyjnie dostępne płytki szklane 10 cm × 20 cm)	TLC	-	Merck KGaA, Darmstadt, Niemcy
ThermoQuest Hypersil C18 nr kat. 3718-062	HPLC	150 mm × 4.6 mm 5 μm	Thermo Fisher Scientific, Karlsruhe, Niemcy
Varian Pursuit 5 C18 nr kat. A3000250C046	HPLC	250 mm × 4.6 mm 5 μm	Varian, Harbor City, CA, USA

2. SPRZĘT I APARATURA

Poniżej przedstawiono wykaz sprzętu i aparatury stosowanej podczas prowadzenia badań wchodzących w skład niniejszej rozprawy doktorskiej:

- Chromatograf cieczowy firmy Varian model 920 (Varian, Harbor City, CA, USA) wyposażony w autosampler (900-LC), pompę gradientową, termostat, detektor spektrofotometryczny DAD (Varian 330 DAD), detektor rozproszenia światła ELSD (Varian 380-LC) oraz oprogramowanie Galaxie;
- Chromatograf cieczowy LC-MS (Varian, Palo Alto, CA, USA) wyposażony w pompę Varian ProStar, detektor-spektrometr masowy Varian 100-MS, a także oprogramowanie Varian MS Workstation wersja 6.9.1;
- Spektrometr mas Thermo LCQ Deca XP z jonizacją ESI;
- Spektrometr IR Magna 560 Nicolet FT-IR (Nicolet, Francja);
- Mikroskop optyczny Axio Scope A1 firmy Zeiss z cyfrową rejestracją obrazu (Zeiss, Oberkochen, Niemcy);
- Skaningowy mikroskop elektronowy firmy Joel model JSM-7600F (Tokio, Japonia);
- Polarymetr 341 z automatycznym zapisem danych firmy Perkin-Elmer (Waltham, MS, USA);
- Turbidymetr z automatycznym zapisem danych firmy Vernier Software & Technology model TRB-BTA (Beaverton, OR, USA);
- Densytometr C60 firmy Desaga (Heidelberg, Niemcy), wyposażony w program ProQuant firmy Desaga, współpracujący z systemem Windows;
- Komory chromatograficzne firmy Camag (Muttenz, Szwajcaria);
- Przystawka TLC-MS firmy Camag (Muttenz, Szwajcaria);
- Kalibrowane kapilary do nanoszenia próbek stosowane w chromatografii cienkowarstwowej firmy Camag (Muttenz, Szwajcaria);
- Waga analityczna model SBC 31 firmy Scaltec (Heiligenstadt, Niemcy);
- Drobny sprzęt laboratoryjny (kolby miarowe, pipety, szkiełka zegarkowe, szalki Pietriego, szkiełka mikroskopowe).

3. METODYKA PROWADZONYCH BADAŃ

3.1. TECHNIKA CHROMATOGRAFII CIENKOWARSTWOWEJ (TLC)

Technikę chromatografii cienkowarstwowej wykorzystano do badania inwersji chiralnej i/lub samorzutnej peptyzacji aminokwasów takich, jak *L*-Hyp oraz *L*-Ser, *D*-Ser oraz *DL*-Ser. Roztwory badanych aminokwasów zostały sporządzone, a następnie przechowywane w szczelnie zamkniętych naczyniach w temperaturze pokojowej przez odpowiednio 37 dni w przypadku *L*-Hyp oraz 11 dni w przypadku *L,D,DL*-Ser. Przed rozpoczęciem analiz chromatograficznych zarówno do świeżo sporządzonego roztworu, jak i do roztworów przechowywanych dodano odpowiednią ilość selektorów chiralnych; dla *L*-Hyp selektorem był octan manganu(II), natomiast dla *L,D,DL*-Ser azotan(V) cynku(II). W obu przypadkach dodano równomolowe ilości wspomnianych soli. Stosowane fazy stacjonarne, składy faz ruchomych oraz stężenia poszczególnych analitów zostały zebrane w Tab. 13.

Tab. 13. Warunki prowadzonych analiz chromatograficznych

Analit	**Stężenie analitu [mg·ml^{-1}] ([mol · dm^{-3}])**	**Rozpuszczalnik**	**Faza stacjonarna**	**Skład fazy ruchomej**
L-Hyp	1 ($7{,}63\cdot10^{-3}$)	acetonitryl – woda (7:3 *v/v*)	mikrokrystaliczna celuloza	2-butanol – pirydyna – lodowaty kwas octowy – woda (30:20:6:24, *v/v*)
L-Ser *D*-Ser *DL*-Ser	1 ($9{,}44\cdot10^{-3}$)	metanol–woda (7:3 *v/v*)	mikrokrystaliczna celuloza	1-propanol–0.5 % woda amoniakalna (7:3, *v/v*)

Przed rozpoczęciem analizy płytki chromatograficzne były aktywowane przez 30 min w temperaturze 110^{o}C. Próbki były nanoszone na płytkę chromatograficzną 1,5 cm od brzegów płytki oraz 1 cm od dolnej krawędzi, w ilości 5 µl. Chromatogramy były rozwijane na wysokość 8 cm (*L*-Hyp) oraz 7 cm (*L*-Ser, *D*-Ser oraz *DL*-Ser) przez ok. 2 godziny. Rozwinięte płytki chromatograficzne suszono na powietrzu przez

ok. 30 minut, a następnie wywoływano 0,5% roztworem ninhydryny rozpuszczonej w 2-propanolu. Tak przygotowane płytki chromatograficzne skanowano z użyciem densytometru skaningowego Desaga. Profile stężeniowe rejestrowano przy długości fali λ=485 nm (*L*-Hyp) oraz λ=550 nm (*L*-Ser, *D*-Ser oraz *DL*-Ser), a także wykonano pomiary w trybie fluorescencji (dla *L*-Hyp, przy długości fali λ=462 nm). Wszystkie eksperymenty zostały trzykrotnie powtórzone.

3.2. SPRZĘŻENIE CHROMATOGRAFII CIENKOWARSTWOWEJ ZE SPEKTROMETRIĄ MAS (TLC-MS)

Połączenie chromatografii cienkowarstwowej (TLC) ze spektrometrią mas (MS) daje możliwość identyfikacji substancji rozdzielonych przy pomocy chromatografii cienkowarstwowej. Płytki chromatograficzne były przygotowywane w analogiczny sposób, jak przedstawiono w rozdziale 3.1., z pominięciem etapu wywoływania płytki. Pierwszym krokiem podczas prowadzenia badań było wyeluowanie badanej substancji (*L*-Hyp oraz produktów rozdziału) z płytki chromatograficznej wodą przy pomocy interfejsu TLC-MS, a następnie zarejestrowanie widm mas badanych związków. Substancje były eluowane kolejno z poszczególnych plamek chromatograficznych, a następnie analizowane techniką LC-MS z jonizacją ESI (ESI – *eng. electrospray ionization*) i analizatorem pułapką jonową. Warunki prowadzonej detekcji były następujące:

- jonizacja: pozytywna;
- temperatura komory rozpylania: T=50°C;
- temperatura gazu: T=250°C;
- ciśnienie gazu: 25 psi;
- napięcie na igle: 5 kV;
- napięcie na kapilarze: 50V.

3.3. TECHNIKA WYSOKOSPRAWNEJ CHROMATOGRAFII CIECZOWEJ (HPLC)

Podczas prowadzonych badań wykorzystano technikę HPLC z detekcją ELSD oraz DAD w celu monitorowania zmian stężenia badanych aminokwasów w czasie ich przechowywania. Badania te były wykonywane w trybie ciągłym z wykorzystaniem chromatografu cieczowego firmy Varian, opisanego w rozdziale 2. Warunki analiz chromatograficznych oraz sposób przygotowania próbek zostały zebrane w Tab. 14 i 15.

Tab. 14. Warunki prowadzonych analiz techniką wysokosprawnej chromatografii cieczowej (HPLC) (cz.1)

Analit	**Stężenie analitu [mg·ml^{-1}] ([mol · dm^{-3}])**	**Rozpuszczalnik**	**Kolumna**	**Faza ruchoma**
L-Ser *D*-Ser *DL*-Ser	1 $9{,}44\cdot10^{-3}$	metanol-woda (7:3 *v/v*)	ThermoQuest Hypersil C18 nr kat. 3718-062	1% kwas octowy: acetonitryl (90:10 *v:v*)
L-Met	2 $1{,}34\cdot10^{-2}$	metanol-woda (7:3 *v/v*)	ThermoQuest Hypersil C18 nr kat. 3718-062	1% kwas octowy: acetonitryl (90:10 *v:v*)
L-Ser-*L*-Met	1 – 2 $9{,}44\cdot10^{-3}$ – $1{,}34\cdot10^{-2}$	metanol-woda (7:3 *v/v*)	ThermoQuest Hypersil C18 nr kat. 3718-062	1% kwas octowy: acetonitryl (90:10 *v:v*)
L-His	2 $1{,}29\cdot10^{-2}$	metanol-woda (7:3 *v/v*)	ThermoQuest Hypersil C18 nr kat. 3718-062	1% kwas octowy: metanol (50:50 *v:v*)
L-Thr	1 $8{,}39\cdot10^{-3}$	metanol-woda (7:3 *v/v*)	ThermoQuest Hypersil C18 nr kat. 3718-062	1% kwas octowy: metanol (50:50 *v:v*)
L-His-*L*-Thr	2 – 1 $1{,}29\cdot10^{-2}$ – $8{,}39\cdot10^{-3}$	metanol-woda (7:3 *v/v*)	ThermoQuest Hypersil C18 nr kat. 3718-062	1% kwas octowy: metanol (50:50 *v:v*)
L-Phe-*L*-Pro	1 – 1 $6{,}05\cdot10^{-3}$ – $8{,}69\cdot10^{-3}$	acetonitryl-woda (7:3 *v/v*)	Varian Pursuit 5 C18 nr kat. A3000250C046	metanol-woda (40:60 *v:v*)

Tab. 15. Warunki prowadzonych analiz techniką wysokosprawnej chromatografii cieczowej (HPLC) (cz.2)

Analit	Temp. pracy kolumny [^{o}C]	Objętość próbki [µl]	Szybkość przepływu [ml·min^{-1}]	Czas analizy [min]	Czas prowadzenia badań [h]
L-Ser *D*-Ser *DL*-Ser	35	3	0,8	8	40
L-Met	35	3	0,8	8	30
L-Ser-*L*-Met	35	3	0,8	8	30
L-His	35	3	1	8	30
L-Thr	35	3	1	8	30
L-His-*L*-Thr	35	3	1	8	30
L-Phe-*L*-Pro	35	30	0,25	20	250

3.4. SPRZĘŻENIE CHROMATOGRAFII CIECZOWEJ ZE SPEKTROMETRIĄ MAS (HPLC-MS, LC-MS) ORAZ SPEKTROMETRIA MAS (MS)

Badania z wykorzystaniem spektrometrii mas były prowadzone w trzech różnych układach:

- HPLC-MS – podczas badań techniką HPLC-ELSD proces peptyzacji aminokwasów był dodatkowo kontrolowany z użyciem detektora mas;
- LC-MS – procesy peptyzacji były kontrolowane z użyciem układu LC-MS podczas przechowywania roztworów; układ zawierał jedynie prekolumnę;
- MS – próbki świeże oraz przechowywane przez pewien okres czasu były analizowane z użyciem spektrometru mas.

Pomiary prowadzono z wykorzystaniem spektrometrów mas opisanych w rozdziale 2, a badane roztwory zostały przygotowane w taki sam sposób, jak w przypadku badań w układzie HPLC-ELSD.

Warunki analiz prowadzonych w układach HPLC-MS oraz LC-MS były następujące:

- jonizacja pozytywna/negatywna: ESI;
- temperatura komory rozpylania: 50^{o}C;
- temperatura gazu: 350^{o}C;
- ciśnienie gazu: 25 psi;
- napięcie na kapilarze: 50 V;
- napięcie na igle: 5 kV.

W przypadku wykonywania analiz z wykorzystaniem spektrometru mas (MS) warunki prowadzenia detekcji były następujące:

- jonizacja pozytywna/negatywna: ESI;
- napięcie na kapilarze: 50 V;
- napięcie na igle: 5 kV;
- temperatura igły: 250 ^{o}C.

3.5. MIKROSKOPIA OPTYCZNA

Analizy przy pomocy mikroskopu optycznego opisanego w rozdziale 2 prowadzono dla roztworu *L*-Phe–*L*-Pro o stężeniu poszczególnych aminokwasów równym 10 mg · ml^{-1} przechowywanego przez okres jednego roku w układzie acetonitryl-woda (7:3, *v/v*) zawierającego mikrowłókna peptydowe. Włókna wyodrębnione z roztworu nanoszono na szkiełko mikroskopowe, a następnie rejestrowano ich obraz stosując powiększenie X50. Analizowano również włókna zawieszone w roztworze. W tym celu kilka mililitrów badanej próbki umieszczono na szalce Pietriego, a następnie rejestrowano obraz roztworu pod mikroskopem stosując powiększenia X50 i X10.

3.6. SKANINGOWA MIKROSKOPIA ELEKTRONOWA (SEM)

W wyniku samoorganizacji aminokwasów w roztworze powstają proste peptydy, które również mogą organizować się w bardziej skomplikowane nano- oraz mikrostruktury, które obserwowano z wykorzystaniem skaningowego mikroskopu elektronowego opisanego w rozdziale 2. Roztwory badanych aminokwasów przygotowano, a następnie przechowywano w szczelnie zamkniętych naczyniach. Tab. 16 przedstawia sposób przygotowania roztworów oraz czas ich przechowywania. Roztwory zawierające nano- oraz mikrostruktury peptydowe nanoszono na mosiężne kołeczki i pozostawiano do odparowania rozpuszczalnika, a następnie wykonywano serie pomiarów mikroskopowych.

Tab. 16. Sposób przygotowania próbek do badań mikroskopowych

Analit	**Stężenie analitu [mg·ml^{-1}] ([mol · dm^{-3}])**	**Rozpuszczalnik**	**Czas przechowywania**
L-Ser	1 $9{,}44\cdot10^{-3}$	metanol-woda (7:3 *v/v*)	1 miesiąc
L-Ser-*L*-Met	1 – 2 $9{,}44\cdot10^{-3}$ – $1{,}34\cdot10^{-2}$	metanol-woda (7:3 *v/v*)	1 miesiąc
L-Cys	0,7 $5{,}77\cdot10^{-3}$	metanol-woda (7:3 *v/v*)	2 tygodnie
L-Pro	1 $8{,}69\cdot10^{-3}$	metanol-woda (7:3 *v/v*)	2 tygodnie
L-Phe	1 $6{,}05\cdot10^{-3}$	metanol-woda (7:3 *v/v*)	3 miesiące
L-Pro-*L*-Cys	1 – 1 $8{,}69\cdot10^{-3}$– $8{,}25\cdot10^{-3}$	metanol-woda (7:3 *v/v*)	2 tygodnie
L-Phe-*L*-Pro	10 – 10 $6{,}05\cdot10^{-2}$ – $8.69\cdot10^{-2}$	acetonitryl-woda (7:3 *v/v*)	1 rok

3.7. SPEKTROSKOPIA W PODCZERWIENI (IR)

Badania spektroskopowe przeprowadzono w celu ustalenia, jakie grupy funkcyjne znajdują się w badanych próbkach, a tym samym w celu potwierdzenia obecności wiązań peptydowych. Widma w podczerwieni zostały zarejestrowane dla mikrowłókien *L*-Phe–*L*-Pro, próbek stałych *L*-Phe, *L*-Pro oraz dla ich równomolowej mieszaniny. Widma rejestrowano dla próbek badanych związków w pastylce KBr (3 mg próbki na 150 g KBr) w zakresie długości fal od 4000 do 400 cm^{-1} z zastosowaniem spektrometru FTIR opisanego w rozdziale 2.

3.8. TURBIDYMETRIA

Badania turbidymetryczne pozwalają zaobserwować efekty wytrącania się nierozpuszczalnych, wyższych peptydów, niewidocznych gołym okiem, co ma znaczenie dla zrozumienia mechanizmów samoorganizacji peptydów w nanostruktury. Badania turbidymetryczne dokumentują zmiany zachodzące w świeżo sporządzonym roztworze aminokwasów. Badania te prowadzone były w trybie ciągłym (pomiar wykonywano co 1 minutę) w temp. 23±1 ^{o}C.

Badania turbidymetryczne przeprowadzono dla pojedynczych aminokwasów *L*-Ser, *D*-Ser, *DL*-Ser (czas analizy: 7 dni) oraz dla par aminokwasów białkowych *L*-His–*L*-Thr (czas analizy: 48h) oraz *L*-Phe–*L*-Pro (czas analizy: 26 dni). Roztwory badanych aminokwasów zostały przygotowane w taki sam sposób, jak w przypadku analiz HPLC.

3.9. POLARYMETRIA

Zastosowanie polarymetrii pozwoliło na uzyskanie informacji na temat zmian skręcalności właściwej badanych roztworów aminokwasów (*L*-Ser, *D*-Ser oraz *DL*-Ser) w czasie ich przechowywania. Pomiary prowadzono w trybie ciągłym (w odstępach 1 minuty przez 24h) z zastosowaniem polarymetru Perkin-Elmer (opisanego w rozdziale 2). Podczas pomiarów stosowano długość fali 589 nm, charakterystyczną

dla linii *D* sodu. Celka pomiarowa miała długość 1 dm, objętość wodnego roztworu aminokwasów wynosiła 6 ml, a stężenie 10 $mg \cdot ml^{-1}$ ($1g \cdot 100ml^{-1}$). Skręcalność właściwą $[\alpha]_D$ badanych roztworów obliczono, korzystając z następującego wzoru:

$$[\alpha]_D = \frac{100\alpha}{cd}$$

gdzie: α – kąt skręcania płaszczyzny światła spolaryzowanego; c – stężenie próbki wyrażone w gramach na 100 ml roztworu; d – długość drogi optycznej.

3.10. REAKCJA BIURETOWA

Reakcja biuretowa została po raz pierwszy opisana w 1961 roku [172], a obecnie jest to standardowa procedura analityczna, umożliwiająca łatwe wykrywanie peptydów i białek w różnych cieczach, w tym również w krwi i moczu. Przeprowadzenie próby biuretowej pozwala na wykrycie obecności wiązań peptydowych w badanych roztworach. Pozytywny wynik reakcji biuretowej potwierdza obecność co najmniej dwóch wiązań peptydowych w bezpośrednim sąsiedztwie. Test ten polega na dodaniu odczynnika biuretowego (zawierającego m.in. silną zasadę, np. NaOH oraz jony miedzi Cu^{2+}) do badanego roztworu. Jeśli w roztworze obecne są wiązania peptydowe wówczas roztwór zmienia barwę z niebieskiej na różową (w przypadku dipeptydów) lub fioletową (w przypadku wyższych peptydów). Obecność wolnych aminokwasów nie zmienia barwy odczynnika biuretowego. Za zmianę barwy odpowiedzialne są jony miedzi, które w obecności silnej zasady tworzą anionowe związki kompleksowe z grupami peptydowymi.

Odczynnik biuretowy używany podczas prowadzenia doświadczeń zawierał: 78,6 g $CuSO_4 \cdot 7H_2O$, 10 g $NaKC_4H_4O_6 \cdot 4H_2O$, 50 ml 10% (*w*/*w*) NaOH rozcieńczonych wodą do objętości 1 dm^{-3}. Stężenie jonów miedzi Cu^{2+} wynosiło 0,26 $mol \cdot dm^{-3}$, a wodorotlenku sodu 2,7 $mol \cdot dm^{-3}$.

Reakcja biuretowa została przeprowadzona dla metanolowo-wodnych roztworów *L*-Ser oraz *L*-Met, a także dla mikrostruktur peptydowych par aminokwasów *L*-Phe–*L*-Pro oraz *L*-Pro–*L*-Cys, wydzielonych z roztworu poprzez dekantację, a następnie wysuszonych na wolnym powietrzu. Dla tak przygotowanych próbek przeprowadzono próbę biuretową poprzez dodanie odczynnika biuretowego.

3.11. TEST MIKROBIOLOGICZNY

Testy mikrobiologiczne przeprowadzano dla wszystkich przechowywanych roztworów badanych aminokwasów na Wydziale Biologii Uniwersytetu Śląskiego w Katowicach, dwiema metodami.

Pierwsza metoda polegała na wprowadzeniu roztworów aminokwasów do pożywki stałej oraz ciekłej. Pożywka stała o pH=7,4 zawierała: ekstrakt mięsa (C=2,0 $g \cdot dm^{-3}$), ekstrakt drożdży (C=2,0 $g \cdot dm^{-3}$), roztwór propanolu (C=5,0 $g \cdot dm^{-3}$), roztwór chlorku sodu (C=4,0 $g \cdot dm^{-3}$), roztwór agaru (C=15,0 $g \cdot dm^{-3}$). Pożywka ciekła zawierała: ekstrakt mięsa (C=0,4 $g \cdot dm^{-3}$), roztwór hydrolizatu drożdży (C=1,7 $g \cdot dm^{-3}$), roztwór enzymatycznego hydrolizatu kazeiny (C=5,4 $g \cdot dm^{-3}$), roztwór peptonu (C=4,0 $g \cdot dm^{-3}$), roztwór chlorku sodu (C=3,5 $g \cdot dm^{-3}$).

Pierwszą serię próbek na pożywce stałej z dodatkiem 100 µl badanych roztworów poddawano 7-dniowej inkubacji w temp. 21±1^{o}C, a drugą serię próbek na pożywce ciekłej (50 ml pożywki z dodatkiem 100 µl badanych roztworów) poddawano 14-dniowej inkubacji z ciągłym mieszaniem z szybkością 260 obrotów na minutę w temp. 21±1^{o}C. Następnie otrzymane preparaty badano pod mikroskopem.

Druga metoda polegała na oznaczaniu zawartości białka w badanych próbkach (DNA bakterii) metodą Bradford [173]. Metoda ta charakteryzuje się wysoką czułością i wykorzystuje zdolność wiązania barwnika błękitu brylantowego Coomassie G-250 (ang. *Coomasie Brillant Blue*) z białkiem. Barwnik ten w środowisku kwaśnym ma kolor czerwono-brązowy (maksimum absorpcji przy 465 nm), a po związaniu białka roztwór zmienia kolor na niebieski (maksimum absorpcji przy 595 nm). Badane roztwory aminokwasów zmieszano z odczynnikiem Bradford i mierzono ich absorbancję przy odpowiedniej długości fali.

VI. WYNIKI BADAŃ I DYSKUSJA

1. CHROMATOGRAFICZNE BADANIA OSCYLACYJNEJ INWERSJI CHIRALNEJ (TLC) ORAZ SAMORZUTNEJ PEPTYZACJI (TLC-MS) *L*-HYP

1.1. CHROMATOGRAFIA CIENKOWARSTWOWA *L*-HYP

Pierwszym badanym aminokwasem białkowym była *L*-Hyp, a pierwszą zastosowaną techniką analityczną była chiralna chromatografia cienkowarstwowa. Użycie naturalnej celulozy, która posiada zdolność do skręcania światła spolaryzowanego, jako fazy stacjonarnej umożliwiło rozdział enancjomerów hydroksyproliny. W przeszłości pojawiały się już publikacje na temat rozdziału enancjomerów na fazie celulozowej zakończone sukcesem i dlatego w niniejszej pracy zdecydowano się na zastosowanie tej fazy stacjonarnej do rozdziału oligopeptydów hydroksyproliny oraz *D* i *L*-enancjomerów powstałych w wyniku reakcji oscylacyjnej enancjomeryzacji i peptyzacji. Dodatkowo w celu polepszenia rozdziału enancjomerów hydroksyproliny do badanych roztworów została dodana przed rozpoczęciem analizy równomolowa ilość octanu manganu(II), pełniącego rolę selektora chiralnego polepszającego rozdział chromatograficzny. Zdjęcie wywołanej płytki chromatograficznej przedstawiono na Rys. 29.

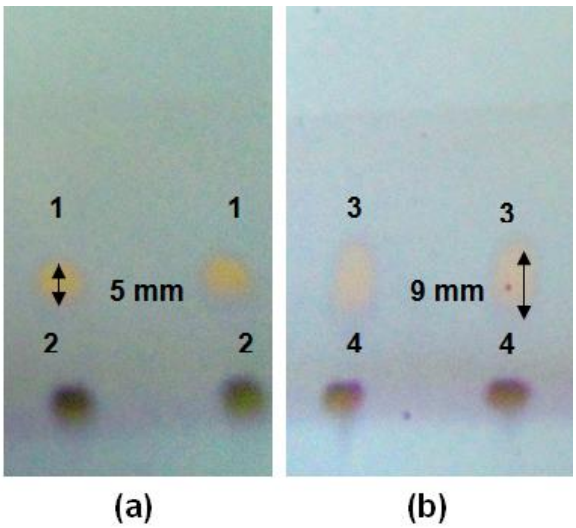

Rys. 29. Chromatogram (a) świeżo sporządzonego roztworu oraz (b) roztworu przechowywanego przez okres 37 dni. 1: *L*-Hyp; 2: produkt reakcji peptyzacji; 3: *L,D*-Hyp; 4: produkt reakcji peptyzacji [174]

Widoczne na chromatogramie (Rys. 29) żółte plamki odpowiadają pojedynczym formom Hyp, natomiast fioletowe – oligopeptydom. Rys. 29(a) prezentuje chromatogram świeżo sporządzonego roztworu *L*-Hyp, natomiast Rys. 29(b) przedstawia chromatogram roztworu *L*-Hyp przechowywanego przez okres 37 dni. Widać wyraźne różnice między Rys. 29(a), a Rys. 29(b). Współczynnik retencji filetowej plamki oligopeptydów Hyp na Rys. 29(a) i (b) wynosi 0,32 ± 0,02. Żółta plamka świeżo sporządzonego roztworu (Rys. 29(a)) jest stosunkowo niewielka (5 mm), a jej współczynnik retencji wynosi 0,58 ± 0,01. Na Rys. 29(b) widać, że żółta plamka jest bardziej rozciągnięta (9 mm), co sugeruje powstanie formy *D*-Hyp w wyniku inwersji chiralnej. Współczynnik retencji *D*/*L*-Hyp wynosi 0,61 ± 0,01. Na podstawie poprzednich badań prowadzonych dla 70% metanolowego roztworu *D*/*L*-Pro, badanego według tej samej procedury analitycznej [175], gdzie rozdział poszczególnych form enancjomerycznych był zupełny, można wnioskować, że rozciągnięta żółta plamka przechowywanego roztworu zawiera zarówno formę *L*, jak i *D*-Hyp. Hydroksyprolina różni się od proliny jedynie dodatkową grupą hydroksylową, przez co jej powinowactwo do fazy stacjonarnej jest większe, a rozdział niepełny. Przez analogię do wyników wcześniejszych badań nad *D*/*L*-Pro wnioskujemy, że *D*-Hyp ma większy współczynnik retencji od formy *L*-Hyp. Płytka chromatograficzna została zdensytometrowana, a otrzymane densytogramy przedstawiono na Rys. 30.

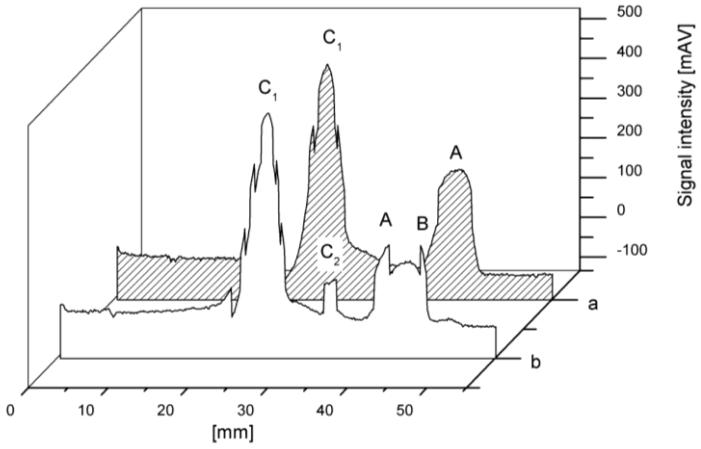

Rys. 30. Densytogramy (a) świeżo sporządzonego roztworu *L*-Hyp oraz (b) roztworu przechowywanego przez 37 dni. Densytogramy zostały wykonane w trybie odbicia przy długości fali λ = 485 nm. A: *L*-Hyp; B: *D*-Hyp; C_1: produkt reakcji peptyzacji (obecny już w świeżo sporządzonej próbce); C_2: produkt reakcji peptyzacji (obecny jedynie w przechowywanym roztworze) [174]

Na Rys. 30 można zauważyć wyraźne różnice między densytogramami próbki przechowywanej przez okres 37 dni (Rys. 30(b)), a próbki świeżo sporządzonego roztworu *L*-Hyp (Rys. 30(a)). Piki A na obu wykresach odpowiadają formom monomerycznym *L*-Hyp, natomiast dodatkowy pik B, obecny jedynie na widmie próbki przechowywanej, potwierdza powstawanie formy *D*-Hyp o wyższym współczynniku retencji. Pik C_1 na Rys. 30 odpowiada plamce fioletowej na chromatogramie (oligopeptydy obecne już w świeżo sporządzonej próbce), natomiast pik C_2 jest obecny jedynie w przechowywanej próbce (Rys. 30(b)) i pojawił się on w wyniku powstania peptydów w procesie oscylacyjnej peptyzacji.

Na Rys. 31 przedstawiono densytogram 2D zmierzony w trybie fluorescencji przy długości fali 465 nm. Rys. 31(a) odpowiada świeżo sporządzonemu roztworowi *L*-Hyp, a Rys. 31(b) odpowiada roztworowi przechowywanemu przez 37 dni. Densytogram przechowywanego roztworu *L*-Hyp jest bogatszy w piki w porównaniu do Rys. 31(a). Pik A odpowiadający monomerycznej formie *L*-Hyp obecny jest na obydwóch densytogramach. Pik B obecny jest tylko na densytogramie przechowywanej próbki i jest to kolejny dowód na powstanie formy enancjomerycznej *D*-Hyp w wyniku oscylacyjnej enancjomeryzacji. Pasmo oligopeptydów (pik C) występuje zarówno w widmie świeżo sporządzonego, jak i przechowywanego roztworu, natomiast pik D pojawił się tylko w przechowywanej próbce, co świadczy o powstaniu produktów kondensacji tego aminokwasu.

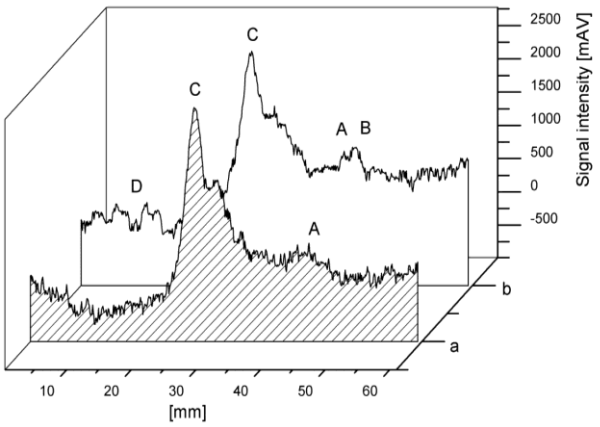

Rys. 31. Densytogramy (a) świeżo sporządzonego roztworu *L*-Hyp oraz (b) roztworu przechowywanego przez 37 dni. Densytogramy zostały wykonane w trybie fluorescencji przy długości fali λ = 462 nm. A: *L*-Hyp; B: *D*-Hyp; C: produkt reakcji peptyzacji (obecny zarówno w świeżo sporządzonej próbce, jak i próbce przechowywanej przez 37 dni); D: produkt reakcji peptyzacji (obecny jedynie w przechowywanym roztworze) [174]

1.2. SPRZĘŻENIE CHROMATOGRAFII CIENKOWARSTWOWEJ ZE SPEKTROMETRIĄ MAS (TLC-MS) DLA *L*-HYP

Połączenie chromatografii cienkowarstwowej ze spektrometrią mas pozwoliło na identyfikację związków rozdzielonych przy pomocy chromatografii cienkowarstwowej. Substancje były eluowane kolejno z poszczególnych plamek chromatograficznych, przedstawionych na Rys. 29. Uzyskane piki chromatograficzne oraz widma mas zostały przedstawione na Rys. 32.

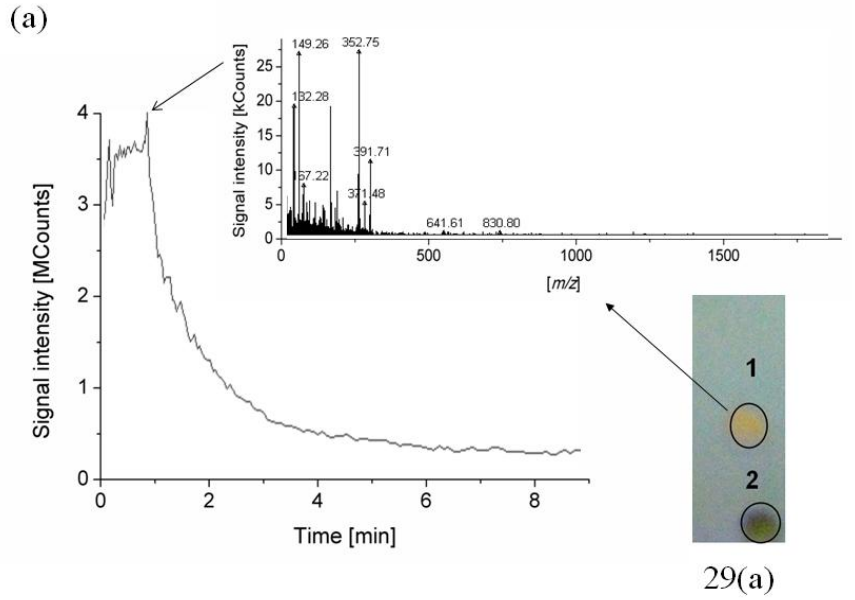

29(a)

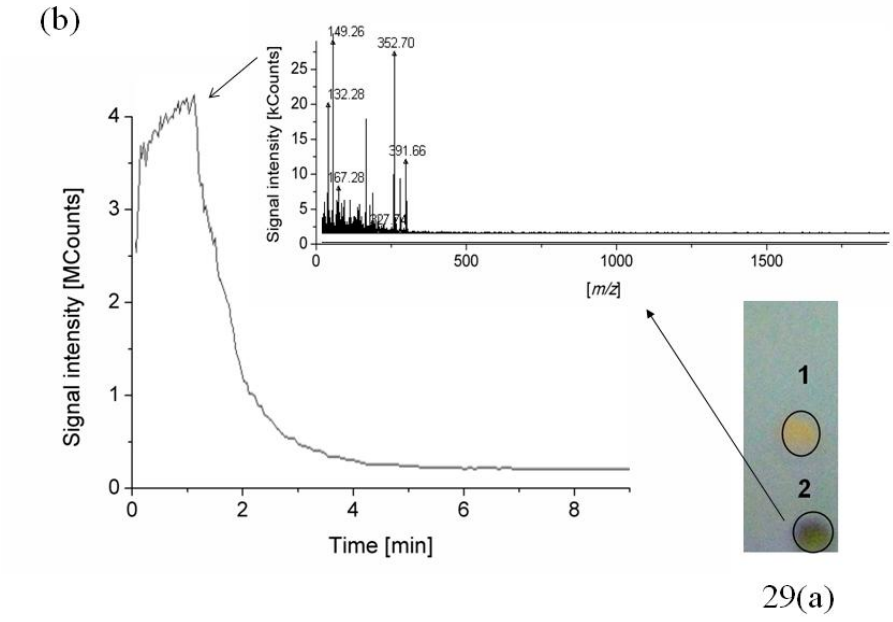

29(a)

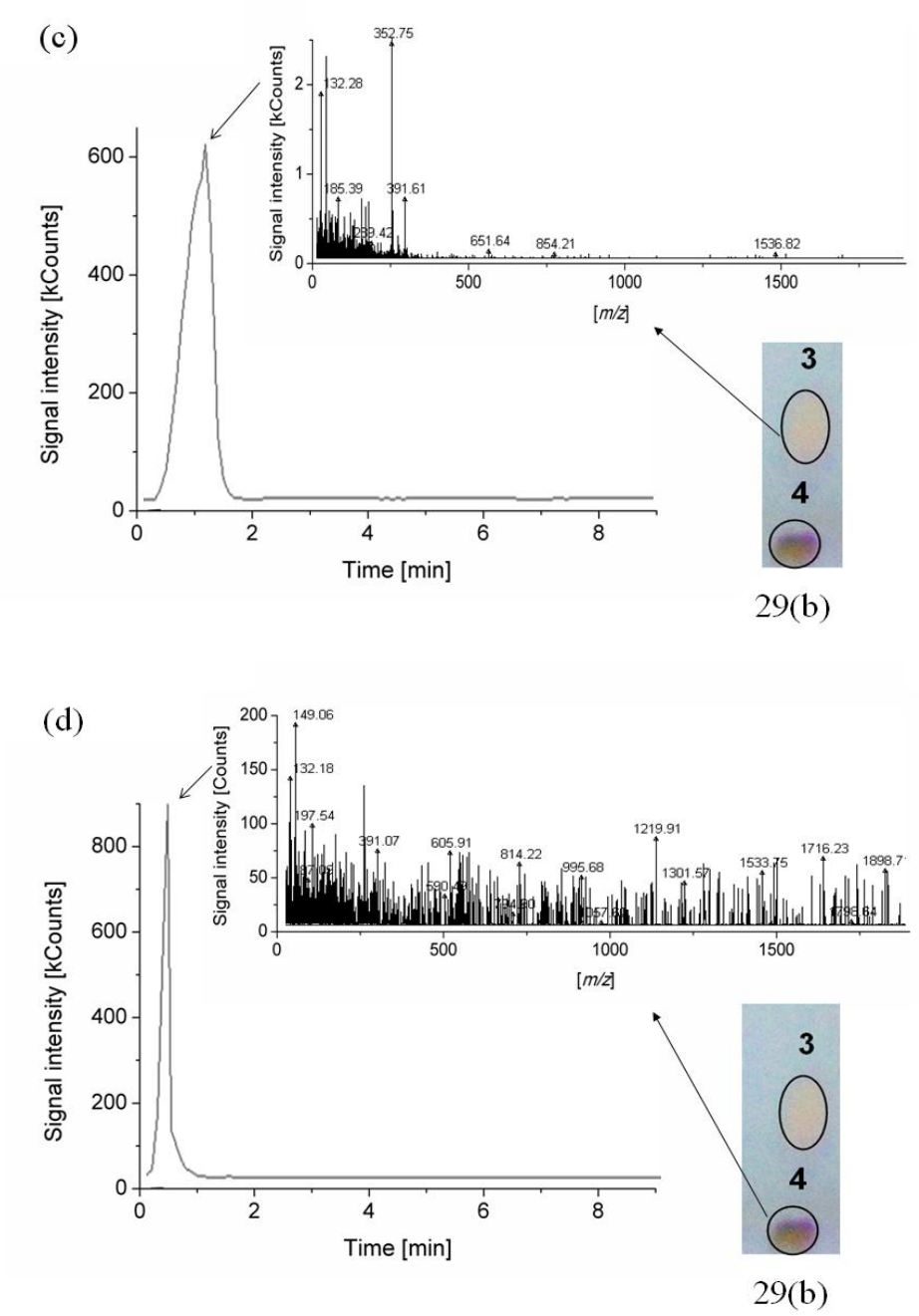

Rys. 32. Chromatogramy oraz widma mas plamek chromatograficznych, przedstawionych na Rys. 29, wyeluowanych z płytki chromatograficznej; (a) widmo mas plamki 1(*L*-Hyp); (b) widmo mas plamki 2 (produkt reakcji peptyzacji); (c) widmo mas plamki 3(*L*,*D*-Hyp); (d) widmo mas plamki 4 (produkt reakcji peptyzacji) [174]

Chromatogramy oraz widma mas przedstawione na Rys. 32(a) oraz 32(b) odpowiadają żółtej plamce *L*-Hyp świeżo sporządzonego roztworu (Rys. 32(a)) oraz fioletowej plamce odpowiadającej produktowi peptyzacji (Rys. 32(b)). Zarówno otrzymane chromatogramy, jak i widma mas są podobne do siebie i można na nich zauważyć wyraźny pik pseudomolekularny hydroksyproliny *m/z* 132 $[Hyp+H]^+$ oraz szereg pików, których masy nie przekraczają *m/z* 400. Piki te najprawdopodobniej można w większości uznać za szumy pochodzące z matrycy (tj. z samej płytki chromatograficznej). Natomiast w przypadku chromatogramów i widm mas próbki przechowywanej przez 37 dni, przedstawionych na Rys. 32(c) (żółta plamka *L/D*-Hyp) oraz Rys. 32(d) (fioletowa plamka polikondensatu) można przede wszystkim zauważyć, że widma mas różnią się znacząco między sobą. Widmo mas monomerycznej formy *L/D*-Hyp nie zawiera peptydów, a jedynie piki charakterystyczne dla analitu oraz dla matrycy. Natomiast widmo mas plamki fioletowej posiada również pik pochodzący od hydroksyproliny, jak i piki matrycy. Ponadto na widmie mas pojawiły się dodatkowe piki polikondensatów, których intensywności stanowią ok. 50% intensywności piku macierzystego. Jako przykłady mogą posłużyć piki: *m/z* 606 i 1717, prawdopodobnie odpowiadające następującym strukturom: $[Hyp_5+Na]^+$ oraz $[Hyp_{15}+Na]^+$.

Porównując widma mas próbki świeżej i przechowywanej przez okres 37 dni można zauważyć, że dla świeżej próbki widoczne są jedynie piki hydroksyproliny oraz matrycy, natomiast dla próbki przechowywanej przez okres 37 dni widoczne są dodatkowe piki polikondensatów hydroksyproliny, co potwierdza zajście samorzutnej oligopeptyzacji.

Przedstawione wyniki świadczą o zajściu procesów inwersji chiralnej i peptyzacji. Obserwacja zaistniałych procesów była możliwa dzięki zastosowaniu techniki chromatografii cienkowarstwowej (TLC) na fazie celulozowej oraz dodaniu równomolowej ilości octanu manganu(II), jak również dzięki zastosowaniu chromatografii cienkowarstwowej z zastosowaniem detekcji mas (TLC-MS) i densytometrii.

2. BADANIA OSCYLACYJNEJ INWERSJI CHIRALNEJ ORAZ SAMORZUTNEJ PEPTYZACJI SER

Podczas badań enancjomerów i racematu Ser wykorzystano różne techniki analityczne takie, jak chromatografię cienkowarstwową, wysokosprawną chromatografię cieczową, spektrometrię mas, turbidymetrię oraz polarymetrię. Prowadzone badania miały na celu porównanie dynamiki peptyzacji i inwersji chiralnej *L*-Ser, *D*-Ser oraz ich mieszaniny (*DL*-Ser).

2.1. CHROMATOGRAFIA CIENKOWARSTWOWA *L*-SER, *D*-SER I *DL*-SER

Pierwszą zastosowaną techniką była chiralna chromatografia cienkowarstwowa. Niestety ze względu na trudności ogólnie dotyczące rozdziałów chiralnych, nie udało się dobrać takiej fazy ruchomej, która umożliwiłaby rozdział enancjomerów Ser. Udało się jednak zaobserwować różnicę w dynamice peptyzacji Ser w zależności od konfiguracji. Na Rys. 33 znajdują się densytogramy odpowiednich pasm chromatograficznych (Rys. 33(A)) zarówno dla świeżo sporządzonych roztworów *L*-Ser, *D*-Ser i *DL*-Ser, jak i dla roztworów przechowywanych przez okres 11 dni oraz zdjęcie wywołanej płytki chromatograficznej (Rys. 33(B)).

(A)

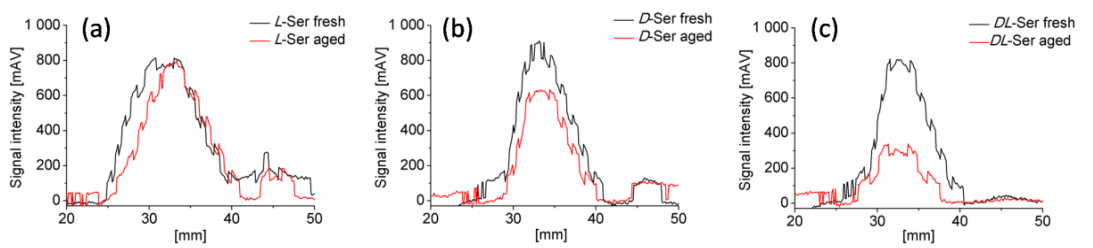

(B)

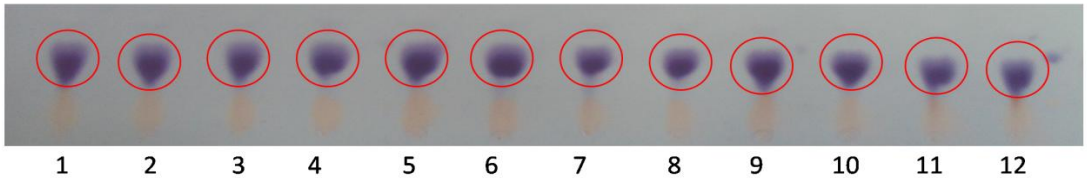

Rys. 33. (A) Densytogramy uzyskane dla świeżo sporządzonego roztworu (a) *L*-Ser, (b) *D*-Ser i (c) *DL*-Ser oraz dla roztworu przechowywanego przez okres 11 dni; (B) zdjęcie rozwiniętej płytki chromatograficznej gdzie: (1)-(2) świeżo sporządzony roztwór *L*-Ser; (3)-(4) roztwór *L*-Ser przechowywany przez 11 dni; (5)-(6) świeżo sporządzony roztwór *D*-Ser; (7)-(8) roztwór *D*-Ser przechowywany przez 11 dni; (9)-(10) świeżo sporządzony roztwór *DL*-Ser; (11)-(12) roztwór *DL*-Ser przechowywany przez 11 dni [176]

Badania z zastosowaniem chromatografii cienkowarstwowej sprzężonej z densytometrią wykazały, że największą dynamikę peptyzacji wykazuje roztwór binarny dwóch enancjomerów Ser. Różnica stężeń między przechowywanym a świeżym roztworem *DL*-Ser była największa. Intensywność piku na densytogramie (Rys. 33(c)) dla świeżo sporządzonego roztworu *DL*-Ser sięga 836,45 mAV, a dla roztworu przechowywanego zaledwie 332,86 mAV. Mniejszą dynamikę peptyzacji wykazał roztwór *D*-Ser, gdzie na Rys. 33(b) pik na densytogramie odpowiadający przechowywanemu roztworowi *D*-Ser osiągnął wartość 621,08 mAV, a świeżemu 958,00 mAV. Roztwór *L*-Ser wykazał najmniejszą dynamikę peptyzacji, a piki na densytogramie na Rys. 33(a) wykazały bardzo zbliżoną wartość (824,87 mAV dla roztworu świeżo sporządzonego, oraz 792,27 mAV dla roztworu przechowywanego przez 11 dni). Natomiast na zdjęciu wywołanej płytki chromatograficznej (Rys. 33(B)(1)-(12)) nie widać znaczącej różnicy między pasmami chromatograficznymi odpowiadającymi za świeże i przechowywane roztwory aminokwasów. Wszystkie pasma odpowiadające za monomeryczne formy aminokwasów osiągają tą samą wartość $R_F = 0{,}32 \pm 0{,}02$.

2.2. WYSOKOSPRAWNA CHROMATOGRAFIA CIECZOWA *L*-SER, *D*-SER I *DL*-SER

Zastosowanie wysokosprawnej chromatografii cieczowej z detektorem rozproszenia światła (HPLC-ELSD) umożliwiło obserwację zmian stężeń badanych aminokwasów, a tym samym potwierdziło zajście oscylacyjnej peptyzacji w roztworach *L*-Ser, *D*-Ser oraz *DL*-Ser. W trakcie monitorowania badanych aminokwasów ich stężenia zmieniały się w sposób oscylacyjny. Zmiany stężeń aminokwasów były spowodowane powstawaniem i rozpadem peptydów badanych aminokwasów. Przykładowe chromatogramy otrzymane podczas prowadzenia badań zostały przedstawione na Rys. 34.

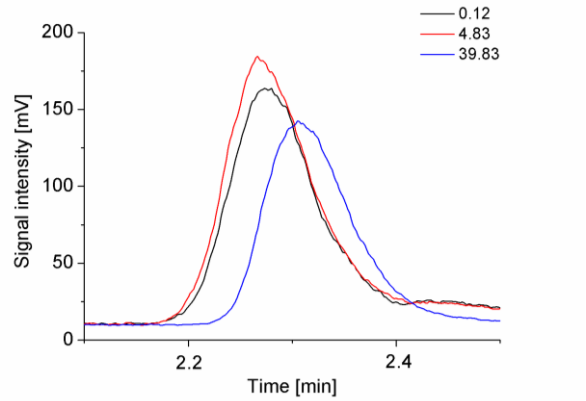

Rys. 34. Przykładowe chromatogramy *L*-Ser zarejestrowane przy pomocy detektora ELSD po upływie 0,12; 4,83; 39,83 h [176]

Zaprezentowane chromatogramy otrzymane z monitorowania *L*-Ser przez okres 40 h pokazują, jak wysokości pików *L*-Ser zmieniają się w trakcie przechowywania roztworu aminokwasu, co potwierdza zajście peptyzacji. Zaprezentowane na Rys. 34 wyniki zostały zarejestrowane zaraz na początku analizy (w 0,12 h), po 4,83 h analizy i na końcu trwania analizy.

Wykres zmian stężeń badanych aminokwasów w czasie trwania analizy został przedstawiony na Rys. 35.

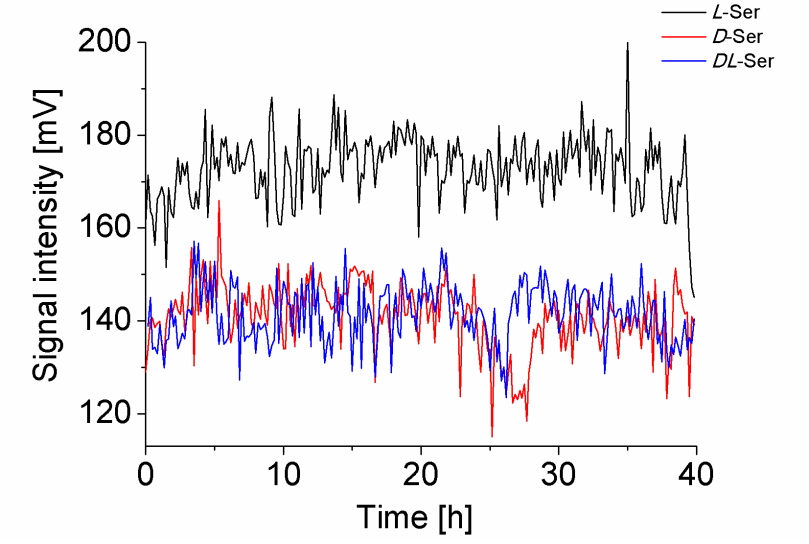

Rys. 35. Zmiany wysokości pików chromatograficznych *L*-Ser, *D*-Ser oraz *DL*-Ser w funkcji czasu zarejestrowane przy pomocy detektora ELSD w przedziale czasowym 0-40 h przechowywania próbki [176]

Na Rys. 35 przedstawiono zmiany maksimów wysokości pików chromatograficznych zarejestrowane w czasie 40 h trwania analiz zarówno dla pojedynczych enancjomerów, jak i mieszaniny dwuskładnikowej. Widać tutaj, że we wszystkich roztworach aminokwasów stężenia zmieniały się w sposób niemonotoniczny, co potwierdza, iż badany proces ma charakter oscylacyjny. Zmiany te są spowodowane powstawaniem peptydów i są bardzo zbliżone dla roztworu *D*-Ser (114,9-165,9 mV) i *DL*-Ser (123,4-157,1 mV). Dla roztworu *L*-Ser (145,03-201,44 mV) przedział zmian stężeń utrzymuje się na najwyższym poziome, co wykazuje, że peptyzacja *L*-Ser zachodzi w najsłabszej mierze. Przedstawione wyniki pokrywają się z wynikami uzyskanymi podczas analiz prowadzonych techniką TLC.

2.3. SPEKTROMETRIA MAS – *L*-SER, *D*-SER I *DL*-SER

W celu potwierdzenia, że roztwory badanych związków zawierają peptydy oraz sprawdzenia, jakie produkty obecne są w roztworach, wykonano analizę przechowywanych roztworów *L*-, *D*- i *DL*-Ser techniką spektrometrii mas. Uzyskane widma mas zostały przedstawione na Rys. 36.

(a)

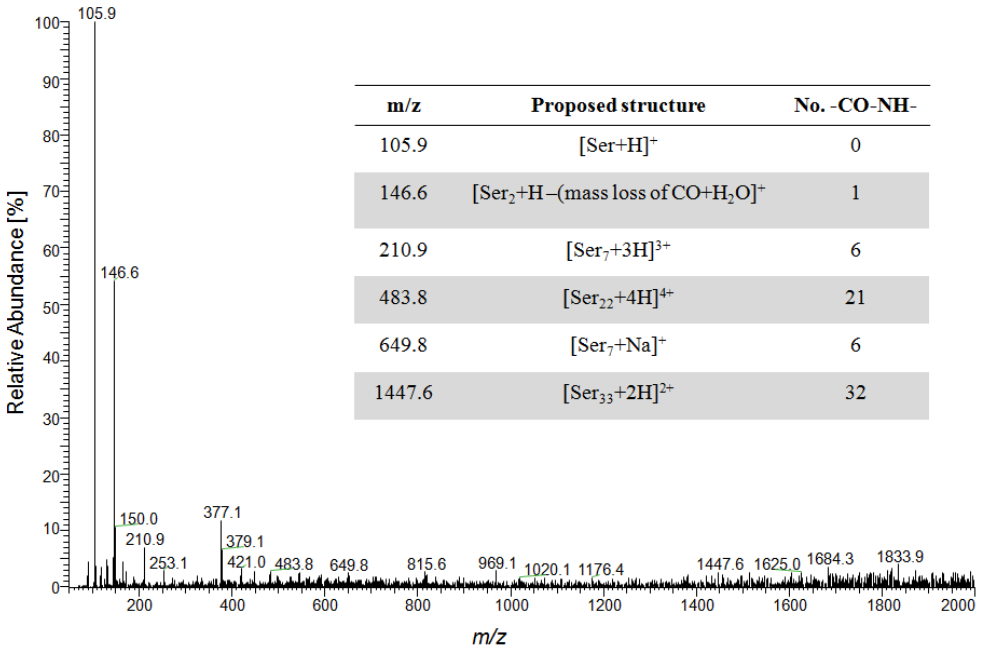

m/z	Proposed structure	No. -CO-NH-
105.9	$[Ser+H]^+$	0
146.6	$[Ser_2+H-(\text{mass loss of } CO+H_2O)]^+$	1
210.9	$[Ser_7+3H]^{3+}$	6
483.8	$[Ser_{22}+4H]^{4+}$	21
649.8	$[Ser_7+Na]^+$	6
1447.6	$[Ser_{33}+2H]^{2+}$	32

(b)

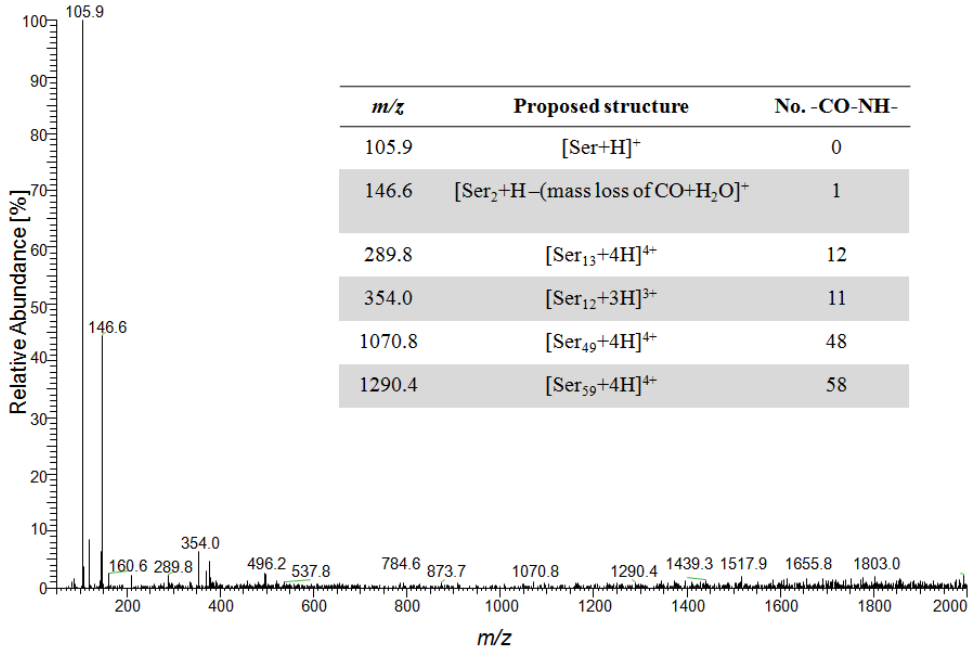

m/z	Proposed structure	No. -CO-NH-
105.9	$[Ser+H]^+$	0
146.6	$[Ser_2+H-(\text{mass loss of } CO+H_2O)]^+$	1
289.8	$[Ser_{13}+4H]^{4+}$	12
354.0	$[Ser_{12}+3H]^{3+}$	11
1070.8	$[Ser_{49}+4H]^{4+}$	48
1290.4	$[Ser_{59}+4H]^{4+}$	58

(c)

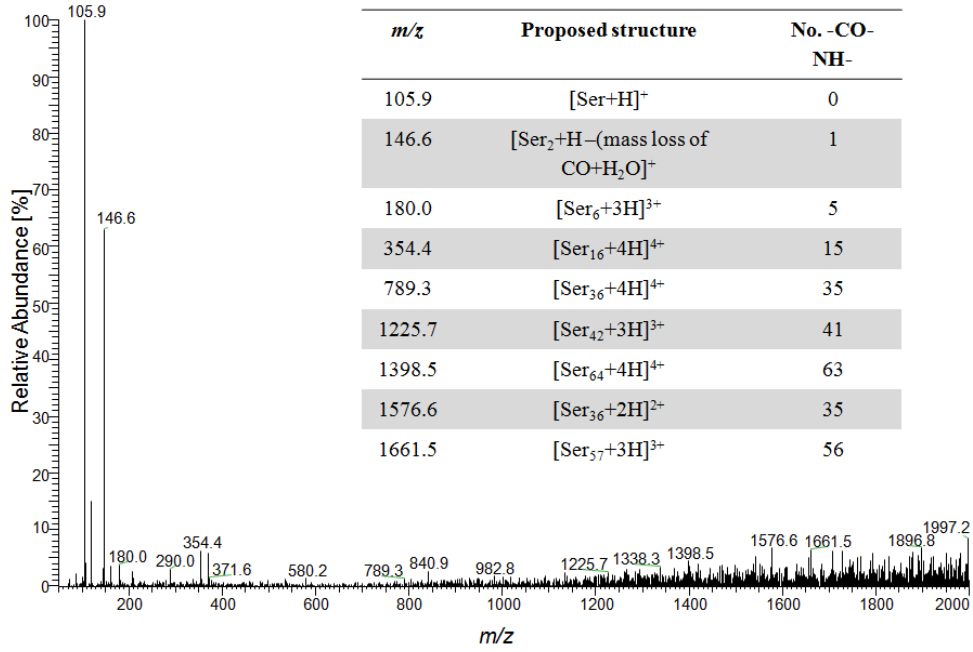

m/z	Proposed structure	No. -CO-NH-
105.9	$[Ser+H]^+$	0
146.6	$[Ser_2+H-(\text{mass loss of } CO+H_2O)]^+$	1
180.0	$[Ser_6+3H]^{3+}$	5
354.4	$[Ser_{16}+4H]^{4+}$	15
789.3	$[Ser_{36}+4H]^{4+}$	35
1225.7	$[Ser_{42}+3H]^{3+}$	41
1398.5	$[Ser_{64}+4H]^{4+}$	63
1576.6	$[Ser_{36}+2H]^{2+}$	35
1661.5	$[Ser_{57}+3H]^{3+}$	56

Rys. 36. Widma mas oraz tabele zawierające wybrane sygnały analityczne obecne w widmach mas przechowywanych próbek (a) *L*-Ser, (b) *D*-Ser i (c) *DL*-Ser [176]

Przedstawione widma mas potwierdzają różną dynamikę procesu peptyzacji badanych aminokwasów. Na podstawie wyników z TLC wysnuto wniosek, iż *DL*-Ser peptyzuje najszybciej, natomiast *L*-Ser oraz *D*-Ser peptyzują znacznie wolniej. Na Rys. 36(a)-(b) widać, że w wyniku przechowywania roztworów aminokwasów (*L*-Ser oraz *D*-Ser) powstały peptydy, których masy sięgają 2000 Da, a otrzymane widma mas są do siebie podobne. W przypadku widma mas *DL*-Ser przedstawionego na Rys. 36(c) również są obecne piki pochodzące od peptydów, jednak ich intensywności są znacznie większe, niż w przypadku pojedynczych enancjomerów Ser, co dodatkowo potwierdza różną dynamikę peptyzacji badanych enancjomerów i racematu Ser.

2.4. TURBIDYMETRYCZNE I POLARYMATRYCZNE BADANIA *L*-SER, *D*-SER I *DL*-SER

W celu sprawdzenia, czy w badanych roztworach aminokwasów powstają struktury peptydowe, wykonano badania turbidymetryczne. Na Rys. 37 zostały przestawione wykresy zmian mętności poszczególnych badanych roztworów.

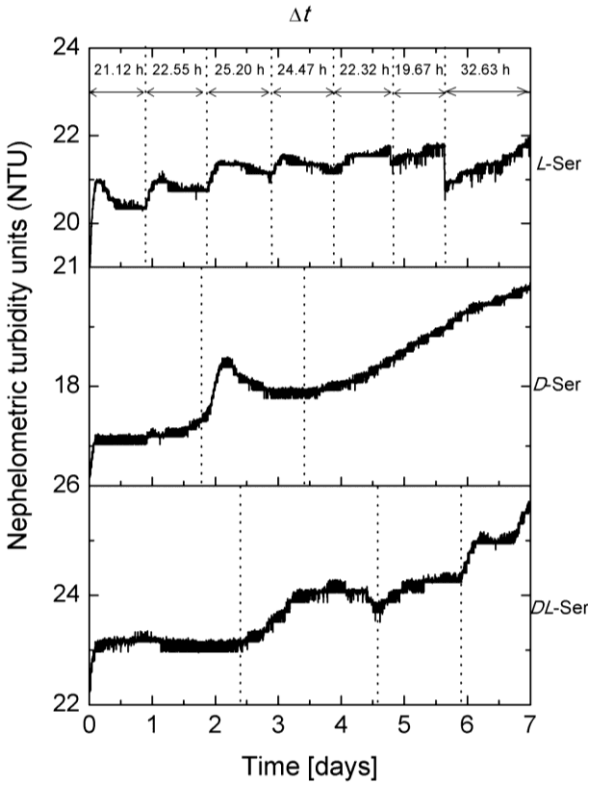

Rys. 37. Zmiany mętności roztworów *L*-Ser, *D*-Ser oraz *DL*-Ser zarejestrowane w trybie ciągłym przez okres 7 dni [177]

W przypadku wszystkich przebadanych roztworów mętność zmienia się w sposób niemonotoniczny. Najciekawsze rezultaty analizy turbidymetrycznej zostały otrzymane dla *L*-Ser. W tym przypadku zaobserwowano 24-godzinne cykle zmiany zmętnienia, natomiast w przypadku *D*-Ser obserwujemy jedynie jeden wyraźny skok mętności między drugim, a trzecim dniem przechowywania próbki. Ostatni wykres dla *DL*-Ser jest jakby połączeniem dwóch poprzednich wykresów: początkowo obserwujemy jeden wyraźny skok mętności między trzecim, a piątym dniem przechowywania próbki, a następnie rozpoczynają się dobowe cykle, jak w przypadku *L*-Ser.

W celu sprawdzenia, czy badane aminokwasy ulegają reakcji inwersji chiralnej, wykonano badania polarymetryczne. Na Rys. 38 zostały przedstawione wyniki badań polarymetrycznych dla *L*-Ser, *D*-Ser oraz *DL*-Ser.

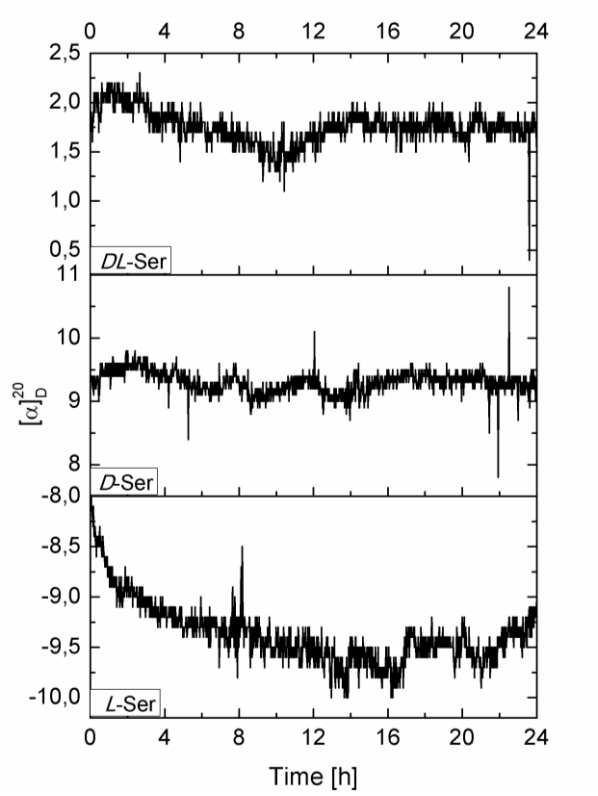

Rys. 38. Oscylacyjne zmiany skręcalności właściwej $[\alpha]_D$ w funkcji czasu dla wodnych roztworów *L*-Ser, *D*-Ser oraz *DL*-Ser

Na przedstawionych wykresach można zaobserwować, iż skręcalność właściwa w przypadku wszystkich badanych roztworów zmienia się w sposób niemonotoniczny. W przypadku *L*-Ser skręcalność właściwa oscylacyjnie maleje od -7,80^o do -10,00^o (wartość literaturowa skręcalności właściwej $[\alpha]_D$ dla wodnego roztworu *L*-Ser wynosi -7,589^o± 0,060 [178]), natomiast w przypadku *D*-Ser wartość ta oscyluje wokół wartości +9^o (wartość literaturowa skręcalności właściwej $[\alpha]_D$ dla wodnego roztworu *D*-Ser wynosi +7,495± 0,060 [178]). Skręcalność właściwa roztworu *DL*-Ser jest połączeniem dwóch poprzednich wykresów – początkowo maleje, a następnie oscyluje wokół jednej wartości (+1,75^o).

3. CHROMATOGRAFICZNE BADANIA SAMORZUTNEJ PEPTYZACJI *L*-MET

3.1. WYSOKOSPRAWNA CHROMATOGRAFIA CIECZOWA *L*-MET

W pierwszym etapie prowadzonych badań został przeprowadzony monitoring zmian stężenia *L*-Met w czasie przechowywania tego aminokwasu. Badania w układzie HPLC-ELSD były prowadzone w trybie ciągłym przez 30 godzin. Wykres zmian wysokości piku chromatograficznego (a więc i zmian stężenia monomerycznej *L*-Met) w funkcji czasu został przedstawiony na Rys. 39.

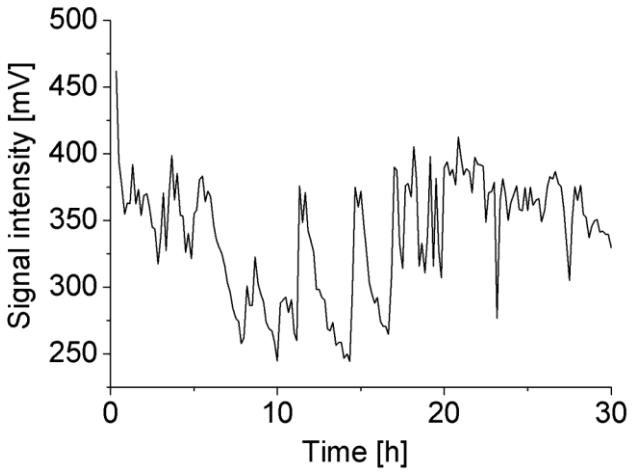

Rys. 39. Zmiany wysokości piku chromatograficznego *L*-Met w funkcji czasu, zarejestrowane przy pomocy detektora ELSD w przedziale czasowym 0-30h przechowywania próbki [179]

Na przedstawionym wykresie można zaobserwować zarówno spadek, jak i wzrost stężenia badanego aminokwasu. Początkowy spadek stężenia *L*-Met świadczy o tworzeniu się peptydów w trakcie przechowywania roztworu, a obserwowane wzrosty stężenia monomerycznej formy aminokwasu świadczą o rozpadzie powstałych peptydów do formy monomerycznej *L*-Met. Dodatkowo przedstawiona krzywa ma charakter nieliniowy, co potwierdza oscylacyjny przebieg reakcji peptyzacji.

3.2. SPEKTROMETRIA MAS – *L*-MET

Aby stwierdzić, czy w badanym roztworze znajdują się peptydy, wykonano analizę HPLC-MS, dla świeżo sporządzonego roztworu *L*-Met i dla próbki po upływie 168,5 h przechowywania, a otrzymane widma mas zostały przedstawione na Rys. 40.

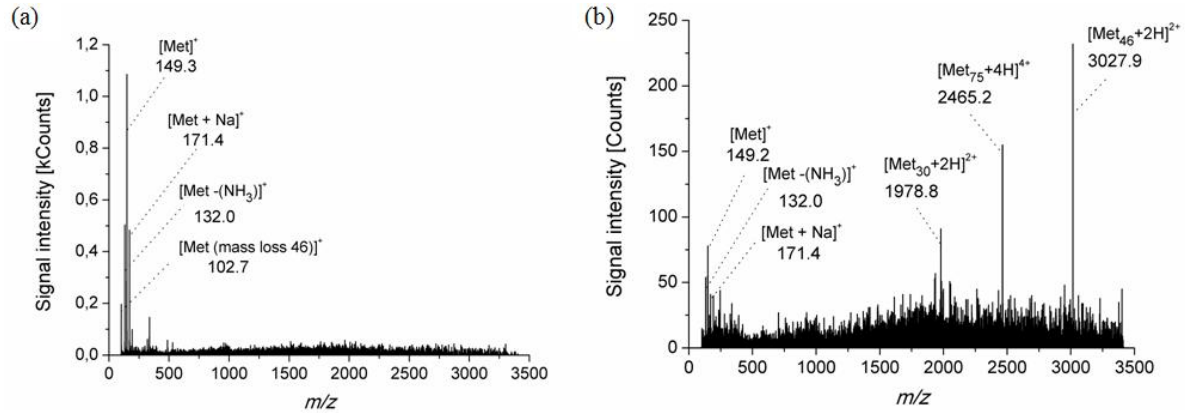

Rys. 40. Widma mas zarejestrowane dla *L*-Met po upływie: (a) 0,20 h; (b) 168,5 h czasu przechowywania wykonane przy pomocy układu HPLC-MS

Widma mas roztworu *L*-Met potwierdzają, że reakcja samorzutnej peptyzacji zachodzi podczas przechowywania roztworu aminokwasu. Na Rys. 40(a) zaprezentowano widmo mas świeżo sporządzonego roztworu (po upływie 0,20 h), natomiast na Rys. 40(b) widmo mas roztworu przechowywanego przez 168,5 h. Różnice pomiędzy zaprezentowanymi widmami są znaczne. Na widmie świeżo sporządzonego roztworu widoczny jest pik molekularny $[Met]^+$, pseudomolekularny $[Met+Na]^+$ oraz dwa piki fragmentacyjne, $[Met-(NH_3)]^+$ oraz [Met (mass loss 46)]$^+$, odpowiadające pikom prezentowanym w literaturze [180], natomiast piki pochodzące od peptydów mają niewielką intensywność. W przypadku widma mas próbki przechowywanej przez 168,5 h sytuacja jest odwrotna: pik molekularny stanowi jedynie

nieco ponad 30% intensywności piku pochodzącego od peptydu o *m/z* 3027,9 odpowiadającego strukturze $[Met_{46}+2H]^{2+}$. Na widmie obecne są również charakterystyczne piki fragmentacyjne $[Met\text{-}(NH_3)]^+$, oraz [Met (mass loss 46)]$^+$, a także pik pseudomolekularny $[Met+Na]^+$. Intensywność pików pochodzących od peptydów jest znacząca, co potwierdza, że w przechowywanej próbce zaszła reakcja samorzutnej peptyzacji.

4. CHROMATOGRAFICZNE BADANIA SAMORZUTNEJ PEPTYZACJI PARY AMINOKWASÓW *L*-SER – *L*-MET

4.1. WYSOKOSPRAWNA CHROMATOGRAFIA CIECZOWA *L*-SER – *L*-MET

Kolejnym etapem prowadzonych badań było połączenie aminokwasów w układ dwuskładnikowy (*L*-Ser–*L*-Met), oraz monitorowanie przebiegu reakcji oscylacyjnej peptyzacji. Pierwszym krokiem był monitoring zmian stężenia badanych aminokwasów w trybie ciągłym z wykorzystaniem układu HPLC-ELSD. Przykładowy chromatogram pokazujący dobry rozdział do linii podstawowej badanych związków został przedstawiony na Rys. 41.

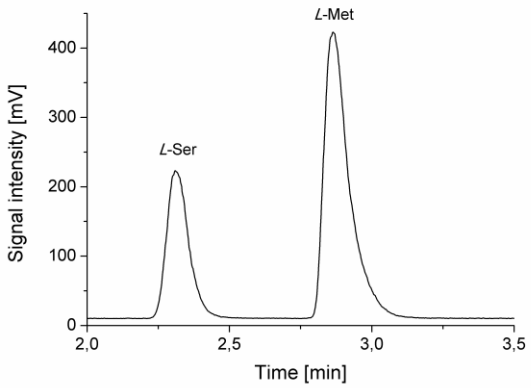

Rys. 41. Przykładowy chromatogram *L*-Ser–*L*-Met zarejestrowany przy pomocy detektora ELSD [179]

Na Rys.42(a)-(c) zostały zaprezentowane wykresy zmian stężeń badanych aminokwasów w funkcji czasu. Na Rys. 42(a) oraz Rys. 42(b) zostały przedstawione wykresy zmiany stężeń *L*-Ser i *L*-Met w układzie jednoskładnikowym, a na Rys. 42(c) w układzie dwuskładnikowym.

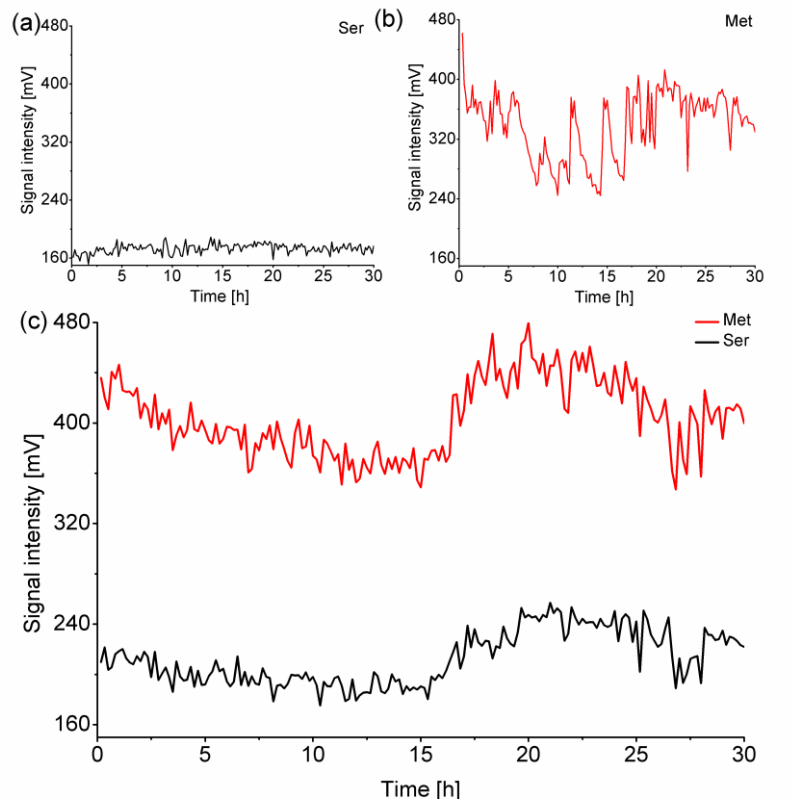

Rys. 42. (a) Zmiany wysokości piku chromatograficznego w funkcji czasu dla *L*-Ser; (b) Zmiany wysokości piku chromatograficznego w funkcji czasu dla *L*-Met; (c) Zmiany wysokości pików chromatograficznych w funkcji czasu dla układu *L*-Ser–*L*-Met zarejestrowane przy pomocy detektora ELSD (0-30h) [179]

Na podstawie przedstawionych wykresów trzydziestogodzinnej rejestracji wysokości pików aminokwasów dla układów jednoskładnikowych *L*-Ser oraz *L*-Met, a także dla układu dwuskładnikowego *L*-Ser–*L*-Met można zauważyć, iż stężenia badanych aminokwasów zarówno w przypadku badań układów jedno-, jak i dwuskładnikowych zmieniają się w sposób niemonotoniczny, co potwierdza, iż badany proces ma charakter oscylacyjny. Ponadto amplitudy zmian stężeń aminokwasów w układach jednoskładnikowych są znacznie większe, niż w przypadku układu dwuskładnikowego. Sugeruje to, że proces peptyzacji oraz rozpadu powstałych peptydów do monomerycznych form aminokwasów charakteryzuje się różną dynamiką. Kolejną ważną obserwacją jest fakt, iż badając aminokwasy w układach jednoskładnikowych otrzymano dwie zupełnie różne krzywe. W przypadku *L*-Ser linia trendu jest bardziej uporządkowana, ma mniejsze amplitudy zmian stężeń w porównaniu do wykresu *L*-Met, na którym obserwuje się wyraźne, gwałtowne skoki

stężeń badanego aminokwasu. Natomiast w przypadku układu dwuskładnikowego *L*-Ser–*L*-Met otrzymano dwie w pełni zsynchronizowane krzywe, czyli gdy stężenie jednego z aminokwasów rośnie to stężenie drugiego również rośnie i odwrotnie. Taki wynik sugeruje tworzenie się w badanym roztworze dwuskładnikowym nie tylko homopeptydów, ale również heteropeptydów. Można również stwierdzić, że proces peptyzacji oraz rozpadu powstałych peptydów w przypadku mieszaniny dwuskładnikowej przypomina bardziej przypadek pojedynczej *L*-Met nawet wówczas, gdy amplitudy zmian stężeń obu aminokwasów nie są tak duże, jak w przypadku układu jednoskładnikowego *L*-Met to ogólny trend pozostaje zachowany – początkowy spadek stężenia, a następnie jego wzrost. Nie można jednak pominąć wpływu Ser w tym przypadku podejrzewa się, że oba aminokwasy współdziałają ze sobą *L*-Met odpowiada za ogólny trend krzywej, natomiast *L*-Ser za amplitudy zmian stężeń.

4.2. SPEKTROMETRIA MAS – *L*-SER – *L*-MET

W celu określenia, czy w przechowywanych roztworach aminokwasów znajdują się zarówno homo- jak i heteropeptydy pochodne *L*-Ser i *L*-Met wykonano dodatkowe badania techniką HPLC-MS. Na Rys. 43 przedstawiono przykładowy chromatogram oraz odpowiednie widma mas zarejestrowane dla roztworu *L*-Ser–*L*-Met przechowywanego przez okres 9 dni.

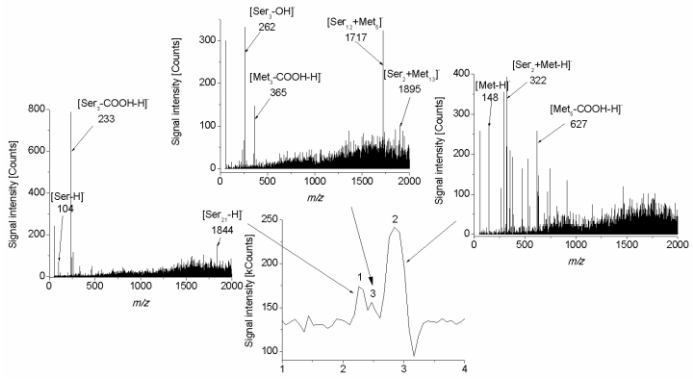

Rys. 43. Chromatogram oraz widma mas zarejestrowane dla układu dwuskładnikowego *L*-Ser–*L*-Met: (1) Ser; (2) Met; (3) główny produkt peptyzacji z wykorzystaniem techniki HPLC-MS [179]

Otrzymane widma mas potwierdzają obecność zarówno homo-, jak i heteropeptydów w roztworze badanych aminokwasów. Na widmie mas piku 1 (Ser) dominuje pik o *m/z* 233 odpowiadający $[Ser_3\text{-}COOH\text{-}H]^-$, ale obecny jest również pik

pseudomolekularny aminokwasu $[Ser-H]^-$ o *m/z* 104; reszta pików odpowiadających peptydom wykazuje niewielką intensywność. W przypadku widma mas Met (2) obecny jest pik pseudomolekularny $[Met-H]^-$ o *m/z* 148, ale widać tutaj znaczną dominację pików odpowiadających peptydom. Na chromatogramie (Rys. 43) można również zaobserwować pik 3, będący głównym produktem peptyzacji aminokwasów. W przypadku widma mas produktu (pik 3) nieobecne są piki molekularne aminokwasów, natomiast jest szereg pików pochodzących od heteropeptydów, jak np. o *m/z* 1717 oraz 1895 odpowiadające następującym strukturom $[Ser_{12}+Met_5]^-$ oraz $[Ser_2+Met_{13}]^-$.

5. BADANIA SAMORZUTNEJ PEPTYZACJI *L*-HIS, *L*-THR ORAZ ICH MIESZANINY DWUSKŁADNIKOWEJ (*L*-HIS – *L*-THR)

5.1. BADANIA POJEDYNCZYCH AMINOKWASÓW BIAŁKOWYCH (*L*-HIS, *L*-THR)

5.1.1. BADANIE SAMORZUTNEJ PEPTYZACJI *L*- HIS

Kolejnym aminokwasem poddanym serii badań pod kątem samorzutnej peptyzacji była *L*-His. Wykres zmian wysokości piku chromatograficznego (a więc i zmian stężenia monomerycznej *L*-His) w funkcji czasu został przedstawiony na Rys. 44 (0-30h).

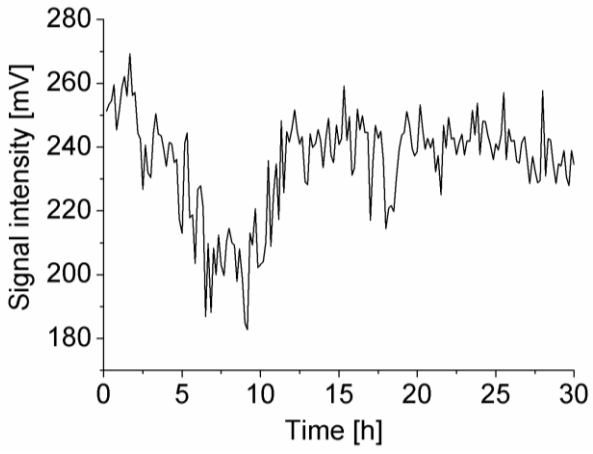

Rys. 44. Zmiany wysokości piku chromatograficznego *L*-His w funkcji czasu zarejestrowane przy pomocy detektora ELSD w przedziale czasowym 0-30h przechowywania próbki

Na przedstawionym wykresie pokazano, że w pierwszych godzinach po sporządzeniu roztworu *L*-His stężenie tego aminokwasu gwałtownie maleje. Zmiana stężenia *L*-His jest spowodowana szybką peptyzacją. Duża zdolność His do tworzenia peptydów bezpośrednio w układzie HPLC-ELSD spowodowała, że duże cząsteczki peptydów osadzały się na kolumnie, co praktycznie uniemożliwiło ich wymywanie z układu.

W celu sprawdzenia, jakie produkty powstały w badanym roztworze, wykonano analizę HPLC-MS oraz LC-MS, a otrzymane widma mas pokazano na Rys. 45 i 46.

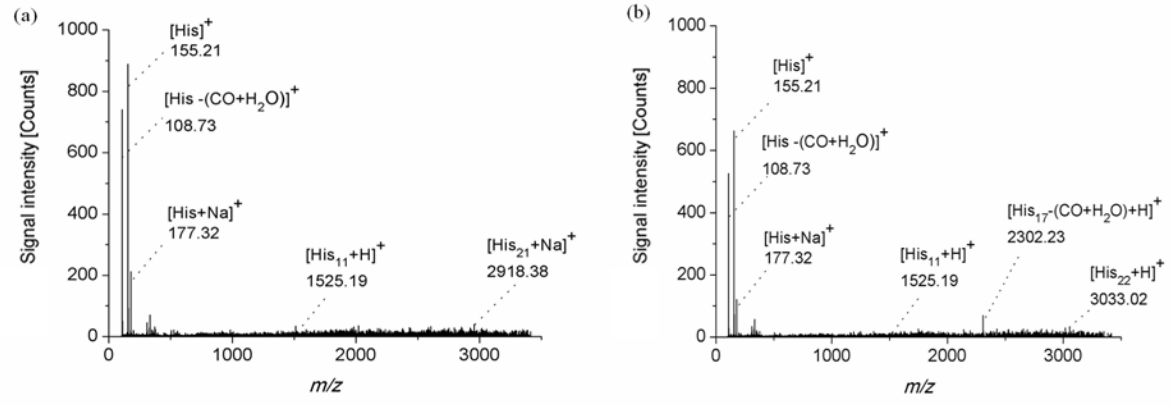

Rys. 45. Widma mas zarejestrowane dla *L*-His: a) po upływie 4,00 h; b) po upływie 52,50 h czasu przechowywania wykonane przy pomocy układu HPLC-MS [181]

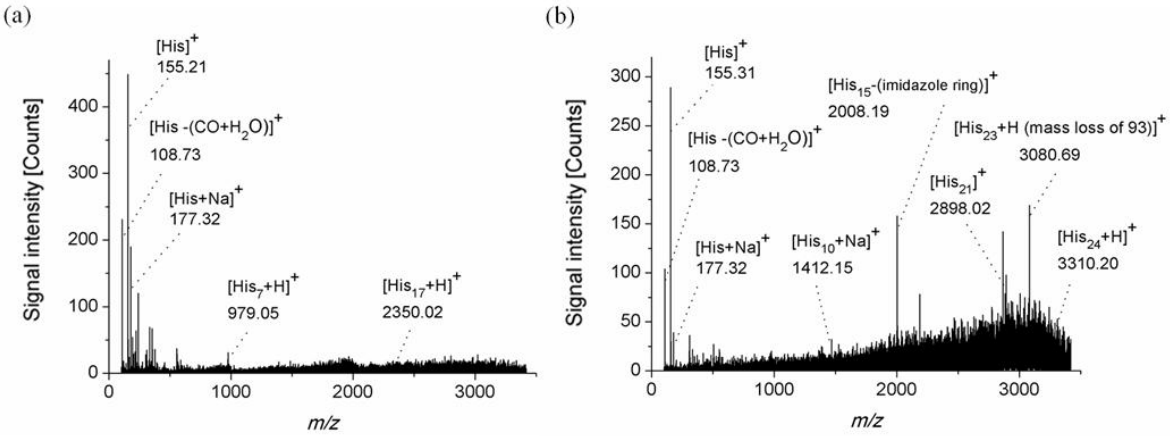

Rys. 46. Widma mas zarejestrowane dla *L*-His: (a) po upływie 0,20 h; (b) po upływie 1031,5 h wykonane przy pomocy układu LC-MS [181]

Widma wykonane w układzie HPLC-MS różnią się między sobą nieznacznie (Rys. 45(a)-(b)). Pod wpływem przechowywania próbki obserwujemy wyraźny spadek intensywności piku monomeru His (*m/z* = 155,21), a także pików: fragmentacyjnego *m/z* 108,73 $[His(-CO+H_2O)]^+$ [180] i pseudomolekularnego *m/z* 177,32 $[His+Na]^+$, pojawiają się również nieco bardziej intensywne piki peptydów, lecz różnica nie jest znacząca. Jednak His ma tendencję do zatrzymywania się na kolumnie, jej peptyzacja jest szybka, a powstałe peptydy są na tyle duże, że nie przechodzą wystarczająco szybko przez układ chromatograficzny. Aby wykluczyć efekt zatrzymywania się większych molekuł peptydów His na kolumnie, co nastąpiło podczas analizy techniką HPLC, zastosowano technikę LC-MS z wykorzystaniem jedynie prekolumny.

Wyniki analizy LC-MS przedstawiono na Rys. 46(a)-(b). Na Rys. 46(a) pokazano widmo mas zarejestrowane zaraz po sporządzeniu roztworu histydyny (0,20 h) i na nim widać dominujący pik pochodzący od His o wartości *m/z* równej 155,21. Wyraźny jest również pik o *m/z* 177,32, który również odpowiada formie monomerycznej His lecz z przyłączonym atomem sodu. Obecne są również piki o większych wartościach *m/z*, jak np. piki 979,05 i 2350,03, odpowiadające kolejno strukturom $[His_7+H]^+$ i $[His_{17}+H]^+$, jednak intensywność pików odpowiadających peptydom jest znikoma w porównaniu z pikiem głównym (*m/z* 155,21). Na Rys. 46(b) przedstawiono widmo mas zarejestrowane po upływie 1031,50 h od sporządzenia roztworu His. Na widmie tym widać intensywny sygnał formy monomerycznej His (*m/z* 155,31), ale podobną intensywność mają też piki odpowiadające peptydom o *m/z* 1412,15, 2008,19 i 2898,02, które kolejno można przyporządkować strukturom: $[His_{10}+Na]^+$, $[His_{15}$-(pierścień imidazolowy)$]^+$ i $[His_{21}]^+$. Przedstawione widma mas pokazują, iż wcześniejsze przypuszczenie dotyczące osadzania się peptydów His na kolumnie w układzie HPLC było słuszne, co widać na widmie przechowywanej próbki, gdzie piki peptydów pochodnych His dochodzą do *m/z* 3500 Da.

5.1.2. BADANIE SAMORZUTNEJ PEPTYZACJI *L*-THR

Roztwór *L*-Thr również został poddany badaniom w układzie HPLC-ELSD podczas jego przechowywania, a wykres zmian wysokości piku chromatograficznego w funkcji czasu został przedstawiony na Rys. 47.

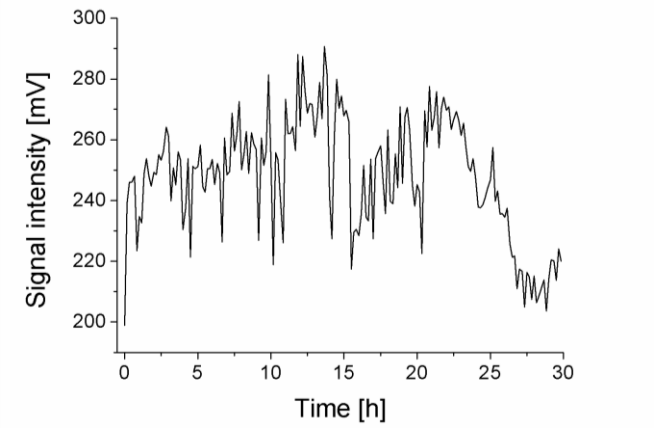

Rys. 47. Zmiany wysokości piku chromatograficznego *L*-Thr w funkcji czasu zarejestrowane przy pomocy detektora ELSD w przedziale czasowym 0-30h przechowywania próbki

Na krzywej przedstawionej na Rys. 47 można zaobserwować zarówno spadek, jak i wzrost stężenia aminokwasu, co świadczy o tym, iż peptydy zarówno powstają, jak i rozpadają się do formy monomerycznej. Dodatkowo nieliniowy charakter otrzymanej krzywej potwierdza, że badana reakcja ma charakter oscylacyjny. W celu udowodnienia, że w badanym roztworze powstają peptydy, przeprowadzono analizę HPLC-MS, a otrzymane widma mas zostały przedstawione na Rys. 48. Analiza HPLC-MS potwierdziła, iż wraz z upływem czasu przechowywania aminokwasu ilość powstałych peptydów wzrosła.

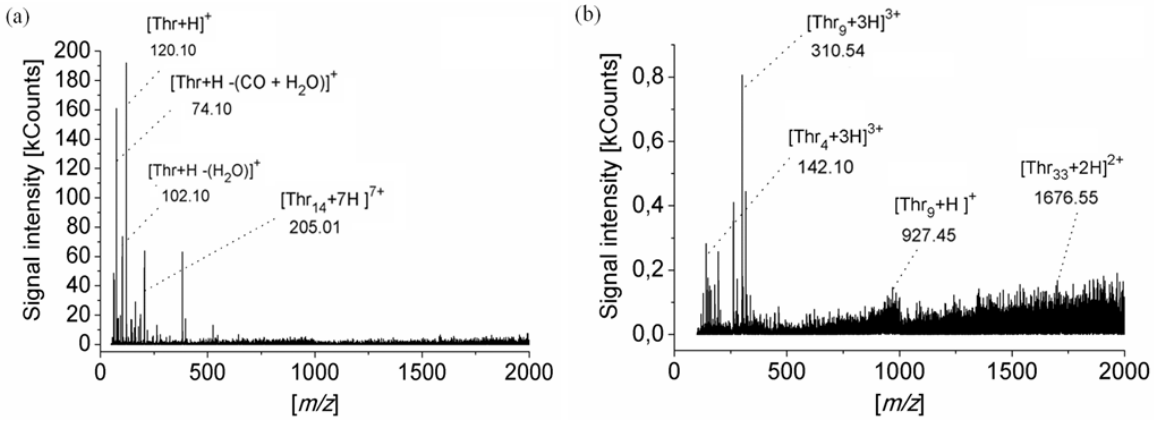

Rys. 48. Widma mas zarejestrowane dla *L*-Thr: (a) po upływie 0,20 h; (b) po upływie 135,20 h czasu przechowywania wykonane przy pomocy układu HPLC-MS

5.2. BADANIE SAMORZUTNEJ PEPTYZACJI UKŁADU DWUSKŁADNIKOWEGO *L*-HIS–*L*-THR

5.2.1. CHROMATOGRAFICZNE BADANIA *L*-HIS–*L*-THR

Kolejnym etapem prowadzonych badań było sprawdzenie jak połączenie *L*-His oraz *L*-Thr w układ dwuskładnikowy wpłynie na dynamikę procesu peptyzacji, oraz czy w wyniku samorzutnej peptyzacji powstaną również heteropeptydy badanych aminokwasów. Na Rys. 49 został przedstawiony przykładowy chromatogram badanej pary związków, który pokazuje, że piki pochodzące od aminokwasów były dobrze rozdzielone do linii podstawowej.

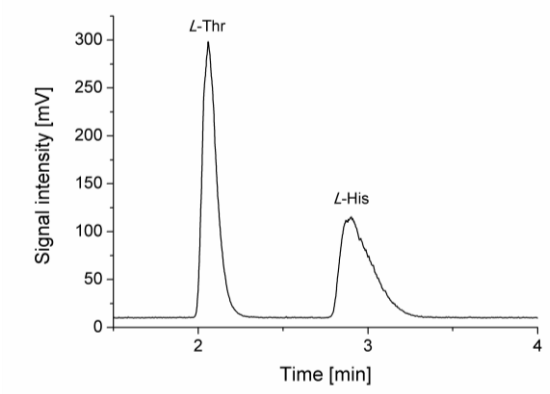

Rys. 49. Przykładowy chromatogram zarejestrowany przy pomocy detektora ELSD dla badanej pary związków [179]

Badania z wykorzystaniem układu HPLC-ELSD były prowadzone w trybie ciągłym przez 30 godzin, a wykresy zmian stężeń badanych aminokwasów w funkcji czasu zostały zaprezentowane na Rys. 50(a)-(c). Na Rys. 50(a) oraz 50(b) przedstawiono wykresy zmiany stężeń *L*-His i *L*-Thr w układach jednoskładnikowych, a na Rys. 50(c) w układzie dwuskładnikowym.

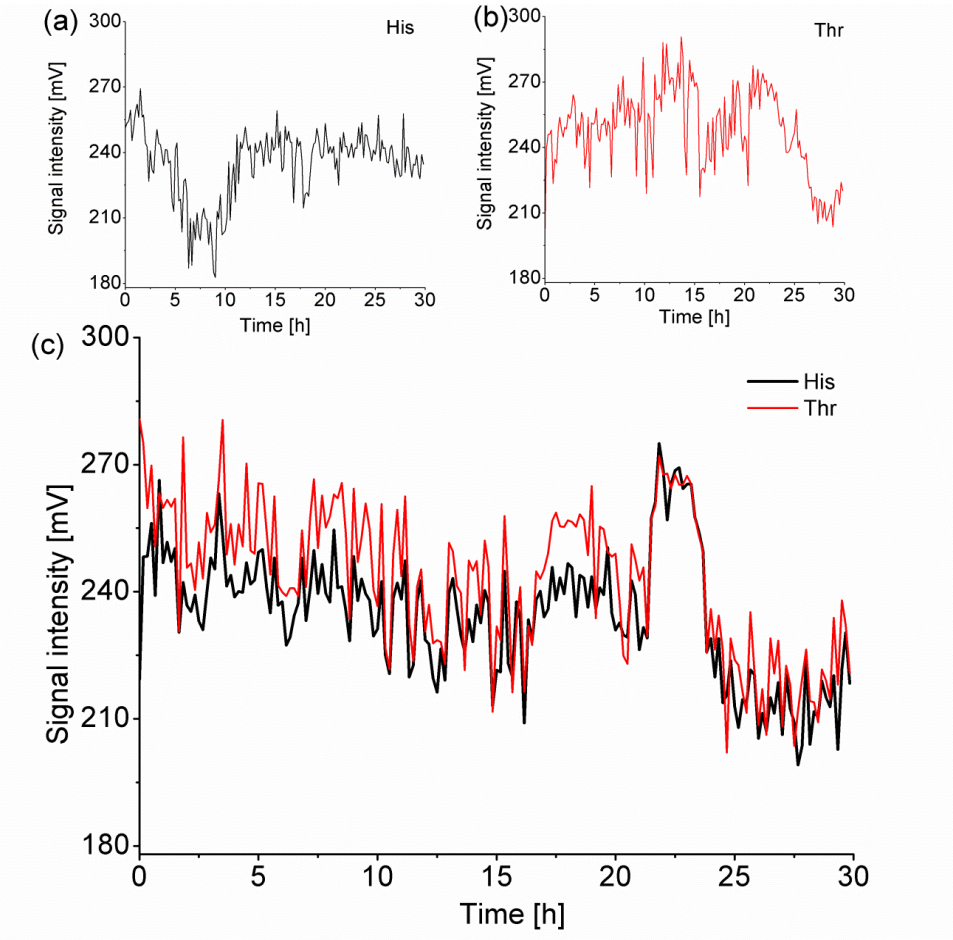

Rys. 50. (a) Zmiany wysokości piku chromatograficznego w funkcji czasu *L*-His; (b) Zmiany wysokości piku chromatograficznego w funkcji czasu *L*-Thr; (c) Zmiany wysokości pików chromatograficznych w funkcji czasu dla *L*-His–*L*-Thr zarejestrowane przy pomocy detektora ELSD (0-30h) [179]

Na podstawie przedstawionych wykresów można zauważyć, iż badane aminokwasy w układzie dwuskładnikowym w początkowej części eksperymentu idą niezależnie od siebie, a linia trendu nie jest zdeterminowana przez żaden z badanych związków i nie przypomina zachowań aminokwasów w układach jednoskładnikowych. Natomiast po upływie 15 godzin prowadzonych badań, można zauważyć, że zamiany na krzywej Thr są podobne jak w układzie His–Thr, co może sugerować wpływ na trend krzywej tego aminokwasu w układzie dwuskładnikowym. Warto również podkreślić, iż badając pojedyncze aminokwasy otrzymano dwie zupełnie różne krzywe, natomiast połączenie aminokwasów w parę His–Thr sprawiło, iż zmiany stężeń aminokwasów stały się silnie zsynchronizowane. Widoczna zależność między zmianami stężeń badanych aminokwasów w układzie dwuskładnikowym sugeruje, iż tworzą się nie tylko homopeptydy, ale również heteropeptydy.

5.2.2. SPEKTROMETRIA MAS UKŁADU DWUSKŁADNIKOWEGO *L*-HIS–*L*-THR

W celu potwierdzenia, iż w badanym roztworze aminokwasów obecne są peptydy oraz w celu przeprowadzenia ich identyfikacji wykonano badania techniką MS. Otrzymane widma mas wraz z tabelami zawierającymi wybrane sygnały analityczne znajdują się na Rys. 51.

Badania techniką MS zostały przeprowadzone dla przechowywanego przez okres 8 miesięcy dwuskładnikowego roztworu *L*-His–*L*-Thr. Na Rys. 51(a)-(b) przedstawiono widma mas układu *L*-His–*L*-Thr w jonizacji zarówno pozytywnej (Rys. 51(a)), jak i negatywnej (Rys. 51 (b)). Na otrzymanych widmach mas obserwujemy piki pseudomolekularne badanych aminokwasów ($[His+H]^+$, $[His-H]^-$, $[Thr+H]^+$, $[Thr-H]^-$). Można również zaobserwować liczne piki pochodzące od peptydów powstałych w wyniku reakcji samorzutnej peptyzacji. Na przedstawionych widmach dominują heteropeptydy, lecz można również zaobserwować pojawianie się homopeptydu takiego, jak $[Thr_3+2H]^{2+}$, o *m/z* 160,5. Wśród licznych heteropeptydów można wyróżnić dwa typy powstałych związków. Pierwszy to taki, w którym występuje znaczna przewaga jednego z badanych aminokwasów, a jako przykład mogą posłużyć następujące piki o *m/z* 484,9 ($[His_9+Thr_2+3H]^{3+}$), 775,8 ($[His_2+Thr_{12}+2Na]^{2+}$), 308,8 ($[His_3+Thr_8-4H]^{4-}$), 1316,0 ($[His_8+ Thr_2]^-$). Drugi typ to taki, w którym aminokwasy łączą się w stosunku stechiometrycznym, tutaj jako przykład może posłużyć następujący heteropeptyd $[Thr_2+His_2-3H]^{3-}$ o *m/z* równym 163,7. Otrzymane wyniki potwierdzają, że w układach wieloskładnikowych powstają również heteropeptydy.

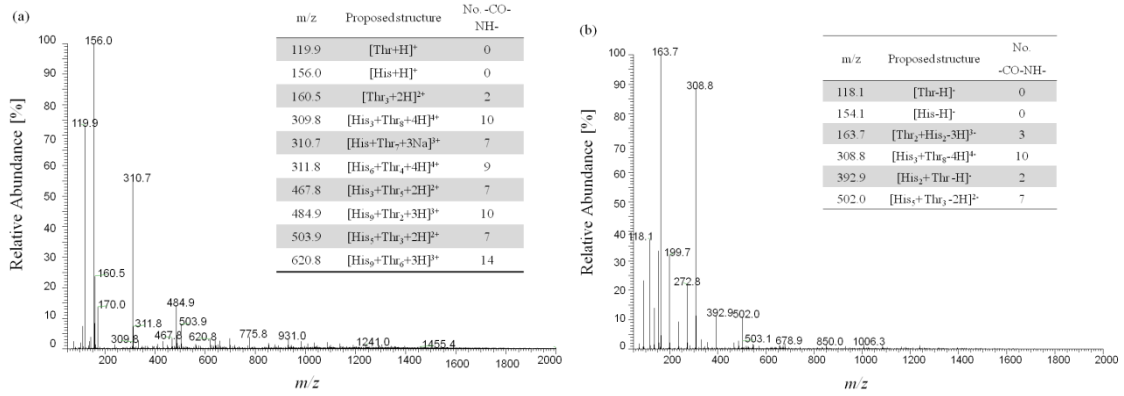

m/z	Proposed structure	No. -CO-NH-
119.9	$[Thr+H]^+$	0
156.0	$[His+H]^+$	0
160.5	$[Thr_3+2H]^{2+}$	2
309.8	$[His_3+Thr_8+4H]^{4+}$	10
310.7	$[His+Thr_7+3Na]^{3+}$	7
311.8	$[His_6+Thr_4+4H]^{4+}$	9
467.8	$[His_3+Thr_5+2H]^{2+}$	7
484.9	$[His_9+Thr_2+3H]^{3+}$	10
503.9	$[His_5+Thr_3+2H]^{2+}$	7
620.8	$[His_9+Thr_6+3H]^{3+}$	14

m/z	Proposed structure	No. -CO-NH-
118.1	$[Thr-H]^-$	0
154.1	$[His-H]^-$	0
163.7	$[Thr_2+His_2-3H]^{3-}$	3
308.8	$[His_3+Thr_8-4H]^{4-}$	10
392.9	$[His_2+Thr-H]^-$	2
502.0	$[His_5+Thr_3-2H]^{2-}$	7

Rys. 51. Widma mas oraz tabele zawierające wybrane sygnały analityczne obecne na tych widmach dla roztworu *L*-His-*L*-Thr przechowywanego przez okres 8 miesięcy (a) jonizacja pozytywna; (b) jonizacja negatywna [179]

5.2.3. BADANIA TURBIDYMETRYCZNE *L*-HIS–*L*-THR

Dodatkowo wykonano badania turbidymetryczne, które pozwalają zaobserwować efekty niewidoczne gołym okiem, co ma znaczenie dla zrozumienia mechanizmów samoorganizacji aminokwasów. Na Rys. 52 przedstawiono wykres zmian mętności roztworu *L*-His–*L*-Thr**.** Na przedstawionym wykresie obserwujemy zmiany mętności, co może świadczyć o tworzeniu się peptydów. Ponadto zmiany te mają charakter niemonotoniczny, co dodatkowo potwierdza, iż badana reakcja ma charakter oscylacyjny.

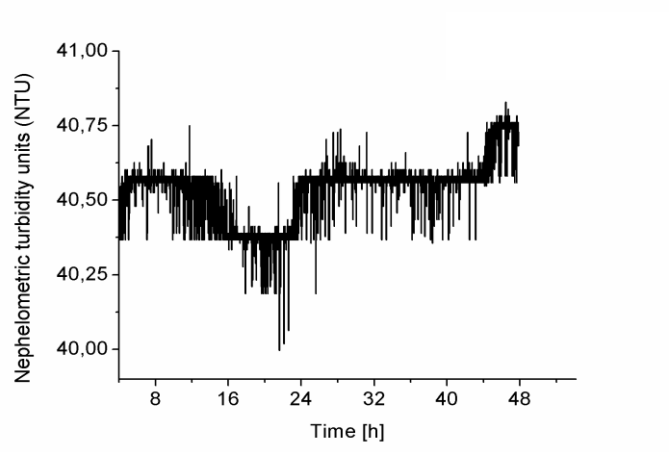

Rys. 52. Zmiany mętności roztworu pary aminokwasów *L*-His i *L*-Thr (0-48 h)

6. BADANIE SAMORZUTNEJ PEPTYZACJI UKŁADU DWUSKŁADNIKOWEGO AMINOKWASÓW *L*-PHE–*L*-PRO, ORAZ SAMOORGANIZACJI POWSTAŁYCH PEPTYDÓW DO NANOSTRUKTUR PEPTYDOWYCH

Kolejną parą badanych aminokwasów był układ *L*-Phe–*L*-Pro. Badania prowadzono z wykorzystaniem technik HPLC-ELSD, HPLC-DAD i LC-MS, a następnie badanie otrzymanych nanostruktur peptydowych prowadzono z wykorzystaniem technik LC-MS, IR, mikroskopii optycznej, SEM oraz turbidymetrii.

6.1. CHROMATOGRAFICZNE BADANIA SAMORZUTNEJ PEPTYZACJI UKŁADU *L*-PHE–*L*-PRO

Pierwszym ważnym krokiem badawczym było przeanalizowanie dynamiki procesu samorzutnej peptyzacji (układu *L*-Phe–*L*-Pro). W wyniku takiego procesu mogą tworzyć się zarówno homo- jak i heteropeptydy badanych aminokwasów. Na Rys. 53 przedstawiono niektóre możliwe produkty peptyzacji pary *L*-Phe–*L*-Pro do tri peptydów włącznie. Jak widać kombinacji jest wiele przy kondensacji jedynie trzech cząsteczek, a w miarę przyłączania kolejnych aminokwasów do łańcucha peptydowego ilość możliwych kombinacji gwałtownie wzrasta.

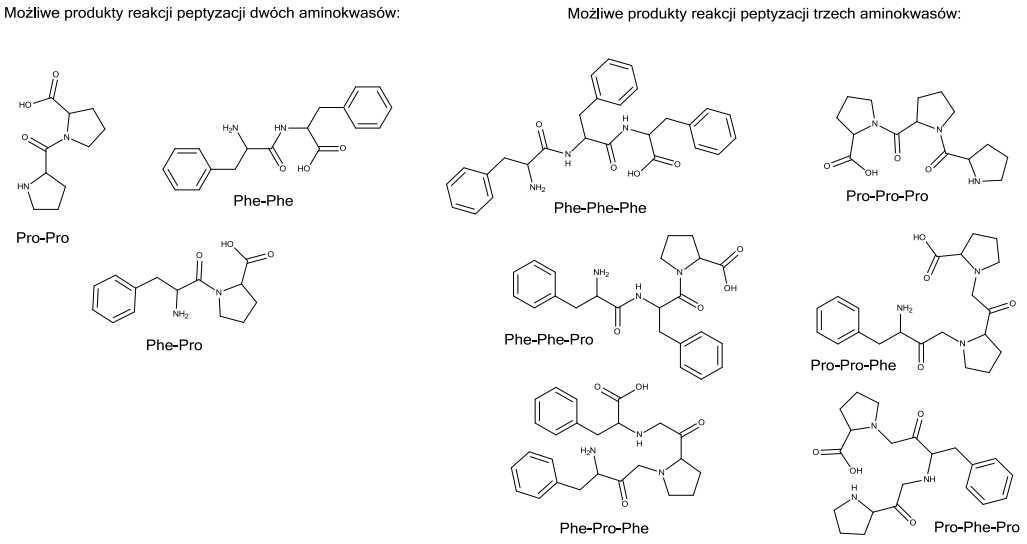

Rys. 53. Możliwe produkty peptyzacji w układzie (*L*-Phe–*L*-Pro) dla di- oraz tripeptydów

Podczas badań prowadzonych dla pary aminokwasów białkowych *L*-Phe–*L*-Pro techniką HPLC zastosowano dwa detektory: DAD oraz ELSD. Na Rys. 54 zaprezentowano przykładowy chromatogram, zarejestrowany na początku prowadzonych badań (po 2,9 h od sporządzenia roztworu) przy pomocy detektora ELSD. Na przedstawionym chromatogramie wyraźnie widać piki pochodzące od badanych aminokwasów, oraz można zauważyć, iż rozdział aminokwasów był pełny do linii podstawowej.

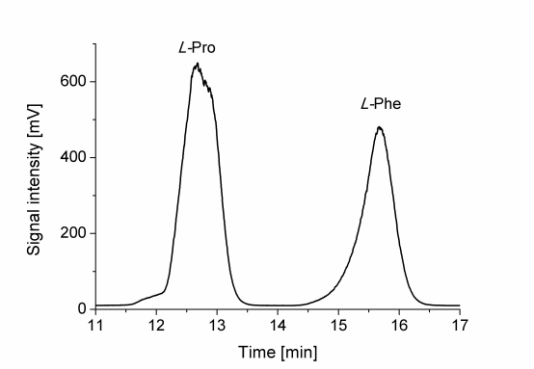

Rys. 54. Przykładowy chromatogram pary aminokwasów *L*-Phe-*L*-Pro zarejestrowany przy pomocy detektora ELSD badanej po upływie 2,9 h

Aby pokazać ogromne zróżnicowanie obrazu chromatograficznego, jakie zaobserwowano podczas 250 godzin monitorowania dynamiki procesu peptyzacji, na Rys. 55 przedstawiono cztery przykładowe chromatogramy, zarejestrowane podczas prowadzonych badań.

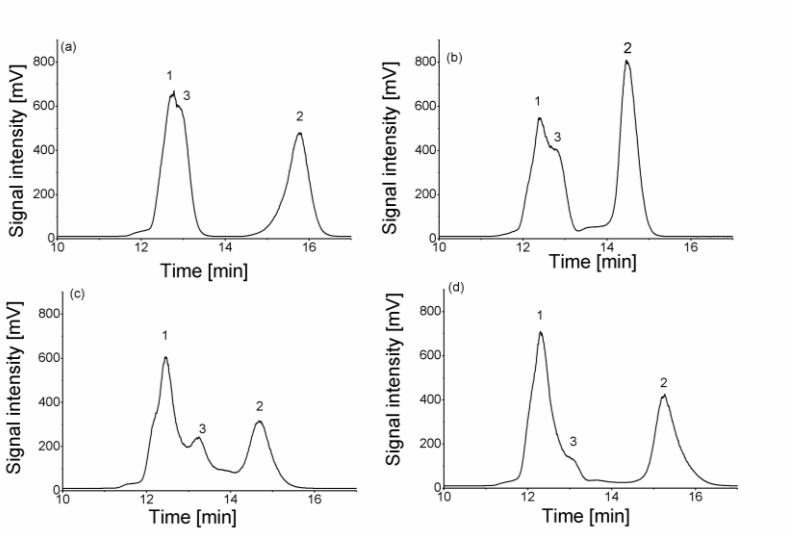

Rys. 55. Przykładowe chromatogramy badanej pary związków (*L*-Phe–*L*-Pro) zarejestrowane przy pomocy detektora ELSD po upływie (a) 4.00 h, (b) 28.20 h, (c) 74.40 h oraz (d) 206.80 h. (1) Pro, (2) Phe oraz (3) główny produkt peptyzacji [182]

Na przedstawionych chromatogramach można zauważyć obecność głównego produktu peptyzacji pary *L*-Phe–*L*-Pro (pik 3), pojawiającego się między pikami Pro (1), a Phe (2), którego stężenie znacznie zmienia się podczas trwania analizy. Obecność piku (3) pomiędzy pikami obu aminokwasów świadczy o jego podobnych właściwościach i podobnej masie molowej do związków wyjściowych. Czas retencji poszczególnych związków również zmienia się podczas przechowywania roztworu. Czas retencji *L*-Pro mieści się w granicach od 12,04 do 12,78 min, czas retencji *L*-Phe od 14,46 do 15,81 min, natomiast czas retencji głównego produktu peptyzacji od 13,31 do 14,17 min. Obserwowane, niezależne zmiany czasów retencji są skutkiem działania mechanizmu rugowania. Dążąc do jak najkrótszych czasów analizy (w celu lepszego śledzenia dynamiki badanego procesu), musimy zgodzić się na kompromis związany z rozdzielczością. W związku z tym piki aminokwasów, a także piki produktu peptyzacji wykazują obserwowany efekt przesunięcia.

Dla lepszego zobrazowania oscylacyjnych zmian stężeń *L*-Phe i *L*-Pro sporządzono wykres zmian wysokości pików chromatograficznych (tożsamych ze zmianami odpowiednich stężeń) w funkcji czasu (Rys. 56). Ponieważ na chromatogramach zaobserwowano pojawienie się piku pochodzącego od peptydu, odpowiedni wykres również znalazł się na Rys. 56.

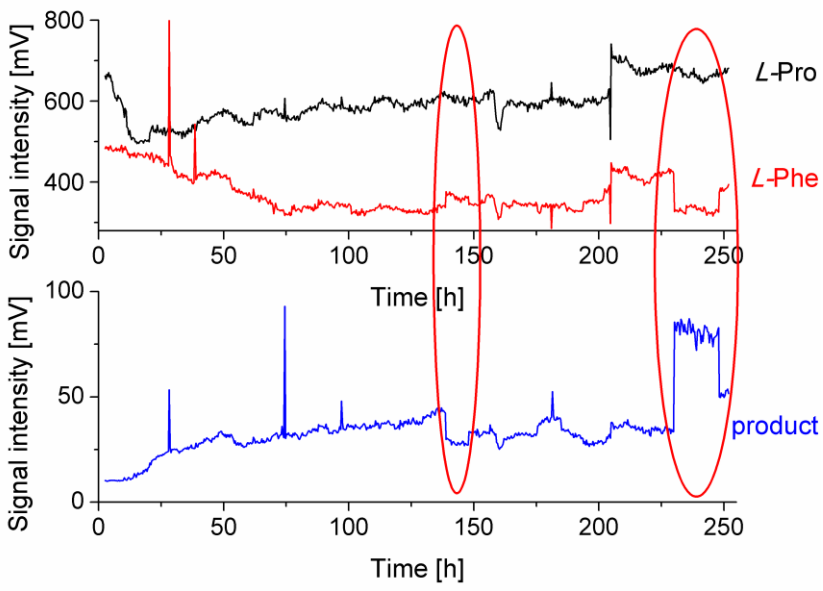

Rys. 56. Zmiany wysokości pików chromatograficznych *L*-Phe, *L*-Pro oraz głównego produktu peptyzacji w funkcji czasu, zarejestrowane przy pomocy detektora ELSD w przedziale czasowym 0-250 h przechowywania próbki [183]

Widać wyraźnie, iż zmiany stężeń aminokwasów oraz peptydu są silnie skorelowane. Czerwonymi owalami zostały zaznaczone te fragmenty wykresu, które potwierdzają, iż obserwowany produkt składa się z obu wyjściowych aminokwasów. Pierwszym owalem został zaznaczony fragment, na którym stężenie obu aminokwasów rośnie przy jednoczesnym spadku stężenia produktu (od 130 do 150 h). Drugim owalem zaznaczono ten fragment wykresu (od 225 do 250 h), na którym stężenia obu aminokwasów maleją przy jednoczesnym wzroście stężenia produktu. Ponadto na Rys. 56 dostrzegamy niemonotoniczne zmiany stężeń świadczące o oscylacyjnym charakterze obserwowanego procesu. Zaznaczone fragmenty potwierdzające samorzutne tworzenie się heteropeptydów, a także ich rozpad do wyjściowych związków powiększono i przedstawiono na Rys. 57.

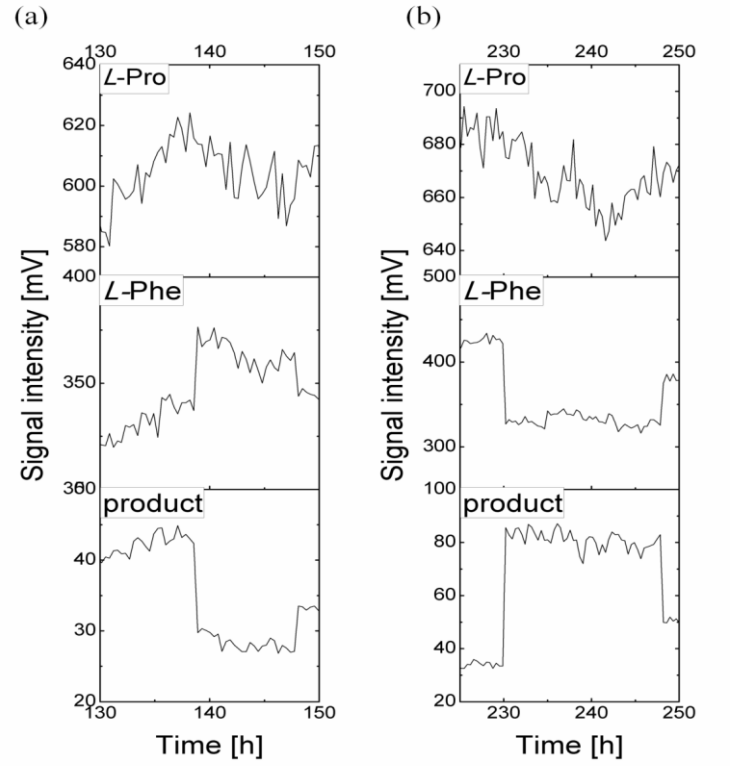

Rys. 57. Powiększone fragmenty Rys. 56 przedstawiające zmiany wysokości pików chromatograficznych *L*-Phe, *L*-Pro oraz głównego produktu peptyzacji; (a) 130-150 h; (b) 225-250 h [183]

Badania chromatograficzne były prowadzone z jednoczesnym wykorzystaniem dwóch detektorów, ELSD oraz DAD. Rys. 58 przedstawia wykresy zależności wysokości pików chromatograficznych *L*-Phe w funkcji czasu zarejestrowane przez detektory ELSD oraz DAD (cały czas trwania analizy – 250 h). Zaprezentowane zestawienie przedstawia pełną synchronizację przebiegu krzywych na obu wykresach, co wyklucza jakiekolwiek błędy związane z działaniem detektora ELSD, jak np. wahania napięcia bądź niestabilność detektora, a potwierdza poprawność obserwacji badanych procesów.

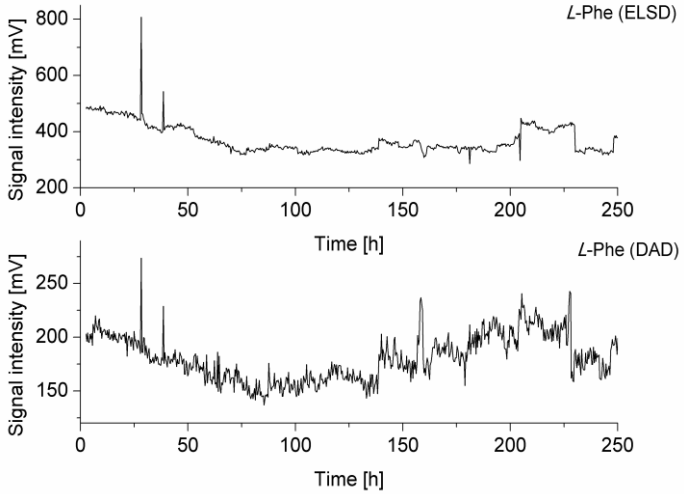

Rys. 58. Zmiany wysokości piku chromatograficznego dla *L*-Phe w funkcji czasu (0-250h) zarejestrowane przy pomocy detektora ELSD oraz DAD

6.2. SPEKTROMETRIA MAS UKŁADU *L*-PHE-*L*-PRO

W celu dodatkowego sprawdzenia czy w przechowywanej próbce układu dwuskładnikowego *L*-Phe–*L*-Pro obecne są zarówno homo- jak i heteropeptydy badanych aminokwasów oraz w celu ich identyfikacji przeprowadzone zostały badania techniką LC-MS. Na Rys. 59 przedstawiono otrzymane chromatogramy oraz widma mas.

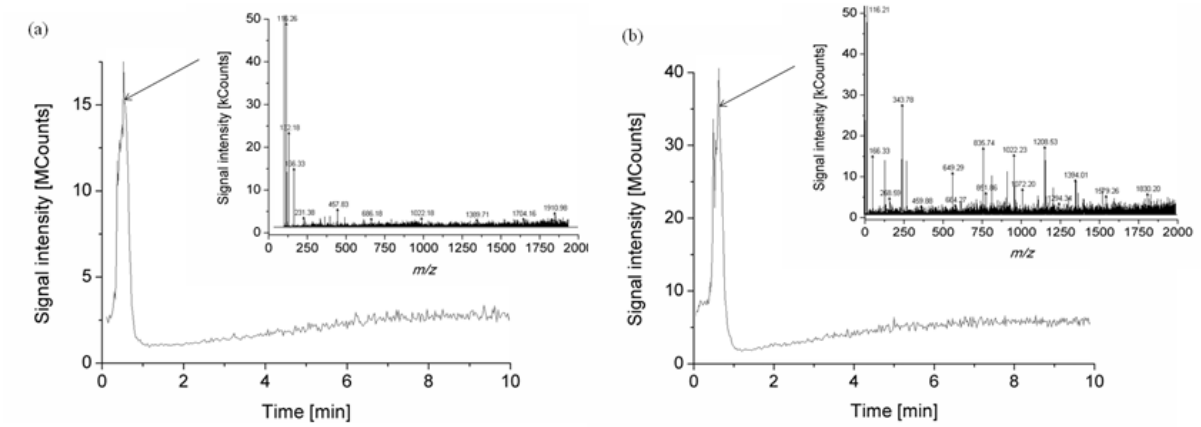

Rys. 59. Chromatogramy oraz widma mas dla (a) świeżo sporządzonego roztworu *L*-Phe–*L*-Pro oraz (b) roztworu przechowywanego przez okres 122 dni [183]

Na Rys. 59(a) przedstawiono chromatogram wraz z widmem mas dla próbki świeżo sporządzonego roztworu *L*-Phe–*L*-Pro, natomiast na Rys. 59(b) przedstawiono widmo mas próbki przechowywanej przez okres 122 dni. Porównując zaprezentowane widma mas widać wyraźną różnicę między widmami świeżo sporządzonego roztworu, a roztworu przechowywanego przez okres 122 dni. Na widmie świeżo sporządzonego roztworu (Rys. 59(a)) obecne są piki pseudomolekularne obu aminokwasów $[Pro+H]^+$, oraz $[Phe+H]^+$ o *m/z* równych odpowiednio 116 oraz 166, a także nieliczne piki pochodzące od peptydów, których intensywność jest niewielka. Natomiast na widmie mas próbki przechowywanej przez okres 122 dni (Rys. 59(b)) obecne są również piki pseudomolekularne wyjściowych aminokwasów, a także piki pochodzące od peptydów, których intensywność jest znacznie większa, niż w przypadku świeżo sporządzonego roztworu. Można zaobserwować wśród tych pików zarówno piki odpowiadające homopeptydom, np. $[Phe_3]^+$ o wartości *m/z* równej 460, jak i heteropeptydom wyjściowych aminokwasów, jak np. $[(Phe)_6(Pro)_7]^+$ o wartości *m/z* równej 1579,26.

6.3. BADANIA SAMOORGANIZACJI PEPTYDÓW *L*-PHE-*L*-PRO

Po jednorocznym okresie przechowywania próbki w szczelnie zamkniętym naczyniu w temp. 21± 1^{o}C, w badanym roztworze zaobserwowano pojawienie się włókien peptydowych. Pierwszym krokiem badawczym było wykonanie testów mikrobiologicznych mających na celu wykluczenie obecności mikroorganizmów w badanej próbce przechowywanej przez długi okres czasu. Badania mikrobiologiczne wykonano dwiema metodami, które zostały opisane w rozdziale 3.11. W żadnej z badanych próbek nie zaobserwowano pojawienia się mikroorganizmów.

6.3.1. MIKROSKOPIA OPTYCZNA ORAZ SKANINGOWA MIKROSKOPIA ELEKTRONOWA NANO- ORAZ MIKROWŁÓKIEN PEPTYDOWYCH POWSTAŁYCH W UKŁADZIE *L*-PHE–*L*-PRO

Układ dwuskładnikowy aminokwasów białkowych *L*-Phe–*L*-Pro rozpuszczonych w 70% wodnym roztworze acetonitrylu przez okres jednego roku ulegał równoległym reakcjom inwersji chiralnej oraz samorzutnej peptyzacji. W wyniku tych dwóch procesów w roztworze powstały białe włókna, widoczne na Rys. 60(a). Ilość włókien występujących w roztworze zmieniała się od prawie przeźroczystego roztworu do gęstej zawiesiny włókien, aby następnie znów spaść do bardzo niskiego poziomu. Taka pulsacja roztworu była procesem ciągłym i dynamicznym. Na Rys. 60(b) pokazano fiolkę odwróconą do góry dnem z gęstą zawiesiną mikrowłókien. Na Rys. 60(c) przedstawiono przykładowy obraz wykonany mikroskopem optycznym, przedstawiający mikrowłókno Phe–Pro wyciągnięte z roztworu, a na Rys. 60(d)-(e) przedstawiono mikrowłókna zawieszone w roztworze.

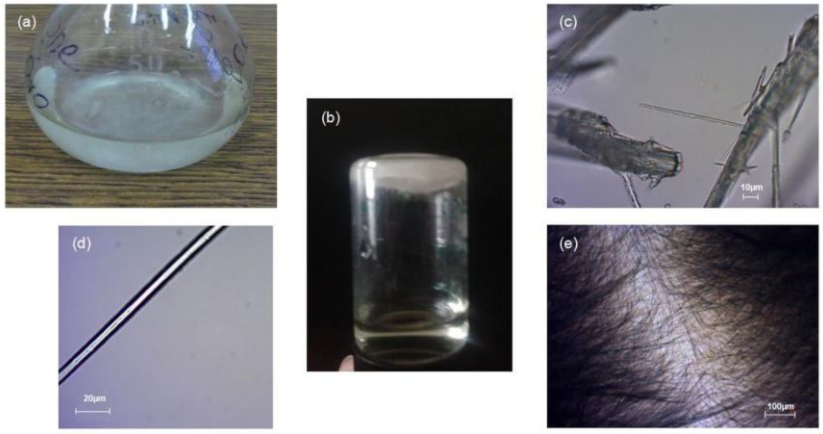

Rys. 60. (a) Kolba miarowa z mikrowłóknami w układzie Phe-Pro zawieszonymi w roztworze; (b) fiolka zawierająca włókna Pro-Phe odwrócona do góry dnem; (c) mikrowłókna wyciągnięte z roztworu (powiększenie X50); (d) pojedyncze mikrowłókno w roztworze (powiększenie X50); (e) mikrowłókna zawieszone w roztworze (powiększenie X10). Skala została dopasowana indywidualnie do każdego zdjęcia [184]

Następnie, aby lepiej zbadać otrzymane struktury oraz sprawdzić, czy na pewno są to włókna peptydowe, a nie np. mikrorurki, oraz aby zobaczyć czy w roztworze poza mikrostrukturami peptydowymi są obecne również nanostruktury peptydowe, wykonano serię badań z użyciem skaningowego mikroskopu elektronowego (SEM). Otrzymane mikrografie przedstawiono na Rys. 61.

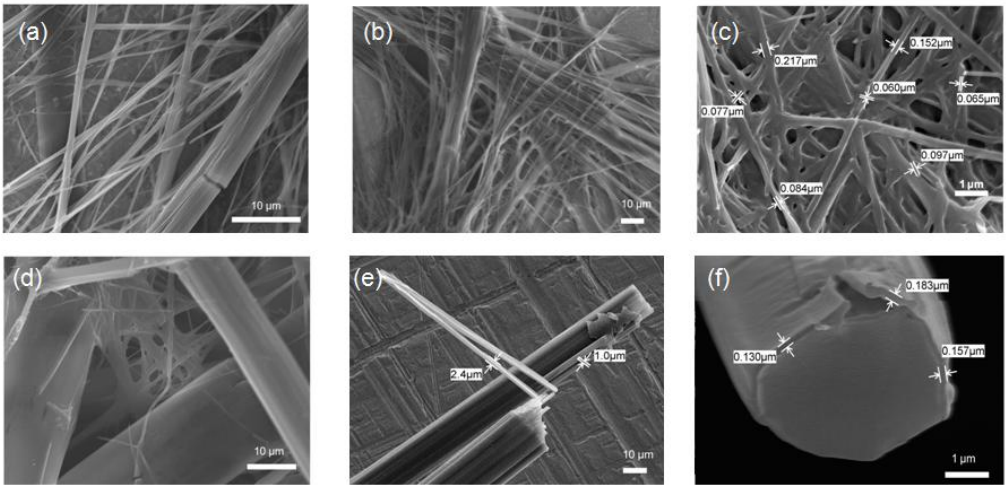

Rys. 61. (a)-(c): Mikrografie przedstawiające włókna Phe-Pro pozyskane z roztworu znad osadu pozostawionego do wyschnięcia. (d)-(f): Zdjęcia SEM włókien Phe-Pro wyciągniętych z roztworu; powiększenia (a) X2700; (b) X800; (c) X13000; (d) X900; (e) X1900; (f) X17000. Na rysunkach (c), (e) oraz (f) zostały zaznaczone wymiary włókien. Skala została dopasowana indywidualnie do każdego zdjęcia [182]

Przedstawione mikrografie włókien Phe-Pro pokazują, że większość struktur osiąga rozmiary mikro, ale obecne są również struktury mniejsze, o wielkościach nano (o szerokości mniejszej niż 0,1 μm). Spośród włókien zawieszonych w roztworze, a niewidocznych gołym okiem (Rys. 61(a)-(c)), znaczna przewaga włókien osiąga rozmiary nano. W przypadku włókien wyciągniętych z roztworu, których masy są na tyle duże, że wypadają w formie osadu na dnie fiolki (Rys. 61(d)-(e)) przeważają mikrowłókna. Można również zauważyć, że większe mikrowłókna są zbudowane z nanowłókien ściśle upakowanych w jedną większą całość, co pokazano na Rys. 61(e).

6.3.2. SPEKTROSKOPIA W PODCZERWIENI (IR)

Aby potwierdzić założenia, że otrzymane nano- oraz mikrowłókna są oligopeptydami, wykonano badania z wykorzystaniem spektroskopii IR. Badano próbki włókien Phe–Pro, mieszaniny równowagowej *L*-Phe i *L*-Pro, a także próbki pojedynczych aminokwasów. Otrzymane widma zostały przedstawione na Rys.62.

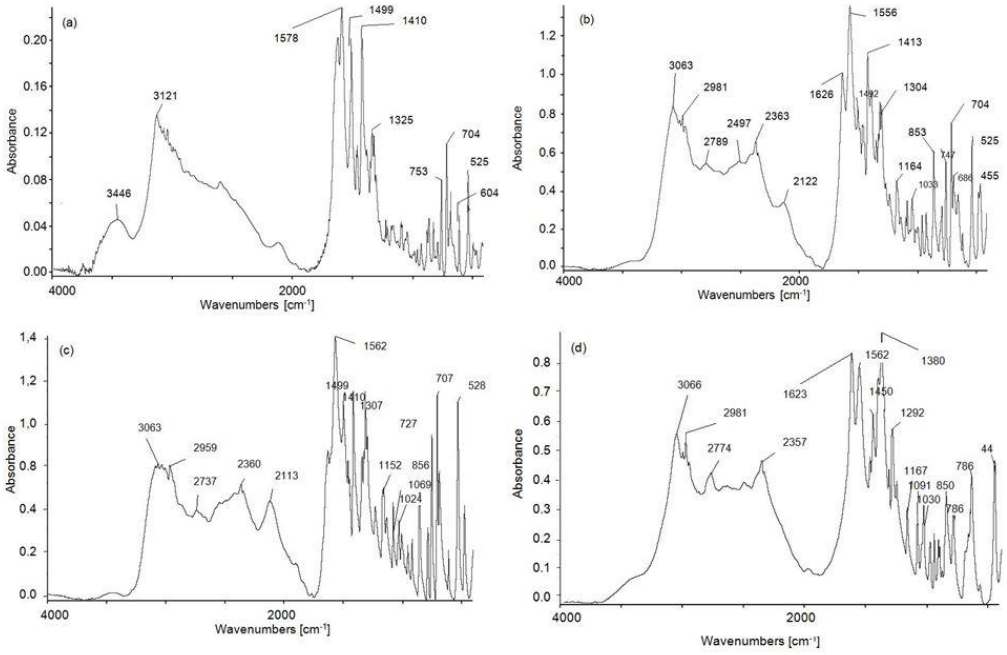

Rys. 62. Widma absorpcyjne IR w zakresie długości fal od 4000 do 400 cm^{-1}, wykonane w pastylkach KBr dla (a) próbki włókien Phe-Pro, (b) mieszaniny *L*-Phe i *L*-Pro w stosunku wagowym 1:1, (c) próbki *L*-Pro, (d) próbki *L*-Phe [184]

Porównanie otrzymanych widm absorpcyjnych w podczerwieni wskazuje na wyraźne różnice między próbką włókien peptydowych (Rys. 62(a)), a pozostałymi widmami aminokwasów (Rys. 62(b)-(d)). Widmo mieszaniny równowagowej wyjściowych aminokwasów (Rys. 62(b)) odzwierciedla pewną addytywność widm pojedynczych aminokwasów Pro (Rys. 62(c)) oraz Phe (Rys. 62(d)). Porównując widmo włókien peptydowych z pozostałymi widmami aminokwasów można zauważyć dwie zasadnicze różnice. Pierwsza z nich to znacznie niższa absorpcja włókien peptydowych w porównaniu z aminokwasami. Drugą ważną różnicą jest znacznie uproszczony kształt widma w zakresie od 3400 do 1800 cm^{-1}, a jest to obszar, w którym widoczne są oddziaływania międzycząsteczkowe, takie jak wiązania wodorowe. Opisane różnice wynikają prawdopodobnie z faktu, iż większość grup –COOH oraz $–NH_2$ aminokwasów we włóknach peptydowych bierze udział w wiązaniach peptydowych (–CO-NH–), co zmniejsza zdolność cząsteczki do tworzenie wiązań wodorowych. Z drugiej strony znaczne podobieństwo wszystkich widm w zakresie od 1250 do 450 cm^{-1} potwierdza, że włókna peptydowe zbudowane są *L*-Phe oraz *L*-Pro.

6.3.3. SPEKTROMETRIA MAS NANO- ORAZ MIKROWŁÓKIEN PEPTYDOWYCH

Kolejną techniką zastosowaną w celu potwierdzenia, że w badanym roztworze obecne są peptydy była technika LC-MS. Otrzymane widma mas dla próbki świeżo sporządzonego roztworu oraz dla roztworu przechowywanego przez okres 1 roku (roztwór znad osadu włókien peptydowych) przedstawiono na Rys. 63. Na widmie mas świeżo sporządzonego roztworu (Rys. 63(a)) widoczne są dwa dominujące piki, pochodzące od wyjściowych aminokwasów oraz piki o niewielkiej intensywności pochodzące od peptydów. Natomiast w widmie mas próbki przechowywanej przez okres jednego roku – zawierającej nano oraz mikrowłókna peptydowe (Rys. 63(b)), dominują piki peptydów o masach sięgających do 3500 Da, a piki molekularne wyjściowych aminokwasów mają niewielką intensywność. Wyniki te również potwierdzają, że nano- oraz mikrowłókna peptydowe zbudowane są z oligopeptydów wyjściowych aminokwasów.

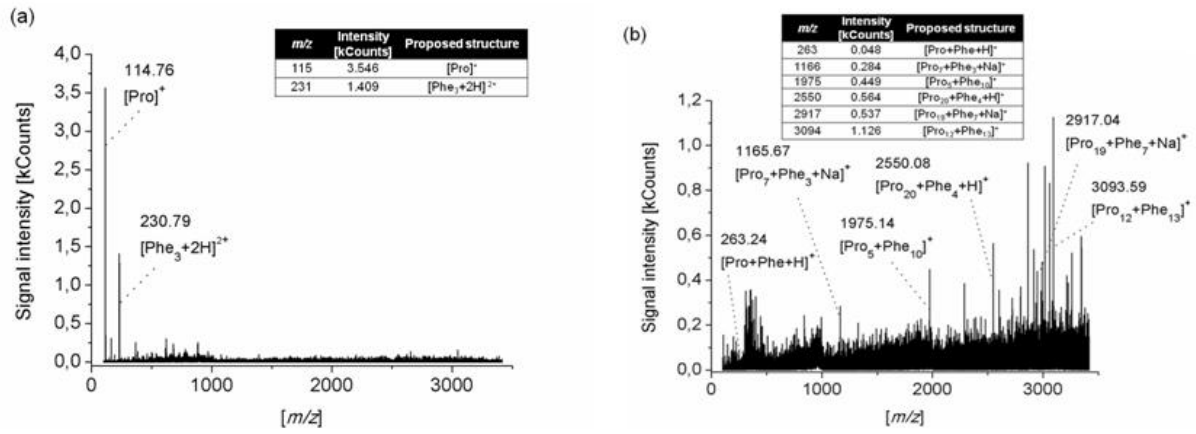

Rys. 63. Widma mas oraz tabele zawierające wybrane sygnały analityczne obecne na widmach mas (a) świeżo sporządzonego roztworu *L*-Phe–*L*-Pro; (b) roztworu włókien peptydowych Phe-Pro po roku przechowywania próbki, zarejestrowane przy pomocy układu LC-MS [182]

6.4. BADANIA TURBIDYMETRYCZNE UKŁADU *L*-PHE–*L*-PRO

W przechowywanych roztworach aminokwasów powstają układy dwufazowe, gdzie w fazie ciekłej obecne są monomeryczne aminokwasy i rozpuszczalne peptydy, natomiast fazę stałą stanowią nierozpuszczalne peptydy. W układach dwufazowych oscylacyjny charakter samorzutnej peptyzacji może być zauważony nawet gołym okiem, jako sekwencyjna zmiana ilości wytrąconych peptydów. W skrajnych przypadkach układ aminokwasów może oscylować między postacią całkowicie przezroczystą (brak zauważalnej obecności peptydów) oraz opalizującą (gdzie widoczne są swobodnie unoszące się cząstki peptydów), co sprawia wrażenie pulsowania takiego roztworu. Takie sekwencyjne przechodzenie od przezroczystego roztworu do opalizującej zawiesiny ilustruje Rys. 64.

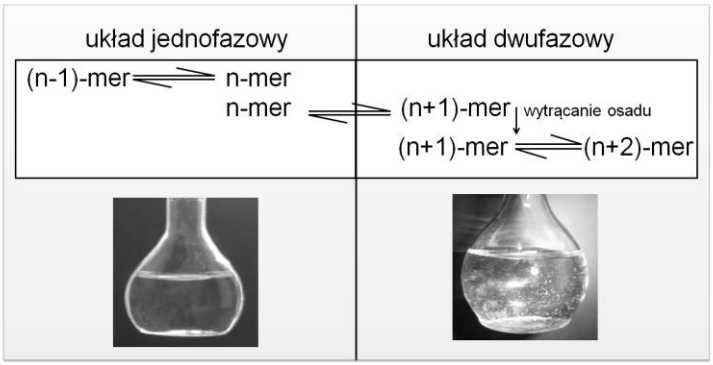

Rys. 64. Schemat przejść fazowych w roztworze aminokwasów [184]

Pulsującą niestabilność nano- i mikrostruktur peptydowych jako odwracalne przechodzenie od niższych, rozpuszczalnych peptydów do peptydów wyższych (wytrącających się w postaci osadu w układach dwufazowych) można śledzić poprzez rejestrację zmian mętności badanych roztworów techniką turbidymetrii w trybie ciągłym. Badania turbidymetryczne pozwalają na zaobserwowanie efektów niewidocznych gołym okiem, co ma znaczenie dla zrozumienia mechanizmów samoorganizacji peptydów w nanostruktury. Na Rys. 65 przedstawiono zmiany zachodzące w świeżo sporządzonym roztworze *L*-Phe–*L*-Pro. Na przedstawionym wykresie obserwujemy zmiany mętności, co świadczy o tworzeniu się peptydów, których obecność w roztworze nie jest widoczna gołym okiem. Ponadto zmiany mętności mają charakter niemonotoniczny, co dodatkowo potwierdza, iż reakcja peptyzacji ma charakter oscylacyjny.

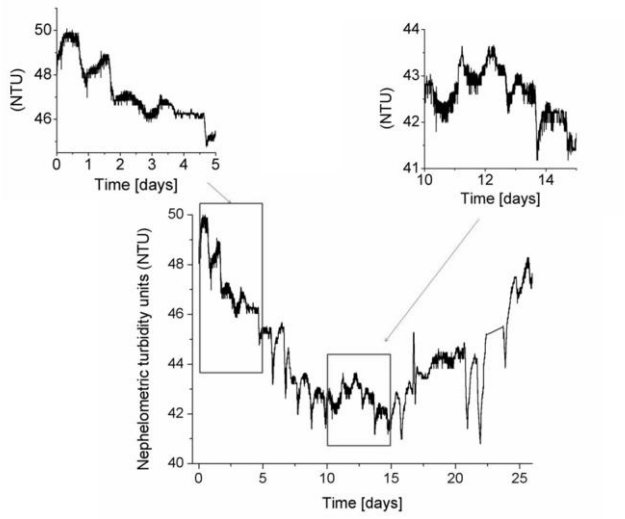

Rys. 65. Zmiany zmętnienia roztworu pary aminokwasów *L*-Phe-*L*-Pro (0-26 dni) [184]

Dodatkowo można zauważyć powtarzające się cykle gwałtownych spadków i wzrostów zmętnienia roztworu aminokwasów, co dokładniej zostało pokazane na Rys. 66. Zmiany zmętnienia aminokwasów wykazują rytm okołodobowy i mieszczą się w zakresie od 19,66 do 26,80 h. Podobną prawidłowość można zaobserwować na wykresie zmian stężeń badanych aminokwasów (Rys. 67), gdzie cykl zmian waha się od 16,80 do 25,67 h.

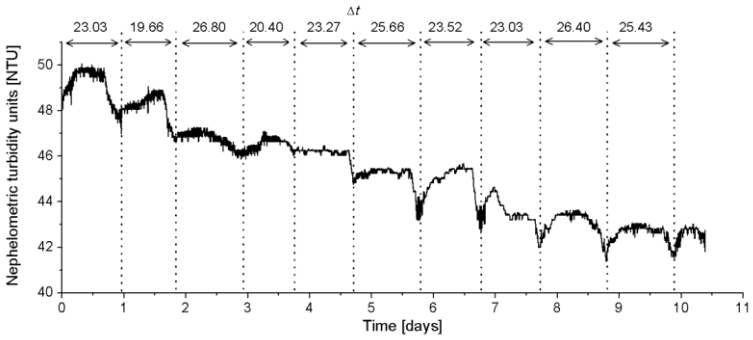

Rys. 66. Zmiany zmętnienia roztworu pary aminokwasów *L*-Phe–*L*-Pro (0-11dni) z zaznaczonymi dobowymi zmianami zmętnienia [177]

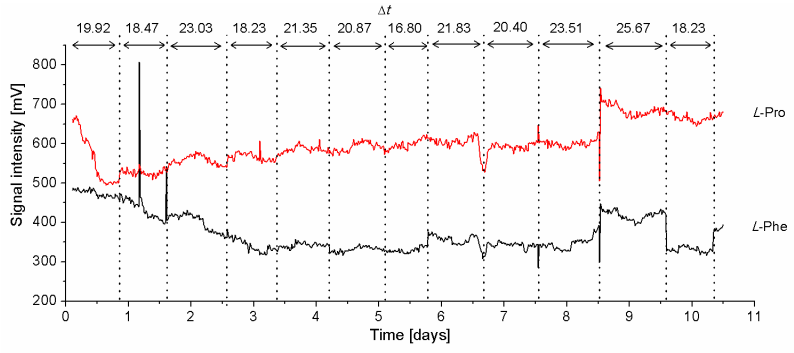

Rys. 67. Zmiany wysokości pików chromatograficznych *L*-Phe, *L*-Pro zarejestrowane przy pomocy detektora ELSD w przedziale czasowym 0-11 dni przechowywania próbki z zaznaczonymi dobowymi zmianami stężenia aminokwasów [177]

7. BADANIE WPŁYWU BUDOWY STRUKTURALNEJ AMINOKWASÓW NA RODZAJ OTRZYMANEJ NANOSTRUKTURY PEPTYDOWEJ

7.1. PORÓWNANIE NANOSTRUKTUR PEPTYDOWYCH *L*-PHE, *L*-PRO, *L*-CYS, *L*-PHE–*L*-PRO ORAZ *L*-PRO–*L*-CYS

Do badań nad wpływem budowy strukturalnej wyjściowych aminokwasów na otrzymaną nanostrukturę peptydową wybrano następujące pojedyncze aminokwasy *L*-Phe, *L*-Pro, *L*-Cys, a także pary tych aminokwasów *L*-Phe–*L*-Pro oraz *L*-Pro–*L*-Cys. Aminokwasy dobrano w taki sposób, aby sprawdzić, który aminokwas determinuje kształt otrzymanych nanostruktur, a także, który determinuje szybkość tworzenia się tych struktur. Zarówno badane pojedyncze aminokwasy, jak i ich pary ulegają reakcjom oscylacyjnej peptyzacji i/lub inwersji chiralnej tworząc peptydy, które samoorganizują

się w nanostruktury, co zostało potwierdzone badaniami chromatograficznymi dla pojedynczych aminokwasów *L*-Phe [185], *L*-Pro [119], *L*-Cys [186], jak i dla par aminokwasów *L*-Phe–*L*-Pro [183] oraz *L*-Pro–*L*-Cys [187].

Pierwszą ważną różnicą między badanymi aminokwasami jest ich różna szybkość tworzenia nanostruktur peptydowych w roztworach. W przypadku pary aminokwasów *L*-Phe–*L*-Pro czas tworzenia się struktur wynosił jeden rok, natomiast w przypadku pary *L*-Pro–*L*-Cys pierwsze mikrostruktury były widoczne już po upływie kilku dni od sporządzenia roztworu. Na Rys. 68 przedstawiono zdjęcie fiolki zawierającej roztwór *L*-Pro–*L*-Cys zaraz po sporządzeniu roztworu (Rys. 68(a)), w czwartej dobie od sporządzenia roztworu już z widocznymi strukturami w roztworze aminokwasów (Rys. 68(b)), oraz po upływie miesiąca od sporządzenia roztworu (Rys. 68(c)).

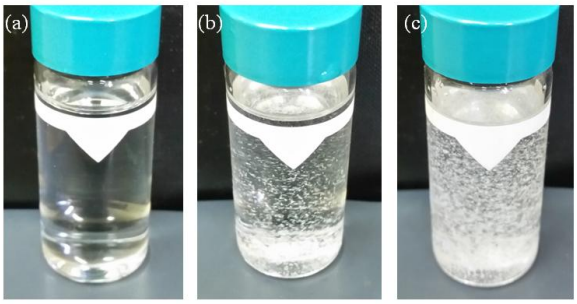

Rys. 68. Zdjęcia fiolek zawierających roztwór *L*-Pro–*L*-Cys po upływie (a) 1 h; (b) 4 dni; (c) 4 tygodni od chwili sporządzenia roztworu

Aby przyjrzeć się bliżej wytrąconym strukturom wykorzystano skaningową mikroskopię elektronową (SEM). W tym celu przygotowano roztwory zarówno pojedynczych aminokwasów wchodzących w skład układów dwuskładnikowych, jak i mieszanin tych aminokwasów. Mikrografie struktur powstałych w przechowywanych roztworach pojedynczych aminokwasów przedstawiono na Rys. 69, natomiast mikrografie struktur powstałych w układach dwuskładnikowych zaprezentowano na Rys. 70.

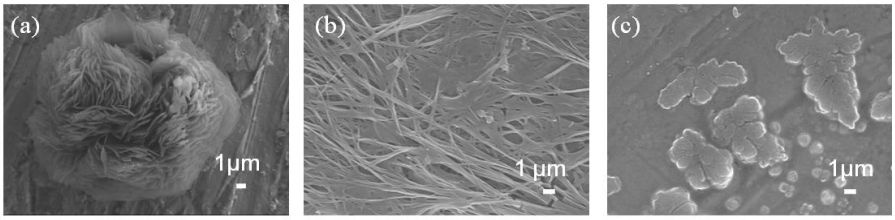

Rys. 69. Mikrografie przestawiające struktury peptydowe pojedynczych aminokwasów (a) Cys, (b) Phe, (c) Pro po upływie (a) 2 tygodni, (b) 3 miesięcy, (c) 1 miesiąca od sporządzenia roztworu; powiększenia (a) X3300, (b) X3300, (c) X5000. Skala została dopasowana indywidualnie do każdego zdjęcia [187]

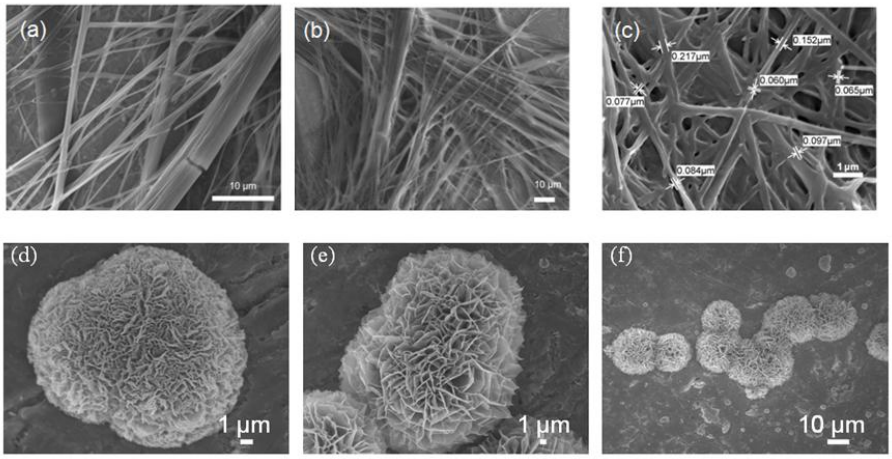

Rys. 70. Mikrografie przestawiające struktury peptydowe par aminokwasów (a)-(c): włókna Phe–Pro po upływie 1 roku; (d)-(f) sfery Pro–Cys po upływie 2 tygodni od sporządzenia roztworu; powiększenia (a) X2700; (b) X800; (c) X13000; (d) X5000; (e) X3000; (f) X900. Skala została dopasowana indywidualnie do każdego zdjęcia [187], [182]

Jak przedstawiono na Rys. 69, w przypadku pojedynczych przechowywanych roztworów aminokwasów otrzymano cztery różne struktury, co dobitnie świadczy o tym, iż rodzaj otrzymanych nano- oraz mikrostruktur peptydowych zależy od budowy strukturalnej wyjściowego aminokwasu. W przypadku Cys (Rys. 69(a)) otrzymana struktura jest sferyczna, co prawdopodobnie wynika z obecności trzech grup funkcyjnych (–COOH, $–NH_2$, –SH), które umożliwiają powstawanie trójwymiarowych struktur. Obecność grupy tiolowej umożliwia tworzenie się mostków disiarkowych, które są dodatkowym elementem wpływającym na kulistość otrzymywanych struktur. Kolejnym badanym aminokwasem była Phe (Rys. 69(b)), posiadająca jedynie dwie grupy funkcyjne oraz zawadę steryczną w postaci pierścienia benzenowego, przez co tworzy nano- oraz mikrowłókna peptydowe. W przypadku ostatniego aminokwasu Pro

(Rys.69(c)), posiadającego również dwie grupy funkcyjne (–COOH oraz –NH) otrzymano płaską nieregularną strukturę i to obecność pierścienia pirolidynowego (zamiast pierwszorzędowej grupy aminowej) spowodowała tak drastyczną różnicę w kształcie otrzymanej struktury, w porównaniu z pozostałymi aminokwasami.

Układy dwuskładnikowe dobrano w taki sposób, aby sprawdzić, czy i jak badane aminokwasy determinują kształt otrzymanych nano- oraz mikrostruktur peptydowych. Badano pary aminokwasów z jednym wspólnym czynnikiem – Pro (*L*-Phe–*L*-Pro oraz *L*-Pro–*L*-Cys). Na Rys. 70(a)-(c) zaprezentowano mikrografie układu dwuskładnikowego *L*-Phe–*L*-Pro, natomiast na Rys. 70(d)-(f) zaprezentowano mikrografie układu *L*-Pro–*L*-Cys. Takie połączenie aminokwasów w układy dwuskładnikowe pokazało, iż w przypadku pierwszej pary aminokwasów (*L*-Phe–*L*-Pro), gdzie otrzymano nano- oraz mikrowłókna peptydowe, to Phe determinuje kształt otrzymanej nanostruktury. W przypadku drugiego badanego układu (*L*-Pro–*L*-Cys), gdzie para aminokwasów samoorganizuje się w nano- oraz mikrosfery peptydowe, to Cys odpowiada za kształt otrzymanej struktury. Ponadto otrzymane wyniki ilustrują wpływ grupy tiolowej w cząsteczce cysteiny na kulisty kształt otrzymanych struktur oraz dowodzą, że tworzenie się mostków disiarkowych jest kluczowe w powstawaniu nanosfer peptydowych. Można również zauważyć, że powierzchnia sfery pojedynczego aminokwasu (Cys) jest dość nieregularnie zbudowana z luźno upakowanych płatków, natomiast dodatek innego aminokwasu – Pro – wpłynął znacząco na powierzchnię otrzymanej sfery peptydowej, której powierzchnia jest również zbudowana z płatków, jednak ich rozmieszczenie jest bardzo regularne.

7.2. BADANIA MIKROSKOPOWE UKŁADU DWUSKŁADNIKOWEGO *L*-SER–*L*-MET

Kolejnym układem dwuskładnikowym, wytypowanym do badań nad wpływem budowy strukturalnej wyjściowych aminokwasów na kształt otrzymanej nanostruktury był układ *L*-Ser–*L*-Met oraz pojedynczy aminokwas, *L*-Ser. Układ ten został wybrany ze względu na strukturę chemiczną *L*-Met, która obok *L*-Cys jest aminokwasem siarkowym, z tą różnicą, że Cys posiada wolną grupę –SH, przez co może tworzyć mostki disiarkowe, natomiast cząsteczka Met posiada zablokowaną grupę siarkową. Celem przeprowadzonych badań było sprawdzenie, czy obecność siarki

w analizowanym układzie również spowoduje tworzenie się nano- oraz mikrosfer peptydowych. Wykonano badania mikroskopowe z wykorzystaniem skaningowego mikroskopu elektronowego (SEM). Otrzymane nanostruktury *L*-Ser oraz układu dwuskładnikowego *L*-Ser–*L*-Met zostały przedstawione na Rys. 71.

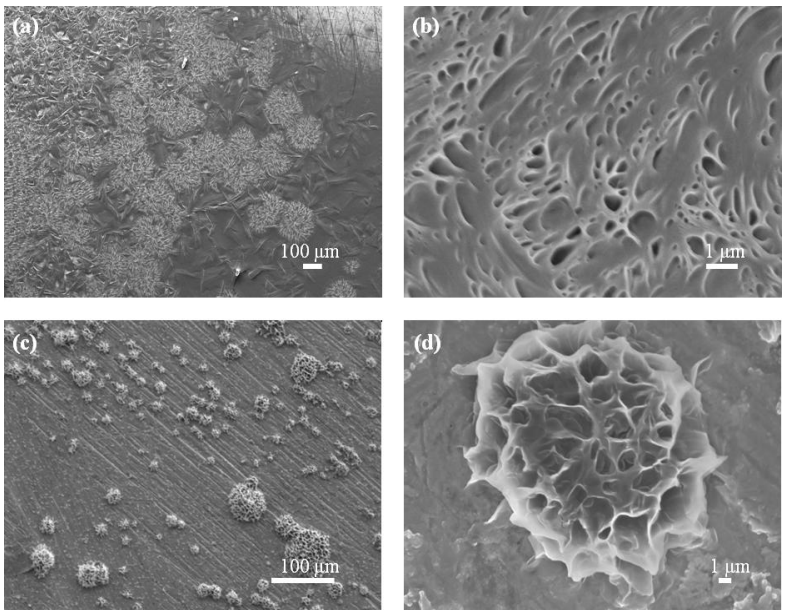

Rys. 71. Mikrografie przedstawiające (a)-(b) proste nieregularne struktury Ser zarejestrowane dla roztworu *L*-Ser przechowywanego przez okres jednego miesiąca; (c)-(d) trójwymiarowe struktury peptydowe układu dwuskładnikowego *L*-Ser-*L*-Met, zarejestrowane dla roztworu przechowywanego przez okres jednego miesiąca. Powiększenia (a) X 50; (b) X 10000; (c) X 200; (d) X 4300; skala została dopasowana indywidualnie do każdego zdjęcia

Na podstawie przedstawionych mikrografii można zaobserwować, iż peptydy Ser organizują się w płaskie nieregularne struktury (Rys. 71(a)-(b)), natomiast dodatek Met do układu aminokwasów sprawia, że otrzymane struktury stały się trójwymiarowe (Rys. 71(c)-(d)), jednak powierzchnia otrzymanych struktur również jest nieregularna, tak jak w przypadku struktur otrzymanych dla układu jednoskładnikowego *L*-Ser. W aktualnie omawianym przypadku nie można jednoznacznie stwierdzić, który aminokwas determinuje kształt otrzymanej nanostruktury, gdyż seryna jest odpowiedzialna za strukturę powierzchni, natomiast dodatek metioniny do badanego układu dodaje badanym strukturom trzeci wymiar.

8. MODELOWANIE PROCESÓW SAMOORGANIZACJI PROSTYCH PEPTYDÓW DO NANO- ORAZ MIKROSTRUKTUR PEPTYDOWYCH ORAZ ICH PULSACYJNYCH ZMIAN

Na podstawie badań przeprowadzonych dla układu dwuskładnikowego aminokwasów *L*-Phe–*L*-Pro skonstruowano model teoretyczny, opisujący sposób powstawania nierozpuszczalnych nanostruktur w roztworze aminokwasów, a także dalsze oscylacyjne zmiany stężenia rozpuszczalnych struktur pozostających w roztworze. Model został opracowany we współpracy z prof. Irwingiem R. Epsteinem z Brandeis University w Waltham, Massachusetts (USA). Pierwszym modelem teoretycznym opisującym proces oscylacyjnej inwersji chiralnej i oscylacyjnej kondensacji pojedynczego związku chiralnego był model opracowany dla kwasu *L*-mlekowego [188]. Model ten następnie został rozbudowany dla układów dwuskładnikowych na przykładzie mieszaniny Pro-Hyp [119]. Ponieważ podczas tworzenia najnowszego modelu nie posiadano danych kinetycznych dotyczących poszczególnych etapów procesu oligomeryzacji i agregacji, zastosowano procedurę „coarse-graining", opracowaną przez Coveneya i Wattisa [189], która zakłada traktowanie procesów wieloetapowych jako pojedynczych pseudo kroków o określonej liczbie agregacji i stałej szybkości. Najnowszy model powstały dla opisu samoorganizacji prostych peptydów do nano- oraz mikrostruktur peptydowych oraz ich dalszych pulsacyjnych zmian składa się z następujących równań:

$n_1\mathrm{M} \rightarrow \mathrm{P}$	szybkość = $k_o\mathrm{M}$	(oligomeryzacja)	(1)
$n_2\mathrm{P} \rightarrow \mathrm{C}$	szybkość = $k_u\mathrm{P}$	(niekatalizowana agregacja)	(2)
$2\mathrm{C} + n_2\mathrm{P} \rightarrow 3\mathrm{C}$	szybkość = $k_c\mathrm{C}^2\mathrm{P}$	(katalizowana agregacja)	(3)
$\mathrm{C} \rightarrow$ produkty	szybkość = $k_d\mathrm{C}$	(rozkład)	(4)

gdzie *M* oznacza monomery aminokwasów, *P* oznacza peptydy o średniej długości n_1, a *C* jest agregatem zawierającym n_2 oligomerów. W początkowym etapie reakcji

monomery *M* tworzą peptydy *P*, które powoli ulegają agregacji do struktur *C*, które następnie stają się szablonem do tworzenia następnych agregatów *C* w autokatalizowanej agregacji. Ostatecznie powstałe agregaty rozpadają się do produktów.

Aby uwzględnić tworzenie się nanostruktur peptydowych, wprowadzono dodatkowe równania:

$$2C \rightarrow F \qquad \text{szybkość} = k_f\theta(C-C_t)C^2 \qquad \text{(powstawanie nanowłókien)} \qquad (5)$$

$$F \rightarrow 2C \qquad \text{szybkość} = k_r[1-\theta(C-C_t)]F \qquad \text{(ponowny rozpad nanowłókien)} \qquad (6)$$

gdzie *F* oznacza nanowłókna peptydowe, θ jest funkcją skokową Heaviside'a, która przyjmuje wartość 1 dla dodatnich argumentów i wartość 0 dla argumentów ujemnych bądź równych zero. Tak więc, nanowłókna mogą powstać tylko wtedy, gdy stężenie powstałych agregatów przekroczy pewną wartość krytyczną C_t, oraz wszystkie włókna się rozpadną wówczas, gdy stężenie agregatów spadnie poniżej tej wartości. Wykorzystanie funkcji skokowej jest podobne do procedury stosowanej podczas modelowania powstawania pierścieni Liesganga [190].

W przypadku modelowania procesu peptyzacji dla dwuskładnikowego układu aminokwasów należy zastosować zestaw sześciu równań ((1)-(6)) dla każdego z monomerów M_1 i M_2. Dodatkowo należy również wprowadzić równanie opisujące oddziaływania pomiędzy monomerami kiedy, np. dwa peptydy mogą współdziałać ze sobą poprzez katalizę krzyżową [119], przy czym agregaty jednego monomeru mogą katalizować agregację oligomerów innego monomeru:

$$2C_1 + n_{22}P_2 \rightarrow 2C_1 + C_2 \qquad \text{szybkość} = k_{cc1}C_1^2P_2 \qquad \text{(1-2 kataliza krzyżowa)} \qquad (7)$$

Na Rys. 72 została przedstawiona symulacja, w której jedynie związek 1 (Pro) katalizuje agregację związku 2 (Phe), a $k_{cc2} = 0$. Należy tutaj zwrócić uwagę na stosunkowo gładką krzywą zmian stężenia oligomeru, przy bardziej nieregularnej krzywej oscylacji nanowłókien peptydowych, zwłaszcza w późniejszym czasie trwania procesu, co pokrywa się z wynikami prowadzonych eksperymentów.

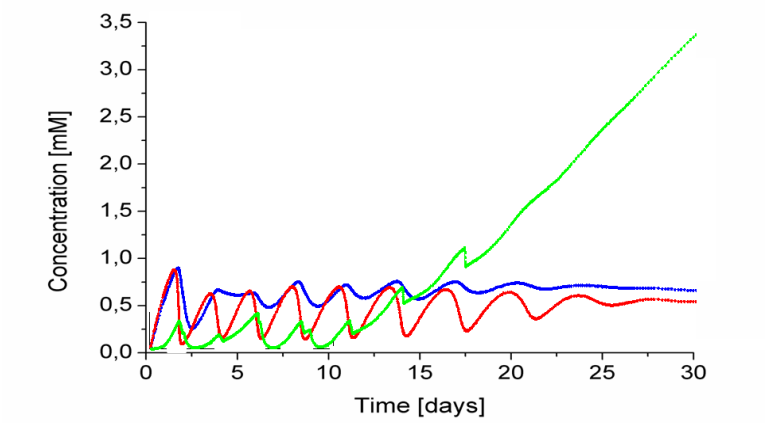

Rys. 72. Symulacja drgań oscylacyjnych stężeń oligomerów i nanostruktur w układzie dwuskładnikowym aminokwasów *L*-Phe-*L*-Pro (o stężeniach 6,05 · 10^{-2} mol · dm^{-3} Phe oraz 8,69 · 10^{-2} mol · dm^{-3} Pro). Wykres czerwony oraz niebieski przedstawia zmiany stężenia oligomerów Phe oraz Pro. Natomiast zielony wykres przedstawia 50×całkowite stężenie nanowłókien peptydowych (Phe-Pro). Parametry równań (1)-(7) (indeks 1 odnosi się do Pro, a indeks 2 do Phe): k_{01} = 1,0 · 10^{-7} s^{-1}, k_{u1} = 3,5 × 10^{-7} s^{-1}, k_{c1} = 1,8 · 10^{3} $M^{-2}s^{-1}$, k_{d1} = 3,5 ·10^{-5} s^{-1}, k_{f1} = 7,0 ·10^{-5} $M^{-1}s^{-1}$, k_{r1} = 7,0 ·10^{-5} s^{-1}, n_{11} = 5, n_{21} = 8, C_{t1} = 5,0 · 10^{-4} M, k_{02} = 1,7· 10^{-7} s^{-1}, k_{u2} = 5,5 · 10^{-7} s^{-1}, k_{c2} = 4,2 · 10^{3} $M^{-2}s^{-1}$, k_{d2} = 5,0 · 10^{-5} s^{-1}, k_{f2} = 7,0 · 10^{-5} $M^{-1}s^{-1}$, k_{r2} = 7,0 · 10^{-5} s^{-1}, n_1 = 3, n_2 = 6, C_{t2} = 2,0 ·10^{-4} M, k_{cc1} = 1,7 ·10^{2} $M^{-2}s^{-1}$ [182]

9. REAKCJA BIURETOWA

Reakcja biuretowa wykrywa obecność co najmniej dwóch wiązań peptydowych będących w bezpośrednim wzajemnym sąsiedztwie i polega na dodaniu odczynnika biuretowego do badanego roztworu. Jony miedzi(II) zawarte w tym odczynniku zmieniają barwę z niebieskiej na fioletową, co jest wynikiem tworzenia się kompleksu pomiędzy jonami miedzi(II), a co najmniej dwoma grupami peptydowymi.

Test ten został wykonany dla przechowywanych przez miesiąc roztworów aminokwasów *L*-Ser oraz *L*-Met, a zdjęcia probówek z badanymi roztworami aminokwasów zostały przedstawione na Rys. 73. Przechowywane roztwory aminokwasów zawierały samorzutnie powstałe peptydy, o czym świadczy pozytywny wynik testu biuretowego. W przypadku *L*-Ser (Rys. 73(a)) można zaobserwować fioletowy pierścień oraz fioletowy roztwór, natomiast w przypadku *L*-Met (Rys. 73(b)) obserwujemy fioletowe zabarwienie piany nad roztworem.

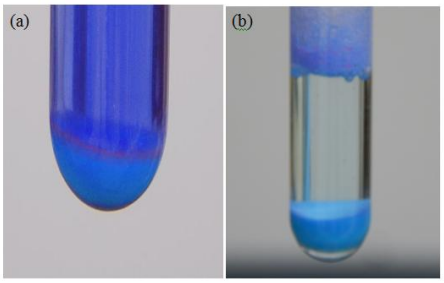

Rys. 73. Zdjęcia probówek z pozytywnym wynikiem próby biuretowej (a) *L*-Ser; (b) *L*-Met

Kolejną grupą roztworów, jaką poddano testowi biuretowemu stanowiły układy dwuskładnikowe aminokwasów *L*-Phe–*L*-Pro oraz *L*-Pro–*L*-Cys. W tym przypadku z roztworów wyodrębniono metodą dekantacji mikrostruktury obecne w roztworach, a następnie tak wyodrębnione i wysuszone substancje poddano działaniu odczynnika biuretowego. Wyniki testu zostały przedstawione na Rys. 74 oraz 75. Obie przeprowadzone reakcje biuretowe dla struktur peptydowych dały wynik pozytywny objawiający się fioletowym zabarwieniem struktur, a także roztworu w przypadku pary aminokwasów *L*-Phe–*L*-Pro.

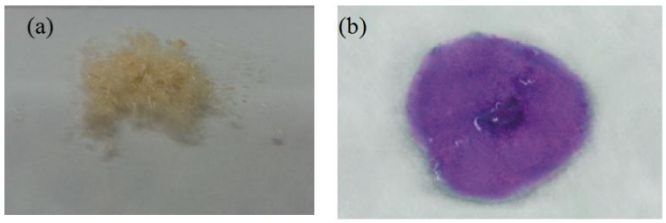

Rys. 74. (a) Żółte struktury mikropeptydowe układu *L*-Phe–*L*-Pro wyodrębnione z roztworu oraz (b) struktury zawierające kroplę odczynnika biuretowego (zdjęcia wykonano na szkiełku mikroskopowym)

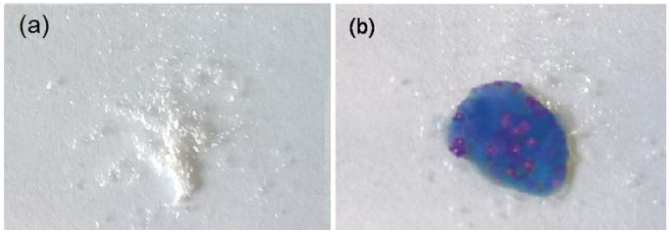

Rys. 75. (a) Białe struktury mikropeptydowe układu *L*-Pro–*L*-Cys wyodrębnione z roztworu przechowywanego oraz (b) struktury zawierające kroplę odczynnika biuretowego (zdjęcia wykonano na szkiełku mikroskopowym)

Pozytywne wyniki przeprowadzonych reakcji dodatkowo potwierdzają zajście reakcji samorzutnej peptyzacji aminokwasów białkowych w roztworach acetonitrylowo-wodnych i metanolowo-wodnych.

VII. PODSUMOWANIE I WNIOSKI

Na podstawie przedstawionych wyników badań można wyciągnąć następujące wnioski:

- Analiza TLC, przeprowadzona dla *L*-Hyp, potwierdziła występowanie procesu oscylacyjnej inwersji chiralnej, a także dzięki zastosowaniu detektora mas (TLC-MS) udowodniono, iż w roztworze równolegle zachodzi proces samorzutnej peptyzacji Hyp.
- Na podstawie badań *L*-, *D*- i *DL*-Ser stwierdzono, że badane związki wykazują różną dynamikę peptyzacji, co jest związane z ich konfiguracją przestrzenną. Na podstawie badań trzema technikami analitycznymi (TLC, HPLC-ELSD i MS) stwierdzono, że racemat (*DL*-Ser) charakteryzuje się najszybszą samorzutną peptyzacją, forma *L*-Ser zaś najwolniejszą, natomiast forma *D*-Ser ma dynamikę peptyzacji pośrednią.
- Analiza turbidymetryczna *L*-, *D*- i *DL*-Ser wykazała różnice w otrzymanych wykresach. Wykazano, że w roztworze *L*-Ser zachodzą cykliczne okołodobowe zmiany zmętnienia roztworu, w przypadku *D*-Ser obecny jest jedynie jeden skok mętności, natomiast racemat daje wykres będący kombinacją wykresów odpowiadających *L*-, i *D*-Ser.
- Badania polarymetryczne potwierdziły, iż proces samorzutnej inwersji chiralnej zachodzi w roztworach aminokwasów białkowych.
- Analiza HPLC-ELSD potwierdziła oscylacyjny charakter reakcji peptyzacji w przypadku wszystkich rozpatrywanych w niniejszej pracy aminokwasów.
- Badania układów dwuskładnikowych *L*-Ser–*L*-Met i *L*-His–*L*-Thr przeprowadzone techniką HPLC-ELSD pokazały, że zmiany stężeń poszczególnych aminokwasów w układzie dwuskładnikowym są silnie ze sobą zsynchronizowane.
- Badania układów dwuskładnikowych *L*-Ser–*L*-Met, *L*-His–*L*-Thr i *L*-Phe–*L*-Pro, przeprowadzone z wykorzystaniem spektrometrii mas potwierdziło, że w układach dwuskładnikowych powstają zarówno homo- jak i heteropeptydy wyjściowych aminokwasów.

- Przeprowadzone badania turbidymetryczne także potwierdziły oscylacyjny charakter procesów peptyzacji, a także wykazały okołodobowy cykl zmian mętności *L*-*α*-aminokwasów białkowych.
- Badania mikroskopowe układu Phe–Pro potwierdziły, że w przechowywanym roztworze aminokwasów w wyniku samorzutnej peptyzacji obecne są proste peptydy, które ulegają samoorganizacji do nano- oraz mikrostruktur peptydowych.
- Wykonane badania z wykorzystaniem spektroskopii IR potwierdziły, że otrzymane struktury peptydowe zbudowane są z oligopeptydów wyjściowych aminokwasów.
- Stwierdzono, że obecność Cys w badanym układzie dwuskładnikowym determinuje szybkość peptyzacji aminokwasów, a następnie samoorganizacji peptydów do nanostruktur peptydowych, a także determinuje kształt otrzymanej nanostruktury peptydowej w przypadku układu *L*-Pro–*L*-Cys. W przypadku układu *L*-Phe–*L*-Pro to Phe determinuje kształt otrzymanych struktur.
- Na podstawie badań SEM układu dwuskładnikowego *L*-Ser–*L*-Met oraz oraz układu jednoskładnikowego *L*-Ser stwierdzono, że Ser determinuje strukturę powierzchni otrzymanych struktur peptydowych, natomiast Met dodaje trzeci wymiar otrzymanym strukturom.
- We współpracy z prof. Irwingiem R. Epsteinem stworzono model teoretyczny opisujący tworzenie się nano- oraz mikrostruktur peptydowych w roztworach aminokwasów białkowych, oraz objaśniający mechanizmy zachodzące podczas tworzenia się nano- oraz mikrostruktur peptydowych.
- Wykonane testy biuretowe ostatecznie potwierdziły, iż proces samorzutnej peptyzacji zachodzi w roztworach aminokwasów białkowych.

VIII. BIBLIOGRAFIA

[1] M. Ghadiri, J. R. Granja, R. A. Milligan, D. McRee and N. Khazanovich, "Self-assembling organic nanotubes based on a cyclic peptide architecture," *Nature,* vol. 366, pp. 324-327, 1993.

[2] M. Ghadir, J. Granja and L. Buehler, "Artificial transmembrane ion channels from self-assembling peptide nanotubes," *Nature,* vol. 369, pp. 301-304, 1994.

[3] M. Engels, D. Bashford and M. R. Ghadiri, "Structure and Dynamics of Self-Assembling Peptide Nanotubes and the Channel-Mediated Water Organization and Self-Diffusion.A Molecular Dynamics Study," *Journal of the American Chemical Society,* vol. 117, pp. 9151-9158, 1995.

[4] P. Sadatmousav, T. Mamo and P. Chen, "Diethylene glycol functionalized self-assembling peptide nanofibers and their hydrophobic drug delivery potential," *Acta Biomaterialia,* vol. 8, pp. 3241-3250, 2012.

[5] D. M. Ryan and B. L. Nilsson, "Self-assembled amino acids and dipeptides as noncovalent hydrogels for tissue engineering," *Polymer Chemistry,* vol. 3, pp. 18-33, 2012.

[6] S. Debnath, S. Roy and R. V. Ulijn, "Peptide Nanofibers with Dynamic Instability through Nonequilibrium Biocatalytic Assembly," *Journal of the American Chemical Society,* vol. 45, pp. 16789-16792, 2013.

[7] B. He, X. Yuan and D. Jiang, "Molecular self-assembly guides the fabrication of peptide nanofiber scaffolds for nerve repair," *RCS Advances,* vol. 4, pp. 2361-23621, 2014.

[8] A. B. Seabra and N. Durán, "Biological applications of peptides nanotubes: An overview," *Peptides,* vol. 4, pp. 47-54, 2013.

[9] E. Gazit, "Self-assembled peptide nanostructures: the design of molecular building blocks and their technological utilization," *Chemical Society Reviews,* vol. 36, pp. 1263-1269, 2007.

[10] I. Żak, "Aminokwasy i pochodne," in *Chemia medyczna*, Katowice, ŚAM, 2001, pp. 221-235.

[11] L. N. Vauquelin and P. J. Robiquet, "The discovery of a new plant principle in Asparagus sativus," *Annales de Chimie,* vol. 57, pp. 88-93, 1806.

[12] W. H. Wollaston, "On cystic oxide, a new species of urinary calculus," *Philosophical Transactions of the Royal Society of London,* vol. 100, pp. 223-230, 1810.

[13] S. K. Mohanty, P. Jayasri and A. Elumalai, "Isolation of amino acids from the leaves of cicer," *International Journal of Medicinal Chemistry & Analysis,* vol. 2, pp. 73-75, 2012.

[14] G. C. Barrett and D. T. Elmore, Amino Acids and Peptides, Cambridge University Press, 1998.

[15] R. Murray, D. Granner, P. Mayes and V. Rodwell, Biochemia Harpera, Warszawa: Wydawnictwo Lekarskie PZWL, 1995.

[16] E. Bańkowski, Biochemia. Podręcznik dla studentów uczelni medycznych, Wrocław: Elsevier Urban & Partner, 2010.

[17] J. M. Berg, J. L. Tymoczko and L. Stryer, Biochemia, Warszawa : Wydawnictwo Naukowe PWN, 2009.

[18] B. D. Hames and N. M. Hooper, Krótkie wykłady – Biochemia, Warszawa: Wydawnictwo Naukowe PWN, 2009.

[19] R. Morrison and R. Boyd, Chemia Organiczna tom 1, Warszawa: Wydawnictwo Naukowe PWN, 1985.

[20] G. Hallas, Stereochemia związków organicznych, Łódź: Państwowe Wydawnictwo Naukowe, 1971.

[21] H. D. Jakubke and H. Jeschkeit, Aminokwasy, peptydy, białka, Warszawa: Państwowe Wydawnictwo Naukowe, 1989.

[22] E. Bańkowski, Biochemia. Podręcznik dla studentów studiów licencjackich i magisterskich, Wrocław: MedPharm Polska, 2006.

[23] C. Ollivaux, D. Soyez and J. Toullec, "Biogenesis of D-amino acid containing peptides/proteins: where, when and how?," *Journal of peptide science,* vol. 20, pp. 595-612, 2014.

[24] P. M. Helfman and J. Bada, "L. Aspartic acid racemization in tooth enamel from living humans," *Proceedings of the National Academy of Sciences,* vol. 72, pp. 2891-2894, 1975.

[25] N. Fujii, K. Satoh, K. Harada and Y. Ishibashi, " Simultaneous stereoinversion and isomerization at specific aspartic acid residues in αA-crystallin from human lens," *Journal of Biochemistry ,* vol. 116, pp. 663-669, 1994.

[26] A. E. Roher, J. D. Lowenson, S. Clarke, C. Wolkow, R. Wang, R. J. Cotter, I. M. Reardon, H. A. Zurcher-Neely, R. L. Heinrikson, M. J. Ball and B. D. Greenberg, "Structural alterations in the peptide backbone of β-amyloid core protein may account for its deposition and stability in Alzheimer's disease," *Journal of Biological Chemistry,* vol. 268, pp. 3072-3083, 1993.

[27] K. Hamase, A. Morikawa and K. Zaitsu, "D-Amino acids in mammals and their diagnostic value," *Journal of Chromatography B,* vol. 781 , pp. 73-91, 2002.

[28] S. A. Fuchs, R. Berger and T. J. de Koning, "D-Serine: The right or wrong isoform?," *Brain Research,* vol. 1404, pp. 104-117, 2011.

[29] S. Doonan, Białka i peptydy, Warszawa: Wydawnictwo Naukowe PWN, 2008.

[30] K. Kulka and A. Rejowski, Biochemia, Olsztyn: Wydawnictwo ART, 1998.

[31] C. Branden and J. Tooze, Introduction to Protein Structure, Nowy Jork: Garland Science, Taylor & Francis Group, 1999.

[32] "Protein Structure - A Brief Introduction - Struktura α-helisy," 09 08 2016. [Online]. Available: http://bioinfo.au-kbc.org.in/books/bi/bi.html.

[33] "Beta-Sheet (Molecular Biology) - Struktura β-harmonijki," 09 08 2016. [Online]. Available: http://what-when-how.com/molecular-biology/beta-sheet-molecular-biology/.

[34] A. Kessel and N. Ben-Tal, Introduction to proteins: structure, function, and motion, Nowy Jork: CRC Press, Taylor & Francis Group, 2011.

[35] G. A. Petsko and D. Ringe, Protein Stucture and Function, Londyn: New Science Press, 2004 .

[36] G. Wu, Amino acids Biochemistry and Nutrition, New York: CRC Press Taylor & Francis Group, 2013.

[37] M. Kohlmeier, Nutrient Metabolism: Structures, Functions, and Genetic, Londyn: Academic Press , 2003.

[38] Carl Roth, "Karta charakterystyki produktu - *L*-Cysteina," 2016.

[39] Sigma-Aldrich, "Karta charakterystyki produktu - *L*-Cysteina," 2016.

[40] W. E. Knox, "Sir Archibald Garrod's "Inborn Errors of Metabolism." I. Cystinuria," *The American Journal of Human Genetics,* vol. 10, pp. 3-32, 1958 .

[41] C. S. Biyania and J. J. Cartledgeb, "Cystinuria-Diagnosis and Management," *EAU-EBU Update Series,* vol. 4, pp. 175-183, 2006.

[42] P. Krombach, G. Wendt-Nordahl and T. Knoll, "Cystinuria and Cystine Stones," in *Urinary Tract Stone Disease*, Londyn, Springer-Verlag, 2011, pp. 207-215.

[43] T. Knoll, A. Zollner, G. Wendt-Nordahl, M. S. Michel and P. Alken, "Cystinuria in childhood and adolescence: recommendations for diagnosis, treatment, and follow-up," *Pediatric Nephrology,* vol. 20, pp. 19-24, 2005.

[44] G. Ariceta, J. A. Camacho, M. Fernández-Obispo, A. Fernández-Polo, J. Gamez, J. García-Villoria, E. L. Monteczuma, P. Leyes, N. Martín-Begué, F. Oppenheimer, M. Perelló, G. P.Morell, R. Torra, A. V. Santandreu and A. Güell, "Cystinosis in adult and adolescent patients: Recommendations for the comprehensive care of cystinosis," *Nefrología,* vol. 35, pp. 304-321, 2015.

[45] P. Karam, R. S. Alhamra, G. Nemer and J. Usta, "Spectrum of mutations in Lebanese patients with phenylalanine hydroxylase deficiency," *Gene,* vol. 515, pp. 117-122, 2013.

[46] Carl Roth, "Karta charakterystyki produktu - *L*-Fenyloalanina," 2016.

[47] Sigma-Aldrich, "Karta charakterystyki produktu - *L*-Fenyloalanina," 2016.

[48] A. Folling, "Ueber Ausscheidung von Phenylbrenztraubensaeure in den Harn als Stoffwechselanomalie in Verbindung mit Imbezillitaet," *Hoppe-Seyler's Zeitschrift für physiologische Chemie,* vol. 227, pp. 169-176, 1934.

[49] H. Bickel, J. W. Gerrard and E. M. Hickmans, "Influence of phenylalanine intake on phenylketonuria," *Lancet,* vol. 2, pp. 812-819, 1953.

[50] R. Guthrie and A. Susi, "A simple phenylalanine method for detecting phenylketonuria in large populations of newborn infants," *Pediatrics,* vol. 32, pp. 338-343, 1963.

[51] J. G. Loeber, "Neonatal screening in Europe; the situation in 2004," *Journal of Inherited Metabolic Disease,* vol. 30, pp. 430-438, 2007.

[52] I. Ozalp, T. Coskun, A. Tokatli, H. Kalkanoğlu, A. Dursun, S. Tokol, G. Köksal, M. Özgüç and R. Köse, "Newborn PKU screening in Turkey: at present and organization for future," *Turkish Journal of Pediatrics,* vol. 43, pp. 97-101, 2001.

[53] J. Zschocke, J. P. Mallory, H. G. Eiken and N. C. Nevin, " Phenylketonuria and the peoples of Northern Ireland," *Human Genetics,* vol. 100, pp. 189-194, 1997.

[54] P. Guldberg, K. F. Henriksen, I. Sipila, F. Guttler and A. dela Chapelle, "Phenylketonuria in a low incidence population: molecular characterisation of mutations in Finland," *Journal of Medical Genetics,* vol. 32, pp. 976-978, 1995.

[55] G. J. Borrajo, "Newborn screening in Latin America at the beginning of the 21st century," *Journal of Inherited Metabolic Disease,* vol. 30, pp. 466-481, 2007.

[56] J. Y. Zhan, Y. F. Qin and Z. Y. Zhao, "Neonatal screening for congenital hypothyroidism and phenylketonuria in China," *World Journal of Pediatrics,* vol. 5, pp. 136-139, 2009 .

[57] J. Jiang, X. Ma, X. Huang, X. Pei, H. Liu, Z. Tan and L. Zhu, "A survey for the incidence of phenylketonuria in Guangdong, China," *The Southeast Asian Journal of Tropical Medicine and Public Health,* vol. 34, p. 185, 2003 .

[58] S. Pangkanon, W. Charoensiriwatana, N. Janejai, W. Boonwanich and S. Chaisomchit, "Detection of phenylketonuria by the newborn screening program in Thailand," *The Southeast Asian Journal of Tropical Medicine and Public Health,* vol. 40, pp. 525-529, 2009.

[59] K. Aoki, M. Ohwada and T. Kitagawa, "Long-term Long-term follow-up study of patients with phenylketonuria detected by the newborn screening programme in Japan," *Journal of inherited metabolic disease,* vol. 30, p. 608, 2007.

[60] B. Neumeister, Diagnostyka laboratoryjna, Seria Poradników Klinicznych, Elsevier Health Sciences, 2013.

[61] S. Jarochowicz and A. Mazur, "Fenyloketonuria – choroba metaboliczna uwarunkowana genetycznie," *Przegląd Medyczny Uniwersytetu Rzeszowskiego,* vol. 1, pp. 76-90, 2007.

[62] Ł. Gawiński and T. H. Wierzba, "Wpływ histydyny na zmienność rytmu serca u szczura," *Annales Academiae Medicae Gedanensis* , vol. 36, pp. 53-61, 2006.

[63] U. B. Hendgen-Cotta, M. Kelm and T. Rassaf, "Myoglobin functions in the heart," *Free Radical Biology and Medicine,* vol. 73, pp. 252-259, 2014.

[64] Carl Roth, "Karta charakterystyki produktu - *L*-Histydyna".

[65] Sigma-Aldrich, "Karta charakterystyki produktu - *L*-Histydyna," 2016.

[66] N. Bert, "Histidinemia Current Status," *American journal of diseases of children,* vol. 113, pp. 88-92, 1967.

[67] H. Levy, "Histidinemia," Orphanet Encyclopedia, 2002.

[68] S. M. Krane, "The importance of proline residues in the structure, stability and susceptibility to proteolytic degradation of collagens," *Amino Acids,* vol. 35, pp. 703-710, 2008.

[69] D. Matthew and R. T. Raines, "Collagen Structure and Stability," *Annual Review of Biochemistry,* vol. 78, pp. 929-958, 2009.

[70] Y. Liu, G. He, K. Q. Wang, W. Xu and H.Zhou, "Hydroxyproline supplementation on the performances of high plant protein source based diets in turbot (*Scophthalmus maximus L.*)," *Aquaculture ,* vol. 433, pp. 476-480, 2014.

[71] Sigma-Aldrich, "Karta charakterystyki produktu - *trans*-4-Hydroxy-*L*-proline," 2016.

[72] R. Wang, W. R. Wilcox and S. D. Cederbaum, "Chapter 92 - Amino Acid Metabolism," in *Emery and Rimoin's Essential Medical Genetics*, Academic Press, 2013, pp. 1-42.

[73] J. H. Mueller, "A new sulphur-containing amino acid isolated from casein," *Proceedings of The Society for Experimental Biology and Medicine ,* vol. 19, pp. 161-163, 1922.

[74] J. H. Mueller, "A new sulfur-containing amino-acid isolated from the hydrolytic products of protein," *Journal of Biological Chemistry,* vol. 56, pp. 157-169, 1923.

[75] G. Barger and F. P. Coine, "The amino-acid methionine; constitution and synthesis," *Biochemical Journal,* vol. 22, pp. 1417-1425, 1928.

[76] T. Willke, "Methionine production—a critical review," *Applied Microbiology and Biotechnology,* vol. 98, pp. 9893-9914, 2014.

[77] Sigma Aldrich, "Karta charakterystyki produktu - *L*-metionina," 2016.

[78] "Chemical Synthesis Database," 2016. [Online]. Available: http://www.chemsynthesis.com/base/chemical-structure-293.html.

[79] T. Kumar, G. S. Sharma and L. R. Singh, "Homocystinuria: Therapeutic approach," *Clinica Chimica Acta,* vol. 458, pp. 55-62, 2016.

[80] M. F. El-Said, R. Badii, M. S. Bessisso, N. Shahbek, M. G. El-Ali, M. El-Marikhie, M. El-Zyoid, M. S. Salem, A. Bener, G. F. Hoffmann and J. Zschocke, "A common mutation in the CBS gene explains a high incidence of homocystinuria in the Qatari population," *Human Mutation,* vol. 27, p. 719, 2006.

[81] E. R. Naughten, S. Yap and P. D. Mayne, " Newborn screening for homocystinuria: Irish and world experience," *European Journal of Pediatrics,* vol. 157, pp. 84-87, 1998.

[82] H. Jurkowska, M. Kaczor-Kamińska, P. Bronowicka-Adamska and M. Wróbel, "γ–Liaza cystationinowa," *Postępy Higieny i Medycyny Doświadczalnej,* vol. 68, pp. 1-9, 2014.

[83] Y. H. Chiena, S. C. Chianga, A. Huanga and W. L. Hwua, "Spectrum of hypermethioninemia in neonatal screening," *Early Human Development,* vol. 81, pp. 529-533 , 2005.

[84] R. Willstätter, " Synthese der Hygrinsäure," *Berichte der Deutschen Chemischen Gesellschaft,* vol. 33, pp. 1160-1166, 1900.

[85] E. Fischer, "Zeitschrift fur Physiologische Chemie Ueber die Hydrolyse des Caseins durch Salzsäure," *Hoppe-Seyler's Zeitschrift für physiologische Chemie,* vol. 33, pp. 151-176, 1901.

[86] Sigma-Aldrich, "Karta charakterystyki produktu - *L*-Prolina".

[87] "Chemical Synthesis Database," 2016. [Online]. Available: http://www.chemsynthesis.com/base/chemical-structure-8661.html

[88] C. L. Clelland, L. L. Read, A. N. Baraldi, C. P. Bart, C. A. Pappas, L. J. Panek, R. H. Nadrich and J. D. Clelland, "Evidence for association of hyperprolinemia with schizophrenia and a measure of clinical outcome," *Schizophrenia Research,* vol. 131, pp. 139-145, 2011.

[89] E. Cramer, "Ueber die Bestandteile der Seide," *Journal für praktische chemie,* vol. 96, pp. 76-98, 1865.

[90] E. Fischer and H. Leuchs, "Synthese des Serins, der l-Glucosaminsaure und anderer Oxyaminosauren,"*Berichte der deutschen chemischen Gesellschaft,* vol. 1902, pp. 3787-3805, 1902.

[91] A. W. El-Hattab, "Serine biosynthesis and transport defects," *Molecular Genetics and Metabolism,* pp. 153-159, 2016.

[92] Sigma-Aldrich, "Karta charakterystyki produktu - *L*-seryny," 2016.

[93] B. Chauhan, Principles of Biochemistry and Biophysics, Firewall Media, 2008.

[94] R. H. McCoy, C. E. Meyer and W. C. Rose, "Feeding Experiments with Mixtures of Highly Purified Amino Acids. VIII. Isolation and Identification of a New Essential Amino Acid," *Journal of Biological Chemistry,* vol. 112, pp. 283-302, 1935.

[95] I. Contineanu, A. Neacşu, D. Gheorghe, S. Tănăsescu and Ş. Perişanu, "The thermochemistry of threonine stereoisomers," *Thermochimica Acta,* vol. 563, pp. 1-5, 2013.

[96] Sigma-Aldrich, "Karta charakterystyki produktu - *L*-treoniny," 2016.

[97] "Chemical Synthesis Database," 2016. [Online]. Available: http://www.chemsynthesis.com/base/chemical-structure-40361.html .

[98] L. Gosen, "Organic acidemias: a methylmalonic and propionic focus," *Journal of Pediatric Nursing* , vol. 23, pp. 225-233, 2008.

[99] S. Malvagia, C. A. Haynes, L. Grisotto, D. Ombrone, S. Funghini, E. Moretti, K. S. McGreevy, A. Biggeri, R. Guerrini, R. Yahyaoui, U. Garg, M. Seeterlin, D. Chace, V. R. D. Jesus and G. l. Marca, "Heptadecanoylcarnitine (C17) a novel candidate biomarker for newborn screening of propionic and methylmalonic acidemias," *Clinica Chimica Acta,* vol. 450, pp. 342-348, 2015.

[100] M. Msharrafieh, M. Al-Ghoul, F. Zaknoun, H. El-Rassy, S. El-Joubeily and R. Sultan, "Simulation of geochemical banding I: Acidization-precipitation experiments in a ferruginous limestone rock," *Chemical Geology,* vol. 440, pp. 42-49, 2016.

[101] M. Orlik, Reakcje oscylacyjne porządek i chaos, Warszawa: Wydawnictwa Naukowo - Techniczne, 1996.

[102] S. Kinoshita, Pattern Formations and Oscillatory Phenomena, Elsevier, 2013.

[103] K. U. Torii, "Two-dimensional spatial patterning in developmental systems," *Trends in Cell Biology,* vol. 22, pp. 438-446, 2012.

[104] S. Kondoa, "The reaction-diffusion system: a mechanism for autonomous pattern formation in the animal skin," *Genes to Cells,* vol. 7, pp. 535-541, 2002.

[105] B. P. Belousov, "Периодически действующая реакция и ее механизм [Periodically acting reaction and its mechanism]," *Сборник рефератов по радиационной медицине,* p. 147:145, 1959.

[106] A. M. Zhabotinsky, "Периодический процесс окисления малоновой кислоты растворе [Periodical process of oxidation of malonic acid solution]," *Биофизика,* vol. 9, pp. 306-311, 1964.

[107] R. J. Field, E. Koros and R. M. Noyes, "Oscillations in Chemical Systems," *Journal of the American Chemical Society ,* vol. 94, pp. 8649- 8664, 1972.

[108] M. Sajewicz, M. Gontarska and T. Kowalska, "HPLC-DAD evidence of the oscillatory chiral conversion of phenylglycine," *Journal of Chromatographic Science,* vol. 52, pp. 329-333, 2014.

[109] M. Sajewicz, M. Gontarska, D. Kronenbach and T. Kowalska, "On the Spontaneous Abiotic Peptization of Phenylglycine in an Aqueous Medium," *Acta Chromatographica,* vol. 22, pp. 151-160, 2009.

[110] M. Sajewicz, M. Gontarska, D. Kronenbach, M. Leda, T. Kowalska and I. R. Epstein, "Condensation oscillations in the peptidization of phenylglycine," *Journal of Systems Chemistry ,* vol. 7, pp. 1-16, 2010.

[111] M. Sajewicz, D. Kronenbach, M. Gontarska, M. Wróbel, R. Piętka and T. Kowalska, "TLC in search for structural limitations of spontaneous oscillatory in-vitro chiral conversion. a-Hydroxybutyric and mandelic acids," *Journal of Planar Chromatography – Modern TLC,* vol. 22, pp. 241-248, 2009.

[112] M. Sajewicz, M. Gontarska, D. Kronenbach, E. Berry and T. Kowalska, "Condensation Oscillations in the Condensation of Mandelic Acid," *Acta Chromatographica,* vol. 24, pp. 1-13, 2012.

[113] M. Sajewicz, M. Matlengiewicz, D. Kronenbach, M. Gontarska and T. Kowalska, "On the Spontaneous Condensation of Selected Hydroxy Acids," *Acta Chromatographica,* vol. 21 , pp. 259-271, 2009.

[114] M. Sajewicz, M. Leda, M. Gontarska, D. Kronenbach, T. Kowalska and I. Epstein, "Spontaneous oscillatory in vitro chiral conversion of simple carboxylic acids and its possible mechanism," *Journal of Physical Organic Chemistry,* vol. 23,pp. 1066-1073, 2010.

[115] M. Sajewicz, R. Piętka and T. Kowalska, "Chiral separation of S-(+)- and R-(-)-ibuprofen by thin-layer chromatography. An improved analytical procedure," *Journal of Planar Chromatography - Modern TLC,* vol. 17, pp. 173-176, 2004.

[116] M. Sajewicz, R. Piętka, A. Pieniak and T. Kowalska, "Application of thin-layer chromatography (TLC) to investigating oscillatory instability of the selected profen enantiomers," *Acta Chromatographica,* vol. 15, pp. 131-149, 2005.

[117] M. Sajewicz, R. Piętka and T. Kowalska, "Chiral separations of ibuprofen and propranolol by TLC. A study of the mechanism and thermodynamics of retention," *Journal of Liquid Chromatography & Related Technologies,* vol. 28, pp. 2499-2513, 2005.

[118] M. Sajewicz, M. Gontarska, D. Kronenbach, E. Berry and T. Kowalska, "An HPLC–DAD and LC–MS study of condensation oscillations with S(+)-ketoprofen dissolved in acetonitrile," *Journal of Chromatographic Science,* vol. 50, pp. 237-244, 2012.

[119] M. Sajewicz, M. Dolnik, T. Kowalska and I. R. Epstein, "Condensation dynamics of L-proline and L-hydroxyproline in solution," *RSC Advances,* vol. 4, pp. 7330-7339, 2014.

[120] J. Castillo, L. Sasso and W. E. Svendsen, Self-Assembled Peptide Nanostructures: Advances and Applications in Nanobiotechnology, Denvers, MA, USA: Pan Stanford, 2013.

[121] Y. Sun, A. Shieh, S. H. Kim, S. King, A. Kim, H. L. Sun, C. M. Croce and J. R. Parquette, "The self-assembly of a camptothecin-lysine nanotube," *Bioorganic & Medicinal Chemistry Letters,* vol. 26, pp. 2834-2838, 2016.

[122] R. Huang, Y. Wang, W. Qi, R. Su and Z. He, "Chemical catalysis triggered self-assembly for the bottom-up fabrication of peptide nanofibers and hydrogels," *Materials Letters,* vol. 128, pp. 216-219, 2014.

[123] K. Shi, Y. Fang, Q. Kan, J. Zhao, Y. Gan and Z. Liu, "Surface functional modification of self-assembled insulin nanospheres for improving intestinal absorption," *International Journal of Biological Macromolecules,* vol. 74, pp. 49-60, 2015.

[124] N. Habibi, N. Kamaly, A. Memic and H. Shafiee, "Self-assembled peptide-based nanostructures: Smart nanomaterials toward targeted drug delivery," *Nano Today,* vol. 11, pp. 41-60, 2016.

[125] R. J. Brea, C. Reiriz and J. R. Granja, "Towards functional bionanomaterials based on self-assembling cyclic peptide nanotubes," *Chemical Society Reviews,* vol. 39, pp. 1448-1456, 2010.

[126] S. Zhang, T. Holmes, C. Lockshin and A. Rich, "Spontaneous assembly of a self-complementary oligopeptide to form a stable macroscopic membrane," *PNAS,* vol. 90, pp. 3334-3338, 1993.

[127] T. C. Holmes, S. deLacalle, X. Su, G. Liu, A. Rich and S. Zhang, "Extensive neurite outgrowth and active synapse formation on self-assembling peptide scaffolds," *PNAS,* vol. 97, pp. 6728-6733, 2000.

[128] R. V. Ulijn and A. M. Smith, "Designing peptide based nanomaterials," *Chemical Society Reviews,* vol. 37, pp. 664-675, 2008.

[129] C. Tang, F. Qiu and X. Zhao, "Molecular Design and Applications of Self-Assembling Surfactant-Like Peptides," *Journal of Nanomaterials,* vol. 2013, pp. 1-9, 2013.

[130] B. Caughey and P. T. Lansbury, "Protofibrils, pores, fibrils, and neurodegeneration: separating the responsible protein aggregates from the innocent bystanders," *Annual Review of Neuroscience,* vol. 26, pp. 267-298, 2003.

[131] R. Nelson, M. R. Sawaya, M. Balbirnie, A. O. Madsen, C. Riekel, R. Grothe and D. Eisenberg, "Structure of the cross-β spine of amyloid-like fibrils," *Nature,* vol. 435, pp. 773-778, 2005.

[132] Y. Compta, M. Buongiorno, N. Bargalló, F. Valldeoriola, E. Muñoz, E. Tolosa, R. J., A. Cámara, M. Fernández and M. J. Martí, "White matter hyperintensities, cerebrospinal amyloid-β and dementia in Parkinson's disease," *Journal of the Neurological Sciences,* vol. 367, pp. 284-290, 2016.

[133] M. Buongiorno, Y. Compta and M. J. Martí, "Amyloid-β and τ biomarkers in Parkinson's disease–dementia," *Journal of the Neurological Sciences ,* vol. 310, pp. 25-30, 2011.

[134] J. Miklossy, H. Qing, A. Radenovic, A. Kis, B. Vileno, F. Làszló, L. Miller, R. N. Martins, G. Waeber, V.Mooser, F. Bosman, K. Khalili, N. Darbinian and P. L. McGeer, "Beta amyloid and hyperphosphorylated tau deposits in the pancreas in type 2 diabetes," *Neurobiology of Aging,* vol. 31, pp. 1503-1515, 2010.

[135] K. Tenidis, M. Waldner, J. Bernhagen, W. Fischle, M. Bergmann, M. Weber, M. Merkle, W. Voelter, H. Brunner and A. Kapurniotu, " Identification of a penta- and hexapeptide of islet amyloid polypeptide (IAPP) with amyloidogenic and cytotoxic properties," *Journal of Molecular Biology,* vol. 295, pp. 1055-1071, 2000.

[136] R. Azriel and E. Gazit, "Analysis of the minimal amyloid-forming fragment of the islet amyloid polypeptide," *Journal of Biological Chemistry,* vol. 276, pp. 34156-34161, 2001.

[137] E. Gazit, "A possible role for π-stacking in the self-assembly of amyloid fibrils," *FASEB Journal,* vol. 16, pp. 77-83, 2002.

[138] E. Gazit, "Self Assembly of Short Aromatic Peptides into Amyloid Fibrils and Related Nanostructures," *Prion,* vol. 1, pp. 32-35, 2007.

[139] Y. Mazor, S. Gilead, I. Benhar and E. Gazit, "Identification and characterization of a novel molecular-recognition and self-assembly domain within the islet amyloid polypeptide," *Journal of Molecular Biology,* vol. 322, pp. 1013-1024, 2002.

[140] M. Reches and E. Gazit, "Casting metal nanowires within discrete self-assembled peptide nanotubes," *Science,* vol. 300, pp. 625-627, 2003.

[141] L. Adler-Abramovich, M. Reches, V. L. Sedman, S. Allen, S. J. B. Tendler and E. Gazit, "Thermal and Chemical Stability of Diphenylalanine Peptide Nanotubes: Implications for Nanotechnological Applications," *Langmuir,* vol. 22, pp. 1313-1320, 2006.

[142] N. Kol, L. Adler-Abramovich, D. Barlam, R. Z. Shneck, E. Gazit and I. Rousso, "Self-Assembled Peptide Nanotubes Are Uniquely Rigid Bioinspired Supramolecular Structures," *Nano Letters,* vol. 5, pp. 1343-1346, 2005.

[143] Y. Song, S. R. Challa, C. J. Medforth, Y. Qiu, R. K. Watt, D. Pena, J. E. Miller, F. vanSwol and J. A. Shelnutt, "Synthesis of peptide-nanotube platinum-nanoparticle composites," *Chemical Communications,* pp. 1044-1045, 2004.

[144] X. Han, C. Huang, X. Chen, Y. Lu and W. Yang, "Anodic electrogenerated chemiluminescence of self-assembled peptide nanotubes in an aqueous system," *Chemical Communications,* vol. 51, pp. 14720-14723, 2015.

[145] J. S. Lee, I. Yoon, J. Kim, H. Ihee, B. Kim and C. B. Park, " Self-Assembly of Semiconducting Photoluminescent Peptide Nanowires in the Vapor Phase," *Angewandte Chemie International Edition,* vol. 50, pp. 1164-1167, 2011.

[146] R. Huang, W. Qi, R. Su, J. Zhaoa and Z. Hea, "Solvent and Surface Controlled Self-assembly of diphenylalanine Peptide: from Microtubes to Nanofibers," *Soft Matter,* vol. 7, pp. 6418-6418, 2011.

[147] R. Huang, R. Su, W. Qi, J. Zhao and Z. He, "Hierarchical, interface-induced self-assembly of diphenylalanine: formation of peptide nanofibers and microvesicles," *Nanotechnology,* vol. 22, p. 245609, 2011.

[148] S. Yuran, Y. Razvag and M. Reches, "Coassembly of Aromatic Dipeptides into Biomolecular Necklaces," *ACS Nano,* vol. 6, pp. 9559-9566, 2012.

[149] S. Yuran and M. Reches, "Formation of Ordered Biomolecular Structures by the Self-assembly of Short Peptides," *Journal of Visualized Experiments,* vol. 81, p. e50946, 2013.

[150] Q. Li, Y. Jia, L. Dai, Y. Yang and J. Li, "Controlled Rod Nanostructured Assembly of Diphenylalanine and Their Optical Waveguide Properties," *ACS Nano,* vol. 9, pp. 2689-2695, 2015.

[151] A. Nuraeva, S. Vasilev, D. Vasileva, P. Zelenovskiy, D. Chezganov, A. Esin, S. Kopyl, K. Romanyuk, V. Y. Shur and A. L. Kholkin, "Evaporation-Driven Crystallization of Diphenylalanine Microtubes for Microelectronic Applications," *Crystal Growth & Design* , vol. 16, pp. 1472-1479, 2016.

[152] A. M. Smith, R. J. Williams, C. Tang, P. Coppo, R. F. Collins, M. L. Turner, A. Saiani and R. V. Ulijn, "Fmoc-Dipheny lalanine Self Assembles to a Hydrogel via a Novel Architecture Based on π–π Interlocked β-Sheets," *Advanced Materials,* vol. 20, pp. 37-41, 2008.

[153] C. Tang, A. M. Smith, R. F. Collins, R. V. Ulijn and A. Saiani, "Fmoc-Diphenylalanine Self-Assembly Mechanism Induces Apparent pKa Shifts," *Langmuir* , vol. 25, pp. 9447-9453, 2009.

[154] M. Reches and E. Gazit, "Formation of Closed-Cage Nanostructures by Self-Assembly of Aromatic Dipeptides," *Nano Letters* , vol. 4, pp. 581-585, 2004.

[155] F. Zhang, G. S. Shi, L. F. Ren, F. Q. Hu, S. L. Li and Z. J. Xie, "Designer selfassembling peptide scaffold stimulates pre-osteoblast attachment, spreading and proliferation," *Journal of Materials Science: Materials in Medicine*, vol. 20, pp. 1475-1481, 2009.

[156] S. Kyle, A. Aggeli, E. Ingham and M. J. McPherson, "Recombinant self-assembling peptides as biomaterials for tissue engineering," *Biomaterials*, vol. 31, pp. 9395-9405, 2010.

[157] H. Meng, L. Y. Chen, Z. Y. Ye, S. T. Wang and X. J. Zhao, "The Effect of a SelfAssembling Peptide Nanofiber Scaffold (Peptide) When Used as a Wound Dressing for the Treatment of Deep Second Degree Burns in Rats," *Journal of Biomedical Materials Research Part B-Applied Biomaterials,* vol. 89B, pp. 379-391, 2009.

[158] F. Li, J. Wang, F. S. Tang, J. Lin, Y. Zhang, E. Y. Zhang, C. Wei, Y. K. Shi and X. Zhao, "Fluorescence Studies on a Designed Self-Assembling Peptide of RAD16-II as a Potential Carrier for Hydrophobic Drug," *Journal of Nanoscience and Nanotechnology,* vol. 9, pp. 1611-1614, 2009.

[159] O. A. Carballo-Molina and I. Velasco, "Hydrogels as scaffolds and delivery systems to enhance axonal regeneration after injuries," *Frontiers in Cellular Neuroscience,* vol. 9, pp. 1-12, 2015.

[160] J. Kisiday, M. Jin, B. Kurz, H. Hung, C. Semino, S. Zhang and A. J. Grodzinsky, "Self-assembling peptide hydrogel fosters chondrocyte extracellular matrix production and cell division: Implications for cartilage tissue repair," *Proceedings of the National Academy of Sciences,* vol. 99, pp. 9996-10001, 2002.

[161] H. Yang, S. Y. Fung, M. Pritzker and P. Chen, "Ionic-Complementary Peptide Matrix for Enzyme Immobilization and Biomolecular Sensing," *Langmuir,* vol. 25, pp. 7773-7777, 2009.

[162] J. H. Kim, S. Y. Lim, D. H. Nam, J. Ryu, S. H. Ku and C. B. Park, "Self-assembled, photoluminescent peptide hydrogel as a versatile platform for enzyme-based optical biosensors," *Biosensors & Bioelectronics,* vol. 26, pp. 1860-1865, 2011.

[163] J. H. Kim, J. Ryu and C. B. Park, "Selective Detection of Neurotoxin by Photoluminescent Peptide Nanotubes," *Small,* vol. 7, pp. 718-722, 2011.

[164] M. Yemini, M. Reches, E. Gazit and J. Rishpon, "Peptide nanotube-modified electrodes for enzyme-biosensor applications," *Analytical Chemistry,* vol. 77, pp. 5155-5159, 2005.

[165] B. Khalilzadeh, N. Shadjou, M. Eskandani, H. N. Charoudeh, Y, Omidiac and M. R. Rashidi, "A reliable self-assembled peptide based electrochemical biosensor for detection of caspase 3 activity and apoptosis," *RSC Advances,* vol. 5, pp. 58316-58326, 2015.

[166] D. Mena, Z. P. Zhang, Y. C. Guo, D. H. Zhu, L. J. Bi, J. Y. Deng, Z. Q. Cui, H. P. Wei and X. E. Zhang, "An auto-biotinylated bifunctional protein nanowire for ultra-sensitive molecular biosensing," *Biosensors & Bioelectronics,* vol. 26, pp. 1137-1141, 2010.

[167] E. C. Cho, J. W. Choi, M. Y. Lee and K. K. Koo, " Fabrication of an electrochemical immunosensor with self-assembled peptide nanotubes," *Colloids and Surfaces A: Physicochemical and Engineering Aspects,* vol. 313, pp. 95-99, 2008.

[168] M. R. Ghadiri, J. R. Granja and L. K. Buehler, "Artificial transmembrane ion channels from self-assembling peptide nanotubes," *Nature,* vol. 369, pp. 301-304, 1994.

[169] W. S. Horne, C. M. Wiethoff, C. Cui, K. M. Wilcoxen, M. Amorin, M. R. Ghadiri and G. R. Nemerow, "Antiviral cyclic D,L-alpha-peptides: Targeting a general biochemical pathway in virus infections," *Bioorganic & Medicinal Chemistry,* vol. 13, pp. 5145-5153, 2005.

[170] A. Montero, P. Gastaminza, M. Law, G. Cheng, F. V. Chisari and M. R. Ghadiri, "Self-Assembling Peptide Nanotubes with Antiviral Activity against Hepatitis C Virus," *Chemistry & Biology,* vol. 18, pp. 1453-1462, 2011.

[171] A. Dehsorkhi, V. Castelletto and I. W. Hamley, "Self-assembling amphiphilic peptides," *Journal of Peptide Science* , vol. 20, pp. 453-467, 2014.

[172] H. Freeman, J. Smith and J. Taylor, "Crystallographic studies of the biuret reaction. I. Potassium bis-biuret cuprate(II) tetrahydrate, K2[Cu(NHCONHCONH)2].4H2O," *Acta Crystallographica,* vol. 14, pp. 407-418, 1961.

[173] M. M. Bradford, "A rapid and sensitive method for the quantitation of microgram quantities of protein utilizing the principle of protein-dye binding," *Analytical Biochemistry,* vol. 72, pp. 248-254, 1976.

[174] A. Maciejowska, A. Godziek, M. Sajewicz and T. Kowalska, "Chiral Conversion and Condensation of L-Hydroxyproline in an Abiotic Liquid System," *Acta Chromatographica,* vol. 26, pp. 355-369, 2014.

[175] M. Sajewicz, M. Matlengiewicz, M. Juziuk, M. Penkala, M. Weloe, M. Schulz and T. Kowalska, "Thin-layer chromatographic evidence of proline peptidization in solution and its thin-layer chromatographic enentiosparation," *Journal of Liquid Chromatography & Related Technologies,* vol. 36, pp. 2497-2511, 2013.

[176] A. Godziek, A. Maciejowska, M. Sajewicz and T. Kowalska, "Dynamics of Spontaneous Peptidization of L-,D- and DL-Serine in an Abiotic Solution as Investigated with Use of TLC-Densitometry and the Auxiliary Chromatographic Techniques," *Journal of Chromatographic Science,* vol. 54, pp. 1090-1095, 2016.

[177] A. Maciejowska, A. Godziek, M. Sajewicz and T. Kowalska, "Circadian Rhythm of Spontaneous non-Linear Peptidization with Proteinogenic Amino Acids in Abiotic Solutions versus Homochirality," *Acta Chromatographica,* vol. 29, pp. 135-142, 2017

[178] W. Kunz, Specific Ion Effects, USA: World Scientific Publishing, 2010.

[179] A. Maciejowska, A. Godziek, M. Sajewicz and T. Kowalska, "Investigation of Spontaneous Non-Linear Peptidization Dynamics and Mechanism with Selected α-Amino Acid Pairs," *Reaction Kinetics, Mechanisms and Catalysis,* vol. 118, pp. 129-142, 2016.

[180] M. Piraud, C. Vianey-Saban, K. Petritis, C. Elfakir, J. P. Steghens, A. Morla and D. Bouchu, "ESI-MS/MS analysis of underivatised amino acids: a new tool for the diagnosis of inherited disorders of amino acid metabolism. Fragmentation study of 79 molecules of biological interest in positive and negative ionization mode," *Rapid Communications in Mass Spectrometry* , vol. 17, pp. 1297-1311, 2003.

[181] A. Godziek, A. Maciejowska, M. Sajewicz and T. Kowalska, "HPLC Monitoring of Spontaneous Non-Linear Peptidization Dynamics of Selected Amino Acids in Solution," *Journal of Chromatographic Science,* vol. 53, pp. 401-410, 2015.

[182] A. Maciejowska, A. Godziek, E. Talik, M. Sajewicz, T. Kowalska and I. R. Epstein, "Spontaneous Pulsation of Peptide Microstructures in an Abiotic Liquid System," *Journal of Chromatographic Science,* vol. 54, pp. 1301-1309, 2016.

[183] M. Sajewicz, A. Godziek, A. Maciejowska and T. Kowalska, "Condensation dynamics of the L-Pro–L-Phe and L-Hyp–L-Phe binary mixtures in solution," *Journal of Chromatographic Science,* vol. 53, pp. 31-37, 2015.

[184] A. Godziek, A. Maciejowska, E. Talik, R. Wrzalik, M. Sajewicz and T. Kowalska, "On spontaneously pulsating proline-phenylalanine peptide microfibers," *Current Protein & Peptide Science,* vol. 17, pp. 106-116, 2016.

[185] A. Maciejowska, A. Godziek, M. Sajewicz and T. Kowalska, "Turbidity patterns of spontaneous peptidization in an aqueous abiotic system and possible secondary peptide structures", *Reaction Kinetics, Mechanisms and Catalysis*, vol. 120, pp. 421-437, 2017

[186] A. Godziek, A. Maciejowska, E. Talik, M. Sajewicz and T. Kowalska, "Thin-Layer Chromatographic Investigation of L-Cysteine in Solution," *Journal of Planar Chromatography*, vol. 28, pp. 144-151, 2015.

[187] A. Godziek, A. Maciejowska, E. Talik, M. Sajewicz and T. Kowalska, "Scanning electron microscopic confirmation of spontaneous heteropeptide formation in abiotic solutions of selected α-amino acid pairs," *Israel Journal of Chemistry,* vol. 56, pp. 1057- 1066, 2016.

[188] M. Sajewicz, M. Dolnik, D. Kronenbach, M. Gontarska, T. Kowalska and I. R.Epstein, "Oligomerization Oscillations of L-Lactic Acid in Solution," *Journal of Physical Chemistry A*, vol. 115, pp. 14331-14339, 2011.

[189] P. V. Coveney and J. A. D. Wattis, "Coarse-graining and renormalization group methods for the elucidation of the kinetics of complex nucleation and growth processes," *Molecular Physics*, vol. 104, pp. 177-185, 2006.

[190] T. Antal, M. Droz, J. Magnin, Z. Rácz and M. Zrinyi, "Derivation of the Matalon-Packter Law for Liesegang Patterns," *Journal of Chemical Physics,* vol. 109, pp. 9479-9486, 1998.

IX. LISTA PRAC WŁASNYCH TEMATYCZNIE ZWIĄZANYCH Z ROZPRAWĄ DOKTORSKĄ

1. A. Maciejowska, **A. Godziek**, M. Sajewicz, T. Kowalska, "Chiral Conversion and Condensation of *L*-Hydroxyproline in an Abiotic Liquid System", *Acta Chromatographica*, **26**, 355-369, 2014
2. M. Sajewicz, **A. Godziek**, A. Maciejowska, T. Kowalska, "Condensation dynamics of the *L*-Pro–*L*-Phe and *L*-Hyp–*L*-Phe binary mixtures in solution", *Journal of Chromatographic Science*, **53**, 31-37, 2015
3. **A. Godziek,** A. Maciejowska, M. Sajewicz, T. Kowalska, "HPLC Monitoring of Spontaneous Non-Linear Peptidization Dynamics of Selected Amino Acids in Solution", *Journal of Chromatographic Science*, **53**, 401-410, 2015
4. **A. Godziek**, A. Maciejowska, E. Talik, R. Wrzalik, M. Sajewicz, T. Kowalska, "On spontaneously pulsating proline-phenylalanine peptide microfibers", *Current Protein & Peptide Science*, **17**, 100-16, 2016
5. A. Maciejowska, **A. Godziek**, M. Sajewicz, T. Kowalska, „Investigation of Spontaneous Non-Linear Peptidization Dynamics and Mechanism with Selected α-Amino Acid Pairs", *Reaction Kinetics, Mechanisms and Catalysis*, **118**, 129-142, 2016
6. **A. Godziek**, A. Maciejowska, M. Sajewicz, T. Kowalska, „Dynamics of Spontaneous Peptidization of *L*-,*D*- and *DL*-Serine in an Abiotic Solution as Investigated with Use of TLC-Densitometry and the Auxiliary Chromatographic Techniques", *Journal of Chromatographic Science*, **54**, 1090–1095, 2016
7. A. Maciejowska, **A. Godziek**, E. Talik, M. Sajewicz, T. Kowalska, I. R. Epstein, "Spontaneous Pulsation of Peptide Microstructures in an Abiotic Liquid System", *Journal of Chromatographic Science*, **54**, 1301-1309, 2016
8. **A. Godziek**, A. Maciejowska, E. Talik, M. Sajewicz, and T. Kowalska, „Scanning electron microscopic confirmation of spontaneous heteropeptide formation in abiotic solutions of selected *α*-amino acid pairs", *Israel Journal of Chemistry*, **56**, 1057– 1066, 2016
9. A. Maciejowska, **A. Godziek**, M. Sajewicz, T. Kowalska, „Circadian Rhythm of Spontaneous non-Linear Peptidization with Proteinogenic Amino Acids in Abiotic Solutions versus Homochirality", *Acta Chromatographica*, **29**, 135-142, 2017

X. LISTA POZOSTAŁYCH PRAC WŁASNYCH

1. **A. Godziek**, A. Maciejowska, E. Talik, M. Sajewicz, T. Kowalska, "Thin-Layer Chromatographic Investigation of *L*-Cysteine in Solution", *Journal of Planar Chromatography*, **28,** 144-151, 2015
2. A. Maciejowska, **A. Godziek**, E. Talik, M. Sajewicz, T. Kowalska, "Investigation of Spontaneous Chiral Conversion and Oscillatory Peptidization of L-Methionine by Means of TLC and HPLC", *Journal of Liquid Chromatography & Related Technologies*, **38**, 1164-1171, 2015
3. A. Maciejowska, **A. Godziek**, M. Sajewicz, T. Kowalska, "Turbidity patterns of spontaneous peptidization in an aqueous abiotic system and possible secondary peptide structures", *Reaction Kinetics, Mechanisms and Catalysis*, **120**, 421-437, 2017
4. **A. Godziek,** A. Maciejowska, M. Sajewicz, and T. Kowalska, *Spontaneous Chiral Conversion and Peptidization of Amino Acids Traced by Means of TLC–MS*; w "Planar Chromatography – Mass Spectrometry", rozdział 19 w pracy zbiorowej pod red. T. Kowalskiej, M. Sajewicza i J. Shermy, Chromatographic Science Series, Vol. 110, ISBN 9781498705882, CRC Press, Taylor & Francis Group, Boca Raton, FL, USA, 2015

XI. LISTA PUBLIKACJI KONFERENCYJNYCH

Wystąpienia ustne:

1. **A. Godziek**, A. Maciejowska, E. Talik, T. Kowalska, M. Sajewicz, *Investigation of the peptide nanofibers and nanospheres formation by chromatographic and microscopic techniques,* XXXVIII Sympozjum nt. „Chromatograficzne metody badania związków organicznych", 26-29 maj 2015, Katowice – Szczyrk
2. **A. Godziek**, A. Maciejowska, T. Kowalska, M. Sajewicz, *Niekonwencjonalne zastosowanie znanych technik analitycznych do badania reakcji samorzutnej peptyzacji aminokwasów białkowych w roztworach abiotycznych*, VI Ogólnopolska Konferencja Studencka „ Nowoczesne metody doświadczalne w fizyce, chemii i inżynierii", 27-29 listopad 2015, Lublin

Postery:

1. M. Sajewicz, **A. Godziek**, A. Maciejowska, T. Kowalska, *Chromatograficzne badanie reakcji oscylacyjnych wybranych aminokwasów*, VII Seminarium Naukowe nt. "Aktualne Problemy Chemii Analitycznej", 17 maj 2013, Katowice
2. **A. Godziek**, A. Maciejowska, M. Sajewicz, T. Kowalska, *HPLC/DAD, HPLC/ELSD, and LC-MS investigation of spontaneous oscillatory reactions of L-phenylalanine and L-hydroxyproline in 70% aqueous acetonitrile solutions,* XXXVI Sympozjum nt. „Chromatograficzne metody badania związków organicznych", 5-7 czerwiec 2013, Katowice – Szczyrk
3. A. Maciejowska, **A. Godziek**, M. Sajewicz, T. Kowalska, *Chromatographic methods of investigating spontaneous oscillatory reactions of L-phenylalanine and L-proline in aqueous solutions,* XXXVI Sympozjum nt. „Chromatograficzne metody badania związków organicznych", 5-7 czerwiec 2013, Katowice – Szczyrk
4. **A. Godziek**, A. Maciejowska, M. Sajewicz, T. Kowalska, *Zastosowanie metod chromatograficznych do badania reakcji oscylacyjnych L-fenyloalaniny oraz L-hydroksyproliny*, Pomiędzy Naukami Zjazd Fizyków i Chemików II Ogólnopolska Konferencja dla Studentów i Doktorantów, 27 wrzesień 2013, Chorzów

5. A. Maciejowska, **A. Godziek**, M. Sajewicz, T. Kowalska, *Badanie reakcji oscylacyjnych pary aminokwasów (L-fenyloalaniny i L-proliny) metodami chromatograficznymi*, Pomiędzy Naukami Zjazd Fizyków i Chemików II Ogólnopolska Konferencja dla Studentów i Doktorantów, 27 wrzesień 2013, Chorzów
6. **A. Godziek**, A. Maciejowska, M. Sajewicz, T. Kowalska, *Badanie reakcji samorzutnej peptyzacji wybranych aminokwasów w roztworach niewodnych*, Zimowy Zjazd Sekcji Studenckiej Polskiego Towarzystwa Chemicznego, 7 grudzień 2013, Łódź
7. A. Maciejowska, **A. Godziek**, M. Sajewicz, T. Kowalska, *Badanie reakcji samorzutnej peptyzacji wybranych aminokwasów w roztworach wodnych*, Zimowy Zjazd Sekcji Studenckiej Polskiego Towarzystwa Chemicznego, 7 grudzień 2013, Łódź
8. **A. Godziek**, A. Maciejowska, M. Sajewicz, T. Kowalska, *Chromatographic evidence of oscillatory inversion and condensation of L-cysteine*, X Międzynarodowej Konferencji pt. Chromatografia jonowa 2014, 9-10 kwiecień 2014, Zabrze
9. A. Maciejowska, **A. Godziek**, M. Sajewicz, T. Kowalska, *Investigation of oscillatory reaction of L-methionine by chromatographic methods*, X Międzynarodowej Konferencji pt. Chromatografia jonowa 2014, 9-10 kwiecień 2014, Zabrze
10. **A. Godziek**, A. Maciejowska, M. Sajewicz, T. Kowalska, *Chromatograficzne badania oscylacyjnej peptyzacji i inwersji chiralnej L-treoniny i L-cysteiny*, VIII Seminarium Naukowe nt. "Aktualne Problemy Chemii Analitycznej", 16 maj 2014, Katowice
11. A. Maciejowska, **A. Godziek**, M. Sajewicz, T. Kowalska, *L-Seryna oraz L-metionina, jako przykład związków ulegających reakcji oscylacyjnej peptyzacji*, VIII Seminarium Naukowe nt. "Aktualne Problemy Chemii Analitycznej", 16 maj 2014, Katowice
12. **A. Godziek,** A. Maciejowska, E. Talik, R. Wrzalik, M. Sajewicz, T. Kowalska, *Investigation of self-organization of selected amino acids in aqueous solutions*, 4. Konferencja Polskiego Towarzystwa Spektrometrii Mas, 25-29 maj 2014, Trzebnica

13. A. Maciejowska, **A. Godziek,** M. Sajewicz, T. Kowalska, *LC/MS Investigation of oscillatory condensation of selected amino acids,* 4. Konferencja Polskiego Towarzystwa Spektrometrii Mas, 25-29 maj 2014, Trzebnica
14. **A. Godziek**, A. Maciejowska, M. Sajewicz, E. Talik, R. Wrzalik, T. Kowalska, *Peptide nanofibers from the self-assembly of amino acids (L-proline and L-phenylalanine),* XXXVII Sympozjum nt. „Chromatograficzne metody badania związków organicznych", 11-13 czerwiec 2014, Katowice – Szczyrk
15. A. Maciejowska, **A. Godziek**, M. Wszołek, J. Klimek, A. Kulosa, M. Sajewicz, T. Kowalska, *Chromatographic investigation of spontaneous reactions of sulphur amino acids*, XXXVII Sympozjum nt. „Chromatograficzne metody badania związków organicznych", 11-13 czerwiec 2014, Katowice – Szczyrk
16. **A. Godziek**, A. Maciejowska, E. Talik, M. Sajewicz, T. Kowalska, *Peptide nano- and microfibers as an example of self-organization of amino acids in an abiotic system,* Oscillations & Dynamic Instabilities in Chemical Systems Gordon Research Conference Self-Organization and Complexity, 13-18 lipiec 2014, Girona
17. A. Maciejowska, **A. Godziek**, E. Talik, T. Kowalska, M. Sajewicz, *Spontaneous self-organization of L-cysteine to nano- and microspheres*, Oscillations & Dynamic Instabilities in Chemical Systems Gordon Research Conference Self-Organization and Complexity, 13-18 lipiec 2014, Girona
18. **A. Godziek,** A. Maciejowska, M. Sajewicz, T. Kowalska, *HPLC-ELSD, HPLC-MS, and LC-MS Investigation of Spontaneous Oscillatory Reactions of L-Histidine*, 7th Central European Conference "Chemistry towards Biology", 9-12 wrzesień 2014, Katowice - Chorzów
19. A. Maciejowska, **A. Godziek**, M. Sajewicz, T. Kowalska, *The study of self-organization of the protein amino acid (L-Met) by chromatographic methods*, 7th Central European Conference "Chemistry towards Biology", 9-12 wrzesień 2014, Katowice – Chorzów
20. **A. Godziek**, A. Maciejowska, M. Sajewicz, T. Kowalska, *Badanie stabilności strukturalnej wybranych aminokwasów białkowych technikami chromatograficznymi oraz polarymetrią,* Pomiędzy Naukami Zjazd Fizyków i Chemików III Ogólnopolska Konferencja dla Studentów i Doktorantów, 26 wrzesień 2014, Chorzów

21. **A. Godziek,** A. Maciejowska, M. Sajewicz, T. Kowalska, *Chromatograficzne i polarymetryczne badania samorzutnej oscylacyjnej peptyzacji L-treoniny w układach abiotycznych,* Zimowy Zjazd Sekcji Studenckiej Polskiego Towarzystwa Chemicznego, 13 grudzień 2014, Wrocław
22. A. Maciejowska, **A. Godziek**, M. Sajewicz, T. Kowalska, *Samorzutna inwersja chiralna i peptyzacja L-asparaginy w układach abiotycznych,* Zimowy Zjazd Sekcji Studenckiej Polskiego Towarzystwa Chemicznego, 13 grudzień 2014, Wrocław
23. **A. Godziek,** A. Maciejowska, T. Kowalska, E. Talik, M. Sajewicz, *HPLC-MS investigation of nano- and microstructures formed from monomeric amino acids phenylglycine and cysteine as a result of oscillatory reaction,* 33rd Informal Meeting on Mass Spectrometry, 10-13 maj 2015
24. A. Maciejowska, **A. Godziek,** M. Sajewicz, T. Kowalska, *Spontaneous oscillatory reaction of protein amino acids in an abiotic system – the LC-MS results,* 33rd Informal Meeting on Mass Spectrometry, 10-13 maj 2015
25. **A. Godziek,** A. Maciejowska, J. Chabińska, O. Krzemień, S. Krzemień, M.Sajewicz, T. Kowalska, *Badania reakcji oscylacyjnych wybranych par aminokwasów białkowych (L- Phg- L-Cys, L- His -L- Thr, L- Ser- L- Met),* IX Seminarium Naukowe nt. "Aktualne Problemy Chemii Analitycznej", 15 maj 2015, Katowice
26. A. Maciejowska, **A. Godziek,** M. Mucha, M. Sajewicz, T. Kowalska, *Badanie dynamiki reakcji oscylacyjnych L-Ser i D-Ser w układzie abiotycznym,* IX Seminarium Naukowe nt. "Aktualne Problemy Chemii Analitycznej", 15 maj 2015, Katowice
27. **A. Godziek,** A. Maciejowska, T. Kowalska, M. Sajewicz, *Investigation of dynamics of an oscillatory reaction od L-Ser, D-Ser and DL-Ser in an abiotic system,* 26th International Symposium on Pharmaceutical and Biomedical Analysis (PBA2015), 5-8 lipiec 2015, Tbilisi, Georgia
28. **A. Godziek,** A. Maciejowska, T. Kowalska, M. Sajewicz, *Zastosowanie niestandardowych metod analitycznych do badania aminokwasów białkowych w układach abiotycznych,* Pomiędzy Naukami Zjazd Fizyków i Chemików IV Ogólnopolska Konferencja dla Studentów i Doktorantów, 18 wrzesień 2015, Chorzów

29. A. Maciejowska, **A. Godziek,** E. Talik, M. Sajewicz, T. Kowalska, *Badanie reakcji oscylacyjnej peptyzacji pary aminokwasów białkowych (L-Ser–L-Met)w środowisku abiotycznym,* Pomiędzy Naukami Zjazd Fizyków i Chemików IV Ogólnopolska Konferencja dla Studentów i Doktorantów, 18 wrzesień 2015, Chorzów
30. A. Maciejowska, **A. Godziek,** M. Sajewicz, T. Kowalska, *Badanie cykliczności w reakcjach oscylacyjnych aminokwasów białkowych*, Zimowy Zjazd Sekcji Studenckiej Polskiego Towarzystwa Chemicznego, 5 grudzień 2015, Kraków
31. **A. Godziek**, A. Maciejowska, E. Talik, T. Kowalska, M. Sajewicz, *Badanie procesu peptyzacji układów dwuskładnikowych aminokwasów białkowych*, X Seminarium Naukowe nt. "Aktualne Problemy Chemii Analitycznej", 13 maj 2016, Katowice
32. **A. Godziek**, A. Maciejowska, T. Kowalska, M. Sajewicz, *Chromatograficzne badania wybranych par aminokwasów białkowych,* XI Międzynarodowa Konferencja pt. Chromatografia jonowa 2016, 20-21 kwiecień 2016, Zabrze
33. A. Maciejowska, **A. Godziek,** E. Talik, M. Sajewicz, T. Kowalska, *Investigation of micro- and nanostructures spontaneously formed in monocomponent proteinogenic amino acid solutions,* 39 Sympozjum nt. „Chromatograficzne metody badania związków organicznych", 1-3 czerwiec 2016, Katowice – Szczyrk
34. A. Maciejowska, **A. Godziek**, M. Sajewicz, T. Kowalska, *Patterns of turbidity changes in spontaneous non-linear peptidization of α-amino acids in abiotic solutions,* Oscillations & Dynamic Instabilities in Chemical Systems Gordon Research Conference Chemical Self-Organization Far from Equilibrium, 17-22 lipiec 2016, Stowe, VT, USA
35. **A. Godziek**, A. Maciejowska, E. Talik, M. Sajewicz**,** T. Kowalska, *Tracing of spontaneous non-linear heteropeptide formation with use of scanning electron microscopy and some auxiliary techniques***,** Oscillations & Dynamic Instabilities in Chemical Systems Gordon Research Conference Chemical Self-Organization Far from Equilibrium, 17-22 lipiec 2016, Stowe, VT, USA
36. **A. Godziek**, A. Maciejowska, E. Talik, T. Kowalska, M. Sajewicz**,** *Badanie procesu peptyzacji aminokwasów białkowych w układach dwuskładnikowych (L-Cys-L-Phe),* Pomiędzy Naukami Zjazd Fizyków i Chemików V Ogólnopolska Konferencja dla Młodych Naukowców, 16 wrzesień 2016, Chorzów

37. A. Maciejowska, **A. Godziek**, M. Sajewicz**,** T. Kowalska, *Badanie par aminokwasów białkowych (L-Ser-L-Met oraz L-Thr-L-His) pod kątem reakcji samorzutnej kondensacji,* Pomiędzy Naukami Zjazd Fizyków i Chemików V Ogólnopolska Konferencja dla Młodych Naukowców, 16 wrzesień 2016, Chorzów
38. A. Maciejowska, **A. Godziek**, E. Talik, M. Sajewicz and T. Kowalska, *Scanning electron microscopic and chromatographic evidence of spontaneous heteropeptide formation in the binary α-amino acid solutions,* 13 th International Conference on Fundamental and Applied Aspects of Physical Chemistry, 26-30 wrzesień 2016, Belgrad
39. A. Łągiewka, **A. Godziek**, I. Schisler, Z. Drzazga, M. Sajewicz, T. Kowalska, *Reakcje oscylacyjne aminokwasów białkowych,* Zimowy Zjazd Sekcji Studenckiej Polskiego Towarzystwa Chemicznego, 16 grudzień 2016, Lublin

LISTA PRAC WŁASNYCH TEMATYCZNIE ZWIĄZANYCH Z ROZPRAWĄ DOKTORSKĄ

Acta Chromatographica 26(2014)2, 355–369
DOI: 10.1556/AChrom.26.2014.2.15

Chiral Conversion and Condensation of *L*-Hydroxyproline in an Abiotic Liquid System

A. MACIEJOWSKA, A. GODZIEK, M. SAJEWICZ, AND T. KOWALSKA*

Institute of Chemistry, University of Silesia, 9 Szkolna Street, 40-006 Katowice, Poland
*E-mail: teresa.kowalska@us.edu.pl

Summary. This study is devoted to the thin-layer chromatographic demonstration of spontaneous chiral conversion of *L*-hydroxyproline (*L*-Hyp) to *D*-hydroxyproline (*D*-Hyp), and to its spontaneous peptidization, when dissolved in 70% aqueous methanol and stored at room temperature in a stoppered glass vessel. The adopted enantioseparation conditions were the same ones, as employed earlier for a successful enantioseparation of *L*- and *D*-proline. To this effect, we used microcrystalline cellulose as stationary phase and a quaternary mixture composed of 2-butanol:pyridine:glacial acetic acid:water (30:20:4:24, *v*/*v*) as mobile phase. Structural difference between proline and hydroxyproline consists in the presence of one hydroxyl group per molecule of the latter amino acid, which makes the respective enantioseparation a more difficult task. Consequently, the obtained separation effect was not a complete (i.e., a baseline) resolution of the two Hyp antimers yet a sufficient enough proof of the appearance of *D*-Hyp, apparently due to spontaneous chiral conversion taking place in the course of the *L*-Hyp solution storage and ageing period. The condensation products were discovered both in the fresh and the aged *L*-Hyp solution, yet in the aged sample, the condensation product yields were considerably higher than in the freshly prepared one (as convincingly demonstrated by mass spectrometry). Demonstration of the condensation products was performed with the aid of thin-layer chromatography (TLC), liquid chromatography–mass spectrometry (LC–MS), and thin-layer chromatography–mass spectrometry (TLC–MS).

Key Words: *L*-Hydroxyproline (*L*-Hyp), *D*-hydroxyproline (*D*-Hyp), spontaneous chiral conversion, spontaneous condensation, TLC enantioseparation, LC–MS, TLC–MS

Introduction

In spite of amino acids being widely considered as "the building blocks of life," chemical behavior of nonderivatized amino acids in neutral solvents attracts hardly any attention of chemists and life scientists in general. In the past, spontaneous peptidization of amino acids has been sporadically investigated, and mostly in the framework of the projects focusing on abiogenesis, including laboratory simulations of a prebiotic universe under the environmental conditions imitating a possible origin of biological life. Usually, the employed experimental conditions were quite drastic, in order to repro-

0231–2522 © 2013 Akadémiai Kiadó, Budapest

duce the terrestrial or extraterrestrial environments from before millions of years. Among the best known experiments were those performed by Fox and Harada, and dealing with thermal copolymerization of amino acids to the products resembling proteins and therefore denoted as proteinoids [1, 2].

Spontaneous chiral conversion of amino acids from the *L* form in living mammals (and humans) to the *D* form after the death of an organism has been reported as a natural *post mortem* process, discovered in the fossilized organic remnants. This discovery was made soon after the first successful gas chromatographic enantioseparations of amino acids in the sixties of the 20th century [3, 4]. With a possibility of measuring the *D*/*L* amino acid ratio and knowing the kinetics of chiral conversion with a selection of the protein-building amino acids (and in the first instance, of aspartic acid), an approach has been established of dating the fossilized organic matter (mostly teeth and bones), based on the known amino acid racemization rates [5–8]. However, the amino acid racemization-founded dating techniques, welcomed by archeologists, paleontobiologists, sedimentary geologists, etc., anticipated a strictly linear nature of this structural transformation as a matter of course. An awareness of a nonlinear course of spontaneous racemization most probably would stop scientists from developing an approach known in archeology as "an amino acid clock," or "a molecular clock" [9].

In several papers dating from the eighties and the nineties of the past century (e.g., Refs. [10–13]), a possibility was pointed out of chiral conversion with amino acids dissolved in the acidic and basic media. In our studies, we have first pointed out to the phenomenon of the spontaneous oscillatory chiral conversion of amino acids running both in the aqueous and organic liquids under the mild temperature and pressure conditions (e.g., Refs. [14, 15]). The oscillatory chiral conversion was found to run in parallel with the spontaneous oscillatory peptidization (e.g., Refs. [16–18]). These two processes (oscillatory chiral conversion and oscillatory peptidization) can take place in simple glass vessels stored at room temperature on laboratory shelves.

In paper [16], we provided a simple thin-layer chromatographic evidence of spontaneous peptidization of *L*-proline (*L*-Pro), an important constituent of collagen responsible for the architecture of human and animal tissues. This demonstration was possible due to the specificity of the color reaction between the monomeric *L*-Pro and ninhydrin, which (unlike with the majority of the other monomeric amino acids and with the *L*-Pro-derived peptides) results in a yellow, and not in a purple color effect.

The aim of this study is to perform an analogous thin-layer chromatographic experiment with *L*-hydroxyproline (*L*-Hyp), another important constituent of collagen. In the first instance, we intend to demonstrate spon-

taneous chiral conversion of L-Hyp to D-Hyp. Moreover, we demonstrate the presence of the condensation products derived from L-Hyp, visible both in the fresh and the aged L-Hyp solution (yet in the aged sample, the condensation product yields are perceptibly higher than in the freshly prepared one, as convincingly demonstrated by mass spectrometry). Owing to the hydroxyl group in the Hyp molecule, self-esterification of the Hyp molecules cannot be excluded, although in energetic terms, spontaneous peptidization is more favorable. For the sake of illustration, in *Fig. 1*, we present chemical structures of L-Hyp and D-Hyp in zwitterionic form. In *Fig. 2(a)* and *2(b)*, we present chemical structures of the self-esterified Hyp dimer and the simplest peptidization product, i.e., the Hyp dipeptide, respectively. Apparently, a number of the condensed Hyp units can be much higher than that in a simple dimer, as demonstrated with the aid of mass spectrometry.

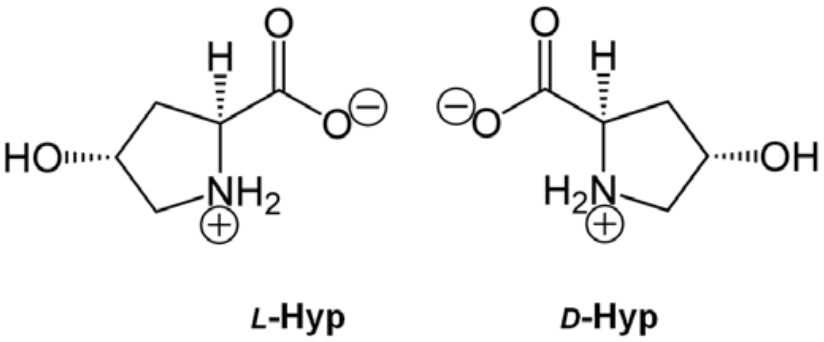

Fig. 1. Chemical structures of L-Hyp and D-Hyp in zwitterionic form

Experimental

Reagents

L-Hyp of the analytical purity grade was purchased from Sigma–Aldrich (St. Louis, MO, USA; cat. no. H-55409). Manganese(II) acetate, pyridine, 2-butanol (Sigma–Aldrich), ninhydrin, and glacial acetic acid (PPH POCh, Gliwice, Poland) used in the experiments were of the analytical purity grade. Methanol (Sigma–Aldrich) and 2-propanol (Roth, Karlsruhe, Germany) were of the high-performance liquid chromatography (HPLC) purity grade. Water was deionized and double distilled in our laboratory by means of the Elix Advantage model Millipore system (manufactured in Molsheim, France).

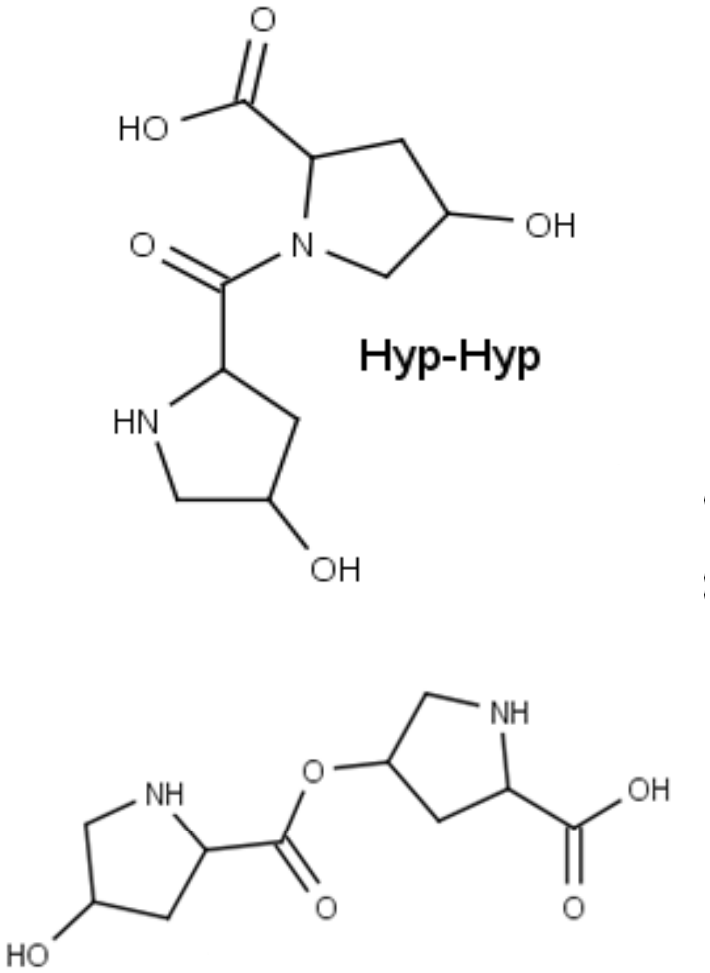

Fig. 2. Chemical structures of (a) self-esterified Hyp dimer and (b) Hyp dipeptide

Thin-Layer Chromatography (TLC)

Thin-layer chromatographic analyses were performed on the commercial 10 cm × 20 cm microcrystalline cellulose plates (layer thickness, 0.10 mm; Merck; cat. no. 1.05730). Concentration of *L*-Hyp in 70% aqueous methanol was 1 mg mL^{-1} for the reflectance densitometry mode and 0.2 mg mL^{-1} for the fluorescence densitometry mode (i.e., 7.63×10^{-3} mol L^{-1} and 1.53×10^{-3} mol L^{-1}, respectively), each time with an equimolar addition of manganese(II) acetate.

The fresh and the aged (37 days storage period) *L*-Hyp samples were chromatographically developed using 2-butanol:pyridine:glacial acetic acid:water (30:20:6:24, *v*/*v*) as a mobile phase. Before applying the samples, the plates were activated by heating for 30 min at 110 °C. Four samples of the fresh *L*-Hyp solution and four samples of the aged *L*-Hyp solution were spotwise applied to the plate (in the 5 μL aliquots), 2 cm apart and 1 cm above the lower edge of the plate. The chromatograms were developed to

the distance of 6 cm, and the development time was ca. 2 h. After that, the plates were dried at ambient air for 30 min, and the chromatograms were visualized by spraying the plates with 0.5% ninhydrin solution in 2-propanol, followed by heating for 5 min at 110 °C.

The obtained chromatograms were densitometrically scanned with use of a Desaga (Heidelberg, Germany) model CD 60 densitometer equipped with Windows-compatible ProQuant software, and they were also recorded with a digital camera. In the reflectance mode, concentration profiles of the development lanes were recorded in visible light from the tungsten/deuterium lamp at the wavelength λ = 485 nm, and in the fluorescence mode, in visible light from the mercury lamp, at the wavelength λ = 465 nm. The dimensions of the scanning rectangular light beam were 0.1 mm × 1.0 mm.

Liquid Chromatography with Mass Spectrometric Detection (LC–MS)

For the LC–MS experiments, concentration of *L*-Hyp in 70% aqueous methanol solution was 1 mg mL^{-1} (i.e., 7.63 × 10^{-3} mol L^{-1}). The analyses were performed for the freshly prepared solutions, and for those after 37 days of the storage period. The LC–MS System Varian (Varian, Palo Alto, CA, USA) was employed, equipped with the Varian ProStar model pump, the Varian 100-MS mass spectrometer, and the Varian MS Workstation v. 6.9.1 software for data acquisition and processing.

The LC separations were carried out for the 5-μL aliquots of the *L*-Hyp solution in the isocratic mode, using the C18 type pre-column (Varian, Harbor City, CA, USA) and methanol as a mobile phase at the flow rate of 0.20 mL min^{-1}. Mass spectrometric detection was carried out in the electrospray ionization (ESI) mode (full ESI–MS scan, positive ionization, spray chamber temperature of 50 °C, drying gas temperature of 350 °C, drying gas pressure of 25 psi, capillary voltage of 50 V, and needle voltage of 5 kV).

Thin-Layer Chromatography with Mass Spectrometric Detection (TLC–MS)

The TLC–MS experiments were performed on the chromatograms of the fresh and the aged *L*-Hyp samples developed in the same way, as earlier described, but without using ninhydrin as a visualizing agent. These analyses were performed to additionally confirm an identity of the chromatographically separated spots by directly eluting them from the chromatographic plates to mass spectrometer. For this purpose, we used a special TLC–MS

device (Camag, Muttenz, Switzerland), enabling a direct elution. In this experiment, elution of the spots from the chromatographic plates was carried out with water. The MS system operated under the following working conditions: the mobile phase was water at the flow rate of 0.10 mL min^{-1}, and the spray chamber temperature was 45 °C. Moreover, from the setup described in the preceding section, the C-18 type pre-column was removed. All the remaining working parameters were the same as described earlier.

Results and Discussion

Thin-Layer Chromatography (TLC)

Microcrystalline cellulose as stationary phase was used in our experiment to check if *L*-Hyp can undergo chiral conversion and condensation, when dissolved in 70% methanol. This chiral sorbent was selected as able to enantioseparate the amino acids, as confirmed in a number of earlier chromatographic studies (e.g., in Refs. [16, 19, 20]). An equimolar amount of manganese(II) acetate was added to the analyzed *L*-Hyp solutions just before the TLC analysis only. Thus, the Hyp molecules acted as complexation ligands for the manganese(II) cation, with different complexation equilibria for the *L*- and *D*-enantiomer (the latter one generated in the course of the spontaneous chiral conversion), which enhanced the enantioseparation. The chromatograms were developed in the 1D mode and visualized with the 0.5% ninhydrin solution in 2-propanol. An example of the visualized chromatograms is given in *Fig. 3*.

In *Fig. 3(a)* and *3(b)*, the chromatograms valid for the freshly prepared *L*-Hyp solution and for the aged one (after 37 days of storage period) are given, respectively. Differences between the chromatograms of the fresh and the aged Hyp sample are evident. Generally, the yellow spots visible on the chromatograms represent the monomeric forms of Hyp, and the purple spots hold for the oligopeptides. Yellow spots on the chromatogram of the freshly prepared *L*-Hyp solution *(Fig. 3(a))* are circular and relatively small (ca. 5 mm in diameter), and their retardation coefficient, R_F, value equals to 0.58 ± 0.01. Yellow spots on the chromatogram of the aged Hyp solution are oblong (ca. 9 mm high), which suggests chiral conversion in the course of the sample storage, and an appearance of the *D*-Hyp form. The retardation coefficient (R_F) of this oblong yellow spot *(Fig. 3(b))* equals to 0.61 ± 0.01. Purple spots visible in *Fig. 3(a)* and *3(b)* at R_F = 0.32 ± 0.02 represent the Hyp-derived oligopeptides.

In our earlier study carried out for *L*,*D*-Pro dissolved in 70% aqueous methanol with use of the same stationary and mobile phase [16], complete

enantioseparation of the *L*- and *D*-Pro species was obtained, and the R_F value valid for *D*-Pro was higher than that for *L*-Pro. A similar outcome was reported in paper [19], where the enantioseparation of three different amino acids on cellulose was performed, always with the higher R_F value for the *D*-isomer and the lower one for the *L*-isomer. However, Hyp differs from Pro with the presence of one hydroxyl group in the Hyp structure; hence, an affinity of Hyp toward stationary phase is higher than that of Pro, and as a result, the enantiomer separation of *L*- and *D*-Hyp is incomplete. Based on our earlier observations with the enantioseparation of Pro [16] and on the results reported in Ref. [19], it can be deduced that the lower part of oblong yellow spot on the chromatogram of the aged Hyp sample *(Fig. 3(b))* represents *L*-Hyp, and the upper part of the same spot holds for *D*-Hyp.

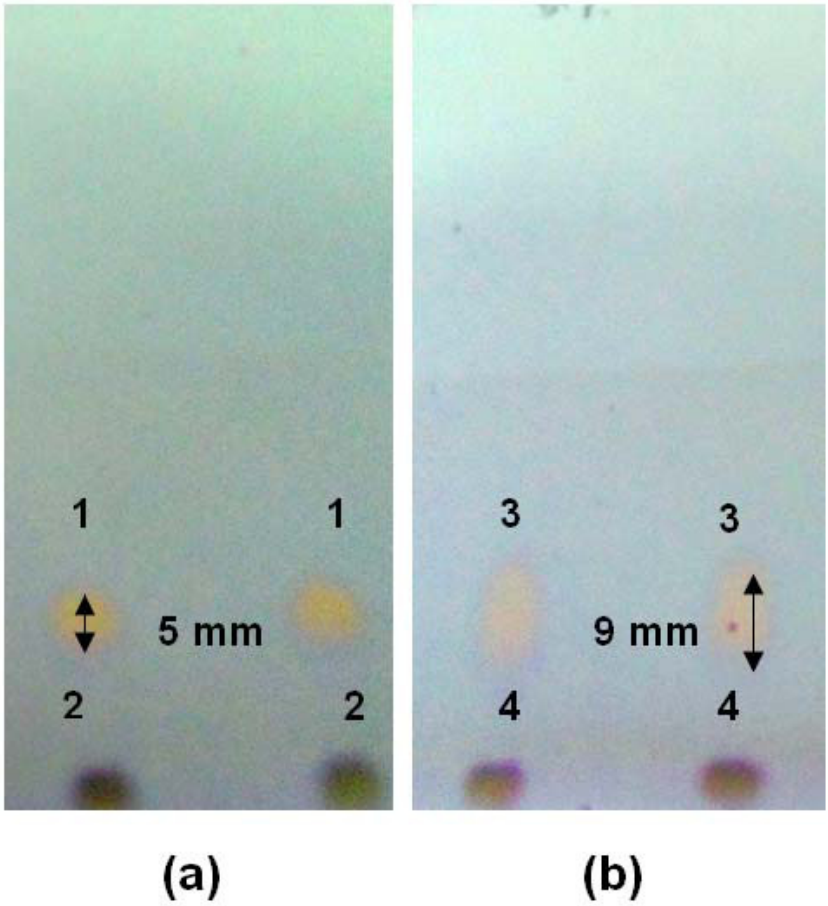

Fig. 3. Chromatograms of (a) freshly prepared *L*-Hyp solution and (b) *L*-Hyp solution after 37 days ageing. 1: *L*-Hyp (yellow spot), 2: condensation products (purple spot), 3: *L*,*D*-Hyp (yellow spot), 4: condensation products (purple spot)

In order to further confirm the above results on chiral conversion and peptidization of the *L*-Hyp solution in 70% aqueous methanol, the visualized chromatograms *(Fig. 3)* were densitometrically scanned both in the reflectance and the fluorescence mode. In *Fig. 4*, we show the densitograms

recorded in the reflectance mode at the wavelength λ = 485 nm from the chromatograms of the freshly prepared and the aged Hyp sample. Differences between these two densitograms are evident. Peak A in both densitograms originates from the monomeric L-Hyp species *(Fig. 4(a)* and *4(b))*, and peak B in the densitogram of the aged Hyp sample *(Fig. 4(b))* originates from the monomeric D-Hyp sample. In other words, peak A in the densitogram of the freshly prepared L-Hyp sample *(Fig. 4(a))* corresponds with the circular yellow spot on the chromatogram shown in *Fig. 3(a)*, and the incompletely separated peaks A and B in the chromatogram of the aged Hyp sample *(Fig. 4(b))* represent the oblong yellow spot on the chromatogram shown in *Fig. 3(b)*. Peak C_1 corresponds with the purple spot visible both on the chromatograms of the freshly prepared and the aged Hyp sample, and based on its color upon visualization with ninhydrin, it originates from oligopeptides. Peak C_2 appears in the densitogram of the aged Hyp sample only, and it most probably is an additional oligopeptidization product.

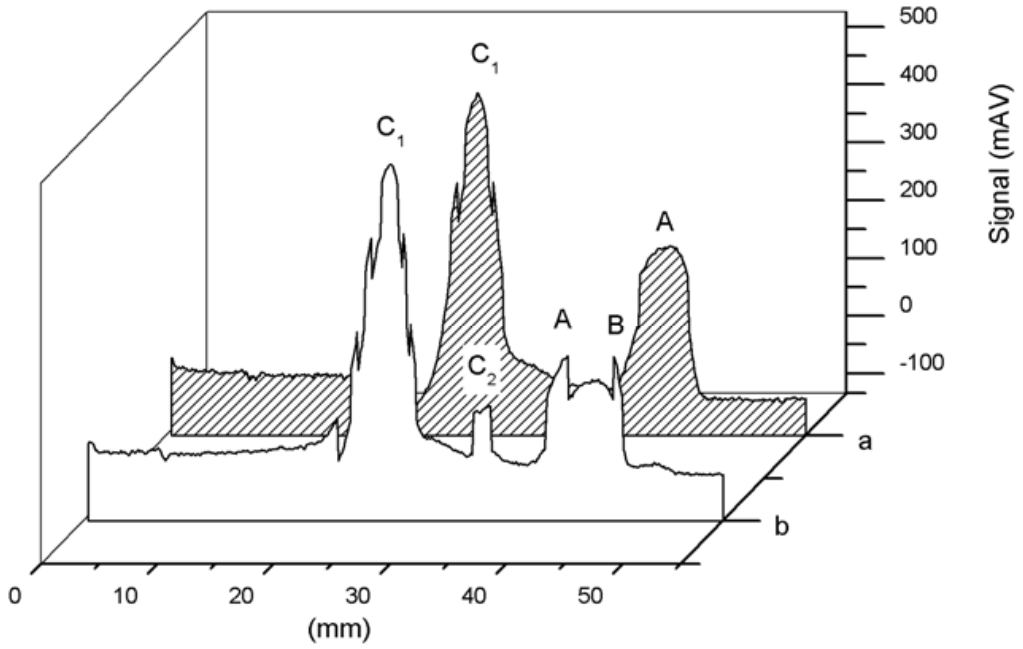

Fig. 4. Densitograms of (a) freshly prepared L-Hyp solution and (b) L-Hyp solution after 37 days ageing recorded in the reflectance mode at the wavelength λ = 485 nm. A: L-Hyp, B: D-Hyp, C_1: condensation products present in the fresh and the aged sample, C_2: condensation products present in the aged sample

The analogous densitograms, yet recorded in the fluorescence mode at the wavelength λ = 465 nm, are shown in *Fig. 5*. The densitogram in *Fig. 5(a)* was recorded from the chromatogram of the freshly prepared L-Hyp sample, and that in *Fig. 5(b)* was recorded from the chromatogram of the Hyp sample after 37 days storage period. The densitogram of the aged sample

shows more peaks than that of the freshly prepared sample. Peak A present in both chromatograms originates from the monomeric *L*-Hyp species, and peak B, which migrates higher than peak A, appears in the densitogram of the aged Hyp sample only. Thus, it is highly probable that peak B represents *D*-Hyp, as a result of chiral conversion. The oligopeptide band denoted as peak C can be seen both in the fresh and the aged Hyp sample, and it corresponds with the purple oligopeptide spots in *Fig. 3*. Peak D appears in the aged Hyp sample only, and it is an evident result of the Hyp condensation. Summing up, the two sets of the densitograms recorded both in the reflectance and fluorescence mode *(Figs. 4* and *5)* confirm the message derived from the chromatograms visualized with ninhydrin as to the spontaneous chiral conversion and spontaneous peptidization in the course of storage of the *L*-Hyp sample.

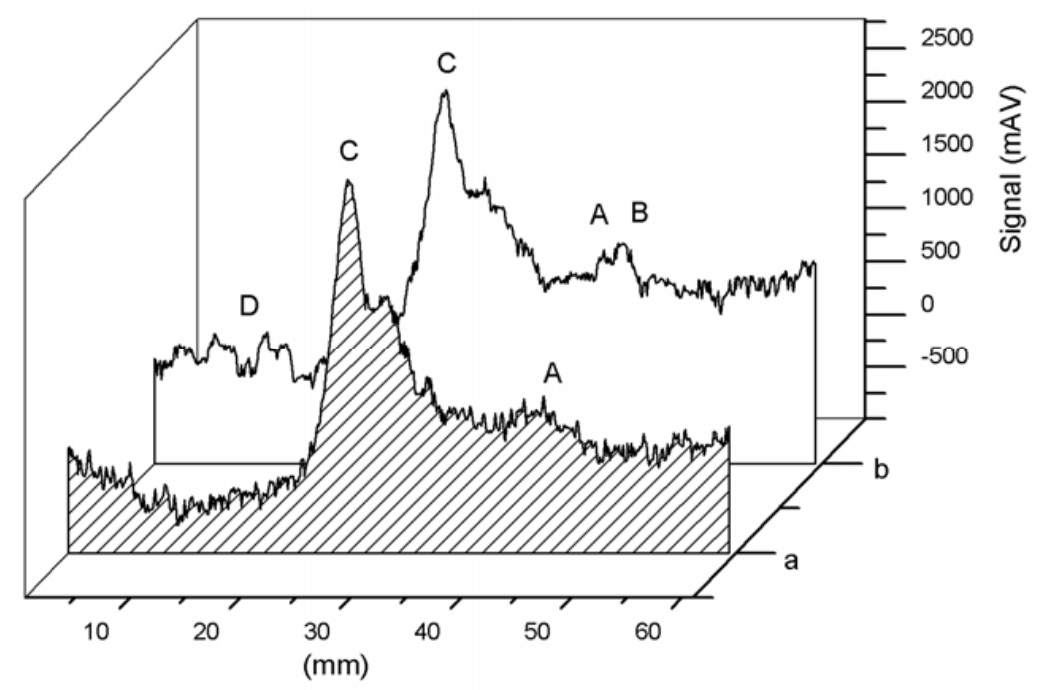

Fig. 5. Densitograms of (a) freshly prepared *L*-Hyp solution and (b) Hyp solution after 37 days ageing recorded in the fluorescence mode at the wavelength λ = 462 nm. A: *L*-Hyp, B: *D*-Hyp, C: condensation products present in the fresh and the aged sample, D: condensation products present in the aged sample

Liquid Chromatography with Mass Spectrometric Detection (LC–MS)

Coupling of liquid chromatography with mass spectrometric detection (LC–MS) provides a handy tool to monitor oligomerization of the investigated amino acid, owing to a possibility of at least partial identification of the oli-

gomerization products. The first step was to pass the samples through the chromatographic pre-column followed by the registration of the mass spectra from the obtained effluents. These two analytical steps were performed both for the freshly prepared L-Hyp solution and for that stored for 37 days at room temperature in a tightly stoppered vessel. The results obtained are shown in *Fig. 6(a)* and *6(b)*.

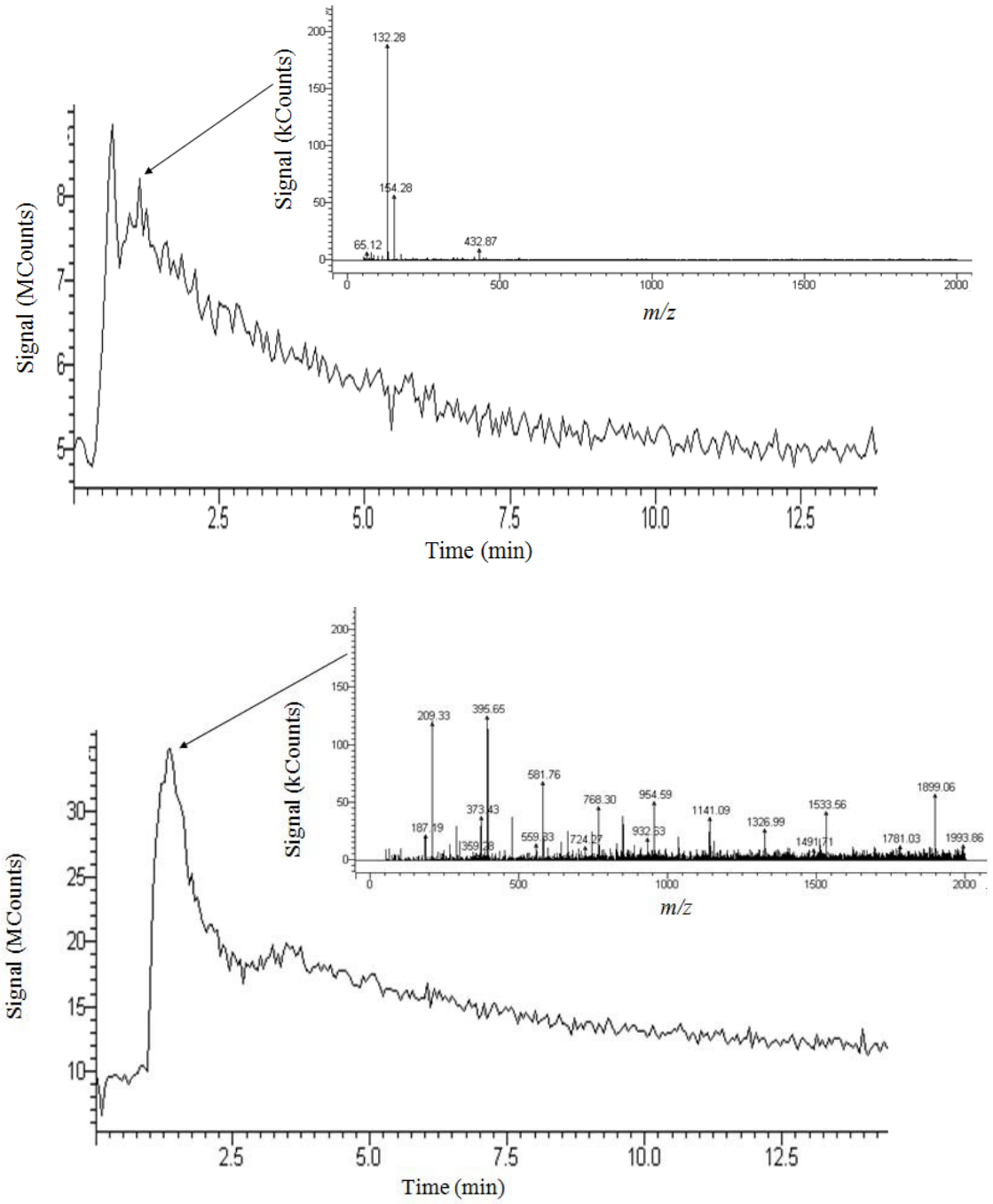

Fig. 6. Signals of the eluted chromatographic spots and mass spectra of the Hyp solution recorded for (a) freshly prepared sample and (b) aged sample after 37 days storage period

The chromatographic peak shapes for the fresh and the aged Hyp sample are not dramatically different, yet the respective mass spectra considerably differ. In the mass spectrum of the freshly prepared L-Hyp solution *(Fig. 6(a))*, the *m/z* values of the two predominant peaks equal to 132 and 154, which can be ascribed to the structures directly derived from L-Hyp, i.e., $[Hyp+H]^+$ and $[Hyp+Na]^+$. There is one more yet less intense peak present at *m/z* 432, which might perhaps be ascribed to the Hyp-derived tetrapeptide fragment. In the mass spectrum of the aged Hyp sample *(Fig. 6(b))*, the molecular ions are hardly visible. Instead, an abundant amount of the peaks characterized by considerable yields and relatively high *m/z* values (up to *m/z* 2000) can be perceived. For the sake of example, one can point out to the peak at *m/z* 1141, which probably originates from the Hyp-derived nonapeptide, and its structure can be given as $[Hyp_9–OH+Na]^+$. Thus, the obtained LC–MS results witness to the spontaneous peptidization of the aged Hyp sample.

Thin-Layer Chromatography with Mass Spectrometric Detection (TLC–MS)

The TLC–MS technique enables mass spectrometric analysis of chromatographic spots separated by means of TLC. In our case, the first step was the elution by means of water of the separated chromatographic spots 1–4 from the developed chromatographic plates *(Fig. 3(a)* and *3(b))*, followed by the registration of the mass spectra of the eluted compounds. Signals of the eluted chromatographic spots, the respective mass spectra, and the thin-layer chromatograms are shown in *Fig. 7(a)–(d)*.

The results produced in *Fig. 7(a)* and *7(b)* correspond, respectively, with the yellow spot 1 of the monomeric L-Hyp and with the purple spot 2 of the oligomerization product from *Fig. 3(a)*. Apparently, these two sets of the data are quite similar. In both mass spectra, peaks at *m/z* 132, 149, and 167 are present, which most probably can be ascribed to $[Hyp+H]^+$, $[Hyp+H_2O]^+$, and $[Hyp+(H_2O)_2]^+$, respectively. The latter two peaks apparently are due to the elution of the chromatographic spots with water. Moreover, in each case, certain number of other peaks can be seen with the *m/z* values below 400. Most probably, these peaks can be ascribed to the constituents of the organic binder eluted with water from the adsorbent layer (peak 1, *Fig. 3(a)*) and to the constituents of the adsorbent binder plus low amounts of the Hyp-derived oligopeptides (peak 2, *Fig. 3(a)*).

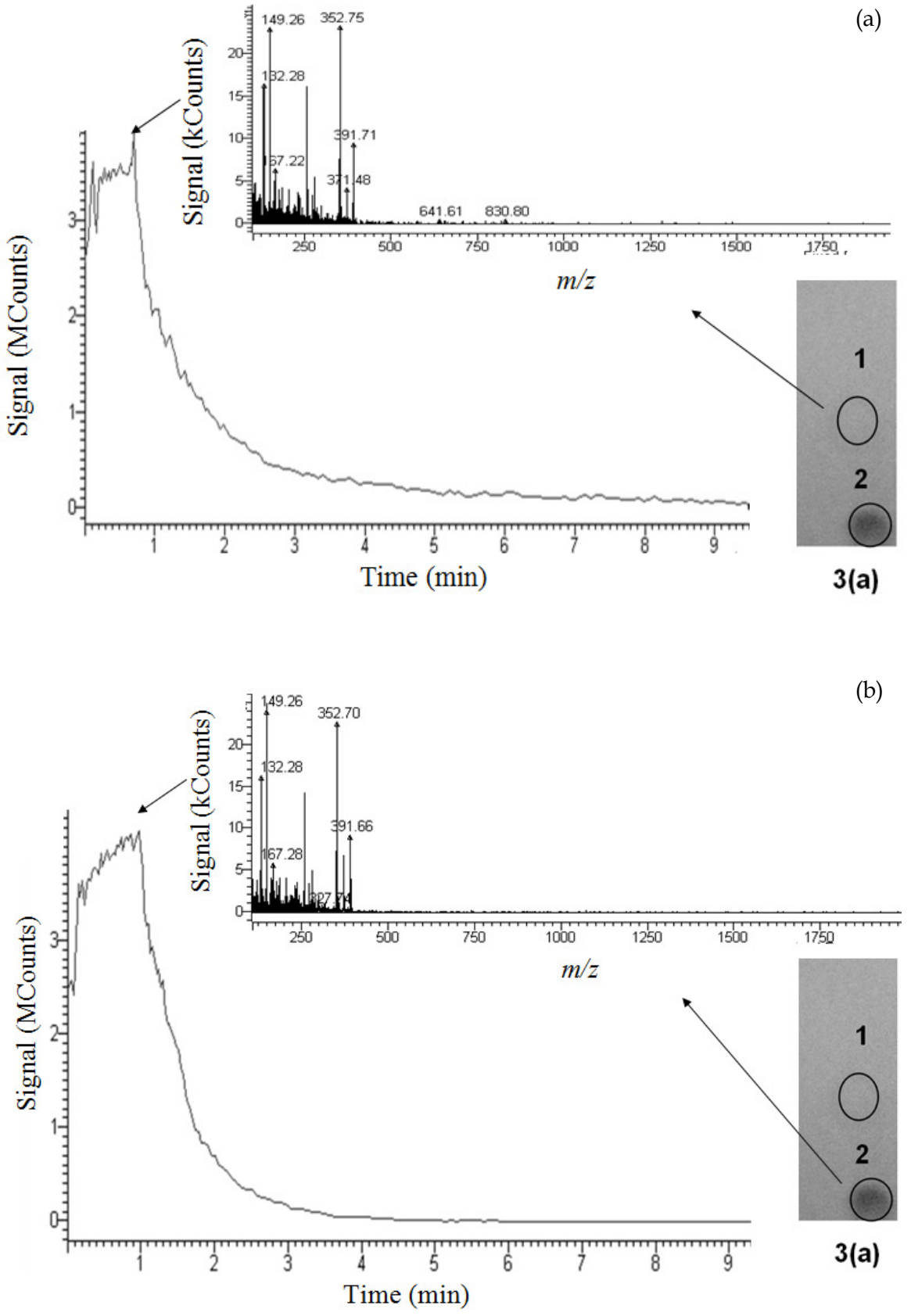
(a)
Signal (MCounts)
Time (min)
Signal (kCounts)
m/z
149.26
352.75
132.28
391.71
167.22
371.48
641.61
830.80
1
2
3(a)
(b)
Signal (MCounts)
Time (min)
Signal (kCounts)
m/z
149.26
352.70
132.28
391.66
167.28
1
2
3(a)

Fig. 7.

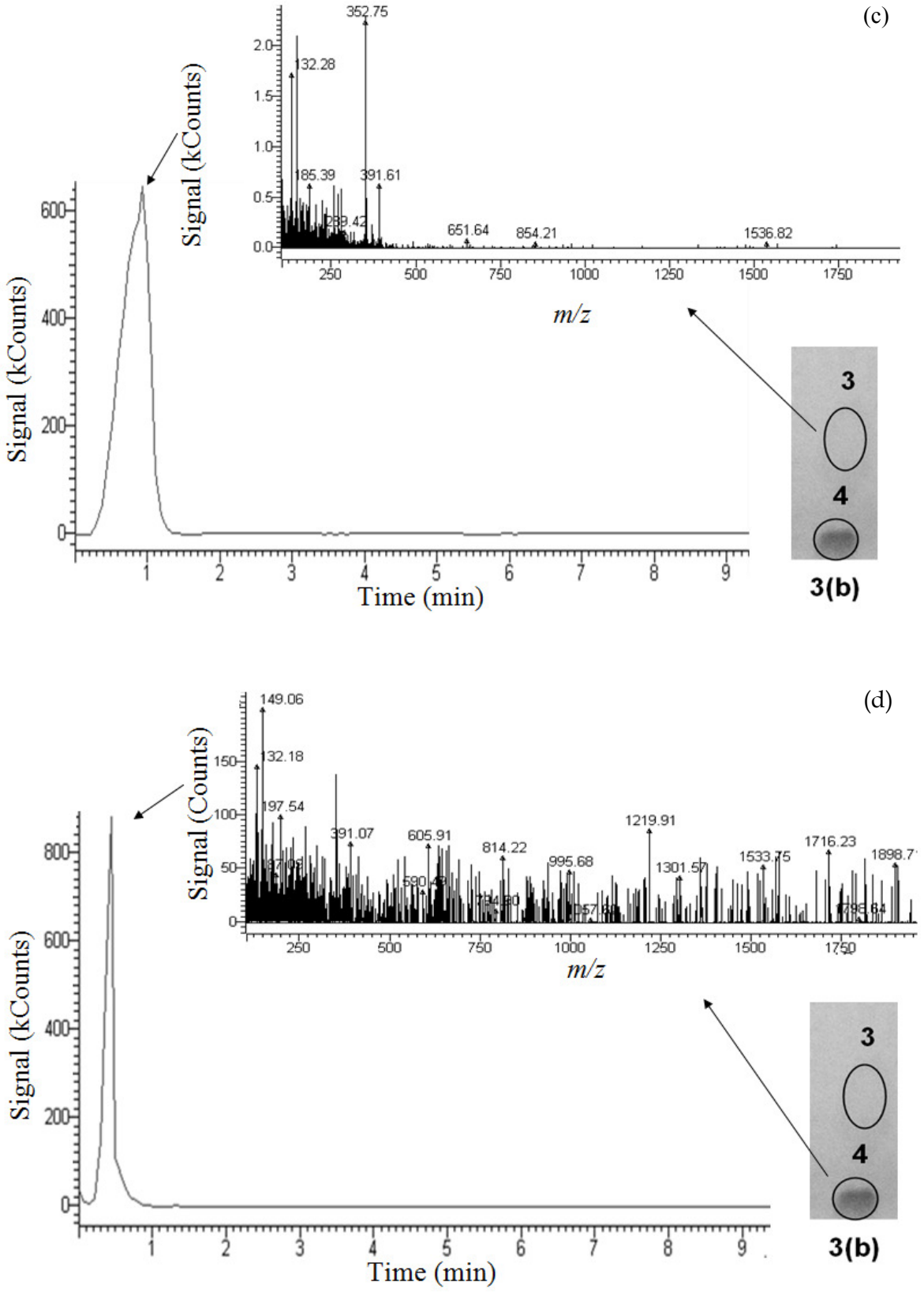

Fig. 7. Thin-layer chromatograms, signals of the chromatographic spots directly eluted from the chromatographic plates, and the respective mass spectra recorded for (a) spot 1, (b) spot 2, (c) spot 3, and (d) spot 4 (see *Fig. 3*)

Signals of the eluted chromatographic spots and mass spectra given in *Fig. 7(c)* and *7(d)* correspond, respectively, with the yellow spot 3 of *L*,*D*-Hyp *(Fig. 3(b))* and the purple spot 4 of the oligopeptides originating from the aged Hyp sample *(Fig. 3(b))*. In the mass spectrum of substances eluted from spot 3 *(Fig. 3(b))*, distinct peak at *m/z* 132 is present, which represents $[Hyp+H]^+$. There are some other peaks also, which can be ascribed to the components of the organic binder eluted from the adsorbent layer, and probably to some simple oligopeptides derived from Hyp, mobile enough to move along the cellulose layer. Such oligopeptide peak can be, e.g., that at *m/z* 289, which can be ascribed to $[Hyp_2+COOH]^+$. In the mass spectrum of peak 4 *(Fig. 3(b))*, the number and the abundance of the oligopeptide peaks are high. As examples, peaks at *m/z* 606, 809, 1533, and 1717 can be ascribed to $[Hyp_5+Na]^+$, $[Hyp_7+He]^+$, $[Hyp_{12}+2Na]^+$, and $[Hyp_{15}+Na]^+$, respectively.

Signal intensities shown in *Fig. 7(a)* and *7(b)* on the one hand (valid for the freshly prepared sample) and for those given in *Fig. 7(c)* and *7(d)* on the other (valid for the aged sample) considerably differ. Intensities of the chromatographic signals in *Fig. 7(a)* and *7(b)* are in the MCount units, and the intensities of the analogous signals in *Fig. 7(c)* and *7(d)* are in the kCount units. Accordingly, the intensities of the mass spectrometric peaks in *Fig. 7(a)*, *7(b)*, and *7(c)* are in the kCount units, and the intensities of the mass spectrometric peaks in *Fig. 7(d)* are in the Count units. These differences among the signal and peak intensities seem in the first instance due to the difficulty in water eluting of higher oligopeptides, specially those from spot 4 *(Fig. 7(d))*. Moreover, mass spectrum representing spot 4 contains peaks originating from an abundance of various different oligopeptides with not very high individual yields (hence, with relatively low intensities of the respective peaks), yet representing a considerable overall consumption of Hyp. This result is one more confirmation of the peptidization process running in the Hyp sample in the course of ageing.

Summing up, the TLC–MS results additionally confirm spontaneous oligopeptidization of Hyp, when stored for the longer periods of time in the 70% aqueous methanol solution.

Conclusion

Storage of the *L*-Hyp solution in an abiotic liquid system results in spontaneous chiral conversion and spontaneous peptidization of the investigated amino acid. An adequate experimental evidence was achieved with the aid of the thin-layer chromatography on the microcrystalline cellulose stationary phase, and owing to an addition of an equimolar amount of manga-

nese(II) acetate to the Hyp solutions, prior to their analysis by means of TLC.

Spontaneous oligopeptidization of Hyp was additionally confirmed by liquid chromatography with mass spectrometric detection (LC–MS) and thin-layer chromatography with mass spectrometric detection (TLC–MS).

References

[1] S.W. Fox and K. Harada, Science, **128**, 1214 (1958)
[2] S.W. Fox, J. Chem. Ed., **34**, 472–479 (1958)
[3] E. Gil-Av, B. Feibush, and R. Charles-Sigler, Tetrahedron Lett., **7**, 1009–1015 (1966)
[4] E. Gil-Av and B. Feibush, Tetrahedron Lett., **8**, 3345–3347 (1967)
[5] H. Elster, E. Gil-Av, and S. Weiner, J. Archaeol. Sci., **10**, 605–617 (1981)
[6] J.F. Bada, Earth Planet. Sci. Lett., **55**, 292–298 (1981)
[7] J.F. Bada, Ann. Rev. Earth Planet Sci., **13**, 241–268 (1985)
[8] G. A. Goodfriend, Nature, **357**, 399–401 (1992)
[9] J.L. Bada and G.D. McDonald, Icarus, **114**, 139–143 (1995)
[10] R. Baum and G.G. Smith, J. Am. Chem. Soc., **108**, 7325–7327 (1986)
[11] T. Shiraiwa, T. Furukawa, T. Tsuchida, S. Sakata, M. Sunami, and H. Kurokawa, Bull. Chem. Soc. Jpn., **64**, 3729–3731 (1991)
[12] G.G. Smith and T. Sivakua, J. Org. Chem., J. Org. Chem., **48**, 627–634 (1983)
[13] H.L. Van Maanen, H. Kleijn, J.T.B.H. Jastrzebski, J. Verveji, A.P.G. Kieboom, and G. Van Koten, J. Org. Chem., **60**, 4331–4338 (1995)
[14] M. Sajewicz, M. Gontarska, D. Kronenbach, and T. Kowalska, Acta Chromatogr., **21**, 151–160 (2009)
[15] M. Sajewicz, M. Gontarska, and T. Kowalska, J. Chromatogr. Sci., DOI:10.1093/chromsci/bmt033
[16] M. Sajewicz, M. Matlengiewicz, M. Juziuk, M. Penkala, M. Weloe, M. Schulz, and T. Kowalska, J. Liq. Chromatogr. Relat. Technol., **36**, 2497–2511 (2013)
[17] M. Sajewicz, M. Matlengiewicz, M. Leda, M. Gontarska, D. Kronenbach, T. Kowalska, and I.R. Epstein, J. Phys. Org. Chem., **23**, 1066–1073 (2010)
[18] M. Sajewicz, M. Gontarska, D. Kronenbach, M. Leda, T. Kowalska, and I.R. Epstein, J. Syst. Chem., **1**, 7 (2010)
[19] S.F. Contractor and J. Wragg, Nature, **208**, 71–72 (1965)
[20] S. Yuasa, A. Shimada, M. Isoyama, T. Fukuhara, and M. Itoh, Chromatographia, **21**, 79–82 (1986)

Accepted by TK

Journal of Chromatographic Science 2015;53:31–37
doi:10.1093/chromsci/bmu006 Advance Access publication March 2, 2014

Article

Condensation Dynamics of the L-Pro-L-Phe and L-Hyp-L-Phe Binary Mixtures in Solution

Mieczysław Sajewicz, Agnieszka Godziek, Anna Maciejowska and Teresa Kowalska*

Institute of Chemistry, University of Silesia, 9 Szkolna Street, 40-006 Katowice, Poland

*Author to whom correspondence should be addressed. Email: teresa.kowalska@us.edu.pl

Received 12 May 2013; revised 14 January 2014

We employ the achiral liquid chromatography with diode array, evaporative light scattering and mass spectrometric detection (HPLC-DAD, HPLC-ELSD and LC-MS) to assess structural instability (understood as spontaneous oscillatory chiral conversion and spontaneous oscillatory condensation) of the two pairs of amino acids, L-proline-L-phenylalanine (L-Pro-L-Phe) and L-hydroxyproline-L-phenylalanine (L-Hyp-L-Phe), in aqueous acetonitrile. In our earlier studies, we managed to demonstrate that single amino acids in aqueous and non-aqueous solutions undergo spontaneous oscillatory chiral conversion and oscillatory condensation. We also investigated condensation in the binary L-Pro-L-Hyp mixture in aqueous solution, and proposed a theoretical model to explain the specific dynamics of this process, which involves mutual catalytic effects of the two amino acids. In this study, we demonstrate oscillatory instability with the other two amino acid pairs in the organic-aqueous solution and reflect on the dynamics of condensation in the investigated cases. The choice of L-Pro and L-Hyp is due to their important role as building blocks of collagen, which is omnipresent in the connective tissues of mammals, and largely responsible for tissue architecture and strength. L-Phe is one of the 20 exogenous amino acids and is a building block of the majority of naturally occurring proteins.

Introduction

The spontaneous oscillatory chiral conversion of the low-molecular-weight carboxylic acids dissolved in the aqueous and non-aqueous abiotic systems was first discovered with profen drugs (1, 2), and later the phenomenon was found general enough to occur with many chiral derivatives of acetic, propionic and butyric acid with the chirality center located either on the α-C or on the β-C atom (3, 4). It was also found out that the oscillatory chiral conversion of the discussed compounds was accompanied by the oscillatory oligomerization.

With amino acids, an ability to undergo spontaneous peptidization in aqueous solution was first demonstrated with the use of the biuret test upon an example of L-phenylglycine (5), and later with some other amino acids as well, using the high-performance liquid chromatography with diode-array detection (HPLC–DAD) and liquid chromatography with mass spectrometric detection (LC–MS) techniques (6). A deeper insight in these phenomena was provided in papers (7–10). The general scheme of the process of chiral conversion with the low-molecular-weight carboxylic acids in aqueous solutions is given in Eq. (1) (11):

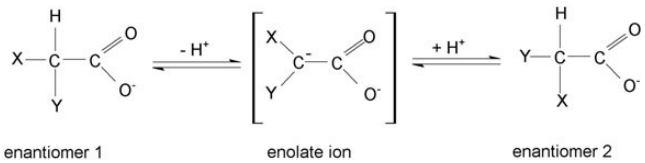

(1)

where X: −R and Y: $-NH_2$, −OH or −Ar.

In anhydrous media and in the presence of trace amounts of water, the probable mechanism of chiral conversion is given in Eq. (2) (12):

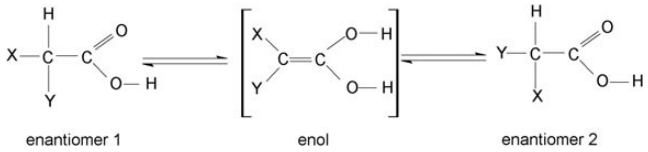

(2)

In the case of amino acids, the process of the parallel oscillatory chiral conversion and oscillatory peptidization can be illustrated by the following scheme given in Eq. (3) (6):

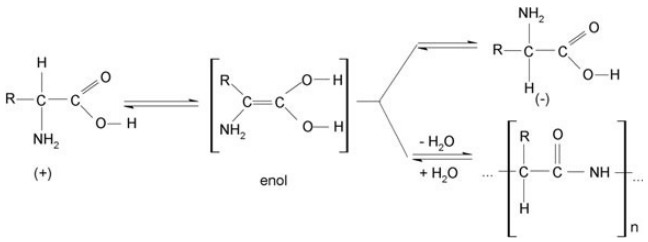

(3)

Some of our results have been cited in the papers dealing with such diverse subjects as prebiotic chemistry and astrophysics (13–17) as the first experimental evidence of the spontaneous chiral oscillatory conversion and spontaneous oscillatory condensation of the selected low-molecular-weight carboxylic acids. In paper (18), we for the first time discussed condensation running in the binary L-Pro-L-Hyp mixture dissolved in 70% aqueous methanol, and proposed a theoretical model to explain the specific dynamics of this process, which took into the account mutual catalytic effect of the two amino acids.

In this study, we extend the discussion on the oscillatory condensation to the other two amino acid pairs. Our choice was L-Pro-L-Phe and L-Hyp-L-Phe dissolved in aqueous acetonitrile. In that way, we intend to provide sufficient experimental evidence on the presence of the hetero-condensation products in the aged samples. The choice of L-Pro and L-Hyp was due to their important role as building blocks of collagen, which is omnipresent in the connective tissues of mammals, and largely responsible for tissue architecture and strength. L-Phe is one out of 20 exogenous amino acids and a building block of the majority of naturally occurring proteins.

© The Author [2014]. Published by Oxford University Press. All rights reserved. For Permissions, please email: journals.permissions@oup.com

Experimental

Reagents

L-Pro and L-Hyp were purchased from Sigma-Aldrich (St. Louis, MO, USA; cat. nos P0380 and H-55409, respectively), and L-Phe was purchased from Merck KGaA (Darmstadt, Germany; cat. no. 1.07256.0025). All amino acids were of the analytical purity grade, acetonitrile was of the high-performance liquid chromatography (HPLC) purity grade (J.T. Baker, Deventer, the Netherlands) and the water was deionized and double distilled in our laboratory by means of the Elix Advantage model Millipore system (manufactured in Molsheim, France).

The investigated binary L-Pro-L-Phe and L-Hyp-L-Phe amino acid solutions in acetonitrile were prepared at the following concentrations of each individual amino acid: 1.0 mg mL^{-1} (i.e., 8.69×10^{-3} mol L^{-1}) L-Pro, 1.0 mg mL^{-1} (i.e., 7.63×10^{-3} mol L^{-1}) L-Hyp, 1.0 mg mL^{-1} (i.e., 6.05×10^{-3} mol L^{-1}) L-Phe in solution with L-Pro and 2.5 mg mL^{-1}(i.e. 15.12×10^{-3} mol L^{-1}) L-Phe in solution with L-Hyp. As solvent, we used 70% aqueous acetonitrile.

High-performance liquid chromatography with evaporative light scattering and diode-array detection

The condensation process starting in each freshly prepared binary amino acid solution was monitored by means of the achiral HPLC with two different detectors (ELSD and DAD). This HPLC mode was employed to separate the oligopeptides from the non-peptidized amino acids and also to fractionate the oligopeptides. The analyses were carried out using the Varian model 920 liquid chromatograph (Varian, Harbor City, CA, USA) equipped with the Varian 900-LC model autosampler, the gradient pump, the Varian model 330 DAD detector, the Varian 380-LC model ELSD detector, the Pursuit 5 C18 (5 μm particle size) column (250 × 4.6 mm, i.d.; Varian; cat. no. A3000250C046) and the Galaxie software for data acquisition and processing. The analyses were carried out for the 30-μL aliquots of the investigated amino acid solutions in the isocratic mode. With the L-Pro-L-Phe mixture, the analyses were carried out in the 20-min intervals for 250 h and methanol–water (40 : 60, v/v) mobile phase at the flow rate of 0.25 mL min^{-1} was used. With the L-Hyp-L-Phe mixture, the analyses were carried out in the 10-min intervals for 160 h, using the acetonitrile–water (30 : 70, v/v) mobile phase at the flow rate of 0.60 mL min^{-1}. The chromatographic column was thermostated at 35°C with use of the Varian Pro Star 510 model column oven. The analyses with the use of these two systems were carried out in the short-time intervals, in order to derive quasi-kinetic information about the oscillatory peptidization processes running in the stored solutions.

High-performance liquid chromatography with mass spectrometric detection

LC–MS analyses were carried out in order to directly demonstrate the presence of the condensation products in the investigated amino acid solutions. They were performed for the freshly prepared solutions of the investigated amino acid pairs and after 122 (L-Pro-L-Phe) and 26 days (L-Hyp-L-Phe) of the storage period. The LC–MS System Varian (Varian, Palo Alto, CA, USA) was employed, equipped with the Varian ProStar model pump, Varian 100-MS mass spectrometer and Varian MS Workstation v. 6.9.1 software for data acquisition and processing.

The LC separation was carried out for the 20-μL aliquots of the investigated binary amino acid mixtures in the isocratic mode, using pre-column C18 (Varian, Harbor City, CA, USA) and 2-propanol mobile phase at the flow rate of 0.20 mL min^{-1}. MS was carried out in the electrospray ionization (ESI) mode (full ESI–MS scan, positive ionization, spray chamber temperature 50°C, drying gas temperature 250°C, drying gas pressure 25 p.s.i., capillary voltage 50 V, needle voltage 5 kV).

Results

HPLC-DAD and HPLC-ELSD of L-Pro-L-Phe and L-Hyp-L-Phe

Storage of the binary L-Pro-L-Phe and L-Hyp-L-Phe solutions in aqueous acetonitrile results in spontaneous and well pronounced changes in chemical composition of the analyzed mixtures. In the course of condensation, homo- and hetero-condensation products can be formed. From L-Pro and L-Phe, only oligopeptides can be derived, yet from the hydroxy-substituted amino acid (L-Hyp), oligopeptides, oligoesters and mixed condensation products (containing both peptide and ester bonds) can be obtained. Just to signalize the complexity of the condensation processes, in Figure 1 we present examples of the Pro-Phe hetero dipeptide, Hyp-Phe hetero dipeptide and Hyp-Phe ester (without taking into the account homodimers and higher oligomers, nor the oscillatory chiral conversion of both amino acids and hence, possible enantiomeric and diastereomeric forms of all these structures). The complexity of the spontaneously generated condensation products can only be appreciated from the perspective of the mass spectra discussed in the forthcoming section.

In order to illustrate the sum of all these effects, we superposed the chromatograms for L-Pro-L-Phe (Figure 2a) and L-Hyp-L-Phe (Figure 2b) registered at the different time intervals with use of ELSD. From the plots shown in Figure 2a and b, it is evident that in the course of the sample storage and ageing, the two predominant peaks in each chromatogram (originating from the two amino acids) slightly change their respective retention

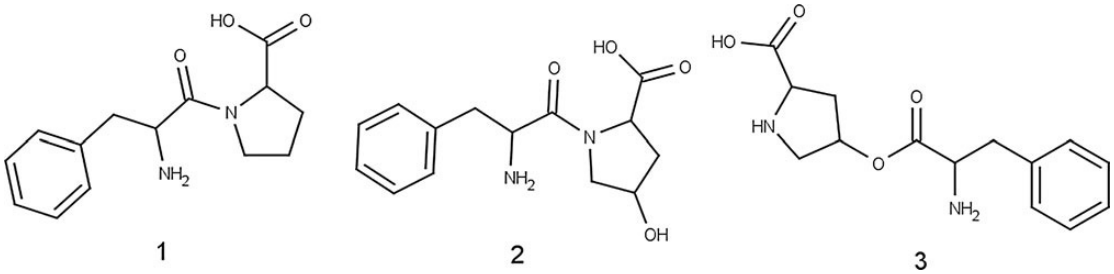

Figure 1. Illustration of the complexity of condensation upon the examples of the mixed heterodimers. (1) Pro-Phe hetero dipeptide, (2) Hyp-Phe hetero dipeptide and (3) Hyp-Phe ester.

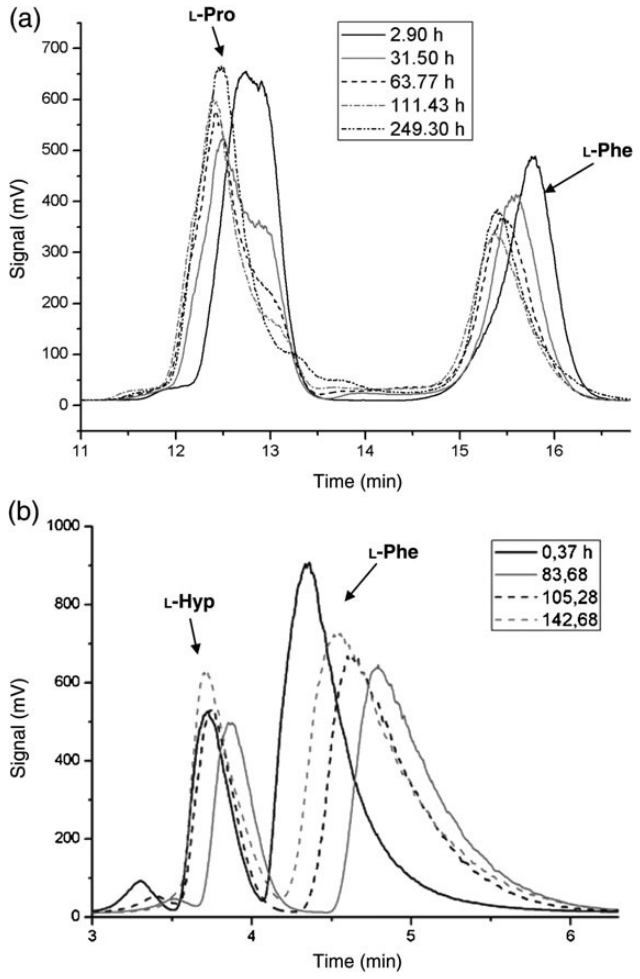

Figure 2. Superposition of the fragments of the selected chromatograms registered with use of the ELSD detector at the different time intervals for the aqueous acetonitrile solutions: (a) L-Pro-L-Phe (after 2.90, 31.50, 63.77, 111.43 and 249.30-h storage time); (b) L-Hyp-L-Phe (after 0.37, 83.68, 105.28 and 142.68-h storage time).

times (t_R). The observed minor changes are due to the displacement mechanism. As we strive for a shortest possible analytical run (in order to gain a quasi-kinetic insight in the dynamics of the investigated process), we have to compromise peak resolution. Hence, the tightly neighboring peaks of amino acids and the resulting condensation products exert the observed displacement effect.

From visual inspection of the plots alone (Figure 2a and b), it is evident that in each case the areas and the heights of the two predominant peaks of the starting compounds undergo nonlinear changes. Moreover, the peaks of the newly formed condensation products emerge. In the case of L-Pro-L-Phe, the main peak of the condensation product appears between those of L-Pro and L-Phe, and its retention time (t_R) falls within the range of 13.31–14.17 min. In the case of L-Hyp-L-Phe, the predominant new peak of the reaction product appears with the retention time shorter than those of L-Hyp and L-Phe, and its retention time is contained in the range of 3.17–3.78 min.

In Figures 3 and 4, we show the time series of the chromatographic peak heights for the two experimental sets. The observed oscillatory changes of the chromatographic peak heights are equivalent to the oscillatory concentration changes of the target species. Plots given in Figure 3a and b illustrate the dynamics of spontaneous peptidization of L-Pro-L-Phe. In Figure 3a, the full time range of the measurements (i.e. 250 h) is given. Respective plots show the time changes of the peak heights for L-Pro (1), L-Phe (2) and the main peptidization product (3). General observation is that at the first stage of the experiment (up to ca. 75 h), concentrations of L-Pro and L-Phe non-monotonously decrease and that of the oligopeptide non-monotonously increases. After that time, a kind of the dynamic equilibrium between peptidization and depeptidization is obtained, with occasionally more pronounced concentration changes. Each plot given in Figure 3a represents ca. 1,000 measuring points and due to that, on the presented graphs all peaks are very densely packed. Therefore in Figure 3b, we zoom the time range from 225 to 250 h for plots 1, 2 and 3 from Figure 3a. In this range, synchronization between the drop of the respective peak heights for L-Pro and L-Phe and the growth of the respective peak height for the peptidization product is clearly visible.

The analogous results valid for L-Hyp-L-Phe are presented in Figure 4a and b. Dynamics of the concentration changes with the two amino acids and the predominant condensation product are fully analogous to those observed in the former case. At the first stage of ageing (up to ca. 40 h), concentrations of L-Hyp and L-Phe non-monotonously decrease and that of the main condensation product non-monotonously increases. In Figure 4a, we show the consecutive stage only, when a kind of the dynamic equilibrium between condensation and the reverse process is achieved and continues for the rest of the measuring time, with occasionally more pronounced concentration changes. In Figure 4b, we zoom the time range from 58 to 59 h for plots 1, 2 and 3 from Figure 4a. In this zoomed range, synchronization between the concentration growth of L-Hyp and L-Phe and the concentration drop of the condensation product is clearly visible.

Finally, a general comment should be made regarding the observed instability of the peak heights and areas (and hence, of the respective concentrations also), discussed in this section. This instability is an evident proof of chemical processes running in the investigated solutions. Control analyses performed with use of the same chromatographic system for the chemically stable compounds (like, e.g., benzoic acid) give evidence of an excellent reproducibility of the respective chromatographic peak heights and areas, with the relative standard deviation values never exceeding 1%.

LC–MS of L-Pro-L-Phe and L-Hyp-L-Phe

LC–MS was another tool to monitor the process of oligocondensation. The chromatograms and the mass spectra valid for the fresh L-Pro-L-Phe sample and for that after 122 days storage period are shown in Figure 5a and b. Although the chromatograms do not considerably differ, the respective mass spectra are quite different. With the fresh L-Pro-L-Phe solution, three major signals are present at m/z 116 ($[Pro + H]^+$), m/z 166 ($[Phe + H]^+$) and m/z 132 ($[Pro + OH]^+$). Also certain signals from the oligopeptides can be seen (e.g., that at m/z 1,389, which can originate from $[(Phe)_6(Pro)_5 + He]^+$). With the aged solution, the major signals at m/z 116 and 166 are still there, yet the mass spectra show many more oligopeptide signals, and with much higher abundances also. Among them, the signals originating from homopeptides are present (e.g., that at m/z 459.88 can be

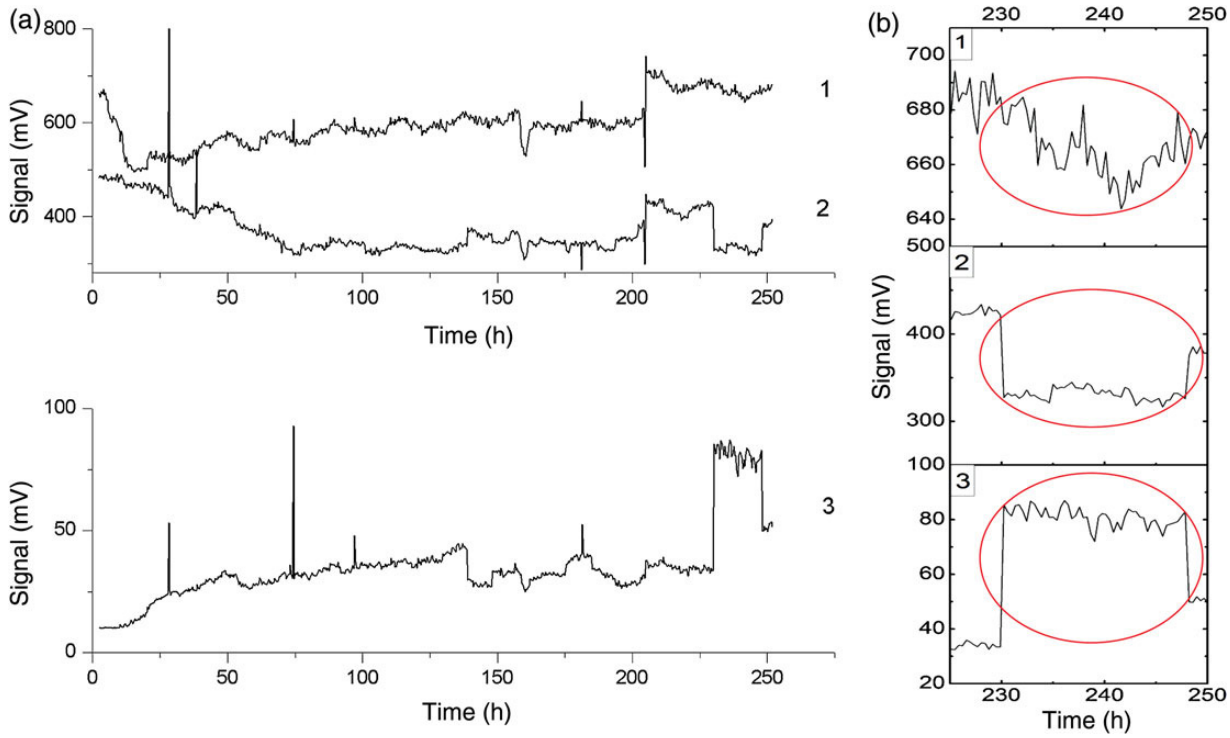

Figure 3. Time series of the chromatographic peak heights for L-Pro-L-Phe in aqueous acetonitrile (registered with ELSD detector): 1, L-Pro; 2, L-Phe; 3, peptidization product. (a) Full time range and (b) time range 225–250 h.

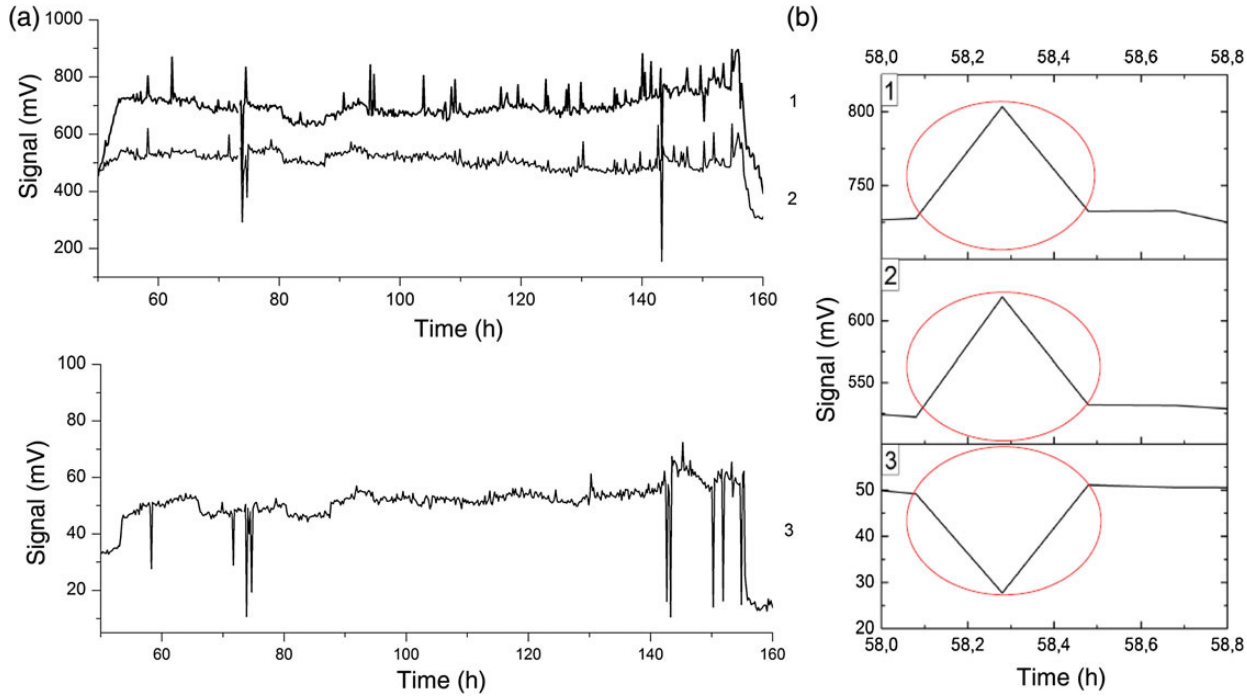

Figure 4. Time series of the chromatographic peak heights for L-Hyp-L-Phe in aqueous acetonitrile (registered with ELSD detector): 1, L-Phe; 2, L-Hyp; 3, condensation product. (a) Time range 50–160 h storage period and (b) time range 58–59 h.

ascribed to phenylalanine tripeptide, $[(Phe)_3]^+$). Most probably, the signals valid for the heteropeptides are also present (e.g., the signal at m/z 1022.23 can hold for $[(Phe)_4(Pro)_4+CO]^+$ and that at m/z 1579,26, might originate from $[(Phe)_6(Pro)_7]^+$).

The chromatograms and the mass spectra valid for the fresh L-Hyp-L-Phe sample and for that after 26 days storage period are shown in Figure 5c and d. Also in this case, the chromatograms of the fresh and the aged sample are quite similar, yet the respective

mass spectra considerably differ. With the fresh sample, the three major signals appear at the same m/z values, as for L-Pro-L-Phe (i.e. at m/z 116, 132 and 166). This time, signal at m/z 116 can be attributed to the fragmentation ion derived from L-Hyp by the detachment of a hydroxyl group ($[\text{Hyp-OH} + 2\text{H}]^+$), that at m/z 132 most probably originates from $[\text{Hyp} + \text{H}]^+$ and that at m/z 166 holds for $[\text{Phe} + \text{H}]^+$. With the aged L-Hyp-L-Phe sample, an abundance of the relatively intense mass spectrometric signals can be seen. This spectrum is richer than the analogous one valid for L-Pro-L-Phe, which apparently is due to the two functionalities with Hyp ($-NH_2$ and OH), which enables both peptidization and esterification. Once again, certain peaks can be attributed to the homocondensates (e.g., those at m/z 1369.58 and 343.93 can be valid for $[(\text{Phe})_9 + \text{CO}]^+$ and $[(\text{Hyp})_3 - \text{OH} + \text{He}]^+$, respectively). Some other peaks can be attributed to heterocondensates (e.g., that at m/z 392.71 can originate from $[(\text{Phe})(\text{Hyp})_2 + \text{H}]^+$, and that at m/z 1589.80 can be derived from $[(\text{Phe})_6(\text{Hyp})_6 - \text{OH} + \text{CO}]^+$).

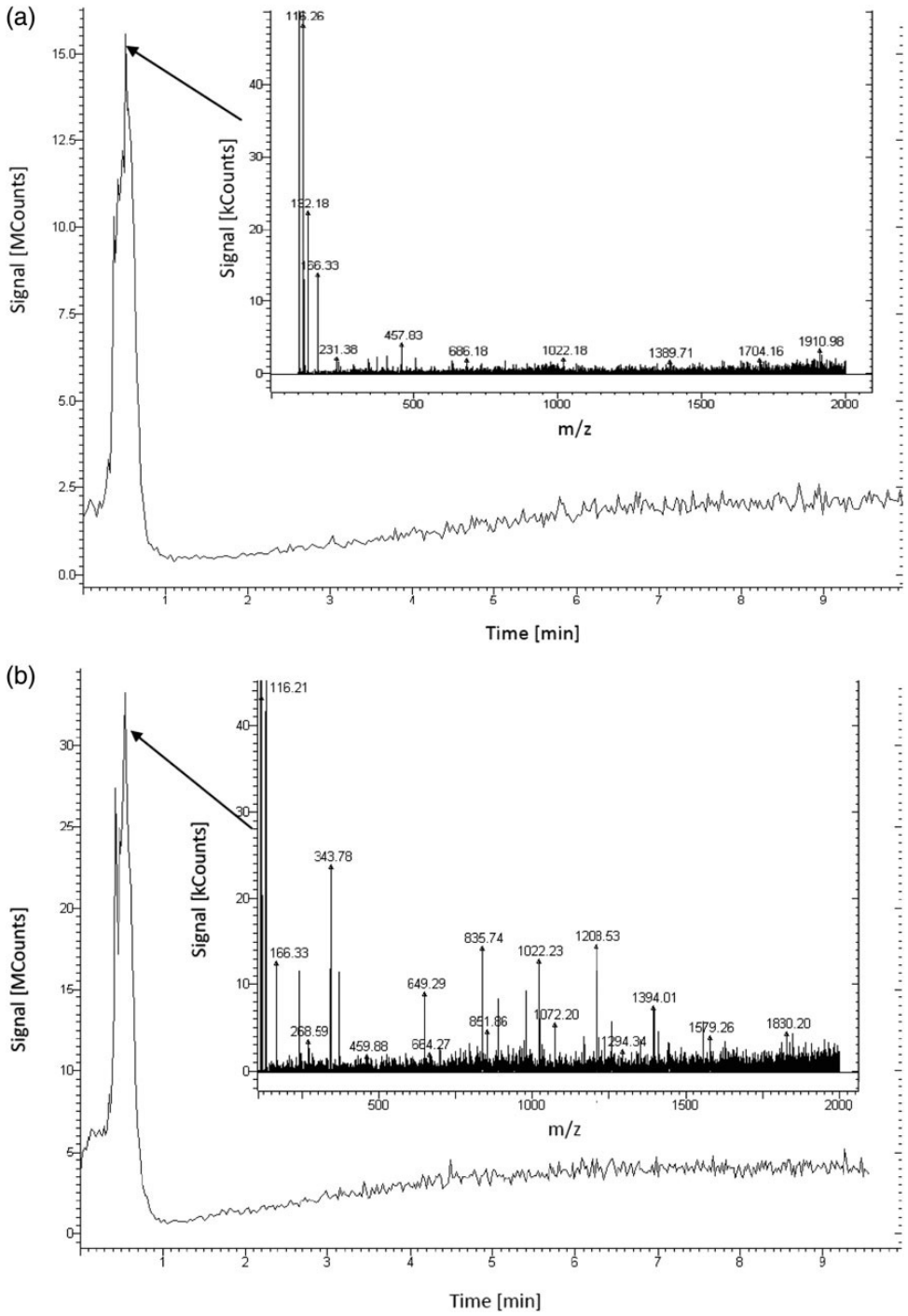

Figure 5. LC chromatograms with mass spectrometric insets for the amino acid pairs dissolved in aqueous acetonitrile. (a) Fresh L-Pro-L-Phe solution, (b) L-Pro-L-Phe solution after 122 days storage period, (c) fresh L-Hyp-L-Phe solution and (d) L-Hyp-L-Phe solution after 26 days storage period.

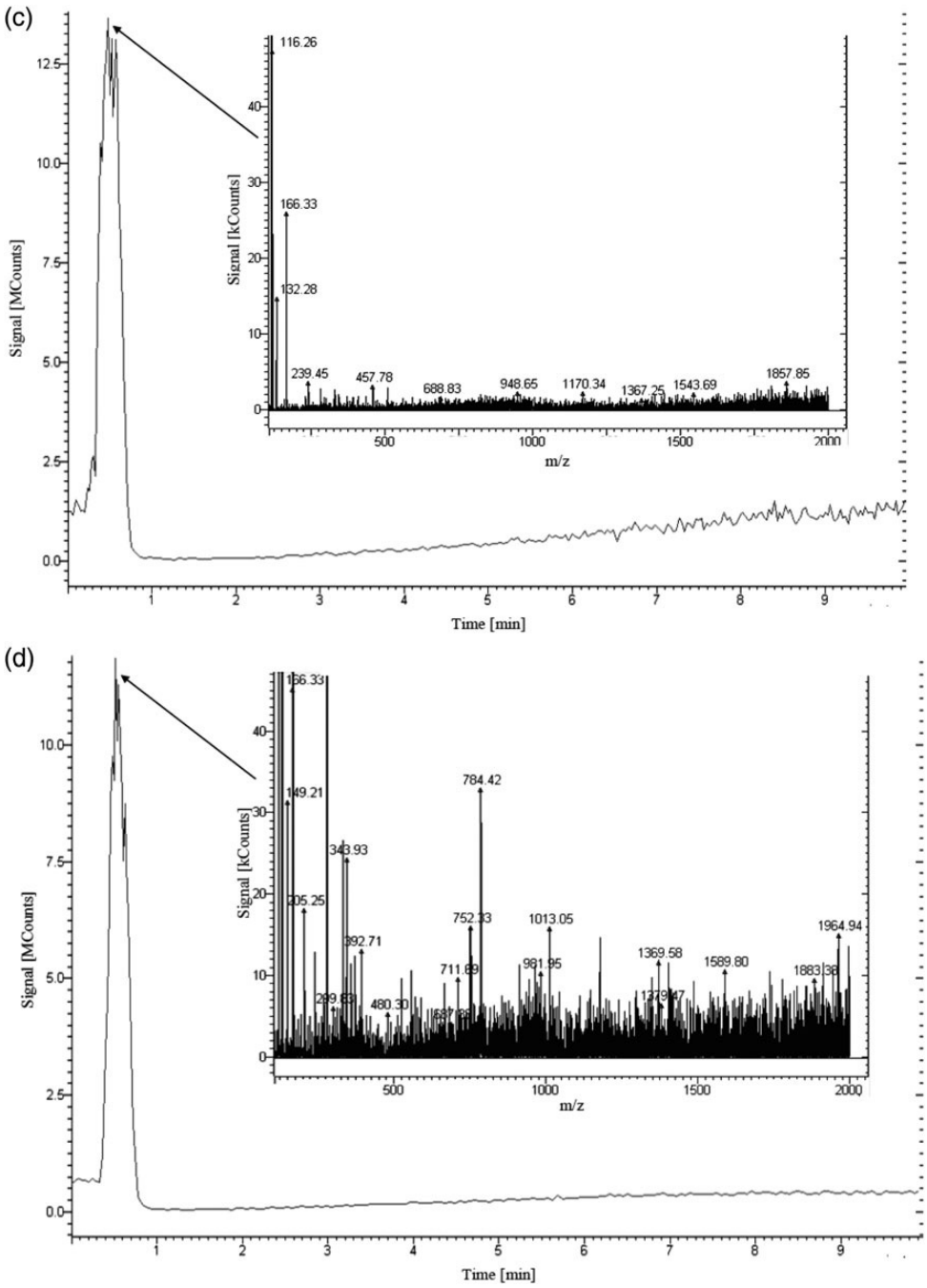

Figure 5. *Continued*.

Discussion

Our interest in spontaneous condensation of amino acids in aqueous and non-aqueous solutions stems from the theory of abiogenesis by Oparin and Haldane (19), and from our understanding of the importance of this class of chemical compounds for life sciences. The hypotheses that emerge from the theory of abiogenesis and refer to the formation of organic compounds, and more specifically, to the formation of peptides and proteins in non-biological processes, certainly need further verification with modern and continuously improving analytical tools.

In our earlier studies, we managed to provide first experimental evidence on spontaneous peptidization of single amino acids in aqueous solutions and on the oscillatory nature of these processes (5–7). In study (18), peptidization of the first amino acid pair (L-Pro-L-Hyp) in aqueous solution was discussed and theoretical models were developed to explain the specific dynamics of this process. These models took into the account mutual catalytic effect of the two amino acids making a pair. Without going too deep into the details of these models, their general feature can be given in the following way. At the first step, both amino acids undergo oligopeptidization. At the second step, the oligopeptides can form higher structures, i.e., the H-bonded supramolecular aggregates and the covalently bonded higher peptides, equally characterizing with the properties of the micelles. This second step is

considered as an uncatalyzed aggregation. The third step is assumed as catalyzed aggregation, which means that the chemical structure of the already formed micelles influences the structure of the new generation micelles. At the fourth step, decomposition of the micelles is anticipated. Each step is described by means of stoichiometric, as well as kinetic equations, separately for each amino acid from a given amino acid pair. An extreme case is that the two amino acids do not cooperate in the condensation process and produce homo-oligopeptides only. In the other three cases, a cooperative condensation occurs, which results in the homo- and hetero-oligocondensates. This coperative condensation can characterize with kinetic predominance of one or the other amino acid from a given pair, or without such predominance at all.

In this study, we focus on the other two amino acid pairs (L-Pro-L-Phe and L-Hyp-L-Phe), when aged in an organic-aqueous solvent. Selection of acetonitrile as a solvent was purposely made in order to verify, if spontaneous mixed peptidization can also run in that environment. In the other words, we tried to check, if a primeval broth concept, generally attributed to Oparin and Haldane, might apply to our solution, and we obtained a positive feedback.

In an attempt to obtain quasi-kinetic evidence with aid of HPLC–DAD and HPLC–ELSD, we had to compromise the quality of separation. As a reward, we managed to convincingly demonstrate the oscillatory nature of the concentration changes with the two amino acids and the main condensation product in a function of time. Selected examples demonstrate perfect time synchronization of the concentration drop with the amino acids of interest and the concentration growth with the main condensation product, or the vice versa (Figure 4a and b, respectively). These results directly confirm the formation of heterocondensates in the investigated solutions, i.e. the cooperative effect assumed in our earlier elaborated model (18). Additional confirmation of the accumulation of the high-molecular-weight condensates was derived from the LC–MS experiments (Figure 5a–d).

Finally, our results seem to conform with the hypothesis formulated in paper (19) and then extensively discussed and theoretically confirmed in papers (13, 20). According to this hypothesis that refers to the chiral substrates, the reason for the condensation oscillations is that heterochiral polymerization is favored over homochiral polymerization. This means that oscillations are favored for heterochiral polymerization and homochiral depolymerization and epimerization.

Conclusions

It was an aim of this study to experimentally demonstrate an ability of selected amino acids (L-Pro, L-Hyp and L-Phe) with key importance for living organisms to spontaneously undergo oscillatory condensation and to form homo- and hetero-condensates. This goal was successfully achieved with aid of HPLC–DAD, HPLC–ELSD and LC–MS. We believe that the importance of the results obtained herewith is due to the fact that they address fundamental issues related to the prebiotic chemical systems and perhaps to the beginning of biological life also.

References

1. Sajewicz, M., Pietka, R., Pieniak, A., Kowalska, T.; Application of thin-layer chromatography (TLC) to investigating oscillatory instability of the selected profen enantiomers; *Acta Chromatographica*, (2005); 15: 131–149.
2. Sajewicz, M., Pietka, R., Pieniak, A., Kowalska, T.; Application of thin-layer chromatography (TLC) to investigate oscillatory instability of the selected profen enantiomers in dichloromethane; *Journal of Chromatographic Science*, (2005); 43: 542–548.
3. Sajewicz, M., Kronenbach, D., Gontarska, M., Wróbel, M., Pietka, R., Kowalska, T.; TLC in search for structural limitations of spontaneous oscillatory in-vitro chiral conversion. α-Hydroxybutyric and mandelic acids; *Journal of Planar Chromatography – Modern TLC*, (2009); 22: 241–248.
4. Sajewicz, M., Kronenbach, D., Gontarska, M., Kowalska, T.; TLC and polarimetric investigation of the oscillatory in vitro chiral conversion of R-β-hydroxybutyric acid; *Journal of Liquid Chromatography and Related Technologies*, (2010); 33: 1047–1057.
5. Sajewicz, M., Gontarska, M., Kronenbach, D., Kowalska, T.; On the spontaneous abiotic peptization of phenylglycine in an aqueous medium; *Acta Chromatographica*, (2009); 21: 151–160.
6. Sajewicz, M., Gontarska, M., Kronenbach, D., Leda, M., Kowalska, T., Epstein, I.R.; Condensation oscillations in the peptidization of phenylglycine; *Journal of Systems Chemistry*, (2010); 1: 7.
7. Sajewicz, M., Gontarska, M., Wojtal, Ł., Kronenbach, D., Leda, M., Epstein, I.R., *et al.* Experimental and model investigation of the oscillatory transenantiomerization of L-α-phenylalanine; *Journal of Liquid Chromatography and Related Technologies*, (2008); 31: 1986–2005.
8. Sajewicz, M., Wrzalik, R., Gontarska, M., Kronenbach, D., Leda, M., Epstein, I.R., *et al.* In vitro chiral conversion, phase separation, and wave propagation in aged profen solutions; *Journal of Liquid Chromatography and Related Technologies*, (2009); 32: 1359–1372.
9. Sajewicz, M., Matlengiewicz, M., Leda, M., Gontarska, M., Kronenbach, D., Kowalska, T., *et al.* Spontaneous oscillatory in vitro chiral conversion of simple carboxylic acids and its possible mechanism; *Journal of Physical Organic Chemistry*, (2010); 23: 1066–1073.
10. Sajewicz, M., Dolnik, M., Kronenbach, D., Gontarska, M., Kowalska, T., Epstein, I.R.; Oligomerization oscillations of L-lactic acid in solutions; *Journal of Physical Chemistry A*, (2011); 115: 14331–14339.
11. Belanger, P., Atkinson, J.G., Stuart, R.S.; Exchange reactions of carboxylic acid salts. Kinetics and mechanism; *Journal of the Chemical Society–Section D: Chemical Communications*, (1969); 1067–1068.
12. Xie, Y., Liu, H., Chen, J.; Kinetics of base catalyzed racemization of ibuprofen enantiomers; *International Journal of Pharmaceutics*, (2000); 196: 21–26.
13. Stich, M., Blanco, C., Hochberg, D.; Chiral and chemical oscillations in a simple dimerization model; *Physical Chemistry Chemical Physics*, (2013); 15: 255–261.
14. Rincon, A.G., Guzman, M.I., Hoffmann, M.R., Colussi, A.J.; Optical absorptivity versus molecular composition of model organic aerosol matter; *Journal of Physical Chemistry A*, (2009); 113: 10517–10529.
15. Paudel, A., Van den Mooter, G.; Influence of solvent composition on the miscibility and physical stability of naproxen/PVP K 25 solid dispersions prepared by cosolvent spray-drying; *Pharmaceutical Research*, (2012); 29: 251–270.
16. Paudel, A., Nies, E., Van den Mooter, G.; Relating hydrogen-bonding interactions with the phase behavior of naproxen/PVP K 25 solid dispersions: evaluation of solution-casted and quench-cooled films; *Molecular Pharmaceutics*, (2012); 9: 3301–3317.
17. Danger, G., Plasson, R., Pascal, R.; Pathways for the formation and evolution of peptides in prebiotic environments; *Chemical Society Reviews*, (2012); 41: 5416–5429.
18. Sajewicz, M., Dolnik, M., Kowalska, T., Epstein, I.R.; Condensation dynamics of L-proline and L-hydroxyproline in solution; *RSC Advances*, (2014); 4: 7330–7339.
19. Pross, A.; *What is Life? How Chemistry Becomes Biology*. Oxford University Press, Oxford, UK, (2012).
20. Plasson, R., Bersini, H., Commeyras, A.; Recycling Frank: spontaneous emergence of homochirality in non-catalytic systems; *Proceeding of the National Academy of Sciences of the Unated States of America*, (2004); 101: 16733–16738.

Journal of Chromatographic Science 2015;53:401–410
doi:10.1093/chromsci/bmu122 Advance Access publication September 19, 2014

Article

HPLC Monitoring of Spontaneous Non-Linear Peptidization Dynamics of Selected Amino Acids in Solution

Agnieszka Godziek, Anna Maciejowska, Mieczysław Sajewicz and Teresa Kowalska*

Institute of Chemistry, University of Silesia, 9 Szkolna Street, Katowice 40-006, Poland

*Author to whom correspondence should be addressed. Email: teresa.kowalska@us.edu.pl

Received 30 June 2014; revised 1 August 2014

This is our new study in a series of publications devoted to exploration of applicability of high-performance liquid chromatography (HPLC) to providing answers to difficult questions from the area of the reaction kinetics and mechanisms with non-linear reactions. Although an excellent analytical performance of HPLC is an indisputable fact, so far its performance as a tool in the kinetic and mechanistic studies has been tested to a lesser extent. In our earlier studies, spontaneous peptidization dynamics of amino acids in solution was demonstrated by means of HPLC upon a few amino acid examples, and on that basis a theoretical model has been developed, anticipating an interdependence of dynamics on chemical structures of amino acids involved. In order to expand the spectrum of experimentally investigated amino acid cases, in this study we present the results valid for three novel amino acids of significant life sciences importance, which differ in terms of peptidization dynamics. Experimental evidence originates from the achiral HPLC with the evaporative light scattering detection and MS detection. A conclusion is drawn that different spontaneous peptidization dynamics of amino acids may significantly influence chemical composition of proteins encountered in living organisms. Hence, a need emerges for systematic physicochemical studies on spontaneous non-linear peptidization dynamics of proteinogenic amino acids in liquid abiotic (but also in the biotic) systems.

Introduction

In the paper (1), spontaneous oscillatory chiral conversion was, for the first time, reported for several propionic acid derivatives, stored for longer periods of time in 70% aqueous ethanol, based on the results originating from TLC (and other instrumental techniques) (2). Later, an analogous evidence of spontaneous chiral conversion obtained with the use of high-performance liquid chromatography with diode-array detection (HPLC-DAD) was presented. We managed to demonstrate that the oscillatory chiral conversion is a general property, which characterizes the low-molecular-weight carboxylic acids from the groups of profen drugs (1), amino acids (3) and hydroxyl acids (4), when dissolved in aqueous or non-aqueous solvents and stored for certain periods of time in solution. Chiral conversion of such compounds can occur according to the two different pathways. In aqueous solutions, the general scheme can be represented as (5)

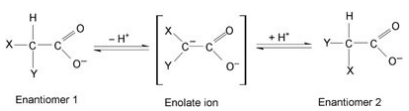

where X: −R (aliphatic) and Y: $-NH_2$, −OH or −Ar (aromatic).

In anhydrous media and in the presence of trace amounts of water, the probable mechanism of chiral conversion is (6)

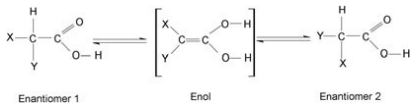

From our earlier investigations, it came out that the oscillatory chiral conversion of the low-molecular-weight carboxylic acids occurs in parallel with the oscillatory condensation, which most probably has thermodynamic justification (2). In papers (7, 8), we presented the results of spontaneous oscillatory condensation for the three binary amino acid systems (*L*-Pro-*L*-Hyp, *L*-Pro−*L*-Phe and *L*-Hyp−*L*-Phe), dissolved in aqueous organic solvents. The parallel processes of chiral conversion and peptidization of amino acids can be illustrated by the following scheme (9):

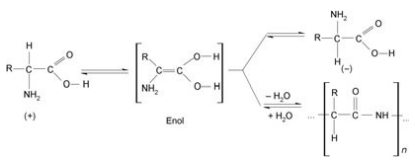

In the paper (7), a theoretical model of spontaneous non-linear peptidization in the binary amino acid systems was developed, particularly focused on heteropeptide formation. This model assumes four different cases, and namely (i) the case, when two amino acids cannot form heteropeptides and even in a binary solution, they spontaneously produce homopeptides only; (ii) the case, when two amino acids of different non-linear peptidization dynamics can form heteropeptides, and dynamics of faster peptidizing amino acid governs an overall dynamics; (iii) the case, when two amino acids of different non-linear peptidization dynamics can form heteropeptides, and dynamics of slower peptidizing amino acid governs an overall dynamics and (iv) the case, when two amino acids of different non-linear peptidization dynamics can form heteropeptides according to cooperative mechanism, where none of the two species governs the process dynamics.

So far, spontaneous non-linear peptidization dynamics has been demonstrated on a set of four amino acids only, i.e., Phg, Phe, Pro and Hyp (2, 7, 8), so the goal of this study is to investigate spontaneous non-linear peptidization dynamics with three novel

© The Author 2014. Published by Oxford University Press. All rights reserved. For Permissions, please email: journals.permissions@oup.com

amino acids, i.e., methionine (Met), histidine (His) and serine (Ser). Met is one of the two sulfur-containing proteinogenic amino acids only and acts as an intermediate in biosynthesis of different phospholipids (10, 11). His and Ser are also proteinogenic amino acids; the former one acts as a precursor of histamine (12, 13), and the latter one participates in biosynthesis of purines and pyrimidines (14) and plays an important role in a catalytic function of many enzymes (15).

Experimental

Reagents

In this experiment, we used three amino acids (i.e., *L*-Met, *L*-His and *L*-Ser) of analytical purity, purchased from Reanal. Methanol was of HPLC purity (Sigma-Aldrich), and water was de-ionized and double distilled in our laboratory by means of the Elix Advantage model Millipore System. Solutions of the investigated amino acids were prepared in water at the concentration equal to $1\ mg\ mL^{-1}$ (i.e., $6.70 \times 10^{-3}\ mol\ L^{-1}$ for *L*-Met, $6.55 \times 10^{-3}\ mol\ L^{-1}$ for *L*-His and $9.52 \times 10^{-3}\ mol\ L^{-1}$ for *L*-Ser).

HPLC with evaporative light scattering detection

Monitoring of spontaneous non-linear peptidization dynamics of the investigated amino acids in water was performed with use of the achiral HPLC. The analyses of freshly prepared amino acid solutions were carried out using the Varian model 920 liquid chromatograph equipped with the Varian 900-LC model autosampler, the gradient pump, the Varian Pro Star 510 model column oven, the Varian 380-LC model evaporative light scattering detection (ELSD) detector, the ThermoQuest Hypersil C18 (5 μm particle size) column and the Galaxie software for data acquisition and processing. The analyses were carried out for the 3-μL aliquots of each investigated amino acid solution, using methanol–water (20:80, v/v) as mobile phase at the flow rate of $0.8\ mL\ min^{-1}$ in the isocratic mode. The column was thermostated at 35°C. The analyses for *L*-Met and *L*-Ser were carried out in the 10-min intervals for 18 and 20 h, respectively, while the analyses of *L*-His were carried out in the 15-min intervals for 10 h.

HPLC with mass spectrometric detection

To prove the presence of the peptides in the investigated amino acid solutions, the HPLC–MS analyses were performed for the freshly prepared amino acid samples and for those after 70.20 h (Met), 52.50 h (His) and 245.40 h (Ser) storage period.

The HPLC system described in the preceding section was additionally equipped with the Varian 100-MS mass spectrometric detector and the Varian MS Workstation v. 6.9.1 software for data acquisition and processing. Mass spectrometric detection was carried out in the ESI mode (ESI-MS scan, positive ionization, spray chamber temperature 50°C, drying gas temperature 350°C, drying gas pressure 25 psi, capillary voltage 50 V, needle voltage 5 kV).

Freshly prepared and aged Met, His and Ser samples were analyzed in the integrated HPLC–ELSD–MS system, equipped with the two detectors. Additionally, freshly prepared and aged His samples in the 20-μL aliquots were analyzed in the LC-MS mode, due to this amino acid's high peptidization rates and a tendency of the resulting peptides to deposit on the chromatographic column. To this effect, the His samples were introduced through the guard column directly to the MS detector. Otherwise, the assumed working parameters of mass spectrometer were the same as those earlier described.

All experiments discussed in this study were performed at least in duplicate, in order to confirm the trends with the amino acid concentration changes and the respective mass spectrometric patterns (as in the case of spontaneous, i.e., uncontrolled, and non-linear processes, it is virtually impossible to commence measurements each time in an identical moment and obtain quantitatively identical results).

Results

HPLC–ELSD of Met, His and Ser

Chemical structures of Met, His and Ser are shown in Figure 1. Met is the $-S-CH_3$ group containing amino acid, His contains an imidazole ring in its structure and Ser is an $-OH$ group containing amino acid. All three are α-amino acids, which can formally be viewed as the *n*-propionic acid derivatives, substituted on C2 and C3 atoms. As they differ in structural terms, this feature should be reflected in differentiated dynamics of their peptidization also, and this study is focused on a comparison of this dynamics.

In order to demonstrate the oscillatory nature of peptidization, samples of the aqueous *L*-Met, *L*-His and *L*-Ser solutions were analyzed for the longer periods of time (Met and Ser in the 10-min intervals, and *L*-His in the 15-min intervals). In Figures 2a–i, we show nine chromatograms valid for Met, recorded in different time intervals. A display of these nine insets is meant to

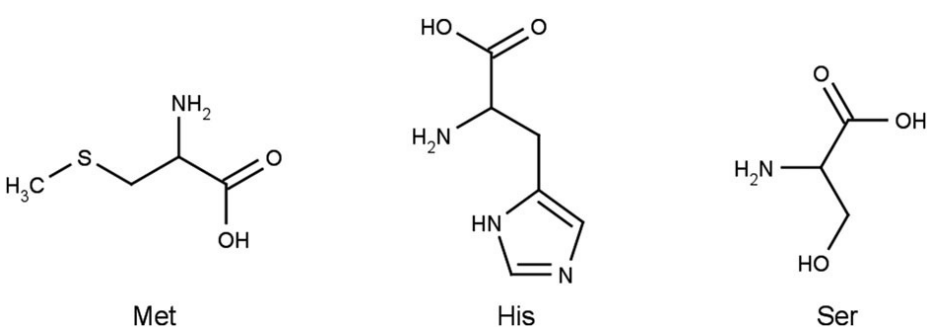

Figure 1. Selected chemical structures of Met, His and Ser.

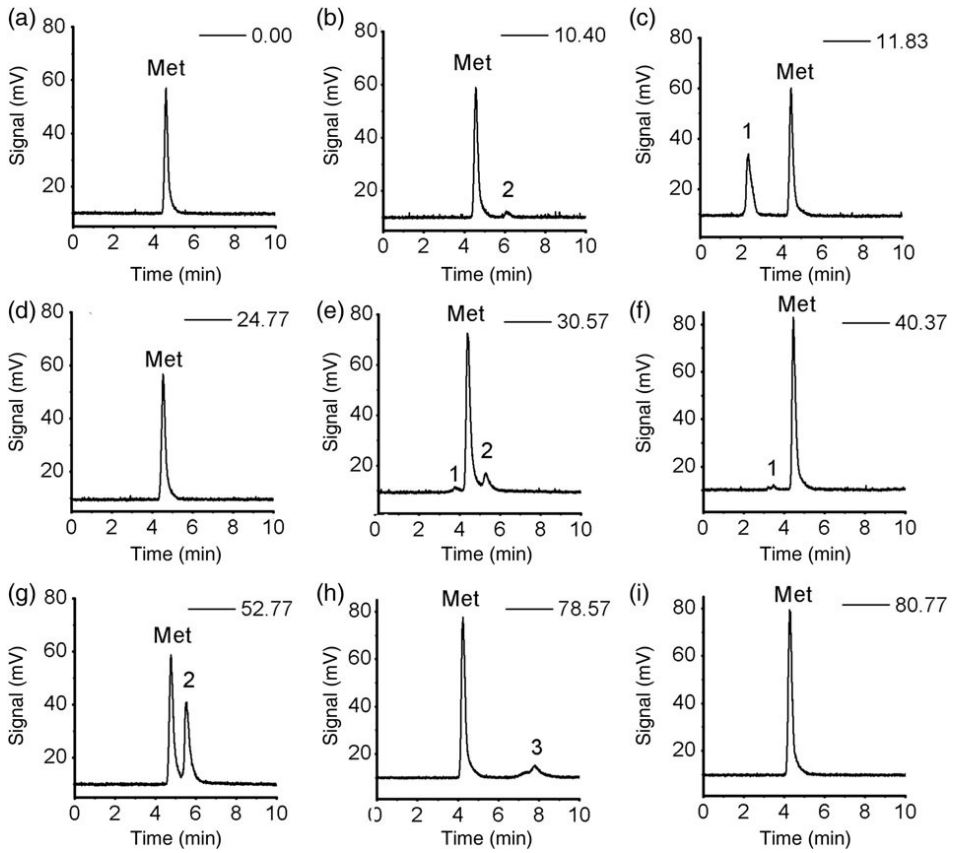

Figure 2. Selected snapshots showing chromatograms of Met ($t_R = 4.46$ min) and the main peptidization products 1 ($t_R = 2.37$ min) 2 ($t_R = 6.11$ min) and 3 ($t_R = 7.80$ min), registered with ELSD, after the different sample storage periods; (a) 0.00 h; (b) 10.40 h; (c) 11.83 h; (d) 27.77 h; (e) 30.57 h; (f) 40.37 h; (g) 52.77 h; (h) 78.57 h and (i) 80.77 h.

demonstrate a spectacular (because irregular) appearance and disappearance of three Met-derived peptidization products, denoted as peak 1 ($t_R = 2.37$ min), peak 2 ($t_R = 6.11$ min) and peak 3 ($t_R = 7.80$ min). In Figure 2a, we can see a single peak of Met ($t_R = 4.46$ min), valid for the freshly prepared solution. In Figure 2b (recorded after 10.40 h sample aging), an additional and eluting slower than Met peak 2 appears. Approximately 1 h later, another and eluting faster than Met peak appears, denoted as peptidization product 1. Occasionally, peptidization products 1 and 2 can be seen simultaneously (as in Figure 2e, recorded after 30.57 h sample aging). After 78.57 h the Met sample aging, peptidization product denoted as peak 3 appears, with the retention time even longer than peak 2 (Figure 2h). It needs adding that each of the three peaks denoted as peptidization products most probably represents more than one peptide type, due to the short time of a single analytical run (10 min), which makes complete peptide separation virtually impossible. In that way, we had to compromise separation in order to gain a quasi-kinetic insight in the dynamic changes of the peak originating from Met. The chromatograms recorded for His and Ser with the aid of the ELSD detector (and for the sake of conciseness, not presented in this study) reflect an analogous tendency with the appearing and disappearing respective peptidization products.

In Figures 3a–c, we show the time series of the chromatographic peak heights for Met, His and Ser, recorded with the ELSD detector. These changes of the peak height represent changing amino acid concentrations in the course of aging. Figure 3a illustrates these changes with Met in the period of 18 h. In the course of the initial *ca.* 2.5 h, one can see the oscillatory concentration drop, due to peptidization. For the next *ca.* 5.5 h, the Met concentration grows in an oscillatory manner, which represents an oscillatory tendency of the peptides to partially dissociate. Starting from the eighth hour of aging, the nonlinear drop of the Met concentration is again observed, which reflects a new shift toward oscillatory peptidization.

In Figure 3b, the time series of the chromatographic peak heights for His in the course of 10 h aging is presented. First, very rapid oscillatory concentration drop is observed for *ca.* 2.5 h. For the rest of the time, the His concentration oscillates within a rather stable value range, which is considerably lower than the initial His concentration. This relative stability is most probably due to clogging the column packing with the higher His-derived peptides. Thus, the packing became coated with the higher peptides and performed like an adsorption column, with most active sites on its surface occupied. One can add that at the end of the experiment, it needed real effort to rinse the chromatographic system (the sensitive ELSD detector

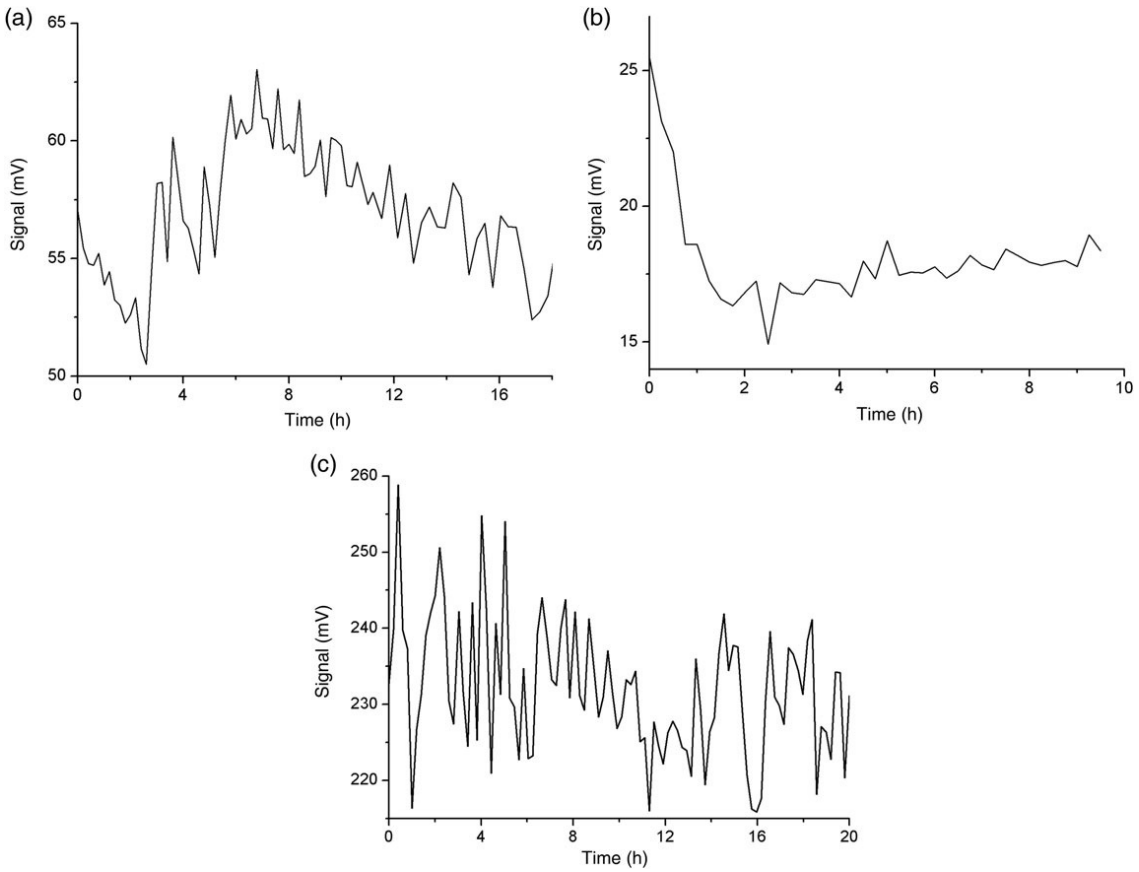

Figure 3. Time series of chromatographic peak heights from amino acids dissolved in water, registered with the ELSD detector for (a) *L*-Met (time range 0–18 h); (b) *L*-His (time range 0–10 h) and (c) *L*-Ser (1) (time range 0–20 h).

included), which lasted *ca.* 1 week and was only possible with the use of methanol, acetonitrile and water in different volume proportions.

In Figure 3c, the time series of the chromatographic peak heights valid for Ser in the course of 20 h aging is presented. A non-linear trend of the respective concentration changes is also evident, although unlike in the former two cases, one cannot point out to any distinct phase in this non-linear pattern. A noteworthy feature is that (unlike with the two other amino acids) in the first half an hour or so, concentration of Ser grows, which might suggest that its commercial form contains certain amount of peptides, which dissociate upon the initial contact with the solvent.

Due to the purposely fixed short sampling intervals (in order to gain a quasi-kinetic insight in the peptidization dynamics), the displacement mechanism showing competition between the monomeric amino acid and the resulting peptides is reflected in certain fluctuations of the retention times (t_R) for the monomeric species. With Met and Ser, these fluctuations were almost negligible (in the range of 4.16–4.77 min and 3.74–4.10 min, respectively). With the rapidly peptidizing His, this fluctuation was higher and the retention time of the His monomer appeared in the range from 6.26 to 8.22 min.

HPLC–MS of Met, His and Ser

Coupling of HPLC with a mass spectrometric detector allowed a deeper insight into the chemical nature of the sample aging products. Mass spectra recorded for the freshly prepared samples and for those after certain storage period are shown in Figure 4.

In Figures 4a and b, the chromatograms and mass spectra valid for Met after 5.00 and 70.20 h aging period are given. Apart from a rather insignificant difference of the retention time (equal to 4.59 and 4.29 min, respectively, for the fresh and the aged sample), changes of the mass spectra due to the sample aging are evident. In the first mass spectrum, the molecular ion of Met at $m/z = 150.25$ ($[\text{Met} + \text{H}]^+$) predominates. Moreover, the fragmentation peaks characteristic of Met can also be seen at $m/z = 131.97$ and 102.76, which correspond with the following structures: $[\text{Met}(-\text{NH}_3)]^+$ and $[\text{Met}(-\text{CO} + \text{H}_2\text{O})]^+$, respectively (16). In the fresh sample, signals originating from the peptides can also be seen, but their intensities equal to the mere 7.5% of molecular ion. In the case of the aged Met sample, the mass spectrum assumes a considerably different pattern. The signal of the molecular ion can hardly be seen and its intensity equals to 0.32 kCounts, yet the signals originating from the spontaneously peptidized species are galore. The most intense signals appear at $m/z = 326.21$, 686.11 and 817.96, and they correspond

with the following structures: $[Met_9 + 4H]^{4+}$, $[Met_5 + H\text{-(mass loss of 22)}]^{+}$ and $[Met_{22} + 4H]^{4+}$.

In Figures 4c and d), the chromatograms and mass spectra valid for His after 4.00 and 52.50 h storage period are given. In this case, mass spectra recorded in the HPLC–MS system only insignificantly differ. The most characteristic symptoms of aging are an intensity drop of the His molecular ion ($m/z = 155.21$), its fragmentation ion at $m/z = 108.73$ ($[His(-CO + H_2O)]^{+}$) (16) and its pseudomolecular ion at $m/z = 177.32$ ($[His + Na]^{+}$). Several more intense peaks originating from the peptides also appear in the course of aging, yet an overall difference between the two mass spectral patterns is almost insignificant, when compared with analogous results obtained for the remaining two amino acids. Based on what was stated in the preceding section on the tendency of His to coat the column packing with peptides, it can be concluded that these peptides largely get stuck on the column and do not appear in the effluent. Therefore, additional analyses were carried out with use of the LC–MS system equipped with a short guard column only, to avoid arresting of the high molecular weight peptides on the column. Respective results are going to be presented in the forthcoming section.

The third investigated amino acid was Ser and in Figures 4e and f, respective chromatograms and mass spectra valid for the freshly prepared sample and for that after 245.40 h aging

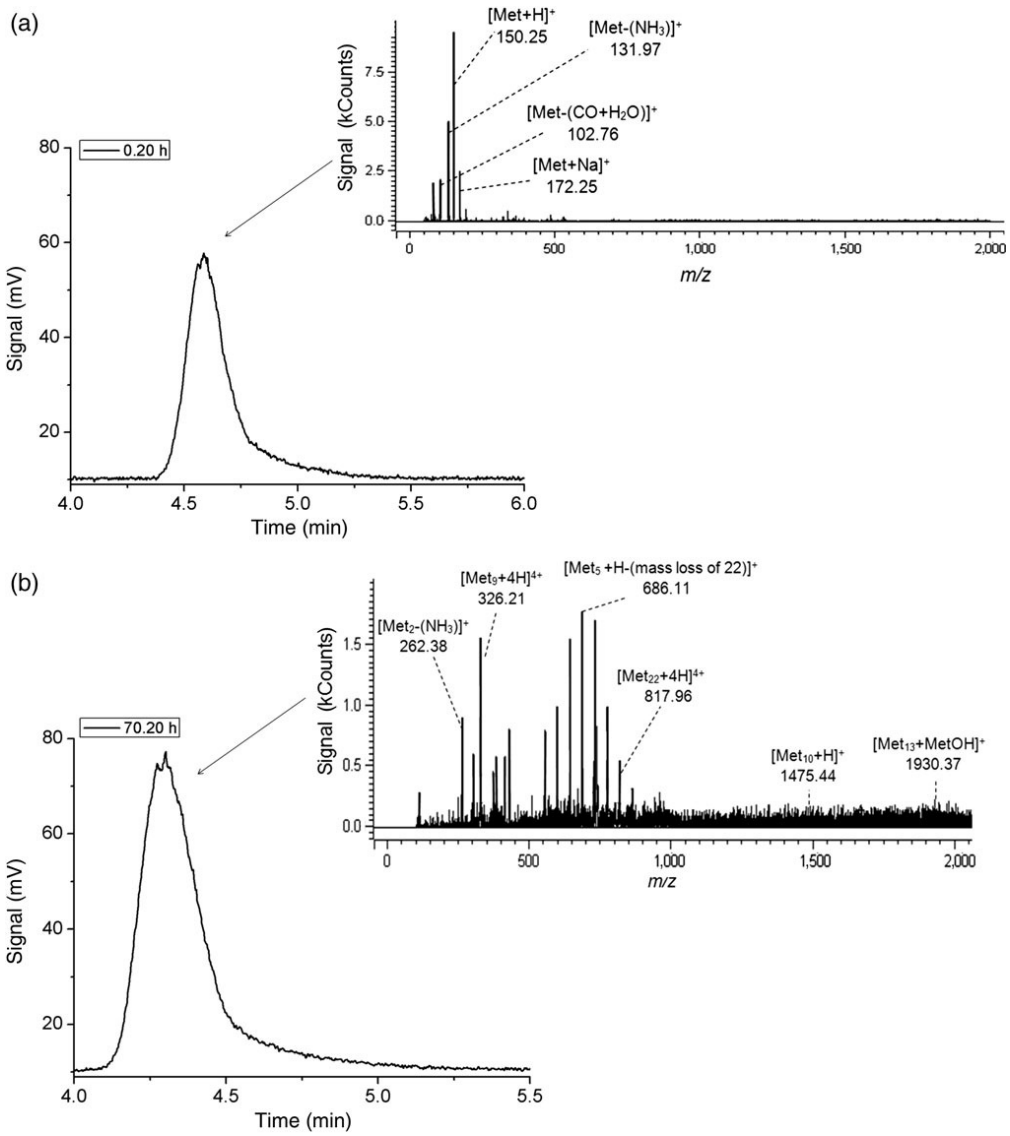

Figure 4. HPLC–MS chromatograms and respective mass spectra recorded from (a) *L*-Met after 0.20 h; (b) *L*-Met after 70.20 h; (c) *L*-His after 4.00 h; (d) *L*-His after 52.50 h; (e) *L*-Ser after 0.20 h and (f) *L*-Ser after 245.40 h.

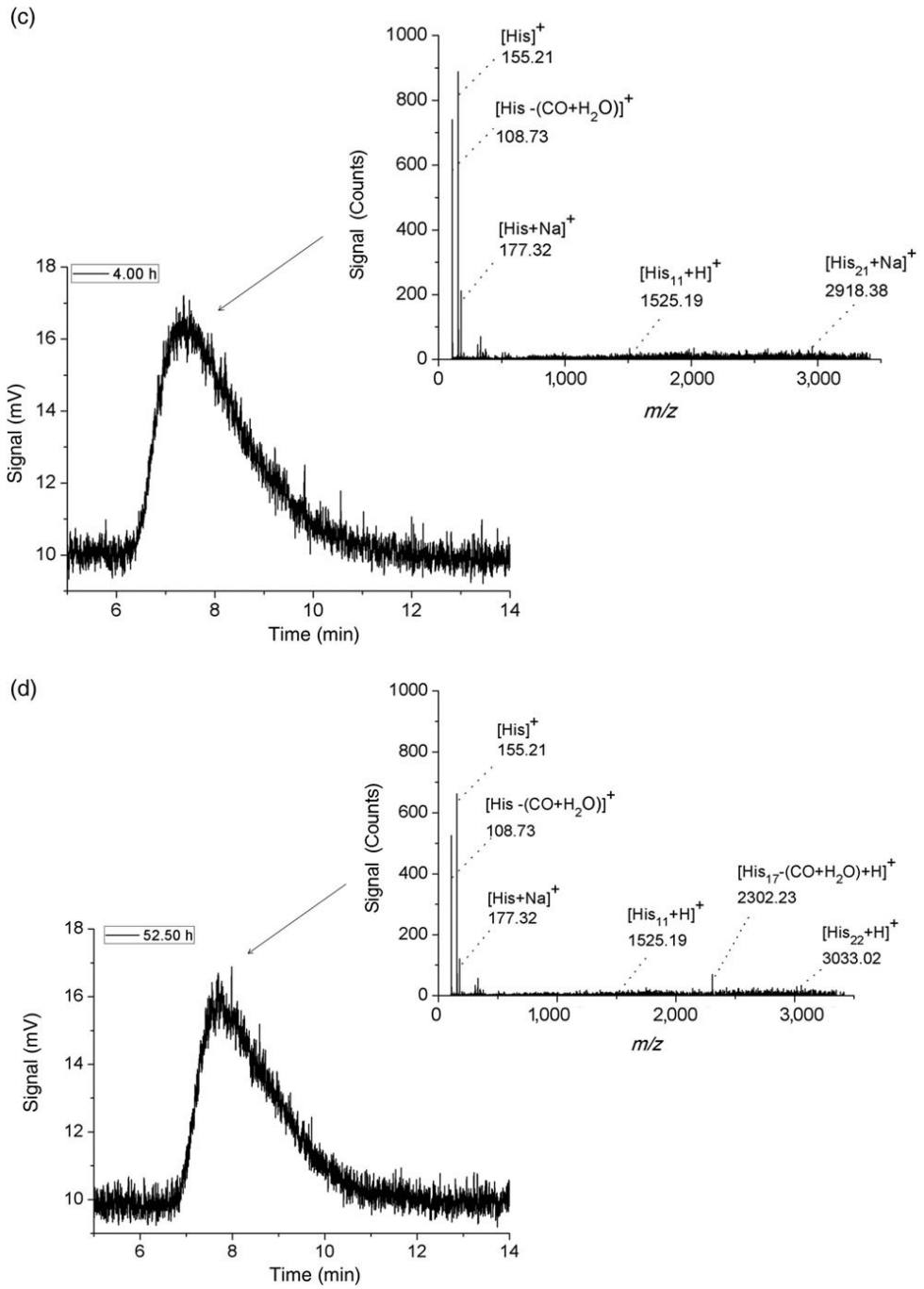

Figure 4. *Continued*

period are given. When two chromatograms are compared, in the aged sample an additional peak can be seen, attributed to the reaction products. At a first glance, there is no spectacular difference between the mass spectra of the fresh and the aged sample. After a closer look, however, a considerable intensity drop of the molecular ion of Ser ($m/z = 104.80$) can be noticed, which from 323.32 Counts for the fresh sample drops to 123.12 Counts in the course of 245 h aging. In the mass spectrum of the aged Ser sample, the predominant peak appears at $m/z = 351.26$, which corresponds with the Ser

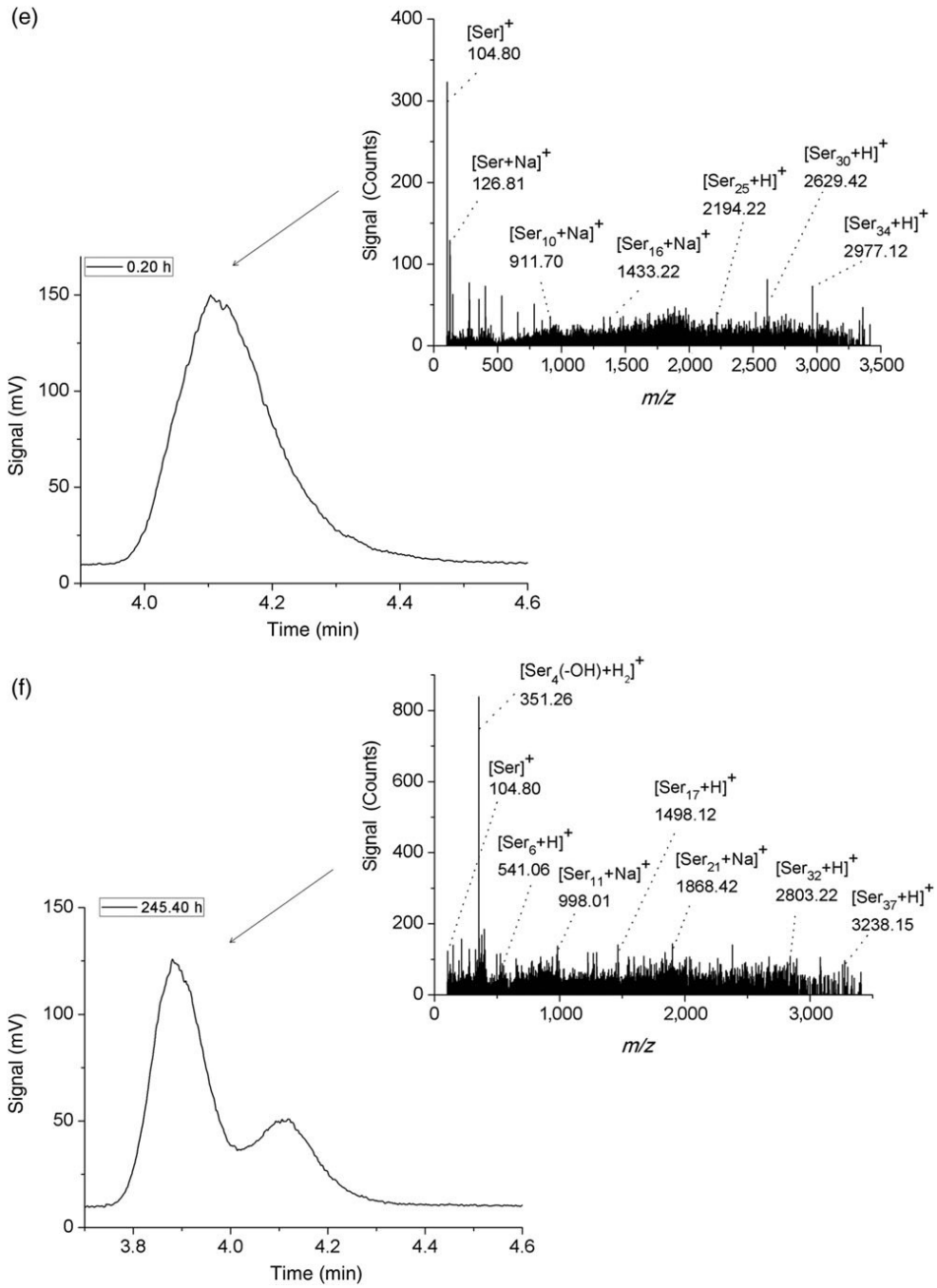

Figure 4. *Continued*

tetrapeptide minus one water molecule split off through the fragmentation of one Ser molecule, $[Ser_4(-H_2O) + H]^+$ (16). Last but not least, an overall intensity increase of the mass spectrometric signals in the aged Ser sample is observed, due to accumulation of considerable peptide amounts at the expense of monomeric Ser.

LC–MS of His

In order to avoid depositing of the His-derived peptides on the chromatographic column (as it was the case with the HPLC–ELSD and HPLC–MS system), the LC–MS system equipped with the short guard column was additionally employed. The obtained mass spectra are given in Figures 5a and b.

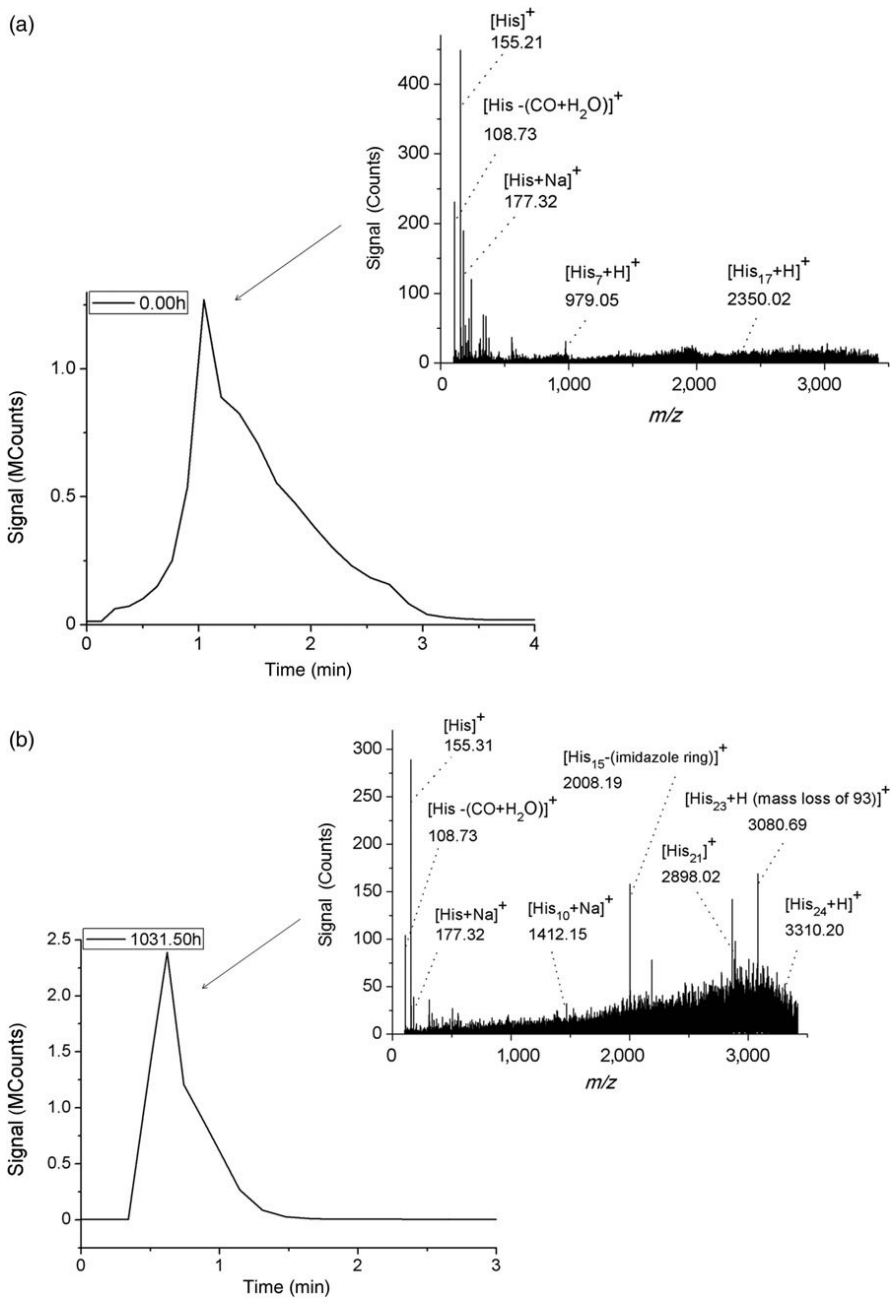

Figure 5. LC–MS chromatograms and respective mass spectra recorded from (a) *L*-His after 0.00 h and (b) 1031.50 h.

In Figure 5a, the chromatogram and the mass spectrum registered immediately after dissolution of His in water (i.e., after 0.00 h storage period) are given. In this spectrum, the predominant molecular signal of His at $m/z = 155.21$ ($[His]^+$) and yet another signal at $m/z = 177.32$, also representing the monomeric His with an attached sodium ion ($(His + Na)^+$) can be seen. Signals with the higher m/z values (e.g., 979.05 and 2350.03, attributed to the $[His_7 + H]^+$ and $[His_{17} + H]^+$ ions, respectively), can also be seen. However, the intensities of the signals originating from the peptides are negligible, when compared with that of the molecular ion at $m/z = 155.21$.

In Figure 5b, we show the chromatogram and the mass spectrum valid for the His sample after 1031.50 h storage period. In this spectrum, an intense signal derived from monomeric His (at

$m/z = 155.31$) can be seen, but the other signals in this spectrum originating from peptides at $m/z = 1412.15$, 2008.19 and 2898.02 ($[His_{10} + Na]^+$, $[His_{15}$-(imidazole ring)$]^+$ and $[His_{21}]^+$) characterize with the intensities comparable with that of the molecular ion.

Mass spectra presented in this section confirm our earlier hypothesis as to deposition of the higher molecular weight peptides on column packing in the HPLC–MS system. In the mass spectra originating from the LC–MS system, signals with the m/z values up to 3,500 units can be perceived. It cannot be excluded that even higher peptides are present in the aged His sample, which cannot however be registered due to technical limitations of our LC–MS setup.

Discussion

The main objective of this study consists in further exploration of applicability of the HPLC technique to tracing the reaction kinetics and mechanisms with the non-linear chemical processes of spontaneous chiral conversion and peptidization, involving selected amino acids and running in colorless solutions. Although an excellent performance of HPLC is a long-established and indisputable fact, so far it has attracted lesser attention as a robust and occasionally unique tool in the kinetic and mechanistic studies.

The results presented in this study add to the experimental evidence on the ability of amino acids to undergo spontaneous and oscillatory peptidization in an abiotic aqueous system. Differences in chemical structure of the investigated compounds are reflected in the dynamics of their peptidization. No doubt, the fastest peptidizing amino acid was His, to the point of rapidly depositing higher peptides on the column packing and practically disabling the chromatographic process. This is evidently due to the presence of two amino groups per one His molecule, the first-order amino group in the α position of the aliphatic skeleton and the second-order amino group in the imidazole ring. Thus, His can easily be involved in the two peptide (–CO–NH–) bonds per one amino acid molecule and hence, in the formation of the 3D condensation products. Ser is also equipped with two functionalities, i.e., the $-NH_2$ and –OH group, thus being able to form two bonds per one amino acid molecule, i.e., the peptide and the ester bond, and to form the 3D condensation products. This ability is reflected in the respective pattern of the time series of the chromatographic peak heights (see Figure 3c), which shows an oscillatory yet systematic concentration drop with monomeric Ser. Met is equipped with one functionality other than the carboxylic group, i.e., with the $-NH_2$ group, thus being able to form linear (2D) peptides only. This statistically lower ability of Met (as compared with His and Ser) to spontaneously peptidize is reflected in the respective pattern of the time series of the chromatographic peak heights valid for Met (see Figure 3a). After an initial drop of the Met concentration and formation of certain amounts of peptides, a well-pronounced and lasting for several hours trend is observed of the oscillatory peptide dissociation, unlike with two other amino acids. Only then Met begins to again peptidize.

In our view, spontaneous structural instability of peptides, especially in abiotic systems, should attract more interest than it has done so far, especially from the side of physical chemists, biochemists peptide researchers, etc. Instability of peptides in biotic environments is a well-known fact and even so to say taken for granted, when provoked, e.g., by an enzymatic or bacterial action. On the other hand, peptides in abiotic systems tend to be viewed as rather stable entities and this stability is largely awaited from the side of bionanotechnologists, who expect to develop peptide nano- and microstructures into the scaffolds in tissue engineering, applicable in regenerative medicine, use them in easily controlled drug delivery systems, etc. An interesting overview on this subject matter is provided in (17). From our long-term involvement in non-linear chemistry in general, and in spontaneous oscillatory chiral conversion and condensation of the low-molecular-weight carboxylic acids in particular, it comes out that all such compounds (amino acids included) characterize with an inherent instability in abiotic systems, the property which first has to be in-depth explored, and only then exploited to the advantage of broadly understood life sciences.

Conclusion

This study contributes to the amino acid and peptide knowledge with the HPLC and MS patterns demonstrating different and molecular structure-related dynamics of spontaneous non-linear peptidization in the abiotic systems of Met, His and Ser, three proteinogenic amino acids playing vital roles in metabolic patterns of living organisms. Experimental evidence presented in this study provides partial justification of an earlier developed theoretical model of co-peptidization in the binary amino acid systems, which anticipates differentiated peptidization dynamics of different species as the heteropeptide building blocks.

Acknowledgement

A.G. acknowledges the financial support of the DoktoRIS project, co-financed by the European Union within the European Social Fund.

References

1. Sajewicz, M., Pietka, R., Pieniak, A., Kowalska, T.; Application of thin-layer chromatography (TLC) to investigating oscillatory instability of the selected profen enantiomers; *Acta Chromatographica*, (2005); 15: 131–149.
2. Sajewicz, M., Gontarska, M., Kowalska, T.; HPLC/DAD evidence of the oscillatory chiral conversion of phenylglycine; *Journal of Chromatographic Science*, (2014); 52: 329–333.
3. Sajewicz, M., Kronenbach, D., Gontarska, M., Wróbel, M., Pietka, R., Kowalska, T.; TLC in search for structural limitations of spontaneous oscillatory in-vitro chiral conversion. α-hydroxybutyric and mandelic acids; *Journal of Planar Chromatography—Modern TLC*, (2009); 22: 241–248.
4. Sajewicz, M., Kronenbach, D., Gontarska, M., Kowalska, T.; TLC and polarimetric investigation of the oscillatory in vitro chiral conversion of *R*-β-hydroxybutyric acid; *Journal of Liquid Chromatography and Related Technologies*, (2010); 33: 1047–1057.
5. Belanger, P., Atkinson, J.G., Stuart, R.S.; Exchange reactions of carboxylic acid salts; Kinetics and mechanism; *Journal of the Chemical Society—Section D: Chemical Communication*, (1969); 1067–1068.
6. Xie, Y., Liu, H., Chen, J.; *International Journal of Pharmaceutics*, (2000); 196: 21–26.
7. Sajewicz, M., Dolnik, M., Kowalska, T., Epstein, I.R.; Condensation dynamics of *L*-proline and *L*-hydroxyproline in solution; *RSC Advances*, (2014); 4: 7330–7339.
8. Sajewicz, M., Godziek, A., Maciejowska, A., Kowalska, T.; Condensation dynamics of the *L*-Pro-*L*-Phe and *L*-Hyp-*L*-Phe binary mixtures in

8. Sajewicz, M., Godziek, A., Maciejowska, A., Kowalska, T.; Condensation dynamics of the *L*-Pro-*L*-Phe and *L*-Hyp-*L*-Phe binary mixtures in solution; *Journal of Chromatographic Science*, (2015); 53: 31–37
9. Sajewicz, M., Matlengiewicz, M., Leda, M., Gontarska, M., Kronenbach, D., Kowalska, T., *et al.* Spontaneous oscillatory in vitro chiral conversion of simple carboxylic acids and its possible mechanism; *Journal of Physical Organic Chemistry*, (2010); 23: 1066–1073.
10. Sundler, R., Akkeson, B.; Regulation of phospholipid biosynthesis in isolated rat hepatocytes. Effect of different substrates; *Journal of Biological Chemistry*, (1975); 250: 3359–3367.
11. Murata, Y., Watanabe, T., Sato, M., Momose, Y., Nakahara, T., Oka, S., *et al.* Dimethyl sulfoxide exposure facilitates phospholipid biosynthesis and cellular membrane proliferation in yeast cells; *Journal of Biological Chemistry*, (2003); 278: 33185–33193.
12. Vaziri, P., Dang, K., Anderson, G.H.; Evidence for histamine involvement in the effect of histidine loads on food and water intake in rats; *Journal of Nutrition*, (1997); 127: 1519–1526.
13. Chen, Z., Li, W.D., Zhu, L.J., Shen, Y.J., Wei, E.Q.; Effects of histidine, a precursor of histamine, on pentylenetetrazole-induced seizures in rats; *Acta Pharmacologica Sinica*, (2002); 23: 361–366.
14. Malathi, V.G., Ramakrishnan, T.; Biosynthesis of nucleic acid purines in *Mycobacterium tuberculosis* $H_{37}R_v$; *Biochemical Journal*, (1966); 98: 594–597.
15. Snell, K.; Enzymes in serine metabolism in normal, developing and neoplastic rat tissues; *Advances in Enzyme Regulation*, (1984); 22: 325–400.
16. Piraud, M., Vianey-Saban, C., Petritis, K., Elfakir, C., Steghens, J.P., Morla, A., *et al.* ESI-MS/MS analysis of underivatised amino acids: a new tool for the diagnosis of inherited disorders of amino acid metabolism. Fragmentation study of 79 molecules of biological interest in positive and negative ionisation mode; *Rapid Communications in Mass Spectrometry*, (2003); 17: 1297–1311.
17. Castillo, J., Sasso, L., Svendsen, W.E. (ed). *Self-Assembled Peptide Nanostructures: Advances and Applications in Nanobiotechnology.* CRC Press Taylor & Francis Group, Boca Raton, FL, USA, (2012).

Send Orders for Reprints to reprints@benthamscience.ae

Current Protein and Peptide Science, 2016, *17*, 000-000

On Spontaneously Pulsating Proline-Phenylalanine Peptide Microfibers

Agnieszka Godziek[1], Anna Maciejowska[1], Ewa Talik[2], Roman Wrzalik[3], Mieczysław Sajewicz[1], and Teresa Kowalska[1,*]

[1]*University of Silesia, Institute of Chemistry, Department of General Chemistry and Chromatography, 9, Szkolna Street, 40-006 Katowice, Poland;* [2]*University of Silesia, Institute of Physics, Department of Physics of Crystals, 4, Uniwersytecka Street, 40-007 Katowice, Poland;* [3]*University of Silesia, Institute of Physics, Department of Biophysics and Molecular Physics, 1A, 74 Pulku Piechoty Street, 41-500 Chorzów, Poland*

Please provide corresponding author(s) photograph
size should be 4" x 4" inches

Abstract: Earlier, we have collected an experimental evidence showing that low molecular weight chiral carboxylic acids (amino acids included) can spontaneously undergo an oscillatory chiral conversion and an oscillatory condensation in abiotic aqueous and non-aqueous liquid systems, stored for certain amount of time under mild external conditions. These earlier findings are summarized in the introductory part of this study. In the second part, a preliminary report is given on spontaneous pulsation of peptide microfibers in the aged proline–phenylalanine (Pro–Phe) solution in 70% aqueous acetonitrile. The experimental evidence originates from a number of advanced analytical techniques. In view of our earlier and present findings, a presumption is made that the mechanism of spontaneous pulsation (formation and decay) of Pro-Phe microfibers is directly related to the oscillatory chiral conversion and oscillatory peptidization. The entity of the discussed results pointing out to spontaneous and uncontrolled instability of peptide structures might be a bad prognostic for employing such structures in nanobiotechnology.

Keywords: Amino acids, spontaneous oscillatory chiral conversion, spontaneous oscillatory peptidization, pulsating oligopeptide structures.

EARLIER FINDINGS ON SPONTANEOUS OSCILLATORY CHIRAL CONVERSION AND SPONTANEOUS OSCILLATORY CONDENSATION OF CHIRAL LOW MOLECULAR WEIGHT CARBOXYLIC ACIDS

Spontaneous Oscillatory Chiral Conversion

Chiral conversion of many compounds, mainly from the group of nonsteroidal anti-inflammatory drugs (NSAIDs), has been abundantly reported right from the development of the chromatographic enantioseparation techniques, which took place in the sixties of the previous century. A comprehensive review covering publications on this topic and originating from the first four decades of investigations is presented in paper [1]. These publications deal with chiral conversions running either in living organisms, or in biological *in vitro* systems, hence apparently catalyzed by the biotic environment. Since that time, numerous new papers on the same topic have been published, none of them, however, witnessing to the oscillatory nature of this steric transformation. In the review book published by Wolf in 2008 [2], an overview was provided of chromatographic and electrophoretic techniques applied to tracing chiral conversion of various different compounds both in biotic and abiotic systems, yet no evidence has been produced of the oscillatory nature of such phenomena.

*Address correspondence to this author at the [1]University of Silesia, Institute of Chemistry, Department of General Chemistry and Chromatography, 9, Szkolna Street, 40-006 Katowice, Poland; E-mail: ???????????

In paper [3], the phenomenon of spontaneous oscillatory chiral conversion was for the first time reported with *S*(+)-ibuprofen, *S*(+)-ketoprofen, and *S,R*(±)-2-phenylpropionic acid as the test analytes, stored for longer periods of time in 70% aqueous ethanol. This discovery was made with aid of the chiral thin-layer chromatography (TLC) and the primary feature of the obtained experimental results was symptomatic instability of the retardation parameter (R_F) with the investigated chiral compounds, as schematically presented in Fig. (**1**).

Owing to densitometric detection, an additional thin-layer chromatographic confirmation of the oscillatory chiral conversion was obtained in form of characteristic changes of the investigated analytes' concentration profiles [3]. Schematic presentation of densitometric evidence upon an example of 2-phenylpropionic acid is given in Fig. (**2**). In this case, symmetric concentration profiles were ascribed to the *S*(+) and *R*(−)-2-phenylpropionic acid, respectively (Figs. **2b,d**), whereas the non-symmetric profiles (Figs. **2c,e,f**) were characteristic of the partially separated scalemic *S*(+)- and *R*(−)2-phenylpropionic acid mixtures.

In paper [4], an analogous evidence of the spontaneous chiral conversion was presented, this time obtained with use of HPLC-DAD. The chromatographic experiment was performed for the scalemic mixture of *L*-Phg and *D*-Phg on the chiral stationary phase with chiral *D*-penicillamine ligands, dedicated exclusively to the enantioseparation of underivatized amino acids. The results obtained are summarized in

1389-2037/16 $58.00+.00 © 2016 Bentham Science Publishers

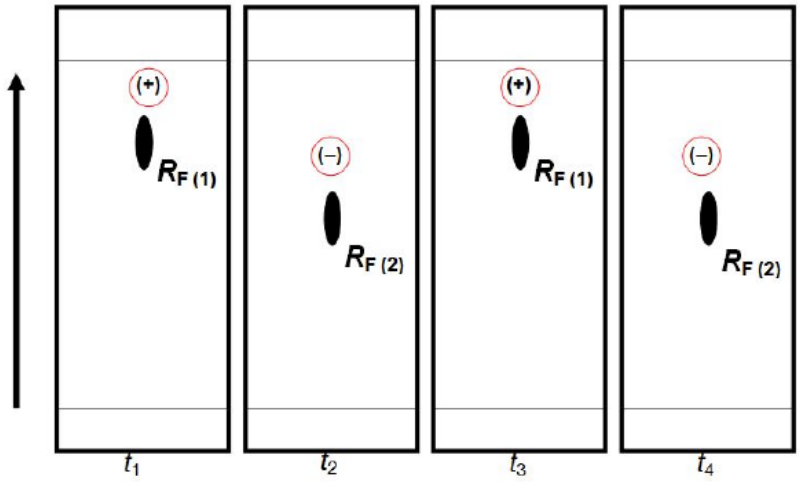

Fig. (1). Schematic representation of oscillatory changes of the R_F position of ibuprofen (and the other investigated profens) on the planar chromatogram in the function of storage time in 70% aqueous ethanol, valid for the periodic chiral conversion from (+) to (–) and back (reproduced with modification from (3)).

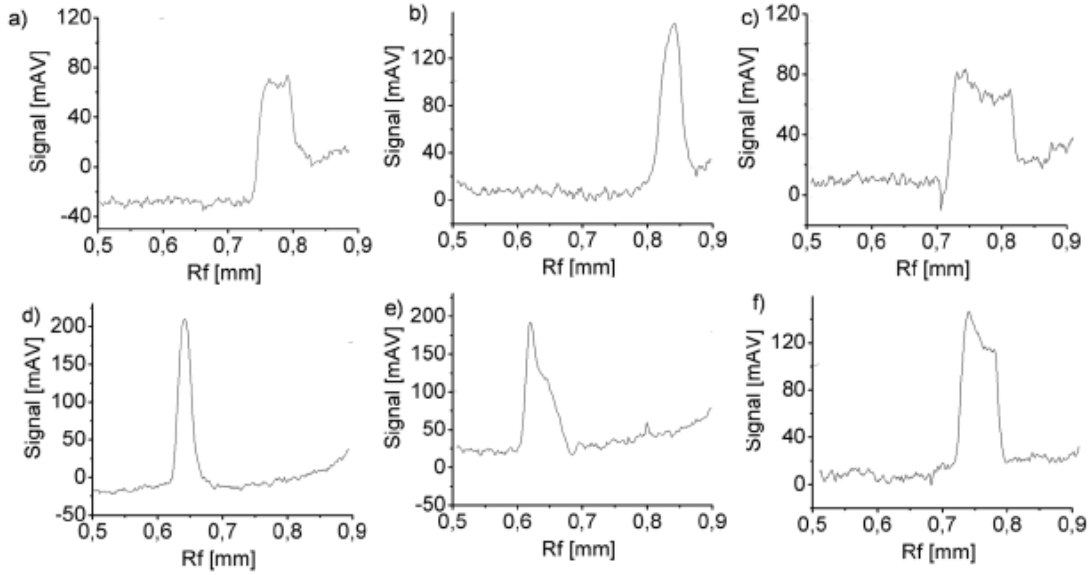

Fig. (2). Sequence of the densitometric concentration profiles of 2-phenylpropionic acid after: (a) 0 h (racemic mixture); (b) 22.5 h (*S*(+) form); (c) 27.5 h (scalemic mixture); (d) 46.5 h (*R*(-) form); (e) 51.5 h (shift from *R*(-) form to scalemic mixture); and (f) 70.5 h (scalemic mixture); sample storage time at ambient temperature (22±1°C). Changes of the concentration profiles are accompanied by the changing R_F values. Stationary phase: silica gel impregnated with *L*-arginine; mobile phase: ACN–MeOH–H_2O, 5:1:0.75, *v*/*v* (reproduced from (3)).

Fig. (**3a**). For the first six hours, the nonlinear peak height changes valid for *L*-Phg and *D*-Phg are observed. Then, the coalescence of the two peaks can be seen lasting for ca. twelve hours (apparently due to the formation of the non-chiral enolate ion, identical for the two enantiomers), After that period of time, the coalesced peaks separate and again, the nonlinear peak height changes valid for *L*-Phg and *D*-Phg can be observed. The UV spectra recorded with use of the DAD detector for the two separated *L*-Phg and *D*-Phg peaks on the one hand and for the single coalesced peak on the other show striking difference, which strongly serves in support of our assumption (see Fig. **3b**).

In fact, chromatographic evidence of the spontaneous oscillatory chiral conversion was obtained in our studies by means of TLC and HPLC for a wide selection of profens, amino acids, and hydroxy acids. Chiral conversion of these compounds can occur according to the two different pathways. In aqueous solutions, the general scheme can be represented as [5]:

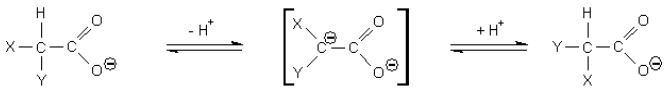

where X: -R (aliphatic) and Y: -NH_2, -OH, or –Ar (aromatic).

In anhydrous media and in the presence of trace amounts of water, the probable mechanism of chiral conversion is [6]:

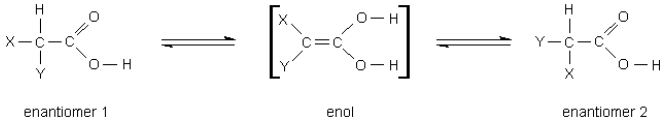

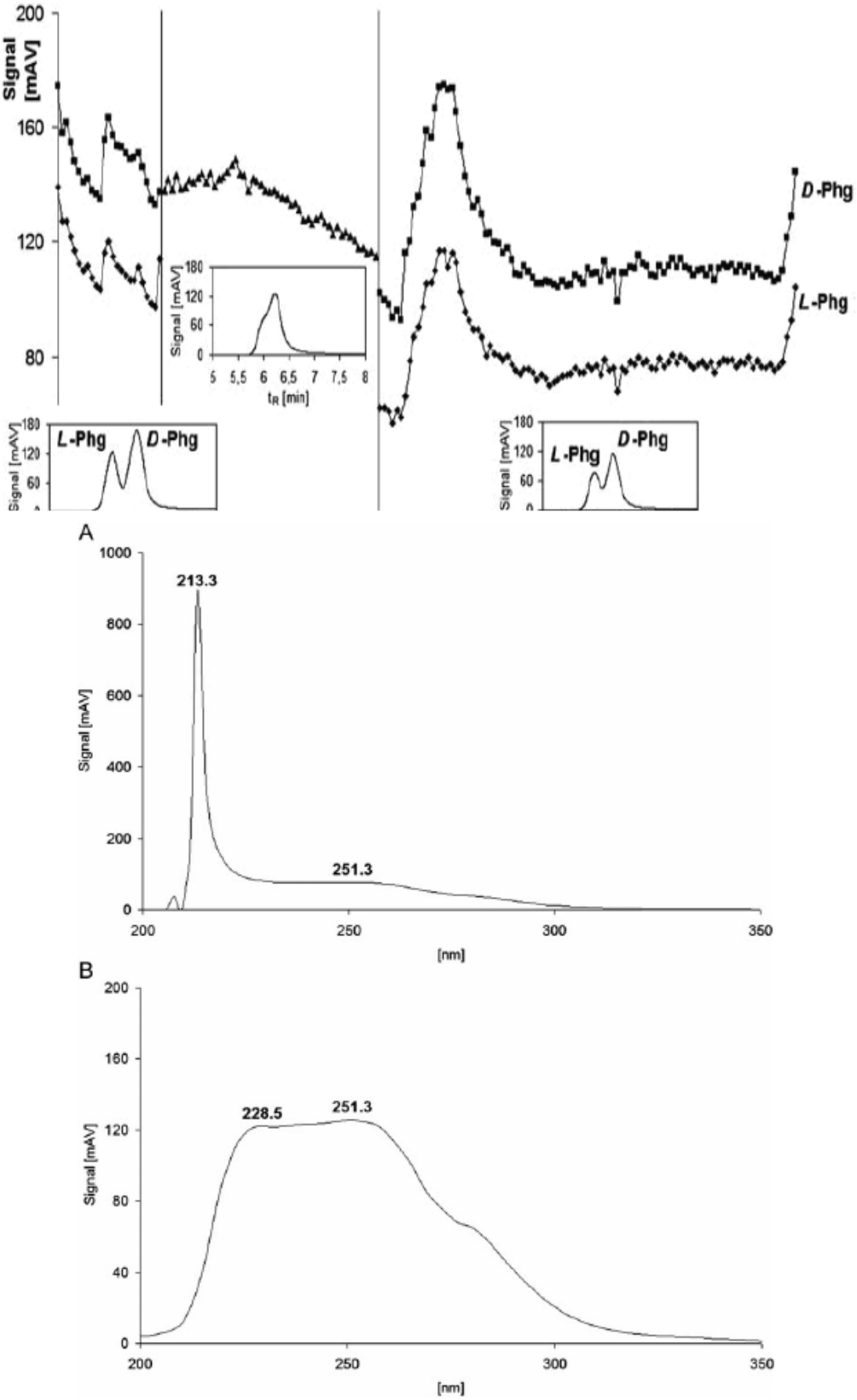

Fig. (3). (a) *L*-Phg and *D*-Phg peak height changes in the function of sample storage time for the chiral HPLC–DAD chromatograms of the *L*-Phg–*D*-Phg solution in the mixture of 2 mM copper(II) sulfate–water–2-propanol (95:5, v/v). Time ranges of the enantiomer peak separation and the enantiomer peak coalescence are additionally illustrated by the chromatogram insets. (b) UV Spectra recorded with the DAD chromatographic detector, valid for (A) each of the two enantioseparated Phg peaks (with maxima at 213.3 and 251.3 nm), and (B) the single coalesced peak (with maxima at 222.8 and 251.3 nm) (reproduced from (4)).

From our earlier investigations, it comes out that the oscillatory chiral conversion of the low molecular weight carboxylic acids is accompanied by the oscillatory condensation. In the consecutive section, a brief overview of our findings on this issue is provided.

Spontaneous Oscillatory Condensation

By oscillatory condensation, we understand formation and decay of condensation products, happening in turns. This decay does not necessarily need to be complete; there can just be a few monomeric units temporarily split off and later again bonded. Thin-layer chromatography is not the most advisable analytical technique to trace such phenomena, and for more than one reason. The main contraindication is a limited mobility of the higher molecular weight species on planar adsorbents, which often act as solid phase extractors, isolating immobile macromolecules from less mobile species by stopping them right on the start. However, it needs mentioning that at least once, TLC has been successfully used for the demonstration of the oscillatory condensation of the silicon-derived species, as shown in papers [7,8].

We started our investigations on spontaneous condensation of the chiral low molecular weight carboxylic acids from proving with use of biuret test that spontaneous peptidization of Phg really occurs [9]. To this effect, three samples (*R*-Phg, *S*-Phg, and *R,S*-Phg) were dissolved in 70% aqueous ethanol at room temperature and left for three days in stoppered glass vessels. After that period of time, biuret test was performed for each stored solution and convincing purple outcome was obtained, witnessing to the presence of the Phg-derived peptides. In the past, spontaneous peptidization of amino acids has been sporadically investigated, and mostly in the framework of the projects focusing on abiogenesis, including laboratory simulations of a prebiotic universe under the environmental conditions imitating possible origin of biological life. Usually, the employed experimental conditions were quite drastic, in order to reproduce the terrestrial or extraterrestrial environments from before the millennia. Among the best known experiments were those performed by Fox and Harada, and dealing with thermal copolymerization of amino acids to the products resembling proteins and therefore denoted as proteinoids [10,11].

To investigate the oscillatory nature of spontaneous peptidization of amino acids and spontaneous condensation of *L*-lactic acid, we used a number of advanced analytical techniques, yet HPLC with the evaporative light scattering (ELSD), diode array (DAD), and mass spectrometric (MS) detection contributed the most.

In papers [12-14], we presented the results of our investigations dealing with spontaneous oscillatory condensation of selected profens, amino acids, and *L*-lactic acid. Chromatographic check was done in two different ways. We recorded either the oscillatory concentration changes of the main compound, or the analogous concentration changes of the condensation products in a quasi-continuous manner. Additionally, in certain time intervals, mass spectra of ageing samples were recorded, to show an increasing number of the condensed species, with gradual growth of the respective *m*/*z* values. Moreover, in papers [12-14], theoretical models were proposed to explain the oscillatory mechanism of spontaneous oscillatory peptidization.

In papers [15,16], we presented the results of spontaneous oscillatory condensation of the three binary amino acid systems (*L*-Pro–*L*-Hyp, *L*-Pro–*L*-Phe, and *L*-Hyp–*L*-Phe), dissolved in aqueous organic solvents. Also in this case, we recorded the oscillatory concentration changes of the two amino acids, and of the main condensation product. The chromatographic response and the respective mass spectra witness to the formation of homo and hetero oligopeptides, derived from the amino acid pairs. For the sake of illustration, in (Fig. **4**) we present selected results originating from paper [16].

Oscillatory nature of chiral conversion and condensation suggests that the mechanisms of these two processes are interrelated. In paper [4], we made an assumption that there might be a thermodynamic dependence between the endothermic process of chiral conversion and the condensation process, which most probably is exothermic (as it comes out from multiple reports on thermodynamics of chemical condensation processes). With amino acids, the parallel processes of chiral conversion and peptidization can be illustrated by the following scheme [12]:

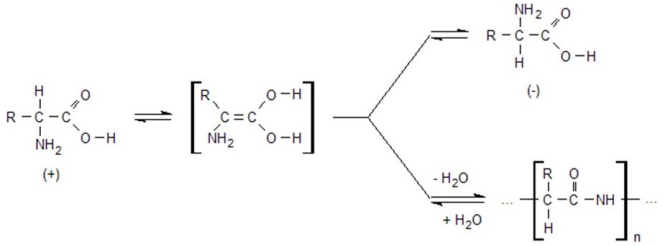

A long-term (e.g., lasting one year) ageing of chiral low molecular weight carboxylic acids can result in high condensation yields, as demonstrated upon the case of *S*(+)-ibuprofen and *R,S*(±)-ketoprofen dissolved in 70% aqueous ethanol, and then stored for one year in a tightly stoppered glass vessel [17]. Considerable condensation yields with these two profens resulted in phase separation of the initially homogenous 70% aqueous ethanol solutions and emulsification of each layer by the respective higher molecular weight condensation products. Emulsification of the one year old *S*(+)-ibuprofen and *R,S*(±)-ketoprofen solutions in 70% aqueous ethanol was confirmed by Raman spectroscopic analysis of the "white pupil", as shown in Fig. (**5**).

Spontaneous oscillatory chiral conversion and spontaneous oscillatory condensation drew our attention as natural phenomena and hence, monitored with use of analytical tools and interpreted with aid of theoretical models, based on stoichiometric and kinetic equations. Theoretical models are proposed and extensively discussed in papers [12-15,17,18]. Chronologically first model interpreted the phenomenon of spontaneous chiral conversion alone and it was named the model of two linked templators [18]. It assumed intermolecular interactions between a given enantiomer (as a catalytically acting template) and a species in an intermediate state (either enol, or an enolate ion). As a result, enol (or enolate ion) eventually assumed steric configuration of an enantiomer that it has been earlier bonded to (basically, through polar intermolecular interactions and the H-bonds).

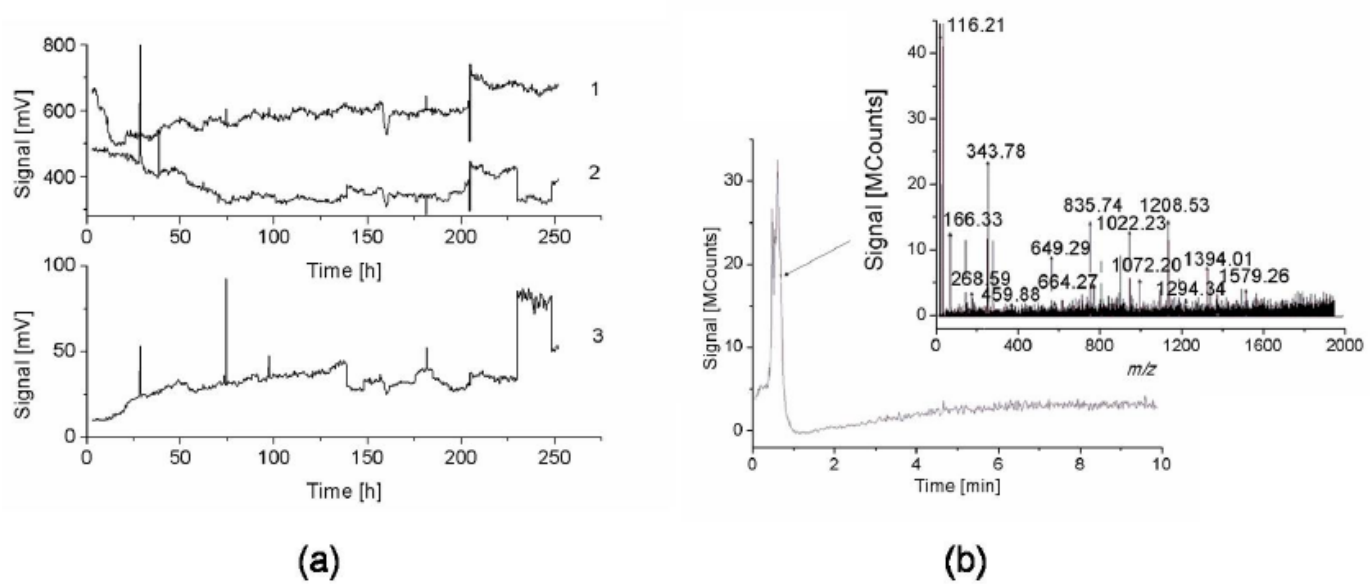

Fig. (4). (a) Time series of the chromatographic peak heights for Pro–Phe in acetonitrile (HPLC-ELSD); 1, Pro; 2, Phe; 3, main peptidization product. (b) LC chromatogram with mass spectrometric inset for the Pro–Phe solution after 122 days storage period (reproduced from (16)).

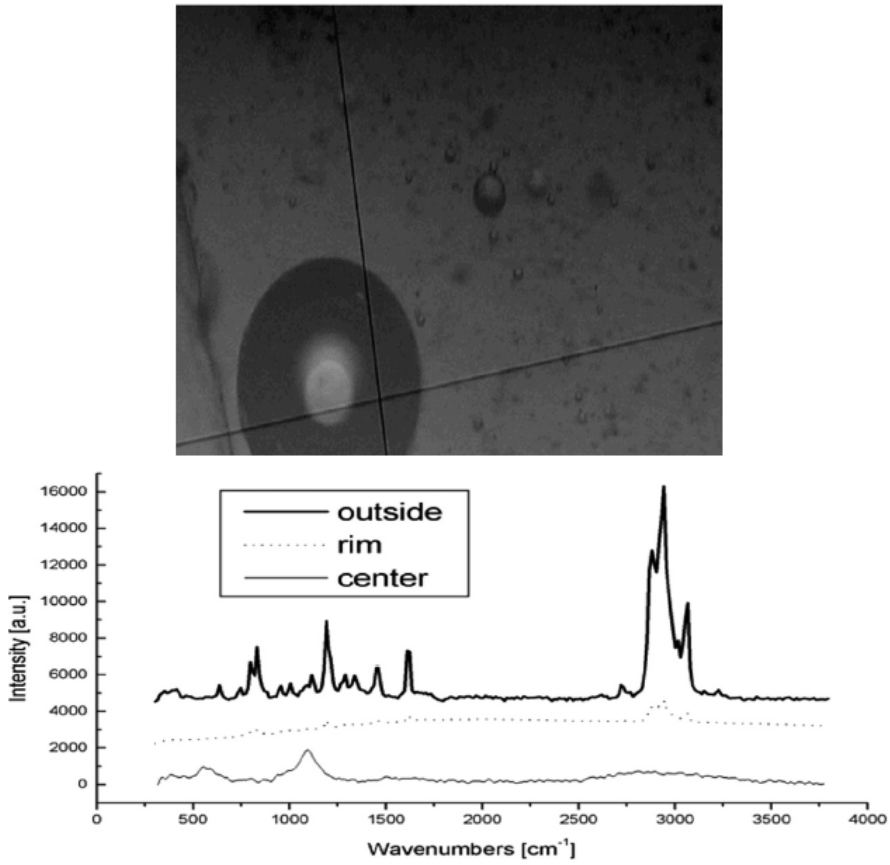

Fig. (5). (a) An example of a single concentric pattern of the microemulsion droplet recorded in the upper layer of ibuprofen solution with pure water constituting the ‘‘white pupil’’; (b) Raman spectra collected from the ‘‘white pupil’’, the dark rim, and the outside of the pattern shown in Figure 5(a) (reproduced from (17)).

The most recent theoretical approach is given in paper [15] and it handles peptidization of a pair of amino acids in an aqueous solution. To this effect, four models have been developed to explain the specific dynamics of this process. They took into the account mutual catalytic effect of the two amino acids making a pair. Their common general feature can be given, as follows. At the first step, both amino acids undergo oligopeptidization. At the second step, oligopeptides can undergo an uncatalyzed aggregation to form the H-bonded supramolecular aggregates and the covalently

bonded higher peptides (characterizing with the properties of the micelles). The third step is assumed as catalyzed aggregation, which means that the chemical structure of the already formed micelles influences the structure of the new generation micelles. At the fourth step, decomposition of the micelles is anticipated. Each step is characterized by means of stoichiometric and kinetic equations, separately for each amino acid from a given amino acid pair. An extreme case is that the two amino acids do not cooperate in the condensation process and produce homo-oligopeptides only (model 1). In the other three cases (models 2-4), homo- and heteropeptides can be formed with kinetic predominance of a faster or a slower peptidizing amino acid from a given pair, or as a result of a cooperative effect.

Current Findings on Spontaneously Pulsating Pro-Phe Oligopeptide Nano- and Microfibers

After one year storage period at 21±1°C, we focused on 70% aqueous acetonitrile solution of a Pro–Phe mixture (the same which was earlier investigated for the period of 250 h; see Fig. **4** [16]). The first step was microbiological tests for possible presence of microorganisms in the Pro–Phe liquid sample after one year long storage period. In our laboratory, this is routine procedure with all organic samples after the long storage periods. These tests are performed using the solid and liquid media. Composition of solid medium: meat extract, 2 g L^{-1}; yeast extract, 2 g L^{-1}, peptone, 5 g L^{-1}, sodium chloride, 4 g L^{-1}; agar, 15 g L^{-1}, pH = 7.4. Composition of liquid medium: meat extract, 0.4 g L^{-1}; enzymatic casein hydrolysate, 5.4 g L^{-1}; yeast hydrolysate, 1.7 g L^{-1}; peptone, 4.0 g L^{-1}; sodium chloride, 3.5 g L^{-1}.

With the solid medium, 100-μL Pro–Phe liquid samples were introduced and incubated for seven days at the same temperature at which stock solution had been stored earlier (ca. 21°C). This experiment was repeated in triplicate. To 50 mL of the liquid medium, we added 100-μL aged Pro–Phe liquid samples and then incubated the samples for fourteen days at ambient temperature (ca. 21°C) with continuous shaking (260 rpm). This experiment was also repeated in triplicate. In none of the samples was growth of microorganisms observed. Longer incubation periods were not employed, due to the risk of sample infection.

As a control, we carried out a protein determination by the Bradford method [19] and also measured the light absorbance at λ = 260 nm in order to check for the presence of DNA in the two samples. The Bradford test gave a negative result, and the spectrophotometric measurement revealed no DNA in our samples. We therefore concluded that no microorganisms were present in the aged Pro–Phe liquid sample.

Originally, our sample was composed of 10 mg mL^{-1}(i.e., 8.69×10^{-2} mol L^{-1}) *L*-Pro (Sigma-Aldrich, St Louis, MO, USA) and 10 mg mL^{-1}(i.e., 6.05×10^{-2} mol L^{-1}) *L*-Phe (Merck KGaA, Darmstadt, Germany), dissolved in a mixture of the HPLC purity grade acetonitrile (J.T. Baker, Deventer, The Netherlands), and the double distilled and de-ionized water by means of the Elix Advantage model Millipore system (Millipore, Molsheim, France) (70:30, *v*/*v*). In the course of one year, spontaneous oscillatory chiral conversion of *L*-amino acids to the *D* form has taken place, as well as spontaneous oscillatory peptidization. As a result, *L*- and *D*-Pro, and *L*- and *D*-Phe must have been formed due to spontaneous chiral conversion, and the homo- and heteropeptides as well.

Upon visual inspection of the aged solution, the following observation was made. Namely, an originally colorless and macroscopically homogenous solution in the course of one year spontaneously turned to a heterogeneous suspension, with white fibers floating therein (Fig. **6a**). However, the amount of fibers was fluctuating from very low abundances to higher abundances (giving the system a milky and opalescent look), and then back to very low abundances. This pulsation was dynamic and continuous (although counted in hours rather than minutes). The gelated agglomeration of fibers captured in the moment of their highest abundance is shown in Fig. (**6b**). In Fig. (**6c**), we present a sample of solid Pro–Phe fibers extracted from the solution and registered in the transition light with use of the Axio Scope A1 model Zeiss optical microscope (Zeiss, Oberkochen, Germany) and in Figs. (**6d,e**), we show the optical microscope pictures of a single microfiber and an agglomeration of microfibers suspended in the solution, respectively.

On the three pictures shown in Figs (**6c-e**), respective size bars are shown, which allow estimating dimensions of the recorded fibers (which on average prove in a range of ca. 1-2 μm diameter and less than 100 μm length). As the investigated solution was originally composed of *L*-Pro and *L*-Phe only, and in view of our earlier findings on common and spontaneous oscillatory peptidization of amino acids, it seems inevitable that chemically, the observed fibers are peptides. Moreover, we concluded that the dynamic formation of fibers is due to the stepwise obtaining of a critical number of the condensed monomeric amino acid units. Above that level, oligopeptides apparently become insoluble in 70% aqueous acetonitrile and therefore precipitate in the fiber form. In the course of spontaneous decay, fibers again lower the number of the condensed monomeric units below the critical condensation level and dissolve in 70% aqueous acetonitrile. This spectacularly pulsating mechanism remains in agreement with our earlier discovery of spontaneous oscillatory peptidization with amino acids.

Next we intended to decide, if the observed fibers are hollow inside (i.e., if they are tubes rather than fibers). Moreover, we intended to know, if there are nanofibers in the suspension, and not exclusively microfibers. To this effect, we needed greater magnification power, so that the next series of the pictures was taken with the Jeol JSM-7600F model scanning electron microscope (SEM) (Joel, Peabody, MA, USA). Selected micrographs are shown in Fig. (**7**). The micrographs presented in (Fig. **7**), show that the investigated Pro-Phe fibers are mostly of the micro size, but some of them are of the nano size also (i.e., with the fiber width below 0.1 μm). Among the fibers floating in solution and practically invisible to human eye (Figs. **7a-c**), there are more nanofibers than among those which due to their much higher weight appeared as a sediment in the vial (Figs. **7d-f**). It also became evident that practically all microfibers are the nanofiber bunches tightly stuck together and in certain way resembling the spaghetti bunches. In the other words, no nano- or microtubes were formed in solution, although

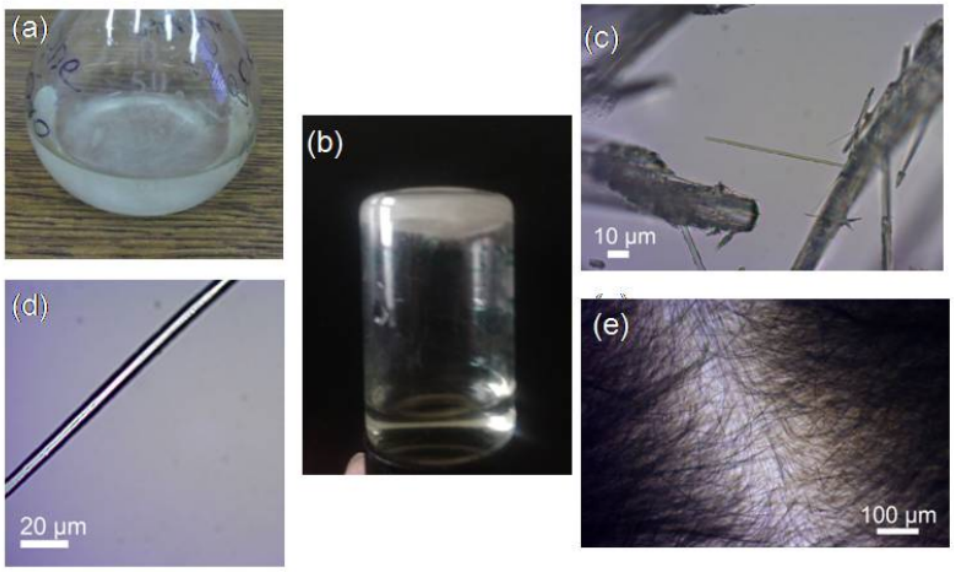

Fig. (6). (a) Volumetric flask with fibers suspended in solution; (b) a sediment of gelated fibers in a vial turned upside down; optical microscope pictures of (c) solid microfibers extracted from the solution (X50); (d) single microfiber suspended in the solution (X50); (e) agglomeration of microfibers suspended in the solution (X10). Size bars make insets in each individual microscope picture.

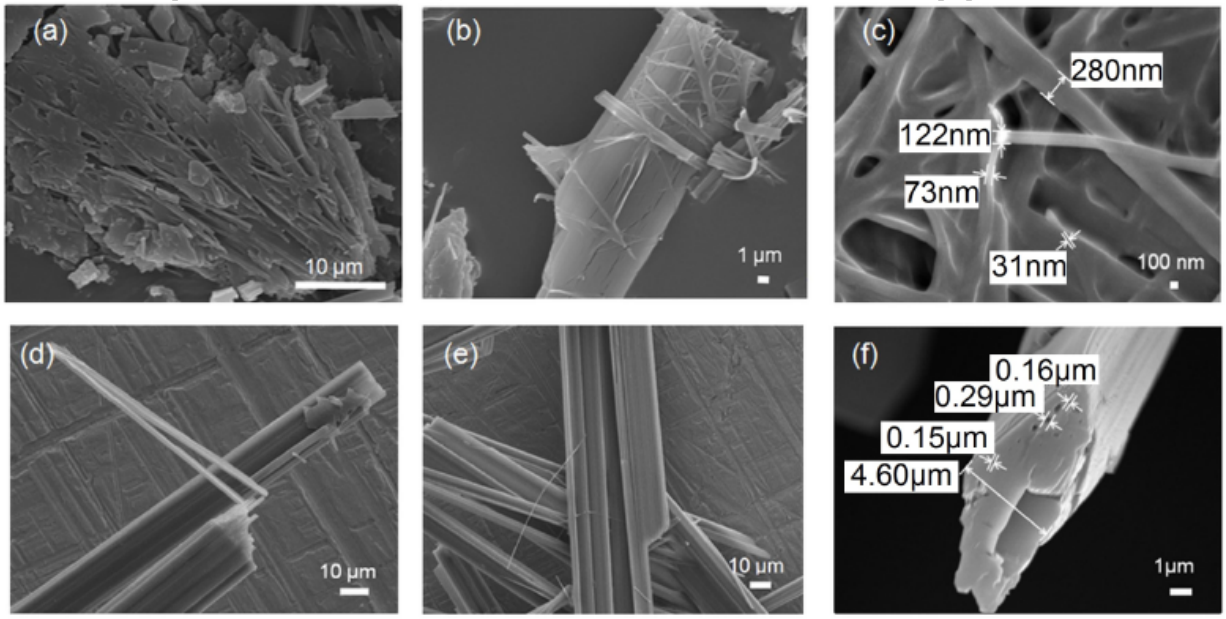

Fig. (7). (a)-(c): Scanning electron micrographs of fibers floating in solution; (d)-(f): scanning electron micrographs of fiber sediment in the vial with magnification of (a) X2700; (b) X3500; (c) X30000; (d) X900; (e) X650; (f) X7000. In (c) and (f), diameters of certain fibers are indicated. Size bars make insets in each individual picture.

occasionally not all nanofibers were stuck very closely together (thus leaving hollow spaces among the neighbouring threads like, *e.g.,* in Fig. **7e**).

In order to confirm our assumption as to the oligopeptide nature of the obtained fibers, two analytical tests were performed. The first test was performed with use of the IR absorption spectroscopy. To this effect, we first picked a sample of solid fibers from the aqueous acetonitrile suspension, dried it in ambient air on a microscope slide, and then recorded its IR spectrum in the wavelength range from 4000 to 400 cm^{-1} with use of the model Magna 560 Nicolet FT-IR spectrophotometer (Nicolet, Grenoble, France). This spectrum was recorded from the KBr pellet (ca. 3 mg fiber sample per 150 g crystalline KBr), and the analogous spectra were recorded for the mechanical 1:1 (w/w) Pro-Phe mixture, and the solid Pro and Phe samples. The obtained spectra are shown in Fig. (**8**).

A comparison of the IR absorption spectra given in (Figs. **8a-d**) reveals a symptomatic difference between the fiber spectrum (Fig. **8a**) on the one hand, and the remaining three spectra (Figs. **8b-d**) on the other. With (Figs. **8b-d**), similarity of all spectral envelopes is evident. Moreover, (Fig. **8b**) valid for the mechanically obtained 1:1 (w/w) Pro-Phe mixture reflects additivity of the IR spectra valid for pure Pro (Fig. **8c**) and pure Phe (Fig. **8d**). There is, however, no such additivity, if the IR spectrum of fibers (Fig. **8a**) is compared

with the remaining three spectra (Figs. **8b-d**). Two most striking differences between the IR spectrum of fibers and those valid for the other samples are: (i) much lower absorbance of fibers, as compared with the rest; and (ii) largely simplified shape of the fiber spectrum in the wavenumber range from ca. 3400 to ca. 1800 cm^{-1} (where an efficiency of intermolecular interactions through the H-bonds is pronounced the best). Effects (i) and (ii) apparently originate from the fact that in the fibers, the amino acid functional groups (-COOH and $-NH_2$) are almost entirely engaged in peptide bonds (-CO-NH-), hence an ability of fibers to act through intermolecular H-bonds drastically diminishes. On the other hand, the subtle structure of the spectrum in the wavenumber range from ca. 1250 to ca. 450 cm^{-1} valid for the fibers resembles those of the remaining three IR spectra, which is a proof that the fibers indeed originate from Pro and Phe. Thus a conclusion can be drawn that the IR spectroscopic evidence supports the oligopeptide nature of the obtained fibers.

The second instrumental test was performed with use of mass spectrometry. Mass spectra were recorded in positive ionization mode by means of the Varian MS-100 mass spectrometer (Varian, Harbor City, CA, USA), operating in the ESI MS mode for the 70% aqueous acetonitrile solution which contained the lower and therefore soluble oligopeptide fraction (with the fiber suspension filtered off). An example of the obtained mass spectrum is given in Fig. (**9**). Mass spectrum of the soluble oligopeptide fraction formed in the course of the prolonged ageing of the Pro-Phe solution reveals a good number of the species with the *m/z* values within the range from 2000 to 3000 and higher. For ten distinct signals, the oligopeptide structures were proposed, as shown in Table **1**. Seven signals were attributed to the hetero type oligopeptides, and molar proportions of Pro and Phe in five such signals are either equal, or close to 1:1, i.e., in analogy to those in the original Pro-Phe solution. Thus one can anticipate that the filtered off fibers also represent homo and hetero oligopeptides, although with higher numbers of the condensed monomeric amino acid units.

Table 1. Selection of some intense mass spectrometric signals for soluble oligopeptides from the Pro-Phe solution in 70% aqueous acetonitrile (see Fig. 9), with possible structures attributed to them.

Signal (m/z)	Proposed ion
216	$[Pro_2+He]^+$
812	$[Pro_8+H_2O]^+$
1498	$[Pro_9+Phe_4+H_3O]^+$
2014	$[Pro_8+Phe_8+CO_2]^+$
2458	$[Pro_{10}+Phe_{10}]^+$
2754	$[Pro_{10}+Phe_{12}+H_2]^+$
2866	$[Pro_{11}+Phe_{12}+OH]^+$
2886	$[Pro_{11}+Phe_{12}+H_2O+H_3O]^+$
3220	$[Pro_{10}+Phe_{15}+CO]^+$
3220	$[Pro_{33}+H]^+$

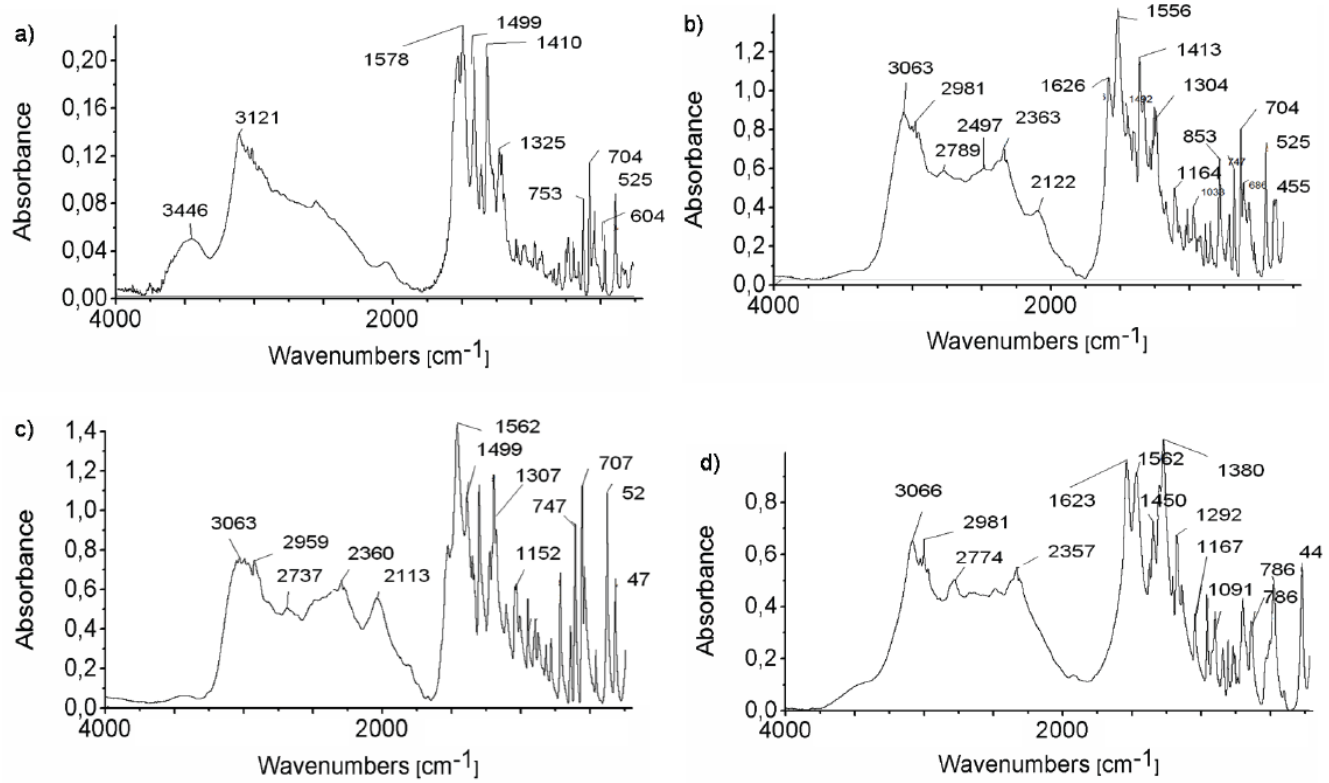

Fig. (8). The IR absorption spectra recorded in the wavelength range from 4000 to 400 cm^{-1} from KBr pellets for (a) solid fiber sample, (b) 1:1 (w/w) mixture of Pro and Phe, (c) Pro sample, and (d) Phe sample.

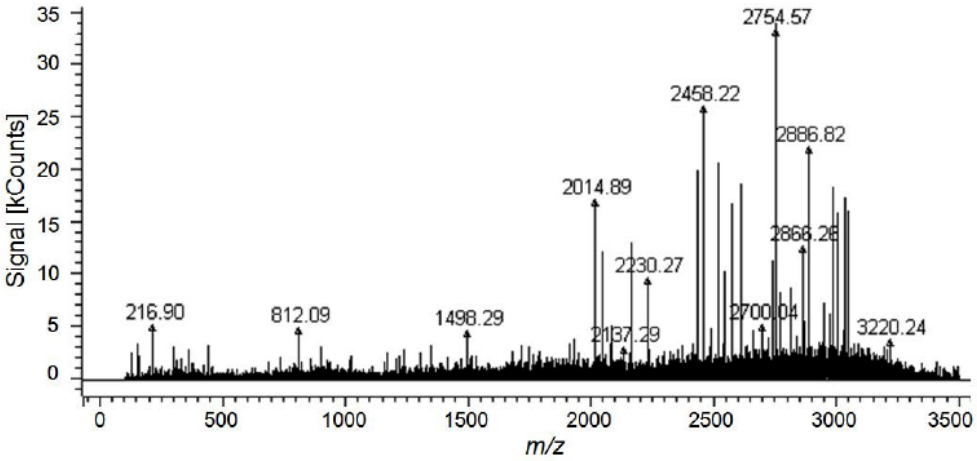

Fig. (9). Mass spectrum recorded in the ESI MS mode with positive ionization for the soluble oligopeptide fraction of the aged Pro-Phe solution in 70% aqueous acetonitrile (with fibers filtered off).

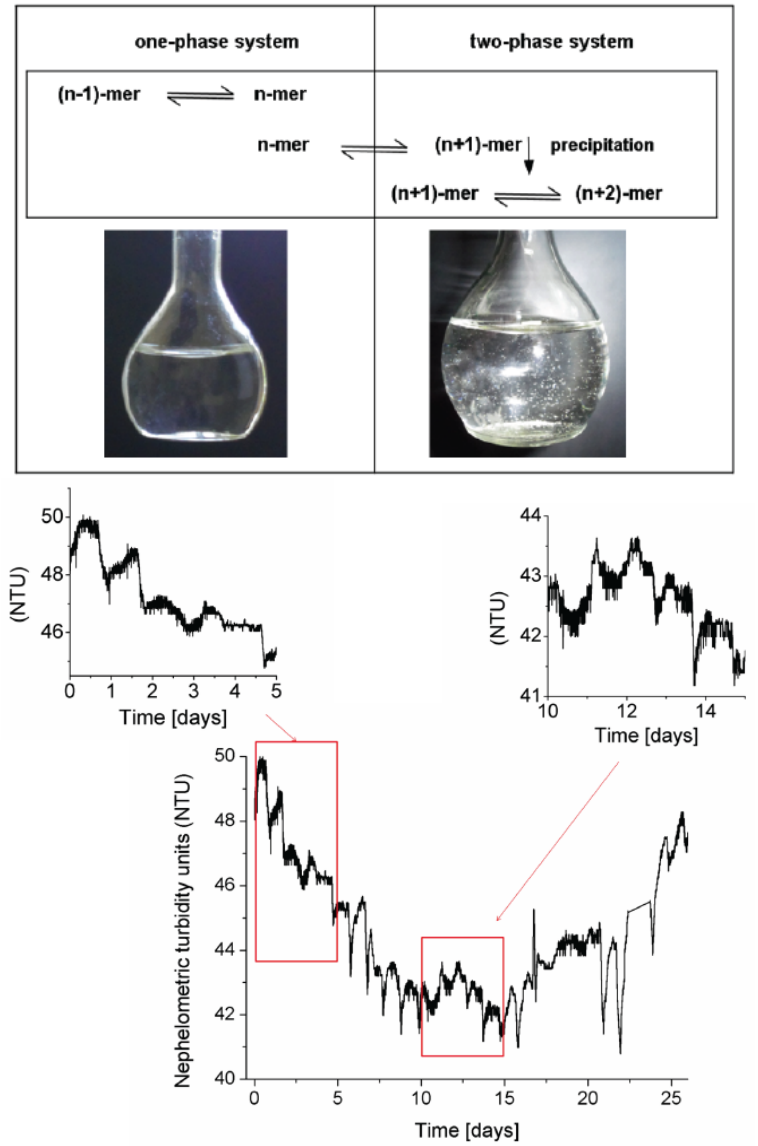

Fig. (10). (a) Schematic illustration of pulsating instability of peptide nano- and microstructures as a reversible change from a lower molecular weight soluble species (dissolved in the one-phase system) to a higher molecular weight insoluble species (precipitated to give a two-phase system); (b) Turbidity changes (in nephelometric turbidity units, NTU) for the Pro-Phe solution in the range of 0 ÷ 26 days sample storage period. Insets emphasize non-linear nature of turbidity changes in shorter time intervals

The results presented in this paper focus on dynamic instability of peptides in solution, apparently caused by peptidization/hydrolysis with participation of monomeric amino acids and by self-assembly/disassembly of the peptide-based supramolecular entities. Seemingly analogous phenomena have earlier been reported in other papers, although fundamental difference between our findings and those earlier reported is that our pulsations were perceived in abiotic amino acid systems, whereas in other cases, action of different biocatalysts was involved (e.g., in paper [20], pulsations were attributed to the presence of the enzyme α-chymotrypsin, and those reported in papers [21,22] to the presence of the phosphatase/kinase system). Moreover, no other report except of ours connects peptide instability with spontaneous oscillatory chiral conversion of the monomeric amino acids as an inevitable initial step of the pulsating instability considered. In view of our present and previous findings on spontaneous oscillatory chiral conversion and oscillatory peptidization, it seems only logical to assume that the pulsating formation and decay of the oligopeptide fibers is a property inherent of amino acids, which can well pronounce in abiotic systems. Schematic illustration of a reversible change from a lower molecular weight soluble species (fully dissolved in the one-phase system) to a higher molecular weight insoluble species is given in Fig. (**10a**). This pulsating shift from the lower to higher yields of insoluble peptide particles can be confirmed experimentally with use of turbidimeter, when peptide particles are still too small to be perceived by human eye. In Fig. (**10b**), the time series is presented of turbidity changes (registered in the nephelometric turbidity units, NTU) for the Pro-Phe solution in 70% aqueous acetonitrile stored for the period of 26 days. Turbidimetric measurements were performed with use of the Turbidity Sensor (model TRB-BTA, Vernier Software & Technology, Beaverton, OR, USA), enabling acquisition of the turbidity results in continuous mode. The non-linear plot given in (Fig. **10b**) represents the pulsating instability effect discussed in this paragraph, i.e., the changing yields of insoluble peptide particles formed in solution in the course of ageing.

In the case described in this study, it took ca. one year for the abiotic Pro–Phe solution to produce visually perceptible pulsating fiber formation and decay (and a much shorter period of 26 days to perceive the same effect with aid of turbidimeter). As demonstrated in paper [20], the potential of amino acids to undergo the oscillatory fiber formation can be biocatalytically enhanced, yet up to our own experience, its true background seems inherent exclusively of the amino acids involved and their ability to spontaneously undergo the oscillatory chiral conversion and peptidization.

CONCLUSIONS

Up to our best knowledge, this is the first documented report on spontaneous (i.e., non-catalyzed) pulsation under mild external conditions (an unshaken sample storage for the period of one year at 21±1°C) of Pro–Phe oligopeptide microfibers in an abiotic aqueous organic solvent. The oligopeptide molecular characteristics was supported by the results originating from IR spectroscopy and mass spectrometry, and the microfiber structure was proved with use of optical and electron microscopy. The mechanism of the dynamic pulsation of the oligopeptide microfibers seems directly related to our earlier findings on the mechanisms of spontaneous oscillatory chiral conversion and spontaneous oscillatory condensation with the low molecular weight chiral carboxylic acids. So far, no theoretical model of peptide pulsation has yet been developed, although some efforts have already been undertaken and the goal might probably be reached in not a very distant future.

CONFLICT OF INTEREST

The author(s) confirm that this article content has no conflicts of interest.

ACKNOWLEDGEMENT

One author (A.G.) acknowledges the financial support of the DoktoRIS project, co-financed by the European Union within the European Social Found.

REFERENCES

[1] Wsol, V.; Skalova, L.; Szotakova, B. Chiral inversion of drugs: Coincidence or principle? *Curr. Drug Metab*., **2004**, 5, 517-533.

[2] Wolf, C. Dynamic Stereochemistry of Chiral Compounds – Principles and Applications, RCS Publishing, Cambridge, UK, **2008.**

[3] Sajewicz, M.; Piętka, R.; Pieniak, A.; Kowalska, T. Application of thin-layer chromatography (TLC) to investigating oscillatory instability of the selected profen enantiomers. *Acta Chromatogr*., **2005**, 15, 131- 149.

[4] Sajewicz, M.; Gontarska, M.; Kowalska, T. HPLC/DAD evidence of the oscillatory chiral conversion of phenylglycine. *J. Chromatogr. Sci.*, **2014**, 52, 329-333.

[5] Belanger, P.; Atkinson, J.G.; Stuart, R.S. Exchange reactions of carboxylic acid salts; Kinetics and mechanism. *Chem. J. Chem. Soc. D: Commun*., **1969**, 1067-1068.

[6] Xie, Y.; Liu, H.; Chen, J. Kinetics of base catalyzed racemization of ibuprofen enantiomers. *Int. J. Pharm*., **2000**, 196, 21-26.

[7] Ivanov, P.V.; Maslova, V.I.; Bondareva, N.G.; Yur'eva, O.A.; Kozlova, N.V; Chernyshev, E.A.; Odintsov, K.Y.; Zykunova, E.A. Concentration oscillations in the condensation of organosilanols. *Russ. Chem. Bull*., **1997**, 46, 2138-2141.

[8] Chernyshev, E.A.; Ivanov, P.V; Golubykh, D.N. Intermediates of chemical assembling of oligoorganosiloxanes in hydrolysis of organochlorosilanes. *Russ. Chem. Bull*., **2001**, 50, 1998-2009.

[9] Sajewicz, M.; Gontarska, M.; Kronenbach, D.; Kowalska, T. On the spontaneous abiotic peptization of phenylglycine in an aqueous medium. *Acta Chromatogr*., **2009**, 21, 151-160.

[10] Fox, S.W.; Harada, K. Thermal copolymerization of amino acids to a product resembling protein. *Science*, **1958**, 128, 1214.

[11] Fox, S.W. The chemical problem of spontaneous generation. *J. Chem. Ed*., **1957**, 34, 472-479.

[12] Sajewicz, M.; Matlengiewicz, M.; Leda, M.; Gontarska, M.; Kronenbach, D.; Kowalska, T.; Epstein, I.R. Spontaneous oscillatory *in vitro* chiral conversion of simple carboxylic acids and its possible mechanism. *J. Phys. Org. Chem*., **2010**, 23, 1066-1073.

[13] Sajewicz, M.; Gontarska, M.; Kronenbach, D.; Leda, M.; Kowalska, T.; Epstein, I.R. Condensation oscillations in the peptidization of phenylglycine. *J. Syst. Chem.*, **2010**, 1:7; DOI:10.1186/1759-2208-1-7.

[14] Sajewicz, M.; Dolnik, M.; Kronenbach, D.; Gontarska, M.; Kowalska, T.; Epstein, I.R. Oligomerization oscillations of *L*-lactic acid in solution. *J. Phys. Chem. A,* **2011**, 115, 14331-14339.

[15] Sajewicz, M.; Dolnik, M.; Kowalska, T.; Epstein, I.R. Condensation dynamics of *L*-proline and *L*-hydroxyproline in solution. *RSC Advances*, **2014**, 4, 7330-7339.

[16] Sajewicz, M.; Godziek, A.; Maciejowska, A.; Kowalska, T. Condensation dynamics of the *L*-Pro-*L*-Phe and *L*-Hyp-*L*-Phe binary mixtures in solution. *J. Chromatogr. Sci.*, **2015**, 53, 31-37.

[17] Sajewicz, M.; Wrzalik, R.; Gontarska, M.; Kronenbach, D.; Leda, M.; Epstein, I.R.; Kowalska, T. *In vitro* chiral conversion, phase

separation and wave propagation in aged profen solutions. *J. Liq. Chromatogr. Relat. Technol*., **2009**, 32, 1359-1372.

[18] Sajewicz, M.; Gontarska, M.; Wojtal, Ł.; Kronenbach, D.; Leda, M.; Epstein, I.R.; Kowalska, T. Experimental and model investigation of the oscillatory transenantiomerization of *L*-α-phenylalanine. *J. Liq. Chromatogr. Relat. Technol*., **2008**, 31, 1986-2005.

[19] Bradford, M.M. A rapid and sensitive method for the quantitation of microgram quantities of protein utilizing the principle of protein-dye binding. Anal Biochem 1976, 72:248-254.

[20] Debnath, S.; Roy, S.; Ulijn, R.V. Peptide nanofibers with dynamic instability through nonequilibrium biocatalytic assembly. *J. Am. Chem. Soc*., **2013**, 135, 16789-16792.

[21] von Maltzahn, G.; Min, D.-H.; Zhang, Y.; Park, J.-H.; Harris, T.J.; Sailor, M.; Bhatia, S.N. Nanoparticle self-assembly directed by antagonistic kinase and phosphatase activities. *Adv. Mater*., **2007**, 19, 3579−3583.

[22] Webber, M.J.; Newcomb, C.J.; Bitton, R.; Stupp, S.I. Switching of self-assembly in a peptide nanostructure with a specific enzyme. *Soft Matter* **2011**, 7, 9665−9672.

Received: ???????????????? **Revised:** ???????????????? **Accepted:** ????????????????

Reac Kinet Mech Cat (2016) 118:129–142
DOI 10.1007/s11144-015-0972-7

Investigation of spontaneous non-linear peptidization dynamics and mechanism with selected α-amino acid pairs

Anna Maciejowska[1] · Agnieszka Godziek[1] · Mieczysław Sajewicz[1] · Teresa Kowalska[1]

Received: 7 November 2015 / Accepted: 15 December 2015 / Published online: 22 December 2015
© The Author(s) 2015. This article is published with open access at Springerlink.com

Abstract The goal of this study was to provide experimental evidence on the dynamics and mechanism of spontaneous oscillatory peptidization in an abiotic system with three α-amino acid pairs (*L*-Met-*L*-Ser, *L*-His-*L*-Thr, and *L*-Cys-*L*-Phg), and to discuss these data in the context of an earlier established theoretical model. For each individual α-amino acid in a monocomponent and binary system, the dynamics of peptidization was traced with aid of the high performance liquid chromatograph with the evaporative light scattering detector. As an auxiliary technique, mass spectrometry (MS) was employed to scrutinize structures of the resulting peptides. With *L*-Met-*L*-Ser and *L*-His-*L*-Thr, the dynamics of one amino acid (*L*-Met and *L*-Thr, respectively) dominated over that of its counterpart. With *L*-Cys-*L*-Phg, no such predominance of the dynamics of one α-amino acid over that of its counterpart was observed. Mass spectrometric results confirmed the formation of heteropeptides with each investigated α-amino acid pair. With *L*-Met-*L*-Ser, *L*-His-*L*-Thr, and *L*-Cys-*L*-Phg, synchronization of the oscillatory behavior in the binary systems was observed, witnessing to mutual cross-catalysis of the two counterparts, assumed by case 4 of the theoretical model.

Keywords Binary alpha-amino acid systems · Spontaneous peptidization dynamics · Abiotic amino acid solutions · High performance liquid chromatography · Mass spectrometry

✉ Teresa Kowalska
teresa.kowalska@us.edu.pl

[1] Institute of Chemistry, University of Silesia, 9 Szkolna Street, 40-006 Katowice, Poland

Introduction

The research on spontaneous oscillatory chiral conversion of the low molecular weight carboxylic acids was initiated over a decade ago with a paper demonstrating this phenomenon upon an example of *S*(+)ibuprofen [1] and later it was confirmed as a general phenomenon with a selection of other compounds from the groups of profen drugs, hydroxyl acids and amino acids (e.g., [2–4]). Then it was found out that spontaneous oscillatory chiral conversion of the aforementioned compounds is accompanied by spontaneous oscillatory condensation of the same compounds and the two processes are running in the parallel [5–7]. Papers [1–7] furnish general information on the possible molecular mechanisms of these two oscillatory processes, which involve a non-chiral enol/enolate ion intermediary step and can be illustrated by the scheme given in Fig. 1 (for the sake of this study, illustrating the case of amino acids).

Although the experiments presented in papers [1–4] were the first ones to demonstrate spontaneous chiral oscillations, this phenomenon had been assumed earlier by Stich et al. [8] in their theoretical model. Chiral oscillations were directly anticipated in a theoretical activation-polymerization-epimerization-depolymerization (APED) model by Plasson et al. [9], whereas some other models [10–12] had to be modified or reinterpreted in order to account for chiral, rather than just mere chemical oscillations.

In paper [13], the high performance liquid chromatographic results were presented on spontaneous peptidization dynamics for *L*-Pro, *L*-Hyp, and *L*-Pro-*L*-Hyp in 70 % aqueous methanol. It was demonstrated that in the monocomponent amino acid solutions, each compound underwent peptidization with its own dynamics, whereas in a binary solution, both amino acids followed the predominant peptidization dynamics of *L*-Pro. Based on these experimental results, a theoretical model was developed which assumed four different peptidization cases in the binary amino acid mixtures. Case 1 does not assume any cross-catalysis between the two amino acids in a binary solution, so that the peptidization products can only be homopeptides derived from each individual amino acid. Cases 2 and 3 anticipate one or another amino acid apt to cross-catalysis, respectively, and the formation of the homo- and heteropeptides in the system. Case 4 assumes cross-catalysis of both partners and formation of the homo- and heteropeptides also. It can be distinguished from the remaining cases 1–3 by the unique synchronization of the oscillatory

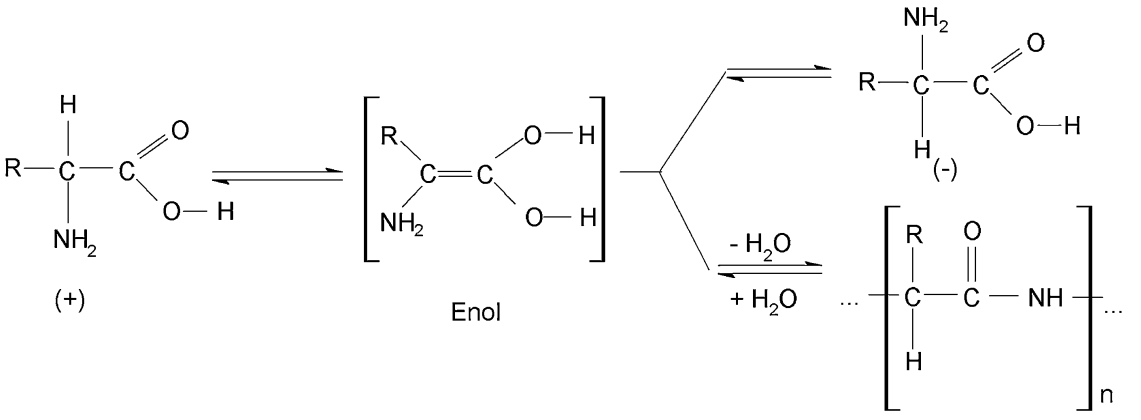

Fig. 1 The parallel processes of chiral conversion and peptidization of an amino acid

behavior of both partners in a binary system. Recently, a striking finding related to the spontaneous non-linear peptidization of amino acids was described in papers [14, 15], namely pulsating changes of the insoluble and hence precipitated higher peptides, which can be perceived even with human eye and instrumentally traced with use of turbidimeter operating in the continuous registration mode.

Continuing our investigations on the peptidization dynamics of α-amino acids in the abiotic binary mixtures, in this paper, we present new experimental results obtained for the three randomly selected α-amino acid pairs (*L*-Met-*L*-Ser, *L*-His-*L*-Thr, and *L*-Cys-*L*-Phg). Chemical structures and molecular weights (MW) of the amino acids involved are given in Table 1. The main objective of this study was to compare the peptidization dynamics in the monocomponent amino acid solutions against those in the binary mixtures, in the context of their respective chemical structures and the earlier developed theoretical model. The main analytical technique to trace peptidization dynamics was high performance liquid chromatography with the evaporative light scattering detection (HPLC-ELSD), and as an auxiliary instrumental technique, mass spectrometry (MS) was used to scrutinize chemical structures of the obtained peptides.

Experimental

Reagents

In our experiment, we used *L*-Ser, *L*-Met, *L*-Cys, *L*-Thr and *L*-His (Reanal, Budapest, Hungary), and *L*-Phg (Sigma-Aldrich, St Louis, MO, USA). All amino

Table 1 Chemical structures and molecular weights (MW) of α-amino acids investigated in pairs *L*-Met-*L*-Ser, *L*-His-*L*-Thr, and *L*-Cys-*L*-Phg

L-Met-*L*-Ser	*L*-His-*L*-Thr	*L*-Cys-*L*-Phg
L-Met	*L*-His	*L*-Cys
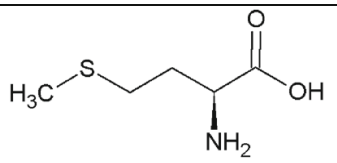	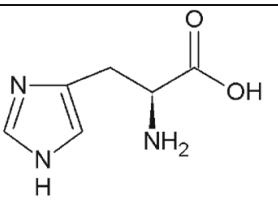	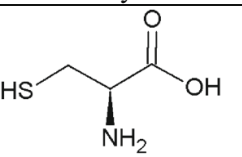
MW = 149.21	MW = 155.15	MW = 121.16
L-Ser	*L*-Thr	*L*-Phg
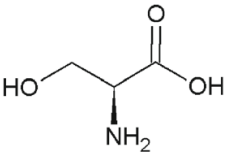	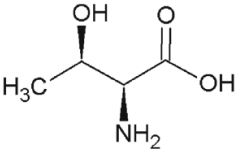	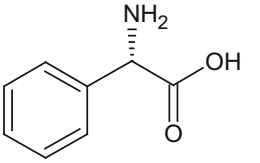
MW = 105.09	MW = 119.12	MW = 151.16

acids were of analytical purity. Methanol and acetonitrile (Sigma-Aldrich) were of HPLC purity. Water was de-ionized and double distilled in our laboratory by means of the Elix Advantage model Millipore System (Molsheim, France).

For the HPLC/ELSD, HPLC/MS, and MS experiments, we prepared the 1.0 mg mL^{-1} solutions of *L*-Phg, *L*-Thr, *L*-Ser, and *L*-Cys (i.e., 6.61×10^{-3} mol L^{-1} for *L*-Phg, 8.39×10^{-3} mol L^{-1} for *L*-Thr, 9.52×10^{-3} mol L^{-1} for *L*-Ser, and 8.25×10^{-3} mol L^{-1} for L-Cys) in 70 % aqueous MeOH, and the 2.0 mg mL^{-1} solutions of *L*-His and *L*-Met (i.e., 1.29×10^{-2} mol L^{-1} for *L*-His and 1.34×10^{-2} mol L^{-1} for *L*-Met) in 70 % aqueous MeOH. The 70 % aqueous methanol, known for its strong antiseptic properties, was selected in order to protect the amino acid solutions purposely stored for longer periods of time from the microbial action.

HPLC with evaporative light scattering detection

The condensation process instantaneously commencing in each freshly prepared monocomponent and binary amino acid solution was monitored by means of the achiral HPLC with the ELSD detector. This HPLC mode was employed to separate the oligopeptides from the non-peptidized amino acids and also to fractionate the oligopeptides. The analyses were carried out using the Varian model 920 liquid chromatograph (Varian, Harbor City, CA, USA) equipped with the Varian 900-LC model autosampler, the gradient pump, the Varian 380-LC model ELSD detector, and the Galaxie software for data acquisition and processing. For the analysis of *L*-Met-*L*-Ser and *L*-His-*L*-Thr, the Hypersil C18 (5 μm particle diameter) column (150 mm × 4.6 mm i.d.; ThermoQuest; cat. no. 3718-062) was used, and for the analysis of *L*-Cys-*L*-Phg, the Pursuit 5 C18 (5 μm particle diameter) column (250 mm × 4.6 mm i.d.; Varian; cat. no. A3000250C046) was employed.

All analyses were carried out in the isocratic mode. With *L*-Met-*L*-Ser and *L*-His-*L*-Thr, the injected sample aliquots were 3 μL, and with *L*-Cys-*L*-Phg, the injected sample aliquots were 5 μL. With the monocomponent *L*-Met and *L*-Ser solutions, and the binary *L*-Met-*L*-Ser mixture, acetonitrile: 1 % aqueous CH_3COOH (10:90, *v/v*) was employed as a mobile phase, at a flow rate of 0.8 mL min^{-1}. With the monocomponent *L*-His and *L*-Thr solutions, and the binary *L*-His-*L*-Thr mixture, methanol: 1 % aqueous CH_3COOH (50:50, *v/v*) was employed as a mobile phase, at a flow rate of 1.0 mL min^{-1}. With the monocomponent *L*-Cys and *L*-Phg solutions, and the binary *L*-Cys-*L*-Phg mixture, methanol:water (20:80, *v/v*) was employed as a mobile phase, at a flow rate of 0.8 mL min^{-1}. The chromatographic columns were thermostatted at 35 °C in the Varian ProStar 510 model column oven. The analyses of the *L*-Met-*L*-Ser, *L*-His-*L*-Thr and *L*-Cys-*L*-Phg systems were carried out for 30 h in the 8-min intervals.

HPLC with mass spectrometric detection

The high performance liquid chromatographic system described in the preceding section was additionally equipped with the Varian 100-MS mass spectrometric detector and the Varian MS Workstation v. 6.9.1 software for data acquisition and

processing. The mass spectrometric detection was carried out for the *L*-Met-*L*-Ser solution in 70 % aqueous methanol aged for 9 days. The working MS conditions were the following ones: the ESI mode (ESI–MS scan, negative ionization, spray chamber temperature 50 °C, drying gas temperature 350 °C, drying gas pressure 25 psi, capillary voltage 50 V, needle voltage 5 kV).

MS

For the mass spectrometric analyses, we used the Thermo LCQ Deca XP Plus MS system. The analyses were carried out for the binary *L*-His-*L*-Thr and *L*-Cys-*L*-Phg solutions in 70 % aqueous methanol aged for 8 and 1 month, respectively. The working MS conditions were the following ones: the ESI mode (ESI–MS scan, positive and negative ionization, capillary voltage 50 V, needle voltage 5 kV, and needle temperature 250 °C).

Results and discussion

A basic requirement to reliably trace concentration changes of individual amino acids in a binary solution as a function of time is to employ a chromatographic system that allows the baseline separation of the amino acid pairs. Moreover, the

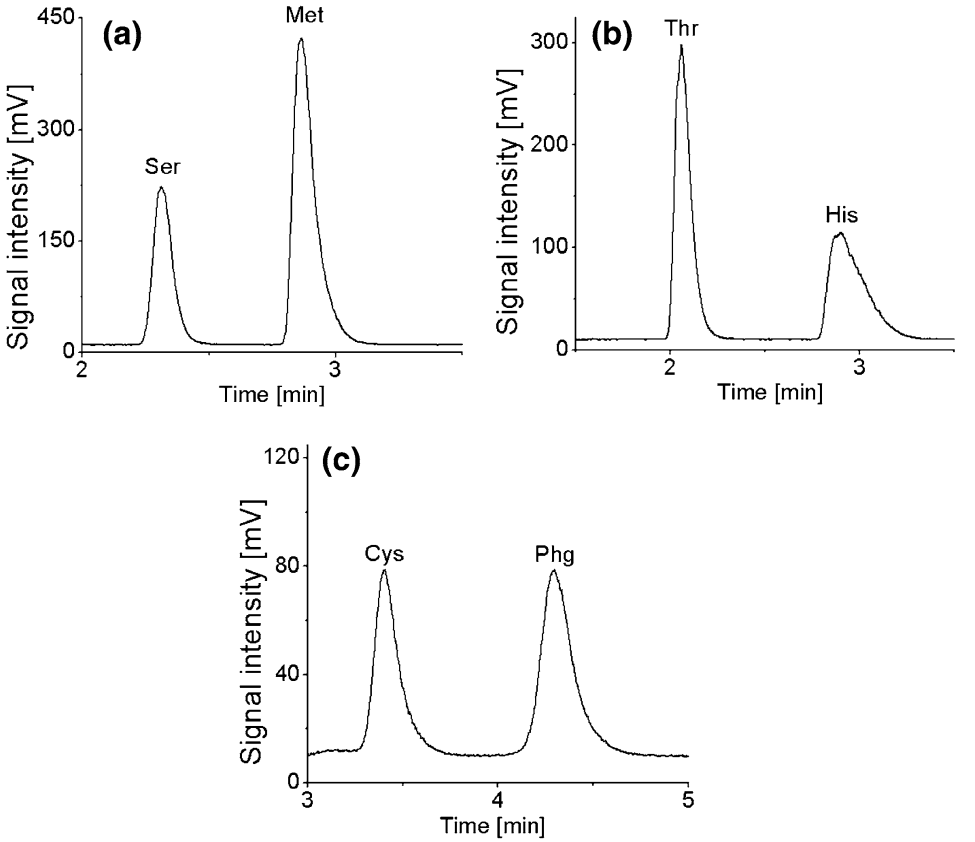

Fig. 2 The base-line separations of the investigated amino acids in the binary mixtures with use of the employed HPLC-ELSD system: **a** Met-Ser; **b** His-Thr; **c** Cys-Phg

shorter is an individual analytical run, the more detailed kinetic information can be obtained on the dynamics of peptidization. The HPLC-ELSD working conditions assumed in this study fully satisfy the aforementioned requirements. Each chromatographic run was carried out for 8 min only (i.e., sampling was automatically done in the 8-min intervals). The baseline separation of each investigated amino acid pair was obtained, as shown in Fig. 2. The retention times of *L*-Met and *L*-Ser were 3.1 ± 0.2 and 2.5 ± 0.2 min, those of *L*-His and *L*-Thr were 3.1 ± 0.2 and 2.1 ± 0.1 min, and those of *L*-Cys and *L*-Phg were 3.5 ± 0.1 and 4.4 ± 0.1 min.

HPLC-ELSD of *L*-Met, *L*-Ser, and *L*-Met-*L*-Ser

In the course of the 30-h lasting ageing of the monocomponent *L*-Met and *L*-Ser solutions and the binary *L*-Met-*L*-Ser mixture, the chromatographic peak heights of individual amino acids were changing in a non-linear fashion, unequivocal with the respective non-linear concentration changes (Figs. 3a–3c). Based on the plots given in Figs. 3a–3c, the following observations were made. First, the amplitudes of the oscillatory concentration changes with *L*-Met in the monocomponent solution were

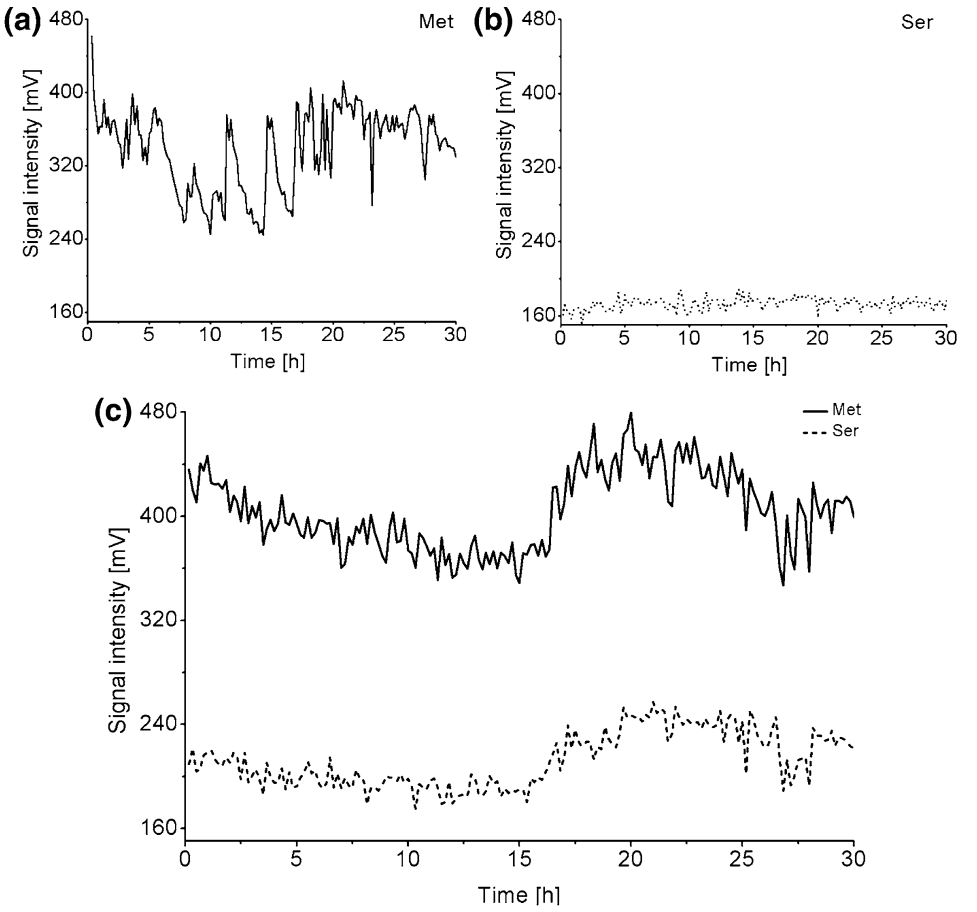

Fig. 3 Time series of the chromatographic peak heights for Met-Ser in 70 % aqueous methanol (registered with ELSD detector): **a** single Met; **b** single Ser; **c** Met and Ser in a binary mixture. The 0–30 h storage period

in the range of 100 mV signal intensity units (Fig. 3a), whereas with the monomeric *L*-Ser and the binary *L*-Met-*L*-Ser solution, they were by one magnitude order lower (Fig. 3b and c). These results indicate that the peptidization process of *L*-Met in the monocomponent solution characterizes with different dynamics from that in the binary solution. Second, the oscillatory patterns of the time series of the chromatographic peak heights valid for *L*-Met and *L*-Ser in the binary *L*-Met-*L*-Ser system are perfectly synchronized (Fig. 3c), witnessing to mutual cross-catalysis of the two counterparts, assumed by case 4 of the theoretical model [13]. Third, the oscillatory patterns of *L*-Ser and *L*-Met in the monocomponent solutions look different from one another (Figs. 3a and 3b), yet in the binary mixture both of them roughly resemble that of pure *L*-Met (even, if the amplitudes of the concentration changes in the former case are lower than in the latter one). This observation suggests that the dynamics of peptidization in the binary *L*-Met-*L*-Ser solution is controlled by that of *L*-Met (which contains 4 carbon atoms in its aliphatic chain against three carbon atoms of *L*-Ser). Thus, it can be assumed that the higher aliphatic chain length of *L*-Met more effectively hinders intermolecular interactions of the $–NH_2$ and –COOH functionalities and hence, *L*-Met controls an

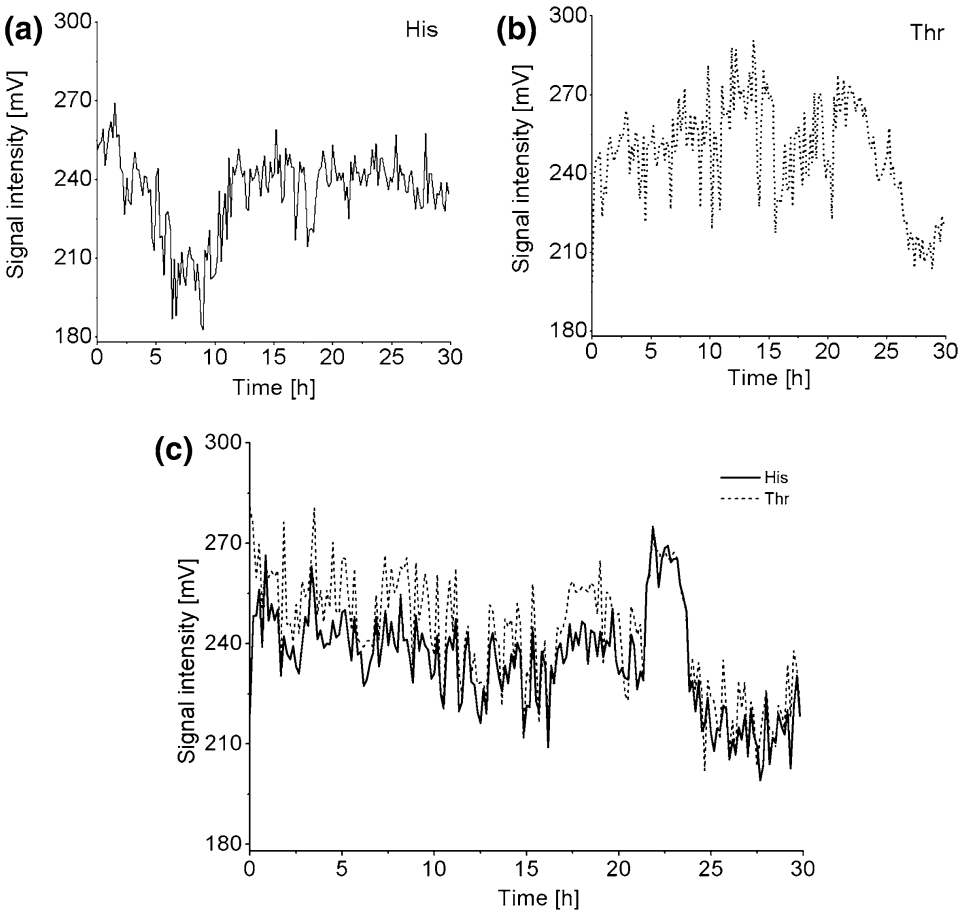

Fig. 4 Time series of the chromatographic peak heights for His-Thr in 70 % aqueous methanol (registered with ELSD detector): **a** single His; **b** single Thr; **c** His and Thr in a binary mixture. The 0–30 h storage period

overall peptidization dynamics (and more specifically, the rate of the heteropeptides formation).

HPLC-ELSD of *L*-His, *L*-Thr, and *L*-His-*L*-Thr

The second investigated amino acid pair was *L*-His-*L*-Thr. The time series of the peak heights for *L*-His and *L*-Thr in the monocomponent amino acid solutions and in the *L*-His-*L*-Thr binary system are presented in Figs. 4a–4c. Based on these plots, the following observations were made. First, the amplitudes of the oscillatory peak height changes are similar for the amino acids in the monocomponent and the binary systems, and remain in the range of several dozen mV signal intensity units. Second, the oscillatory patterns of the time series of the chromatographic peak heights valid for *L*-His and *L*-Thr in the binary system are well enough synchronized (Fig. 4c), again witnessing to mutual cross-catalysis of the two counterparts, assumed by case 4 of the theoretical model [13]. Third, the time series patterns valid for *L*-His and *L*-Thr in the monocomponent solutions are not similar (Figs. 4a and 4b), yet in the binary mixture it looks somewhat different (Fig. 4c). Although for the initial 15-h ageing, the oscillatory patterns valid for *L*-His and *L*-Thr do not resemble those for the monocomponent systems, later (i.e., starting from the 15 h ageing) they start

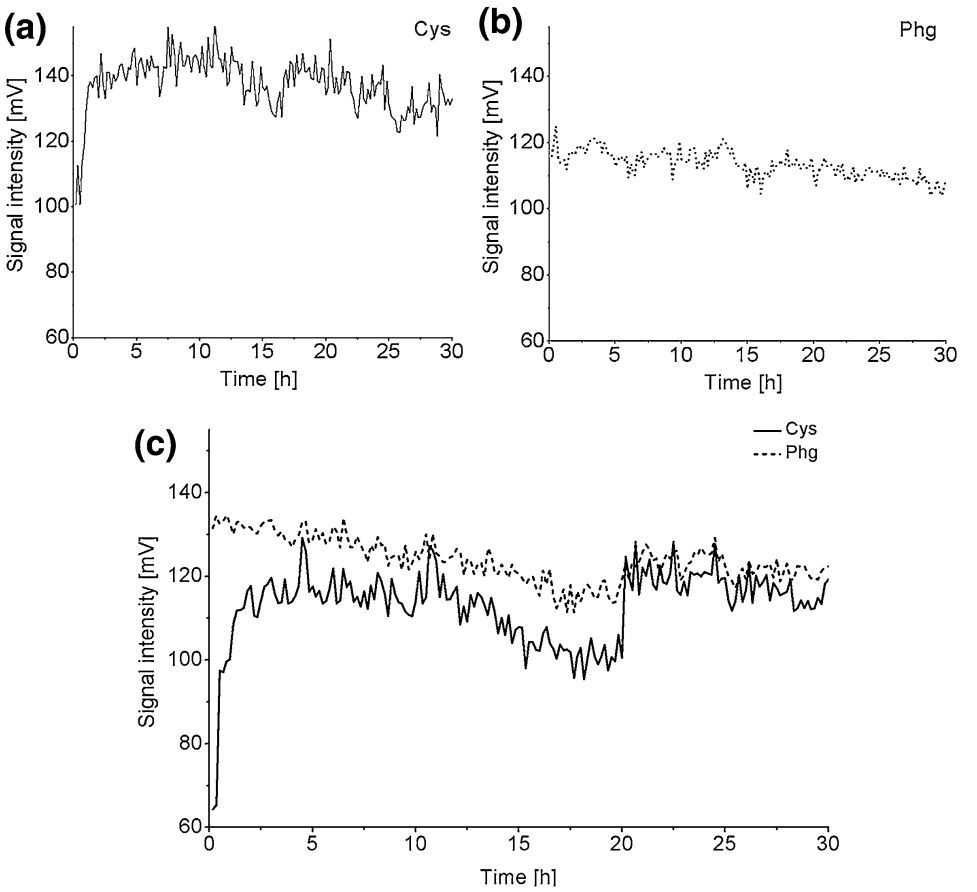

Fig. 5 Time series of the chromatographic peak heights for Cys-Phg in 70 % aqueous methanol (registered with ELSD detector): **a** single Cys; **b** single Phg; **c** Cys and Phg in a binary mixture. The 0–30 h storage period

resembling pattern valid for the monomeric *L*-Thr. This observation suggests that starting from that moment, the dynamics of peptidization in the binary *L*-His-*L*-Thr solution becomes controlled by that of *L*-Thr. This predominance of *L*-Thr can be due to four carbon atoms in its aliphatic chain against three carbon atoms of *L*-His. However, *L*-His contains a bulk imidazole group in its structure, also able to obstruct intermolecular interactions of the $–NH_2$ and –COOH functionalities, and *L*-Thr contains the -OH group, which allows a competitive condensation pattern through esterification. Probably these are the main reasons why the predominance of the *L*-Thr pattern is not instantaneous.

HPLC-ELSD of *L*-Cys, *L*-Phg, and *L*-Cys-*L*-Phg

In the course of the 30-h ageing of the monocomponent *L*-Cys and *L*-Phg solutions and the binary *L*-Cys-*L*-Phg system, the non-linear changes of the chromatographic peak heights with both amino acids were observed, unequivocal with the respective concentration changes (Figs. 5a–5c). Based on these plots, the following observations were made. First, the amplitudes of the *L*-Cys peak height oscillations in the monocomponent system are higher than those of *L*-Phg, and the same observation is valid for the initial ca. 20 h of the binary system also. In the final 10 h of the binary sample storage, the oscillatory amplitudes for both amino acids become comparable with each other. Second, starting from the third hour of the binary sample storage, concentration changes of *L*-Cys and *L*-Phg are well enough synchronized (Fig. 5c), witnessing to mutual cross-catalysis of the two counterparts, assumed by case 4 of the theoretical model [13]. Third, the oscillatory patterns of *L*-Cys and *L*-Phg in the monocomponent systems are not similar (Figs. 5a and 5b) and in the binary mixture, none of these two oscillatory patterns predominates. Although the aliphatic chains of *L*-Cys and *L*-Phg contain 3 and 2 carbon atoms, respectively, their condensation abilities are substantially different. *L*-Cys contains not only the $–NH_2$ and –COOH functionalities in its molecule, but also a reactive thiol (–SH) group, responsible for spontaneous formation of disulfide bridges and hence, for the ternary structure and the spherical shape of the *L*-Cys-derived proteins and peptides [16, 17]. On the other hand, an aromatic ring in molecular structure of *L*-Phg can partially shield its $–NH_2$ and –COOH functionalities, thus hampering the peptidization dynamics of *L*-Phg.

HPLC–MS of *L*-Met-*L*-Ser

The HPLC–MS analysis was performed for the aged *L*-Met-*L*-Ser sample (after 9 days ageing) and its goal was to check, if peptidization spontaneously carried out in this binary system results in both, homo- and heteropeptides (or in homopeptides only). In Fig. 6, we give an HPLC–MS chromatogram and the mass spectra recorded for chromatographic peak 1 (Ser), peak 2 (Met), and peak 3 (the main peptidization product). With peak 1 (Ser), we observe the predominant signal at *m/z* 233, which can be attributed to the homopeptide structure $[Ser_3\text{-}COOH–H]^-$, yet signal at *m/z* 104 originating from the Ser molecular ion ($[Ser\text{-}H]^-$) is also present. The remaining signals are of low intensity only and they can be attributed to peptides. With peak 2 (Met), signal at *m/z* 148 originating from the Met molecular

ion ([Met-H]$^-$) is present, but signals originating from peptides are predominant. With peak 3 (the main peptidization product), the molecular ions derived from Ser and Met are absent, but a good number of signals originating from heteropeptides can be observed (e.g., signals at *m/z* 1717 and 1895, which can be attributed to $[Ser_{12}+Met_5]^-$ and $[Ser_2+Met_{13}]^-$, respectively). To sum up, peptidization spontaneously running in the *L*-Met-*L*-Ser sample results both, in homo- and heteropeptides.

MS of *L*-His-*L*-Thr and *L*-Cys-*L*-Phg

Investigations by means of MS were carried out for the aged binary solutions of *L*-His-*L*-Thr and *L*-Cys-*L*-Phg. In Fig. 7, we show mass spectra recorded for the binary *L*-His-*L*-Thr system in the positive (Fig. 7a) and negative ionization mode (Fig. 7b), respectively. In Figs. 8a and 8b, the analogous mass spectra are presented, valid for the aged *L*-Cys-*L*-Phg system. In all these spectra, signals originating from molecular ions of the investigated α-amino acids can be seen (i.e., originating from the $[His+H]^+$, $[His-H]^-$, $[Thr+H]^+$, $[Thr-H]^-$, $[Cys-H]^-$, and $[Phg+H]^+$ ion). The most interesting signals are, however, those originating from the spontaneously formed peptides. These signals are abundant and the predominant number thereof originates from heteropeptides, although signals originating from homopeptides are encountered as well. For the sake of example, let us point out to such homopeptides, as $[Thr_3+2H]^{2+}$ (*m/z* 160.5; Fig. 7a), and $[Cys_2+2Na]^{2+}$, $[Phg_8+2H]^{2+}$, and $[Cys_5+Na]^+$ (*m/z* 135.0, 540.2, and 556.0; Fig. 8a). Generally, the observed heteropeptides can be divided into two groups. In one group, an evident quantitative predominance of one amino acid over its counterpart is observed and the following

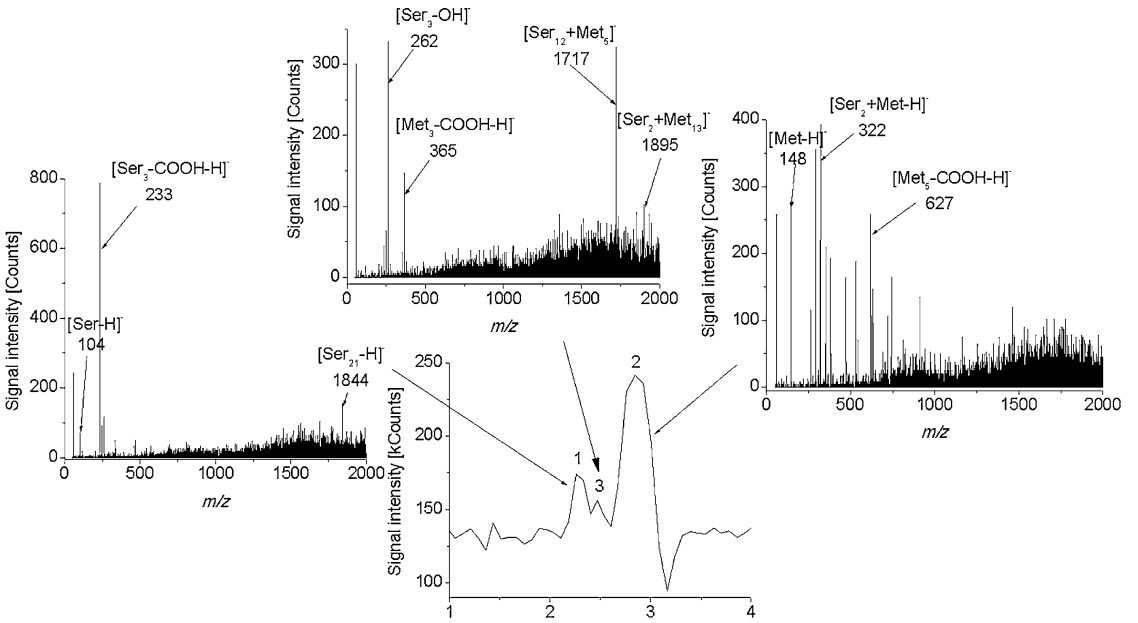

Fig. 6 The HPLC–MS chromatogram recorded for the aged Met-Ser solution in 70 % aqueous methanol and the respective mass spectra recorded for Ser (*peak 1*), Met (*peak 2*), and main peptidization product (*peak 3*)

(a)

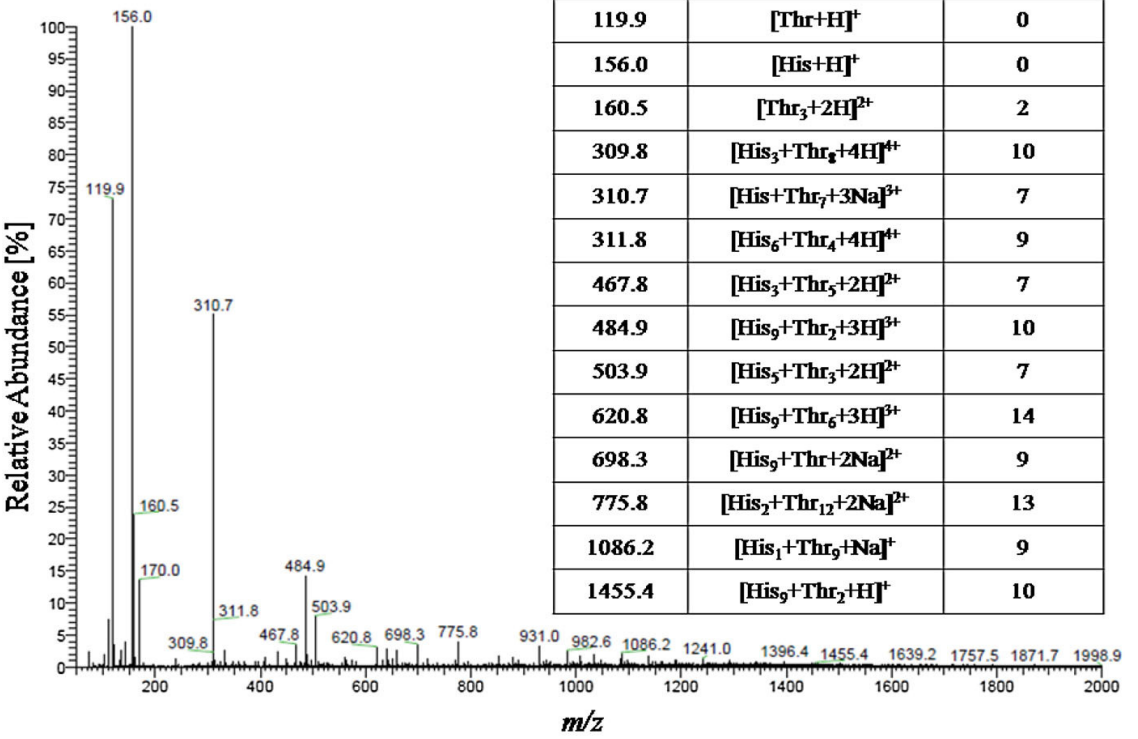

m/z	Proposed structure	No. -CO-NH-
119.9	$[Thr+H]^+$	0
156.0	$[His+H]^+$	0
160.5	$[Thr_3+2H]^{2+}$	2
309.8	$[His_3+Thr_8+4H]^{4+}$	10
310.7	$[His+Thr_7+3Na]^{3+}$	7
311.8	$[His_6+Thr_4+4H]^{4+}$	9
467.8	$[His_3+Thr_5+2H]^{2+}$	7
484.9	$[His_9+Thr_2+3H]^{3+}$	10
503.9	$[His_5+Thr_3+2H]^{2+}$	7
620.8	$[His_9+Thr_6+3H]^{3+}$	14
698.3	$[His_9+Thr+2Na]^{2+}$	9
775.8	$[His_2+Thr_{12}+2Na]^{2+}$	13
1086.2	$[His_1+Thr_9+Na]^+$	9
1455.4	$[His_9+Thr_2+H]^+$	10

(b)

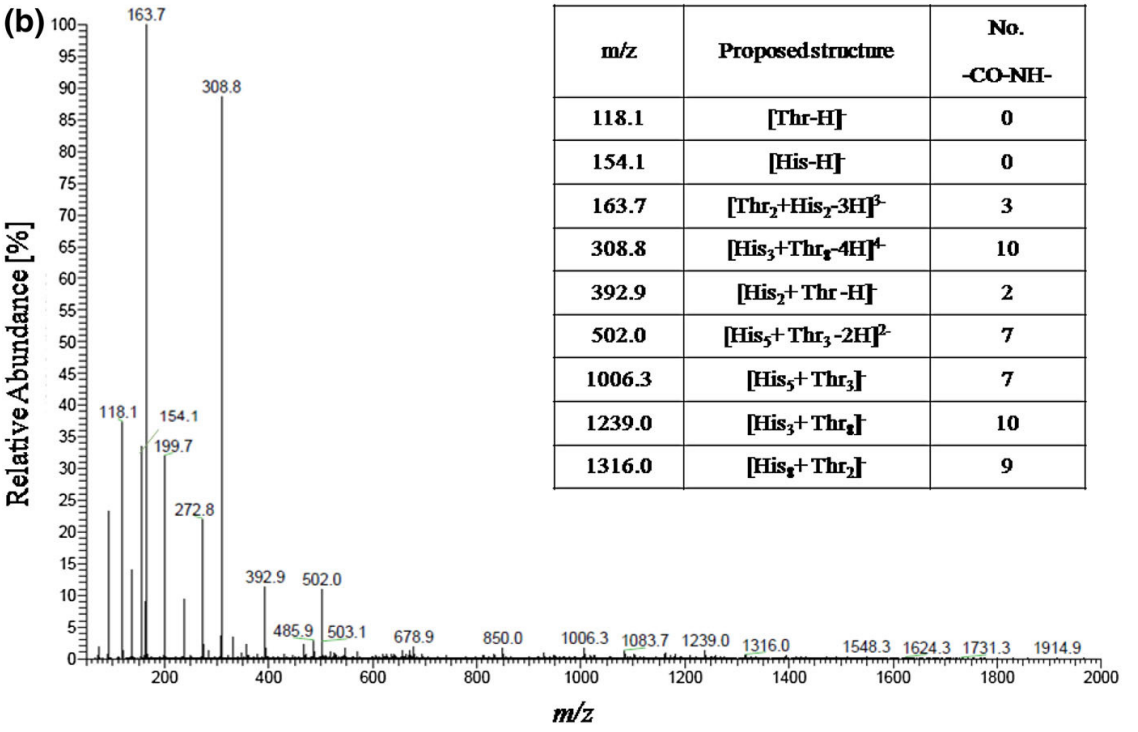

m/z	Proposed structure	No. -CO-NH-
118.1	$[Thr-H]^-$	0
154.1	$[His-H]^-$	0
163.7	$[Thr_2+His_2-3H]^{3-}$	3
308.8	$[His_3+Thr_8-4H]^{4-}$	10
392.9	$[His_2+Thr-H]^-$	2
502.0	$[His_5+Thr_3-2H]^{2-}$	7
1006.3	$[His_5+Thr_3]^-$	7
1239.0	$[His_3+Thr_8]^-$	10
1316.0	$[His_8+Thr_2]^-$	9

Fig. 7 Mass spectra recorded in the **a** positive and **b** negative ionization mode for the His-Thr solution in 70 % aqueous methanol aged for 8 months, suggested chemical structures of certain cations and anions, and the respective numbers of peptide bonds (–CO–NH–)

(a)

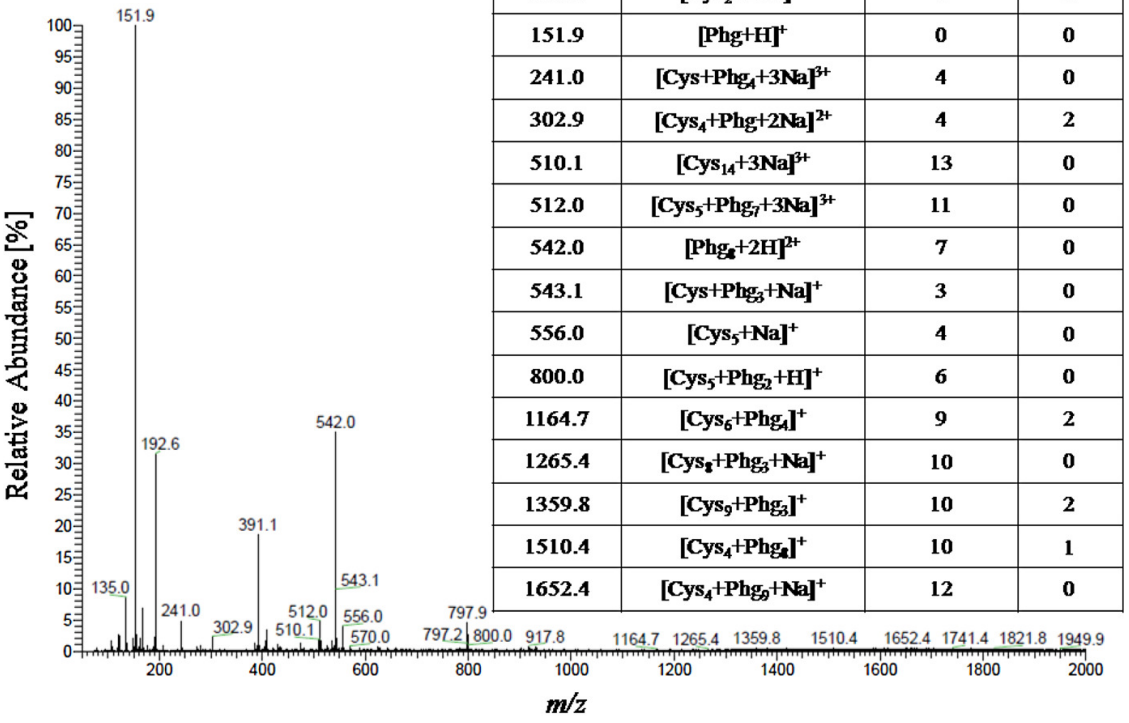

m/z	Proposed structure	No. -CO-NH-	No. -S-S-
135.0	$[Cys_2+2Na]^{2+}$	1	0
151.9	$[Phg+H]^{+}$	0	0
241.0	$[Cys+Phg_4+3Na]^{3+}$	4	0
302.9	$[Cys_4+Phg+2Na]^{2+}$	4	2
510.1	$[Cys_{14}+3Na]^{3+}$	13	0
512.0	$[Cys_5+Phg_7+3Na]^{3+}$	11	0
542.0	$[Phg_8+2H]^{2+}$	7	0
543.1	$[Cys+Phg_3+Na]^{+}$	3	0
556.0	$[Cys_5+Na]^{+}$	4	0
800.0	$[Cys_5+Phg_2+H]^{+}$	6	0
1164.7	$[Cys_6+Phg_4]^{+}$	9	2
1265.4	$[Cys_8+Phg_3+Na]^{+}$	10	0
1359.8	$[Cys_9+Phg_3]^{+}$	10	2
1510.4	$[Cys_4+Phg_8]^{+}$	10	1
1652.4	$[Cys_4+Phg_9+Na]^{+}$	12	0

(b)

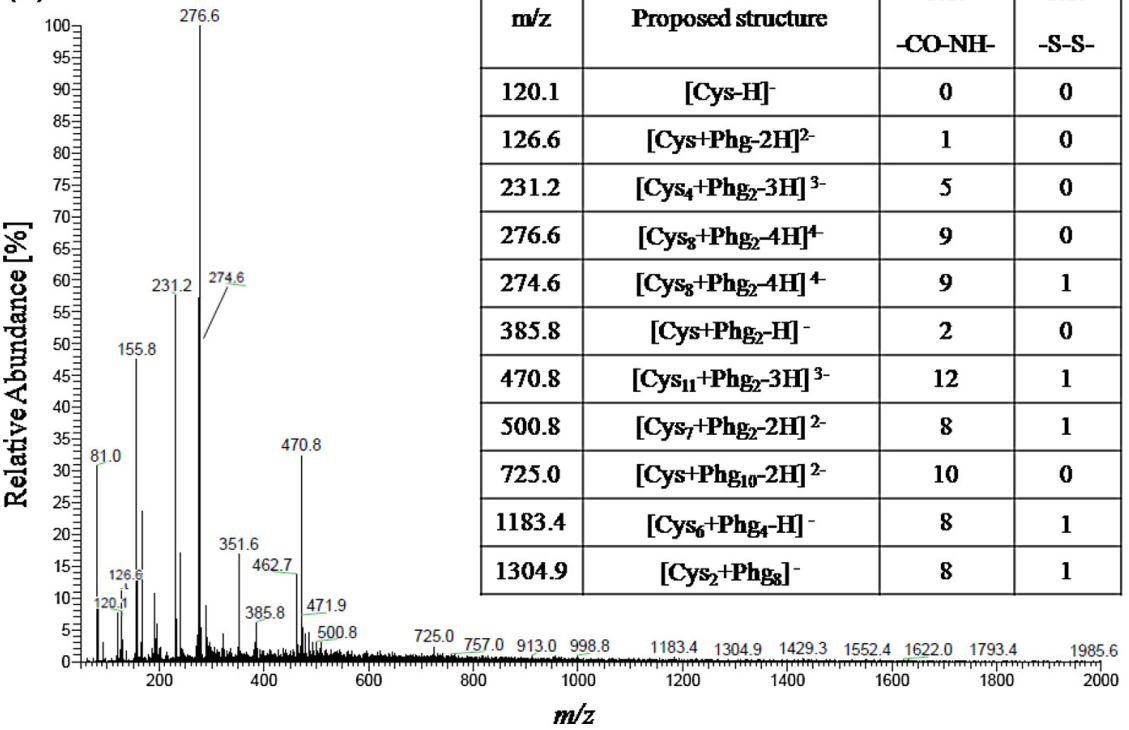

m/z	Proposed structure	No. -CO-NH-	No. -S-S-
120.1	$[Cys-H]^{-}$	0	0
126.6	$[Cys+Phg-2H]^{2-}$	1	0
231.2	$[Cys_4+Phg_2-3H]^{3-}$	5	0
276.6	$[Cys_8+Phg_2-4H]^{4-}$	9	0
274.6	$[Cys_8+Phg_2-4H]^{4-}$	9	1
385.8	$[Cys+Phg_2-H]^{-}$	2	0
470.8	$[Cys_{11}+Phg_2-3H]^{3-}$	12	1
500.8	$[Cys_7+Phg_2-2H]^{2-}$	8	1
725.0	$[Cys+Phg_{10}-2H]^{2-}$	10	0
1183.4	$[Cys_6+Phg_4-H]^{-}$	8	1
1304.9	$[Cys_2+Phg_8]^{-}$	8	1

Fig. 8 Mass spectra recorded in the **a** positive and **b** negative ionization mode for the aged Cys-Phg solution in 70 % aqueous methanol aged for 1 month, suggested chemical structures of certain cations and anions, and the respective numbers of peptide bonds (–CO–NH–) and disulfide bridges (–S–S–)

signals can be given as an example: *m/z* 484.9, $[His_9+Thr_2+3H]^{3+}$; *m/z* 775.8, $[His_2+Thr_{12}+2Na]^{2+}$; *m/z* 308.8, $[His_3+Thr_8-4H]^{4-}$; *m/z* 1316.0, $[His_8+Thr_2]^{-}$; *m/z* 543.1, $[Cys+Phg_3+Na]^{+}$; *m/z* 1265.4, $[Cys_8+Phg_3+Na]^{+}$, *m/z* 470.8, $[Cys_{11}+Phg_2-3H]^{3-}$; and *m/z* 725.0, $[Cys+Phg_{10}-2H]^{2-}$. The other group contains heteropeptides in the molecular ratio of 1:1 (e.g., $[Thr_2+His_2-3H]^{3-}$ and $[Cys+Phg-2H]^{2-}$ at *m/z* 163.7 and 126.6, respectively.

Conclusions

The experimental results presented in this study show that with each investigated α-amino acid pair (*L*-Met-*L*-Ser, *L*-His-*L*-Thr, and *L*-Cys-*L*-Phg), synchronization of the oscillatory concentration changes of the monomeric amino acids is observed, witnessing to mutual cross-catalysis of the two counterparts. These results serve as an experimental confirmation of case 4 of the theoretical model presented elsewhere. Case 4 seems to be the most physical one from the point of view of the law of mass action, because it anticipates intermolecular interactions among all molecules present in a given system. Additional experimental support is provided by the mass spectrometric evidence on the heteropeptide formation with each investigated binary system. An effect of molecular structure of the amino acids involved (and more specifically, the shielding effect of the $–NH_2$ and –COOH functionalities with aliphatic chains) on an overall dynamics of peptidization is perceptible as well as an influence of the other functionalities present in certain molecules (–OH with *L*-Thr and –SH with *L*-Cys).

Acknowledgments We thank Prof. Irving R. Epstein for enlightening discussions of the dynamics of amino acid condensation in binary solutions. One author (A.G.) acknowledges the financial support of the DoktoRIS project, co-financed by the European Union within the European Social Found.

Open Access This article is distributed under the terms of the Creative Commons Attribution 4.0 International License (http://creativecommons.org/licenses/by/4.0/), which permits unrestricted use, distribution, and reproduction in any medium, provided you give appropriate credit to the original author(s) and the source, provide a link to the Creative Commons license, and indicate if changes were made.

References

1. Sajewicz M, Piętka R, Pieniak A, Kowalska T (2005) Acta Chromatogr 15:131–149
2. Sajewicz M, Grygierczyk G, Gontarska M, Kowalska T (2007) J Liq Chromatogr Relat Technol 30:2185–2192
3. Sajewicz M, Kronenbach D, Gontarska M, Wróbel M, Pietka R, Kowalska T (2009) J Planar Chromatogr-Mod TLC 22:241–248
4. Sajewicz M, Gontarska M, Wojtal Ł, Kronenbach D, Leda M, Epstein IR, Kowalska T (2008) J Liq Chromatogr Relat Technol 31:1986–2005
5. Sajewicz M, Gontarska M, Kronenbach D, Berry E, Kowalska T (2012) J Chromatogr Sci 50:237–244
6. Sajewicz M, Matlengiewicz M, Leda M, Gontarska M, Kronenbach D, Kowalska T, Epstein IR (2010) J Phys Org Chem 23:1066–1073

7. Sajewicz M, Dolnik M, Kronenbach D, Gontarska M, Kowalska T, Epstein IR (2011) J Phys Chem A 115:14331–14339
8. Stich M, Blanco C, Hochberg D (2013) Phys Chem Chem Phys 15:255–261
9. Plasson R, Bersini H, Commeyras A (2004) Proc Natl Acad Sci USA 101:16733–16738
10. Hyver C (1985) J Chem Phys 83:850–851
11. Bykov VI, Gorban AN (1987) Chem Eng Sci 42:1249–1251
12. Peacock-Lopez E, Radov DB, Flesner CS (1997) Biophys Chem 65:171–178
13. Dolnik M, Sajewicz M, Kowalska T, Epstein IR (2014) RSC Adv 4:7330–7339
14. Godziek A, Maciejowska A, Talik E, Wrzalik R, Sajewicz M, Kowalska T (2016) Curr Protein Pept Sci **(in press)**
15. Maciejowska A, Godziek A, Sajewicz M, Kowalska T (2017) Acta Chromatogr. doi:10.1556/1326.2017.29.1.00
16. Godziek A, Maciejowska A, Talik E, Sajewicz M, Kowalska T (2015) J Planar Chromatogr-Mod TLC 28:144–151
17. Carny O, Gazit E (2005) FASEB J 19:1051–1055

Journal of Chromatographic Science, 2016, Vol. 54, No. 7, 1090–1095
doi: 10.1093/chromsci/bmw036
Advance Access Publication Date: 14 March 2016
Article

Article

Dynamics of Spontaneous Peptidization of L-, D- and DL-Serine in an Abiotic Solution as Investigated with Use of TLC-Densitometry and the Auxiliary Chromatographic Techniques

Agnieszka Godziek, Anna Maciejowska, Mieczysław Sajewicz, and Teresa Kowalska*

Institute of Chemistry, University of Silesia, 9 Szkolna Street, Katowice 40-006, Poland

*Author to whom correspondence should be addressed. Email: teresa.kowalska@us.edu.pl

Received 13 December 2015; Revised 9 February 2016

Abstract

From our earlier investigations, it comes out that proteinogenic amino acids can undergo spontaneous oscillatory reactions of chiral inversion and peptidization. L-Serine (L-Ser) is an important proteinogenic amino acid with many vital functions in human and mammalian organisms, e.g., it is responsible for good condition of the nervous cell membranes. It undergoes spontaneous oscillatory processes of chiral inversion and peptidization, and the goal of this study was to compare the dynamics of its peptidization with that of D-Ser and DL-Ser (racemate). The main analytical technique used in our experiment was TLC-densitometry, and the auxiliary chromatographic techniques were HPLC–evaporative light scattering detector and LC–MS. The results obtained witness to the differences in peptidization dynamics of the two Ser enantiomers (L and D) and of the racemic mixture thereof (DL). It was shown that DL-Ser characterizes with the higher, and L- and D-Ser with the lower peptidization yields.

Introduction

The research on spontaneous oscillatory chiral conversion of the low-molecular-weight carboxylic acids was initiated a decade ago with an article demonstrating this phenomenon upon an example of *S*(+)-ibuprofen (1), and later it was confirmed as a general phenomenon with a selection of other compounds from the groups of profen drugs, hydroxyl acids and amino acids (e.g., (2–4)). Then, it was found out that spontaneous oscillatory chiral conversion of the aforementioned compounds is accompanied by spontaneous oscillatory condensation of the same compounds and the two processes are running in the parallel (5–7). Studies (1–7) furnish general information on possible molecular mechanisms of these two oscillatory processes, which involve a non-chiral enol/enolate ion intermediary step and can be illustrated by the scheme given in Figure 1A (for the sake of this study, showing an example of L-Ser).

So far, spontaneous peptidization of amino acids in abiotic media has not attracted sufficient interest from the side of the amino acid and protein researchers and an evident proof of this lack of interest is, e.g., a poor choice of the HPLC columns available on the market and dedicated to the enantioseparation of native, underivatized amino acids. In the past, spontaneous peptidization of amino acids has been sporadically investigated, and mostly by those interested in abiogenesis and the development of a prebiotic universe under the environmental conditions stimulating the origin of biological life. In model experiments, the employed working conditions used to be quite drastic, in order to reproduce the terrestrial or extraterrestrial environments from before the millennia. Among the best-known experiments are those performed by Fox and Harada, and dealing with thermal copolymerization of amino acids to the products resembling proteins and therefore denoted as proteinoids (8, 9).

Our interest in spontaneous oscillatory processes running in abiotic liquid systems and involving amino acids resulted in the investigation of chiral conversion (10, 11) and peptidization (e.g., (12–15)), using mainly TLC-densitometry (11–13) and HPLC (14–16) with

© The Author 2016. Published by Oxford University Press. All rights reserved. For Permissions, please email: journals.permissions@oup.com

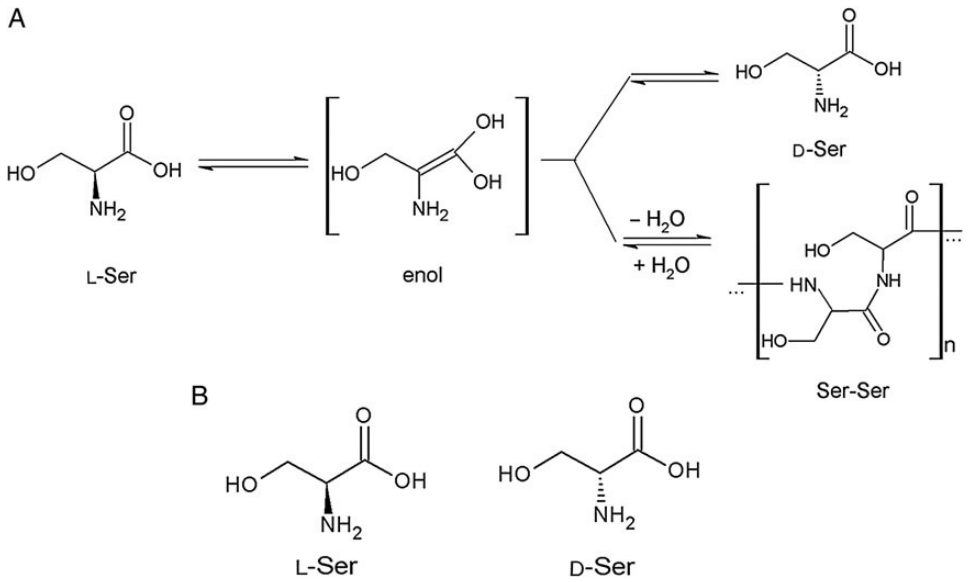

Figure 1. (A) The parallel processes of chiral conversion and peptidization of L-Ser; and (B) chemical structures of L-Ser and D-Ser.

different detectors [diode array detector (DAD), evaporative light scattering (ELSD) and MS] as analytical tools. In some of these investigations, we focused on peptidization of binary amino acid mixtures and a possibility of the heteropeptide formation (e.g., (14, 16, 17)). Selection of the binary amino acid mixtures (e.g., L-Pro-L-Phe, L-Hyp-L-Phe, and L-Pro-L-Hyp) with different peptidization dynamics of each counterpart was deliberate, in order to trace its impact on an overall dynamics of co-peptidization. In the study of Sajewicz *et al.* (16), a theoretical model was developed extensively discussing four logical cases of peptidization dynamics with two different amino acids present in the solution. Case 1 does not assume any intermolecular interactions between the two counterparts, which results in formation of homopeptides only. In that case, peptidization dynamics of the two amino acids resembles those of pure amino acids in monocomponent solutions. Cases 2–4 anticipate different cooperative effects with (i) one amino acid governing an overall peptidization dynamics, (ii) another amino acid governing an overall peptidization dynamics and (iii) peptidization dynamics in the mixture different from those valid for the single peptidization counterparts.

Amino acid enantiomers are two different yet structurally very similar compounds. The aim of this study was to compare peptidization dynamics of two enantiomers in an abiotic solution versus their peptidization dynamics in a binary mixture. Moreover, we were searching for an experimental evidence of heteropeptide formation in an enantiomer mixture. Our choice was L- and D-Ser, because of the importance of the proteinogenic L-Ser as a building block of the mammalian and human proteins (Figure 1B). Our interest in Ser was instigated by a growing amount of information on an effective chiral conversion of L-Ser to D-Ser in various different brain regions of mammals under a catalytic influence of serine racemase (e.g., (18–20)). Although the role of this chiral conversion in the metabolic pathway is not yet fully understood, this finding undermines an established concept of L-homochirality of the mammalian and human proteins. Moreover, certain scientific reports point out to a possible role of D-Ser played in neuropsychiatric and neurodegenerative conditions (e.g., (21, 22)). Another interesting feature of L-Ser is its documented ability to relatively easily racemize, which was perceived by geochemists involved in the protein geochronological studies (23, 24).

Experimental

Reagents

In this experiment, we used L-Ser purchased from Reanal (Budapest, Hungary), and D-Ser and DL-Ser purchased from Sigma-Aldrich (St Louis, MO, USA). All amino acids were of analytical purity. Methanol, 1-propanol (Sigma-Aldrich, St. Louis, MO, USA) and 2-propanol (Merck, Darmstadt, Germany) were of HPLC purity. Ninhydrin, zinc (II) nitrate, glacial acetic acid and ammonia (PHH POCh, Gliwice, Poland) were also of analytical purity. Water was de-ionized and double distilled in our laboratory by means of the Elix Advantage model Millipore System (Molsheim, France).

TLC-densitometric comparison of peptidization yields with L-, D- and DL-Ser

Thin-layer chromatographic experiments were performed on the commercial 20 × 20 cm plates pre-coated with microcrystalline cellulose (Merck; cat. no. 1.05716). Concentrations of L-Ser, D-Ser and DL-Ser in 70% aqueous methanol were 1 mg mL^{-1} (i.e., 9.44×10^{-3} mol L^{-1}). The L-Ser solution in 70% aqueous methanol was used for the microscopic measurements as well.

Chromatographic plates were activated by heating for 30 min at 110°C prior to applying the amino acid samples. Just before the chromatographic analysis, zinc(II) nitrate was added to the six samples, i.e., to the fresh L-, D- and DL-Ser solutions, and the L-, D- and DL-Ser solutions after 11 days of aging (the molar ratio of amino acid-to-zinc(II) nitrate was 1:1). The 1-propanol–0.5% aqueous ammonia (7:3, v/v) mixture was used as the mobile phase. Samples were spotwise applied to the plates in the 5-μL aliquots, 1.5 cm apart and 1 cm above the lower edge of the plate. The chromatograms were developed to the distance of 7 cm, and the development time was ca. 2 h. After the development, the plates were dried and the chromatograms were visualized by spraying the plates with the 0.5% ninhydrin solution in 2-propanol, followed by heating for 5 min at 110°C.

The visualized chromatograms were densitometrically scanned with use of a Desaga (Heidelberg, Germany) model CD 60 densitometer

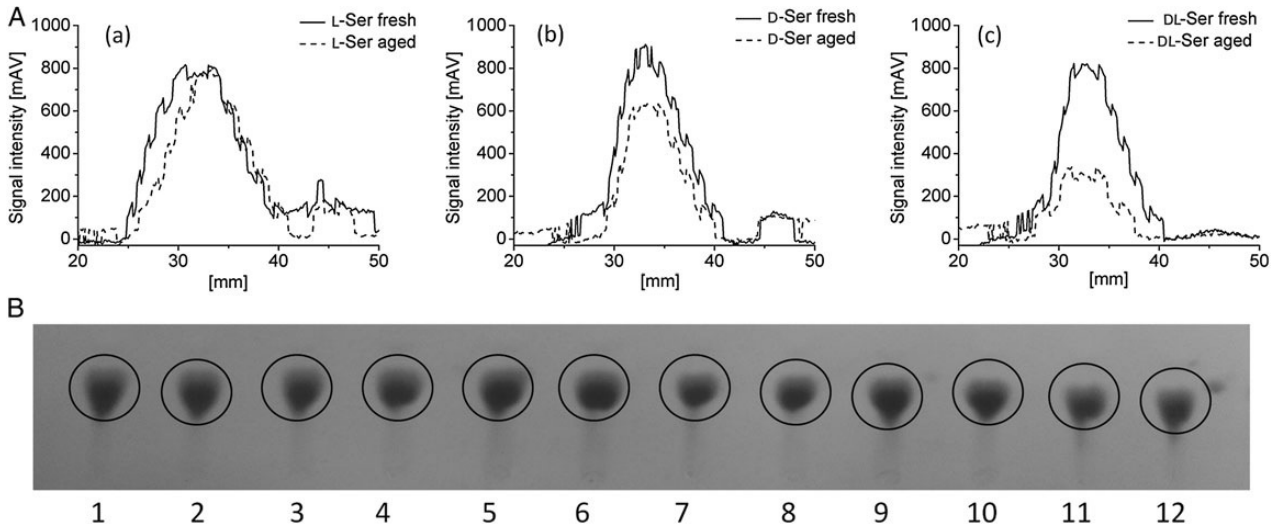

Figure 2. (A) Densitograms obtained for the freshly prepared solution of (a) L-Ser, (b) D-Ser and (c) DL-Ser, and for the solutions thereof stored for the period of 11 days. (B) Picture of the developed chromatogram, where (1, 2): freshly prepared L-Ser solution; (3, 4): L-Ser solution aged for 11 days; (5, 6): freshly prepared D-Ser solution; (7, 8): D-Ser solution aged for 11 days; (9, 10): freshly prepared DL-Ser solution and (11, 12): DL-Ser solution aged for 11 days.

equipped with the Windows-compatible ProQuant software. Concentration profiles of the development lanes were recorded in the reflectance mode at the carefully selected wavelength, $\lambda = 550$ nm. The obtained results were additionally recorded with a digital camera. All TLC experiments were performed in triplicate.

HPLC-ELSD comparison of peptidization dynamics with L-, D- and DL-Ser

Monitoring of spontaneous non-linear peptidization dynamics of L-, D- and DL-Ser was performed with use of the achiral HPLC-ELSD. The L-, D- and DL-Ser solutions were prepared in 70% aqueous methanol at the concentration equal to 1 mg mL^{-1} (i.e., 9.44×10^{-3} mol L^{-1}), then placed in an autosampler and recording of the chromatograms for the L-, D- and DL-Ser sample was carried out in the 8-min intervals for the period of 40 h. The analyses were carried out using the Varian model 920 liquid chromatograph equipped with the Varian 900-LC model autosampler, the gradient pump, the Varian Pro Star 510 model column oven, the Varian 380-LC model ELSD detector (Varian Inc., Palo Alto, CA, USA), the ThermoQuest Hypersil C18 (150 × 4.6 mm i.d.; 5 µm particle size) column and the Galaxie software for data acquisition and processing. Other working conditions are as follows: sample aliquots, 3 µL; mobile phase composition, acetonitrile–1% aqueous CH_3COOH (10:90, v/v); and mobile phase flow rate, 0.8 mL min^{-1} (in the isocratic mode). The column was thermostatted at 35°C.

MS evidence of peptidization of L-, D- and DL-Ser

To prove the presence of the peptides in the investigated amino acid solutions, the mass spectrometric analysis was performed for the samples of L-, D- and DL-Ser in 70% aqueous methanol, aged for 9 months. For this investigation, we used Thermo LCQ Deca XP Plus MS system (Thermo Scientific, Waltham, MA, USA) under the following working conditions: the ESI mode (ESI–MS scan, positive ionization, capillary voltage 50 V, needle voltage 5 kV and needle temperature 250°C). All MS experiments discussed in this study were performed at least in duplicate.

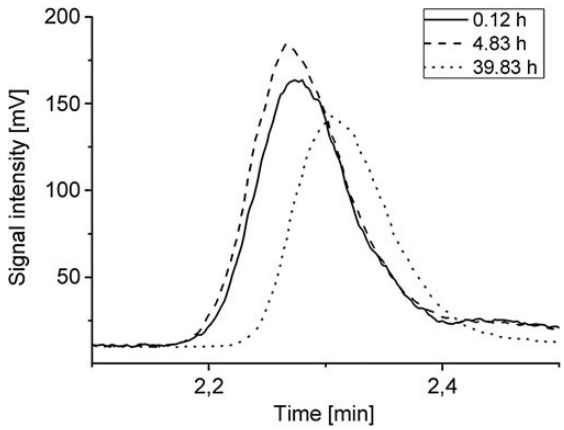

Figure 3. Superposition of the selected HPLC-ELSD chromatograms recorded for L-Ser in 70% aqueous methanol after 0.12, 4.83 and 39.83 h storage time.

Results

TLC-densitometric comparison of peptidization yields with L-, D- and DL-Ser

Different peptidization dynamics of L-, D- and DL-Ser dissolved in 70% methanol were demonstrated with use of the thin-layer chromatography. In Figure 2A, the densitograms are presented valid for the freshly prepared solutions of L-, D- and DL-Ser, and also for those aged for 11 days. In Figure 2B, the picture of the chromatogram is presented, showing the chromatographic spots of the freshly prepared solutions of L-, D- and DL-Ser, and also of those aged for 11 days. The retardation coefficient (R_F) values of the monomeric Ser (L, D and DL) are equal to 0.32 ± 0.02.

HPLC-ELSD comparison of peptidization dynamics with L-, D- and DL-Ser

The HPLC-ELSD technique was used to demonstrate the non-linear concentration changes of the investigated amino acids in the course of time, thus revealing an oscillatory nature of peptidization in the solutions of L-, D- and DL-Ser.

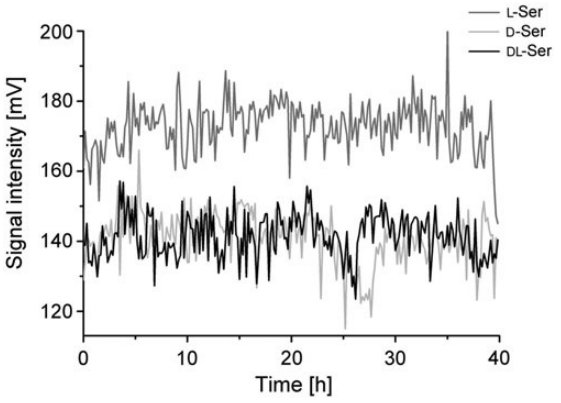

Figure 4. Time series of chromatographic peak heights for L-Ser, D-Ser and DL-Ser in 70% aqueous methanol registered with the ELSD detector.

In Figure 3, superposition is shown of three chromatograms valid for L-Ser and registered for the fresh sample (after 0.12 h aging) and for those after 4.8 and 39.83 h aging. In Figure 4, we show the time series of the peak heights registered for the L-, D- and DL-Ser samples in the course of 40 h aging.

MS evidence of peptidization of L-, D- and DL-Ser

The mass spectrometric results prove that amino acids stored in an abiotic environment undergo spontaneous peptidization. In Figures 5A–C, the mass spectra that were recorded for the L-Ser, D-Ser and DL-Ser samples stored for the period of 9 months are given.

Discussion

TLC-densitometric comparison of peptidization yields with L-, D- and DL-Ser

First, it has to be emphasized that the enantioseparation of amino acids still is a very challenging analytical task. However, TLC-densitometry of amino acids and, more specifically, the enantioresolution thereof can be achieved in a more straightforward and easier manner than with the other chromatographic techniques. There are at least two reasons, which justify this statement. One reason is that for the direct enantioseparation of amino acids (i.e., for that without a preliminary derivatization) only one chiral HPLC column is available on the market, whereas TLC-densitometry offers a possibility of an in-home preparation of a wide selection of dedicated and reasonably well-performing chiral stationary phases and/or a variety of specially devised mobile phases. Another reason is that the enantioresolution of chiral counterparts obtained with aid of TLC-densitometry is preserved on a chromatographic plate, thus enabling further investigations. This conclusion is based on our long-time experience, and it can also be derived from the monograph on chromatographic analysis of amino acids, with a considerable part dedicated to the achievements of the enantioseparation with aid of TLC-densitometry (25).

From our earlier investigations, it comes out that amino acids can undergo spontaneous oscillatory inversion and peptidization (although Ser has never been investigated before). The current comparison of the Ser enantiomers shows that the peptidization dynamics of L-, D- and DL-Ser dissolved in 70% aqueous methanol considerably differ. Investigations with use of TLC revealed that the most dynamic peptidization process takes place with the racemic Ser mixture (DL-Ser). Namely, the band intensity of the monomeric DL-Ser obtained for the fresh sample equaled to 836.45 mAV, and the analogous signal obtained from the aged sample equaled to 332.86 mAV only, showing a concentration drop equal to 503.59 mAV (Figure 2A-C). In the case of D-Ser, the analogous band intensity values were 958.00 and 621.08 mAV, respectively, with the band intensity drop equal to 336.92 mAV, which is a proof of the lower peptidization yields (Figure 2A-B). The least dynamic peptidization was observed with L-Ser. In this case, band intensities of the monomeric L-Ser in the fresh sample and in that after 11 days aging were practically the same and equal to 824.87 mAV. It needs adding that chromatographic spots of the monomeric L-, D- and DL-Ser in the fresh and aged samples (visualized with ninhydrin; Figure 2B) do not show the effect of peptidization as clearly as do the respective densitograms.

HPLC-ELSD comparison of peptidization dynamics with L-, D- and DL-Ser

The superposition of the three chromatograms valid for L-Ser and registered for the fresh sample (after 0.12 h aging) and for those after 4.83 and 39.83 h aging (Figure 3) was made for the sake of comparison to emphasize the general trend of sample aging, which was the concentration drop of the monomeric L-Ser as a result of peptidization. The analogous trend was observed with D-Ser and DL-Ser, too.

In Figure 4, we showed the time series of the peak heights registered for the L-, D- and DL-Ser samples in the course of 40 h aging. From the obtained plots, it is evident that the amino acid concentrations were changing in a non-linear (oscillatory) fashion. Changes in the L-, D- and DL-Ser concentrations are well expressed in terms of the peak intensity changes. For L-, D- and DL-Ser, the respective oscillatory peak intensity ranges are 145.03–201.44, 114.90–165.90 and 123.40–157.10 mV. The oscillation range of the peak maxima valid for L-Ser is somewhat higher than those valid for D-Ser and DL-Ser. This result remains in conformity with those originating from TLC-densitometry as an additional proof that with D- and DL-Ser, higher peptidization yields are observed compared with L-Ser (and hence, the intensity ranges of the respective peak maxima for the monomeric D- and DL-Ser are lower than that valid for L-Ser).

MS evidence of peptidization of L-, D- and DL-Ser

Mass spectra obtained for L-, D- and DL-Ser confirm differentiated peptidization dynamics with these three amino acids. From the TLC results, a conclusion can be drawn that the peptidization rate with DL-Ser is the higher one, whereas peptidization rates with L-Ser and D-Ser are lower. From Figures 5A and B, it can be seen that the mass spectra valid for the aged L- and D-Ser samples after the 9-month storage period are quite similar to one another in this sense that relative intensities of the respective peptides are rather low when compared against the predominant molecular ion at *m/z* 105.9. In Figure 5C, the mass spectrum valid for the DL-Ser sample is given, with the predominant molecular ion at *m/z* 105.9, yet with relative intensities of the spontaneously formed peptides considerably higher than those observed for individual enantiomers (Figures 5A and B). Moreover, in Figures 5A–C the tabulated proposals are presented of the possible peptide structures attributed to the selected *m/z* signals in the respective mass spectra. In certain cases, the numbers of the corresponding peptide bonds (–CO–NH–) are equal to several dozens.

Conclusion

The goal of this study was to demonstrate different peptidization dynamics of L-, D- and DL-Ser, and it was obtained with the use of the TLC-densitometry as the main analytical technique, and HPLC-ELSD

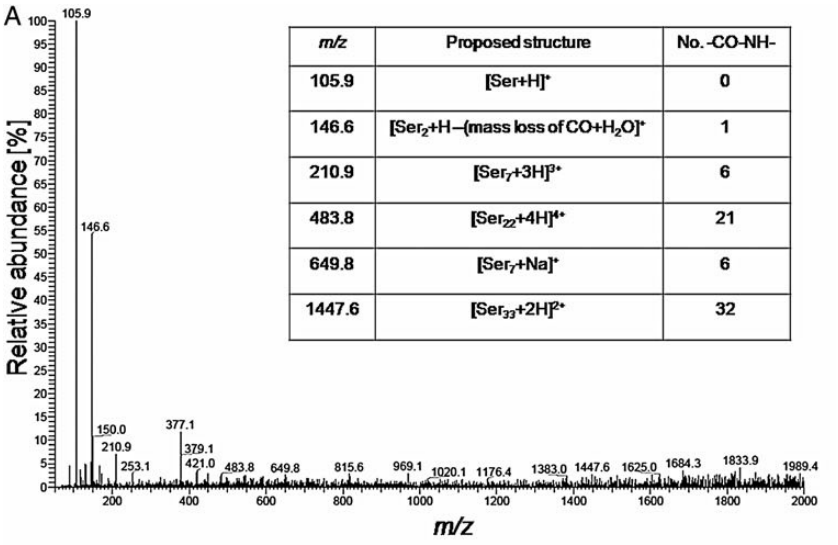

m/z	Proposed structure	No. -CO-NH-
105.9	$[Ser+H]^+$	0
146.6	$[Ser_2+H-(mass\ loss\ of\ CO+H_2O)]^+$	1
210.9	$[Ser_7+3H]^{3+}$	6
483.8	$[Ser_{22}+4H]^{4+}$	21
649.8	$[Ser_7+Na]^+$	6
1447.6	$[Ser_{33}+2H]^{2+}$	32

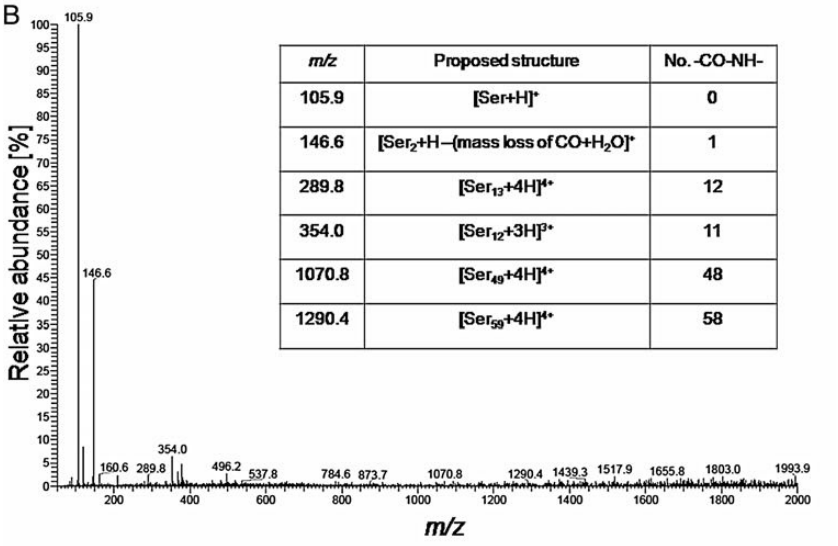

m/z	Proposed structure	No. -CO-NH-
105.9	$[Ser+H]^+$	0
146.6	$[Ser_2+H-(mass\ loss\ of\ CO+H_2O)]^+$	1
289.8	$[Ser_{13}+4H]^{4+}$	12
354.0	$[Ser_{12}+3H]^{3+}$	11
1070.8	$[Ser_{49}+4H]^{4+}$	48
1290.4	$[Ser_{59}+4H]^{4+}$	58

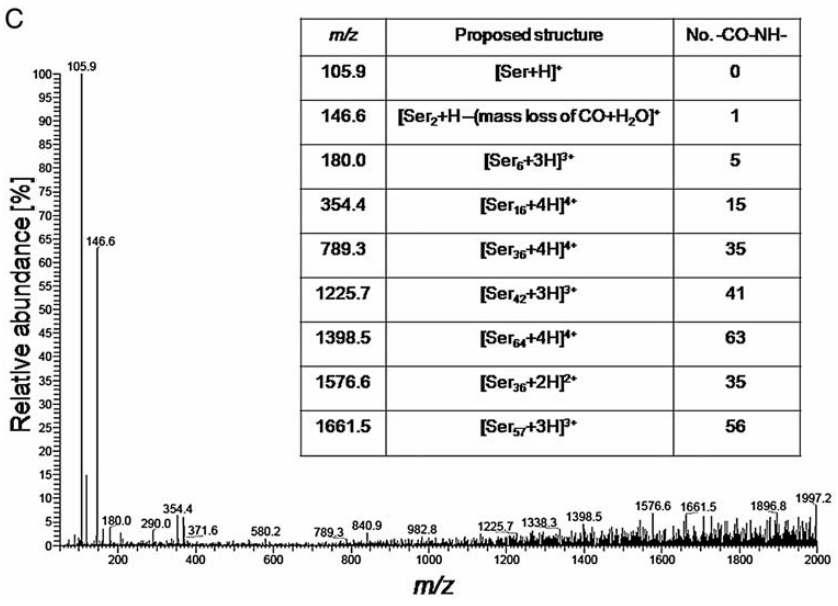

m/z	Proposed structure	No. -CO-NH-
105.9	$[Ser+H]^+$	0
146.6	$[Ser_2+H-(mass\ loss\ of\ CO+H_2O)]^+$	1
180.0	$[Ser_6+3H]^{3+}$	5
354.4	$[Ser_{16}+4H]^{4+}$	15
789.3	$[Ser_{36}+4H]^{4+}$	35
1225.7	$[Ser_{42}+3H]^{3+}$	41
1398.5	$[Ser_{64}+4H]^{4+}$	63
1576.6	$[Ser_{36}+2H]^{2+}$	35
1661.5	$[Ser_{57}+3H]^{3+}$	56

Figure 5. Mass spectra registered with use of LC–MS and implemented with the tabulated interpretation of the selected *m/z* signals for the aged samples of (A) L-Ser, (B) D- and (C) DL-Ser, respectively.

and LC–MS as the auxiliary chromatographic techniques. Although each chromatographic technique contributed in its own way to adding to a multidimensional picture of the phenomenon investigated, the experimental evidence furnished by TLC-densitometry can be regarded as the most straightforward and therefore the most comprehensive also. On the basis of the results originating from the three different chromatographic techniques, it was unequivocally established that DL-Ser undergoes a more rapid spontaneous oscillatory peptidization process, whereas peptidization of L- and D-Ser is perceptibly slower. At this stage, the reason for the difference in peptidization rates between L- and D-Ser is not yet clear.

Acknowledgment

A.G. acknowledges the financial support of the DoktoRIS project, co-financed by the European Union within the European Social Fund.

References

1. Sajewicz, M., Piętka, R., Pieniak, A., Kowalska, T.; Application of thin-layer chromatography (TLC) to investigating oscillatory instability of the selected profen enantiomers; *Acta Chromatography*, (2005); 15: 131–149.
2. Sajewicz, M., Grygierczyk, G., Gontarska, M., Kowalska, T.; Enantioseparation of *S,R*-(±)-ketoprofen on plain silica gel layers with achiral mobile phase; *Journal of Liquid Chromatography & Related Technologies*, (2007); 30(15): 2185–2192 (special TLC issue).
3. Sajewicz, M., Kronenbach, D., Gontarska, M., Wróbel, M., Pietka, R., Kowalska, T.; TLC in search for structural limitations of spontaneous oscillatory in-vitro chiral conversion. α-hydroxybutyric and mandelic acids; *Journal of Planar Chromatography—Modern TLC*, (2009); 22: 241–248.
4. Sajewicz, M., Gontarska, M., Wojtal, Ł., Kronenbach, D., Leda, M., Epstein, I.R., *et al*. Experimental and model investigation of the oscillatory transenantiomerization of L-*α*-phenylalanine; *Journal of Liquid Chromatography & Related Technologies*, (2008); 31(13): 1986–2005 (special TLC issue).
5. Sajewicz, M., Gontarska, M., Kronenbach, D., Berry, E., Kowalska, T.; An HPLC–DAD and LC–MS study of condensation oscillations with *S* (+)-ketoprofen dissolved in acetonitrile; *Journal of Chromatographic Science*, (2012); 50: 237–244.
6. Sajewicz, M., Matlengiewicz, M., Leda, M., Gontarska, M., Kronenbach, D., Kowalska, T., *et al*. Spontaneous oscillatory in vitro chiral conversion of simple carboxylic acids and its possible mechanism; *Journal of Physical Organic Chemistry*, (2010); 23: 1066–1073.
7. Sajewicz, M., Dolnik, M., Kronenbach, D., Gontarska, M., Kowalska, T., Epstein, I.R.; Oligomerization oscillations of L-lactic acid in solutions; *The Journal of Physical Chemistry A*, (2011); 115: 14331–14339.
8. Fox, S.W., Harada, K.; Thermal copolymerization of amino acids to a product resembling protein; *Science*, (1958); 128: 1214.
9. Fox, S.W.; The chemical problem of spontaneous generation; *Journal of Chemical Education*, (1957); 34: 472–479.
10. Sajewicz, M., Gontarska, M., Kowalska, T.; HPLC/DAD evidence of the oscillatory chiral conversion of phenylglycine; *Journal of Chromatographic Science*, (2014); 52: 329–333.
11. Godziek, A., Maciejowska, A., Talik, E., Sajewicz, M., Kowalska, T.; Thin-layer chromatographic investigation of L-cysteine in solution; *Journal of Planar Chromatography—Modern TLC*, (2015); 28: 144–151.
12. Sajewicz, M., Matlengiewicz, M., Juziuk, M., Penkala, M., Weloe, M., Schulz, M., *et al*. Thin-layer chromatographic evidence of proline peptidization in solution and its thin-layer chromatographic enantioseparation; *Journal of Liquid Chromatography & Related Technologies*, (2013); 36 (17): 2497–2511 (special TLC issue).
13. Godziek, A., Maciejowska, A., Sajewicz, M., Kowalska, T.; Spontaneous chiral conversion and peptidization of amino acids traced by means of TLC–MS. In Kowalska, T., Sajewicz, M., Sherma, J. (eds). *Planar chromatography—mass spectrometry*, Chromatographic Science Series, Vol. 110. CRC Press, Francis and Taylor, Boca Raton, USA, (2015), pp. 345–366. , ISBN: 9781498705882.
14. Sajewicz, M., Godziek, A., Maciejowska, A., Kowalska, T.; Condensation dynamics of the L-Pro-L-Phe and L-Hyp-L-Phe binary mixtures in solution; *Journal of Chromatographic Science*, (2015); 53: 31–37.
15. Godziek, A., Maciejowska, A., Sajewicz, M., Kowalska, T.; HPLC monitoring of spontaneous non-linear peptidization dynamics of selected amino acids in solution; *Journal of Chromatographic Science*, (2015); 53: 401–410.
16. Sajewicz, M., Dolnik, M., Kowalska, T., Epstein, I.R.; Condensation dynamics of L-proline and L-hydroxyproline in solution; *RSC Advances*, (2014); 4: 7330–7339.
17. Godziek, A., Maciejowska, A., Talik, E., Wrzalik, R., Sajewicz, M., Kowalska, T.; On spontaneously pulsating proline—phenylalanine peptide microfibers; *Current Protein & Peptide Science*, (2016); 17: 106–116.
18. Wolosker, H., Sheth, K.N., Takahashi, M., Mothet, J.P., Brady, R.O. Jr., Ferris, C.D., *et al*. Purification of serine racemase: biosynthesis of the neuromodulator D-serine; *Proceedings of the National Academy of Sciences of the United States of America*, (1999); 96: 721–725.
19. Baumgart, F., Rodriguez-Crespo, I.; D-Amino acids in the brain: the biochemistry of brain serine racemase; *FEBS Journal*, (2008); 275: 3538–3545.
20. Wolosker, H., Dumin, E., Balan, L., Foltyn, V.N.; D-Amino acids in the brain: D-serine in neurotransmission and neurodegeneration; *FEBS Journal*, (2008); 275: 3514–3526.
21. Goff, D.C., Coyle, J.T.; The emerging role of glutamate in the pathophysiology and treatment of schizophrenia; *The American Journal of Psychiatry*, (2001); 158: 1367–1377.
22. Mothet, J.P., Rouaud, E., Sinet, P.M., Potier, B., Jouvenceau, A., Dutar, P., *et al*.; A critical role for the glial-derived neuromodulator D-serine in the age related deficits of cellular mechanisms of learning and memory; *Aging Cell*, (2006), 5: 267–274.
23. Demarchi, B., Collins, M., Bergstrom, E., Dowle, A., Penkman, K., Thomas-Oates, J., *et al*. New experimental evidence for in-chain amino acid racemization of serine in a model peptide; *Analytical Chemistry*, (2013); 85: 5835–5842.
24. Kaiser, K., Brenner, R.; Hydrolysis-induced hydrolysis of amino acids; *Limnology Oceanography Methods*, (2005); 3: 318–325.
25. Bhushan, R., Martens, J.; *Amino acids: chromatographic separation and enantioresolution*. HBN Publishing, New York, USA, (2010).

Journal of Chromatographic Science, 2016, Vol. 54, No. 8, 1301–1309
doi: 10.1093/chromsci/bmw073
Advance Access Publication Date: 4 May 2016

Article

Spontaneous Pulsation of Peptide Microstructures in an Abiotic Liquid System

Anna Maciejowska[1], Agnieszka Godziek[1], Ewa Talik[2], Mieczysław Sajewicz[1], Teresa Kowalska[1,*], and Irving R. Epstein[3]

[1]Department of General Chemistry and Chromatography, Institute of Chemistry, University of Silesia, 9 Szkolna Street, Katowice, Poland, [2]Department of Physics of Crystals, University of Silesia, 4 Uniwersytecka Street, 40-007 Katowice, Poland, and [3]Department of Chemistry, Brandeis University, MS 015, Waltham, MA 02454-9110, USA

*Author to whom correspondence should be addressed. Email: teresa.kowalska@us.edu.pl

Received 17 July 2015; Revised 19 March 2016

Abstract

We report observations of pulsating peptide formation and depeptidization in 70% aqueous acetonitrile solutions of L-Pro-L-Phe and L-Cys, resulting in the oscillatory appearance and disappearance of solid masses of microfibers and microspheres, respectively. We monitor the concentration changes of the monomeric amino acids by high-performance liquid chromatography. The concentration of all amino acid solutions used is 1.0 mg mL^{-1}, due to solubility limitations in 70% aqueous acetonitrile. The nonlinear concentration changes of L-Pro, L-Phe and L-Cys, and the amounts of the main peptidization products observed within our monitoring periods (for L-Pro–L-Phe, 250 h, and for L-Cys, 70 h) are typically from several to 20% of the original monomer concentrations. We follow the formation and decay of the insoluble peptides by turbidimetry. We also investigate the materials formed using scanning electron microscopy and mass spectrometry. We carry out numerical simulations on a simple model that reflects the main features of spontaneous pulsation of peptide fiber or sphere formation in this abiotic liquid system.

Introduction

The formation of oligomers and polymers from monomeric building blocks is one of the key steps in most scenarios proposed for the origin and evolution of life. In particular, the formation of peptides from amino acids is of considerable interest, as is the question of how a preference for a single chirality may have developed in the earliest life forms.

In earlier work, we reported the spontaneous oscillatory chiral conversion of several classes of monomeric species (1–3), including amino acids (4), after a period of storage in aqueous or nonaqueous solvents. Two general schemes have been suggested to explain chiral conversion of such compounds, depending on the polarity of the solvent. In aqueous solutions, the assumed conversion pathway is via the enolate ion (5), and in anhydrous media or in the presence of small amounts of water, the probable mechanism of chiral conversion is via the enol structure (6).

Our earlier investigations revealed that the oscillatory chiral conversion of low molecular weight carboxylic acids occurs in parallel with oscillatory condensation. The parallel processes of chiral conversion and peptidization of amino acids can be illustrated by Scheme 1 (7).

In seeking to understand oscillatory condensation in three binary amino acid systems (L-Pro–L-Hyp, L-Pro–L-Phe and L-Hyp–L-Phe) dissolved in aqueous organic solvents (8, 9), we developed a theoretical model (8) of spontaneous peptidization in binary amino acid systems that include heteropeptide formation. The model allows for various degrees of cooperativity and control of the dynamics by one or both monomeric species.

To date, our experimental studies of spontaneous oscillatory chiral conversion and oscillatory condensation have been carried out in single-phase liquid systems, and our only analytical tool to monitor the changing concentration of the starting reagent(s) (e.g., an optically pure enantiomeric amino acid) has been high-performance liquid chromatography (HPLC). We have noted, however, that longer (several weeks or months) storage periods of such compounds can result in precipitation of higher *n*-mers as peptide nano- and microstructures, insoluble in our solvent system. In the two-phase systems thus formed,

© The Author 2016. Published by Oxford University Press. All rights reserved. For Permissions, please email: journals.permissions@oup.com

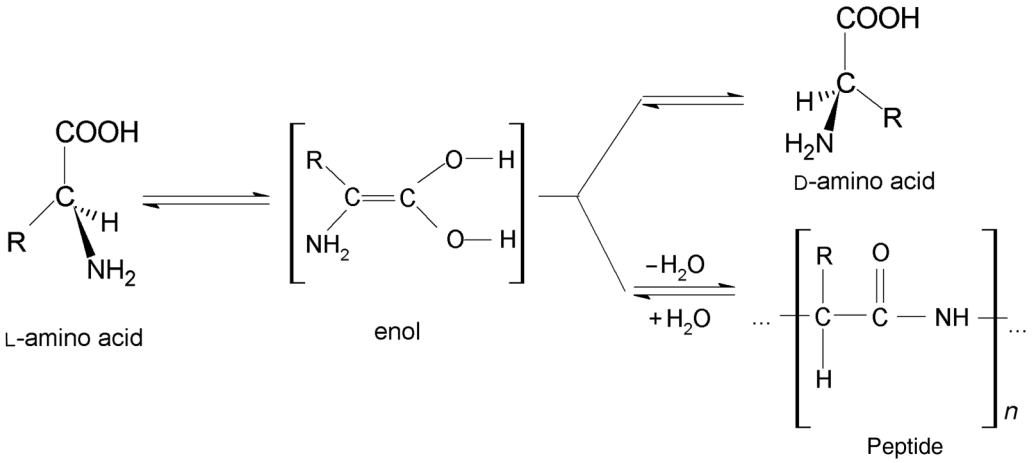

Scheme 1. Chiral conversion and peptidization of an amino acid molecule running in the parallel.

additional analytical tools such as scanning electron microscopy, mass spetroscopy and turbidimetry can be utilized to characterize and monitor the solid particles. A preliminary study employing these additional analytical tools to investigate an apparent instability of the higher peptide *n*-mers was presented in paper (10). Stability, or at least controllable behavior, of peptide nano- and microstructures is an issue of vital importance, especially from the perspective of biotechnology. Short, linear self-assembling peptides with predictable behavior should be attractive as building blocks for nanodevices (11) such as nanocarriers for drug delivery or scaffolds for tissue engineering. The self-assembling properties of diphenylalanine (12), which is a fragment of the Alzheimer's β-amyloid protein, are of particular interest. On the other hand, reports have recently appeared of biocatalyzed dynamic instability of peptide nanofibers (13), and of the destructive role of certain solvents (particularly water and lower aliphatic alcohols), undermining the stability of diphenylalanine nanotubes (14, 15).

The aim of the present study is to systematically investigate the dynamics of the long-term peptidization of a binary amino acid sample (L-Pro–L-Phe) and a single amino acid sample (L-Cys) in an abiotic solution (70% acetonitrile + 30% water), in which accumulation of insoluble nano- and microstructures is observed. In both samples, we first noticed visually, and then confirmed by turbidimetry, spontaneous pulsations of sequentially increasing and decreasing amounts of solid. To our knowledge, this is the first systematic investigation of such an effect in an abiotic liquid system. Schematic illustration of a reversible change from a lower molecular weight soluble species (fully dissolved in the one-phase system) to a higher molecular weight insoluble species is given in Figure 1 , along with snapshots of the one- and two-phase systems.

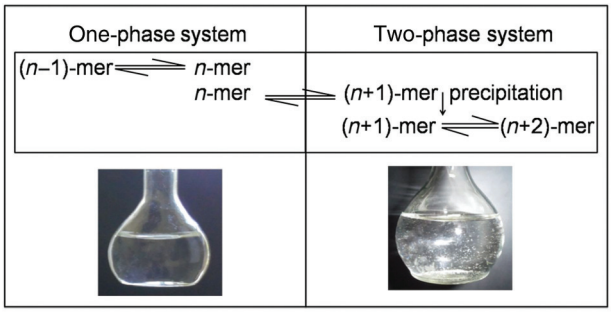

Figure 1. Schematic illustration of pulsating instability of peptide nano- and microstructures as a reversible change from a lower molecular weight soluble species (dissolved in the one-phase system) to a higher molecular weight insoluble species (precipitated to give a two-phase system).

Experimental

Reagents

L-Proline (L-Pro), L-phenylalanine (L-Phe) and L-cysteine (L-Cys) were purchased from Sigma-Aldrich, Merck and Reanal, respectively. All amino acids were of analytical purity, acetonitrile was of HPLC purity (J.T. Baker) and water was deionized and double distilled by means of an Elix Advantage Millipore system.

The binary L-Pro–L-Phe solution in 70% aqueous acetonitrile used in the 250 h ("short") chromatographic experiment had a concentration of 1.0 mg mL^{-1} (8.69×10^{-3} mol L^{-1}) L-Pro and 1.0 mg mL^{-1} (6.05×10^{-3} mol L^{-1}) L-Phe. The binary L-Pro–L-Phe solution in 70% aqueous acetonitrile stored for up to 1 year ("long" term) and used for the mass spectrometric, scanning electron microscopic and turbidimetric measurements had a concentration of 10 mg mL^{-1} (8.69×10^{-2} mol L^{-1}) L-Pro and 10 mg mL^{-1} (6.05×10^{-2} mol L^{-1}) L-Phe. The L-Cys solution in 70% aqueous acetonitrile (stored for up to 26 days and used for all measurements) had a concentration of 0.7 mg mL^{-1} (5.77×10^{-3} mol L^{-1}). All samples were stored at 21 ± 1°C.

High-performance liquid chromatography with evaporative light scattering detection

We employed high-performance liquid chromatography with evaporative light scattering detection (HPLC-ELSD) to separate peptides from monomeric amino acids. The analyses were carried out using a Varian model 920 liquid chromatograph equipped with a 900-LC autosampler, gradient pump, 380-LC ELSD detector and Pursuit 5 C18 (5 μm particle size) Varian column (250 × 4.6 mm i.d.) for L-Pro–L-Phe, ThermoQuest Hypersil C18 column (150 × 4.6 mm i.d.; 5 μm particle size) for L-Cys and Galaxie software for data acquisition and processing. The chromatographic columns were thermostatted at 35°C using a Varian Pro Star 510 column oven.

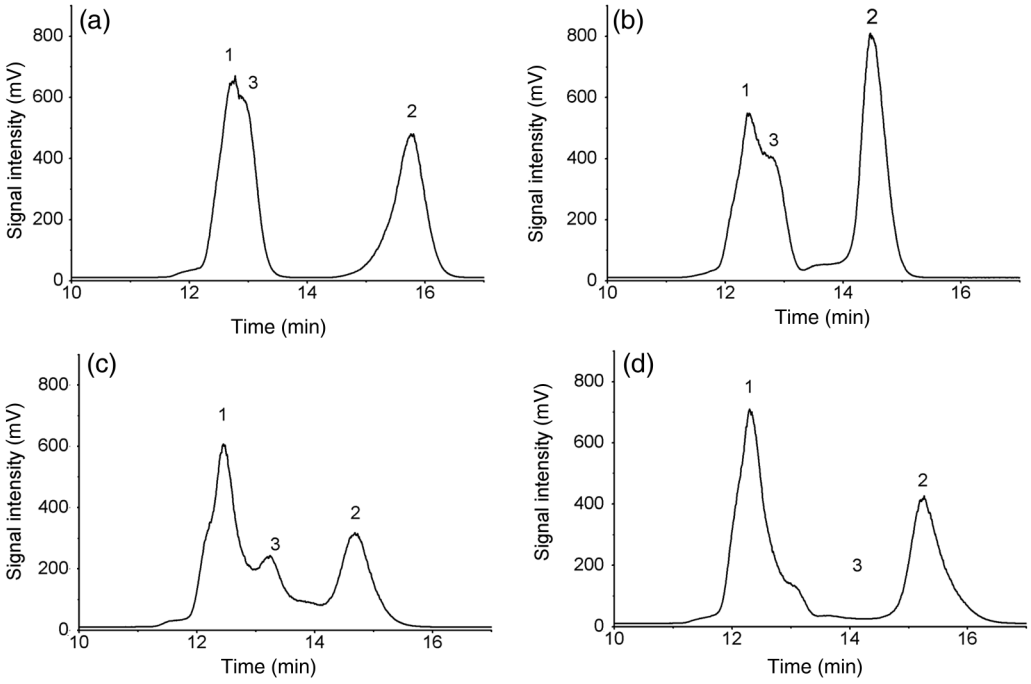

Figure 2. Examples of chromatograms obtained for the L-Pro–L-Phe system after (a) 4.00 h, (b) 28.20 h, (c) 74.40 h and (d) 206.80 h sample aging. (1) Pro, (2) Phe and (3) the main peptidization product.

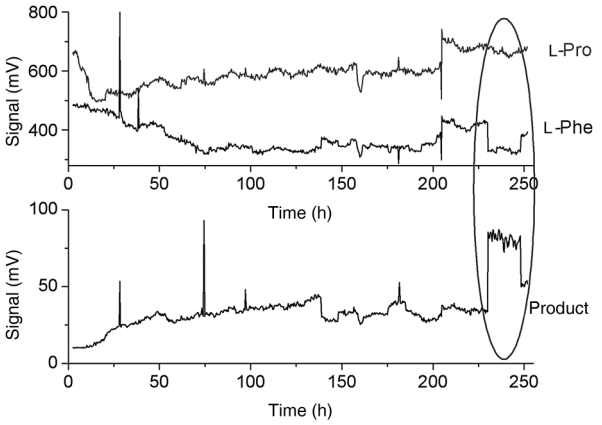

Figure 3. Time series of chromatographic peak heights for L-Pro, L-Phe and the main peptidization product in an L-Pro–L-Phe solution in 70% aqueous acetonitrile (registered over the course of 250 h). Plot fragment marked with an oval shows the time range with a simultaneous decrease of the Pro and Phe concentrations and an increase of the main peptidization product concentration (9).

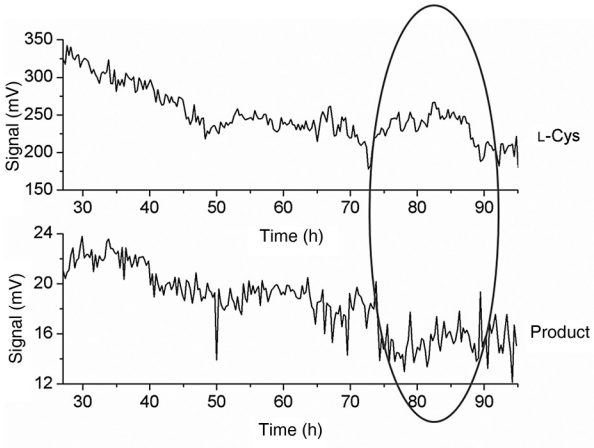

Figure 4. Time series of chromatographic peak heights for L-Cys and the main peptidization product in an L-Cys solution in 70% aqueous acetonitrile solution (registered in the range of 25–95 h). Plot fragment marked with an oval shows the time range with a simultaneous decrease of the Cys concentrations and an increase of the main peptidization product concentration (16).

With the L-Pro–L-Phe sample, chromatographic analyses were carried out for 250 h at 20-min intervals in the isocratic mode. We used 30 μL sample aliquots and a methanol–water (40 : 60, v/v) mobile phase at a flow rate of 0.25 mL min^{-1}. With L-Cys, the chromatographic analyses were carried out for 95 h at 10-min intervals in the isocratic mode using 10 μL sample aliquots and a methanol–water (80 : 20, v/v) mobile phase at a flow rate of 0.80 mL min^{-1}. In both cases, relatively short sampling time intervals were chosen in order to derive quasi-kinetic information about the oscillatory peptidization.

Mass spectrometry

All mass spectra were recorded in the positive ionization mode on a Varian MS-100 mass spectrometer (extended ESI-MS scan, positive ionization, spray chamber temperature 50°C, drying gas temperature 250°C, drying gas pressure 25 psi, capillary voltage 50 V, needle voltage 5 kV) for the 70% aqueous acetonitrile solutions of L-Pro–L-Phe and L-Cys, which contained the soluble peptide fraction only (the self-assembled microparticle suspensions were separated by sedimentation).

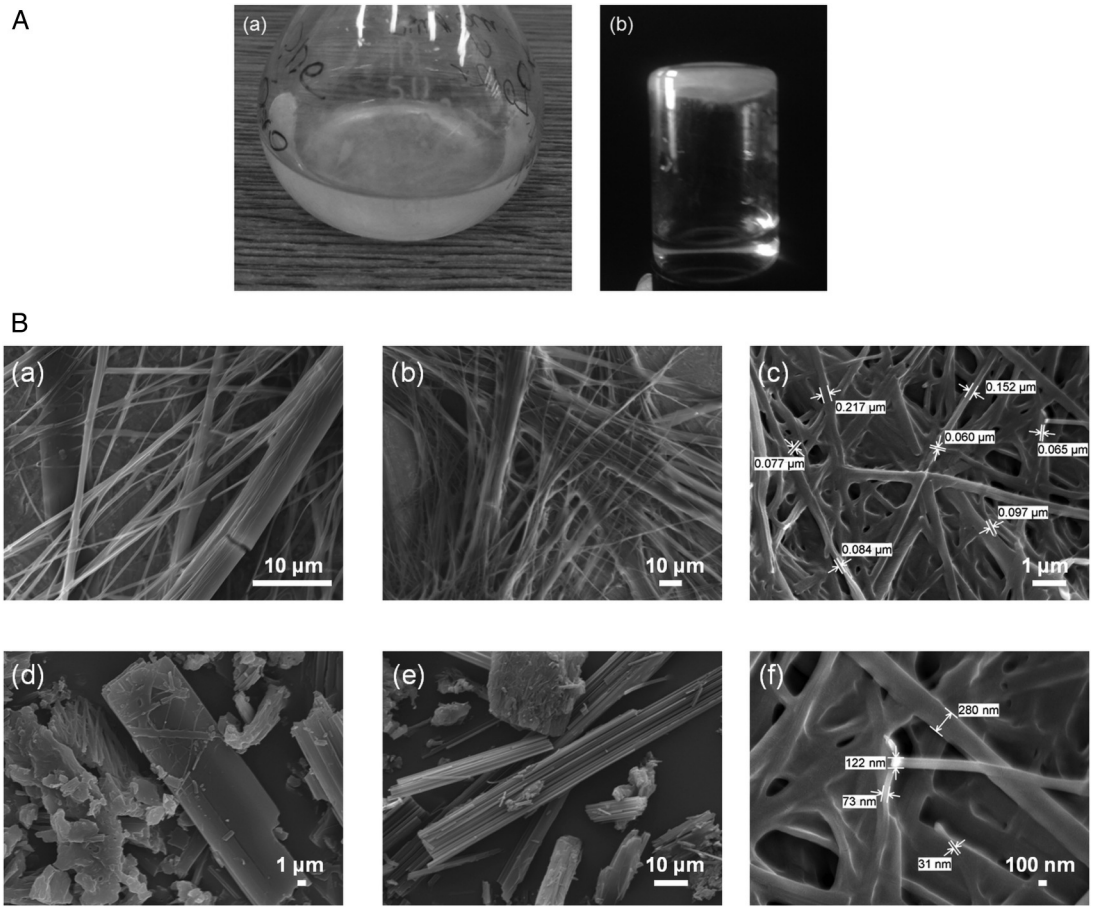

Figure 5. (A, a) Volumetric flask with Pro–Phe fibers suspended in solution; (b) the Pro–Phe fiber sediment in a vial turned upside down. (B, a–f): Scanning electron micrographs of Pro–Phe fibers from the solution residue evaporated to dryness, with a magnification of (a) ×2,700, (b) ×800, (c) ×13,000, (d) ×300, (e) ×1,300 and (f) ×30,000. In (c) and (f), the diameters of certain fibers are indicated.

Scanning electron microscopy

Visualization of nano- and microparticles was performed with a JEOL JSM-7600F model scanning electron microscope (SEM). With the Pro–Phe sample after a 1-year aging period and with Cys after 2 weeks of aging, visualization was performed for microparticles obtained from the respective solutions evaporated to dryness.

Turbidimetry

To obtain quantitative measurements of the nonlinear (pulsating) behavior of peptide nano- and microstructures, we performed measurements with a turbidity sensor (TRB-BTA, Vernier Software & Technology, Beaverton, OR, USA) that allowed continuous monitoring of turbidity. For these experiments, ~15 mL aliquots of the Pro–Phe and Cys solutions in 70% aqueous acetonitrile were freshly prepared and placed in the instrument vials. In both cases, the respective turbidity changes were continuously registered for 26 days. To confirm the qualitative reproducibility of the results, the turbidity measurements were repeated twice.

As the amino acid samples were dissolved in 70% aqueous acetonitrile, the stability of the turbidity was controlled for water, acetonitrile and 70% aqueous acetonitrile as reference solvents over the course of 1 day. In each case, the turbidity was quite stable.

Finally, we performed microbiological tests for the possible presence of microorganisms in the Pro–Phe and Cys liquid samples after storage periods of 1 year and 2 weeks, respectively, following the procedure described in detail in reference (10). These tests revealed no DNA in our samples, and we therefore concluded that they were free of any microorganisms.

Results

This study focuses mainly on the long-term aging of binary (L-Pro–L-Phe) and single (L-Cys) amino acid samples in an abiotic aqueous acetonitrile solution and, more specifically, on spontaneous formation of peptides up to the point of them becoming insoluble and hence precipitating. The shift from a homogeneous one-phase liquid system to an inhomogeneous two-phase liquid–solid system with insoluble higher molecular weight species floating in the solution revealed the intermittent formation and decay of higher peptides, as shown in Figure 1. We therefore sought to characterize this phenomenon by monitoring concentration changes of the monomeric amino acids in a short-term aging experiment by HPLC-ELSD (which is a challenging analytical task, due to the almost instantaneous appearance of peptides in gradually aging solutions and, consequently, to the need to separate them from the monomeric species, which is far from easy (16)). Examples of chromatograms that illustrate how we monitored concentration changes of the monomeric amino acids and the almost instantaneous appearance of peptide in a short-term aging experiment are shown in

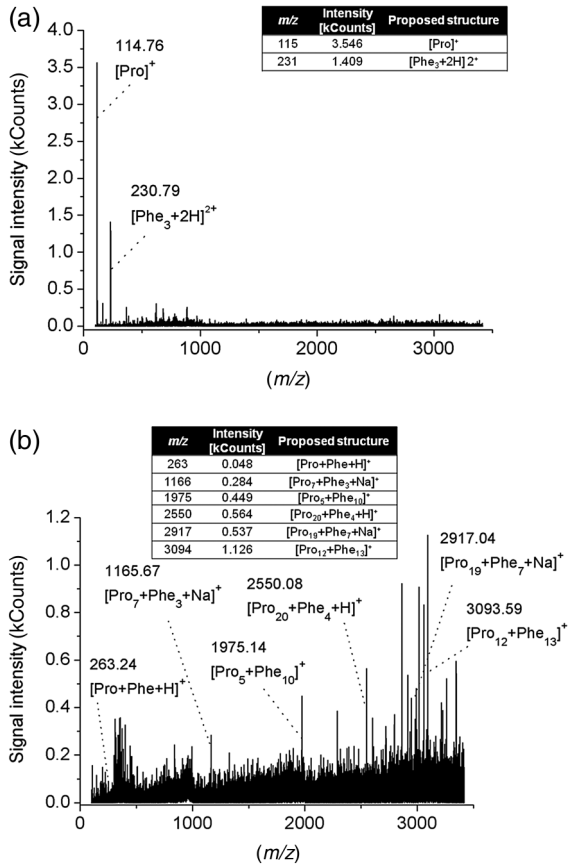

Figure 6. Mass spectra recorded for (a) fresh and (b) the 1-year-old Pro–Phe solution in 70% aqueous acetonitrile, and possible structures attributed to selected signals.

Figure 2 for the binary L-Pro–L-Phe system. The chromatograms in this figure demonstrate that in order to obtain results of quasi-kinetic significance (i.e., with sampling at 10- or 20-min intervals), we were forced to compromise the quality of peak resolution. However, deconvolution of the partially overlapping bands enables reliable estimation of the peak heights, and consequently, of the concentration changes of all monomeric α-amino acids of interest. Additionally, we examined the peptides from the long-term experiment using scanning electron microscopy and mass spectrometry. We employed a turbidimeter in a continuous registration mode to follow the pulsation resulting from the repeated appearance and disappearance of solid precipitate. The results of these measurements are discussed below.

We note that this study is meant as a methodological example of the application of chromatography to the challenging physicochemical task of monitoring spontaneous nonlinear processes. Such an approach is likely to be of interest not only for chromatographers but also for those involved in tracing nonlinear processes, who are limited by a lack of adequate analytical tools.

Short-term measurements of condensation dynamics

Pro–Phe

We studied earlier the dynamics of monomeric L-Pro and L-Phe in the binary L-Pro–L-Phe system with the use of HPLC-ELSD (9), which we summarize briefly here. Under our experimental conditions, the retention time (t_R) of Pro falls in the range of 12.04–12.78 min, that of Phe is in the range of 14.46–15.81 min and that of the main peptidization product lies between 13.31 and 14.17 min. To obtain quasi-kinetic results, we had to keep the time for each chromatographic run short (20 min), and we took the chromatographic peak heights as proportional to the respective concentrations of Pro, Phe and the main peptidization product. In Figure 3, we show time series of these chromatographic peak heights for the three species considered. From the shape of the three plots, the nonmonotonic character of the concentrations of Pro, Phe and the main peptidization product over the course of the 250 h measurement is evident. We have marked with an oval the most dramatic period, during which the concentrations of both amino acids decrease, while the concentration of the main peptidization product increases. This interdependence between the dynamics of the monomeric amino acid concentrations and that of the main peptidization product is probably due to formation of the heteropeptide. However, the shapes of these two plots are not "mirror images" over the entire time range because the two monomeric amino acids also produce smaller quantities of other peptides in addition to the main peptidization product but at different rates (as we demonstrate later with mass spectra).

Cys

Analogous results for L-Cys have been presented in ref. (17) and are summarized here. The retention time (t_R) of Cys is in the range of 3.97–4.23 min and that of its main peptidization product is in the range of 3.76–4.00 min. In Figure 4, we show a time series of chromatographic peak heights for monomeric Cys and its main peptidization product. The oscillatory changes in the concentrations of monomeric cysteine and its main peptidization product are evident. Again, we have marked with an oval a period during which the concentration of monomeric Cys decreases, while that of its main peptidization product increases. This interdependence apparently results from the consumption of Cys to give the main peptidization product. However, various other peptide types are formed simultaneously at lower concentrations and with different kinetics, so that the interdependence between the time course of Cys and that of its main peptidization product varies over the course of our experiment.

Long-term measurements of condensation dynamics

Pro–Phe

After 1 year in the calibration flask at 21 ± 1°C, the initially homogeneous Pro–Phe sample (with 10 times higher initial concentrations of L-Pro and L-Phe than in the short-term study) became a heterogeneous suspension, with white fibers freely floating therein (Figure 5A(a)). This observation is consistent with our earlier experience with the long-term aging of chiral carboxylic acids in solution (18), which also generated high condensation yields and macroscopic effects perceptible upon visual inspection. Remarkably, the amount of fibers perceptibly fluctuated from low to high, and then back to low. An agglomeration of the fibers captured near the moment of their highest abundance is shown in Figure 5A(b).

To gain deeper insight into the structure of the fibers generated in the solution, we took a series of SEM images from the solution residue evaporated to dryness. Selected micrographs are shown in Figure 5B. From the micrographs in Figure 5B(a–e), it is evident that the observed microfibers are in fact self-assembled nanofiber bundles stuck together, in a fashion resembling spaghetti bunches (occasionally leaving hollow spaces between neighboring fibers). These nano- and microfiber structures resemble those seen in SEM images in other studies of peptide assemblies (13, 19). We suggest that the visually perceptible

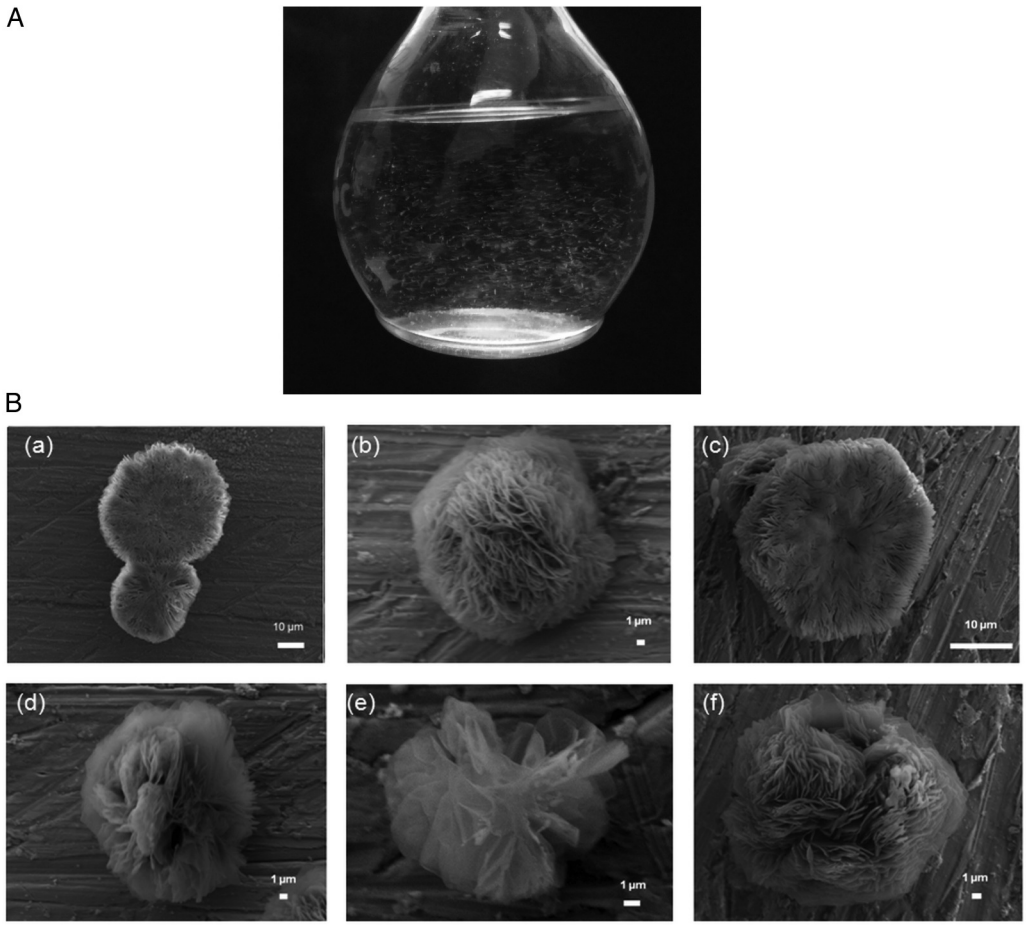

Figure 7. (A) Volumetric flask with Cys-derived microstructures suspended in solution. (B, a–f) Scanning electron micrographs of Cys microstructures from the solution residue evaporated to dryness, with a magnification of (a) ×1,000, (b) ×3,000, (c) ×2,300, (d) ×3,300, (e) ×5,500 and (f) ×3,300.

fiber formation and decay result from the stepwise attainment of a critical number of condensed monomer amino acid units, above which peptides at sufficiently high concentration become insoluble in 70% aqueous acetonitrile, precipitating in fiber form. Spontaneous hydrolytic decay reduces the number of condensed monomeric units below the solubility level, allowing them to redissolve. This mechanism generates the observed pulsation of fiber density (as shown schematically and in snapshots in Figure 1).

To provide more direct evidence of peptide formation, we utilized mass spectrometry. Mass spectra were recorded for the freshly prepared and the aged Pro–Phe solutions in the extended range from 100 to 3,500 *m/z*. Examples are shown in Figure 6(a and b). In the mass spectrum of the freshly prepared Pro–Phe solution (Figure 6a), the two predominant signals are those originating from the amino acids of interest. One of them can be attributed to the $[Pro]^+$ ion (*m/z* 115; 3.5 kCounts signal intensity) and the other to the $[Phe_3+2H]^{2+}$ ion (*m/z* 231; 1.4 kCounts signal intensity). In the mass spectrum of the Pro–Phe solution that was aged for 1 year, an abundance of signals can be seen. We attribute structures to several of those with the highest intensities in the inset to Figure 6b.

Cys

The spontaneous peptidization of L-Cys is faster than that of L-Pro–L-Phe. Hence, we were able to observe pulsation of the Cys-derived peptide suspension after a relatively short period of 2 weeks. A volumetric flask containing a relatively high yield of this suspension is shown in Figure 7A. To investigate the microstructures in more depth, we evaporated an aged Cys solution to dryness and took a series of SEM images. The micrographs in Figure 7B show clear evidence of globular nanoparticle assemblies. The globular form, which resembles that of other self-assembled Cys-derived peptides (20), probably results from the availability of three functionalities per cysteine molecule, i.e., –COOH, $–NH_2$ and –SH (when compared with two functionalities per proline and phenylalanine molecule, resulting in linear peptides).

Mass spectra of the fresh and the aged Cys samples are shown in Figure 8(a and b) in the extended range from 100 to 3,500 *m/z*. A mass spectrum of freshly prepared Cys solution is shown in Figure 8a; the predominant signal originates from the $[Cys]^+$ ion (*m/z* 121; 12.8 kCounts signal intensity). Although aging of the Cys solution lasted only 2 weeks, in that time the signal intensity of $[Cys]^+$ dropped to 12.3 kCounts, and non-negligible amounts of the aging products appeared with *m/z* values around and above 3,000 (Figure 8b). We have attributed peptide structures to selected signals in this spectrum as summarized in the inset to this figure. The relatively intense signals at *m/z* values of 2,780 (2.3 kCounts) and 3,296 (3.9 kCounts) correspond, respectively, to the $[Cys_{26}+H]^+$ ion (20 peptide bonds and 5 disulfide bonds) and the $[Cys_{31}+H]^+$ ion (25 peptide bonds and 5 disulfide bonds).

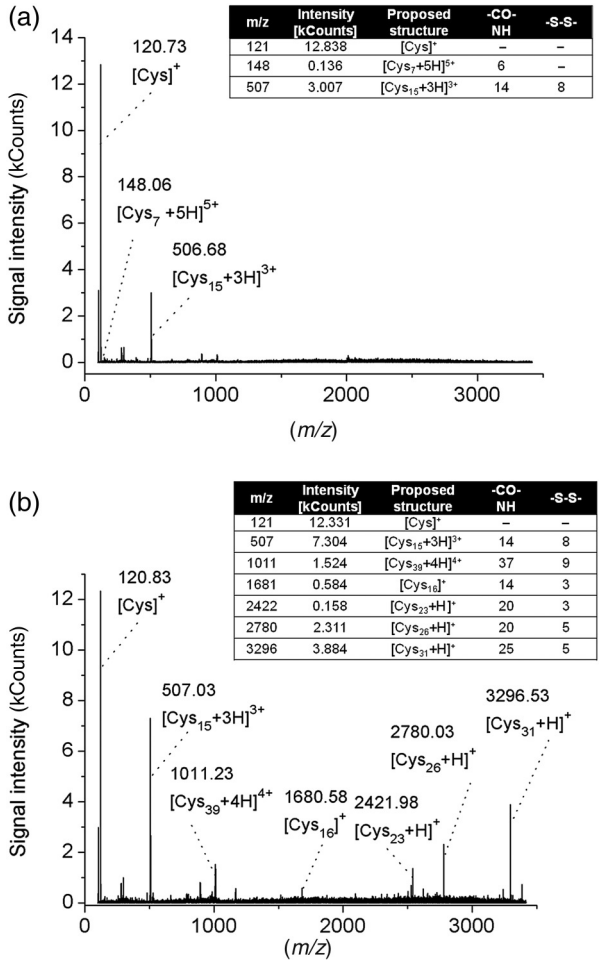

Figure 8. Mass spectra recorded for (a) the fresh and (b) the 2-week-old Cys solution in 70% aqueous acetonitrile, and possible structures attributed to selected signals.

Turbidimetry

Turbidity changes recorded for the Pro–Phe and Cys systems in the continuous registration mode are shown in Figure 9(a and b). From these data, it is evident that the dynamics of the turbidity changes differ between the Pro–Phe (Figure 9a) and the Cys (Figure 9b) systems. This is apparently due to the different molecular structures of the three amino acids involved, with three functionalities able to participate in peptidization of each Cys molecule versus two functionalities per Pro or Phe molecule. As controls, we present the time dependence of the turbidity for water, acetonitrile and 70% aqueous acetonitrile over 24 h (Figure 9c). The stable turbidity values for all three solvents are quite different from the dynamic behavior of the amino acid solutions. We interpret increases in turbidity to correspond to growing amounts of nano- and microparticles suspended in the solution, owing to the progress of the peptidization process. A decrease in turbidity can arise from dissociation of higher, insoluble peptides to lower, soluble ones, and/or from sedimentation of the higher insoluble peptides at the bottom of the measuring vial. Although more complex interpretations are possible, it is evident that, in amino acid solutions stored for long periods of time, the peptidization process progresses in a nonmonotonic fashion, with sequentially increasing and decreasing amounts of insoluble peptides suspended in the liquid phase and responsible for the pulsation effect.

Modeling

In an effort to understand oscillatory behavior observed in the oligomerization of lactic acid, we developed a simple model based on the key hypothesis that oligomers can assemble to form an aggregate that is capable of serving as a template for the formation of more aggregates (21). We subsequently extended the model to treat oscillatory condensation found in mixtures of L-proline and L-hydroxyproline (8). Because we lacked kinetic data about the individual steps of the oligomerization and aggregation processes, we employed a coarse-graining procedure (22) that treats each of these multistep processes as a single pseudo-step characterized by an effective species size and rate constant. The rate constants, which are effectively averages over multiple elementary steps involving oligomers and aggregates of different sizes, were obtained by varying these parameters until rough qualitative agreement with the experimental turbidity data, particularly the typical length of an oscillatory cycle, was obtained. Given the crudeness of the model and the high variability of the data, no attempt at more detailed fitting was made.

With a slight modification of the notation employed in our earlier work, the basic model consists of the following equations:

$$n_1\mathrm{M} \rightarrow \mathrm{P} \quad \text{rate} = k_\mathrm{o}\mathrm{M} \quad \text{(oligomerization)} \tag{1}$$

$$n_2\mathrm{P} \rightarrow \mathrm{C} \quad \text{rate} = k_\mathrm{u}\mathrm{P} \quad \text{(uncatalyzed aggregation)} \tag{2}$$

$$2\mathrm{C} + n_2\mathrm{P} \rightarrow 3\mathrm{C} \quad \text{rate} = k_\mathrm{c}\mathrm{C}^2\mathrm{P} \quad \text{(catalyzed aggregation)} \tag{3}$$

$$\mathrm{C} \rightarrow \text{products} \quad \text{rate} = k_\mathrm{d}\mathrm{C} \quad \text{(decomposition)} \tag{4}$$

Here, M represents monomers (amino acid molecules), P stands for a typical oligomeric peptide of average length n_1 and C is a typical catalytic aggregate, which contains, on average, n_2 oligomers. In the early stages, monomers form peptides, which slowly aggregate. Once the templating species, C, is formed, the aggregation process becomes autocatalytic. Aggregates can decay into products, which are assumed not to play a role in the dynamics.

To account for the formation of solid nanofibers, we introduce two additional steps:

$$2\mathrm{C} \rightarrow \mathrm{F} \quad \text{rate} = k_f\theta(C - C_\mathrm{t})C^2 \quad \text{(fiber formation)} \tag{5}$$

$$\mathrm{F} \rightarrow 2\mathrm{C} \quad \text{rate} = k_r[1 - \theta(C - C_\mathrm{t})]\mathrm{F} \quad \text{(fiber redissolution)} \tag{6}$$

where F represents nanofibers and θ is the Heaviside step function, which is 1 if its argument is positive and 0 if it is negative or zero. Thus, fiber formation occurs only when the concentration of aggregates exceeds a critical value, C_t, and any fibers present redissolve if C lies below this threshold. The use of the step function is similar to the procedure employed in some models of Liesgang band formation (23). Equations (1–6) enable us to simulate the behavior of a solution of a single amino acid, e.g., our cysteine system. Figure 10a shows the result of such a simulation.

To treat a mixture of amino acids, we employ a set of six equations, analogous to Eqs. (1)–(6), for each of the monomers M_1 and M_2, and the species that result from it. In addition, we allow the two peptides to interact via cross-catalysis (8), whereby aggregates of one monomer can catalyze the aggregation of oligomers of the other monomer, e.g.,

$$2\mathrm{C}_1 + n_{22}\mathrm{P}_2 \rightarrow 2\mathrm{C}_1 + \mathrm{C}_2 \quad \text{rate} = k_{cc1}\mathrm{C}_1^2\mathrm{P}_2 \quad (1-2 \text{ cross catalysis}) \tag{7}$$

Interchanging indices 1 and 2 gives the equation describing catalysis of species 1 aggregation by species 2. In Figure 10b, we present the results of a simulation in which only species 1 (Pro) catalyzes the

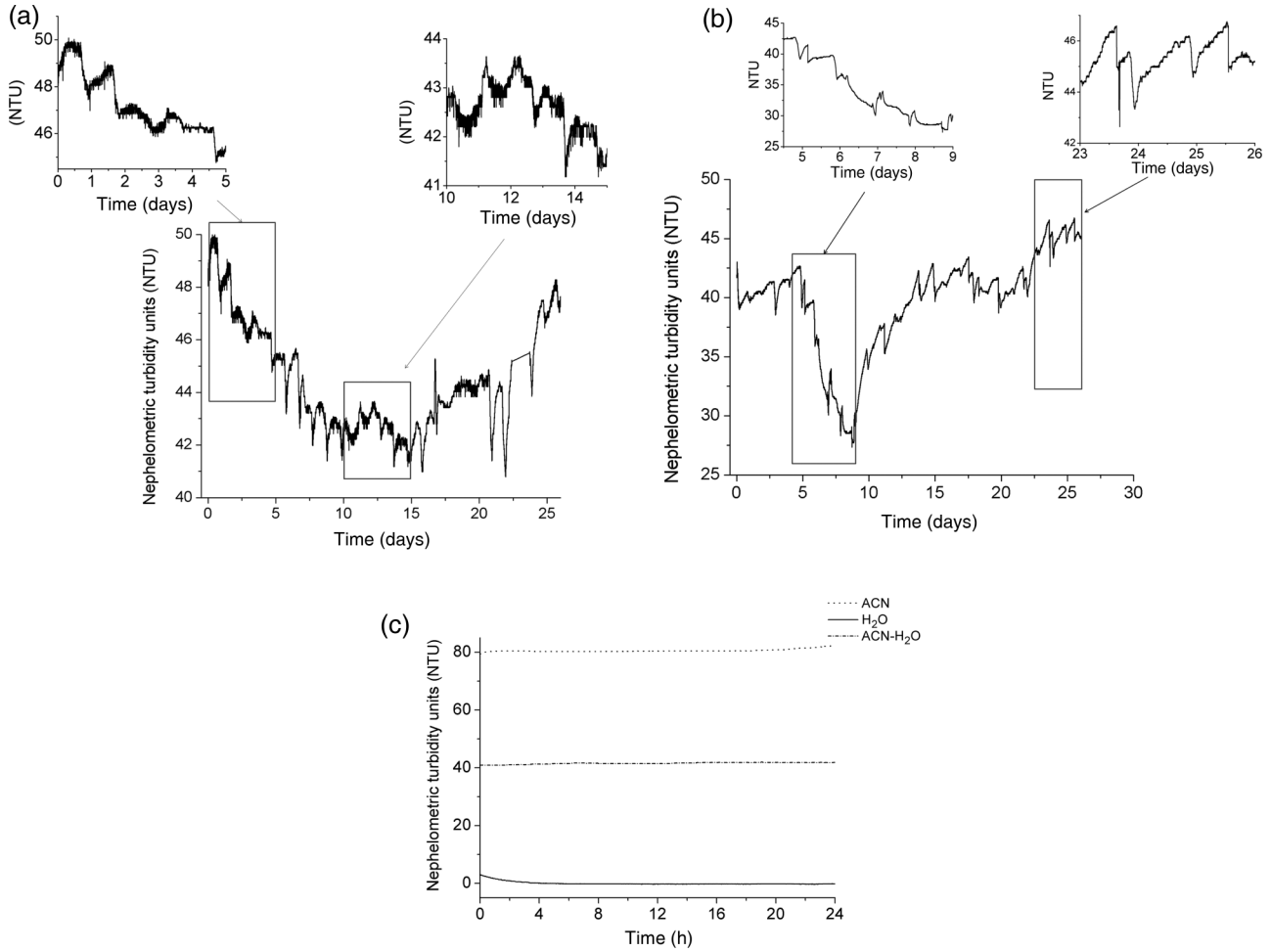

Figure 9. Turbidity changes (in nephelometric turbidity units, NTU) for (a) a Pro–Phe solution (10) and (b) a Cys solution between 0 and 26 days. Insets emphasize the nonmonotonic nature of turbidity changes in shorter time intervals. (c) Turbidity changes (in nephelometric turbidity units, NTU) for acetonitrile (ACN), water (H_2O) and 70% aqueous ACN registered for 24 h.

aggregation of species 2 (Phe), i.e., Eq. (7) is included, and $k_{cc2} = 0$. Qualitatively similar results can be obtained by allowing mutual cross-catalysis.

In both cases, we note the relatively smooth oscillation of the oligomer concentration and the more irregular, spiky nature of the oscillations in the amount of nanofiber, consistent with our observations. At long time periods, the oscillations damp out and the concentration of nanofibers builds up to a steady state. The simulated nanofiber concentration is, as expected, smoother than the turbidimetric measurements because the simulations give a spatial average over the entire sample as opposed to the local sampling of the turbidimeter.

Discussion

The HPLC-ELSD technique used in this study can be regarded as a first-choice instrumental option to reveal nonlinear concentration changes of the monomeric amino acids and the lower soluble peptides present in the liquid phase. The turbidity results presented in this study are complementary to those obtained with HPLC-ELSD in that they reflect nonlinear changes in the amounts of higher insoluble peptides. SEM enables visualization of insoluble peptides and visual comparison thereof with analogous structures available from the literature. MS provides the data that allow structural characterization of at least some peptidization products. Modeling provides theoretical justification of spontaneous pulsation of peptide microstructures visualized with the use of SEM and turbidimetry, anticipating physical phenomena traced with the use of HPLC-ELSD.

Conclusion

To our knowledge, this study represents the first systematic investigation of spontaneous uncatalyzed pulsation of peptide nano- and microstructures in an abiotic liquid system. The multiple analytical techniques employed, bolstered by our model simulations, strongly support the notion that peptide nano- and microparticles may form and decompose in an oscillatory fashion. More detailed study of both the structural and kinetic aspects of this system is clearly necessary before more precise conclusions can be formed. Nonetheless, the results obtained provide potential clues to processes that may be of importance in biotechnology, where the formation of such particles may need to be taken into account in designing and controlling processes, and in the origin of life, where fibrous materials generated from simple biomonomers might provide a vehicle for compartmentalization and/or catalysis.

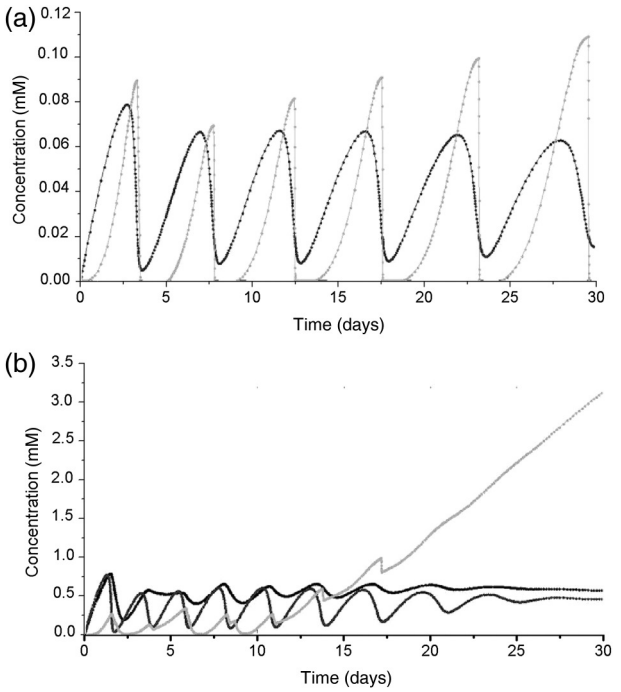

Figure 10. Simulation of oscillations in the concentrations of oligomers and nanofibers in solutions initially containing amino acids dissolved in 70% acetonitrile. (a) Cys solution with initial [Cys] = 5.77×10^{-3} mol L^{-1}. Black trace shows concentration of oligomers; gray trace is 100 × concentration of nanofibers. Parameters in Eqs (1–6): $k_0 = 2.25 \times 10^{-7}$ s^{-1}, $k_u = 3.0 \times 10^{-7}$ s^{-1}, $k_c = 6.3 \times 10^5$ M^{-2} s^{-1}, $k_d = 7.5 \times 10^{-5}$ s^{-1}, $k_f = 6.0 \times 10^{-4}$ M^{-1} s^{-1}, $k_r = 1.2 \times 10^{-5}$ s^{-1}, $n_1 = 3$, $n_2 = 6$ and $C_t = 2.0 \times 10^{-5}$ M; (b) Pro–Phe solution initially containing 8.69×10^{-2} mol L^{-1} Pro and 6.05×10^{-2} mol L^{-1} Phe. Upper and lower black traces are concentrations of Pro and Phe oligomers, respectively. Gray trace is 50× total concentration of nanofibers (Pro + Phe). Parameters in Eqs (1–7) (subscript 1 refers to Pro, subscript 2 to Phe): $k_{01} = 1.0 \times 10^{-7}$ s^{-1}, $k_{u1} = 3.5 \times 10^{-7}$ s^{-1}, $k_{c1} = 1.8 \times 10^3$ M^{-2} s^{-1}, $k_{d1} = 3.5 \times 10^{-5}$ s^{-1}, $k_{f1} = 7.0 \times 10^{-5}$ M^{-1} s^{-1}, $k_{r1} = 7.0 \times 10^{-5}$ s^{-1}, $n_{11} = 5$, $n_{21} = 8$, $C_{t1} = 5.0 \times 10^{-4}$ M, $k_{02} = 1.7 \times 10^{-7}$ s^{-1}, $k_{u2} = 5.5 \times 10^{-7}$ s^{-1}, $k_{c2} = 4.2 \times 10^3$ M^{-2} s^{-1}, $k_{d2} = 5.0 \times 10^{-5}$ s^{-1}, $k_{f2} = 7.0 \times 10^{-5}$ M^{-1} s^{-1}, $k_{r2} = 7.0 \times 10^{-5}$ s^{-1}, $n_1 = 3$, $n_2 = 6$, $C_{t2} = 2.0 \times 10^{-4}$ M, $k_{cc1} = 1.7 \times 10^2$ M^{-2} s^{-1}.

Acknowledgements

We thank Professor John Pojman for suggesting the use of continuous turbidimetry. A.G. acknowledges the financial support of the DoktoRIS project, co-financed by the European Union within the European Social Found. I.R.E. was supported by the U.S. National Science Foundation (grant CHE-1362477) and the W.M. Keck Foundation.

References

1. Sajewicz, M., Piętka, R., Pieniak, A., Kowalska, T.; Application of thin-layer chromatography (TLC) to investigating oscillatory instability of the selected profen enantiomers; *Acta Chromatographica*, (2005); 15: 131–149.
2. Sajewicz, M., Kronenbach, D., Gontarska, M., Wróbel, M., Piętka, R., Kowalska, T.; TLC in search for structural limitations of spontaneous oscillatory in-vitro chiral conversion. α-Hydroxybutyric and mandelic acids; *Journal of Planar Chromatography – Modern TLC*, (2009); 22: 241–248.
3. Sajewicz, M., Kronenbach, D., Gontarska, M., Kowalska, T.; TLC and polarimetric investigation of the oscillatory in vitro chiral conversion of *R*-*β*-hydroxybutyric acid; *Journal of Liquid Chromatography and Related Technologies*, (2010); 33: 1047–1057.
4. Sajewicz, M., Gontarska, M., Kowalska, T.; HPLC/DAD evidence of the oscillatory chiral conversion of phenylglycine; *Journal of Chromatographic Science*, (2014); 52: 329–333.
5. Belanger, P., Atkinson, J.G., Stuart, R.S.; Exchange reactions of carboxylic acid salts; kinetics and mechanism; *Journal of the Chemical Society – Section D: Chemical Communication*, (1969); 1067–1068.
6. Xie, Y., Liu, H., Chen, J.; Kinetics of base catalyzed racemization of ibuprofen enantiomers; *International Journal of Pharmaceutics*, (2000); 196: 21–26.
7. Sajewicz, M., Gontarska, M., Kronenbach, D., Leda, M., Kowalska, T., Epstein, I.R.; Condensation oscillations in the peptidization of phenylglycine; *Journal of Systems Chemistry*, (2010); 1: 7.
8. Sajewicz, M., Dolnik, M., Kowalska, T., Epstein, I.R.; Condensation dynamics of *L*-proline and *L*-hydroxyproline in solution; *RSC Advances*, (2014); 4: 7330–7339.
9. Sajewicz, M., Godziek, A., Maciejowska, A., Kowalska, T.; Condensation dynamics of the *L*-Pro-*L*-Phe and *L*-Hyp-*L*-Phe binary mixtures in solution; *Journal of Chromatographic Science*, (2015); 53: 31–37.
10. Godziek, A., Maciejowska, A., Talik, E., Wrzalik, R., Sajewicz, M., Kowalska, T.; On spontaneously pulsating proline-phenylalanine peptide microfibers; *Current Protein and Peptide Science*, (2016); 17: 106–116.
11. Lakshmanan, A., Zhang, S., Hauser, C.A.E.; Short self-assembling peptides as building blocks for modern nanodevices; *Trends in Biotechnology*, (2012); 30: 155–165.
12. Wang, M.J., Du, L.J., Wu, X.L., Xiong, S.J., Chu, P.K.; Charged diphenylalanine nanotubes and controlled hierarchical self-assembly; *ACS Nano*, (2011); 5: 4448–4454.
13. Debnath, S., Roy, S., Ulijn, R.V.; Peptide nanofibers with dynamic instability through nonequilibrium biocatalytic assembly; *Journal of American Chemical Society*, (2013); 135: 16789–16792.
14. Brandt Andersen, K., Castillo-Leon, J., Hedström, M., Svendsen, W.E.; Stability of diphenylalanine peptide nanotubes in solution; *Nanoscale*, (2011); 3: 994–998.
15. Wu, X.L., Xiong, S.J., Wang, M.J., Shen, J.C., Chu, P.K.; Water-sensitive high-frequency molecular vibrations in self-assembled diphenylalanine nanotubes; *Journal of Physical Chemistry C*, (2012); 116: 9793–9799.
16. Jandera, P., Kucerova, Z., Urban, J.; Retention times and bandwidth in reversed-phase gradient liquid chromatography of peptides and proteins; *Journal of Chromatography A*, (2011); 1218: 8874–8889.
17. Godziek, A., Maciejowska, A., Sajewicz, M., Kowalska, T.; HPLC monitoring of spontaneous non-linear peptidization dynamics of selected amino acids in solution; *Journal of Chromatographic Science*, (2015); 53: 401–410.
18. Sajewicz, M., Wrzalik, R., Gontarska, M., Kronenbach, D., Leda, M., Epstein, I.R., *et al.*; In vitro chiral conversion, phase separation, and wave propagation in aged profen solutions; *Journal of Liquid Chromatography & Related Technologies*, (2009); 32: 1359–1372.
19. Andersen, K.B., Castillo-Leon, J., Hedstrom, M., Svendsen, W.E.; Stability of diphenylalanine peptide nanotubes in solution; *Nanoscale*, (2011); 3: 994–998.
20. Carny, O., Gazit, E.; A model for the role of short self-assembled peptides in the very early stages of the origin of life; *FASEB Journal*, (2005); 19: 1051–1055.
21. Sajewicz, M., Dolnik, M., Kronenbach, D., Gontarska, M., Kowalska, T., Epstein, I.R.; Oligomerization oscillations of *L*-lactic acid in solution; *The Journal of Physical Chemistry A*, (2011); 115: 14331–14339.
22. Coveney, P.V., Wattis, J.A.D.; Coarse-graining and renormalization group methods for the elucidation of the kinetics of complex nucleation and growth processes; *Molecular Physics*, (2006); 104: 177–185.
23. Antal, T., Droz, M., Magnin, J., Rácz, Z., Zrinyi, M.; Derivation of the Matalon-Packter law for Liesegang patterns; *The Journal of Chemical Physics*, (1998); 109: 9479–9486.

Full Paper

Israel Journal of Chemistry

DOI: 10.1002/ijch.201600085

Scanning Electron Microscopic Evidence of Spontaneous Heteropeptide Formation in Abiotic Solutions of Selected α-Amino Acid Pairs

Agnieszka Godziek,[a] Anna Maciejowska,[a] Ewa Talik,[b] Mieczysław Sajewicz,[a] and Teresa Kowalska*[a]

Dedicated to the memory of Professor Emanuel Gil-Av

Abstract: Spontaneous nonlinear peptidization of the monomeric and enantiomerically pure α-amino acids in abiotic aqueous and nonaqueous solutions is still regarded by some as a somewhat puzzling phenomenon, and therefore it needs additional experimental authentication. In our earlier studies, we employed several analytical techniques to prove its occurrence. In this study, we present the scanning electron microscopic (SEM) evidence of spontaneous heteropeptide formation in the binary *L*-Cys–*L*-Phe, *L*-Cys–*L*-Phg, and *L*-Cys–*L*-Pro mixtures dissolved in 70% aqueous methanol. With each α-amino acid pair, one amino acid (*L*-Cys) is equipped with three functionalities (–SH, $-NH_2$, and –COOH), enabling formation of the spherical homopeptide microstructures, while its counterpart (*L*-Phe, *L*-Phg, or *L*-Pro, respectively) is equipped with the two functionalities only ($-NH_2$ or =NH, and –COOH). The SEM micrographs of the peptidization products originating from the three investigated α-amino acid pairs show three different, yet spherical, structures, which seem suggestive of the heteropeptide formation involving both *L*-Cys and its counterpart α-amino acid. Additional confirmation of heteropeptide formation is furnished by high performance liquid chromatography (HPLC), the biuret test, and mass spectrometry (MS).

Keywords: electron microscopy · liquid chromatography · mass spectrometry · spherical heteropeptides · spontaneous peptidization

1. Introduction

Spontaneous nonlinear formation of peptides from the monomeric and enantiomerically pure α-amino acids running in abiotic liquid systems in parallel with spontaneous nonlinear chiral conversion was first reported in Refs. [1,2]. Under "spontaneous peptidization" and "spontaneous chiral conversion", we understand two processes running without any purposely induced external stimuli, and therefore, they are opposite to those enzymatically catalyzed in a biotic environment, or following a specially devised laboratory procedure in an abiotic environment (although self-catalysis obviously cannot be excluded). In fact, these two processes have not been observed with α-amino acids alone, but with a wider selection of the low molecular weight chiral carboxylic acids, such as profen drugs[3,4] and hydroxyl acids,[5,6] so it can be justifiably speculated that these two processes are even more general than our up-to-date understanding thereof. Under nonlinear processes, the time-dependent variations of the respective concentrations of a given enantiomeric or peptide species are understood (as a result of chiral conversion or peptidization, respectively). Below, the mechanisms are presented for chiral conversion (Scheme 1a), peptidization (Scheme 1b), and the two processes running in parallel (Scheme 1c), upon the examples of Cys and Pro which will be discussed in the experimental part of this study.

Earlier, no such observation had been made with the monomeric α-amino acids dissolved in abiotic aqueous or nonaqueous media, in the absence of a catalyst. Moreover, selected peptide structures tend to be viewed as fairly stable units (e.g., Refs. [7–9]), often with some negative health repercussions (e.g., as a cause of the age-related neurodegenerative diseases; e.g., Refs. [9–11]) or to the contrary, they can be utilized in various different bio-

[a] A. Godziek, A. Maciejowska, M. Sajewicz, T. Kowalska
Institute of Chemistry
University of Silesia
9 Szkolna Street
40-006
Katowice
Poland
e-mail: teresa.kowalska@us.edu.pl

[b] E. Talik
Institute of Physics
University of Silesia
4 Uniwersytecka Street
40-007
Katowice
Poland

© 2016 Wiley-VCH Verlag GmbH & Co. KGaA, Weinheim

Israel Journal of Chemistry

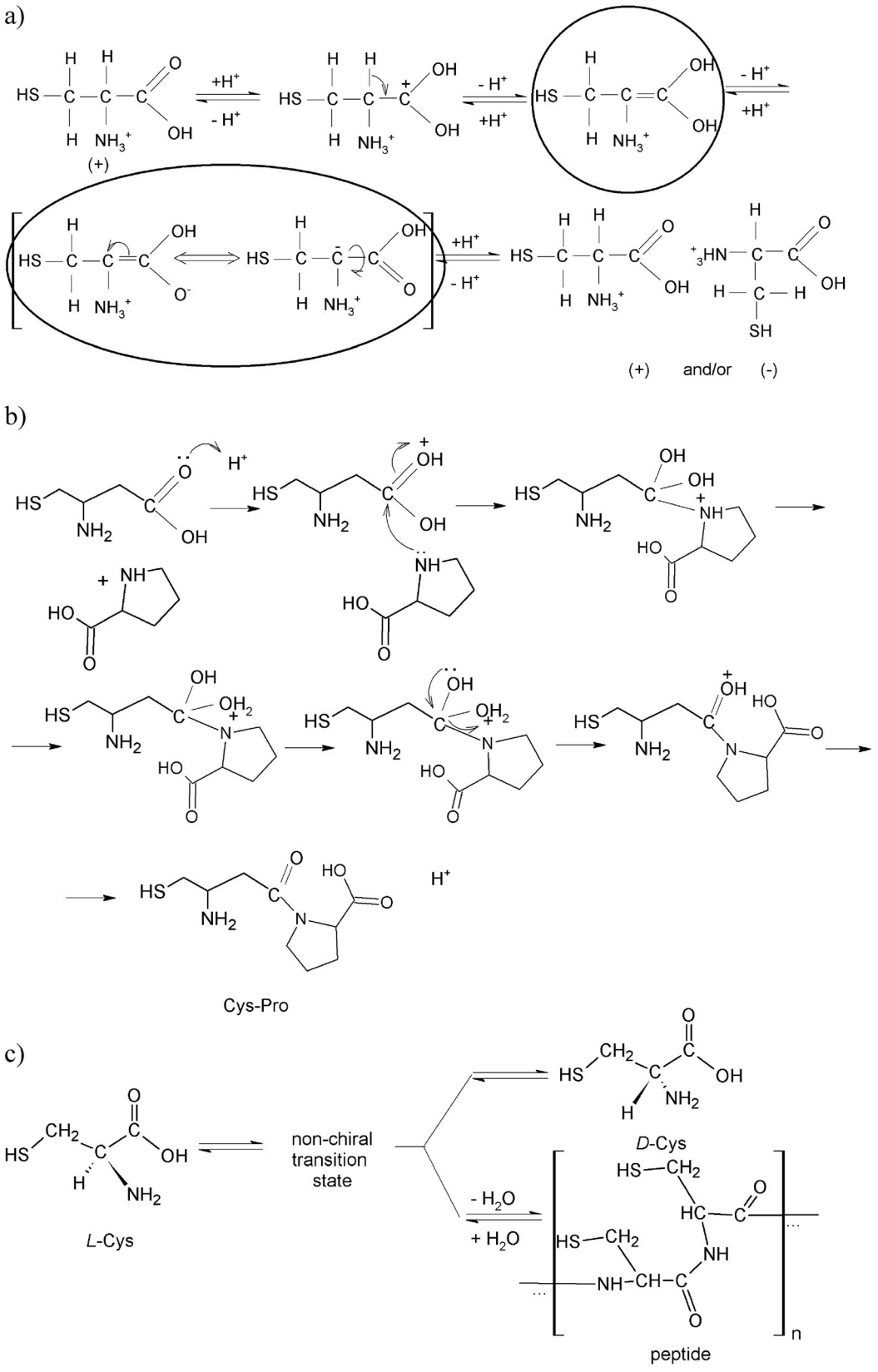

Scheme 1. Molecular mechanisms of the processes running in the *L*-Cys–*L*-Pro system dissolved in an aqueous medium: a) chiral conversion of *L*-Cys to *D*-Cys (intermediary nonchiral structures are marked with black ovals); b) heterodipeptide formation (Cys-Pro); and c) chiral conversion (*L*-Cys to *D*-Cys) and peptidization $(Cys\text{-}Cys)_n$ running in parallel.

 © 2016 Wiley-VCH Verlag GmbH & Co. KGaA, Weinheim

medical nanotechnology contexts, owing to their biocompatibility (e.g., Refs. [9,12,13]). Numerous reports on the lack of peptide stability in abiotic solutions refer to their decay (e.g., hydrolysis) rather than to their spontaneous formation (the latter process being the leitmotif of our own investigations), and they tend to ascribe such phenomena to basically external stimuli, such as pH, temperature, the chemical nature of the solvents, etc.[14–16]

Spontaneous peptidization of α-amino acids has been documented in our earlier studies with the use of several analytical techniques, and in the first instance, with the use of high-performance liquid chromatography (HPLC)[17] and thin-layer chromatography (TLC),[18] both with mass spectrometric detection. HPLC and TLC with alternative detection systems,[17,18] turbidimetry with continuous data registration,[19,20] and scanning electron microscopy (SEM)[21] were applied as auxiliary techniques. In Ref. [22], we reflected on the possible thermodynamic justification of spontaneous chiral conversion of the low molecular-weight chiral carboxylic acids upon an example of phenylglycine. Although such processes can be regarded as endothermic, they can most probably be relatively easily initialized, e.g., by a transfer of thermal energy or ultraviolet (UV) light from the environment to the system. On the contrary, one can expect spontaneous peptidization (as a specific form of condensation) to run with a weak exothermic effect. Some of our experimental results with a clearly kinetic importance gave rise to the development (in collaboration with the Epstein group at Brandeis University, Waltham, MA working on the nonlinear chemical dynamics) of theoretical models of the oscillatory chiral conversion and peptidization (e.g., Refs. [2,6]). Although SEM is a powerful instrumental technique able to provide interesting information on various different peptide nano- and microstructures held together by supramolecular forces (e.g., Ref. [9]), its hitherto reported practical applications to tracing spontaneous peptidization of the monomeric α-amino acid units are still rather sporadic.[19,21]

Due to the fact that spontaneous peptidization of α-amino acids from the monomeric molecular units is still viewed by some as somewhat puzzling, and because the potential of SEM in this application field has not yet been fully exploited, the aim of this study is to demonstrate the usefulness of SEM to document the formation of the heteropeptide structures in solutions of the three α-amino acid pairs (*L*-Cys–*L*-Phe, *L*-Cys–*L*-Phg, and *L*-Cys–*L*-Pro). *L*-Cys is the simplest sulfur-containing proteinogenic amino acid equipped with three functionalities (–SH, $–NH_2$, and –COOH), which are responsible for the spherical structure of its own homopeptides,[23] whereas *L*-Phe, *L*-Phg, and *L*-Pro are equipped with a set of two functionalities each ($–NH_2$ or =NH, and –COOH). It was preliminarily assumed that spontaneous peptidization taking place in the three binary α-amino acid mixtures, each of them containing *L*-Cys as a structural motif with the three functionalities, would result in an easily recognizable spherical morphology of the respective heteropeptides. As auxiliary techniques, HPLC, the biuret test, and mass spectrometry (MS) were applied. Nevertheless, we additionally performed microbiological tests for the possible presence of microorganisms in the α-amino acid solutions stored for one month or more, following the procedure described in detail in Ref. [2]. These tests revealed no DNA in our samples, and we therefore concluded that they were free of contamination from any microorganisms.

2. Results and Discussion

The chemical structures and molecular weights of the four *L*-α-amino acids (i.e., *L*-Cys, *L*-Phe, *L*-Phg, and *L*-Pro) investigated in the framework of this study are given in Table 1. Spontaneous formation of the condensation products as a result of ageing of the four monocomponent and the three binary α-amino acid samples in an antiseptic solvent (70% aqueous methanol) was traced with use of SEM. For a confirmatory purpose, HPLC, the biuret test, and MS were used as auxiliary analytical techniques.

Table 1. Chemical structures and molecular weights (MW, $g\,mol^{-1}$) of α-amino acids investigated in this study (*L*-Cys, *L*-Phe, *L*-Phg, and *L*-Pro).

L-Cys	*L*-Phe	*L*-Phg	*L*-Pro
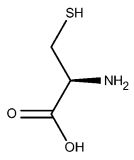	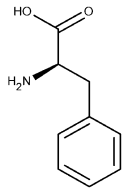	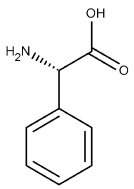	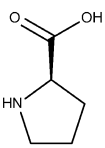
MW = 121.16	MW = 165.19	MW = 151.16	MW = 115.13

2.1 Scanning Electron Microscopy

To demonstrate the heteropeptide formation in the aged binary solutions (*L*-Cys–*L*-Phe, *L*-Cys–*L*-Phg, and *L*-Cys–*L*-Pro), the scanning electron micrographs were registered to compare the precipitates obtained from the aged monocomponent (Figure 1) and the binary (Figure 2) solutions in 70% aqueous methanol.

The nano- and microstructures of solid precipitates derived from the four monocomponent α-amino acids are presented in Figure 1. A difference evident among them is apparently due to their different molecular structures. In the case of *L*-Cys, the spherical morphology is observed (Figure 1a), most probably due to the three functionalities present in the *L*-Cys molecule (–COOH, –

© 2016 Wiley-VCH Verlag GmbH & Co. KGaA, Weinheim

Israel Journal of Chemistry

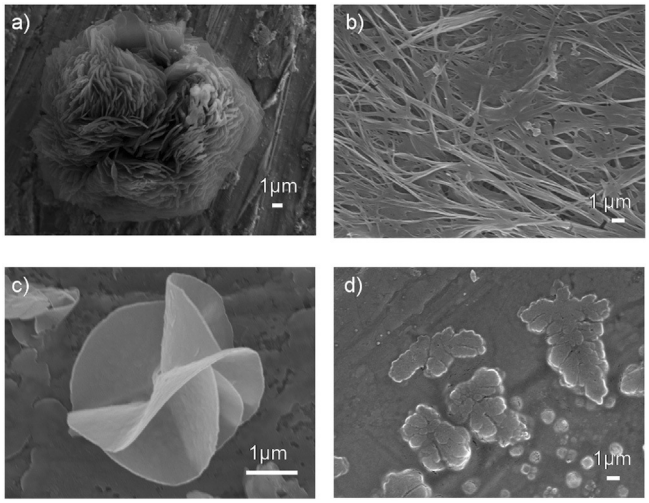

Figure 1. Scanning electron micrographs recorded for a) Cys, b) Phe, c) Phg, and d) Pro dissolved in 70% aqueous methanol; aged for: a) 2 weeks, b) 3 months, and c), d) one month, and then evaporated to dryness. Magnification: a) X3300, b) X3300, c) X20000, and d) X5000. Size bars are inset in each individual picture.

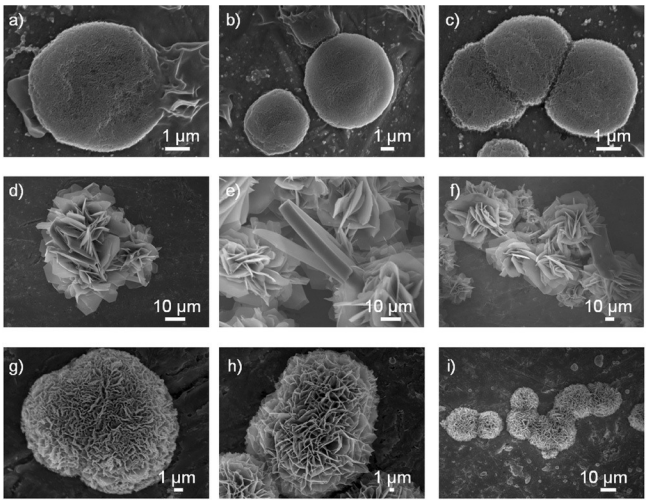

Figure 2. Scanning electron micrographs recorded for: a–c) *L*-Cys–*L*-Phe, d–f) *L*-Cys–*L*-Phg, and g–i) *L*-Cys–*L*-Pro system dissolved in 70% aqueous methanol, aged for two weeks and then evaporated to dryness. Magnification: a) X14000, b) X5000, c) X3500, d) X500, e) X1100, f) X1100, g) X5000, h) X3000, i) X900. Size bars are inset in each individual picture.

NH_2, and –SH), which enable formation of the 3D homopeptides. Moreover, the presence of the thiol group (–SH) in the *L*-Cys molecule can result in the formation of disulfide bridges, additionally contributing to the 3D shape of the precipitate. *L*-Phe characterizes with two functionalities (–COOH and $–NH_2$) and the phenyl ring as a steric hindrance, able to obstruct peptidization. Consequently, the *L*-Phe-derived homopeptides are fibrous in shape (Figure 1b). From the aged *L*-Phg sample equipped with two functionalities (–COOH and NH_2), sheet-like homopeptide structures are obtained, which are rolled in several planes, resembling flower petals, or flakes (Figure 1c). From *L*-Pro with two functionalities (–COOH and =NH), flat irregular structures are obtained. This irregularity in shape is apparently due to the presence of a pyrrolidine ring with the =NH functionality in the *L*-Pro molecule.

Micrographs of the precipitates derived from the binary α-amino acid samples are presented in Figure 2. It was our intent to use SEM to assess the morphology of the peptides formed in the binary systems and to decide, if the heteropeptide structures are visually recognizable among them. In fact, from each amino-acid pair, spherical precipitate structures were obtained, apparently demonstrating the fact that *L*-Cys was involved in the respective heteropeptide structures. With *L*-Cys–*L*-Phe, very regular and smooth spherical structures developed (Figures 2a–2c). With *L*-Cys–*L*-Phg, also spherical structures were obtained, although built of the irregular petal-like substructures (Figures 2d–2f). With *L*-Cys–*L*-Pro, again spherical structures were obtained, constructed of the regular petal-like substructures (Figures 2g–2i).

Thus, the spherical morphology of the precipitates obtained from the aged *L*-Cys–*L*-Phe, *L*-Cys–*L*-Phg, and *L*-Cys–*L*-Pro solutions was considered as a confirmatory factor which allowed the conclusion that the heteropeptides were formed in each examined sample. *L*-Cys not only governed the shape of the obtained precipitates, but also the formation rates thereof. Namely, the precipitate originating from the monocomponent *L*-Cys sample and from those derived from the three binary systems were perceived by the human eye after ageing for only two weeks. In the case of *L*-Phe and *L*-Pro, the analogous duration was three months and one month, respectively. Understandably, among the obtained peptides, not only heteropeptides were formed, but also homopeptides originating from each individual α-amino acid counterpart, as will be shown in Section 2.4 (mass spectrometry results).

2.2 HPLC

The achiral HPLC-ELSD technique has been used in our earlier studies to demonstrate the progress of peptidization, demonstrating sequential peptide formation and decay in the course of ageing.[1,2,19,21] An important prerequisite is the baseline separation of the two amino acids in an employed HPLC system, at least in the initial period of running the experiment. In this study, we present a detailed example of an HPLC scrutiny of the ageing process upon the *L*-Cys–*L*-Phe system, using the ELSD and DAD detectors. For the remaining two cases (*L*-Cys–*L*-Phg and *L*-Cys–*L*-Pro), basic HPLC results are shown.

In Figure 3, an entity of the HPLC results referring to the binary *L*-Cys–*L*-Phe system monitored in the course

 © 2016 Wiley-VCH Verlag GmbH & Co. KGaA, Weinheim

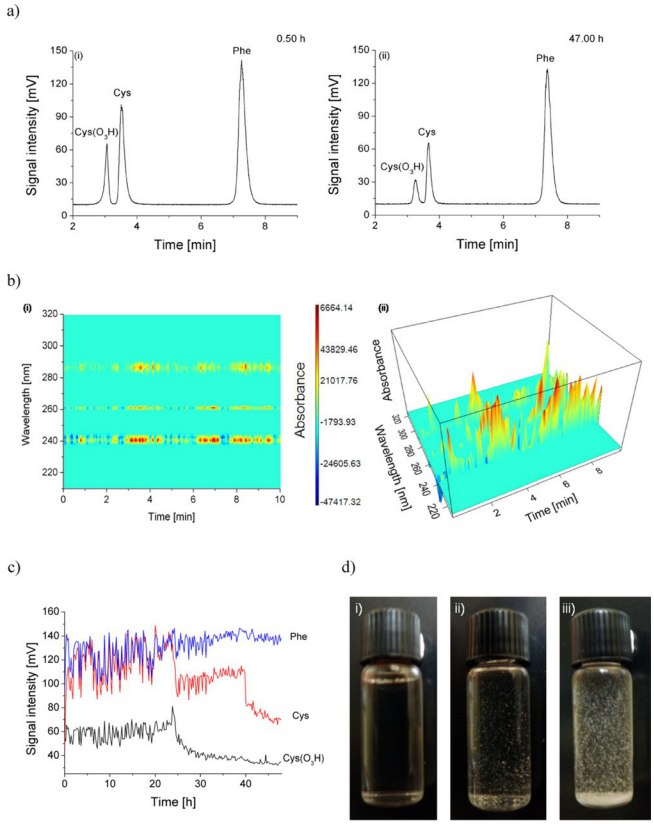

Figure 3. a) The HPLC-ELSD chromatograms recorded for the *L*-Cys–*L*-Phe system dissolved in 70% aqueous methanol after (i) 0.50 h and (ii) 47.00 h sample ageing period. b) The (i) 2D and (ii) 3D HPLC-DAD spectrochromatograms recorded for the *L*-Cys–*L*-Phe system after 48.00 h ageing period. c) Time series of the chromatographic peak heights for Cys, Phe, and Cys(O_3H), recorded with the ELSD detector in the course of a 49.00 h ageing period. d) Images of the vials containing the *L*-Cys–*L*-Phe system dissolved in 70% aqueous methanol for: (i) the freshly prepared sample; (ii) the sample after 3 days ageing; and (iii) the sample after one month ageing.

of ageing is presented. First, the chromatograms recorded almost immediately after the sample preparation (Figure 3a (i); ageing period 0.50 h) and after almost two days storage (Figure 3a (ii); ageing period 47.00 h) are presented, which show the baseline resolution of the signals. In both chromatograms, the peaks of the two amino acids (Cys and Phe) are accompanied by that of cysteic acid (Cys(O_3H)). Its presence in the Cys sample is unclear, and it can either be ascribed to rapid oxidation of Cys in the course of the solution making, or it can be a contaminant from the production stage. Otherwise, oxidation of Cys to cysteic acid is inherent in certain metabolic pathways which occur in living organisms and result in many pathological and ageing-related effects.[24] The chromatograms shown in Figure 3a (i) and (ii) clearly show the lowering signal intensities originating from Cys, Phe, and Cys(O_3H), which are equivalent to the respective concentration drops, most probably due to peptidization. For Cys, the observed drop was from 101.50 to 62.51 mV (38.4%); for Phe, it was from 141.42 to 132.53 mV (6.3%); and for Cys(O_3H), it was from 65.38 to 32.20 mV (50.8%).

Additional confirmation of the peptidization process running in the *L*-Cys–*L*-Phe system originates from the spectrochromatogram registered in the 2D and 3D mode (Figure 3b (i) and (ii)) after 47.00 h sample ageing with use of the DAD detector. In this spectrochromatogram, the UV absorption maxima appear at the wavelength ranges of 240, 263, and 288 nm. The maximum in the range of 240 nm is characteristic of the amide groups (the –CO–NH– peptide bonds), the range of 260 nm can suggest the presence of disulfide bridges, and absorption in the range of 280 nm is due to the presence of the phenyl ring in the molecule of Phe.[25,26] Thus, the obtained spectrochromatogram confirms the formation of peptide bonds and sulfide bridges in the aged sample.

In Figure 3c, the chromatographic peak heights recorded for Cys, Phe, and Cys(O_3H) against the ageing time of the Cys-Phe sample (i.e., the so-called time series) for the initial 49.00 h ageing period are presented. Changes of the peak heights, synonymous with the respective concentration changes, evidently are oscillatory in nature. In the initial period of 24 h ageing, the general trend of the concentration change with Phe is an oscillatory drop and after 24 h, an even stronger pronounced drop of the Cys and Cys(O_3H) concentrations is observed. All these concentration drops can be ascribed to the process of peptide formation, with white particles of the precipitate recognizable with naked eyes already after 24 h sample storage. The concentration drop of Cys(O_3H) can serve as proof that cysteic acid is also involved in peptidization. The simplest visual confirmation of the peptidization progress in the *L*-Cys–*L*-Phe system can be furnished by the series of photographs (Figure 3d (i)–(iii)), showing a vial with the freshly prepared and clear Cys-Phe solution, and the same vial after three days and one month ageing, respectively, with the amounts of the precipitate apparently growing with time. These dynamics of ageing going on in the *L*-Cys–*L*-Phe system will be confirmed by the forthcoming mass spectrometric data (Section 2.4).

The application of HPLC-ELSD to tracing the peptidization progress in the binary *L*-Cys–*L*-Phg system is highlighted in Figures 4a and 4b, which illustrate considerable transformation dynamics taking place in the course of ageing. Figure 4a shows the chromatogram registered after 1.72 h sample storage, showing two well-separated peaks, with the respective retention times (t_R) of 3.40 and 4.29 min valid for Cys and Phg, respectively. After 191.12 h (i.e., ca. 8 days) ageing period, signals from the two chromatographic peaks representing Cys and Phg are not seen anymore, and instead, a new peak appears with the retention time $t_R = 4.19$ min. Gradual disappearance of the peak valid for Cys in the course of sample storage demonstrates a considerable consumption of this α-amino

© 2016 Wiley-VCH Verlag GmbH & Co. KGaA, Weinheim

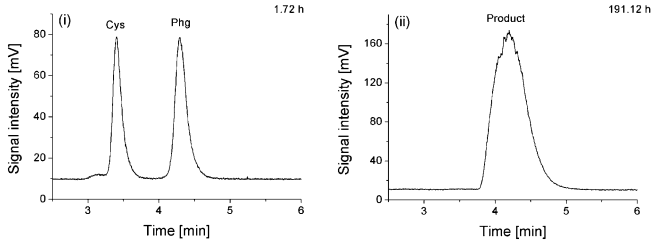

Figure 4. The HPLC-ELSD chromatograms recorded for the *L*-Cys–*L*-Phg system dissolved in 70% aqueous methanol after (i) 1.72 h and (ii) 191.12 h sample ageing period.

acid, most probably due to the peptidization process. The new peak apparently represents the coalesced signals, which may originate from a variety of the ageing products and from not fully consumed monomeric Phg. In that way, HPLC provides a convincing insight into the occurrence and dynamics of peptidization in the *L*-Cys–*L*-Phg system, additionally confirmed with the mass spectrometric results.

Figure 5 shows the chromatogram registered for the binary *L*-Cys–*L*-Pro system. The two peaks representing Cys ($t_R = 15.12$ min) and Pro ($t_R = 14.16$ min) are well resolved. Monitoring the progression of ageing for this pair of α-amino acids in the course of the four-day HPLC experiment did not result in any spectacular change of this chromatographic picture, except for a certain lowering of the peak heights, demonstrating a moderate peptidization progress. The relatively low dynamics of peptidization is also confirmed by the adequate mass spectrometric results.

2.3 Biuret Test

The biuret test, performed on microscopic slides for microgram quantities of the precipitates from the binary *L*-Cys–*L*-Phe, *L*-Cys–*L*-Phg, and *L*-Cys–*L*-Pro system, gave, in each case, an instantaneous positive result, i.e., an intense purple color appeared on the surface of the solid particles, demonstrating the presence of peptide bonds. For the sake of an example, in Figure 6a, we show the microscopic slide with the dried solid particles of the precipitate derived from the *L*-Cys–*L*-Phe system after one month ageing, and in Figure 6b, the same particles are shown, yet upon treatment with a drop of the biuret reagent. Fully analogous results were gained for the peptide particles originating from the remaining two binary α-amino acid systems. It is perhaps noteworthy that the analogous positive effect of the biuret test was documented for the lower (and therefore soluble) peptides originating from the aged *L*-Phe, *D*-Phe, and *rac*-Phe solutions in 70% aqueous methanol, as reported in our earlier study.[27]

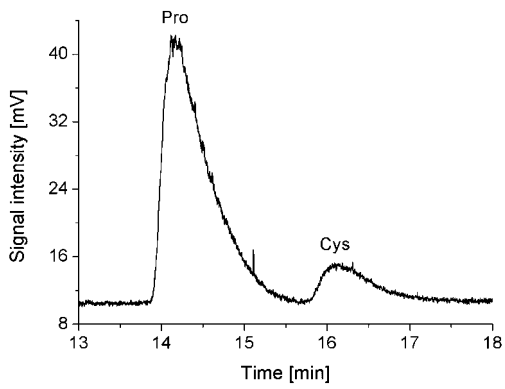

Figure 5. The HPLC-ELSD chromatogram recorded for the freshly prepared sample of the *L*-Cys–*L*-Pro system dissolved in 70% aqueous methanol.

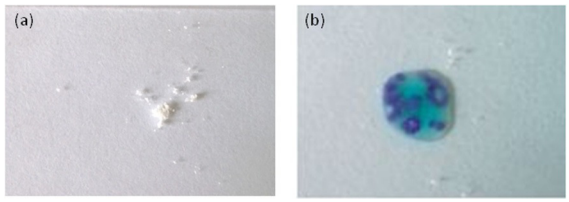

Figure 6. The microscopic slide with white particles of the peptide precipitate: a) separated by decantation from the liquid *L*-Cys–*L*-Phe system after one month ageing and evaporated to dryness; and b) treated with a drop of the biuret reagent to produce purple color as proof of the presence of peptide bonds.

2.4 Mass Spectrometry

Mass spectrometry was used to confirm that in the course of the storage of the investigated binary α-amino acid samples, homo- and heteropeptides were formed. In Figures 7a–7c, the respective mass spectra are presented, implemented with the tabulated data summarizing the *m*/*z* values of the predominant MS signals and suggesting possible structures for these signals, including the respective numbers of peptide bonds and disulfide bridges.

From a comparison of the registered mass spectra, it comes out that peptidization running in the *L*-Cys–*L*-Phe system characterizes with higher yields of the higher molecular-weight peptides than the *L*-Cys–*L*-Phg system, and the last one is the *L*-Cys–*L*-Pro system, which is the least efficient in this respect. These results remain in good agreement with those obtained with the use of HPLC-ELSD. In each spectrum given in Figures 7a–7c, signals originating from the *L*-Cys-derived homopeptides (e.g., signal at *m*/*z* 339.8, corresponding to the $[Cys_{13}–4H]^{4-}$ structure) are observed. Moreover, in each spectrum, signals coming from cysteic acid ($Cys(O_3H)$) (*m*/*z* 81.0 and 168.0),[28] the cystine ($(Cys)_2$) derived pseudomolecular ions with the conjugated $^{35}Cl^-$ or $^{37}Cl^-$ ions (*m*/*z* 274.8 and 276.7, respectively), and Cys with the conjugated $^{35}Cl^-$ ion (*m*/*z* 155.9) are present. Proportional dominance of the *L*-Cys-derived homopeptides over homopep-

© 2016 Wiley-VCH Verlag GmbH & Co. KGaA, Weinheim

a)

m/z	Proposed structure	No. -CO-NH-	No. -S-S-
81.0	$[Cys(O_3H)-H$ (mass loss 87)$]^-$	0	0
155.8	$[Cys + {}^{35}Cl]^-$	0	0
168.0	$[Cys(O_3H)-H]^-$	0	0
274.8	$[(Cys)_2+{}^{35}Cl]^-$	0	1
276.7	$[(Cys)_2+{}^{37}Cl]^-$	0	1
374.8	$[Cys_2 + Cys(O_3H)-H]^-$	2	0
534.6	$[(Cys)_2+Phe_2]^-$	2	1
575.9	$[Cys_4+Phe]^-$	4	1
735.8	$[Cys_7+2(Cys)_2+Phe_7-3H]^{3-}$	15	4
795.3	$[Cys_8+(Cys)_2+Phe_8-3H]^{3-}$	17	1
1162.0	$[Cys_4+Phe_5]^-$	8	2
1442.2	$[Cys_{10}+(Cys)_2+Phe_{11}-2H]^{2-}$	21	3
1551.5	$[Cys_6+Phe_6+{}^{35}Cl]^-$	11	2
1712.2	$[Cys_{19}+(Cys)_2+Phe_{20}-3H]^{3-}$	39	3

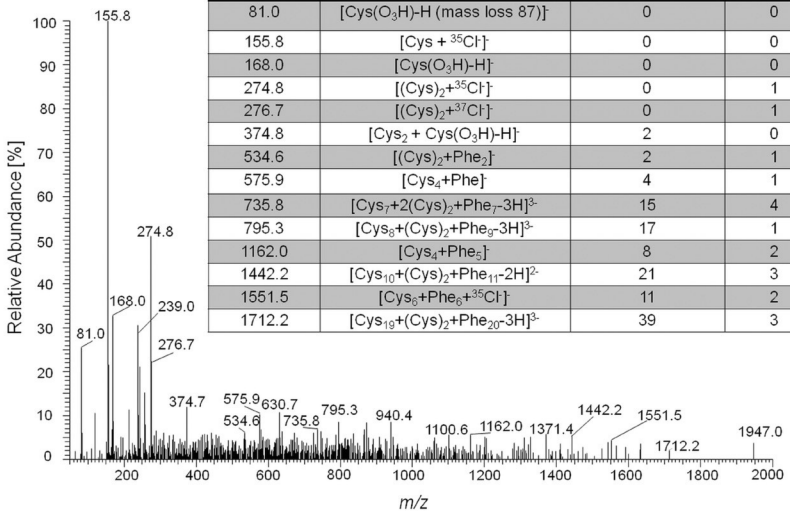

b)

m/z	Proposed structure	No. -CO-NH-	No. -S-S-
81.0	$[Cys(O_3H)-H$ (mass loss 87)$]^-$	0	0
155.9	$[Cys + {}^{35}Cl]^-$	0	0
274.8	$[(Cys)_2+{}^{35}Cl]^-$	0	1
276.8	$[(Cys)_2+{}^{37}Cl]^-$	0	1
289.0	$[Cys_4 + (Cys)_2 + Phg_6 - 5H]^{5-}$	10	1
351.8	$[Cys_7 + (Cys)_2 + Phg_6 - 5H]^{5-}$	13	1
374.8	$[Cys_2 + Cys(O_3H)-H]^-$	2	0
470.9	$[Cys_2 + (Cys)_2 + 2Cys(O_3H) + Phg_5 - 3H]^{3-}$	9	1
596.9	$[Cys_4 + Phg + {}^{35}Cl]^-$	4	0
740.8	$[Cys_5 + Cys(O_3H) + Phg_6 - 2H]^{2-}$	11	0
770.9	$[Cys_6 + (Cys)_2 + Cys(O_3H) + Phg_4 - 2H]^{2-}$	11	1

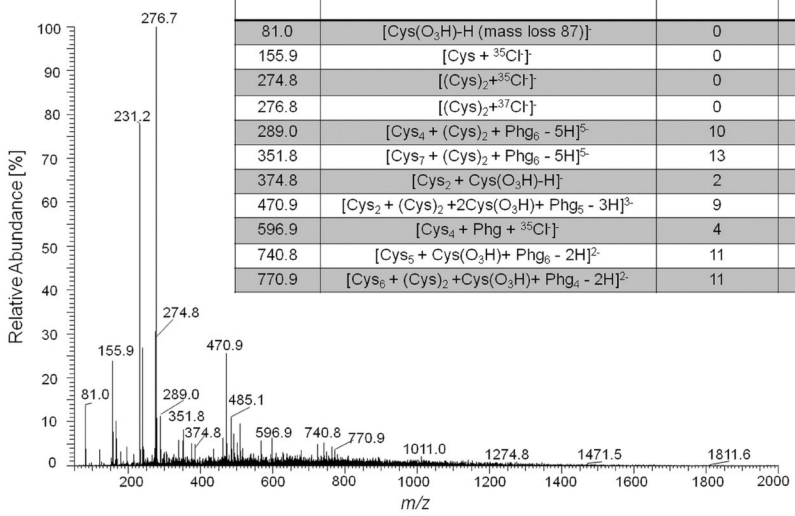

c)

m/z	Proposed structure	No. -CO-NH-	No. -S-S-
81.0	$[Cys(O_3H)-H$ (mass loss 87)$]^-$	0	0
155.9	$[Cys + {}^{35}Cl]^-$	0	0
168.0	$[Cys(O_3H)-H]^-$	0	0
274.8	$[(Cys)_2+{}^{35}Cl]^-$	0	1
339.8	$[Cys_{13} - 4H]^{4-}$	12	0
374.8	$[Cys_2 + Cys(O_3H)-H]^-$	2	0
423.3	$[Cys_3 + Pro - H]^-$	3	0
459.0	$[Cys_8+(Cys)_2 + Pro_8 - 4H]^{4-}$	16	1

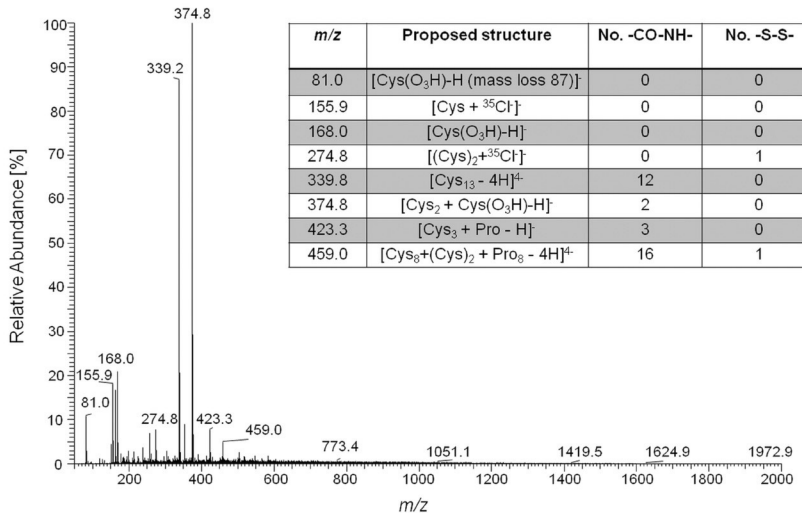

Figure 7. Mass spectra recorded in the negative ionization mode for the: a) *L*-Cys–*L*-Phe; b) *L*-Cys–*L*-Phg; and c) *L*-Cys–*L*-Pro system dissolved in 70% aqueous methanol and aged for 6 weeks, the suggested chemical structures of certain anions, and the respective numbers of peptide bonds (–CO–NH–) and sulfide bridges (–S–S–).

© 2016 Wiley-VCH Verlag GmbH & Co. KGaA, Weinheim

tides of the counterpart amino acids is evident, as the latter signals are usually low intensity and therefore hardly observed. However, in each discussed spectrum, signals originating from the respective heteropeptides are also present, and chemical structures which can be attributed to these signals are tabulated in Figures 7a–7c. In Figure 7a, all signals starting from m/z 534.6 (signal ascribed to $[Cys_2+Phe_2]^-$), are attributed to the Cys-Phe heteropeptides, and in some of them, the molecular contribution from Cys is dominant. In Figure 7b, most signals starting from m/z 289.0 (ascribed to $[Cys_4+(Cys)_2+Phg_6-5H]^{5-}$) are attributed to the Cys-Phg heteropeptides. In the case of the *L*-Cys–*L*-Pro system (Figure 7c), only two signals (at m/z 423.3 and 459.0, ascribed to $[Cys_3+Pro-H]^-$ and $[Cys_8+(Cys)_2+Pro_8\text{-}4H]^{4-}$, respectively) are attributed to the Cys-Pro heteropeptides. Thus, the mass spectrometric evidence is provided which confirms spontaneous formation of homo- and heteropeptides in the aged binary α-amino acid systems, and the dominance of Cys among the condensation products. This evidence remains in good agreement with the SEM results.

2.5 Closing Remarks

Experimental confirmation of the spontaneous formation of heteropeptides in the binary solutions of *L*-Cys–*L*-Phe, *L*-Cys–*L*-Phg, and *L*-Cys–*L*-Pro, obtained with use of HPLC and MS, remains in full agreement with our earlier findings, which are presented in numerous papers (e.g., Refs. [1,2,6,17,19,22]). Micrographs presented in this study provide experimental proof obtained with one more analytical technique (SEM) to show that peptides can be formed from the monomeric and enantiomerically pure α-amino acids in an abiotic aqueous organic system. The hallmarks of the heteropeptide formation in the three different binary α-amino acid systems are spherical microstructures shown in Figure 2, due to the presence of *L*-Cys in each investigated system. These spherical patterns are most probably due to the supramolecular peptide aggregations and clearly resemble spherical supramolecular entities obtained from the Cys-containing tripeptides shown in Ref. [9]. Although it would hardly be possible to establish a critical molar concentration (CMC) at which different homo- and heteropeptides start assembling into supramolecular aggregates kept together by intermolecular forces, it seems largely probable that even if highly diluted, the *L*-Cys monomer with its three functionalities (–SH, $–NH_2$, and –COOH) actively initiates the 3D homo- and hetero-oligopeptides formation, still before the supramolecular aggregates are formed. Moreover, it is worth remembering that peptidization in solution is a process which consists of sequential formation and decay of peptide bonds (with partial reconstitution of the amino-acid monomers).

The research presented in this study can also be viewed as a voice in a dialogue with the report given in Ref. [9] on the formation of the analogous spherical heteropeptide nanostructures from the *L*-Cys containing tripeptides dissolved in the 1,1,1,3,3,3-hexafluoro-2-propanol (HFP) (an analog of 2-propanol, yet devoid of the six hydrogen atoms and therefore employed as a protective solvent, with a minimized ability to form the H-bonds, basically for steric reasons). In that report, the authors proposed a model which assumes the formation of the *L*-Cys containing spherical peptides from peptide sheets by their closure along the two axes (Figure 5 in Ref. [9]), which in view of our earlier and present findings does not necessarily represent a real mechanism for spherical nanostructure formation. Namely, it is not guaranteed that HFP provides sufficient protection of the *L*-Cys containing tripeptides from a split off of the monomeric amino-acid units (due to the nonlinear peptidization process discovered in our earlier studies), so that the formation of the spherical supramolecular entities discussed in Ref. [9] can well start on a monomeric *L*-Cys level, induced by the three functionalities of this particular α-amino acid (a possibility postulated in this study).

3. Conclusion

The nonlinearity of spontaneous peptidization can easily be demonstrated with the use of HPLC. Morphological characterization of the peptides formed in the *L*-Cys-containing binary α-amino acid mixtures (and more specifically, the spherical shape thereof), as performed with use of SEM, strongly suggests that in each case, the heteropeptides are formed. This suggestion is convincingly supported by the biuret test and the respective MS results. SEM proves a very straightforward and robust analytical tool for studying peptidization of α-amino acids in abiotic liquid media.

4. Experimental

4.1 Reagents

In the experiment, we used *L*-Cys hydrochloride monohydrate (Reanal, Budapest, Hungary), *L*-Phe, *L*-Pro (Merck KGaA, Darmstadt, Germany), and *L*-Phg (Sigma-Aldrich, St Louis, MO, USA). All α-amino acids were of analytical purity. Methanol (Sigma-Aldrich) was of HPLC purity. Water was deionized and double distilled in our laboratory by means of the Elix Advantage model Millipore System (Molsheim, France).

For the SEM, HPLC, and MS experiments, concentrations of the investigated α-amino acids in the binary mixtures (dissolved in 70% aqueous MeOH) were $1.0\ mg\,mL^{-1}$ each (i.e., $8.25\times10^{-3}\ mol\cdot L^{-1}$ for *L*-Cys, $6.054\times10^{-3}\ mol\cdot L^{-1}$ for *L*-Phe, $6.15\times10^{-3}\ mol\cdot L^{-1}$ for *L*-

© 2016 Wiley-VCH Verlag GmbH & Co. KGaA, Weinheim

Phg, and 8.69×10^{-3} mol·L^{-1} for *L*-Pro). The 70% aqueous methanol, known for its strong antiseptic properties, was selected to protect the amino-acid solutions from microbial action in the experiments of sample ageing. Storage of samples for the purpose of the SEM, HPLC, and MS analyses was at 22±1 °C.

4.2 Scanning Electron Microscopy

Series of micrographs of the condensation products spontaneously formed as nano- and microstructures in the monocomponent and binary α-amino acid solutions in 70% aqueous methanol were recorded (upon the evaporation of the solvent to dryness) after the sample ageing period of two weeks (*L*-Cys, *L*-Phg, *L*-Cys–*L*-Phe, *L*-Cys–*L*-Phg, and *L*-Cys–*L*-Pro), three months (*L*-Phe), and one month (*L*-Pro) with use of the Jeol JSM-7600F model scanning electron microscope, SEM (Jeol, Japan).

4.3 HPLC

The condensation process instantaneously starting in each freshly prepared binary amino-acid solution was monitored by means of the achiral HPLC with the ELSD and DAD detectors. This HPLC mode was employed to resolve the oligopeptides from the non-peptidized amino acids and to fractionate the oligopeptides. The analyses were carried out using a Varian model 920 liquid chromatograph (Varian, Harbor City, CA, USA) equipped with a Varian 900-LC model auto sampler, a gradient pump, a Varian 380-LC model ELSD detector, and Galaxie software for data acquisition and processing. For the analysis of the *L*-Cys–*L*-Phe and *L*-Cys–*L*-Phg binary systems, the Varian C18 column (250 mm×4.6 mm i.d., 5 μm particle diameter; cat. no. A3000250C046) was used. For the analysis of the *L*-Cys–*L*-Pro binary system, the Hypersil C8 column (250 mm×4.6 mm i.d., 5 μm particle diameter; cat. no. 28205-254630) was used.

All analyses were carried out in the isocratic mode. With *L*-Cys–*L*-Phe and *L*-Cys–*L*-Phg, the injected sample aliquots were 5 μL, and MeOH:H_2O (20:80, v/v) was employed as the mobile phase at a flow rate of 0.8 mL min^{-1}. With *L*-Cys–*L*-Pro, the injected sample aliquots were 3 μL, and MeOH:H_2O (80:20, v/v) was employed as the mobile phase at a flow rate of 0.4 mL min^{-1}. The analysis of the *L*-Cys–*L*-Phe and *L*-Cys–*L*-Phg systems was carried out in 8 min intervals, and that of the *L*-Cys–*L*-Pro system, in 20 min intervals. The chromatographic columns were thermostatted at 35 °C in the Varian ProStar 510 model column oven.

4.4 Biuret Test

The biuret test, first described in 1961,[29] is now a standard analytical procedure enabling easy detection of the presence of peptides and proteins in many liquids (including blood and urine – it is widely used in medical analysis). In the biuret test, the Cu^{2+} ion forms complexes with at least two peptide groups; as a result of this, the system changes color from blue (characteristic of the solvated copper ions) to pink (characteristic of dipeptides) or purple (characteristic of higher peptides). The biuret reagent used in this study contained 78.6 g $CuSO_4\cdot7H_2O$ and 10 g $NaKC_4H_4O_6\cdot4H_2O$, 50 mL 10% (w/w) NaOH, and water, and the total volume was diluted to 1 L. In this solution, the concentration of Cu(II) ions was 0.26 mol L^{-1} and the concentration of NaOH was 2.7 mol L^{-1}.

The biuret test was performed upon the microgram quantities of the peptide precipitates separated from the *L*-Cys–*L*-Phe, *L*-Cys–*L*-Phg, and *L*-Cys–*L*-Pro system by the decantation, deposited on the microscopic slides and evaporated to dryness. Then each sample of the dry precipitate was treated with a drop of the biuret reagent.

4.5 Mass Spectrometry

Mass spectra of the *L*-Cys–*L*-Phe, *L*-Cys–*L*-Phg, and *L*-Cys–*L*-Pro solutions in 70% aqueous methanol aged for 6 weeks were recorded with the use of the Thermo LCQ Deca XP Plus MS system. The working MS conditions were as follows: ESI mode (ESI-MS scan, negative ionization, capillary voltage 50 V, needle voltage 5 kV, and needle temperature 250 °C).

Acknowledgements

One author (A.G.) acknowledges the financial support of the DoktoRIS project, co-financed by the European Union within the European Social Found.

References

[1] M. Sajewicz, M. Matlengiewicz, M. Leda, M. Gontarska, D. Kronenbach, T. Kowalska, I. R. Epstein, *J. Phys. Org. Chem.* **2010**, *23*, 1066–1073.
[2] M. Sajewicz, M. Gontarska, D. Kronenbach, M. Leda, T. Kowalska, I. R. Epstein, *J. Syst. Chem.* **2010**, *1*, 7.
[3] M. Sajewicz, R. Piętka, A. Pieniak, T. Kowalska, *Acta Chromatogr.* **2005**, *15*, 131–149.
[4] M. Sajewicz, M. Gontarska, M. Wróbel, T. Kowalska, *J. Liq. Chromatogr. Relat. Technol.* **2007**, *30*, 2193–2208.
[5] M. Sajewicz, D. Kronenbach, M. Gontarska, M. Wróbel, R. Pietka, T. Kowalska, *J. Planar Chromatogr. Mod. TLC* **2009**, *22*, 241–248.
[6] M. Sajewicz, M. Dolnik, D. Kronenbach, M. Gontarska, T. Kowalska, I. R. Epstein, *J. Phys. Chem. A* **2011**, *115*, 14331–14339.
[7] L. Adler-Abramovich, M. Reches, V. L. Sedman, S. Allen, S. J. B. Tendler, E. Gazit, *Langmuir* **2006**, *22*, 1313–1320.
[8] J. Ryu, C. B. Park, *Biotechnol. Bioeng.* **2010**, *105*, 221–230.
[9] M. Reches, E. Gazit, *Nano Lett.* **2004**, *4*, 581–585.
[10] C. H. Görbitz, *Chem. Commun.* **2006**, *22*, 2332–2334.

© 2016 Wiley-VCH Verlag GmbH & Co. KGaA, Weinheim

[11] A. V. Maltsev, S. Bystryak, O. Galzitskaya, *Ageing Res. Rev.* **2011**, *10*, 440–452.
[12] M. Tokunaga, M. L. Liu, T. Nagai, K. Iwanaga, K. Matsuura, T. Takahashi, M. Kanda, N. Kondo, P. Wang, A. T. Naito, I. Komuro, *J. Mol. Cell. Cardiol.* **2010**, *49*, 972–983.
[13] Y. Ueda, K. Ishii, Y. Toyama, M. Nakamura, H. Okano, *Neurosci. Res.* **2008**, *61*, S93.
[14] S. Debnath, S. Roy, R. V. Ulijn, *J. Am. Chem. Soc.* **2013**, *135*, 16789–16792.
[15] J. G. Samaritoni, A. T. Copes, D. K. Crews, C. Glos, A. L. Thompson, C. Wilson, M. J. O'Donnell, W. L. Scott, *J. Org. Chem.* **2014**, *79*, 3140–3151.
[16] V. Villani, A. M. Tamburro, J. M. Z. Comenges, *J. Chem. Soc. Perkin Trans.* **2000**, *2*, 2177–2184.
[17] A. Godziek, A. Maciejowska, M. Sajewicz, T. Kowalska, *J. Chromatogr. Sci.* **2015**, *53*, 401–410.
[18] M. Sajewicz, M. Matlengiewicz, M. Juziuk, M. Penkala, M. Weloe, M. Schulz, T. Kowalska, *J. Liq. Chromatogr. Relat. Technol.* **2013**, *36*, 2497–2511.
[19] A. Godziek, A. Maciejowska, E. Talik, R. Wrzalik, M. Sajewicz, T. Kowalska, *Curr. Protein Pept. Sci.* **2016**, *17*, 106–116.
[20] A. Maciejowska, A. Godziek, E. Talik, M. Sajewicz, T. Kowalska, I. R. Epstein, *J. Chromatogr. Sci.* **2016**, doi: 10.1093/chromsci/bmw073.
[21] A. Maciejowska, A. Godziek, E. Talik, M. Sajewicz, T. Kowalska, *J. Liq. Chromatogr. Relat. Technol.* **2015**, *38*, 1164–1171.
[22] M. Sajewicz, M. Gontarska, T. Kowalska, *J. Chromatogr. Sci.* **2014**, 52, 329–333.
[23] O. Carny, E. A. Gazit, *FASEB J.* **2005**, *19*, 1051–1055.
[24] E. R. Stadtman, *Ann. N. Y. Acad. Sci.* **2006**, *928*, 22–38.
[25] S. M. Kelly, N. C. Price, *Curr. Protein Pept. Sci.* **2000**, *1*, 349–384.
[26] *Amino Acids, Peptides and Proteins in Organic Chemistry* (Ed.: A. B. Hughes), Wiley-VCH Verlag GmbH & Co. KGaA, Weinheim, **2012**, p. 176–178.
[27] M. Sajewicz, M. Gontarska, D. Kronenbach, T. Kowalska, *Acta Chromatogr.* **2009**, *21*, 151–160.
[28] M. Piraud, C. Vianey-Saban, K. Petritis, C. Elfakir, J. P. Steghens, A. Morla, D. Bouchu, *Rapid Commun. Mass Spectrom.* **2003**, *17*, 1297–1311.
[29] H. C. Freeman, J. E. W. L. Smith, J. C. Taylor, *Acta Cryst.* **1961**, *14*, 407–418.

Received: July 9, 2016
Published online: August 16, 2016

© 2016 Wiley-VCH Verlag GmbH & Co. KGaA, Weinheim

Short Communication

Acta Chromatographica 29(2017)1, 135–142
DOI: 10.1556/1326.2017.29.1.00

Circadian Rhythm of Spontaneous non-Linear Peptidization with Proteinogenic Amino Acids in Abiotic Solutions *versus* Homochirality

A. MACIEJOWSKA, A. GODZIEK, M. SAJEWICZ and T. KOWALSKA*

Institute of Chemistry, University of Silesia, 9 Szkolna Street, 40-006 Katowice, Poland
*E-mail: teresa.kowalska@us.edu.pl

Summary. In this short communication, we report on three striking phenomena of the circadian rhythm. One was observed with the non-linear concentration changes of the monomeric *L*-Cys and the non-linear yields of the *L*-Cys derived peptides, when undergoing spontaneous non-linear peptidization. The other one was observed with the binary *L*-Phe-*L*-Pro system, and the third one with *L*-Ser, *D*-Ser, and *DL*-Ser. So far, no analogous reports have been released on the circadian rhythm of the spontaneous non-linear peptidization of proteinogenic amino acids in a sterile abiotic environment (70% aqueous acetonitrile, or 70% aqueous methanol solutions). At the moment, we cannot find any rational explanation of this phenomenon, yet it seems highly probable that its origin is analogous to or even of a primordial nature for the circadian rhythm phenomena abundantly found in biological samples by other researchers. An experimentally established lack of the circadian rhythm with peptidization of the non-proteinogenic amino acid (*D*-Ser) can encourage us to revisit a still unsolved question of homochirality preconditions.

Key Words: circadian rhythm, proteinogenic amino acids, spontaneous non-linear peptidization, HPLC-ELSD, turbidimetry, homochirality precondition

Experiment

Spontaneous non-linear peptidization of proteinogenic amino acids dissolved in aqueous organic solvents was demonstrated in our earlier reports (e.g., [1–5]), and possible molecular mechanism of this process was also discussed. These investigations were carried out for the solutions containing single amino acids and the amino acid pairs. In paper [5], a theoretical model was proposed assuming four possible cases of spontaneous peptidization in solutions containing a pair of amino acids.

The main analytical tool employed in the aforementioned papers to trace spontaneous non-linear changes of the amino acid concentration in the course of sample storage (and ageing) was high-performance liquid chro-

This is an open-access article distributed under the terms of the Creative Commons Attribution License, which permits unrestricted use, distribution, and reproduction in any medium for non-commercial purposes, provided the original author and source are credited.

First published online: October 21, 2015 *ISSN 2083-5736 © The Author(s)*

matography with evaporative light scattering detection (HPLC–ELSD). With its aid, the monomeric amino acid fraction can be separated from the spontaneously formed peptides and the time series of the changing peak heights valid for the monomeric amino acid witnesses to its non-linear concentration changes in the course of storage. These changes provide an indirect hint as to the non-linear changes of the resulting peptide yields also. Direct evidence of the non-linear changes of peptide yields can be obtained with aid of turbidimetric measurements in continuous mode. Such measurements can reveal non-linear turbidity changes of the amino acid solution (unequivocal with the changing peptide yields) right from the moment of the amino acid dissolution and long before the insoluble higher peptides precipitate, which then can be traced with human eye.

Currently, we intend to focus on our results mostly published elsewhere, yet without earlier pointing out to one of the most striking features of the spontaneous non-linear peptidization of the proteinogenic amino acids, and namely on the circadian rhythm of this process, revealed both with aid of HPLC-ELSD and turbidimetry.

First example demonstrates the circadian rhythm of the non-linear concentration and the yield changes with the monomeric *L*-Cys and the *L*-Cys-derived peptides, respectively, as traced in the course of the 4 days lasting *L*-Cys solution storage. Details concerning the experimental conditions are given elsewhere [6] and here, let us only emphasize that the investigated samples were protected from the day-night light changes (both in the autosampler of the chromatograph and the turbidimetric cell). Moreover, the chromatographic column of the C_{18} type used for the HPLC-ELSD experiments was thermostatted at 35˚C, and turbidimeter was put in a foamed polystyrene box to preserve constant temperature throughout an entire experiment (22±0.5˚C). Last not least, the *L*-Cys sample was prepared in the aseptic 70% aqueous acetonitrile. The results obtained are shown in *Fig 1(a),(b).* Above each of the two plots, roughly estimated periods of the plot shape repetitions are given. In the case of the concentration changes with the monomeric *L*-Cys, these periods range from 23.75 to 24.95 h, and the analogous repetition periods on the plot of the peptide yield changes range from 21.60 to 25.20 h. Taking into account the physical difference between the monomeric *L*-Cys concentration and an overall turbidity of the peptides containing *L*-Cys solution, and the difference in accuracy of the chromatographic and turbidimetric measurements, there is no doubt that the two result sets given in *Fig. 1(a),(b)* unequivocally witness to the circadian rhythm of the *L*-Cys peptidization.

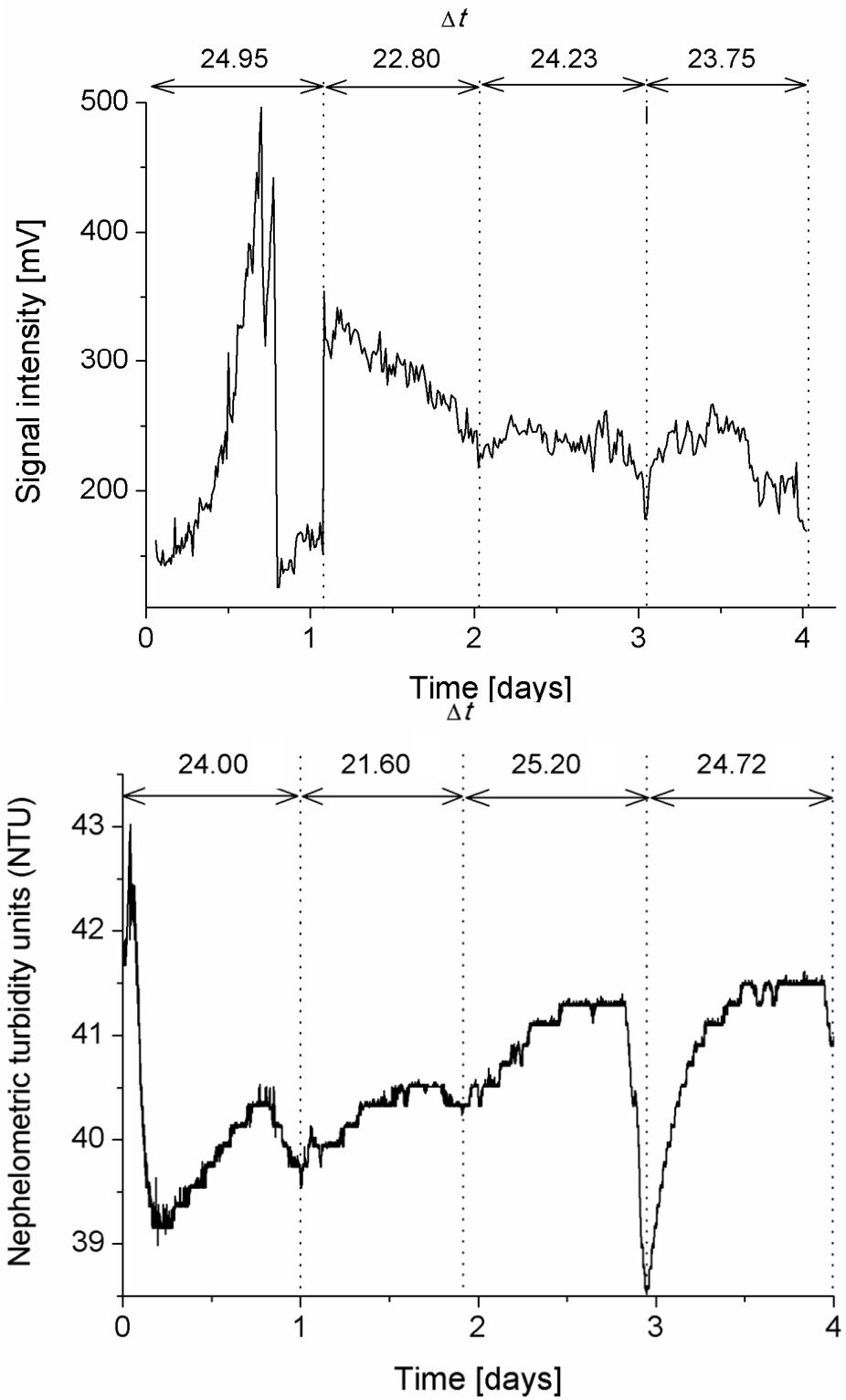

Fig. 1. (a) The chromatographic peak height changes of the monomeric *L*-Cys and (b) the turbidity changes for the *L*-Cys solution in 70% aqueous acetonitrile in the initial 4 days of the sample storage. Concentration of *L*-Cys was equal to 0.7 mg mL^{-1} (5.77×10^{-3} mol L^{-1}). Duration of the plot shape repetition periods (Δt, [h]) is marked above the respective plots

Second example demonstrates the circadian rhythm of the non-linear concentration changes with *L*-Phe and *L*-Pro in the binary *L*-Phe-*L*-Pro system, and the circadian rhythm of the turbidity changes in the same system, as traced in the course of the 11 days lasting sample storage. The HPLC-ELSD results valid for second example were originally presented in paper [3]. The *L*-Phe-*L*-Pro sample was also dissolved in 70% aqueous acetonitrile, and it was protected from the day-night light changes in the autosampler of the chromatograph and the turbidimetric cell, respectively. The chromatographic column of the C_{18} type was thermostatted at 35° and the turbidimeter temperature was kept steady in the previously described way (22±0.5°C). The results obtained are shown in *Fig. 2(a),(b)*. Periodicity of the plot shape repetitions (HPLC-ELSD) valid for *L*-Phe and *L*-Pro ranges from 18.23 to 25.67 h, yet in most cases the repeatability periods are closer to each other and range from 20.40 to 23.51 h *(Fig. 2(a))*. Even more regular is the shape of the registered turbidity plot *(Fig. 2(b))* and in this case, the plot repeatability periods hold between 19.66 and 26.80 h. Thus it can be stated that spontaneous peptidization of *L*-Phe and *L*-Pro in the binary *L*-Phe-*L*-Pro system proceeds in the circadian rhythm.

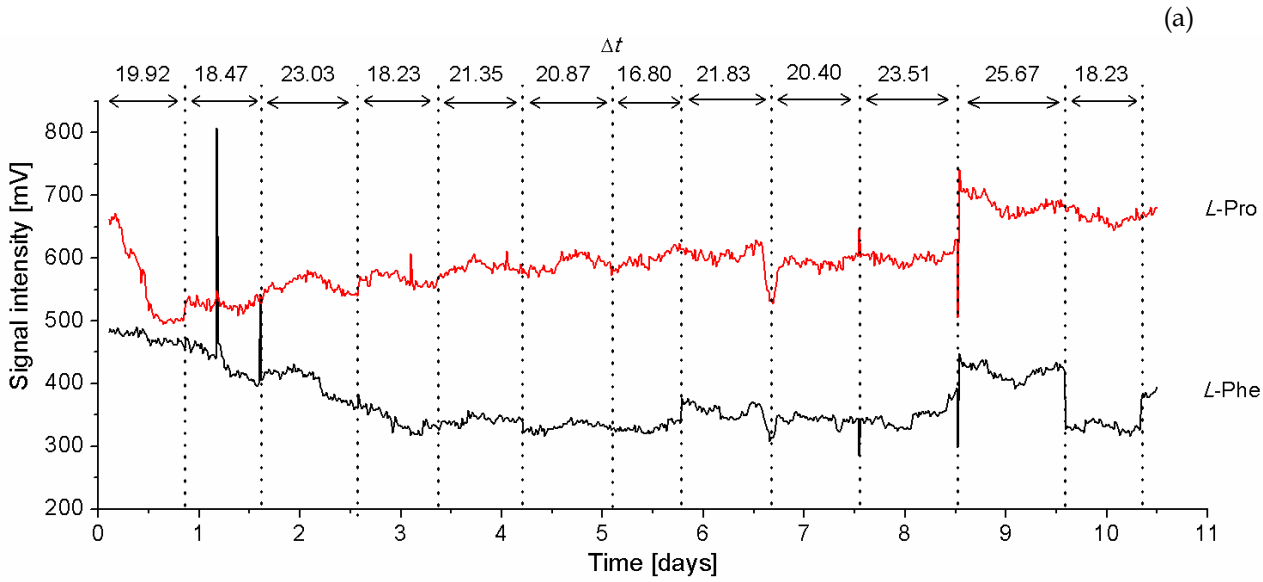

Fig. 2. (a) The chromatographic peak height changes of the monomeric *L*-Phe and *L*-Pro in the binary *L*-Phe-*L*-Pro solution in 70% aqueous acetonitrile and (b) the turbidity changes for the *L*-Phe-*L*-Pro solution in 70% aqueous acetonitrile in the initial 11 days of sample storage. Concentration of *L*-Phe and *L*-Pro was equal to 1.0 and 1.0 mg mL^{-1} (6.05×10^{-3} and 8.69×10^{-3} mol L^{-1}), respectively. Duration of the plot shape repetition periods (Δt, [h]) is marked above the respective plots

(b)

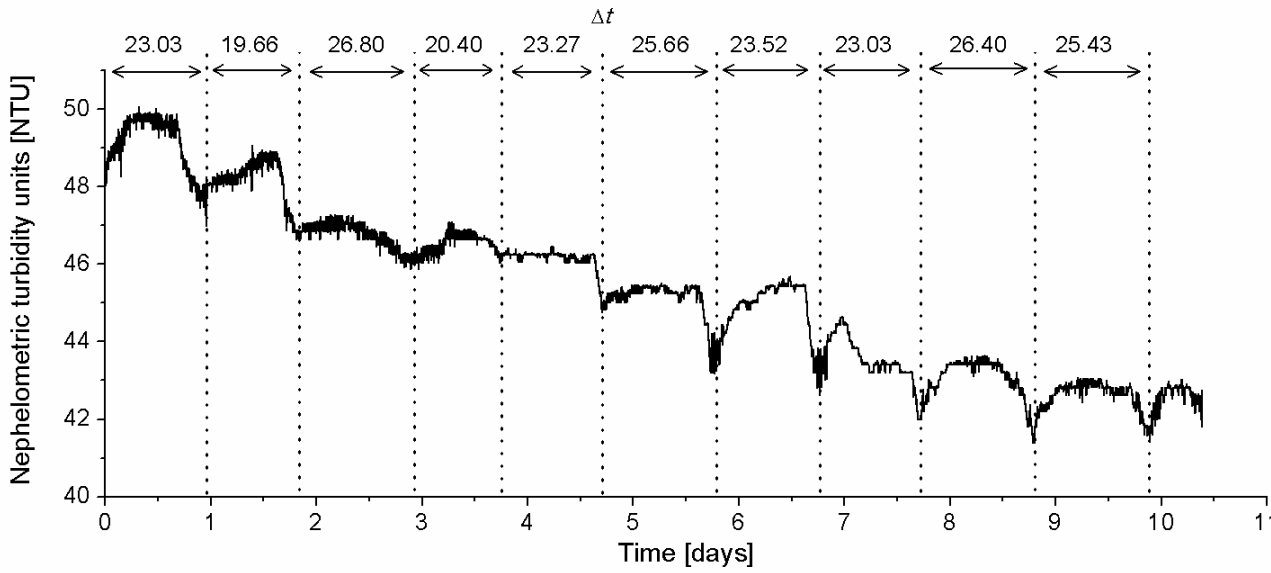

Fig. 2. Cont.

The turbidimetric results of the third experiment are presented for the first time now and they refer to *L*-Ser (proteinogenic amino acid), *D*-Ser (non-proteinogenic amino acid), and *DL*-Ser (the racemic mixture of the Ser enantiomers) dissolved in a strongly antiseptic 70% aqueous methanol. These results were recorded in the course of the 7 days sample storage period and similar to the two aforementioned examples, also in this case the turbidimeter was kept at constant temperature (22±0.5°C) throughout an entire experiment. The results obtained are given in *Fig. 3(a)–(c).* Based on the plot presented in *Fig. 3a* and valid for *L*-Ser, it can be stated that although the plot shape repetition periods differ from 19.66 to 32.63 h, most of them range from 21.12 to 25.20 h, which well corresponds with the circadian rhythm. In the case of *D*-Ser (which is a non-proteinogenic amino acid), no circadian peptidization rhythm is observed and sample turbidity is monotonously growing (in pace with the growing peptide yields), except for one maximum after ca. 2 days storage period *(Fig. 3(b)).* In the case of *DL*-Ser, irregular repetitions of the plot shape pattern are observed, apparently as a kind of a 'compromise' between the regularity of the *L*-Ser pattern and no plot shape repetitions with *D*-Ser *(Fig. 3(c)).* The most amazing outcome of this experiment is that the circadian peptidization rhythm holds for the proteinogenic *L*-Ser only, whereas no such rhythm is observed with the non-proteinogenic *D*-Ser. Thus a supposal can be formulated that maybe the necessary precondition for the homochirality of amino acids in human and

animal tissues is founded on the circadian rhythm of the proteinogenic amino acids involved, although a tedious and thorough experimental confirmation of this supposal is inevitable.

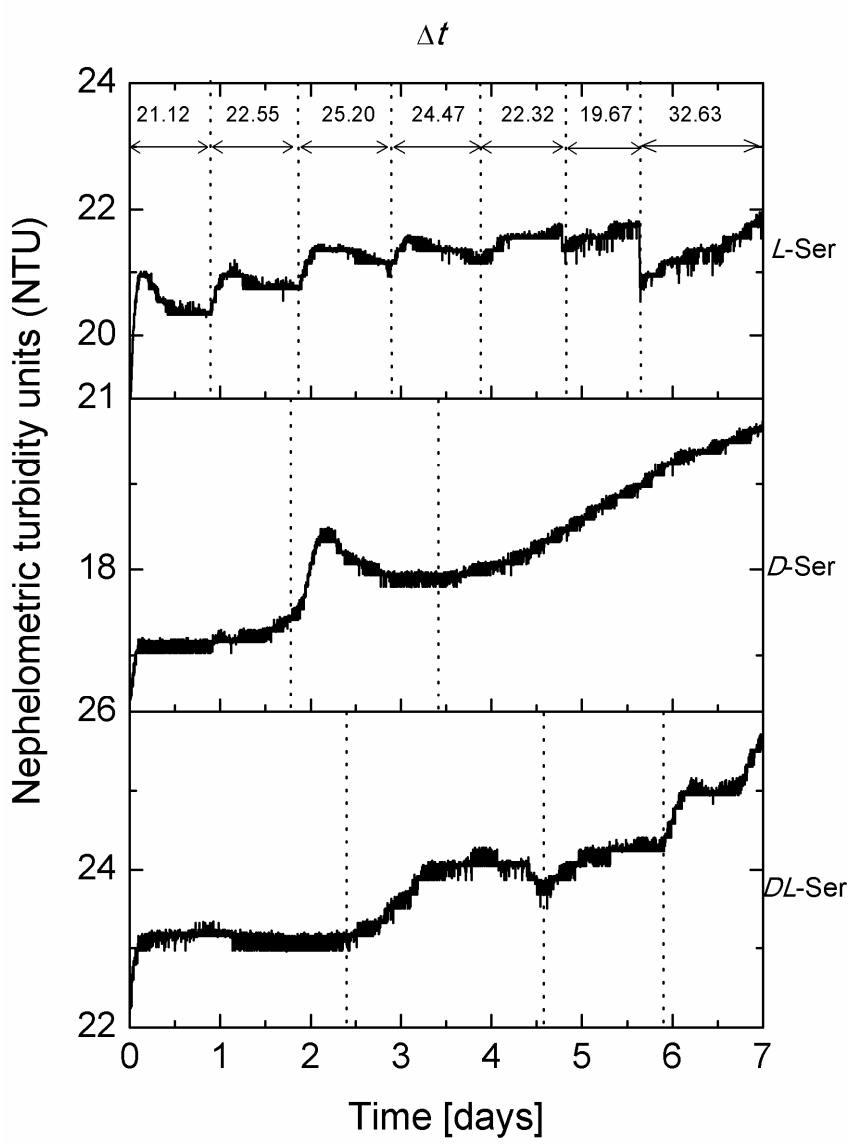

Fig. 3. The turbidity changes for the *L*-Ser, *D*-Ser, and *DL*-Ser solution in 70% aqueous methanol in the initial 7 days of sample storage. Concentration of *L*-Ser, *D*-Ser, and *DL*-Ser was equal to 1.0 mg mL^{-1} (9.44×10^{-3} mol L^{-1}). Duration of the plot shape repetition periods (Δt, [h]) valid for *L*-Ser is marked above the plot of *L*-Ser

Finally, it has to be added that the turbidimetric measurements were performed for all solvents used in our experiments (water, acetronitrile, methanol, 70% aqueous acetonitile, and 70% aqueous methanol), and stability of the turbidity levels was confirmed with each tested solvent system.

Discussion

The circadian rhythm of the peptide concentration changes and the other physiological phenomena has been revealed by many researchers in biological material, and investigated both under the *in vivo* and *in vitro* conditions (e.g., [8–13]). Up to our best knowledge, this is the first report in the literature on the circadian rhythm of the non-linear concentration changes with the monomeric amino acids and the resulting peptides, carried out in full abstraction from any biological matter, and with use of the commercially obtained amino acids of analytical purity and the HPLC purity grade solvents only.

Conclusion

We cannot offer any rational explanation of the circadian rhythm observed with four proteinogenic amino acids discussed in this study (and not taking place with one non-proteinogenic amino acid). It can only be speculated that the proteinogenic amino acids formed in the evolutionary course of biogenesis characterize with physicochemical properties (like, e.g., the pK_a values, the dipole moments, the electric permeabilities, etc.) which in some way promote this circadian rhythm. Moreover, it seems probable that the circadian rhythm of spontaneous non-linear peptidization observed with proteinogenic amino acids is of a primordial nature and the same mechanism is responsible for the circadian rhythms widely observed with biological matter. In other words, maybe the proteinogenic amino acids act as triggers of the circadian clocks abundantly observed in Nature. Last not least, an observation of the circadian peptidization rhythm with *L*-Ser and no such effect with *D*-Ser naturally reminds us of the so far unknown sources of homochirality. In future experiments, the dynamics of spontaneous peptidization with *D*-isomers of proteinogenic amino acids should be tested to find out if the circadian peptidization rhythm occurs with the proteinogenic *L*-amino acids only.

References

[1] M. Sajewicz, M. Matlengiewicz, M. Leda, M. Gontarska, D. Kronenbach, T. Kowalska, and I.R. Epstein, J. Phys. Org. Chem., **23,** 1066–1073 (2010)

[2] M. Sajewicz, M. Gontarska, D. Kronenbach, M. Leda, T. Kowalska, and I.R. Epstein, J. Syst. Chem., **1**:7 (2010); DOI:10.1186/1759-2208-1-7

[3] M. Sajewicz, A. Godziek, A. Maciejowska, and T. Kowalska, J. Chromatogr. Sci., **53,** 31–37 (2015)
[4] A. Godziek, A. Maciejowska, M. Sajewicz, and T. Kowalska, J. Chromatogr. Sci., **53,** 401–410 (2015)
[5] M. Sajewicz, M. Dolnik, T. Kowalska, and I.R. Epstein, RSC Advances, **4,** 7330–7339 (2014)
[6] A. Maciejowska, A. Godziek, E. Talik, M. Sajewicz, T. Kowalska and I.R. Epstein, paper in preparation
[7] A. Godziek, A. Maciejowska, E. Talik, R. Wrzalik, M. Sajewicz, and T. Kowalska, Curry. Protein Pept. Sci. (accepted)
[8] M. Nakajima, K. Imai, H. Ito, T. Nishiwaki, Y. Murayama, H. Iwasaki, T. Oyama, and T. Kondo, Science, **308**, 414–415 (2005)
[9] J.L. Ditty, S.B. Williams, and S.S. Golden, Annu. Rev. Genet. **37,** 513–543 (2003)
[10] C.H. Johnson, Curr. Issues Mol. Biol. **6,** 103–110 (2004)
[11] C.H. Johnson and M. Egli, Nat. Struct. Mol. Biol. **11,** 584–585 (2004)
[12] D. Staiger, J. Shin, M. Johansson, and S.J Davis, Genome Biol., **14,** 208 (2013)
[13] K.M. Vaze and V.K. Sharma, Chronobiol. Intern., **30,** 413–433 (2013)

LISTA POZOSTAŁYCH PRAC WŁASNYCH

Thin-Layer Chromatographic Investigation of L-Cysteine in Solution

Agnieszka Godziek, Anna Maciejowska, Ewa Talik, Mieczysław Sajewicz, and **Teresa Kowalska***

Key Words

Cysteine
Spontaneous chiral inversion
Spontaneous condensation
Thin-layer chromatography–mass spectrometry
High-performance liquid chromatography–evaporative light scattering detection
High-performance liquid chromatography–mass spectrometry

Summary

Spontaneous oscillatory chiral conversion and condensation of low-molecular-weight chiral carboxylic acids have been investigated by our research group for almost 10 years now. However, dynamics of these oscillatory processes substantially differ from one compound to another, moreover, spontaneous chiral conversion and condensation of sulfur-containing amino acids have not been investigated so far. To this effect, we present in this paper the results of our current investigations on spontaneous oscillatory chiral conversion and condensation of L-cysteine (L-Cys), a biologically important sulfur-containing semiessential amino acid. In our thin-layer chromatographic experiments, we employ the Mn(II) and Zn(II) cations to facilitate the enantioseparation of L-Cys from the spontaneously formed D-Cys, to prevent chiral conversion of the *L* form, and to highlight rapid consumption of Cys in the course of condensation. Spontaneous peptidization of Cys is confirmed with use of thin-layer chromatography–mass spectrometry (TLC–MS). Additionally, we emphasize the oscillatory nature of the investigated process with use of high-performance liquid chromatography–evaporative light scattering detection (HPLC–ELSD) and provide a complementary insight in the chemical structure of the spontaneously formed Cys-derived oligopeptides with use of HPLC–MS.

1 Introduction

In our studies carried out in the course of the last decade, much attention has been paid to spontaneous oscillatory processes of chiral conversion and condensation, which occur with the low-molecular-weight chiral carboxylic acids, when dissolved both in aqueous and nonaqueous solvents. In paper [1], the phenomenon of spontaneous oscillatory chiral conversion (revealed by use of thin-layer chromatography (TLC)–densitometry) was for the first time reported for several propionic acid derivatives as the test analytes, stored for longer periods of time in 70% aqueous ethanol. In paper [2], an analogous evidence of spontaneous chiral conversion was presented, this time obtained with use of high-performance liquid chromatography (HPLC)–diode-array detection (DAD). Later, we demonstrated that the oscillatory chiral conversion occurs with low molecular weight carboxylic acids from the groups of amino acids [3] and hydroxyl acids [4]. Chiral conversion of such compounds can occur according to the two different pathways. In aqueous solutions, the general scheme can be represented as [4]:

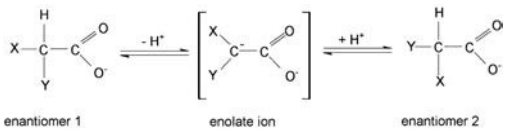

where X: –R (aliphatic) and Y: $–NH_2$, –OH, or –Ar (aromatic).

In anhydrous media and in the presence of trace amounts of water, the probable mechanism of chiral conversion is [6]:

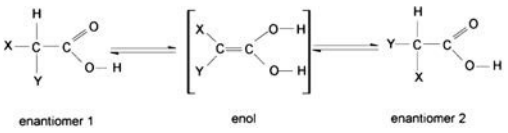

From our earlier investigations, it came out that the oscillatory chiral conversion of the low molecular weight carboxylic acids occurs in parallel with the oscillatory condensation, which most probably has thermodynamic justification [2]. In papers [7, 8], we presented the results of spontaneous oscillatory condensation for the three binary amino acid systems (L-Pro-L-Hyp, L-Pro-L-Phe, and L-Hyp-L-Phe), dissolved in aqueous organic solvents. The parallel processes of chiral conversion and peptidization of low-molecular-weight carboxylic acids can be illustrated by the following scheme, adapted to L-cysteine (L-Cys) dissolved in the aqueous organic medium, which is going to be discussed in this study [9]:

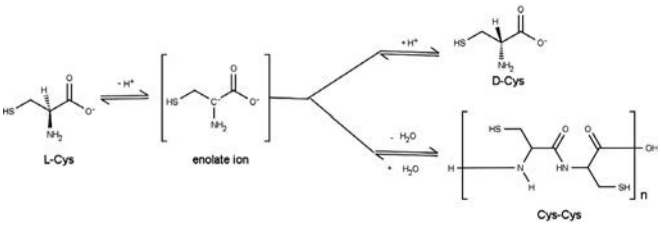

A. Godziek, A. Maciejowska, M. Sajewicz, and T. Kowalska, Institute of Chemistry, University of Silesia, 9 Szkolna Street, 40-006 Katowice, Poland; and E. Talik, Department of Physics of Crystals, Institute of Physics, University of Silesia, 4 Uniwersytecka Street, 40-007 Katowice, Poland.
E-mail: teresa.kowalska@us.edu.pl

0933-4173/$ 20.00 © Akadémiai Kiadó, Budapest
DOI: 10.1556/JPC.28.2015.2.10

An ability of low-molecular-weight carboxylic acids to undergo chiral conversion poses a serious question mark on a possibility of the enantioseparation thereof and, hence, on quantification of the enantiomer ratio, which appears an unstable magnitude fluctuating in the function of time. Due to the parallel process of condensation, a tendency is observed of a gradual dropdown of the monomer concentration in ageing solutions. Due to these two simultaneously running processes, chromatographic analysis of the nonderivatized amino acids becomes a challenging task indeed.

Unlike HPLC, where all separated species end up in an effluent tank, TLC is a handy option which allows unconventional modifications of stationary phases and an *in situ* preservation of the separated species for further examinations. Therefore, TLC is very well suited for studying impact of storage time on amino acids in solution, which bears an obvious importance from the life sciences perspective.

In this study, we focused our attention on L-Cys as an important sulfur-containing semi-essential amino acid, which can be biosynthesized in humans, and yet, due to its relatively low content in food, it is also used as a food additive (denoted as E920). L-Cys is an important building block of proteins that are used throughout the body, and it can physiologically be transformed to glutathione (a powerful antioxidant [10]), or taurine (essential for cardiovascular function, development and function of skeletal muscles, the retina, and the central nervous system [11]).

The main aim of this study was to employ TLC–densitometry and TLC–MS in order to demonstrate an ability of L-Cys to undergo chiral conversion and condensation, when dissolved in an aqueous organic solvent. Confirmation of the TLC results was obtained with aid of high-performance liquid chromatography with evaporative light scattering and mass spectrometric detection (*i.e.,* HPLC–ELSD and HPLC–MS, respectively).

2 Experimental

2.1 Reagents

L-Cys and DL-Cys (both as hydrochlorides) of analytical purity grade were purchased from Reanal (Budapest, Hungary). Manganese(II) acetate, pyridine, 2-butanol (Sigma-Aldrich, St Louis, MO, USA), ninhydrin, zinc(II) nitrate, and glacial acetic acid (PPH POCh, Gliwice, Poland) were also of the analytical purity grade. Methanol, acetonitrile (Sigma-Aldrich), and 2-propanol (Roth, Karlsruhe, Germany) were of the HPLC purity grade. Water was deionized and double distilled in our laboratory by means of the Elix Advantage model Millipore system (Millipore, Molsheim, France).

2.2 Scanning Electron Microscopy (SEM)

Series of micrographs of the L-Cys microspheric condensation products obtained after 2 weeks of the amino acid solution ageing were recorded by use of the Jeol JSM-7600F model scanning electron microscope, SEM (Jeol, Japan). These microspheres were recorded from the L-Cys solution in 70% aqueous acetonitrile evaporated to dryness.

2.3 Thin-Layer Chromatography (TLC)

Two thin-layer chromatographic experiments were performed on the commercial 20 cm × 20 cm microcrystalline cellulose plates (Merck; cat. No. 1.05716). For densitometric scanning of the chromatograms (performed in the reflectance mode), concentration of L-Cys and DL-Cys in 70% aqueous acetonitrile was 0.7 mg mL^{-1} (*i.e.,* 5.77×10^{-3} mol L^{-1}).

In experiment 1, 2-butanol–pyridine–glacial acetic acid–water (30:20:6:24, *v*/*v*) was used as the mobile phase. Plates were activated by heating for 30 min at 110°C prior to applying the amino acid samples. Just before the chromatographic analysis, an equimolar amount of manganese(II) acetate was added to the fresh L-Cys solution, fresh DL-Cys solution, and the L-Cys solution after 60 days ageing, and then, the samples were spotwise applied to the plates in the 5 µL aliquots, 1.5 cm apart, and 1 cm above the lower edge of the plate. The chromatograms were developed to the distance of 7 cm, and the development time was ca. 3 h. After the development, the plates were dried and the chromatograms were visualized by spraying the plates with the 0.5% ninhydrin solution in 2-propanol, followed by heating for 5 min at 110°C.

In experiment 2, first, the stock L-Cys solution was prepared. From this fresh stock L-Cys solution, 1 mL was withdrawn and spiked with an equimolar amount of zinc(II) nitrate, and the remaining lot was stored for ageing. From this 1 mL fresh solution spiked with zinc(II) nitrate, the 5 µL aliquot was spotwise applied to the chromatographic plate. After the 1-h long storage of the Cys stock solution again, 1 mL was withdrawn, spiked with an equimolar amount of zinc(II) nitrate, and from this sample, the 5 µL aliquot was spotwise applied to the chromatographic plate. This procedure in the 1-h intervals was carried out for 5 h. At the end, the chromatographic plate with the Cys samples after 0, 1, 2, 3, 4, and 5 h storage period was developed. Stationary and mobile phase and all other working conditions (except for activation of the plates, which was not done in experiment 2) were the same as in experiment 1.

The visualized chromatograms were densitometrically scanned by use of a Desaga (Heidelberg, Germany) model CD 60 densitometer equipped with the Windows-compatible ProQuant software. Concentration profiles of the development lanes were recorded in the reflectance mode, at the carefully selected wavelength $\lambda = 485$ nm. The obtained results were also recorded with a digital camera. All thin-layer chromatographic experiments were performed in triplicate.

2.4 Thin-Layer Chromatography–Mass Spectrometry (TLC–MS)

The TLC–MS experiments were performed for the chromatograms obtained in the analogous way, as those earlier described in Section 2.3 for experiment 1, yet without using ninhydrin as a visualizing agent. In fact, we focused our attention on one spot with the highest retardation factor ($R_F = 0.60 \pm 0.02$), which appeared yellow upon visualization and was attributed to the least retarded peptide fraction. In this experiment, we employed a TLC–MS interface (CAMAG, Muttenz, Switzerland), which enabled direct elution of individual chromatographic bands from the plate to the LC–MS system. Elution of the target ("yellow") spots was carried out with 50% aqueous methanol. The employed LC–MS System Varian (Varian, Palo Alto, CA, USA)

was equipped with the Varian ProStar model pump, the Varian 100-MS mass spectrometer, and the Varian MS Workstation v. 6.9.1 software for data acquisition and processing. This system operated under the following working conditions: the mobile phase was methanol–water (50:50, *v/v*) at the flow rate of 0.20 mL min^{-1}. Mass spectrometric detection was carried out in the ESI mode (extended ESI–MS scan from *m/z* 100 to 3500, positive ionization; spray chamber temperature, 50°C; drying gas temperature, 350°C; drying gas pressure, 25 psi; capillary voltage, 50 V; needle voltage, 5 kV).

2.5 High-Performance Liquid Chromatography with Evaporative Light Scattering Detection (HPLC–ELSD)

The process of ageing of the fresh prepared L-Cys solution was monitored by use of HPLC–ELSD. Concentration of L-Cys was 0.7 mg mL^{-1} (5.77×10^{-3} mol L^{-1}). The chromatograms were recorded by use of the Varian model 920 liquid chromatograph (Varian, Harbor City, CA, USA) equipped with the Varian 900-LC model autosampler, the gradient pump, the Varian model 330 DAD detector, the Varian 380-LC model ELSD detector, the ThermoQuest Hypersil C18 column (5 µm particle size column), and the Galaxie software for data acquisition and processing. The analyses of the investigated Cys solution were carried out for the 10-µL sample aliquots in the 10-minute intervals for the period of 75 h. Methanol–water (20:80, *v/v*) in the isocratic mode at the flow rate 0.8 mL min^{-1} was used as the mobile phase. The column was thermostated at 35°C in the Varian Pro Star 510 model column oven.

2.6 High-Performance Liquid Chromatography with Mass Spectrometric Detection (HPLC–MS)

The high-performance liquid chromatographic system described in Section 2.5 was additionally equipped with the Varian 100-MS mass spectrometric detector. The detection was carried out under the same working conditions as those described in Section 2.4. By use of mass spectrometric detector, mass spectra were systematically collected for the L-Cys samples analyzed by the HPLC–ELSD system. In this study, we present two mass spectra, one performed for the fresh prepared L-Cys sample, and the other one for that after a 4-day storage period.

3 Results and Discussion

The main goal of this study was to check if L-Cys (which is a proteinogenic amino acid) can undergo spontaneous oscillatory chiral conversion and peptidization. Its choice was due to the important physiological functions of L-Cys in living organisms. For example, it is present in creatine and appears inevitable for the synthesis of collagen, thus, positively affecting structure and appearance of hair, skin, and nails. Detoxificating and antioxidant properties of L-Cys protect liver and brain from damages caused, *e.g.,* by alcohol. Moreover, it can easily bond heavy metals and, hence, facilitate removal thereof from living organisms.

Cys molecule is equipped with three functionalities ($–NH_2$, –COOH, and –SH), which enable bonding other molecules in the three different planes (see **Figure 1a**) and, consequently, facilitate formation of the three-dimensional polycondensate structures. Moreover, in the cysteine condensation products, two types of covalent bonds can appear, *i.e.,* the peptide and the disulfide bonds. In **Figure 1b,** two simplest cysteine condensation products are shown, *i.e.,* cysteine dipeptide and cysteine dimer coupled through the disulfide bond.

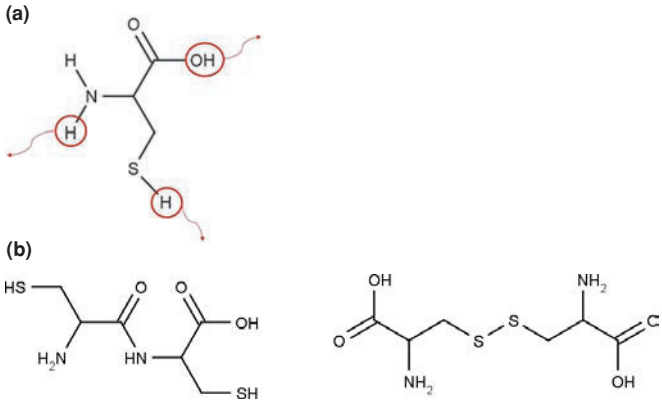

Figure 1

(a) Molecular structure of L-Cys with marked three functionalities able to participate in spontaneous 3D condensation process; (b) structures of the Cys dimers coupled through the peptide (–CO–NH–) and disulfide (–S–S–) bond.

3.1 Scanning Electron Microscopy (SEM)

In order to check if L-Cys can undergo spontaneous condensation process, its solution was prepared in aqueous acetonitrile and stored for a few weeks in a stoppered volumetric flask at room temperature (21 ± 1°C). After less than 14 days storage only, the white spherical microstructures appeared in that flask, perceptible with a naked eye (see **Figure 2a**). In order to get a better insight in

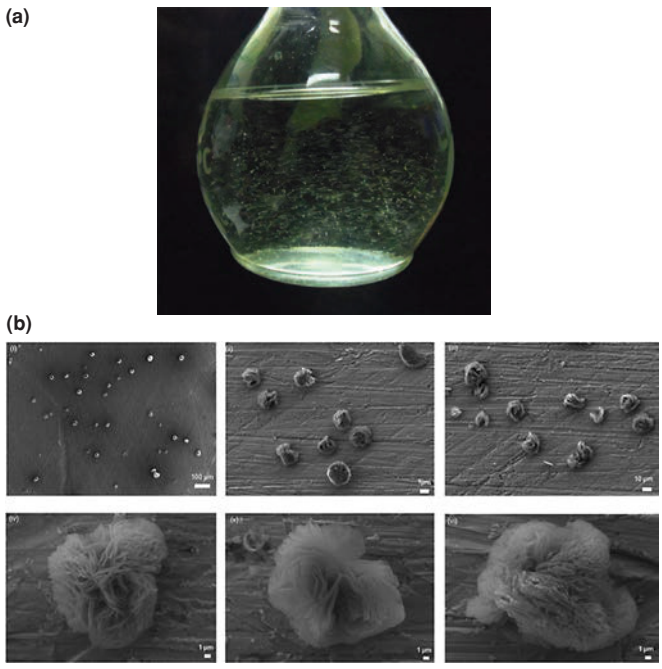

Figure 2

Spontaneous condensation of L-Cys; (a) suspension of Cys-derived oligomers in volumetric flask; (b) (i)–(vi) SEM micrographs of the Cys microstructures from the solution residue evaporated to dryness; magnification of (i) ×90, (ii) ×500, (iii) ×500, (iv) ×3700, (v) ×3700, and (vi) ×4000. Size bars make insets in each individual picture.

these spherical microstructures, their micrographs were recorded by use of a scanning electron microscope (SEM). To this effect, the Cys solution droplet was transferred from the volumetric flask to a brass test knob and left to evaporate to dryness. In **Figure 2b,** the micrographs of the Cys-derived microstructures are shown and their spherical shape is most probably due to the aforementioned three Cys functionalities, which promote the 3D shape of the respective condensation products. These spherical microstructures are fully analogous to those shown in the SEM micrographs in ref. [12] and the rapidity of their formation to the stage when they become visible witnesses to a high formation rate thereof.

3.2 Thin-Layer Chromatography (TLC)

3.2.1 Experiment 1

In experiment 1, we intended to demonstrate spontaneous chiral inversion of L-Cys to the *D* species and in order to facilitate the enantioseparation of the two isomers (*L* and *D*), we used the microcrystalline cellulose precoated chromatographic plates (to benefit from natural chirality of native cellulose). As the investigated samples, we used aqueous acetonitrile solutions of the fresh prepared L-Cys, Cys after 60 days aging, and the fresh prepared DL-Cys. In order to enhance the enantioseparation of the *L* and *D* species, prior to the chromatographic analysis, each of these three samples was spiked with an equimolar amount of manganese(II) acetate. As L-Cys and D-Cys both act as ligands able to chelate the Mn(II) cation and yet the complexation constants for these two chelate types (involving *L* and *D* form) has to be different, an addition of the Mn(II) salt was meant to enhance the enantioseparation effect, primarily exerted by cellulose. Additionally, we intended to use the complexation effect to stop chiral inversion of Cys in the samples just prior to chromatographic analysis and, in that way, to "freeze" the *L*/*D* ratio in the investigated samples. This goal can be obtained through the chelation, as reported elsewhere [12, 13].

The obtained chromatograms were visualized with the 0.5% ninhydrin solution in 2-propanol and then densitometrically scanned. The results obtained are presented in **Figure 3,** in the form of densitograms and photographs, respectively. In qualitative terms, all three chromatograms look similar, yet from a comparison of the chromatograms of L-Cys and DL-Cys, it was easily deduced that the blue spots represent monomeric Cys, and the brown and yellow spots hold for the condensates. In all densitograms shown in Figures 3(1a–c), the predominant peak originates from the condensates fraction and it is present both in the chromatograms of the fresh samples (Figures 3(1a and b)), and in that of the aged one (Figure 3(1c). This predominant peak witnesses to very high condensation rates of Cys and also to possible contamination of the commercial L-Cys sample with the Cys-derived oligopeptides.

In the range of the monomeric cysteine (the blue spots, marked on the densitograms, and the chromatograms with the red circle and red arrow), differences between the fresh and the aged Cys sample are considerable. These differences are particularly well perceptible, when focusing on the enlarged densitograms of the blue spots. Densitogram of the monomeric peak registered from the fresh prepared L-Cys sample shows a single concentration profile (Figure 3(3a)). The densitogram registered from the aged Cys sample shows two partially separated bands (Figure 3(3b)), which resemble those registered from the freshly pre-

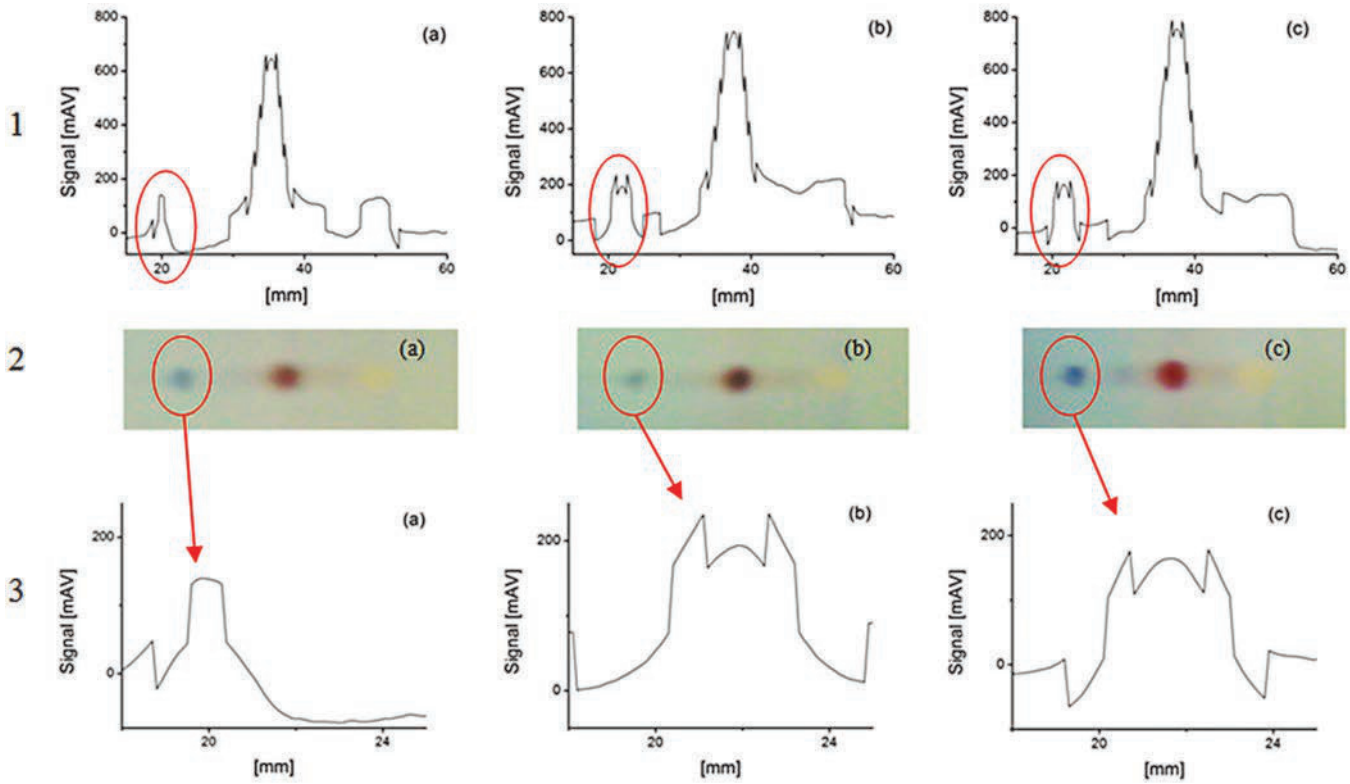

Figure 3

Densitograms and chromatograms of L-Cys solution with equimolar addition of Mn(II) acetate. (a) Fresh prepared L-Cys solution; (b) Cys solution after 60 days ageing; (c) fresh prepared DL-Cys solution. 1: Densitometric scans of the whole chromatograms (a)–(c); 2: photographs of the whole chromatograms (a)–(c); 3: enlarged densitometric scans of the Cys bands (a)–(c). Red circles and arrows indicate the Cys bands.

pared DL-Cys sample (Figure 3(3c)). This resemblance allows a conclusion that, in the course of ageing, L-Cys undergoes chiral inversion according to the mechanism extensively discussed in Introduction.

The R_F values additionally emphasize difference between the fresh and the aged Cys sample, and also similarity between the aged Cys and the fresh DL-Cys sample. For the fresh L-Cys sample, the R_F value of the monomer peak equals to 0.31 ± 0.01, which is the same as those for the lower peaks from the two partially separated monomer bands in the aged Cys and the fresh DL-Cys sample. The R_F value (equal to 0.35 ± 0.01) valid for the upper peak from the two partially separated monomer peaks in the aged Cys sample is the same as that of the upper peak from the partially separated monomer band for the fresh DL-Cys solution. Thus, the retardation coefficient (R_F) value of D-Cys is higher than that of L-Cys, and this sequence remains in agreement with that reported for the derivatized L- and D-Cys in the NP-TLC systems, given in the literature [15].

3.2.2 Experiment 2

Experiment 2 was carried out in a manner similar to experiment 1. Its aim was, however, to demonstrate gradual consumption of monomeric Cys in the course of peptidization. Also, in this case, the cellulose stationary phase as a native chiral separator was employed, and the transition metal cation (Zn(II)) was sequentially added to the investigated sample in the 1-h time intervals, as described in detail in Section 2.3. This additive was meant to hamper chiral inversion and condensation of Cys through the competitive chelating of the cation with amino acid ligands, *i.e.,* to "freeze" the investigated process in the assumed time intervals.

The results in form of the respective densitograms and photographs are presented in **Figure 4.** In Figures 4(1a–f), the whole densitograms of the individual development tracks are shown for the fresh prepared L-Cys solution (Figure 4(1a)), and for the samples stored for 1–5 h. In Figures 4(2a–f), the corresponding photographs are presented and in Figures 4(3a–f); the enlarged fragments of the respective chromatograms showing Cys in the monomeric form (encircled red) can be seen. General characteristics of the densitograms and photographs presented in Figure 4 largely resemble that given in Figure 3. The predominant peak visible in each densitogram (and the corresponding brown spot on the respective photograph) holds for the main fraction of the condensation products, yet it is out of scope of our present discussion.

We focus our attention on the blue spot of the monomeric Cys in Figures 4(2a–f) and on the enlarged densitograms of this fragment in Figures 4(3a–f). Initially, color intensity of the blue spot is high, yet in the 1-h intervals, considerable lowering of its intensity is observed. The enlarged fragments of the densitograms additionally emphasize the bleaching effect with the blue spot. Namely, the intensity of the Cys monomer peak with the fresh prepared solution equals to 170 Mav, and in the course of the 5-h lasting ageing, it drops to the bare 36 mAV. In that way, relatively rapid disappearance of the monomeric Cys band is confirmed, which can only be due to the rapidly progressing spontaneous condensation.

3.2.3 Thin-Layer Chromatography–Mass Spectrometry

In order to confirm spontaneous peptidization of Cys, mass spectra were registered for the selected target ("yellow") spots on all the chromatograms obtained according to the experiment 1 procedure and directly eluted from the respective chromatographic plates to mass spectrometer with use of the TLC–MS interface. These spots were attributed to the peptide fraction with the highest retardation factor value (R_F = 0.60 ± 0.02). For the sake of comparison, in this study, we compare the results obtained for the target ("yellow") spot derived from the freshly prepared DL-Cys solution **(Figure 5a)** and for that valid for the aged Cys solution **(Figure 5b),** as those which illustrate the discussed issue in the most spectacular manner.

The results presented in Figures 5a and b differ considerably. Primary difference consists in the intensity of the eluted liquid chromatographic signals. In the case of the aged Cys solution, this intensity is considerably higher and measured in MCounts (Figure 5b), whereas with the fresh DL-Cys solution, signal intensity is much lower and measured in kCounts only (Figure 5a). This is a persuasive evidence of the peptidization yields considerably growing in the course of ageing.

Further evidence originates from a comparison of the respective mass spectra registered for the discussed target spots. The

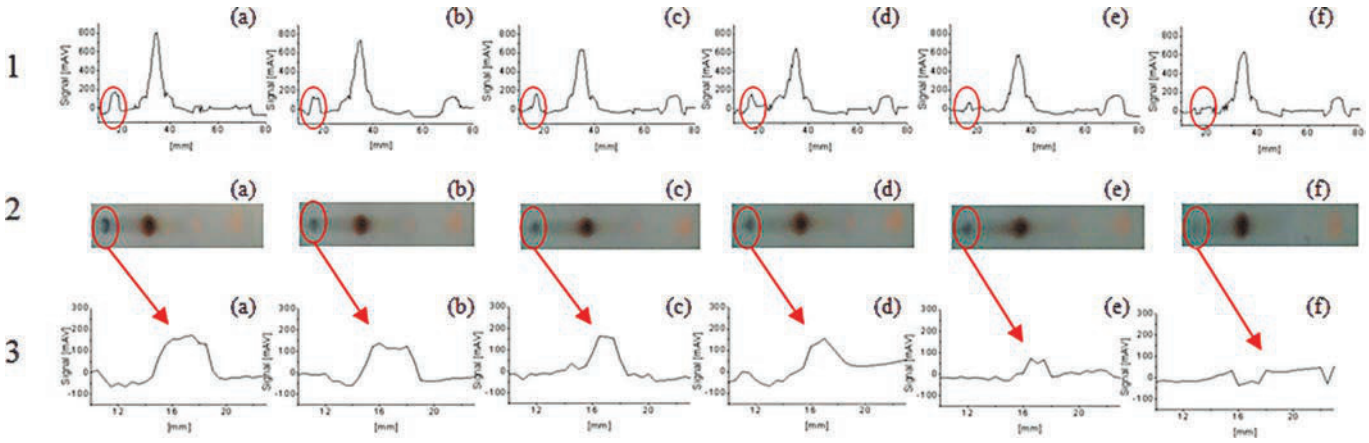

Figure 4

Densitograms and chromatograms of L-Cys solution with equimolar addition of Zn(II) nitrate. (a) Fresh prepared L-Cys solution; (b) Cys solution after 1 h ageing; (c) Cys solution after 2 h ageing; (d) Cys solution after 3 h ageing; (e) Cys solution after 4 h ageing; (f) L-Cys solution after 5 h ageing. 1: Densitometric scans of the whole chromatograms (a)–(f); 2: photographs of the whole chromatograms (a)–(f); 3: enlarged densitometric scans of the Cys bands (a)–(f). Red circles and arrows indicate the Cys bands.

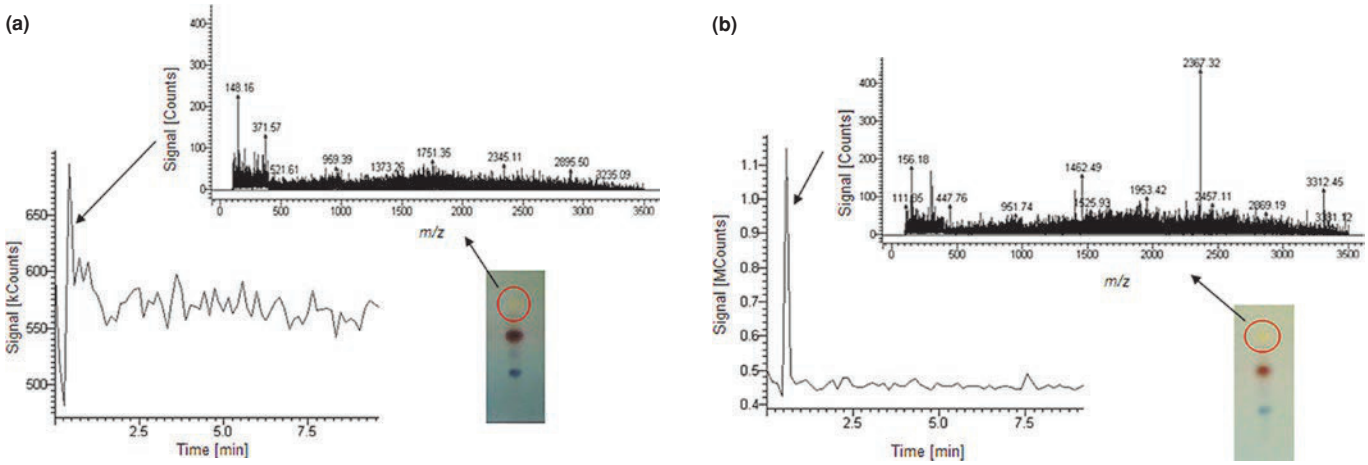

Figure 5

Thin-layer chromatograms, signals of the chromatographic spots representing an oligopeptide fraction (red framed on the respective chromatograms), directly eluted from the chromatographic plates, and the respective mass spectra recorded for the (a) fresh DL-Cys sample and (b) aged L-Cys sample.

most intense peak (229 Counts) present in the mass spectrum of the fresh sample (Figure 5a) appears at *m/z* 148, and it can be attributed to monomeric Cys (in form of the $[Cys+Na+He]^+$ cation). The intensities of peptide signals originating from the fresh sample are much lower than that observed for the signal of the monomer. For the sake of example, let us consider certain peptide signals and the intensities thereof originating from the fresh sample, *i.e.,* those at 371 (133 Counts), 959 (55 Counts), and 1373 (37 Counts). The following ion structures can be, respectively, attributed, to these signals: $[Cys_3+CO_2]^+$ (2 peptide bonds), $[Cys_9+H_2O]^+$ (8 peptide and 2 disulfide bonds), and $[Cys_{13}+H_2O]^+$ (12 peptide and 1 disulfide bond).

Mass spectrum recorded for the target spot derived from the aged L-Cys sample (Figure 5b) characterizes with an abundance of peptide peaks of considerable intensity. Among these peaks, the following ones can be mentioned: *m/z* 2367 (448 Counts), 1462 (159 Counts), and 951 (56 Counts). To these signals, the following structures can be attributed, respectively: $[Cys_{22}+Na]^+$ (17 peptide bonds and 6 disulfide bonds), $[Cys_{14}+H_2]^+$ (13 peptide bonds), and $[Cys_9+He+H_2]^+$(8 peptide bonds). Mass spectrometric characteristics of the target ("yellow") spot convincingly demonstrate a good progress of spontaneous peptidization in the course of the L-Cys ageing.

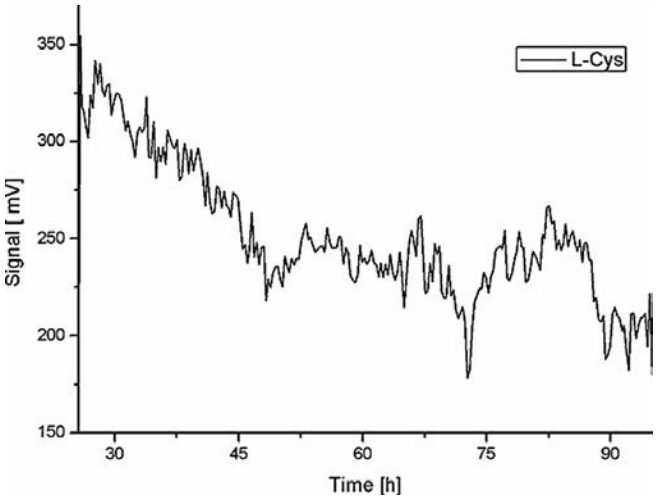

Figure 6

Time series of the chromatographic peak heights for Cys in 70% aqueous acetonitrile.

3.3 High-Performance Liquid Chromatography with Evaporative Light Scattering Detection (HPLC–ELSD)

In order to check, if spontaneous chiral inversion and condensation of Cys (which were demonstrated with the aid of TLC) are oscillatory in nature, an experiment was performed by use of the achiral HPLC–ELSD system. Our goal was to systematically analyze the Cys solution in the course of sample ageing. To this effect, the analyses were carried out in the 10-min intervals for the period of 75 h, in which time, a total number of 450 chromatograms was acquired. These short intervals enabled collecting the chromatographic data with a quasi-kinetic importance. The main attention was paid to quantitative changes of the Cys peak height (equivalent to its concentration changes). In **Figure 6,** the time series of the Cys peak height is presented in the span from the 25th to the 95th measuring hour. Based on this plot, two valid observations can be made. Firstly, it is evident that the change of the Cys peak height is nonmonotonous, which corresponds well with our earlier findings (summarized in the Introduction) as to the oscillatory nature of chiral conversion and peptidization of the low molecular weight carboxylic acids. Secondly, a distinct tendency is observed of sinking the Cys concentration in the function of time (in spite of local ups and downs of the plot, due to the oscillations). This sinking of the Cys concentration reflects gradual consumption of the monomeric species in pace with progressing condensation.

3.4 High-Performance Liquid Chromatography with Mass Spectrometric Detection (HPLC–MS)

By use of HPLC–MS, we managed to get certain insight into the molecular structure of the condensation products. For the sake of comparison, we analyzed both the fresh prepared and the aged Cys samples in the assumed time intervals. In **Table 1,** we show mass spectra recorded for the fresh sample and that after 4 days storage period, along with chemical structures, which can be attributed to certain signals. In the mass spectrum recorded

Table 1

Mass spectra recorded for (a) fresh prepared L-Cys solution and (b) Cys solution after 4 days storage period in 70% aqueous acetonitrile and possible structures attributed to selected signals. Signal intensities, numbers of the assumed peptide, and disulfide bonds in individual structures are indicated in the respective columns.

Sample	Mass spectrum	*m*/z *vs.* Proposed structure				
(a)	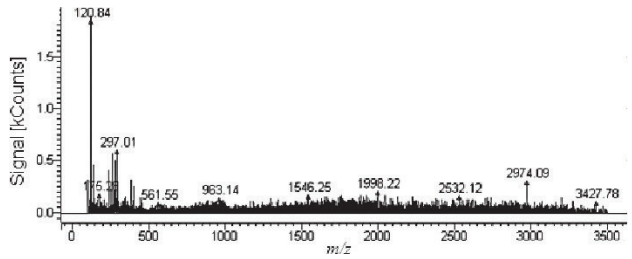	*m*/z	Signal intensity [kCounts]	Proposed structure	–CO–NH–	–S–S–
		120	2.13	$[Cys]^+$	–	–
		561	0.18	$[Cys_5+CO]^+$	4	–
		963	0.10	$[Cys_9+H_2O]^+$	8	–
		1998	0.31	$[Cys_{19}+Na]^+$	18	–
		2532	0.96	$[Cys_{24}+CO]^+$	22	2
		3427	0.20	$[Cys_{33}+H_2O]^+$	32	4
(b)	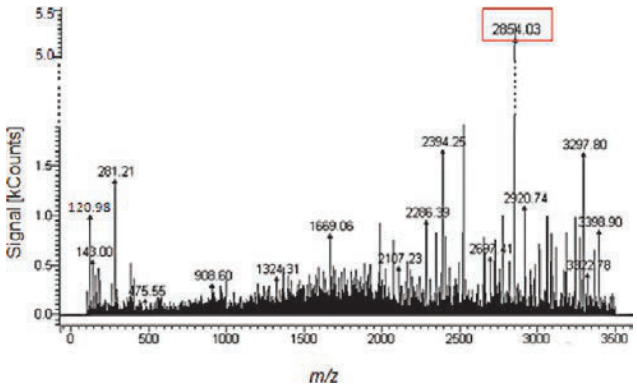	*m*/z	Signal intensity [kCounts]	Proposed structure	–CO–NH–	–S–S–
		120	0.99	$[Cys]^+$	–	–
		143	0.55	$[Cys+Na]^+$	4	–
		1324	0.38	$[Cys_{12}+He]^+$	7	3
		1669	0.82	$[Cys_{16}+He+H]^+$	15	1
		2286	0.95	$[Cys_{22}+H_2]^+$	21	–
		2394	1.66	$[Cys_{23}+H]^+$	21	6
		2697	0.58	$[Cys_{26}+H]^+$	25	–
		2854	5.37	$[Cys_{27}+H_3O]^+$	23	9
		2920	1.09	$[Cys_{28}+H_2]^+$	26	1
		3322	0.41	$[Cys_{32}+H_2O]^+$	31	5
		3398	0.38	$[Cys_{33}+H]^+$	32	10

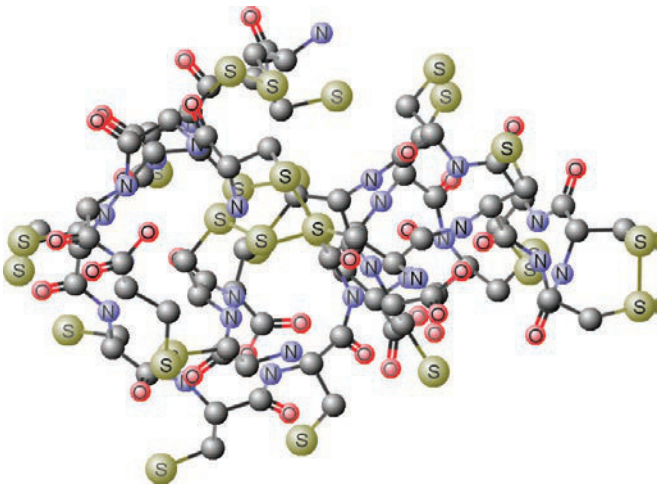

Figure 7

The 3D structure of Cys-derived oligopeptide with *m*/*z* 2854, computationally simulated for the red-framed predominant signal in the mass spectrum of aged Cys (see Table 1).

for the fresh L-Cys solution, the molecular ion originating from the Cys monomer at *m*/*z* 120 is predominant, although much less intense peaks are also recorded (which apparently originate from the peptides). Mass spectrum of the 4-day old sample witnesses to a substantial progress of peptidization, so that the intensities of the signals from peptidization products considerably outgrow that of molecular ion. The predominant peak in the aged sample appears at *m*/*z* 2854, and its intensity is five-fold, when compared with molecular ion. Summing up, the results presented in Table 1 not only confirm the progress of spontaneous peptidization, but also its considerable rate.

In **Figure 7,** we demonstrate the molecular structure of the Cys oligopeptide at *m*/*z* 2854 (red framed in Table 1), simulated with the Marvin Sketch v. 5.11 program. It shows that the presence of the thiol (–SH) group in the amino acid structure promotes spherical shape of a polycondensate molecule, as the oligopeptide at *m*/*z* 2854 (built of 27 Cys units and containing nine –S–S– bridges) already assumes a spherical shape. This tendency is certainly amplified with larger microstructures, as those shown in Figure 2b.

4 Conclusion

– With the aid of TLC, spontaneous chiral conversion and spontaneous peptidization of L-Cys were demonstrated.

– Chelating of transition metal cations (*e.g.,* Mn(II)) with the Cys ligands facilitates enantioseparation on the cellulose adsorbent of the L- and D-Cys enantiomers present in the aged Cys solution.

– Moreover, chelating of transition metal cations (*e.g.,* Zn(II)) with the Cys ligands hampers the spontaneous chiral conversion thereof at any given moment of the solution's storage and ageing period. In that way, the gradual progress of the Cys consumption due to the condensation process was demonstrated in the span of 5 h, in the 1-h intervals.

– With the aid of TLC–MS, peptidization of Cys was demonstrated, and a difference in chemical composition of the different chromatographic bands was emphasized.

– With the aid of HPLC–ELSD, the oscillatory nature of the Cys transformation (*i.e.,* chiral conversion and condensation) was demonstrated.

– With the aid of HPLC–MS, the progress of the spontaneous Cys condensation was demonstrated, providing the molecular-level insights in the formed peptides.

References

[1] *M. Sajewicz, R. Piętka, A. Pieniak, T. Kowalska,* Acta Chromatogr. **15** (2005) 131–149.

[2] *M. Sajewicz, M. Gontarska, T. Kowalska,* J. Chromatogr. Sci. **52** (2014) 329–333.

[3] *M. Sajewicz, D. Kronenbach, M. Gontarska, M. Wróbel, R. Pietka, T. Kowalska,* J. Planar Chromatogr. **22** (2009) 241–248.

[4] *M. Sajewicz, D. Kronenbach, M. Gontarska, T. Kowalska,* J. Liq. Chromatogr. Relat. Technol. **33** (2010) 1047–1057.

[5] *P. Belanger, J.G. Atkinson, R.S. Stuart,* Chem. J. Chem. Soc. D: Commun. (1969) 1067–1068.

[6] *Y. Xie, H. Liu, J. Chen,* Int. J. Pharm. **196** (2000) 21–26.

[7] *M. Sajewicz, M. Dolnik, T. Kowalska, I.R. Epstein,* RSC Adv. **4** (2014) 7330–7339.

[8] *M. Sajewicz, A. Godziek, A. Maciejowska, T. Kowalska,* J. Chromatogr. Sci. **53** (2015) 31–37.

[9] *M. Sajewicz, M. Matlengiewicz, M. Leda, M. Gontarska, D. Kronenbach, T. Kowalska, I.R. Epstein,* J. Phys. Org. Chem. **23** (2010) 1066–1073.

[10] *M. Valko, D. Leibfritz, J. Moncol, M.T.D. Cronin, M. Mazur, J. Telser,* Int. J. Biochem. Cell Biol. **39** (2007) 44–84.

[11] *R.J. Huxtable,* Physiol. Rev. **72** (1992) 101–63.

[12] *O. Carny, E. Gazit,* Fed. Am. Soc. Exp. Biol. J. **19** (2005) 1051–1055.

[13] *R. Guo, Y. Fan, X. Chen, Y. Shen,* J. Agric. Food Chem. **61** (2012) 157–166.

[14] *M. Sajewicz, E. John, D. Kronennbach, M. Gontarska, M. Wróbel, T. Kowalska,* Acta Chromatogr. **21** (2009) 39–55.

[15] *R. Bhushan, J. Martens, Amino Acids*, HNB Publishing, New York, 2010, pp. 76, 85.

Ms received: May 8, 2014
Accepted: June 11, 2014

Journal of Liquid Chromatography & Related Technologies, 38: 1164–1171, 2015
Copyright © Taylor & Francis Group, LLC
ISSN: 1082-6076 print/1520-572X online
DOI: 10.1080/10826076.2015.1028302

Taylor & Francis
Taylor & Francis Group

Investigation of Spontaneous Chiral Conversion and Oscillatory Peptidization of L-Methionine by Means of TLC and HPLC

ANNA MACIEJOWSKA,[1] AGNIESZKA GODZIEK,[1] EWA TALIK,[2] MIECZYSŁAW SAJEWICZ,[1] and TERESA KOWALSKA[1]

[1]*Institute of Chemistry, University of Silesia, Katowice, Poland*
[2]*Department of Physics of Crystals, Institute of Physics, University of Silesia, Katowice, Poland*

Downloaded by [Uniwersytet Slaski W Katowicach], [Teresa Kowalska] at 06:32 08 May 2015

From our earlier studies, it comes out that proteinogenic amino acids undergo spontaneous oscillatory chiral conversion and condensation. An understanding of these phenomena is crucial in view of the fact that amino acids are the building blocks of proteins and peptides present in all living organisms. Moreover, amino acids play an increasingly important role as components of drugs, dietary supplements, and cosmetics. In this study, we trace spontaneous oscillatory reactions of L-methionine (L-Met) with use of thin-layer chromatography with densitometric and mass spectrometric detection, and high-performance liquid chromatography with evaporative light scattering detection. Additional measurements were carried out with use of scanning electron microscopy. The results obtained confirm that L-Met spontaneously undergoes chiral conversion and peptidization. As an outcome of these two processes, peptides are formed of considerably different chemical structures, able to self-organize in nano- and microstructures under the mild ambient conditions without any catalysts.

Keywords: HPLC-ELSD, L-methionine (L-Met), nonlinear peptidization, self-assembled peptide nanostructures, spontaneous chiral conversion, TLC-MS

Introduction

The oscillatory enantiomerization was for the first time reported for several propionic acid derivatives, stored for longer periods of time in 70% aqueous ethanol.[1] Later, an analogous evidence of spontaneous chiral conversion obtained with use of HPLC-DAD was provided. We managed to demonstrate that the oscillatory chiral conversion is a general property which characterizes the low molecular weight carboxylic acids from the groups of profen drugs, amino acids, and hydroxyl acids,[2,3] when dissolved in aqueous or non-aqueous solvents and stored for certain periods of time in solution. Chiral conversion of such compounds can occur according to the two different pathways. In aqueous solutions, the general scheme[4] adapted to the case of L-Met can be represented as found in Scheme 1.

In anhydrous media and in the presence of trace amounts of water, the probable mechanism of chiral conversion is[5] shown in Scheme 2.

Investigations of amino acids show that the processes of oscillatory chiral conversion and oscillatory peptidization occur simultaneously. In papers,[6,7] we presented the results of spontaneous oscillatory condensation for the three binary amino acid systems (L-Pro-L-Hyp, L-Pro-L-Phe, and L-Hyp-L-Phe), dissolved in aqueous organic solvents. The process of chiral conversion and peptidization of amino acids running in parallel[8] and adapted to the case of L-Met can be illustrated as shown in Scheme 3.

In this study, we focus our attention on spontaneous processes of chiral conversion and peptidization running in aqueous acetonitrile solutions of L-Met. We chose this amino acid due to its important functions in human body. L-Met is a donor of methyl groups in the metabolic processes of methyl group transfer, it plays an important role in synthesis of choline and lecithin, promotes normalization of lipid metabolism and hepatic steatosis, and has an anti-atherosclerotic activity. Furthermore, L-Met plays an important role in the activities of adrenal gland, in particular in synthesis of adrenaline, and also in the processes of inactivation of catecholamines, thereby regulating the catecholamine balance. An existence of a close relationship has also been proved between L-Met, folate transformations, and vitamins B6 and B12.[9] Moreover, investigation of spontaneous peptidization of L-Met is important because self-assembled amino acid structures appear very promising for the application in such fields, as biosensing, electronics, diagnostics, drug delivery, tissue repair, and clean-room fabrication processes.[10]

Experimental

Reagents

In our experiment, we used L-Met of analytical purity (for its chemical structure see Figure 1), purchased from Reanal (Budapest, Hungary). Methanol, acetonitrile (Sigma-Aldrich, St. Louis, MO, USA), and 2-propanol (Merck, Darmstadt, Germany) were of HPLC purity. Pyridine, 2-butanol

Address correspondence to: Teresa Kowalska: Institute of Chemistry, University of Silesia, 9 Szkolna Street, 40-006 Katowice, Poland. E-mail: teresa.kowalska@us.edu.pl

Color versions of one or more of the figures in the article can be found online at www.tandfonline.com/ljlc.

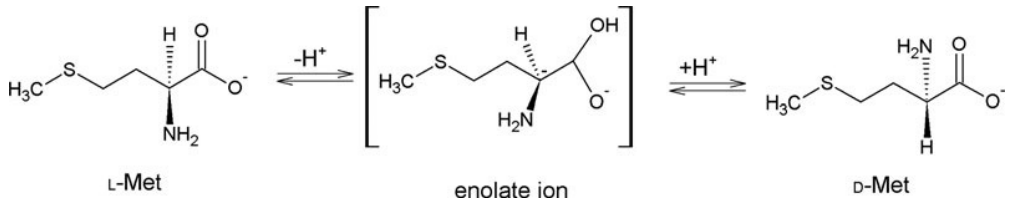

Scheme 1.

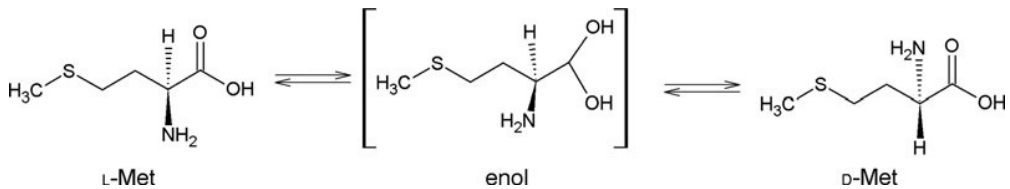

Scheme 2.

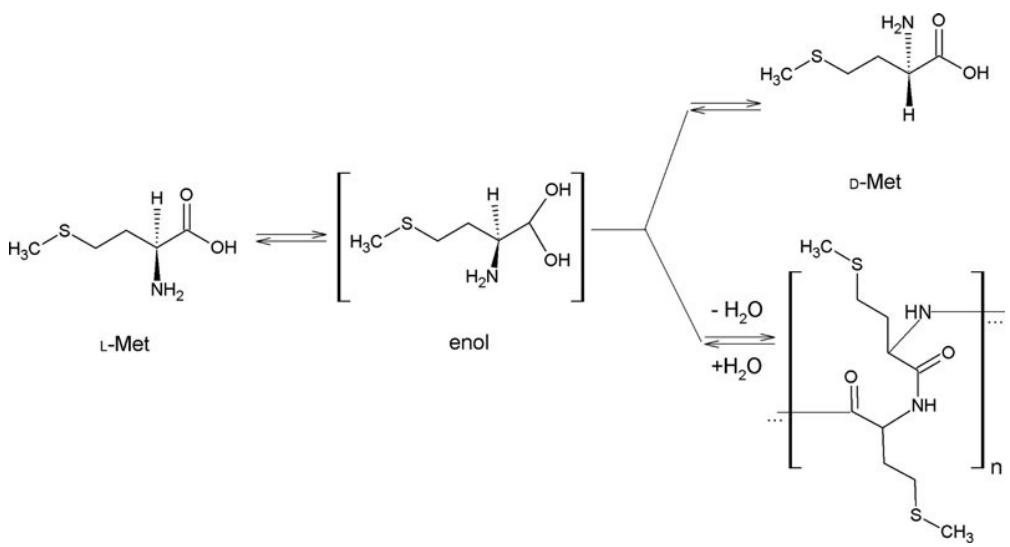

Scheme 3.

Downloaded by [Uniwersytet Slaski W Katowicach], [Teresa Kowalska] at 06:32 08 May 2015

(Sigma-Aldrich), ninhydrin, zinc (II) nitrate, and glacial acetic acid (PHH POCh, Gliwice, Poland) were also of analytical purity. Water was de-ionized and double distilled in our laboratory by means of the Elix Advantage model Millipore System.

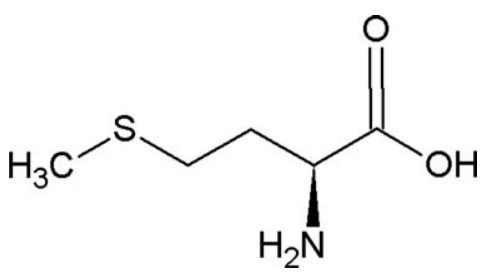

Fig 1. Molecular structure of L-Met.

Thin-Layer Chromatography (TLC)

Thin-layer chromatographic experiments were performed on the commercial 20 cm × 20 cm microcrystalline cellulose plates (Merck; cat. no. 1.05716). Concentration of L-Met in 70% aqueous acetonitrile was 1 mg mL^{-1} (i.e., 6.70×10^{-3} mol L^{-1}). The L-Met solution in aqueous acetonitrile was used for the microscopic measurements as well. The 2-butanol–pyridine–glacial acetic acid–water (30:20:6:24, *v/v*) mixture was used as mobile phase. Samples were spotwise applied to the plates in the 5 µL aliquots, 1.5 cm apart and 1 cm above the lower edge of the plate. The chromatograms were developed to the distance of 7 cm, and the development time was ca. 2 hr. After the development, the plates were dried and the chromatograms were visualized by spraying the plates with the 0.5% ninhydrin solution in 2-propanol, followed by heating for 5 min at 110°C. Two different experiments were carried out, Experiment 1 and Experiment 2.

Downloaded by [Uniwersytet Slaski W Katowicach], [Teresa Kowalska] at 06:32 08 May 2015

In Experiment 1, the stock L-Met solution was first prepared. From this fresh stock L-Met solution, 1 mL was withdrawn and spiked with an addition of zinc (II) nitrate (the molar ratio of amino acid to zinc nitrate was equal to 2:1, as recommended for the most efficient chelating effect with the transition metal cation (e.g., in Ref. [11]), and the remaining lot was stored for ageing. From this 1 mL fresh solution spiked with zinc (II) nitrate, the 5 µL aliquot was spotwise applied to the chromatographic plate. After the 1 hr long storage of the Met stock solution again, 1 mL was withdrawn, spiked with an addition of zinc (II) nitrate, and from this sample the 5 µL aliquot was spotwise applied to the chromatographic plate. This procedure in the 1 hr intervals was carried out for 5 hr. At the end, the chromatographic plate with the Met samples deposited in it after 0, 1, 2, 3, 4, and 5 hr storage period was developed.

In Experiment 2, chromatographic plates were activated by heating for 30 min at 110°C prior to applying the amino acid samples. Just before the chromatographic analysis, zinc (II) nitrate was added to the two Met samples, i.e., the freshL-Met solution and the Met solution after 5 months ageing (again, the molar ratio of amino acid to zinc (II) nitrate was 2:1).

The visualized chromatograms were densitometrically scanned with use of a Desaga (Heidelberg, Germany) model CD 60 densitometer equipped with the Windows-compatible ProQuant software. Concentration profiles of the development lanes were recorded in the reflectance mode, at the carefully selected wavelength $\lambda = 610$ nm. The obtained results were additionally recorded with a digital camera. All thin-layer chromatographic experiments were performed in triplicate.

Thin-Layer Chromatography-Mass Spectrometry (TLC-MS)

The TLC-MS analyses were performed for the chromatograms obtained in the analogous way as those earlier described for Experiment 2, yet without using ninhydrin as a visualizing agent. In this experiment, we employed a TLC-MS interface (Camag, Muttenz, Switzerland), which enabled direct elution of individual chromatographic bands from the plate to the LC-MS system. Elution of the target spots was carried out with acetonitrile. The employed LC-MS System Varian (Varian, Palo Alto, CA, USA) was equipped with the Varian ProStar model pump, the Varian 100-MS mass spectrometer, and the Varian MS Workstation v. 6.9.1 software for data acquisition and processing. This system operated under the following working conditions: As mobile phase, acetonitrile at the flow rate of 0.20 mL min^{-1} was used. Mass spectrometric detection was carried out in the ESI mode (extended ESI-MS scan from *m*/*z* 100 to 3500, positive ionization, spray chamber temperature 50°C, drying gas temperature 350°C, drying gas pressure 25 psi, capillary voltage 50 V, needle voltage 5 kV).

High-Performance Liquid Chromatography with Evaporative Light Scattering Detection (HPLC-ELSD)

Monitoring of spontaneous nonlinear peptidization dynamics of L-Met was performed with use of the achiral HPLC-ELSD. The L-Met solution was prepared in water at the concentration equal to 1 m g mL^{-1} (i.e., 6.70×10^{-3} mol L^{-1}). The analysis of freshly prepared amino acid solution was carried out using the Varian model 920 liquid chromatograph equipped with the Varian 900-LC model autosampler, the gradient pump, the Varian Pro Star 510 model column oven, the Varian 380-LC model ELSD detector, the ThermoQuest Hypersil C18 (150 mm × 4.6 mm i.d.; 5 µm particle size) column, and the Galaxie software for data acquisition and processing. The analyses were carried out for the 3 µL sample aliquots, using methanol–water (20:80, *v*/*v*) as mobile phase at the flow rate of 0.8 mL min^{-1} in the isocratic mode. Column was thermostatted at 35°C. The analysis of the L-Met sample was carried out in the 10 min intervals for the period of 85 hr.

Scanning Electron Microscopy (SEM)

Series of micrographs of the L-Met condensation product (microstructures) obtained from the fresh amino acid solution and that after 5 months ageing were recorded with use of the Jeol JSM-7600 F model scanning electron microscope, SEM (Jeol Ltd., Tokyo, Japan). These micrographs were recorded from the L-Met solution in 70% aqueous acetonitrile evaporated to dryness.

Results and Discussion

Thin-Layer Chromatography

Experiment 1

Usage of chromatographic plates pre-coated with microcrystalline cellulose as a native chiral adsorbent and zinc (II) nitrate as a complexation agent facilitated enantioseparation of D-Met from L-Met. Molar proportion of amino acid to zinc (II) nitrate equal to 2:1 provided the best enantioseparation performance, as established in the trial-and-error approach and suggested in the literature.[11]

In order to monitor the rate of chiral conversion and peptidization, an experiment was performed, described in the "Experimental" section. First, the fresh L-Met sample was prepared and then the 1 mL aliquots have been collected from it in the 1 hr intervals for 5 hr, and immediately mixed with the zinc (II) nitrate solution, as zinc cation is known for its ability to "freeze" amino acid's configuration and consequently, to prevent further chiral conversion.[12] In that way, six samples at different stages of chiral conversion were spotted on to one and the same chromatographic plate and then the chromatogram was developed.

The chromatogram was visualized with ninhydrin and densitometrically scanned. In Figures 2a–2f, six chromatographic lanes and the corresponding densitograms are shown. Figure 2a represents the chromatographic lane and the densitogram for the freshly prepared L-Met sample, whereas Figures 2b–2f represent respective lanes and densitograms for the Met samples after from 1 to 5 hr ageing period. On the chromatograms shown in Figures 2a–2f, the intense purple spot (no. 2) corresponds with monomeric L-Met, a less intense purple spot (no. 1) corresponds with monomeric D-Met, and the yellow spot (no. 3) represents peptide fraction. An advantage of using ninhydrin as a visualizing reagent is that it allows differentiating between

Downloaded by [Uniwersytet Slaski W Katowicach], [Teresa Kowalska] at 06:32 08 May 2015

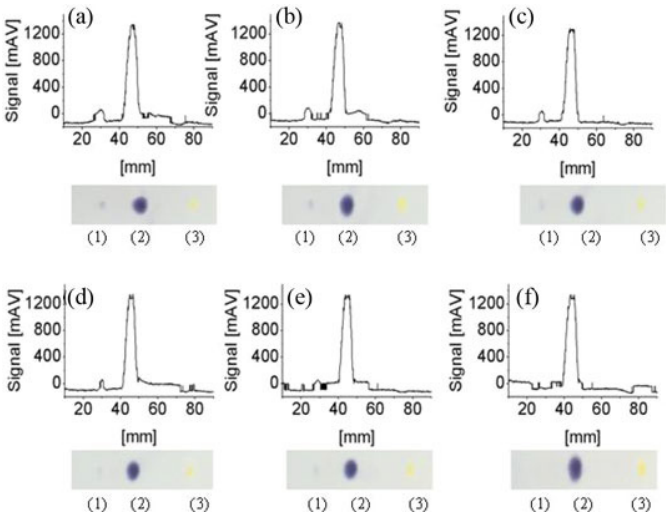

Fig 2. Chromatographic lanes and densitograms of the L-Met solution with an addition of Zn (II) nitrate (molar ratio ofL-Met to zinc (II) nitrate, 2:1). (a) Freshly prepared L-Met solution, and Met solution after (b) 1 hr ageing, (c) 2 hr ageing, (d) 3 hr ageing, (e) 4 hr ageing, and (f) 5 hr ageing.

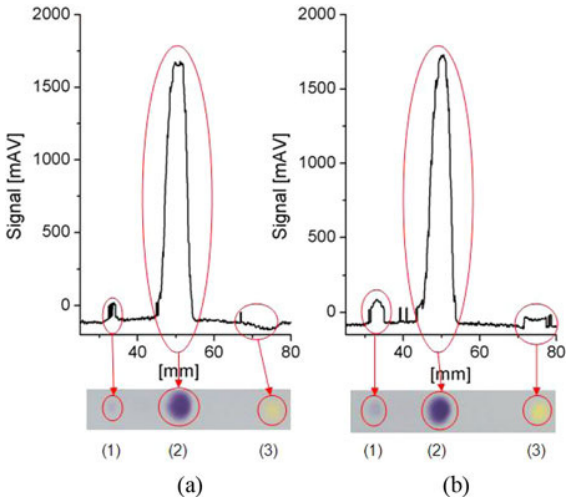

Fig 3. Chromatographic lanes and densitograms for the L-Met solution with an addition of Zn (II) nitrate (molar ratio of L-Met to zinc (II) nitrate, 2:1). (a) Freshly prepared L-Met solution; (b) Met solution after 5 months ageing; 1:D-Met; 2:L-Met; 3: peptide fraction.

purple spots of monomeric amino acids and yellow spot of peptide fraction.

The intense purple spot no. 2 ($R_F = 0.54 \pm 0.02$) originating from monomeric L-Met, characterizes with practically equal signal intensity in each densitogram. Presence of yellow spot no. 3 on all chromatograms ($R_F = 0.92 \pm 0.02$) witnesses to considerable L-Met peptidization rate, although this spot becomes more distinct after 5 hr sample ageing only. Presence of the less purple spot no. 1 originating from D-Met ($R_F = 0.30 \pm 0.02$) in the freshly prepared L-Met sample witnesses to the high rate of chiral conversion, yet its intensity drop in the course of the sample storage period is the most characteristic feature of Experiment 1. This intensity is dropping from 70.56 mAV for peak 1 in the freshly prepared sample to 55.89 mAV after 2 hr storage period, to 44.48 mAV after 4 hr storage period, and to 8.62 mAV after 5 hr storage period. Relatively short (5 hr) storage period of the Met sample and relatively long (1 hr) sampling intervals did not allow perceiving an oscillatory pattern of the amino acid chiral conversion. However, reappearance of the D-Met signal after 5 months sample ageing (discussed in the forthcoming subsection) serves as an indicator of an oscillatory nature of chiral conversion.

Experiment 2

In order to demonstrate a nonlinear nature of chiral conversion in a long-term ageing course, the freshly prepared L-Met sample and that after 5 months storage period were mixed with the zinc (II) nitrate solution in molar proportions of 2:1, and then spotted on to the chromatographic plate. Upon the development, the chromatograms were visualized with ninhydrin and densitometrically scanned. The results obtained for the freshly prepared L-Met sample and for that after 5 months storage period are presented in Figures 3a and 3b, respectively. Again, the chromatographic spots nos. 1–3 were detected in both chromatograms, with the intense purple spot no. 2 originating from monomeric L-Met, the less intense purple spot no. 1 originating from monomeric D-Met, and the yellow spot no. 3 originating from peptide fraction. Spots in the chromatogram and the corresponding concentration profiles in the densitogram were indicated pair-wise with red ovals.

Signal of the intense purple spot no. 2 originating from monomeric L-Met is the highest and it does not considerably change in the course of the 5 months storage period. Signal of less intense purple peak no. 1 (originating from monomeric D-Met) is very low (10.42 mAV) with freshly prepared L-Met sample, yet after the storage period of 5 months, it grows to 85.67 mAV. In Experiment 1, we have seen a decrease of intensity of peak 1 in the course of the initial 5 hr monitoring the process of ageing, and now we observe an intensity growth in the course of 5 months ageing. A comparison of the results originating from Experiment 1 and 2 and valid for peak 1 indirectly points out to a nonlinear pattern of chiral conversion of Met. Yellow spot no. 3 in Figure 3b valid for the peptide fraction after 5 months sample ageing is more intense than spot no. 3 in Figure 3a, valid for the freshly prepared L-Met solution. This is direct proof that the process of sample ageing results in gradual accumulation of peptides.

Thin-Layer Chromatography-Mass Spectrometry

Additional evidence on the reactions spontaneously occurring in the course of the L-Met ageing was obtained with use of TLC-MS. The analyses were carried out for the chromatograms obtained according to the procedure assumed in Experiment 2 and the results are presented in Figures 4 and 5. Figures 4a–4c show the mass spectra recorded for spots no. 1–3 from the chromatogram of the freshly prepared L-Met sample, and Figures 5a–5c show the analogous mass spectra recorded from

Downloaded by [Uniwersytet Slaski W Katowicach], [Teresa Kowalska] at 06:32 08 May 2015

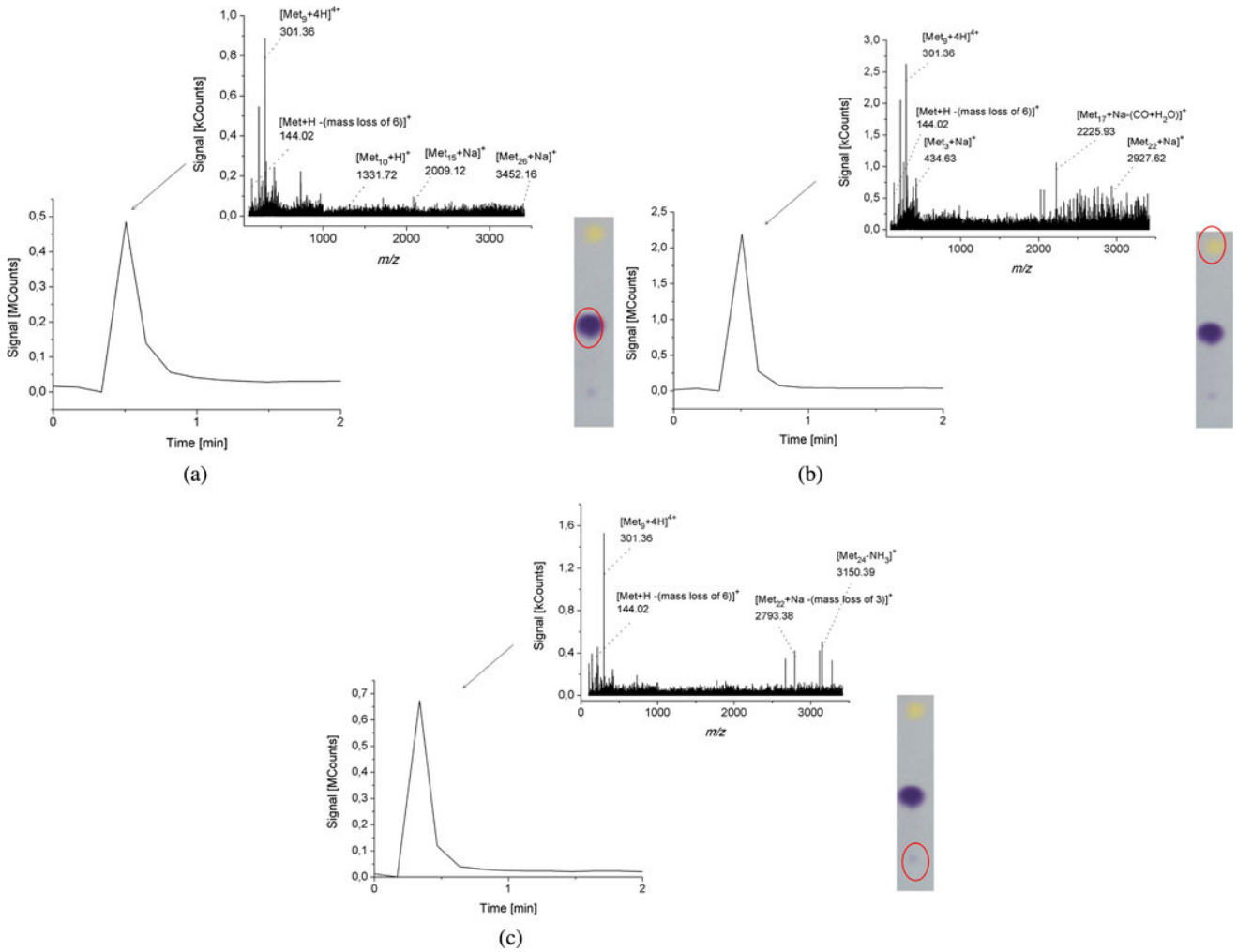

Fig 4. Thin-layer chromatograms, signals of chromatographic spots marked with red oval and directly eluted from the chromatographic plate, and the respective mass spectra recorded for the freshly prepared Met solution; (a) L-Met, (b) peptide fraction, and (c) D-Met.

the chromatogram of the L-Met sample after 5 months ageing. Differences between mass spectra presented in Figures 4 and 5 are evident in spite of an earlier recognized fact that mass spectra recorded directly from the thin-layer chromatograms tend to contain considerable amounts of the noise signals which obscure the signal pattern,[13] which can be the case in this study also. However, let us focus now on the message contained in Figures 4 and 5.

In Figure 4a, the chromatogram and mass spectrum recorded from the freshly prepared sample and valid for the intense purple spot of L-Met is given, and the predominant signal in this spectrum appears at *m/z* 301, which can possibly be attributed to $[Met_9 + 4H]^{4+}$. However, peak of monomeric Met at *m/z* 144 can also be seen, with a loss of 6 Da, due to fragmentation. Last not least, more peaks originating from peptides are present in this spectrum, although their intensities are quite low. In Figure 4b, the chromatogram and mass spectrum valid for the yellow spot of peptide fraction is given. Again, signal at *m/z* 301 is predominant, yet other signals originating from the peptides are also intense (e.g., those at *m/z* 2225 and 2927, which can be attributed to $[Met_{17} + Na - (CO + H_2O)]^+$ and $[Met_{22} + Na]^+$, respectively). The intense peptide signals recorded from the freshly prepared sample witness to an efficient and rapid peptidization process. Data shown in Figure 4c refer to the less intense purple spot valid for monomeric D-Met, resulting from chiral conversion of L-Met. Due to rather low conversion yields, signal intensities are also low, yet the mass spectral pattern valid for this spot fully resembles that recorded for monomeric L-Met (Figure 4a).

Figure 5 shows the chromatograms and mass spectra valid for the aged Met sample and in this case, increased yields of peptides can be seen in each chromatographic spot. Apparently, peptides are not sufficiently enough separated from the purple monomeric L- and D-Met fractions, as confirmed by the photographs taken from the back side of chromatographic plates (Figure 6). From this transparent (glass!) back side of the plate, in the center of each purple spot "yellow eye" can be seen, representing peptides (which remain invisible from the adsorbent side). In Figure 5a, valid for the intense purple spot of L-Met, the predominant signal at *m/z* 144 represents

Downloaded by [Uniwersytet Slaski W Katowicach], [Teresa Kowalska] at 06:32 08 May 2015

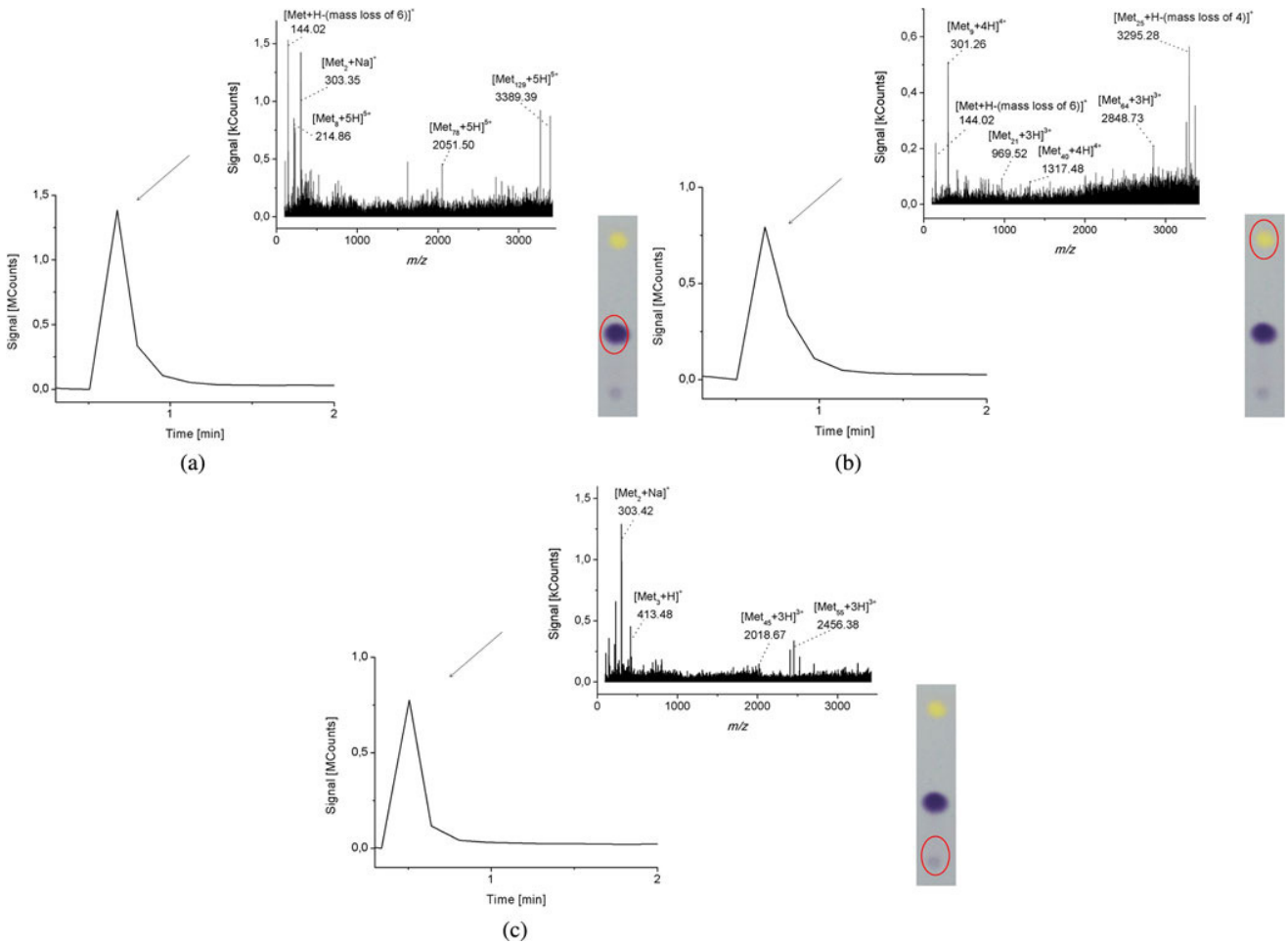

Fig 5. Thin-layer chromatograms, signals of chromatographic spots marked with red oval and directly eluted from the chromatographic plate, and the respective mass spectra recorded for the aged Met solution; (a) L-Met, (b) peptide fraction, and (c) D-Met.

monomeric Met. However, higher signals at, e.g., *m/z* 2051 and 3389 are also present, which can be attributed to $[Met_{78} + 5H]^{5+}$ and $[Met_{129} + 5H]^{5+}$, respectively. In fact, molecular weights of these two peptides are equal to 10,252 and 16,944 Da, respectively, which explains their low mobility in the employed thin-layer chromatographic system, sticking to the monomeric fractions, and formation of "yellow eyes." In Figure 5b, chromatogram and mass spectrum are given for the yellow spot of the peptide fraction. This mass spectrum confirms considerable progress of peptidization in the course of the 5 months sample ageing (as compared with the mass spectrum for the corresponding yellow spot originating from the freshly prepared sample; see Figure 4b). In Figure 5c, valid for the less intense purple spot of D-Met, considerable intensity growth of the predominant peak representing D-Met is observed. This result confirms an efficient chiral conversion of L-Met in the course of the 5 months ageing and corresponds well with the thin-layer chromatographic results summarized in Figure 3.

Fig 6. Photograph of two chromatographic spots of the aged L-Met sample (spot no. 2 in Figure 3b) with clearly visible "yellow eye," taken from the back (glass) side of chromatographic plate.

High-Performance Liquid Chromatography with Evaporative Light Scattering Detection

The experiment carried out with use of the achiral HPLC-ELSD additionally confirmed that L-Met undergoes spontaneous structural transformations in a nonlinear fashion. In Figure 7, four chromatograms are given, randomly selected from ca. 500 chromatograms registered in the 10 min intervals for the period of 85 hr to monitor sample ageing. In Figures 7a and 7d, single peak of Met can be seen (its retention time, $t_R = 4.46$ min), registered for the freshly prepared sample and for that after 80.17 hr ageing period, respectively. In Figures 7b and 7c, the peak of Met is accompanied by those originating from predominant peptidization products. After 11.83 hr sample

Downloaded by [Uniwersytet Slaski W Katowicach], [Teresa Kowalska] at 06:32 08 May 2015

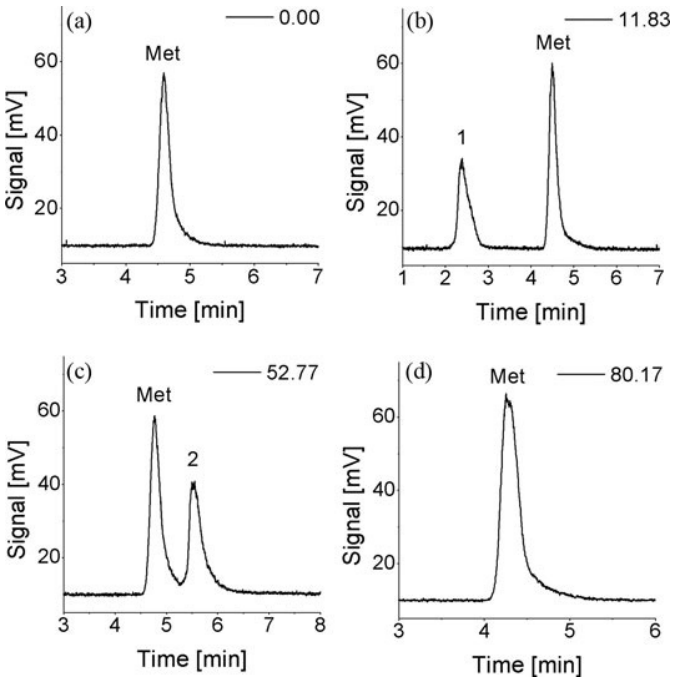

Fig 7. Selected snapshots showing chromatograms of Met and the main peptidization products 1 and 2, registered with ELSD, after the different sample storage periods; (a) 0.00 hr; (b) 11.83 hr; (c) 52.77 hr; (d) 80.77 hr.

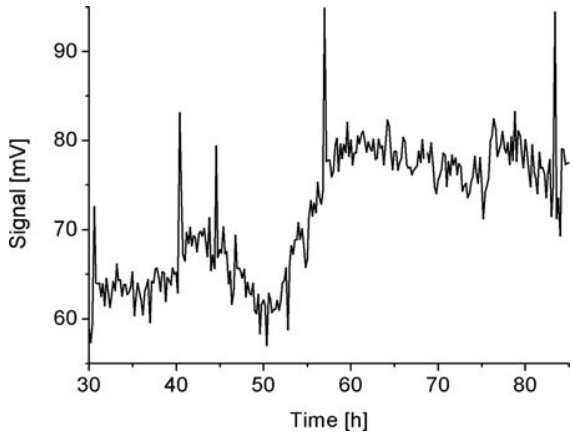

Fig 8. Time series of chromatographic peak heights for Met dissolved in water (time range 25–85 hr).

ageing, peak no. 1 valid for the predominant peptidization product elutes faster than Met (Figure 7b), and after 52.77 hr sample ageing, peak no. 2 of another peptidization product appears, which elutes slower than Met (Figure 7c). Temporary appearance and disappearance of peptidization products alone suffices to prove that structural transformation of L-Met follows a nonlinear pattern. Moreover, the heights of chromatographic peak valid for monomeric Met are plotted against time to give time

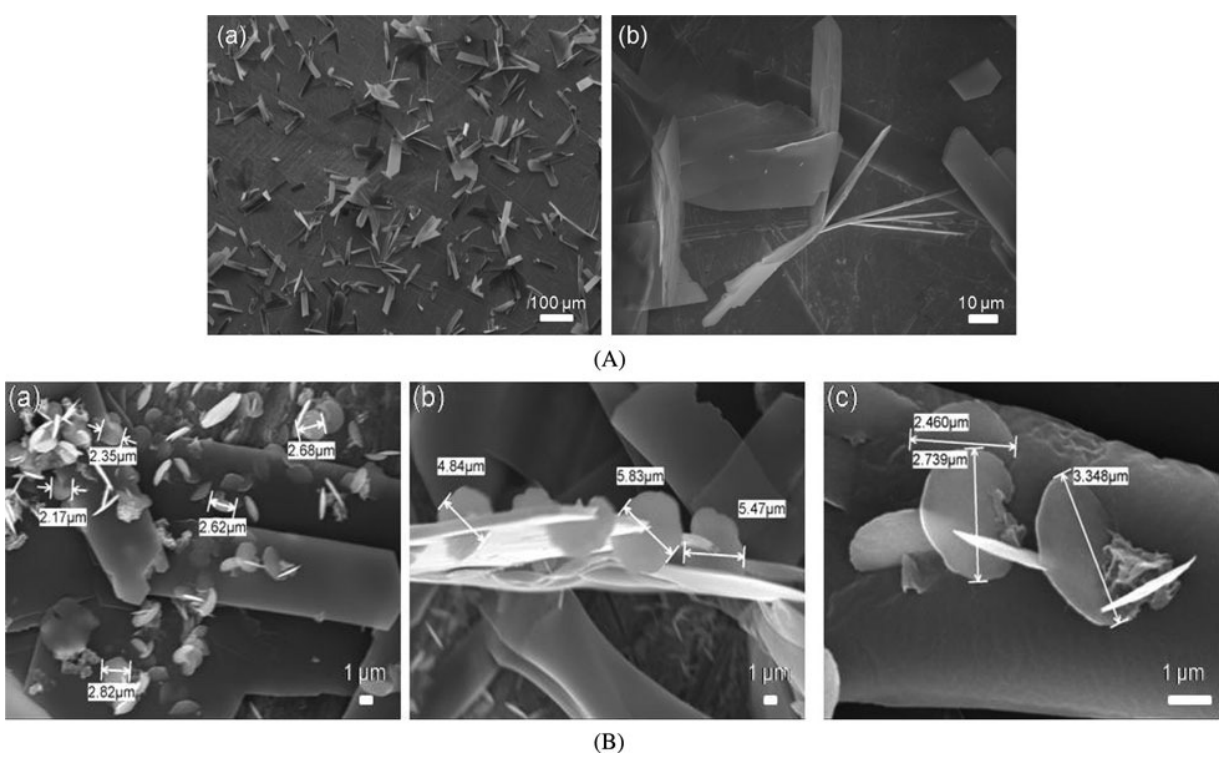

Fig 9. Scanning electron micrographs of the Met from the solution residue evaporated to dryness (A): (a) and (b): from the fresh sample, magnification of (a) X100; (b) X850; (B): (a) and (c): from the age sample, magnification of (a) X3000; (b) X3300; (c) X13000. Size bars make insets in each individual picture.

series of the peak heights (Figure 8). As chromatographic peak heights are directly proportional to the concentrations and the plot is strongly nonlinear, a conclusion can be drawn that the time changes of the Met concentration are oscillatory in nature. On molecular level, these oscillatory changes are due to spontaneous formation (lowering of the peak height) and hydrolytic decay (growth of the peak height) of the Met-derived peptides. What cannot be observed in achiral HPLC, is an additional chiral conversion and hence, stepwise transformation of L-Met to a scalemic L/D mixture.

Scanning Electron Microscopy

Fresh L-Met solution and that after 5 months ageing were analyzed with use of the SEM. Samples of both solutions were deposited on the brass knobs, then evaporated to dryness, and finally the micrographs were registered (Figures 9A and 9B). In Figures 9A(a) and 9A(b), the micrographs valid for the fresh L-Met are given. They show the flat band-like structures, which can well represent the monomeric L-Met crystals. In Figures 9B (a)–9B(c), the results valid for the aged L-Met solution are given. It can be noticed that in the aged sample, along with the flat band-like structures, the flat disc-like structures appear as well (absent from the micrographs of the fresh sample). It can be assumed that these flat disc-like structures originate from peptides formed in the course of the 5 months' ageing process. Once we consider the molecular structure of L-Met (Figure 1), which contains two functional groups (–COOH and $–NH_2$) per one L-Met molecule, one can expect the flat peptide structures. Moreover, an information contained in the literature on a tendency of the L-Met-derived oligomers toward circular forms[13–15] can act in support of our assumption as to the peptide nature of the flat disc-like structures observed on the micrographs shown in Figures 9B(a)–9B(c).

Conclusions

- Application of TLC enables demonstration of spontaneous peptidization and spontaneous chiral conversion of L-Met.
- Chelating of the transition metal cations (e.g., Zn(II)) with the Met ligands facilitates enantioseparation of the L- and D-Met species on the cellulose adsorbent.
- With use of TLC-MS, difference in the *m*/*z* values of the constituents of individual chromatographic bands is shown and moreover, the presence of the Met-derived peptides in the aged Met solution is demonstrated.
- With use of HPLC-ELSD, an oscillatory nature of structural transformation (i.e., peptidization) with Met is demonstrated.
- Application of SEM additionally confirms the presence of the Met derived homopeptides in the aged Met solution, attributing the flat disc-like form to them.

Funding

One author (A.G.) acknowledges the financial support of the DoktoRIS project, co-financed by the European Union within the European Social Found.

References

1. Sajewicz, M.; Piętka, R.; Pieniak, A.; Kowalska, T. Application of Thin-Layer Chromatography (TLC) to Investigating Oscillatory Instability of the Selected Profen Enantiomers. *Acta Chromatogr.* **2005**, *15*, 131–149.
2. Sajewicz, M.; Kronenbach, D.; Gontarska, M.; Wróbel, M.; Piętka, R.; Kowalska, T. TLC in Search for Structural Limitations of Spontaneous Oscillatory In-Vitro Chiral Conversion. α-Hydroxybutyric and Mandelic Acids. *J. Planar Chromatogr. Mod. TLC* **2009**, *22*, 241–248.
3. Sajewicz, M.; Kronenbach, D.; Gontarska, M.; Kowalska, T. TLC and Polarimetric Investigation of the Oscillatory In Vitro Chiral Conversion of *R*-*β*-Hydroxybutyric Acid. *J. Liq. Chromatogr. Related Technol.* **2010**, *33*, 1047–1057.
4. Belanger, P.; Atkinson, J. G.; Stuart, R. S. Exchange Reactions of Carboxylic Acid Salts. Kinetics and Mechanism. *J. Chem. Soc. Sect. D. Chem. Commun.* **1969**, 1067–1068.
5. Xie, Y.; Liu, H.; Chen, J. Kinetics of Base Catalyzed Racemization of Ibuprofen Enantiomers. *Int. J. Pharm.* **2000**, *196*, 21–26.
6. Sajewicz, M.; Dolnik, M.; Kowalska, T.; Epstein, I. R. Condensation Dynamics of L-Proline and L-Hydroxyproline in Solution. *RSC Adv.* **2014**, *4*, 7330–7339.
7. Sajewicz, M.; Godziek, A.; Maciejowska, A.; Kowalska, T. Condensation Dynamics of the L-Pro-L-Phe and L-Hyp-L-Phe Binary Mixtures in Solution. *J. Chromatogr. Sci.* **2014**, *53*, 31–37.
8. Sajewicz, M.; Matlengiewicz, M.; Leda, M.; Gontarska, M.; Kronenbach, D.; Kowalska, T.; Epstein, I. R. Spontaneous Oscillatory In Vitro Chiral Conversion of Simple Carboxylic Acids and Its Possible Mechanism. *J. Phys. Org. Chem.* **2010**, *23*, 1066–1073.
9. Murray, R. K.; Granner, D. K.; Mayes, P. A.; Rodwell, V. W. *Biochemia Harpera*; Wydawnictwo lekarskie PZWL: Warszawa, 1995.
10. Castillo-Leon, J.; Sasso, L.; Svendsen, W. E. *Self-Assembled Peptide Nanostructures*; Pan Stanford Publishing Pte: USA, 2013.
11. Sajewicz, M.; John, E.; Kronenbach, D.; Gontarska, M.; Wróbel, M.; Kowalska, T. How to Suppress the Spontaneous Oscillatory In-Vitro Chiral Conversion of α-Substituted Propionic Acids a Thin-Layer Chromatographic, Polarimetric, and Circular Dichroism Study of Complexation of the Cu(II) Cation with L-Lactic Acid. *Acta Chromatogr.* **2009**, *21*, 39–55.
12. Guo, R.; Fan, Y.; Chen, X.; Shen, Y. Chiral Resolution of Racemic p-Methylsulfonylphenyl Serine EthylEster with Lipases: The Mechanism of Side Reaction and Its Suppression. *J. Agric. Food Chem.* **2013**, *61*, 157–166.
13. Morlock, G. E. Background Mass Signals in TLC/HPTLC-ESI-MS and Practical Advices for Use of TLC-MS Interface. *J. Liq. Chromatogr. Related Technol.* **2014**, *37*, 2892–2914.
14. Naider, F.; Khare, S.; Arshava, B.; Severino, B.; Russo, J.; Becker, J. M. Synthetic Peptides as Probes for Conformational Preferences of Domains of Membrane Receptors. *Biopolymers* **2005**, *80*, 199–213.
15. Goodman, M.; Ribeiro, A. A.; Naider, F. Protected Homo-Oligopeptide Structure: Model for Preferred Conformation of a Linear Methionine Heptapeptide in Chloroform. *Proc. Natl. Acad. Sci. U.S.A.* **1978**, *75*, 4647–4651.

Downloaded by [Uniwersytet Slaski W Katowicach], [Teresa Kowalska] at 06:32 08 May 2015

Reac Kinet Mech Cat (2017) 120:421–437
DOI 10.1007/s11144-017-1157-3

Turbidity patterns of spontaneous peptidization in an aqueous abiotic system and possible secondary peptide structures

A. Maciejowska[1] · A. Godziek[1] · M. Sajewicz[1] · T. Kowalska[1]

Received: 5 January 2017 / Accepted: 4 February 2017 / Published online: 13 February 2017
© The Author(s) 2017. This article is published with open access at Springerlink.com

Abstract The non-linear dynamics of spontaneous peptidization running in 10 monocomponent and binary abiotic liquid systems of *L*- and *D*-Ala and *L*- and *D*-Phe is investigated with use of turbidimetry with continuous registration, high-performance liquid chromatography with light scattering detection (HPLC-ELSD), mass spectrometry (MS), and spectroscopy of far UV circular dichroism (CD). The turbidity patterns represent a sum of the light scattering effects caused by insoluble peptides of unknown yields, structures, and molecular weights. The auxiliary analytical techniques confirm the non-linear nature of peptidization (HPLC-ELSD) and spontaneous formation of the homo- and heteropeptides (MS). CD spectroscopy seems to confirm the presence of the secondary α-helix structures. The similarity of turbidity patterns is revealed with the monocomponent (*L* or *D*) and binary (*L*-*L* or *D*-*D*) systems of equichiral α-amino acids, and dissimilarity of patterns is observed with the binary systems of inequichiral α-amino acids (*L*-*D*). The tentative conclusion is drawn that the peptides assembled of equichiral α-amino acid units are able to assume the secondary (right- or left-handed α-helix) structures, which in a certain way could foster the similarity of turbidity patterns, and the peptides built of inequichiral α-amino acid units cannot ensure an efficient enough stringing of monomer molecules into equichiral heptades to form complete segments of an α-helix. This randomness of the α-amino acids arrangement in the inequichiral peptide molecules most probably manifests itself as a lack of similarity among the respective turbidity patterns.

Electronic supplementary material The online version of this article (doi:10.1007/s11144-017-1157-3) contains supplementary material, which is available to authorized users.

✉ T. Kowalska
teresa.kowalska@us.edu.pl

[1] Institute of Chemistry, University of Silesia, 9 Szkolna Street, 40-006 Katowice, Poland

Keywords Alanine · Phenylalanine · Spontaneous peptidization · Turbidimetric measurements · Secondary peptides structure · α-Helices

Introduction

Spontaneous non-linear formation of peptides from the monomeric and optically pure α-amino acids running in the abiotic liquid systems in parallel with spontaneous non-linear chiral conversion was first reported in papers [1–3]. In fact, these two non-linear processes have not been observed with α-amino acids alone, but with a wider selection of the low molecular weight chiral carboxylic acids such, as profen drugs [4, 5] and hydroxyl acids [6, 7], so it can be justifiably speculated that these two non-linear processes are even more general than our up-to-the-date understanding thereof. Below, the mechanisms are presented of chiral conversion (Scheme 1a), peptidization (Scheme 1b), and the two processes running in the parallel (Scheme 1c), upon an example of *L*-Ala, one of the α-amino acids which will be referred to in the experimental part of this study.

Earlier, no similar observations have been made with α-amino acids dissolved in abiotic aqueous or non-aqueous media, in the absence of a catalyst. Moreover, the selected peptide structures tend to be viewed as fairly stable units (e.g., [8–10]), often with some negative health repercussions (e.g., as a cause of the age-related neurodegenerative diseases [10–12]) or to the contrary, they can be positively employed in various different biomedical nanotechnology contexts, owing to their biocompatibility (e.g., [10, 13, 14]). Numerous reports on the lack of peptide stability in abiotic solutions refer to their decomposition (e.g., hydrolysis) rather than to their spontaneous formation (the latter process being the leitmotif of this study) and they tend to ascribe such phenomena to the external stimuli such, as pH, temperature, chemical nature of solvents, etc. [15–17].

The spontaneous non-linear peptidization of α-amino acids has been documented in our earlier studies with use of several analytical techniques, and in the first instance liquid chromatography (both HPLC and TLC) [18, 19], turbidimetry with continuous data acquisition [20, 21], and scanning electron microscopy (SEM) [22]. Although the least employed analytical technique has been turbidimetry, we consider it as well suited to tracing the dynamics of the aforementioned process, as peptidization almost instantaneously yields insoluble peptides, initially invisible to human eye. This analytical technique is appropriate to the media of rather low turbidity in which the suspended particles are small [23], which is the case in this study. Moreover, turbidimetry has already proved useful in some other investigations, and its particularly attractive feature is that it facilitates the detection of very short-lived pulsing of suspended precipitates, which characterizes many systems and reveals the precipitate mobilization processes (e.g., [24]).

The aim of this study is to trace the turbidity patterns of spontaneous peptidization in the monocomponent and binary *L*-Ala, *D*-Ala, *L*-Phe, and *D*-Phe systems, the latter ones assembled in the equichiral and inequichiral configurations, using turbidimetry with continuous registration. As the auxiliary analytical

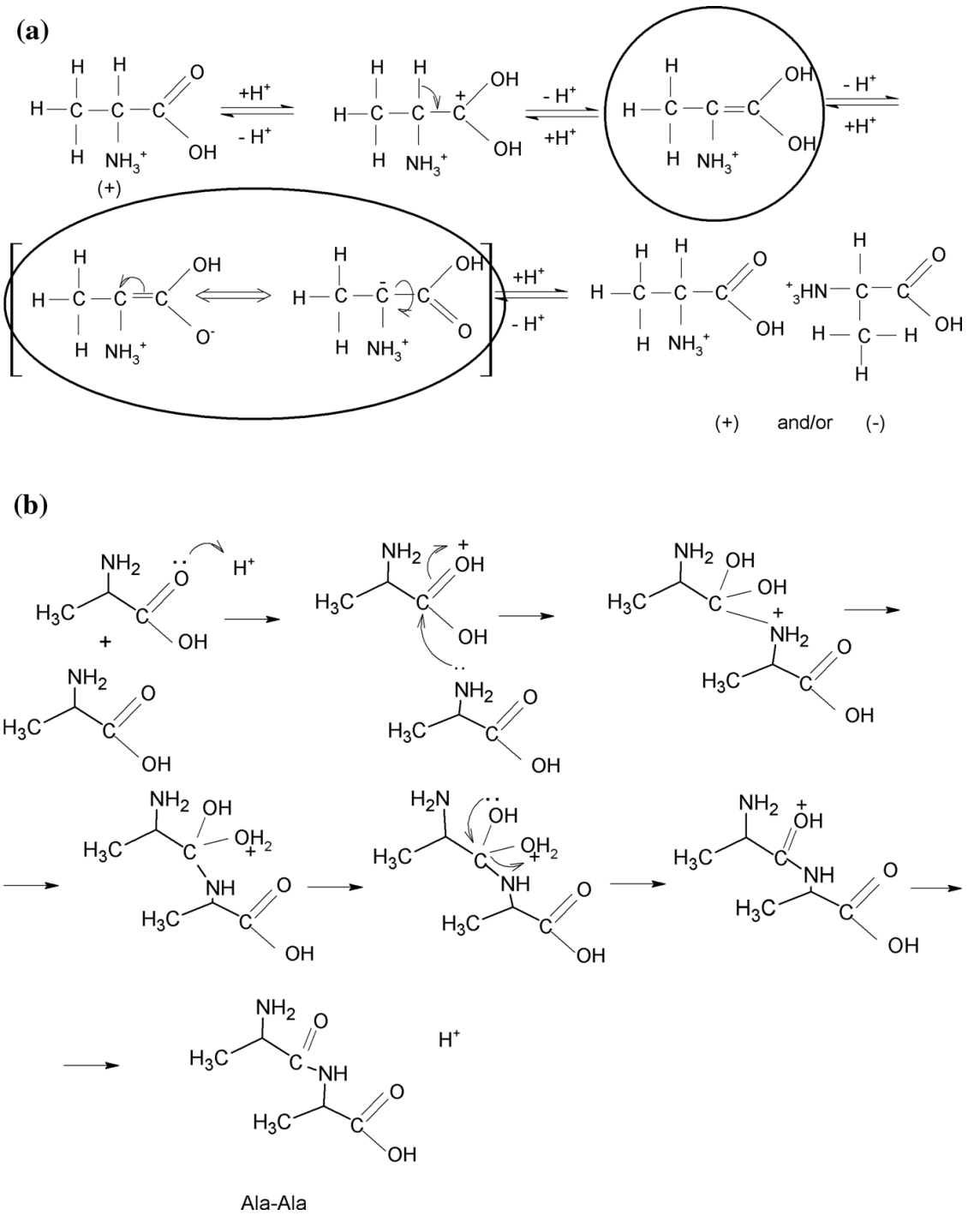

Scheme 1 Molecular mechanisms of the processes running in the monocomponent *L*-Ala system dissolved in an aqueous medium: **a** Chiral conversion of *L*-Ala to *D*-Ala (intermediary non-chiral structures are marked with *black ovals*); **b** homopeptide formation (*L*-Ala-*L*-Ala); and **c** peptidization $(\text{Ala-Ala})_n$ running in the parallel with chiral conversion

techniques, HPLC-ELSD, MS and CD were used, in order to assess the dynamics of the investigated process, the chemical structure of the resulting peptides, and the presence of α-helices in solutions, respectively.

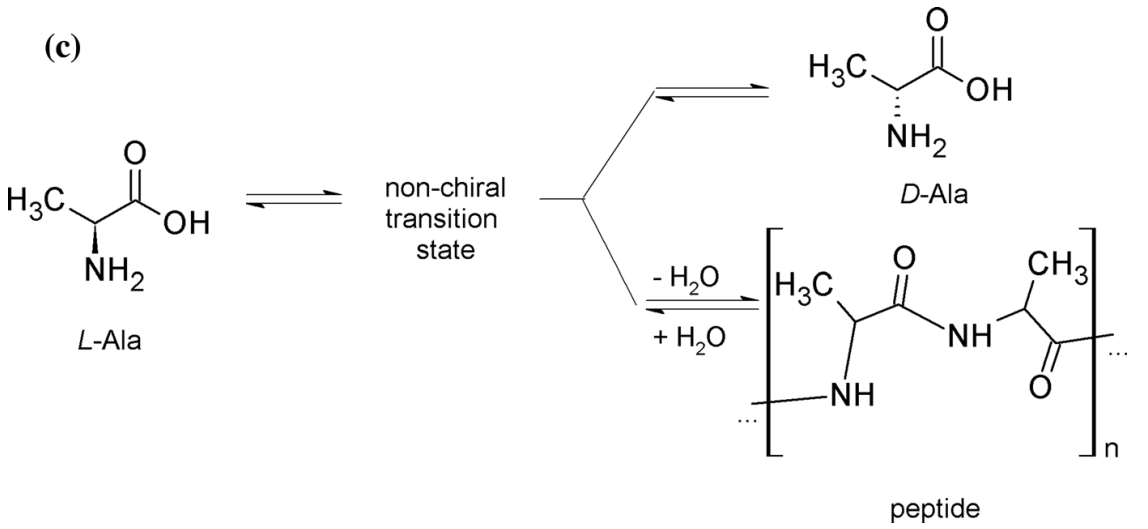

Scheme 1 continued

Experimental

Reagents

We used *L*-Ala and *D*-Phe (Reanal, Budapest, Hungary), *D*-Ala (Sigma-Aldrich, St Louis, MO, USA), and *L*-Phe (Merck KGaA, Darmstadt, Germany). All α-amino acids were of analytical purity. Methanol (Sigma-Aldrich) was of HPLC purity. Glacial acetic acid and conc. hydrochloric acid (PPH POCh, Gliwice, Poland) were of analytical purity. Water was de-ionized and double distilled in our laboratory by means of the Elix Advantage model Millipore System (Molsheim, France).

For all the experiments, concentrations of the investigated α-amino acids in the monocomponent systems were 1.0 mg mL^{-1} (i.e., 1.12 × 10^{-2} mol L^{-1} for *L*-, *D*-, and *DL*-Ala, and 6.05 × 10^{-3} mol L^{-1} for *L*-, *D*-, and *DL*-Phe), and 0.5 mg mL^{-1} (i.e., 5.61 × 10^{-3} for *L*- and *D*-Ala, and 3.03 × 10^{-3} mol L^{-1} for *L*- and *D*-Phe) in the binary systems. The 70% aqueous methanol (i.e., 70% methanol + 30% water, *v*/*v*), known for its strong antiseptic properties, was selected as a solvent in order to protect the α-amino acid solutions from microbial action in the experiments of sample ageing. Sample ageing for the purpose of all the experiments except turbdimetric analysis was carried out just by storage of samples in the transparent and tightly stoppered volumetric flasks on the laboratory shelf, with the natural illumination changes in the day/night cycle. Storage of samples for the purpose of the chromatographic analyses was at 22 ± 1 °C and for the purpose of turbidimetric analyses, at 25.0 ± 0.5 °C. Glacial acetic acid as a control sample for turbidimetric measurements was also dissolved in 70% aqueous methanol at the concentration of 1 mg mL^{-1} (1.67 × 10^{-2} mol L^{-1}).

Turbidimetry

Turbidity measurements were performed for 10 monocomponent and binary α-amino acid systems listed in the preceding section with use of the turbidity sensor

(TRB-BTA, Vernier Software & Technology, Beaverton, OR, USA) that allowed continuous monitoring of turbidity changes. For these experiments, *ca.* 15-mL aliquots of the amino acids solutions in 70% aqueous methanol were freshly prepared and placed in the instrument vials. The respective turbidity changes were registered for the period of 14 days (in 1-min intervals). To confirm the qualitative reproducibility of the results, the turbidity measurements were repeated twice. Moreover, the stability of turbidity measurements was controlled in the course of one day for water, methanol, and 70% aqueous methanol as the reference solvents, and the relative standard deviation (RSD) of these measurements proved very low (0.29% for pure methanol and 0.79% for 70% aqueous methanol). Similarly, turbidity measurements were carried out in the course of one day for the solution of glacial acetic acid (as a simple model of the low molecular weight non-chiral carboxylic acid) in 70% aqueous methanol and again, stability of these results was confirmed by an insignificant relative RSD value (below 0.50%).

HPLC-ELSD

The HPLC-ELSD system was used to monitor concentration changes of the six α-amino acid systems (*L*-, *D*-, and *DL*-Ala, and *L*-, *D*-, and *DL*-Phe) in the function of time. The analyses were carried out using the Varian model 920 liquid chromatograph equipped with the 900-LC autosampler, the gradient pump, the 380-LC ELSD detector, the C18 column (250 mm × 4.6 mm i.d., 5 μm particle diameter; Varian; cat. no. A3000250C046), and the Galaxie software for the data acquisition and processing. The chromatographic column was thermostatted at 35°C using the Varian Pro Star 510 column oven. Chromatographic analyses were carried out over the course of 48 h at the 10-min intervals in the isocratic mode. The 5-μL sample aliquots and the methanol–water (20:80, *v*/*v*) mobile phase at a flow rate of 0.8 mL min^{-1} were used.

LC-MS

Mass spectra of the four binary systems (*L*-Ala-*L*-Phe, *D*-Ala-*D*-Phe, *L*-Ala-*D*-Phe and *D*-Ala-*L*-Phe) dissolved in 70% aqueous methanol aged for four weeks were recorded with use of the Varian MS-100 mass spectrometer. The working MS conditions were the following: ESI-MS scan from *m*/*z* 50–2000, positive ionization, spray chamber temperature 50 °C, drying gas temperature 250 °C, drying gas pressure 25 psi, capillary voltage 50 V, needle voltage 5 kV.

Spectroscopy of far UV circular dichroism (CD)

The circular dichroism spectra in the far UV range (190 ÷ 260 nm) were registered for the monomeric and binary α-amino acid samples analogous to those used for turbidimetric measurements (i.e., for the 10 freshly prepared and 10 aged samples after the four months ageing period), yet diluted in proportion of 1: 25 (v/v) with water. The CD spectrum of the blank sample (0.20 mL 70% aqueous methanol + 4.80 mL H_2O) was also registered and subtracted from each spectrum

of the amino acid solution. The measurements were carried out for the samples placed in the 1-mm cell with use of the J-815 model CD spectrometer (Jasco Electronics Holdings, Johannesburg, South Africa).

Results and discussion

Turbidity patterns

Turbidimetric monitoring of spontaneous peptidization was carried out in the continuous mode (in the 1-min intervals) by the registration of the nephelometric turbidity units (NTU) for the period of 14 days at 25.0 ± 0.5 °C. The patterns of turbidity changes in the function of time are given in Figs. 1a–1c. Based on visual assessment, these patterns can be divided in two groups. Group 1 includes six different monocomponent and binary α-amino acid samples characterizing with a similarity of turbidity patterns among different samples (Figs. 1a and 1b). Group 2 includes four different binary α-amino acid samples characterizing with dissimilarity from the aforementioned six cases and from one another (Fig. 1c).

The first two cases are classified as those belonging to Group 1 (Subgroup 1a), which includes the monocomponent *L*-Ala and *L*-Phe solutions. The respective turbidity patterns look similar to one another, with an initial drop of turbidity followed by its gradual increase, to finally head toward a steady state (Figs. 1ai and 1aii). Frequent and needle-like oscillatory changes most probably have a physical meaning, as they are not artifacts caused by the power supply or temperature instability (the employed measuring system was carefully stabilized). The four cases belonging to Group 1 (Subgroup 1b) are characterized by turbidity patterns also looking similar to one another with spiky oscillations followed by an oscillation damp and the turbidity eventually heading toward a steady state. Subgroup 1b includes two monocomponent solutions (*D*-Ala and *D*-Phe, Fig. 1biii, iv) and two binary solutions (*L*-Ala-*L*-Phe and *D*-Ala-*D*-Phe, Figs. 1bv and 1bvi).

The dissimilar turbidity patterns with four binary α-amino acids solutions (*DL*-Ala, *DL*-Phe, *L*-Ala-*D*-Phe, and *D*-Ala-*L*-Phe) are classified as Group 2. With *DL*-Ala, after an initial turbidity drop lasting less than one day, rather insignificant oscillatory changes of turbidity are observed, very close to a steady state (Fig. 1cvii). With *DL*-Phe, rapid and continuous oscillatory drop of turbidity is observed (Fig. 1cviii). With *L*-Ala-*D*-Phe, an oscillatory drop of turbidity is followed by the oscillations around a steady state, to finish with a well pronounced turbidity growth (Fig. 1cix). With *D*-Ala-*D*-Phe, one observes weak and irregular oscillations of turbidity around a steady state (Fig. 1cx). A reminder can be made that the experimental turbidity patterns (characterized by spiky oscillations and then turbidity building up to a steady state) were modeled in the theoretical section of paper [25].

Let us consider possible reasons of similarity of the turbidity patterns within Group 1 (Figs. 1a and 1b) and dissimilarity within Group 2 (Fig. 1c). With solutions of four optically pure α-amino acids belonging to Group 1 (*L*-Ala, *D*-Ala, *L*-Phe, and *D*-Phe), at the initial peptidization stage, the formation of peptides built of

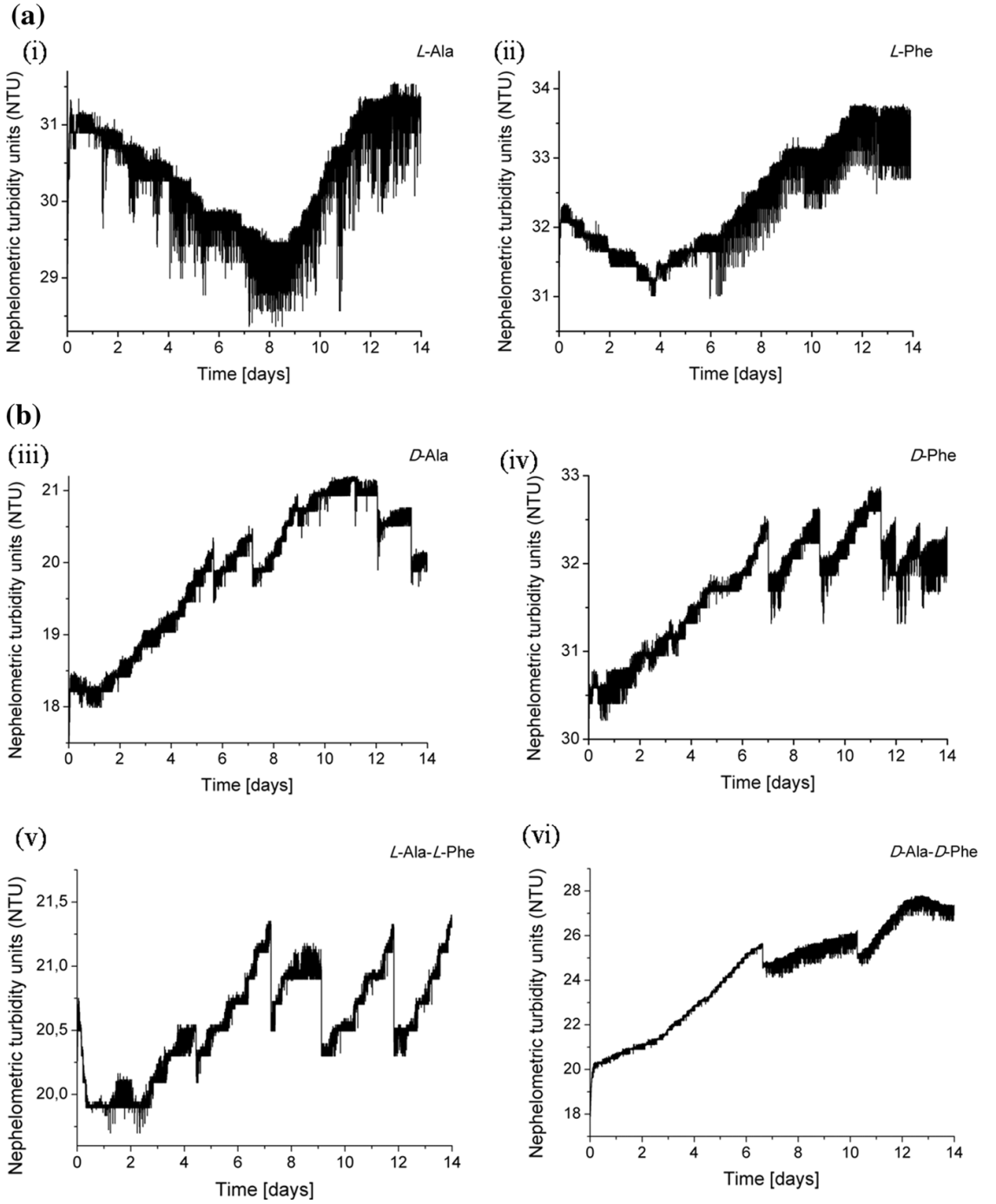

Fig. 1 Patterns of turbidity changes (in nephelometric turbidity units (NTU)) in the function of time for the solutions: **a** (i) *L*-Ala, (ii) *L*-Phe, **b** (iii) *D*-Ala, (iv) *D*-Phe, (v) *L*-Ala-*L*-Phe, (vi) *D*-Ala-*D*-Phe, **c** (vii) *DL*-Ala, (viii) *DL*-Phe, (ix) *L*-Ala-*D*-Phe, and (x) *D*-Ala-*L*-Phe

equichiral α-amino acids is expected (until spontaneous chiral conversion results in accumulation of meaningful amounts of inequichiral counterparts, which is not likely in the initial 14 days of the experiment). It is not certain if these equichiral peptides can assume the secondary α-helix structure under our experimental conditions, yet such a possibility with a consequent formation of the backbone H-bonds between the >CO of peptide group i and the >NH of peptide group $i + 3$

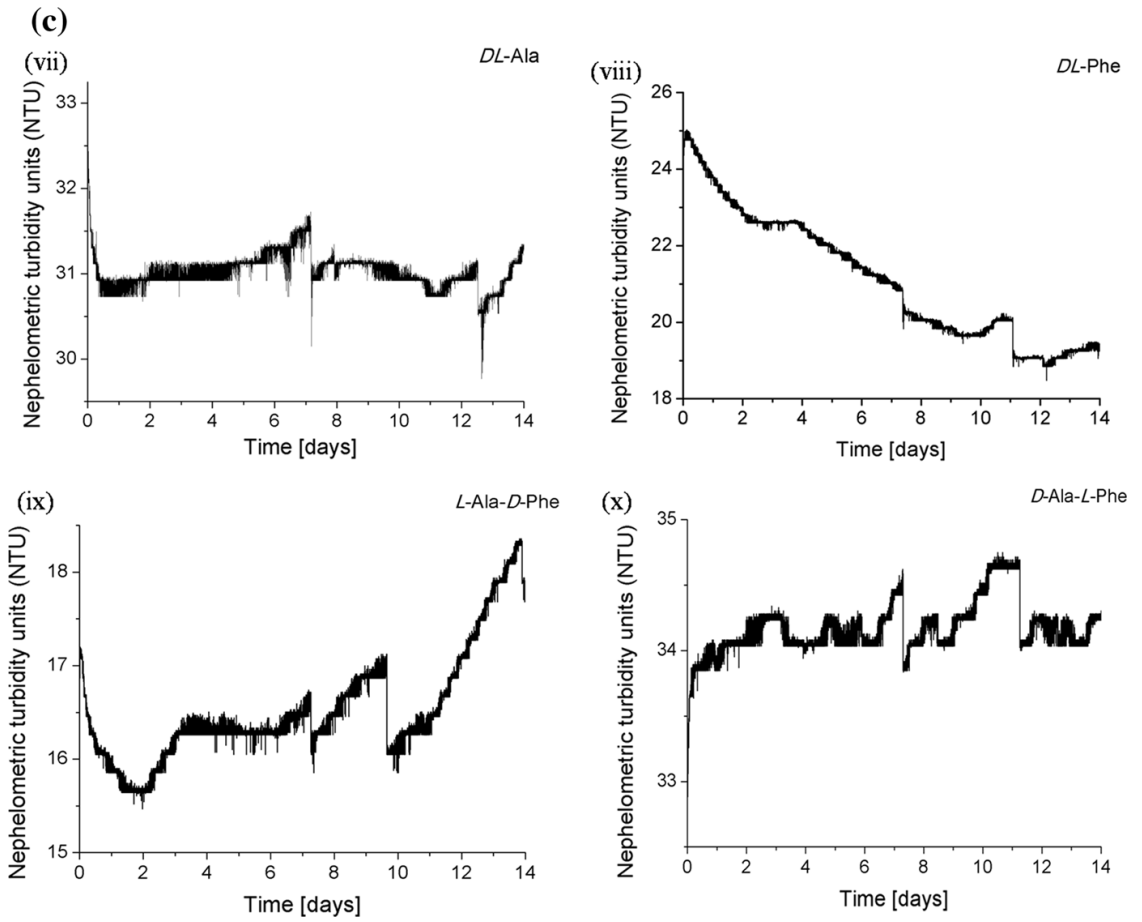

Fig. 1 continued

[26] is anticipated. One has to additionally comment on the difference between the turbidity patterns valid for *L*-Ala and *L*-Phe on the one hand (Figs. 1ai and 1aii) and those valid for *D*-Ala and *D*-Phe on the other (Figs. 1aiii and 1aiv). This difference could be due to the fact that in the former case, the right-handed α-helices are formed and in the latter case the left-handed ones [27], claimed to be somewhat less stable in an aqueous environment [28]. Indirectly, such a difference is confirmed by our earlier turbidity measurements carried out for *L*-Ser and *D*-Ser [29], where the turbidity pattern of *L*-Ser demonstrated the circadian rhythm of turbidity changes, and *D*-Ser did not show such a rhythm. Thus the difference in the handedness of the right- and left-handed α-helices can probably influence the different dynamics of peptidization and consequently, a different light-scattering effect (reflected in the difference of the respective turbidity patterns).

With the solutions of the two binary α-amino acid mixtures belonging to Group 1 (*L*-Ala-*L*-Phe and *D*-Ala-*D*-Phe, (Figs. 1bv and 1bvi), one expects formation of the homo- and heteropeptides. However, both homo- and heteropeptides can assemble in equichiral α-amino acid units, so that the right-handed (*L*-*L*) and the left-handed (*D*-*D*) α-helices can be expected as a possible reason of similarity of the respective turbidity patterns. Herewith, it needs to be added that both Ala and Phe have long been recognized among the most helicogenic α-amino acids [30].

Group 2 differs from Group 1, as it includes four binary mixtures (*DL*-Ala, *DL*-Phe, *L*-Ala-*D*-Phe, and *D*-Ala-*L*-Phe) with the opposite chiral configurations of the two counterparts (either *L*-*D*, or *D*-*L*). Although in this case both homo- and heteropeptides can be formed spontaneously, the preferential formation of heteropeptides is statistically more probable. The heteropeptides in Group 2 are built of inequichiral α-amino acid units, with a random sequence of the *L* and *D* α-amino acids. Since ~3.5 equichiral α-amino acid units are needed per one turn in the α-helix (and the smallest integer number required to ensure two complete α-helical turns is 7 [31]), a random sequence of the *L* and *D* α-amino acid units cannot ensure an efficient enough stringing of equichiral molecules into the equichiral heptade regions (either left-, or right-handed). This randomness of the α-amino acids arrangement in the inequichiral peptide molecules most probably manifests itself as a lack of similarity among the respective turbidity patterns. The turbidimetric results valid for Group 2 indirectly strengthen our assumption as to possible formation of the α-helix structures in spontaneous peptidization with equichiral α-amino acids. However, the formation of peptide α-helices is regarded as a working hypothesis only (conceived by equichirality of the monomeric units involved), although the other molecular level mechanisms cannot be excluded which might eventually complement or replace the α-helix concept.

As controls, we present the time dependence of the turbidity for water, methanol, 70% aqueous methanol and the glacial acetic acid solution in 70% aqueous methanol over 24 h (Fig. 2). Stable turbidity values for the three solvents and the solution of acetic acid (as a simple model of the low molecular weight non-chiral carboxylic acid) apparently differ from the dynamic behavior of the α-amino acid solutions. We interpret increases in turbidity to correspond to the growing amounts of the nano- and microparticles suspended in the solution, owing to the progress of peptidization (because from our partially unpublished experiments performed with use of the scanning electron microscopy, it comes out that insoluble peptides are

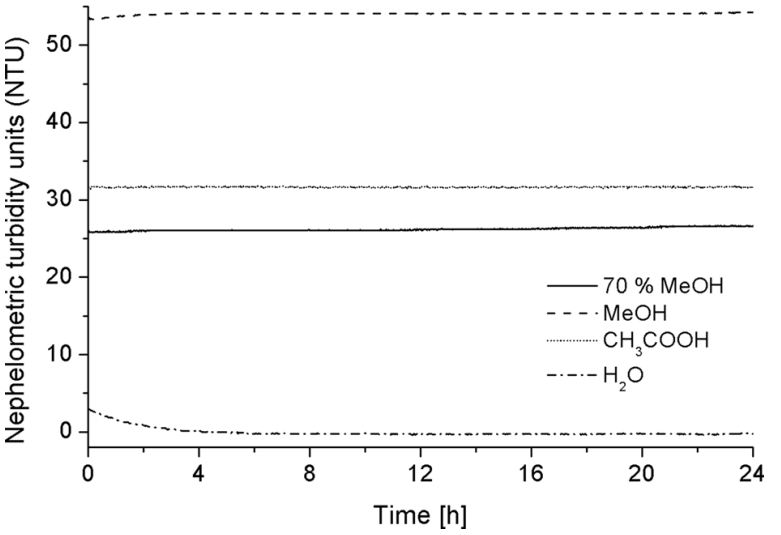

Fig. 2 Turbidity (in nephelometric turbidity units, NTU) for water (H_2O), methanol (MeOH), 70% aqueous MeOH, and 1 mg mL^{-1} solution of glacial acetic acid in 70% aqueous MeOH registered for 24 h

formed almost instantaneously in the solution, much earlier than they can be perceived by human eye). A decrease in turbidity can arise from dissociation of the higher, insoluble peptides to lower soluble ones, and/or from sedimentation of the higher insoluble peptides at the bottom of the measuring vial.

Finally, a general conclusion is drawn that in the α-amino acid solutions stored for the longer periods of time, peptidization progresses in a nonmonotonic fashion. Due to the randomness of size with peptide nano- and microparticles spontaneously formed in each individual experimental cycle, absolute turbidity values can change from one cycle to another, yet the shapes of individual turbidity patterns remain similar independent of the repetitions. Thus we can point out to the similarity of certain turbidity patterns and dissimilarity of the other ones, and speculate on spontaneous formation of the secondary α-heliceous peptide structures in the former case. It is understandable that in view of a lack of standardization in turbidity units, measurement devices and calibration techniques, usage of turbidimetry to analytical determinations can only be empirical and rather qualitative [23].

HPLC-ELSD

Due to specific nature of turbidimetric results which represent a sum of the light scattering effects with insoluble peptides of unknown yields, shapes, and molecular weights present in the investigated solutions, we cannot expect direct correlation thereof with chromatographic results which provide a quantitative insight in peptidization. However, certain analogies between turbidimetric and chromatographic results have been observed.

L-Ala, *D*-Ala, and *DL*-Ala solutions

For the *L*-, *D*-, and *DL*-Ala solutions, the chromatographic peak heights (corresponding to the monomeric Ala concentrations) were recorded in the course of the initial 12 h of samples ageing in the 10-min intervals, with the retention time value (t_R) equal to 3.5 min for each Ala sample. The obtained chromatographic time series are given in Fig. 3. The most important observation is that the plots shown in

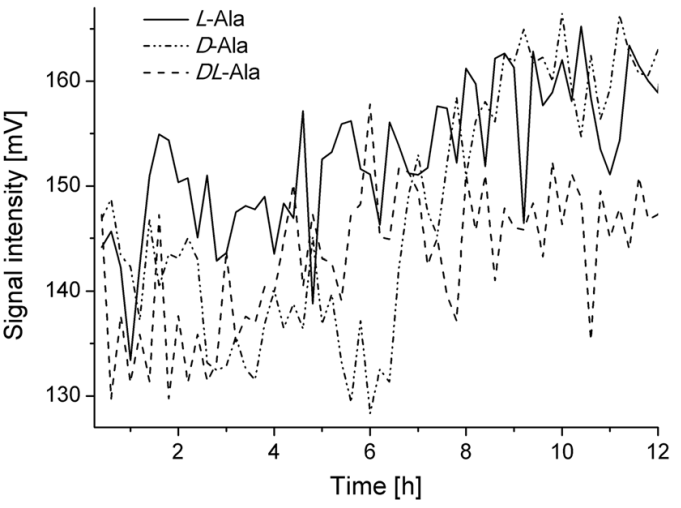

Fig. 3 Time series of the chromatographic peak heights for (*i*) *L*-Ala, (*ii*) *D*-Ala, and (*iii*) *DL*-Ala solution in 70% aqueous methanol (registered over the course of 48 h)

Fig. 3 directly confirm an oscillatory nature of the concentration changes with the monomeric Ala species and indirectly, the oscillatory nature of the peptides formation. High amplitudes of the respective concentration changes often equal to a dozen mV units. However, no similarity such, as synchronization of the oscillation dynamics along the time axis is observed among the time series patterns valid for *L*-, *D*-Ala, and *DL*-Ala.

L-Phe, *D*-Phe, and *DL*-Phe solutions

For the *L*-, *D*-, and *DL*-Phe solutions, the chromatographic peak heights (corresponding to the monomeric Phe concentrations) were recorded in the course of the initial two days of samples ageing in the 10-min intervals, with the retention time value (t_R) equal to 7.5 min for the *L*-, *D*-, and *DL*-Phe sample. The chromatographic time series are given in Fig. 4. The most important observation is that the plots shown in Fig. 4 directly confirm an oscillatory nature of the concentration changes with the monomeric Phe species and indirectly, the oscillatory nature of the peptides formation. Then a certain similarity is observed between the time series patterns valid for *L*- and *D*-Phe, whereas the time series pattern valid for *DL*-Phe is different. Similarity of the *L*- and *D*-Phe patterns consists in synchronization of the oscillation dynamics along the time axis and in high amplitudes of the respective concentration changes, often equaling to several dozen mV units. The time series pattern valid for *DL*-Phe does not show synchronization with the remaining two patterns and the amplitudes of the concentration changes in this latter case are in the range of *ca.* 10 mV only.

LC-MS

The main aim of the LC-MS analysis was to prove that in the binary α-amino acid systems, both homo- and heteropeptides are spontaneously formed. Four binary systems (*L*-Ala-*L*-Phe, *D*-Ala-*D*-Phe, *L*-Ala-*D*-Phe and *D*-Ala-*L*-Phe) were selected

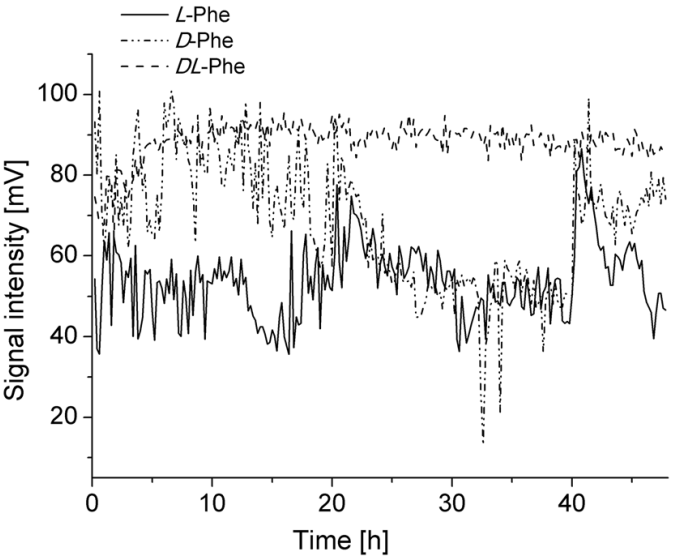

Fig. 4 Time series of the chromatographic peak heights for (*i*) *L*-Phe, (*ii*) *D*-Phe, and (*iii*) *DL*-Phe solution in 70% aqueous methanol (registered over the course of 48 h)

for this investigation and the respective mass spectra recorded. In each spectrum, signal originating from the monomeric Ala cation is registered (*m*/*z* 89.8, $[Ala + H]^+$), and in two spectra (*L*-Ala-*L*-Phe and *L*-Ala-*D*-Phe), signal originating from the monomeric Phe cation is also present (*m*/*z* 165.8, $[Phe + H]^+$). In *L*-Ala-*L*-Phe, three *m*/*z* signals at 350.5, 801.1, and 1867.1 are ascribed, respectively, to the homopeptide cations ($[Ph_7 + 3H]^{3+}$, $[Ala_{11} + H]^+$, and $[Ala_{26} + H]^+$), and six *m*/*z* signals are ascribed to the heteropeptide cations. In *D*-Ala-*D*-Phe, five *m*/*z* signals at 840.7, 871.2, 1342.9, 1452.4 and 1605.2 are ascribed, respectively, to the homopeptide cations ($[Ala_{47} + 4H]^{4+}$, $[Ala_{12}]^+$, $[Phe_9 + H]^+$, $[Ala_{61} + 3H]^{3+}$, and $[Ala_{22} + Na]^+$), and five *m*/*z* signals are ascribed to the heteropeptide cations. In *L*-Ala-*D*-Phe, three *m*/*z* signals at 350.5, 792.0, and 898.6 are ascribed, respectively, to the homopeptide cations ($[Phe_7 + 3H]^{3+}$, $[Ala_{25} + 2H]^{2+}$, and $[Phe_{16} + 3H]^{3+}$), and eight signals are ascribed to the heteropeptide cations. In *D*-Ala-*L*-Phe, one signal at *m*/*z* 1785.3 is ascribed to the homopeptide cation ($[Phe_{12} + H]^+$), and nine signals are ascribed to the heteropeptide cations. Summing up, the obtained mass spectra provide a convincing enough evidence of spontaneous formation of the homo- and heteropeptides in each analyzed binary α-amino acid system. The discussed mass spectra are available as a supplementary material.

We also reflect on molecular proportions between Ala and Phe in the heteropeptides formed in the inequichiral binary solutions. The *m*/*z* signals in *L*-Ala-*D*-Phe at 1389.4, 1470.6, 1821.3, and 1926.6 are ascribed to the $[Ala_{19} + Phe_{19} + 3H]^{3+}$, $[Ala_8 + Phe_6 + H]^+$, $[Ala_{15} + Phe_5 + H]^+$, and $[Ala_2 + Phe_{12}]^+$ cation. The *m*/*z* signals in *D*-Ala-*L*-Phe at 1281.6, 1475.9, 1633.1, 1983.5 are ascribed to the $[Ala_{13} + Phe_{11} + 2H]^{2+}$, $[Ala_6 + Phe_7 + H]^+$, $[Ala_{21} + Phe_{23} + 3H]^{3+}$, and $[Ala_9 + Phe_9 + H]^+$ cation, in order. In many of these heteropeptides, quantitative proportions between the two α-amino acids are either equal to 1:1 (e.g., 19:19), or quite close to this value (e.g., 8:6, 13:11, 21:23, etc.). Although in most cases considerably more than seven monomer units of one species (either Ala, or Phe) are involved, due to randomness of the assembling mechanism one can expect neither equichiral heptades, nor the resulting secondary α-helix structures.

Spectroscopy of far UV circular dichroism (CD)

The far UV circular dichroism performs well, when estimating secondary structures of globular proteins [32–34], yet the analysis of linear peptides is considerably more complicated [35] and mathematical algorithms have to be used to deconvolve the CD spectra in order to assess relative contributions from a variety of secondary structures (α-helices, *β*-sheets, coils etc.). However, we used the CD spectroscopic technique just to qualitatively compare the CD spectra in the range of 190 ÷ 260 nm (characteristic of the secondary linear peptide structures) for the systems composed of equichiral and inequichiral α-amino acid molecules after four months ageing. Respective CD spectra are presented in Figs. 5a–5f and we believe that the predominant contribution to these spectra originates from α-helices (as more complicated secondary structures are less probable as a result of spontaneous peptidization carried out for four months only.

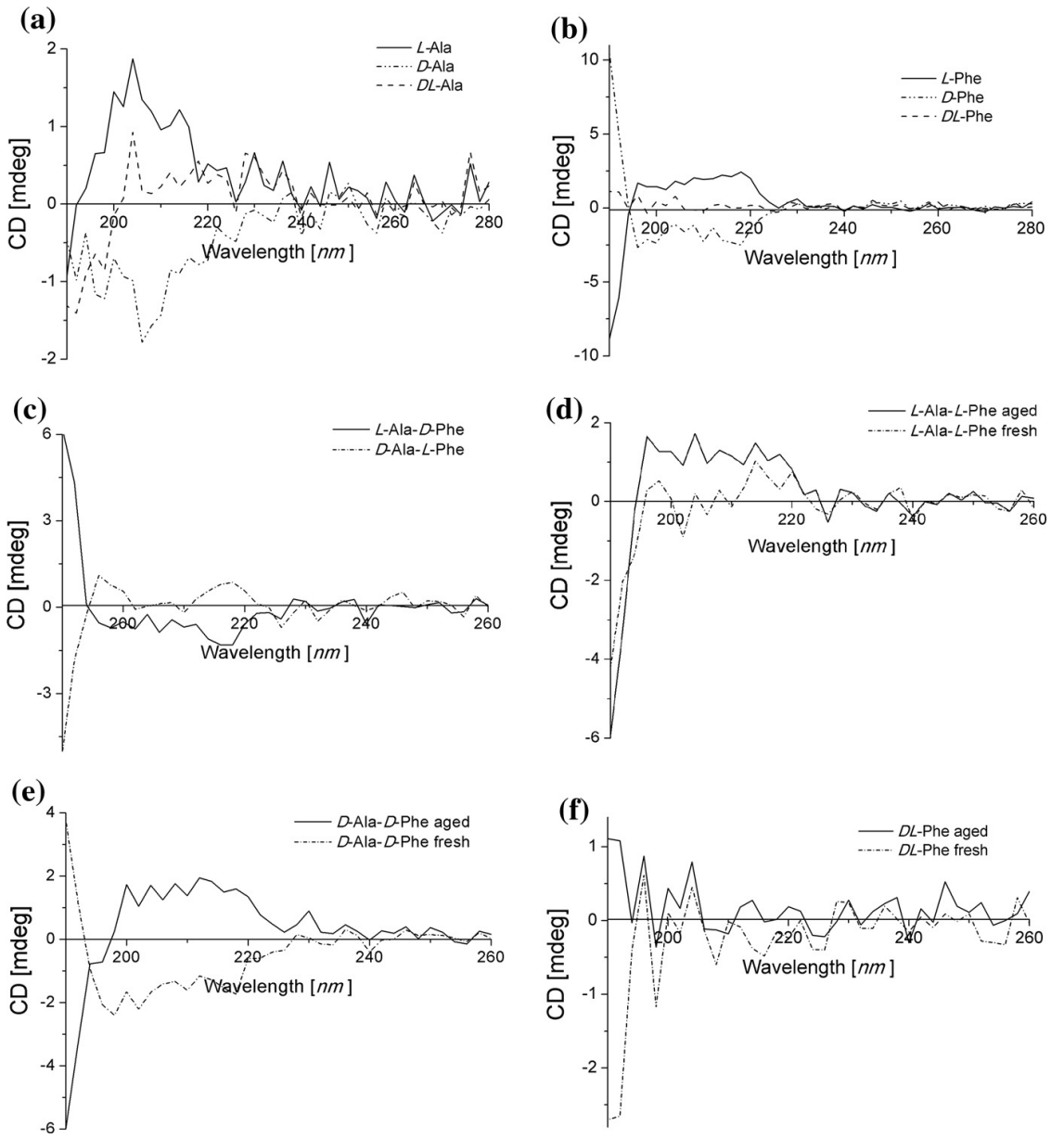

Fig. 5 CD spectra recorded for the solutions of **a** *L*-, *D*-, and *DL*-Ala, **b** *L*-, *D*-, and *DL*-Phe, and **c** *L*-Ala-*D*-Phe and *D*-Ala-*L*-Phe after the four months samples ageing, and for the fresh and aged solutions of **d** *L*-Ala-*L*-Phe, **e** *D*-Ala-*D*-Phe, and **f** *DL*-Phe (after the four months samples ageing)

In Fig. 5a, we compare the CD spectra for *L*-, *D*-, and *DL*-Ala. In the sample of *L*-Ala, two *Cotton* bands characteristic of α-helix can be seen with the first band positive and the second one negative. In the sample *D*-Ala, also two *Cotton* bands can be seen with the first band negative and the second band positive. The CD spectrum for the racemic (*DL*-Ala) sample is considerably less intense than the other two, with the first *Cotton* band positive and the second band negative. Thus, we assume that in the inequichiral (racemic) mixture, the *L*-Ala-derived α-helices predominate and *D*-Ala hardly participates in the helical secondary structures.

In Fig. 5b, we compare the CD spectra for *L*-, *D*-, and *DL*-Phe. For *L*-Phe, two *Cotton* bands can be seen with the first band positive and the second band negative. For *D*-Phe, two *Cotton* bands can be seen with the first band negative and the second

band positive. From the CD spectrum of the racemic (*DL*-Phe) sample, the *Cotton* bands are practically absent and hence, apparently no (or trace amounts) of equichiral α-helices are formed.

In Fig. 5c, we show the CD spectra for the two binary *L*-Ala-*D*-Phe and *D*-Ala-*L*-Phe samples, each one composed of two inequichirial α-amino acids. The spectrum valid for *L*-Ala-*D*-Phe shows two *Cotton* bands, the first band negative (characteristic of *D*-Phe) and the second band positive. Thus we assume that in the investigated sample, the *D*-Phe-derived α-helices are formed. The plot valid for *D*-Ala-*L*-Phe also demonstrates two *Cotton* bands, the first band positive (characteristic of *L*-Phe) and the second band negative. In this case, we assume that in the investigated sample, the *L*-Phe-derived α-helices are formed. Thus in the aged *L*-Ala-*D*-Phe and *D*-Ala-*L*-Phe systems, the observed signs of the respective *Cotton* bands point out to the selective formation of the Phe-derived α-helices, with the monomeric Ala units hardly engaged in the helical structures.

In Fig. 5d, we show CD spectra for the fresh and aged sample of the binary equichiral *L*-Ala-*L*-Phe system. The fresh sample demonstrates a very low intensity CD spectrum characterizing with the first *Cotton* band positive and the second band negative (characteristic of the *L* configuration of both α-amino acids). The reason for an appearance of these two *Cotton* bands in the fresh sample is not quite clear and it can either be due to trace contamination of the commercial monomeric α-amino acids with the peptides, or to fast peptidization upon dissolution. After four months of sample ageing, the intensity of the CD spectrum considerably grows, witnessing to peptidization progress and the higher yields of α-helices in the system.

The most interesting phenomenon is shown in Fig. 5e, which holds for the fresh and aged sample of the binary equichiral *D*-Ala-*D*-Phe system. The fresh sample demonstrates α-helix characterizing with the first *Cotton* band negative and the second band positive (pointing out to the *D* configuration of the amino acids involved). Again, the reason for its appearance in the fresh sample is not quite clear (either due to contamination of the commercial monomeric α-amino acids with certain amounts of peptides, or to fast peptidization upon dissolution). A striking phenomenon though is that after the four months storage period, the CD spectrum confirms the presence of the α-helical structures, yet with the reversed signs of the two *Cotton* bands, i.e., the first band is now positive and the second band is negative (pointing out to the *L* configuration of the amino acids involved). This result witnesses not only to the process of peptidization, but also to chiral conversion in the course of sample ageing.

One more interesting example is furnished by Fig. 5f, which holds for the fresh and aged sample of the racemic *DL*-Phe system. In this case, the intensities of the two plots in the range of 190 ÷ 260 nm are almost negligible (and especially in the range of the first *Cotton* band), which confirms negligible amounts of the α-helix structures only. However, in the range of the second *Cotton* band the negative slope for the fresh sample changes to the positive slope for the aged sample. This result also seems indicative of the process of chiral conversion taking place in the system in the course of sample storage.

Summing up, the CD spectroscopic results confirm spontaneous formation of α-helical secondary structures in the equichiral *L*, *D*, *L*-*L*, and *D*-*D* systems on the one

hand, and either an inability to form α-helices in the inequichiral *DL* system (Figs. 5b and 5f), or the formation of α-helical homochiral peptides in the binary *D*-*L* systems (Figs. 5a and 5c). In this sense, the obtained CD results support our assumptions derived from turbidimetric data and presented earlier. An additional gain of applying the CD spectroscopy is confirmation with its aid of the processes of chiral conversion.

Conclusions

The non-linear turbidity changes with the monocomponent and binary Ala and Phe solutions are due to the oscillatory peptidization process which results in the formation of insoluble higher molecular weight peptides, extensively discussed elsewhere. In this study, the similarity of turbidity patterns is in the main focus of our attention. It is tentatively ascribed to equichirality of all α-amino acid units in a molecule of a given peptide and consequently, to a possible formation of the peptide α-helix structure. Analogously, the dissimilarity of turbidity patterns is tentatively explained by inequichirality of α-amino acid units in the respective peptides. However, the formation of peptide α-helices is regarded as a working hypothesis only, conceived by equichirality of the monomeric units involved and the other molecular level mechanisms leading to the secondary peptide structures cannot be excluded, which might eventually complement or replace the α-helix concept. The HPLC-ELSD data confirm the non-linear nature of peptidization and certain analogies are emphasized between the turbidimetric and chromatographic results. The MS data confirm formation of peptides, and the CD data confirm a possibility of formation of α-helical structures in equichiral α-amino acid systems.

Acknowledgements A.G. acknowledges the financial support of the DoktoRIS project, cofinanced by the European Union within the European Social Found. The authors acknowledge an invaluable help of Prof. Zofia Drzazga and Ms. Izabela Schisler from the Department of Medicinal Physics, University of Silesia, Katowice, Poland with registration of the CD spectra.

Open Access This article is distributed under the terms of the Creative Commons Attribution 4.0 International License (http://creativecommons.org/licenses/by/4.0/), which permits unrestricted use, distribution, and reproduction in any medium, provided you give appropriate credit to the original author(s) and the source, provide a link to the Creative Commons license, and indicate if changes were made.

References

1. Sajewicz M, Matlengiewicz M, Leda M, Gontarska M, Kronenbach D, Kowalska T, Epstein IR (2010) Spontaneous oscillatory in vitro chiral conversion of simple carboxylic acids and its possible mechanism. J Phys Org Chem 23:1066–1073
2. Sajewicz M, Gontarska M, Kronenbach D, Leda M, Kowalska T, Epstein IR (2010) Condensation oscillations in the peptidization of phenylglycine. J Syst Chem 1:7. doi:10.1186/1759-2208-1-7
3. Sajewicz M, Godziek A, Maciejowska A, Kowalska T (2015) Condensation dynamics of the *L*-Pro-*L*-Phe and *L*-Hyp-*L*-Phe binary mixtures in solution. J Chromatogr Sci 53:31–37

4. Sajewicz M, Piętka R, Pieniak A, Kowalska T (2005) Application of thin-layer chromatography (TLC) to investigating oscillatory instability of the selected profen enantiomers. Acta Chromatogr 15:131–149
5. Sajewicz M, Gontarska M, Wróbel M, Kowalska T (2007) Enantioseparation and oscillatory transenantiomerization of S, R-(±)-ketoprofen, as investigated by means of thin layer chromatography with densitometric detection. J Liq Chromatogr Relat Technol 30:2193–2208
6. Sajewicz M, Kronenbach D, Gontarska M, Wróbel M, Piętka R, Kowalska T (2009) TLC in search for structural limitations of spontaneous oscillatory in vitro chiral conversion. α-hydroxybutyric and mandelic acids. Planar Chromatogr-Modern TLC 22:241–248
7. Sajewicz M, Dolnik M, Kronenbach D, Gontarska M, Kowalska T, Epstein IR (2011) Oligomerization oscillations of L-lactic acid in solutions. J Phys Chem A 115:14331–14339
8. Adler-Abramovich L, Reches M, Sedman VL, Allen S, Tendler SJB, Gazit E (2006) Thermal and chemical stability of diphenylalanine peptide nanotubes: implications for nanotechnology applications. Langmuir 22:1313–1320
9. Ryu J, Park CB (2010) High stability of self-assembled peptide nanowires against thermal, chemical and proteolytic attacks. Biotechnol Bioeng 105:221–230
10. Reches M, Gazit E (2004) Formation of closed-cage nanostructures by self-assembly of aromatic dipeptides. Nano Lett 4:581–585
11. Görbitz CH (2006) The structure of nanotubes formed by diphenylalanine, the core recognition motif of Alzheimer's beta-amyloid polypeptide. Chem Commun (Camb) 22:2332–2334
12. Maltsev AV, Bystryak S, Galzitskaya O (2011) The role of β-amyloid peptide in neurodegenerative diseases. Ageing Res Rev 10:440–452
13. Tokunaga M, Liu ML, Nagai T (2010) Implantation of cardiac progenitor cells using self-assembling improves cardiac function after myocardial infarction. J Mol Cell Cardiol 49:972–983
14. Ueda Y, Ishii K, Toyama Y, Nakamura M, Okano H (2008) Transplantation of human neural stem cells for spinal cord injury in primates. Neurosci Res 1:93–93
15. Debnath S, Roy S, Ulijn RV (2013) Peptide nanofibers with dynamic instability through nonequilibrium bioanalytic assembly. J Am Chem Soc 135:16789–16792
16. Samaritoni JG, Copes AT, Crews DeMarcus K (2014) Unexpected hydrolytic instability of N-acylated amino acid amides and peptides. J Org Chem 79:3140–3151
17. Villani V, Tamburro AM, Comenges JMZ (2000) Conformational chaos and biomolecular instability in aqueous solution. J Chem Soc, Perkin Trans 2:2177–2184
18. Godziek A, Maciejowska A, Sajewicz M, Kowalska T (2015) HPLC monitoring of spontaneous nonlinear peptidization dynamics of selected amino acids in solution. J Chromatogr Sci 53:401–410
19. Sajewicz M, Matlengiewicz M, Juziuk M, Penkala M, Weloe M, Schulz M, Kowalska T (2013) Thin-layer chromatographic evidence of proline peptidization in solution and its thin-layer chromatographic enantioseparation. J Liq Chromatogr Relat Technol 36:2497–2511
20. Godziek A, Maciejowska A, Talik E, Wrzalik R, Sajewicz M, Kowalska T (2016) On spontaneously pulsating proline-phenylalanine peptide microfibers. Curr Protein Pept Sci 17:106–116
21. Kowalska T, Sajewicz M (2016) Possibilities and limitations of selected analytical tools to trace nonlinear chemical processes. In: Proceedings of the 13th international conference on fundamental and applied aspects of physical chemistry "Physical Chemistry 2016", Belgrade, Serbia, September 26th–30th, 2016
22. Maciejowska A, Godziek A, Talik E, Sajewicz M, Kowalska T (2015) Investigation of spontaneous chiral conversion and oscillatory peptidization of L-methionine by means of TLC and HPLC. J Liq Chromatogr Relat Technol 38:1164–1171
23. Lawler DM (2005) Turbidity and nephelometry. In: Worsfold P, Townshend A, Poole C (eds) Encyclopedia of analytical science, 2nd edn. Elsevier Academic, San Diego, USA, pp 343–352
24. Lawler DM, Brown RM (1992) A simple and inexpensive turbidity meter for the estimation of suspended sediment concentrations. Hydrol Proc 6:159–168
25. Maciejowska A, Godziek A, Talik E, Sajewicz M, Kowalska T, Epstein IR (2016) Spontaneous pulsation of peptide microstructures in an abiotic liquid system. J Chromatogr Sci 17:106–116
26. Baldwin RL (2003) In search of the energetic role of peptide hydrogen bonds. J Biol Chem 278:17581–17588
27. Mortishire-Smith RJ, Drake AF, Nutkins JC, Williams DH (1991) Left handed α-helix formation by a bacterial peptide. FEBS Lett 278:244–246
28. Lins RD, Ferreira R (2006) The stability of right- and left-handed alpha-helices as a function of monomer chirality. Quim Nova 29:997–998

29. Maciejowska A, Godziek A, Sajewicz M, Kowalska T (2017) Circadian rhythm of spontaneous non-linear peptidization with proteinogenic amino acids in abiotic solutions versus homochirality. Acta Chromatogr 29:135–142
30. Blout ER (1962) The dependence of the conformation of polypeptides and proteins upon of amino acid composition. In: Stahmann MA (eds) Polyamino acids, polypeptides, and proteins. The University of Wisconsin Press, Madison, WI, USA, pp 275–279
31. Gruber M, Lupas AN (2003) Historical review. Another 50th anniversary. New periodicities in coiled coils. Trend Biochem Sci 28:679–685
32. Provencher SV, Glöckner J (1981) Estimation of globular protein secondary structure from circular dichroism. Biochemistry 20:33–37
33. Hennesey JP, Johnson WC (1981) Information content in the circular dichroism of proteins. Biochemistry 20:1085–1094
34. Perczel A, Foxman BM, Fasman GD (1992) How reverse turns may mediate the formation of helical segments in proteins: an x-ray model. Proc Natl Acad Sci USA 89:8210–8214
35. Reed J, Reed TA (1997) A set of constructed type spectra for the practical estimation of peptide secondary structure from circular dichroism. Anal Biochem 254:36–40

19 Spontaneous Chiral Conversion and Peptidization of Amino Acids Traced by Means of TLC–MS

Agnieszka Godziek, Anna Maciejowska, Mieczysław Sajewicz, and Teresa Kowalska

CONTENTS

19.1 SPONTANEOUS OSCILLATORY CHIRAL CONVERSION AND SPONTANEOUS OSCILLATORY PEPTIDIZATION OF AMINO ACIDS

In Reference 1, spontaneous oscillatory chiral conversion for the first time was reported for several propionic acid derivatives, stored for longer periods of time in 70% aqueous ethanol, based on the results originating from thin-layer chromatography (TLC) (and other instrumental techniques). Later, an analogous evidence of spontaneous chiral conversion obtained with use of high-performance liquid

K24794_C019.indd 345 11-09-2015 21:51:11

chromatography with diode-array detection (HPLC–DAD) was presented [2]. It was demonstrated that the oscillatory chiral conversion is a general property that characterizes the low-molecular weight carboxylic acids from the groups of profen drugs [1], amino acids [3], and hydroxyl acids [4], when dissolved in aqueous or nonaqueous solvents and stored for certain periods of time in solution. Chiral conversion of such compounds can occur according to two different pathways. In aqueous solutions, the general scheme is represented as [5] follows:

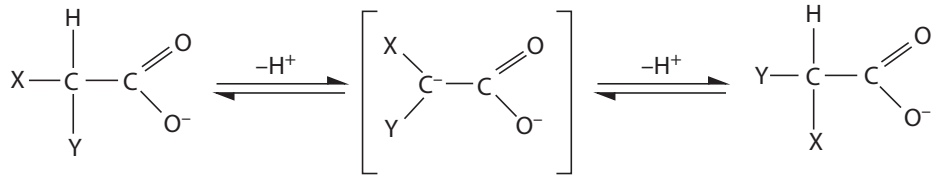

where X: –R (aliphatic) and Y: $–NH_2$, –OH, or –Ar (aromatic).

In anhydrous media and in the presence of trace amounts of water, the probable mechanism of chiral conversion is [6] as follows:

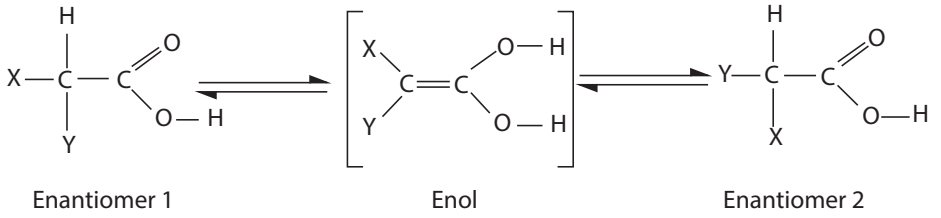

From our earlier investigations, it came out that the oscillatory chiral conversion of the low-molecular weight carboxylic acids occurs in parallel with the oscillatory condensation, which most probably has thermodynamic justification [2]. In Reference 7, the results were presented of spontaneous oscillatory peptidization for three amino acids (L-Met, L-His, and L-Ser) dissolved in water, and in References 8 and 9, the analogous results were given for three binary amino acid systems (L-Pro-L-Hyp, L-Pro-L-Phe, and L-Hyp-L-Phe) dissolved in aqueous organic solvents. The parallel processes of chiral conversion and peptidization of amino acids running in abiotic systems can be illustrated by the following scheme [10]:

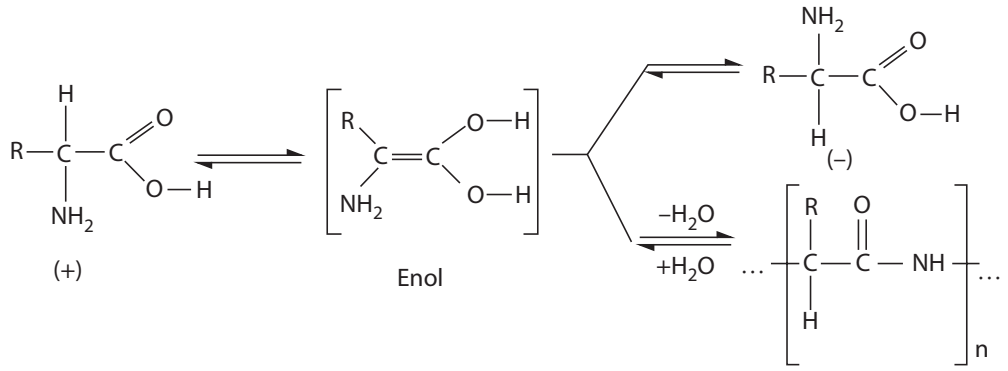

In Reference 8, a theoretical model of spontaneous nonlinear peptidization in the abiotic binary amino acid systems was developed, particularly focused on heteropeptide formation. This model assumes the following four different cases: (1) when two amino acids do not form heteropeptides and even in a binary solution they spontaneously produce homopeptides only; (2) when two amino acids of different nonlinear peptidization dynamics can form heteropeptides, and dynamics of faster peptidizing amino acid governs overall dynamics; (3) when two amino acids of different nonlinear peptidization dynamics can form heteropeptides, and dynamics of slower peptidizing amino acid governs overall dynamics; and (4) when two amino acids of different nonlinear peptidization dynamics can form heteropeptides according to cooperative mechanisms, where none of the two species governs the process dynamics.

Experimental evidence of the oscillatory chiral conversion and oscillatory condensation of amino acids (and of the other low-molecular weight carboxylic acids) is a challenging experimental task. For tracing dynamics of the oscillatory chiral conversion, both TLC and HPLC can be used (e.g., [1,2]), although each technique has its own advantages and shortcomings. For tracing dynamics of the oscillatory condensation, HPLC can be regarded as a technique of choice, due to high rates of the concentration changes, which could hardly be captured by means of TLC. If we, however, have no need to demonstrate the oscillatory nature of chiral conversion and peptidization, then TLC–densitometry proves handy for demonstration of chiral conversion, and TLC–MS proves equally handy for demonstrating peptidization. Unlike HPLC, where all separated species end up in an effluent tank, TLC is a good option that allows unconventional modifications of stationary and mobile phase, and an *in situ* preservation of the separated species for further examinations.

Spontaneous chiral conversion and peptidization of amino acids in abiotic systems means that in a certain way, these two parallel processes run out of control, although their dynamics certainly can be modified by external conditions (such as the solvent type, concentration, temperature, etc.). Thus far, the knowledge of the spontaneous nature of these two processes in abiotic systems has not yet become widespread among biochemists and life scientists in general, in spite of the growing importance of peptide nano- and microstructures for biotechnology. This modern technology branch is increasingly more interested in stable, or at least predictably behaving peptides, which can be employed in regenerative medicine, for delivery of bioactive therapeutics, as scaffolds in tissue engineering, etc. [11,12].

In this chapter, a brief overview is provided of our recent efforts in developing a novel thin-layer chromatographic method of the amino acid enantioseparation with use of chiral stationary phase (native cellulose) and with fortification of the amino acid sample just prior to the chromatographic analysis with the transition metal cation upon the example of Pro [13]. Then, an ability of two proteinogenic amino acids (i.e., Cys and Met) to undergo chiral conversion and peptidization is demonstrated with use of TLC–densitometry and TLC–MS [14,15]. It is shown how TLC–densitometry can provide evidence on spontaneous chiral conversion of amino acids taking place in the course of their storage in aqueous organic solutions. It is also shown how TLC–MS can be used to prove spontaneous peptidization of amino acids in the course of their aging, in spite of considerable and annoying background signals,

which are hard to avoid, when the TLC–MS interface and the TLC–ESI–MS operation mode are used [16].

19.2 ENANTIOSEPARATION OF PROLINE

The choice of L-Pro (Scheme 19.1) for our studies was due to an important role of this proteinogenic amino acid as a building block of collagen, which is omnipresent in the connective tissues of mammals, and largely responsible for tissue architecture and strength. It was our aim to develop a novel approach to the enantioseparation of Pro (which might later be extended to the enantioseparation of other amino acids as well) because up to our best knowledge, direct enantioseparation of Pro by means of TLC has been done only once prior to our own research [17] (which reflects a difficulty of this supposedly easy analytical task). In fact, we revisited an old concept of the thin-layer chromatographic enantioseparations of amino acids on native cellulose adsorbents proposed decades ago (e.g., [18,19]), although introducing considerable modification to it.

Experimental evidence of successful enantioseparation of DL-Pro is given in Reference 13. As native chiral adsorbent, microcrystalline cellulose was used (the 20 cm × 20 cm commercial precoated glass plates; layer thickness, 0.10 mm; Merck; cat. # 1.05716). As the test samples, DL-Pro (for the purpose of the enantioseparation) and L-Pro (as an external standard) were used. Concentrations of both samples in 70% aqueous methanol were 1.0 mg mL^{-1}. In order to enhance the enantioseparation, equimolar amounts of Mn(II) acetate were added to each solution, in order to obtain complexes between the Mn(II) cation and Pro as a chelating agent. Enhancement of the enantioseparation process by fortifying the analyzed racemic mixture with different transition metal cations (e.g., Cu(II), Co(II), Ni(II), and Mn(II)) just prior to analysis proper was tested in our earlier studies focusing on DL-lactic acid [20,21] and positive results were obtained. Apart from enhancing the enantioseparation, complexation of transition metal cations with chiral low-molecular weight carboxylic acids plays one more important role. Namely, bonding of these acids as chelating ligands to the metal cation stops their oscillatory configuration changes and so to say "freezes" (i.e., stabilizes) their respective configurations [21]. Therefore, the concept was adopted in the discussed research also and the complexation mechanism is schematically given here:

$$\text{L-Pro} + \text{Mn(II)} \quad \Leftrightarrow \quad \text{L-Pro} \ldots \text{Mn(II)}; \quad K_1$$

$$\text{D-Pro} + \text{Mn(II)} \quad \Leftrightarrow \quad \text{D-Pro} \ldots \text{Mn(II)}; \quad K_2$$

the enantioseparation condition: $K_1 \neq K_2$

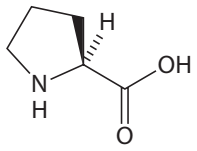

SCHEME 19.1 Chemical structure of Pro.

As mobile phase, 2-butanol–pyridine–glacial acetic acid–water (30:20:6:24, *v*/*v*) was used. The chromatogram was visualized by dipping the plate for 2 s in the 0.5% ninhydrin solution in 2-propanol, followed by heating for 5 min at 110°C.

As a result, the baseline enantioseparation was obtained, as shown in Figure 19.1a. Monomeric Pro is one of these rare amino acids, which develop yellow (and not bluish) color when visualized with ninhydrin. L-Pro used as an external standard (Figure 19.1b) confirmed the identity of the lower yellow spot number 2 as enantiomer L and the upper yellow spot number 3 as enantiomer D, as shown in Figure 19.1a. The respective R_F values were 0.57 ± 0.02 and 0.74 ± 0.02. Brownish-purple spot number 1 ($R_F = 0.32 \pm 0.02$; Figure 19.1) apparently originates from the Pro-derived peptides and it is also fully separated from the monomeric L-Pro spot number 2. The presence of peptides in the two freshly prepared Pro samples witnesses to rapid peptidization of this amino acid (although contamination of the commercial monomeric DL-Pro and L-Pro samples with peptides cannot be excluded).

A method utilizing native cellulose adsorbent and the concept of the amino acid complex formation with the transition metal cation elaborated in Reference 13 was then applied to tracing spontaneous chiral conversion and spontaneous peptidization of the other amino acids, as presented in the forthcoming sections.

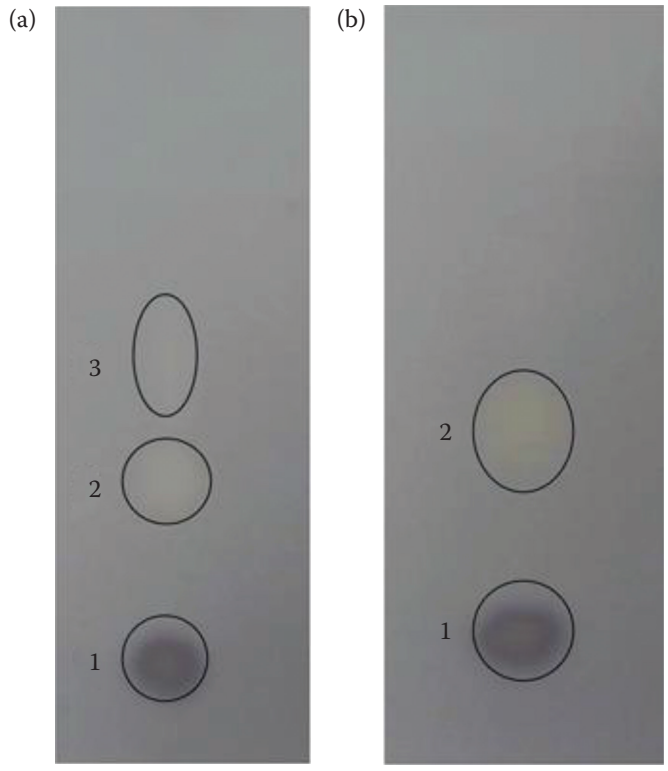

FIGURE 19.1 Pictures of the chromatograms on the cellulose plates stained with ninhydrin and valid for (a) DL-proline and (b) L-proline; (1) proline-derived oligopeptide fraction; (2) L-proline; and (3) D-proline. Samples were applied to the plate in the aliquots of 5 μL, at the concentration of 1.0 mg mL^{-1} amino acid (plus equimolar amount of Mn(II) acetate) and developed with 2-butanol + pyridine + glacial acetic acid + water (30:20:6:24, *v*/*v*). (From Sajewicz, M. et al. 2013. *J. Liq. Chromatogr. Relat. Technol.*, 36: 2497. With permission.)

19.3 SPONTANEOUS CHIRAL CONVERSION AND PEPTIDIZATION OF CYSTEINE

We focused our attention on L-Cys (Scheme 19.2) because of its importance as a sulfur-containing semiessential amino acid, which can be biosynthesized in humans and yet, due to its relatively low content in food, it is also used as a food additive (denoted as E920). L-Cys is an important building block of proteins that are used throughout the body, and it can physiologically be transformed to glutathione (a powerful antioxidant [22]), or taurine (essential for cardiovascular function, development and function of skeletal muscles, the retina, and the central nervous system [23]). Thus, the main aim of this study [14] was to employ TLC–densitometry and TLC–ESI–MS in order to demonstrate an ability of L-Cys to spontaneously undergo chiral conversion and condensation, when dissolved in 70% aqueous acetonitrile.

19.3.1 Thin-Layer Chromatography–Densitometry

Two thin-layer chromatographic experiments with densitometric detection were performed with Cys [14]. In Experiment 1, the main focus was on demonstration of spontaneous chiral conversion of Cys, and in Experiment 2, on demonstration of spontaneous peptidization of Cys in the course of sample aging. Both experiments were performed on chromatographic glassplates precoated with microcrystalline cellulose (Merck; cat. # 1.05716) with use of 2-butanol–pyridine–glacial acetic acid–water (30:20:6:24, *v*/*v*) as mobile phase and using ninhydrin as a visualizing agent (following the protocol described in Section 19.2 [13]). In Experiment 1, the chromatographic plates were activated by heating for 30 min at 110°C prior to applying the amino acid samples, and in Experiment 2, the plates were not activated.

In Experiment 1, L-Cys (for tracing chiral conversion) and DL-Cys (for proving the enantioseparation) were dissolved in 70% aqueous acetonitrile at the concentration of 0.7 mg mL^{-1}. The third sample was the L-Cys solution after 60 days aging. Just before the chromatographic analysis, equimolar amount of Mn(II) acetate was added to each of these three samples (in order to facilitate enantioseparation and stop oscillations). Each sample was spotwise applied to the plate in the 5-μL aliquot. The result in the form of the visualized chromatograms and densitograms is given in Figure 19.2.

In qualitative terms, all three chromatograms look similar, yet from a comparison of the chromatograms of L-Cys and DL-Cys, one can easily deduce that the blue spots represent monomeric Cys, and the brown and yellow spots hold for peptides. In all densitograms shown in Figure 19.2a(i–iii), the predominant peak originates from the peptide fraction and it is present both in the chromatograms of the fresh

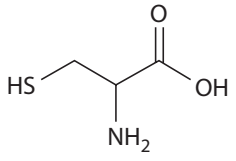

SCHEME 19.2 Chemical structure of Cys.

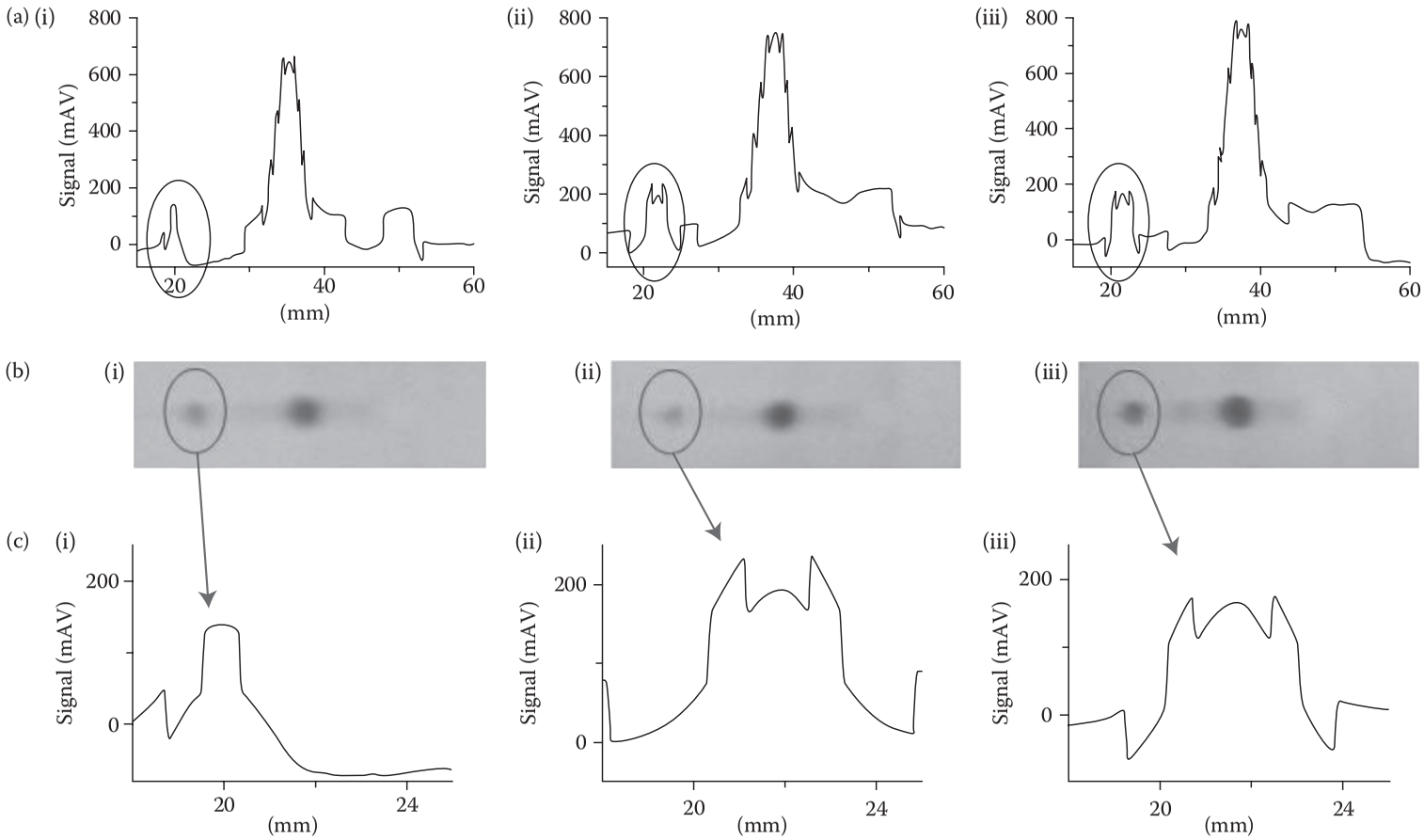

FIGURE 19.2 Densitograms and chromatograms of Cys solution with equimolar addition of Mn(II) acetate. (i) Fresh prepared L-Cys solution; (ii) Cys solution after 60 days' aging; (iii) fresh prepared DL-Cys solution. (a): Densitometric scans of the whole chromatograms (i)–(iii). (b): Photographs of the whole chromatograms (i)–(iii). (c): Enlarged densitometric scans of the Cys bands (i)–(iii). Black circles and arrows indicate the Cys bands. (From Godziek, A. et al. 2015. *J. Planar Chromatogr.—Modern TLC*, 28: 144–151. With permission.)

K24794_C019.indd 351 11-09-2015 21:51:12

samples (Figure 19.2a(i) and (ii)) and in that of the aged one (Figure 19.2a(iii)). This predominant peak witnesses to high condensation rates of Cys and also to a possible contamination of the commercial L-Cys sample with the Cys-derived peptides.

With monomeric cysteine (blue spots marked with black circles and black arrows on densitograms and chromatograms), differences between the fresh and the aged Cys sample are considerable. They are particularly well perceptible, when focusing on the enlarged densitograms of the blue spots. Densitogram of the monomeric peak registered from the freshly prepared L-Cys sample shows a single concentration profile (Figure 19.2c(i)), whereas that registered from the aged Cys sample shows two partially separated bands (Figure 19.2c(ii)). Similarly two partially separated bands can be seen in the densitogram registered from the freshly prepared DL-Cys sample (Figure 19.2c(iii)) and this resemblance allows a conclusion that in the course of aging, L-Cys undergoes chiral conversion according to the mechanism extensively discussed in Section 19.1.

The R_F values additionally emphasize differences between the fresh and the aged Cys sample, and also the similarity between the aged Cys and the fresh DL-Cys sample. For the fresh L-Cys sample, the R_F value of the monomer peak equals to 0.31 ± 0.01, which is the same as that for the lower peaks from the two partially separated monomer bands in the aged Cys and the fresh DL-Cys sample, respectively. The R_F value (equal to 0.35 ± 0.01) valid for the upper peak from the two partially separated monomer peaks in the aged Cys sample is the same as that of the upper peak from the partially separated monomer band for the fresh DL-Cys solution. Thus, the R_F value of D-Cys is higher than that of L-Cys, and this sequence remains in agreement with that reported for the derivatized L- and D-Cys in the NP-TLC systems, reported in the literature [24].

Experiment 2 was carried out in a similar manner to Experiment 1, although its aim was to demonstrate gradual consumption of monomeric Cys in the course of peptidization. To this effect, the stock L-Cys solution was prepared. From this fresh stock, 1 mL was withdrawn and spiked with an equimolar amount of Zn(II) nitrate, and the remaining lot was stored for aging. From this 1-mL fresh spiked solution, the 5-μL aliquot was spotwise applied to the chromatographic plate. After the 1-h long storage period, again 1 mL was withdrawn from the stock solution, spiked with an equimolar amount of Zn(II) nitrate, and from this sample the 5-μL aliquot was spotwise applied to the chromatographic plate. This procedure was repeated in 1-h intervals for 5 h. At the end, one and the same chromatographic plate with the Cys samples after 0-, 1-, 2-, 3-, 4-, and 5-h storage period was developed. The results obtained are shown in Figure 19.3.

In Figure 19.3a(i–vi), the whole densitograms of individual development tracks are shown for the freshly prepared L-Cys solution (Figure 19.3a(i)), and for the samples stored for 1 + 5 h. In Figure 19.3b(i–vi), the corresponding photographs are presented and in Figure 19.3c(i–vi), the enlarged densitogram fragments are given of the respective chromatograms showing Cys in the monomeric form (encircled black). General characteristics of the densitograms and photographs presented in Figure 19.3 largely resemble those given in Figure 19.2. The predominant peak visible in each densitogram (and the corresponding brown spot on the respective picture) holds for the main fraction of the condensation products, yet it is out of the scope of our

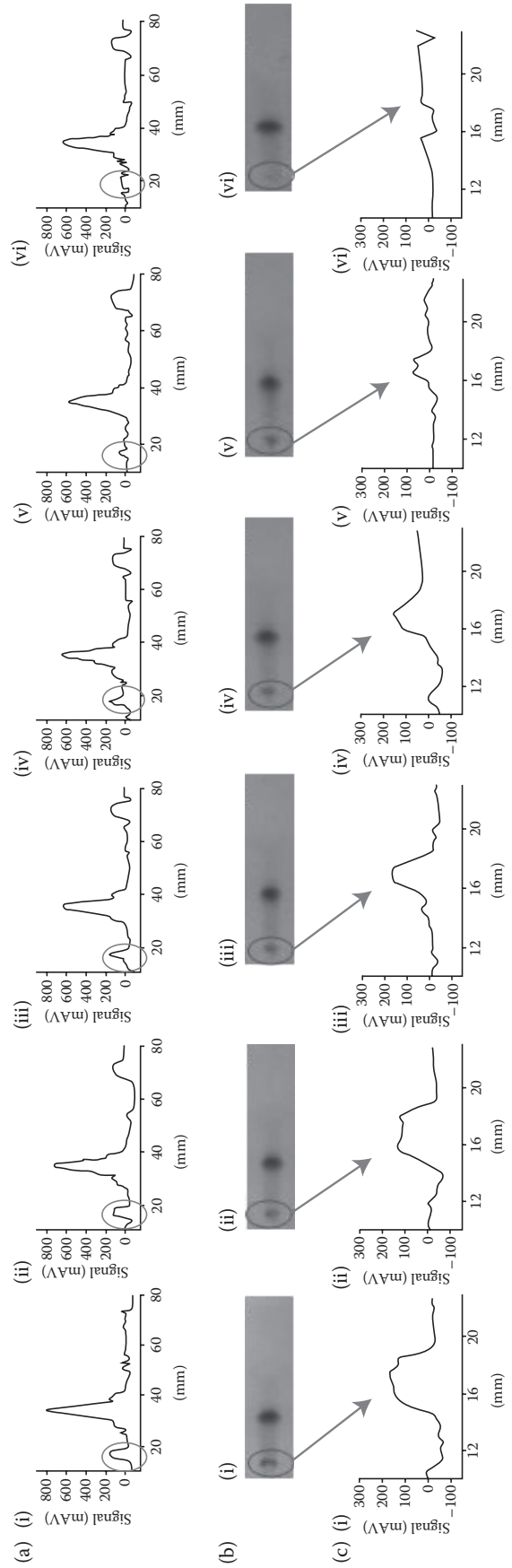

FIGURE 19.3 Densitograms and chromatograms of L-Cys solution with equimolar addition of Zn(II) nitrate. (i) Fresh prepared L-Cys solution; (ii) Cys solution after 1 h aging; (iii) Cys solution after 2 h aging; (iv) Cys solution after 3 h aging; (v) Cys solution after 4 h aging; (vi) L-Cys solution after 5 h aging. (a): Densitometric scans of the whole chromatograms (i)–(vi). (b): Photographs of the whole chromatograms (i)–(vi). (c): Enlarged densitometric scans of the Cys bands (i)–(vi). Black circles and arrows indicate the Cys bands. (From Godziek, A. et al. 2015. *J. Planar Chromatogr.—Modern TLC*, 28: 144–151. With permission.)

discussion. We focus our attention on the blue spot of the monomeric Cys in Figure 19.3b(i–vi), and on the enlarged densitograms of this fragment in Figure 19.3c(i–vi). Initially, color intensity of the blue spot is high, yet in the 1-h interval, considerable lowering of its intensity is observed. The enlarged fragments of the densitograms additionally emphasize the bleaching effect with the blue spot. Namely, the intensity of the Cys monomer peak with the fresh prepared solution equals to 170 mAV and in the course of the 5-h lasting aging, it drops to the bare 36 mAV. In that way, relatively rapid disappearance of the monomeric Cys band is confirmed, which can only be due to the rapidly progressing spontaneous peptidization.

19.3.2 Thin-Layer Chromatography–Electrospray Ionization–Mass Spectrometry

The TLC–ESI–MS experiment was performed for the chromatograms obtained from Experiment 1, yet without using ninhydrin as a visualizing agent [14]. In this experiment, we employed a TLC–MS interface (CAMAG), which enabled direct elution of individual chromatographic bands from the plate to the LC–ESI–MS system. Elution of the target spots was carried out with 50% aqueous methanol. The employed LC–ESI–MS System Varian was equipped with the Varian ProStar model pump, the Varian 100-MS mass spectrometer, and the Varian MS Workstation v. 6.9.1 software for data acquisition and processing. This system operated under the following working conditions: The mobile phase was methanol–water (50:50, *v/v*) at the flow rate of 0.20 mL min^{-1}. Mass spectrometric detection was carried out in the ESI mode (extended ESI/MS scan from *m/z* 100–3500, positive ionization, spray chamber temperature 50°C, drying gas temperature 350°C, drying gas pressure 25 psi, capillary voltage 50 V, needle voltage 5 kV).

In fact, we focused our attention on one spot with the highest retardation factor ($R_F = 0.60 \pm 0.02$), which appeared yellow on visualization and was attributed to the least retarded peptide fraction. For the sake of comparison, we registered mass spectra of the yellow spot originating from the freshly prepared DL-Cys solution (Figure 19.4a) and for that valid for the aged Cys solution (Figure 19.4b), as those which illustrate the sample aging issue in the most spectacular and also direct manner. The results presented in these two figures considerably differ. The primary difference consists in the intensity of the eluted liquid chromatographic signals. In the case of the aged Cys solution, this intensity is considerably higher and measured in MCounts (Figure 19.4b), whereas with the fresh DL-Cys solution, it is much lower and measured in kCounts only (Figure 19.4a). This is convincing evidence of the peptidization yields considerably growing in the course of aging.

Further evidence originates from a comparison of the respective mass spectra registered for the discussed target spots. The most intense peak (229 Counts) present in the mass spectrum of the fresh sample (Figure 19.4a) appears at *m/z* 148 and it can be attributed to monomeric Cys (in the form of the $[Cys + Na + He]^+$ cation). The intensities of peptide signals originating from the fresh sample are much lower than that observed for the signal of the monomer. For the sake of example, let us consider certain peptide signals and the intensities thereof originating from the fresh sample, that is, those at 371 (133 Counts), 959 (55 Counts), and 1373 (37 Counts). The following

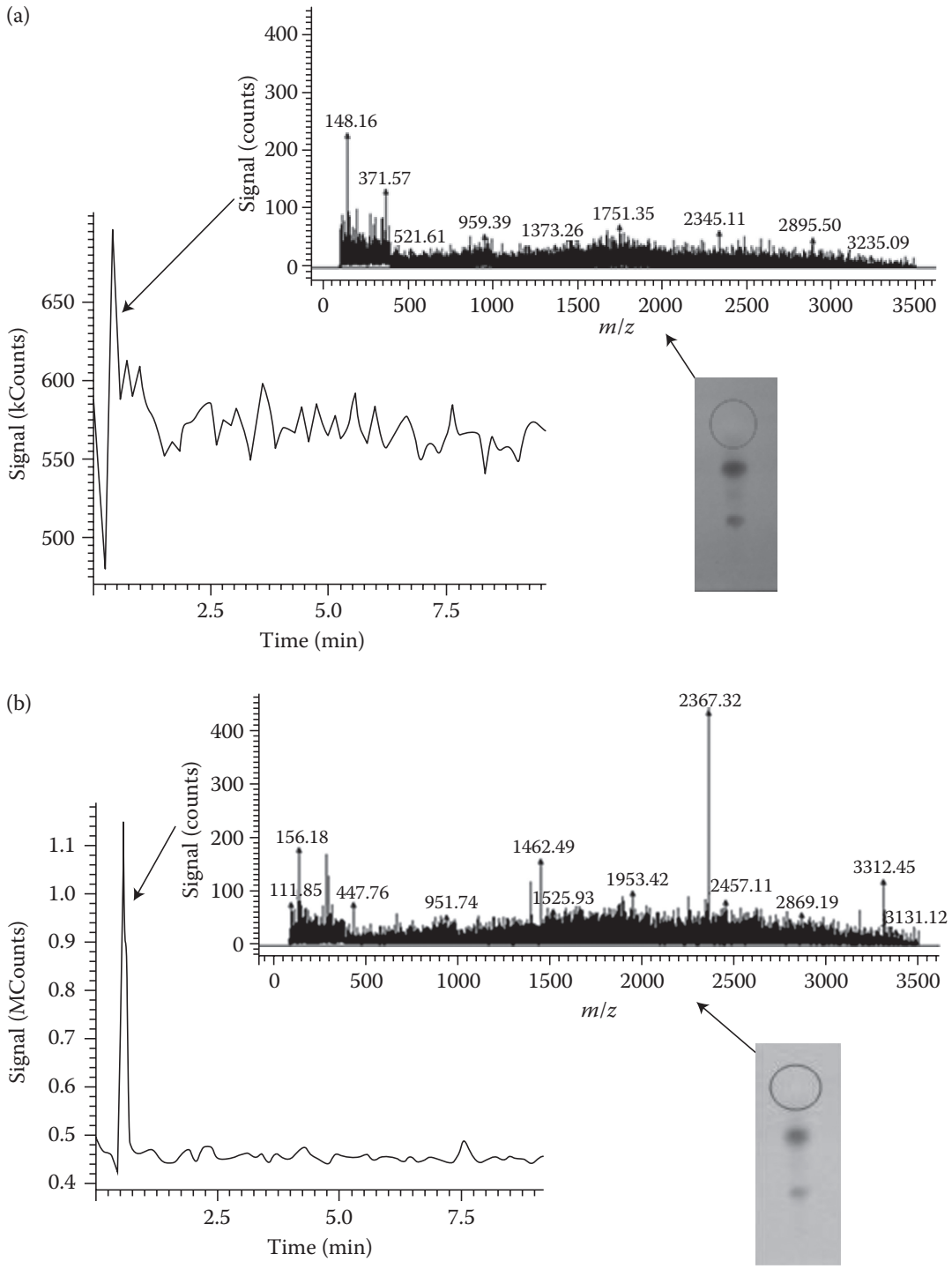

FIGURE 19.4 Thin-layer chromatograms, signals of the chromatographic spots representing an oligopeptide fraction (black framed on the respective chromatograms), directly eluted from the chromatographic plates, and the respective mass spectra recorded for the (a) fresh DL-Cys sample and (b) aged L-Cys sample. (From Maciejowska, A. et al. 2015. *J. Liq. Chromatogr. Relat. Technol*., 38: 1164–1171. With permission.)

ion structures can be attributed to these signals, respectively: $[Cys_3 + CO_2]^+$ (2 peptide bonds), $[Cys_9 + H_2O]^+$ (8 peptide and 2 disulfide bonds), and $[Cys_{13} + H_2O]^+$ (12 peptide and 1 disulfide bond).

Mass spectrum recorded for the yellow spot derived from the aged L-Cys sample (Figure 19.4b) characterizes with an abundance of peptide peaks of considerable intensity. Among these peaks, the following ones can be mentioned: *m/z* 2367 (448 Counts), 1462 (159 Counts), and 951 (56 Counts). To these signals, the following structures can be attributed, respectively: $[Cys_{22} + Na]^+$ (17 peptide bonds and 6 disulfide bonds), $[Cys_{14} + H_2]^+$ (13 peptide bonds), and $[Cys_9 + He + H_2]^+$ (8 peptide bonds). Mass spectrometric characteristics of the yellow spot convincingly demonstrate a good progress of spontaneous peptidization in the course of the L-Cys aging.

19.4 SPONTANEOUS CHIRAL CONVERSION AND PEPTIDIZATION OF METHIONINE

In the study presented in Reference 15, we focused our attention on spontaneous processes of chiral conversion and peptidization running in aqueous acetonitrile solution of L-Met (Scheme 19.3). We chose this amino acid due to its important functions in the human body. L-Met is a donor of methyl groups in the metabolic processes of methyl group transfer; it plays an important role in synthesis of choline and lecithin, promotes normalization of lipid metabolism and hepatic steatosis, and has an antiatherosclerotic activity. Furthermore, L-Met plays an important role in the activities of the adrenal gland, in particular in the synthesis of adrenaline, and in the processes of inactivation of catecholamines, thereby regulating the catecholamine balance. The existence of a close relationship has also been proven between L-Met, folate transformations, and vitamins B6 and B12 [25].

19.4.1 Thin-Layer Chromatography–Densitometry

Two thin-layer chromatographic experiments with densitometric detection were performed with Met [15]. In Experiment 1, the focus was on exposing the dynamics of chiral conversion and peptidization of this amino acid, and in Experiment 2, a nonlinear nature of chiral conversion in a long-term aging course was emphasized. Both experiments were performed with the use of the L-Met solution in 70% aqueous acetonitrile at the concentration of 1.0 mg mL^{-1}. The chromatographic glassplates precoated with microcrystalline cellulose (Merck; cat. # 1.05716), 2-butanol–pyridine–glacial acetic acid–water (30:20:6:24, *v/v*) as mobile phase and ninhydrin as a visualizing agent were employed (following the protocol described in Section 19.2 [13]).

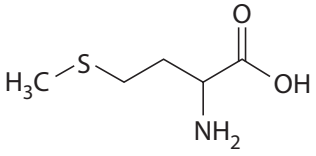

SCHEME 19.3 Chemical structure of Met.

In Experiment 1, the stock L-Met solution was first prepared. From this fresh stock, 1 mL was withdrawn and spiked with an addition of Zn(II) nitrate (the molar ratio of amino acid to Zn(II) nitrate was equal to 2:1, as suggested for an efficient chelating effect with the transition metal cations (e.g., in Reference 21), and the remaining lot was stored for aging. From this 1-mL fresh solution spiked with Zn(II) nitrate, the 5-μL aliquot was spotwise applied to the chromatographic plate. After the 1-h long storage period of stock solution again, 1 mL was withdrawn, spiked with an addition of Zn(II) nitrate, and from this sample, the 5-μL aliquot was spotwise applied to the chromatographic plate. This procedure was carried out in 1-h intervals for 5 h. At the end, the chromatographic plate with the Met samples deposited in it after 0-, 1-, 2-, 3-, 4-, and 5-h storage period was developed. The chromatogram was visualized with ninhydrin and densitometrically scanned (Figure 19.5).

In Figure 19.5a–f, six chromatographic lanes and the corresponding densitograms are shown. Figure 19.5a represents the chromatographic lane and the densitogram for the freshly prepared L-Met sample, whereas Figure 19.5b–f represents respective lanes and densitograms for the Met samples after from 1–5 h aging period. On the chromatograms shown in Figure 19.5a–f, an intense purple-bluish spot (number 2) corresponds

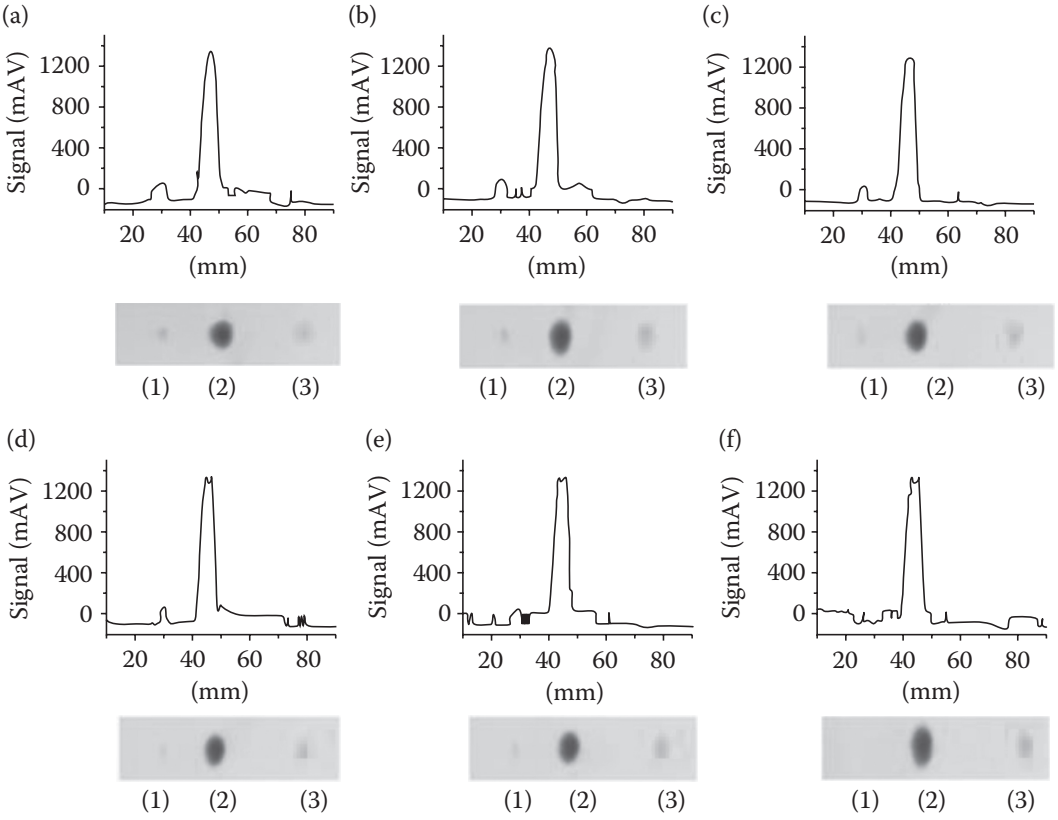

FIGURE 19.5 Chromatographic lanes and densitograms of the L-Met solution with an addition of Zn (II) nitrate (molar ratio of L-Met to zinc (II) nitrate, 2:1). (a) Freshly prepared L-Met solution, and Met solution after (b) 1 h aging, (c) 2 h aging, (d) 3 h aging, (e) 4 h aging, and (f) 5 h aging. (From Maciejowska, A. et al. 2015. *J. Liq. Chromatogr. Relat. Technol.,* 38: 1164–1171. With permission.)

with monomeric L-Met, a less intense purple-bluish spot (number 1) corresponds with monomeric D-Met, and the yellow spot (number 3) represents peptide fraction. One advantage of using ninhydrin as a visualizing reagent is that it allows differentiating between blue or purple-bluish spots of monomeric amino acids and yellow or brown spots of peptide fraction. The intense purple-bluish spot number 2 ($R_F = 0.54 \pm 0.02$) originating from monomeric L-Met, characterizes with practically equal signal intensity in each densitogram. The presence of yellow spot number 3 on all chromatograms ($R_F = 0.92 \pm 0.02$) witnesses to considerable L-Met peptidization rate, although this spot becomes more distinct after 5-h sample aging only. The presence of the less intense purple-bluish spot number 1 originating from D-Met ($R_F = 0.30 \pm 0.02$) in the freshly prepared L-Met sample witnesses to the high rate of chiral conversion, yet its intensity drop in the course of the sample storage period is the most characteristic feature of Experiment 1. This intensity drops from 70.56 mAV for peak 1 in the freshly prepared sample to 55.89 mAV after a 2-h storage period, to 44.48 mAV after a 4-h storage period, and to 8.62 mAV after a 5-h storage period. A relatively short (5 h) storage period of the Met sample and a relatively long (1 h) sampling interval did not allow perceiving an oscillatory pattern of the amino acid chiral conversion. However, reappearance of the D-Met signal after 5 months' sample aging (demonstrated in Experiment 2) serves as an indication of an oscillatory nature of chiral conversion.

In Experiment 2, chromatographic plates were activated by heating for 30 min at 110°C prior to applying the amino acid samples. Just before the chromatographic analysis, Zn(II) nitrate was added to the two Met samples, that is, to the fresh L-Met solution and after 5 months' aging (again, the molar ratio of amino acid to Zn(II) nitrate was 2:1). On the development, the chromatograms were visualized with ninhydrin and densitometrically scanned. The results obtained for the freshly prepared L-Met sample and for that after 5 months' storage period are presented in Figure 19.6a and b, respectively.

Again, the chromatographic spots numbers 1–3 were detected in both chromatograms, with the intense purple-bluish spot number 2 originating from monomeric L-Met, the less intense purple-bluish spot number 1 originating from monomeric D-Met, and the yellow spot number 3 originating from the peptide fraction. Spots in the chromatogram and the corresponding concentration profiles in the densitogram were indicated pair-wise with red ovals. Signal of the intense purple-bluish spot number 2 originating from monomeric L-Met is the highest and its intensity does not considerably change in the course of the 5 months' storage period. Signal of the less intense purple-bluish peak number 1 (originating from monomeric D-Met) is very low (10.42 mAV) with freshly prepared L-Met sample, yet after the storage period of 5 months, it grows to 85.67 mAV. In Experiment 1, we saw a decrease of intensity of peak 1 in the course of the initial 5 h monitoring the process of aging, and now, we observe an intensity growth in the course of the 5 months' aging. A comparison of the results originating from Experiments 1 and 2 and valid for peak 1 indirectly points to a nonlinear pattern of chiral conversion of Met. Yellow spot number 3 in Figure 19.6b valid for the peptide fraction after 5 months' sample aging is more intense than spot number 3 in Figure 19.6a, valid for the freshly prepared L-Met solution. This is a direct proof that the process of sample aging results in gradual accumulation of peptides.

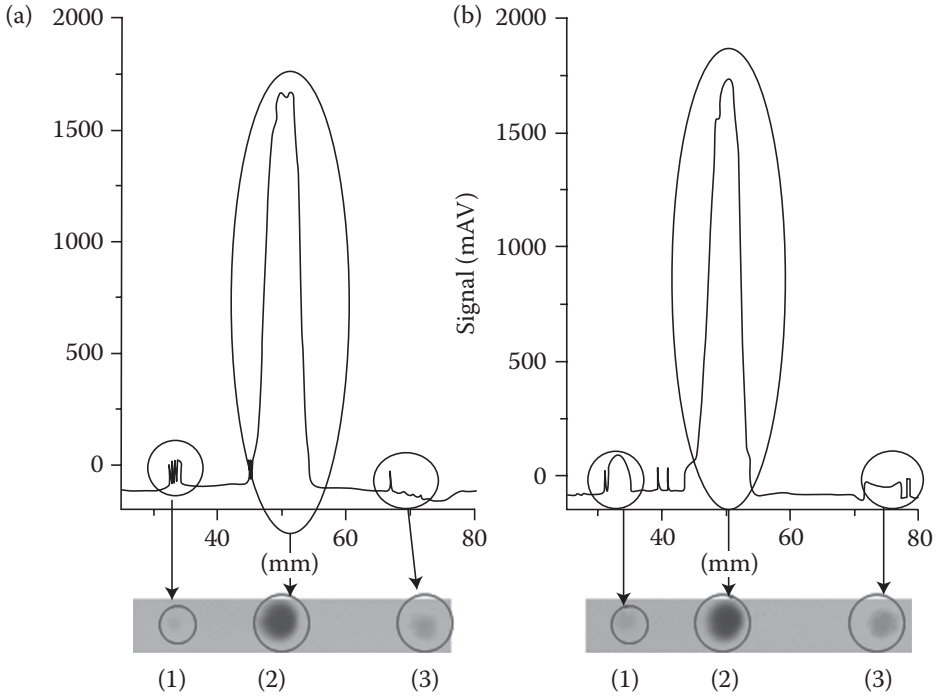

FIGURE 19.6 Chromatographic lanes and densitograms for the L-Met solution with an addition of Zn (II) nitrate (molar ratio of L-Met to zinc (II) nitrate, 2:1). (a) Freshly prepared L-Met solution; (b) Met solution after 5 months' aging; (1) D-Met; (2) L-Met; (3) peptide fraction. (From Maciejowska, A. et al. 2015. *J. Liq. Chromatogr. Relat. Technol.,* 38: 1164–1171. With permission.)

19.4.2 Thin-Layer Chromatography–Electrospray Ionization–Mass Spectrometry

Important evidence on the reactions spontaneously occurring in the course of the L-Met aging was obtained with use of TLC–ESI–MS. The analyses were carried out for the chromatograms obtained according to the procedure assumed for L-Met in Experiment 2 and the results are presented in Figure 19.7. Figure 19.7a, c, and e shows the mass spectra recorded for spots numbers 1–3 from the chromatogram of the freshly prepared L-Met sample, and Figure 19.7b, d, and f shows the analogous mass spectra recorded from the chromatogram of the L-Met sample after 5 months' aging. Mass spectra valid for the freshly prepared and the aged Met sample evidently differ, in spite of an earlier recognized fact that with use of the TLC–MS interface considerable amounts of the background (noise) signals appear, which make interpretation of the spectra a challenging task [16]. Now, let us focus on the message extracted from Figure 19.7.

In Figure 19.7a, the chromatogram and mass spectrum recorded from the freshly prepared sample and valid for an intense purple-bluish spot of monomeric L-Met are given, and the predominant signal in this spectrum appears at *m/z* 301, which can possibly be attributed to $[Met_9 + 4H]^{4+}$. However, peak of monomeric Met at *m/z* 144 can also be seen, with a loss of 6 Da in fragmentation. Last but not least, more peaks

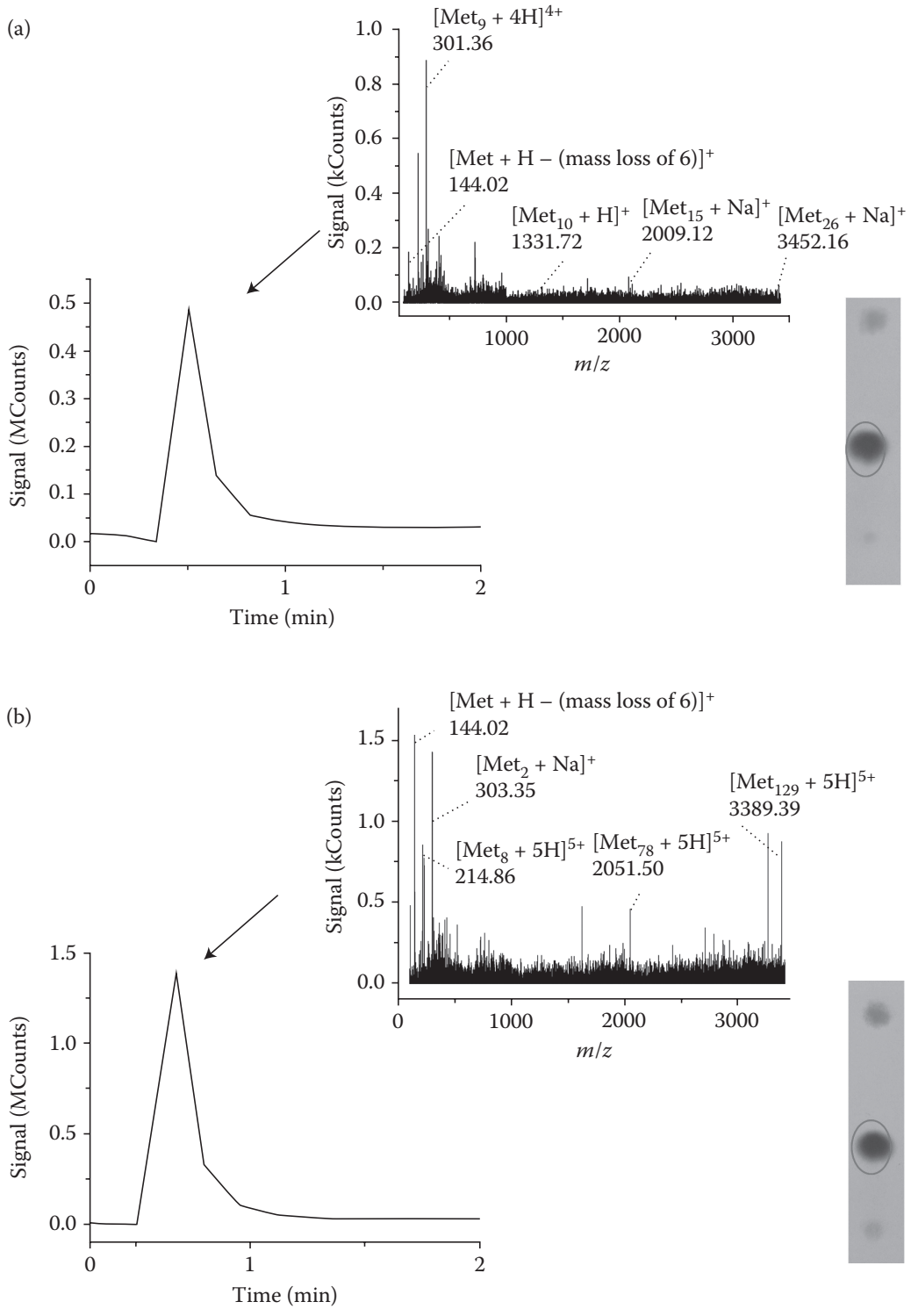

FIGURE 19.7 Thin-layer chromatograms, signals of chromatographic spots marked with red oval and directly eluted from the chromatographic plate, and the respective mass spectra recorded for L-Met fraction in (a) freshly prepared and (b) aged solution, peptide fraction in (c) freshly prepared and (d) aged solution, and D-Met fraction in (e) freshly prepared and (f) aged solution. (From Maciejowska, A. et al. 2015. *J. Liq. Chromatogr. Relat. Technol*., 38: 1164–1171. With permission.) (*Continued*)

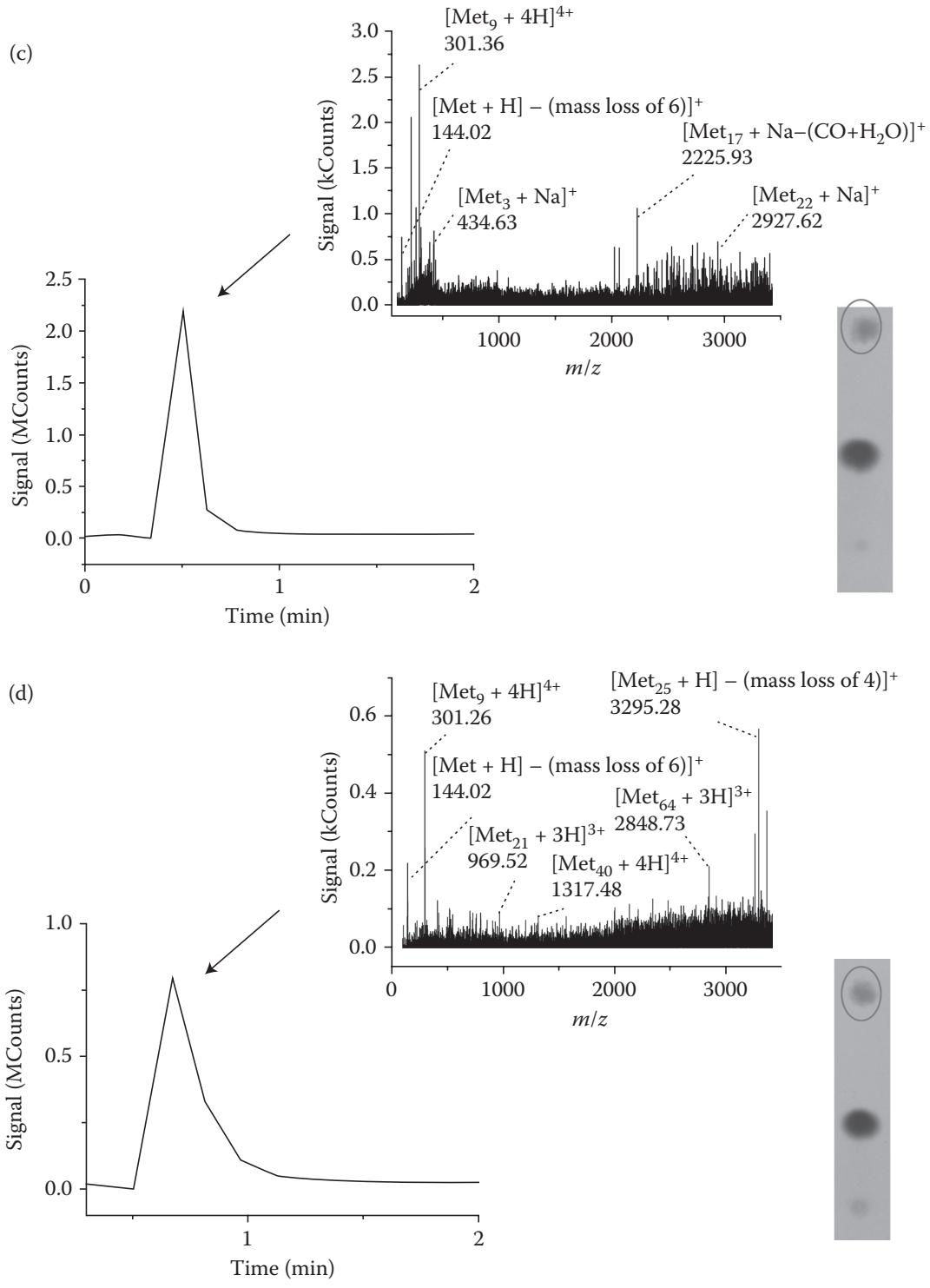

FIGURE 19.7 (Continued) Thin-layer chromatograms, signals of chromatographic spots marked with red oval and directly eluted from the chromatographic plate, and the respective mass spectra recorded for L-Met fraction in (a) freshly prepared and (b) aged solution, peptide fraction in (c) freshly prepared and (d) aged solution, and D-Met fraction in (e) freshly prepared and (f) aged solution. (From Maciejowska, A. et al. 2015. *J. Liq. Chromatogr. Relat. Technol.*, 38: 1164–1171. With permission.) (*Continued*)

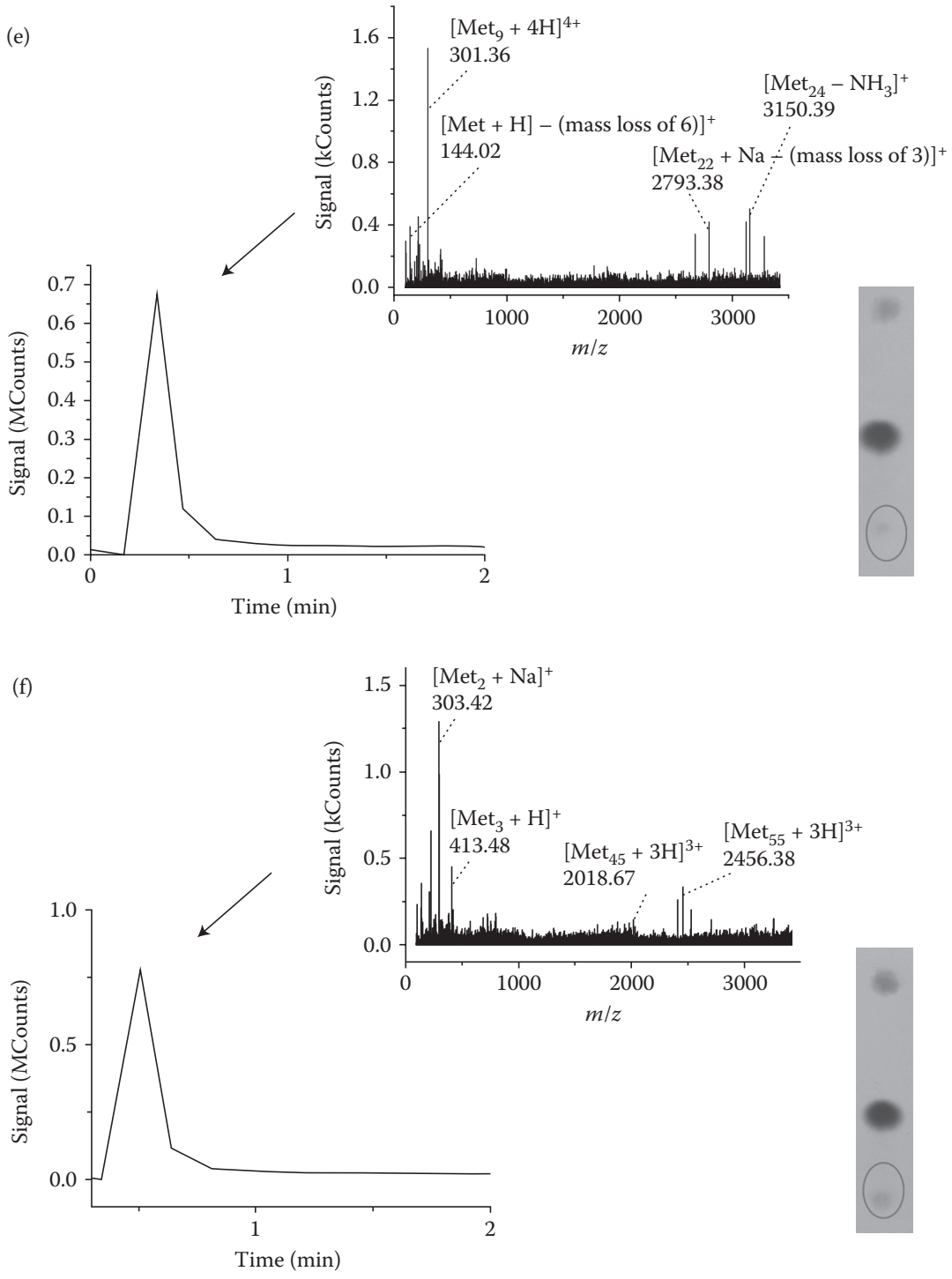

FIGURE 19.7 (Continued) Thin-layer chromatograms, signals of chromatographic spots marked with red oval and directly eluted from the chromatographic plate, and the respective mass spectra recorded for L-Met fraction in (a) freshly prepared and (b) aged solution, peptide fraction in (c) freshly prepared and (d) aged solution, and D-Met fraction in (e) freshly prepared and (f) aged solution. (From Maciejowska, A. et al. 2015. *J. Liq. Chromatogr. Relat. Technol*., 38: 1164–1171. With permission.)

originating from peptides are present in this spectrum, although their intensities are quite low. In Figure 19.7b, valid for an intense purple-bluish spot of Met in the aged sample, the predominant signal at *m/z* 144 represents monomeric Met. However, higher signals at, for example, *m/z* 2051 and 3389 are also present, which can be attributed to $[Met_{78} + 5H]^{5+}$ and $[Met_{129} + 5H]^{5+}$, respectively. In fact, molecular weights of these two peptides are equal to 10,252 and 16,944 Da, respectively, which explains their low mobility in the employed thin-layer chromatographic system, and sticking to the monomeric fraction.

In Figure 19.7c, the chromatogram and mass spectrum recorded from the freshly prepared sample and valid for the yellow spot of peptide fraction are given. Again, signal at *m/z* 301 is predominant, yet other signals originating from the peptides are also intense (e.g., those at *m/z* 2225 and 2927, which might correspond with $[Met_{17} + Na - (CO + H_2O)]^+$ and $[Met_{22} + Na]^+$, respectively). The intense peptide signals recorded from the freshly prepared sample witness to an efficient and rapid peptidization process. In Figure 19.7d, chromatogram and mass spectrum are given valid for the yellow spot of peptide fraction in the aged sample. This mass spectrum confirms considerable progress of peptidization in the course of the 5 months' aging (as compared with that for the corresponding yellow spot from the freshly prepared sample; Figure 19.7c).

Data shown in Figure 19.7e refer to a less intense purple-bluish spot valid for monomeric D-Met, obtained through chiral conversion of L-Met in the freshly prepared solution. Due to rather low conversion yields, signal intensities in this spectrum are relatively low, yet the mass spectral pattern valid for this spot resembles that recorded for the monomeric L-Met in the freshly prepared solution (Figure 19.7a). In Figure 19.7f, valid for the less intense purple-bluish spot of D-Met in the aged sample, considerable intensity growth of the predominant peak representing D-Met is observed. This result confirms an efficient chiral conversion of L-Met in the course of the 5 months' aging and corresponds well with the thin-layer chromatographic results summarized in Figure 19.6.

Surprisingly, many peptides remained unresolved from the monomeric L-Met fraction (Figure 19.7a and b), and from the monomeric D-Met fraction as well. A persuasive evidence of this fact was confirmed by the photograph of the monomeric L-Met fraction taken from the back side of chromatographic plate (Figure 19.8). From this transparent glass backside, a "yellow eye" can be seen in the center of each purple-bluish spot, representing peptides (which remain invisible from the front side of the visualized adsorbent layer). In that way, clear explanation is given why

FIGURE 19.8 Photograph of the back side of a chromatographic plate showing the purple-bluish spot of monomeric L-Met with the "yellow eye" of peptide fraction inside of it. (From Maciejowska, A. et al. 2015. *J. Liq. Chromatogr. Relat. Technol.,* 38: 1164–1171. With permission.)

mass signals originating from peptides were recorded from the purple-bluish spots of monomeric L-Met and D-Met. A more general comment can also be made that an imperfect separation performance of TLC is in certain cases rather incompatible with high sensitivity of mass spectrometry (thus considerably adding to an inconvenience of background signals of different origin, encountered in the TLC–ESI–MS technique and discussed in Reference 16).

19.5 CONCLUSIONS

1. TLC–ESI–MS has to be accompanied by TLC–densitometry and/or videoscanning (photography) of the developed chromatograms, in order to help localize separated chromatographic bands on the adsorbent layers, prior to their elution with use of the TLC–MS interface.
2. In the case of complex samples and the thin-layer fractionation thereof, mass spectra obtained by means of TLC–ESI–MS basically serve as fingerprints, providing information of qualitative or semiquantitative importance. This is due to an imperfect chromatographic separation and an additional eclipsing effect of background signals (extensively discussed in Reference 16), combined with high sensitivity of the mass spectrometric technique.
3. As a confirmation of the above statement, similar complex mass spectra of the fingerprint importance can be quoted, which have been recorded for medicinal plant extracts from the chromatographic thin layers and shown in papers [26–29].
4. In the research discussed in this chapter and dealing with spontaneous chiral conversion and peptidization of amino acids, fingerprint results obtained with use of the TLC–ESI–MS technique serve as convincing evidence of the chiral conversion and peptidization progress and furnish certain information on identity of the formed species.

REFERENCES

1. Sajewicz, M., Piętka, R., Pieniak, A., and Kowalska, T. 2005. Application of thin-layer chromatography (TLC) to investigating oscillatory instability of the selected profen enantiomers, *Acta Chromatogr.*, 15: 131–149.
2. Sajewicz, M., Gontarska, M., and Kowalska, T. 2014. HPLC/DAD evidence of the oscillatory chiral conversion of phenylglycine, *J. Chromatogr. Sci.*, 52: 329–333.
3. Sajewicz, M., Kronenbach, D., Gontarska, M., Wróbel, M., Piętka, R., and Kowalska, T. 2009. TLC in search for structural limitations of spontaneous oscillatory in-vitro chiral conversion. α-hydroxybutyric and mandelic acids, *J. Planar Chromatogr.—Modern TLC*, 22: 241–248.
4. Sajewicz, M., Kronenbach, D., Gontarska, M., and Kowalska, T. 2010. TLC and polarimetric investigation of the oscillatory *in vitro* chiral conversion of r-β-hydroxybutyric acid, *J. Liq. Chromatogr. Relat. Technol.*, 33: 1047–1057.
5. Belanger, P., Atkinson, J.G., and Stuart, R.S. 1969. Exchange reactions of carboxylic acid salts; Kinetics and mechanism, *J. Chem. Soc. D: Chem. Commun.*, 1067–1068.
6. Xie, Y., Liu, H., and Chen, J. 2000. Kinetics of base-catalyzed racemization of ibuprofen enantiomers, *Int. J. Pharm.*, 196: 21–26.

7. Godziek, A., Maciejowska, A., Sajewicz, M., and Kowalska, T. 2015. HPLC monitoring of spontaneous non-linear peptidization dynamics of selected amino acids in solution, *J. Chromatogr. Sci.*, 53: 401–410. DOI: 10.1093/chromsci/bmu122.
8. Sajewicz, M., Dolnik, M., Kowalska, T., and Epstein, I.R. 2014. Condensation dynamics of L-proline and L-hydroxyproline in solution, *RSC Adv.*, 4: 7330–7339.
9. Sajewicz, M., Godziek, A., Maciejowska, A., and Kowalska, T. 2015. Condensation dynamics of the L-Pro-L-Phe and L-Hyp-L-Phe binary mixtures in solution, *J. Chromatogr. Sci.*, 53: 31–37. DOI: 10.1093/chromsci/bmu006.
10. Sajewicz, M., Matlengiewicz, M., Leda, M., Gontarska, M., Kronenbach, D., Kowalska, T., and Epstein, I.R. 2010. Spontaneous oscillatory *in vitro* chiral conversion of simple carboxylic acids and its possible mechanism, *J. Phys. Org. Chem.*, 23: 1066–1073.
11. Shoseyov, O. and Levy, I. (Eds.) 2008. *NanoBioTechnology: BioInspired Devices and Materials of the Future*, Humana Press, Totowa, NJ.
12. Castillo, J., Sasso, L., and Svendsen, W.E. (Eds.) 2013. *Self-Assembled Peptide Nanostructures: Advances and Applications in Nanobiotechnology*, Pan Stanford Publishing, Singapore.
13. Sajewicz, M., Matlengiewicz, M., Juziuk, M., Penkala, M., Weloe, M., Schulz, M., and Kowalska, T. 2013. Thin-layer chromatographic evidence of proline peptidization in solution and its thin-layer chromatographic enantioseparation, *J. Liq. Chromatogr. Relat. Technol.*, 36: 2497–2511.
14. Godziek, A., Maciejowska, A., Talik, E., Sajewicz, M., and Kowalska, T. 2015. Thin-layer chromatographic investigation of L-cysteine in solution, *J. Planar Chromatogr.—Modern TLC*, 28: 144–151.
15. Maciejowska, A., Godziek, A., Talik, E., Sajewicz, M., and Kowalska, T. 2015. Investigation of spontaneous chiral conversion and oscillatory peptidization of L-methionine by means of TLC and HPLC, *J. Liq. Chromatogr. Relat. Technol.*, 38: 1164–1171.
16. Morlock, G.E. 2014. Background mass signals in TLC/HPTLC–ESI–MS and practical advices for use of the TLC–MS interface, *J. Liq. Chromatogr. Relat. Technol.*, 37: 2892–2914.
17. Mack, M., Hauck, H., and Herbert, H. 1988. Enantiomeric separation in TLC with the new HPTLC pre-coated plate CHIR with concentration zone, *J. Planar Chromatogr.—Modern TLC*, 1: 304–308.
18. Fukuhara, T., Isoyama, M., Shimada, A., Itoh, M., and Yuasa, S. 1987. Resolution of six polar DL-amino acids by chromatography on native cellulose. *J. Chromatogr.*, 387: 562–565.
19. Fukuhara, T., Isoyama, M., Shimada, A., Itoh, M., and Yuasa, S. 1987. Resolution of all proteinic DL-amino acids on native cellulose chromatography, *Sci. Rep. Osaka Univ.*, 35: 11–21.
20. Sajewicz, M., John, E., Kronenbach, D., Gontarska, M., and Kowalska, T. 2008. TLC study of the separation of the enantiomers of lactic acid, *Acta Chromatogr.*, 20: 367–382.
21. Sajewicz, M., John, E., Kronenbach, D., Gontarska, M., Wróbel, M., and Kowalska, T. 2009. How to suppress the spontaneous oscillatory in-vitro chiral conversion of α-substituted propionic acids? A thin-layer chromatographic, polarimetric, and circular dichroism study of complexation of the Cu(II) cation with L-lactic acid, *Acta Chromatogr.*, 21: 39–55.
22. Valko, M., Leibfritz, D., Moncol, J., Cronin, M.T.D., Mazur, M., and Telser, J. 2007. Free radicals and antioxidants in normal physiological functions and human disease, *Int. J. Biochem. Cell Biol.*, 39: 44–84.
23. Huxtable, R.J. 1992. Physiological actions of taurine, *Physiol. Rev.*, 72: 101–163.
24. Bhushan, R. and Martens, J. 2010. *Amino Acids*, HNB Publishing, New York, pp. 76, 85.

25. Murray, R.K., Bender, D.A., Botham, K.M., Kennelly, P.J., Rodwell, V.W., and Weil, P.A. 2012. *Harper's Illustrated Biochemistry*, 29th ed., McGraw-Hill, New York.
26. Sajewicz, M., Wojtal, Ł., Hajnos, M., Waksmundzka-Hajnos, M., and Kowalska, T. 2010. Low-temperature TLC–MS of essential oils from five different sage (Salvia) species, *J. Planar Chromatogr.—Modern TLC*, 23: 270–276.
27. Sajewicz, M., Wojtal, Ł., Natić, M., Staszek, D., Waksmundzka-Hajnos, M., and Kowalska, T. 2011. TLC–MS versus TLC–LC–MS fingerprints of herbal extracts. Part I. Essential oils, *J. Liq. Chromatogr. Relat. Technol.*, 34: 848–863.
28. Sajewicz, M., Staszek, D., Natić, M., Wojtal, Ł., Waksmundzka-Hajnos, M., and Kowalska, T. 2011. TLC–MS versus TLC–LC–MS fingerprints of herbal extracts. Part II. Phenolic acids and flavonoids, *J. Liq. Chromatogr. Relat. Technol.*, 34: 864–887.
29. Sajewicz, M., Staszek, D., Natić, M., Waksmundzka-Hajnos, M., and Kowalska, T. 2011. TLC–MS versus TLC–LC–MS fingerprints of herbal extracts. Part III. Application of the reversed phase liquid chromatography systems with C18 stationary phase, *J. Chromatogr. Sci*., 49: 560–567.